Neogene and Quaternary clay minerals in the southern North sea

Rieko Adriaens

Supervisor:
Prof. Dr. Noël Vandenberghe
Co-supervisor:
Prof. Dr. Jan Elsen

Examination Committee:
Prof. Dr. Manuel Sintubin, *chairman*
Prof. Dr. Philippe Muchez
Prof. Dr. Abderrazak El Albani
Prof. Dr. Stephen Louwye
Dr. Michael Fettweis

Dissertation presented in partial fulfilment of the requirements for the degree of Doctor of Science

February 2015

ISBN 978-90-8649-792-8
D/2015/10.705/2

ISSN 0250-7803
Aardkundige Mededelingen 47

DANKWOORD

Done-afgelopen-gedaan !!! Dit doctoraat was een leuke ervaring met veel mooie momenten afgewisseld met de nodige frustraties. Gelukkig is het vooral de eerste groep die bijblijft en dat komt niet in het minste doordat ik gedurende deze periode de steun kreeg van talrijke personen.

Allereerst zou ik graag promotor Noël Vandenberghe bedanken. Ik kon steeds terecht bij u voor vragen, advies en begeleiding - dat heeft me echt vaak vooruit geholpen – maar u liet me ook mijn eigen weg gaan. Gelukkig kon ik ook rekenen op uw grootste talent, namelijk het kristalhelder verwoorden van de essentie van bepaalde zaken. Ik geloof ook dat ik u grondig moet bedanken voor het geduldig nalezen van mijn teksten, ik ben er zeker van dat u regelmatig een West-Vlaamse vloek heeft afgevuurd. Ik zal niet zeggen dat ik niet eens gevloekt hebt na het lezen of horen van uw commentaren, maar dat was dan vooral omdat ik besefte dat u, zoals wel vaker, een punt had. De samenwerking is, zeker wat mij betreft, altijd prima verlopen en ik hoop dat het nog enige tijd zo kan verder gaan. Bovendien wordt 2015 misschien wel eindelijk het jaar van Club... Het zal wel moeten want volgend seizoen zal het een pak moeilijker worden aangezien ze alvast 3 punten op Stayen zullen verliezen…

Verder wil ik ook co-promotor Jan Elsen bedanken voor de ondersteuning, discussies en het nalezen van teksten. Ook de andere leden van de examencommissie Abder El Albani, Michael Fettweis, Stephen Louwye, Philippe Muchez en Manuel Sintubin wens ik grondig te danken voor het zorgvuldig nalezen van mijn teksten en de daarop volgende interessante discussies en suggesties. Verder zou ik ook graag Alain Meunier en Abder El Albani bedanken voor hun goede ontvangst en enorm interessante discussies in Poitiers.

Tijdens dit doctoraat kon ik ook rekenen van een heleboel mensen voor het aanleveren van data, staalnames en hulp hierbij. Marleen De Ceukelaire wil ik graag bedanken voor de vlotte samenwerking, het uitzoeken van boringen bij de Geologische Dienst en zelfs het opsporen van “verdwenen” kernen. Hierbij kon ik ook rekenen op de hulp van Frans Moorkens. Piet Laga wens ik te bedanken om boringen te selecteren, mee te gaan kijken naar kernen en het opsnorren van je vroegere boorbeschrijvingen en foraminiferen-analyses. Ik wil ook graag NIRAS en SCK bedanken dat ik kon werken op materiaal uit hun hoge kwaliteitskernen en Serge Labat voor de praktische begeleiding hierbij. Laurent Wouters en Koen Beerten wil ik bedanken voor het aanleveren van data en reeds beschikbare analyses. Karel De Mey wil ik bedanken voor de toelating tot bemonstering van de “PIDPA”-boring. Rik Houthuys wil ik bedanken voor de discussies over de Vlaamse heuvels. De medewerking van Pim Demecheleer en Koen Vos (SIBELCO-SCR) wordt ook sterk geapprecieerd. Katrien De Nil wil ik bedanken voor het ter beschikking stellen van geologische kaarten. Wim Westerhoff wens ik te bedanken voor de monsters uit het Nederlandse kernhuis. Het BMM en vooral Michael Fettweis wil ik bedanken om de staalname-campagnes met de Belgica mogelijk te maken. Ondanks dat de Belgica mij een stevige zeeziekte bezorgde, was het een heel avontuur! Voorts wil ik ook Hans Verreecken, Joris Vanlede, Jan De Schutter bedanken voor de hulp en toelating voor het nemen van suspensiestalen op verschillende plaatsen in Scheldebekken. Tijdens deze staalnames kon ik rekenen op de ervaren begeleiding van Ivo Mielants, bedankt! Een speciale dankjewel is er ook voor Elin Vanlierde voor het aanleveren van debieten en suspensieconcentraties, de hulp bij de verwerking ervan en de leuke discussies. Ik bedank ook Hans Middelkoop en Kathleen Fontaine voor het aanleveren van nuttige stalen. Ik apprecieer ook de fijne interessante wetenschappelijke samenwerkingen met

Ruben Snellings, Gilles Mertens, Tom Haerinck, Benedicta Ronchi, Alexis Licht, Hemmo Abels, Els Verstrynghe, Lieven Machiels en Jasper Verhaegen. Voorts wil ik ook Wathab Mohammad, Ellen Barrie, Johanna Gauquie, Ruth Fierens, Katherine Lauriks, Nicole Dilissen, Robin Honlet, Mathieu Degros Sofie Hollanders, Elise François, Caroline Van den Heuvel, Jasper Verhaegen en Yaana Bruneel bedanken voor hun geapprecieerde hulp op terrein of in het labo. Ik herinner mij nog levendig dat de Van Veen grijper kwam vast te zitten in de Dender en hem al zwemmend, GSM inclusief, ben moeten gaan bevrijden. Ik geloof dat ik Caroline en Jasper moet bedanken om geen bezwarende foto's te nemen. Het verhaal zal echter blijven bestaan vrees ik…

Ook "nen dikke merci" aan Nancy, Ria en Wathab! Jullie leerden mij eerst de kneepjes van het labowerk en deden nadien een gigantisch aantal kleivoorbereidingen voor mij tijdens dit onderzoek. Heel erg bedankt! Jullie bleven ook altijd meedenken tijdens het labowerk hetgeen ik enorm heb geapprecieerd. De leukste momenten uit mijn doctoraat zijn vaak in het labo geweest om samen met jullie te bekijken hoe we problemen konden oplossen of wegdromen naar gemaakte of toekomstige reizen. Ik kan niet genoeg benadrukken hoezeer ik jullie bijdrage op prijs stel ! Dirk zou ik graag bedanken voor de nodige chirurgische ingrepen en reanimaties van de diffractometers. Ik assisteerde ook graag zodat ik erg veel bij kon leren over de technische kant van de toestellen en de complexiteit van de koelinstallaties. Dat is ook meermaals zeer handig gebleken aangezien de diffractometers systematisch blijken in staking te gaan wanneer jij met verlof bent! Ook de samenwerking met Elvira en Herman ging steeds erg vlot, bedankt voor jullie inzet! Ook Edwin, bedankt ! Je zette me op de juiste klei-weg waardoor ik al tijdens mijn studententijd wegwijs raakte met XRD interpretaties van kleien. Ook tijdens het vakantiewerk in het labo, leerde ik al een hoop bij die achteraf enorm van pas is gekomen. Ik kon ook steeds rekenen op de spontane hulp van Ria Mattheus en Petra Stassaert: bedankt! Tijdens dit doctoraat werkte ik ook erg vaak samen met Gilles aan allerlei projecten waardoor ik erg veel kon bijleren. De exponent van deze succesvolle samenwerking zijn onze deelnames, en uitstekende positionering, in de Reynolds Cup. Ik hou ook prima herinneringen over aan tripjes naar Porto en Dresden ! Ik wens jou, en Qmineral, alle succes toe in de toekomst!

Dit doctoraat zal mij voor altijd bijblijven omwille van de koffiepauzes, afdelingsuitstappen, PhD-midweeks, vrijgezellenfeesten, 7Oaks-bezoekjes, pina-coladas, veldritten, excursies, barbeques, de Muco-for-live actie enzoverder. Deze fantastische momenten werden ook mede mogelijk gemaakt door collega's Koen, Benedicta, Tom, Carl, Kim ,Mathias, Jorik, Julie, Marijke, en natuurlijk nog vele anderen. Bedankt voor deze leuke momenten. Ook de onnavolgbare jaarlijkse weekendjes met "de maten", Bene ("den Benny") en Jean, Stijn en Nathalie en Koen en Cindy waren geweldig. Ik hoop dat we nog vaak de Ardense bossen onveilig mogen maken ! *"Da we nog lang mogen mogen en goe kunnen kunnen !"*

Fréderic "Freddy", trouwe kameraad en mede-STVV supporter, merci voor de gezellige avonden op café of op de voetbal ! Ook de mannen van de basket zijn echte kameraden "*Jaja, ik voel het al…"*

Graag wil ook mijn familie bedanken voor de onvoorwaardelijke steun. In het bijzonder wil ik mijn ouders bedanken om mij steeds alle kansen te geven en mijn eigen keuzes te laten maken. Ik kon ook steeds bij jullie terecht Ook mijn zus Tamara, haar vriend Tom en vooral mijn neefjes Daan en Roel konden erg makkelijk een glimlach op mijn gezicht toveren bij een troebele blik of frustrerende dag.

En dan is er natuurlijk nog Sofie, die mij uit het niets met één blik spontaan kan doen glimlachen. Erg bedankt voor je geduld, je steun en luisterend oor. Je maakt me gelukkig en ik hoop dat dat zo mag blijven voor de rest van ons leven, te beginnen met ons huwelijk in 2015 !!!

Abstract

Although the clay mineral fraction of sediments often holds important information regarding provenance, paleogeography and climatic conditions, the poor reliability of clay mineral quantification in the past has made that the large potential of clay mineralogical analyses has never been fully exploited. However, with the introduction of systematic and standardized preparation procedures and the development of highly-specialized interpretation software, quantitative clay mineralogy by X-ray diffraction analysis has become a reliable and powerful tool in sediment characterization studies.

In this work, quantitative clay mineralogy, complemented with sediment petrological analyses, is used primarily as a tool for lithostratigraphic characterization of the pelletal glauconite-rich Neogene succession of the Campine basin in Belgium. For this purpose, X-ray diffraction was applied on clay material <2µm prepared on oriented clay slides as well as on random oriented powder patterns, the latter allowing decomposition and separate quantification of the 060-region. Results revealed clay-sized glauconite is a systematic and important contributor to the clay fraction of pelletal glauconite-bearing sands in both Miocene and Pliocene deposits but is systematically absent in the clay fraction of intercalated clay laminae. This suggests a relation with pelletal glauconite. This hypothesis is confirmed as the mineralogy of clay-sized and pelletal glauconite is nearly identical. Based on size distributions curves combined with pelletal glauconite dating, it was concluded that pelletal glauconite in the Neogene is massively reworked from older deposits, except for the Antwerp Member, and underwent significant amounts of transport.

This transport caused clay-sized glauconite to be introduced in the clay fraction through the abrasion and/or disintegration of pelletal glauconite upon transport resulting in very similar pelletal and clay-sized glauconite mineralogical characteristics. Nevertheless, the increased expandability of clay-sized glauconite compared to pelletal glauconite shows that the former is more reactive.

The systematic analysis of the different units showed little variability in clay composition of the Berchem Fn and the marine part of the Bolderberg Fm, which contain smectite-rich clay assemblages with relatively high expandable glauconite-smectite. Also the Deurne and Dessel Members of the Diest Formation are characterized by such clay mineral composition which suggests reworking. A significant break in clay and glauconite mineralogy is found in the Diest sand member with the introduction of a glauconite-smectite dominated clay mineralogy which furthermore is low expandable (Diest D1 unit). The clay mineralogical characteristics of this Diest D1 unit are no different from the characteristics of the Hageland Diest sand. In the western part of the Campine basin, a clayey, glauconite-poor sand unit was found, termed the Diest D2 to D3 unit. Results also reveal that the top part of the Diest Formation, although not occurring over the entire Campine basin, consists of ex-situ weathered glauconitic sediments, as indicated by the presence of trioctahedral Fe-vermiculite and kaolinite-expandable minerals.

The main objective in this work was to use quantitative clay mineralogical results in order to better define the stratigraphic boundaries in the Neogene. This was demonstrated for the Diest-Kasterlee-Mol stratigraphic issue where it was shown that clay mineralogy allows to reliably define stratigraphic boundaries and furthermore allows for robust correlations.

Each stratigraphic boundary was defined based on a set of clay mineralogical and sediment petrological parameters. At the Diest-Kasterlee boundary, a transition zone is found in which mineralogical and sediment petrological characteristics typical for the top Diest Fm gradually transition into characteristics typical for the Kasterlee Fm, which consists of fine-grained sands with ca. 5% pelletal glauconite and glauconite-smectite and kaolinite dominating the clay fraction. The base of the Kasterlee is interpreted at the base of this transition zone. This transition zone indicates reworking which is most likely related to the emersion of the Diest Fm during the late-Miocene. The top of the transition zone is defined as the level where no residual

characteristics typical of the Diest Fm are found. The Kasterlee-Mol boundary is defined based on change in kaolinite content and the decrease in pelletal glauconite content. As these criteria also apply to sections where a gravel layer marks the boundary (e.g. Olen and Heist-op-den-berg), the criteria are considered justified. The reliability of the boundary interpretations is furthermore increased by the observation that the defined clay mineral boundaries are also important paleoenvironmental boundaries. The clay fraction of the Poederlee Fm was found to be prone to local variability. At the base, reworked Kasterlee material was found whereas laterally the Poederlee sediment systematically contain more smectite. In the top of the Poederlee Fm, Fe-vermiculite was found in the clay fraction and in pelletal glauconite of severely weathered Fe-sandstones.

Based on the systematic clay mineral analysis of the different units, it is also possible to draw preliminary paleogeographic conclusions. Clay minerals in the different studied Neogene formations origin from several provenances. Firstly, marine detrital clay is dominantly transported from the North Sea and typically results in smectite-rich clay assemblages (Berchem Fm, marine Bolderberg Fm, Deurne and Dessel Members and Diest D2-D3 units of Diest Fm and Poederlee Fm). Secondly, clay-sized glauconite-smectite has no detrital origin but instead is locally derived from pelletal glauconite abrasion or even complete disintegration upon energetic transport. Clay-sized glauconite production can be the dominant clay supplier whenever detrital, marine- or land-derived, clay supply is insignificant, such as in the Diest D1 sand unit. Thirdly, Continentally-derived clays were encountered in the Opgrimbie facies of the Bolderberg Fm, the Mol Fm and in the top Flemish hill sand deposits. The clay composition of all of the former deposits consists dominantly of kaolinite and illite most likely originating from the Ardennes-Rhenish massif in the south to southeast. Fourthly, trioctahedral Fe-vermiculite and kaolinite-expandable minerals were found in the Diest D4 unit and in clay and pelletal glauconite of part of the Poederlee Formation which have a weathered origin, most likely originating from eroded soils. Fifthly, substantial amounts of Neogene clay has a reworked origin, such as the Deurne and Dessel Member of the Diest Fm and the basal deposits of the Kasterlee and Poederlee Formations. Glauconite-smectite in the Mol Formation is also considered as reworked. Furthermore, pelletal glauconite in these units, except for the Antwerp Member, was also massively reworked.

In a second part of the work, quantitative clay mineralogy was used as a provenance indicator of recent muds on the Belgian Continental Shelf (BCS). The qualitative and quantitative clay composition <2µm of the muds was hereby compared with that of the different possible source areas. Through analysis and recalculation of the different tributary rivers of the Scheldt system, it was proven that the clay composition discharged by the Scheldt river system. As all other source areas have a significantly different clay composition, the Scheldt river system must be the main clay supplier of the BCS muds.

Although hydrodynamic modeling shows that the Scheldt is presently not discharging fluvial mud to the BCS, the Scheldt must have massively discharged mud in the past, most likely in the period before anthropogenic influence. The clay composition present on the BCS can be traced back to early-Holocene tidal deposits in the coastal plain but also to Weichselian (MIS-5d), Eemian (MIS-5e) and Saalian (MIS-7) deposits of dominantly fluvial origin. Logically, the clay composition was first introduced in the coastal plain when the paleo-Scheldt river system united all tributary rivers during which the current Scheldt river clay composition was formed for the first time. This most likely happened during the Elsterian when all tributary rivers merged into one river system instead of having a separate existence. The Scheldt river system discharged from then on in westward direction, occupying the Flemish Valley. Most likely, this occurred around 450.000 years BP, during the Elsterian (~MIS12), after a proglacial breakthrough in the North Sea.

During this research, quantitative clay mineralogy was successfully applied in order to bring clarity in stratigraphic as well as in provenance issues. Nevertheless, many open questions remain regarding the significance of the found clay mineral variations and their implications for paleogeographic, climatic and tectonic interpretations.

Nederlandstalige samenvatting

Kleimineralen laten vaak interpretaties toe omtrent herkomstbepaling, paleogeografie, klimaat en tektoniek van sedimenten. In het verleden is echter gebleken dat het potentieel van kleimineralenanalyses nooit volledig benut is en dit vooral omwille van methodologische beperkingen. Echter, de invoering van gestandaardiseerde voorbereidingstechnieken en de ontwikkeling van gesofisticeerde interpretatie software laten toe kleimineralen betrouwbaar op een volledig kwantitatieve manier te bepalen via X-stralen diffractie methodes waardoor het sterk instrument is in de karakterisering van sedimenten. In dit werk wordt deze kwantitatieve kleimineralenanalyse gebruikt om specifieke geologische problemen te analyseren of beter te kunnen begrijpen.

In een eerste case wordt de kleimineralenanalyse in combinatie met een studie van sediment petrologische kenmerken (korrelgrootte, glauconietgehalte) gebruikt in een stratigrafische studie van de Neogene glauconietzanden van het Kempen bekken om finaal de stratigrafische grenzen tussen verschillende eenheden beter te kunnen gaan bepalen. Hiervoor werd een systematische analyse van de verschillende Neogene formaties uitgevoerd met specifieke aandacht voor de grenzen en overgangszones. De systmatische studie wijst uit dat glauconietmineralen niet alleen in bolletjes voorkomen maar ook systematisch in de kleifractie van de Neogene zanden. Deze glauconietklei komt echter niet voor in kleilaminae, hetgeen een relatie met de glauconietbolletjes suggereert. Dit vermoeden wordt alleen maar versterkt doordat de mineralogie van glauconietmineralen in de kleifractie inderdaad nagenoeg identiek is aan die van de bolletjes. Visuele inspectie en korrelgrootteanalyse van de glauconietbolletjes wees uit dat de grote meerderheid, behalve in het Lid van Antwerpen, van de glauconietbolletjes in het Neogeen herwerkt zijn uit oudere afzettingen en in belangrijke mate transport ondergingen. Dit transport zorgde voor abrasie of zelfs het compleet uit elkaar vallen van de bolletjes waardoor glauconietmineralen in de kleifractie terecht kwamen. Aangezien de glauconietmineralen in de kleifractie meer zwellende laagjes bevatten dan de bolletjes toont aan dat het glauconiet in de kleifractie in verhoogde mate reactief is ten opzichte van de glauconietbolletjes.

De systematische analyse van de verschillende eenheden toonde weinig variabiliteit binnen de verschillende eenheden van de Berchem Fm en de eenheden van de Bolderberg Fm met mariene invloeden. De kleifractie van deze eenheden bestaat uit assemblage gedomineerd door smectiet met ook relatief sterk-zwellend glauconiet-smectiet als secundair kleimineraal. Deze kleimineralensamenstelling is ook te vinden in de Deurne en Dessel leden van de Diest Fm, hetgeen duidt op een belangrijke herwerking van sediment. Een belangrijke break in kleimineralogie en glauconietmineralogie is aanwezig in het Diest zand (Diest D1 eenheid) met glauconiet-smectiet als belangrijkste kleimineraal, dat bovendien erg weinig zwellende laagjes bevat. In het westelijk deel van het Kempen bekken, wordt een kleiig, glauconietarm zandfacies gevonden (Diest D2-D3 eenheden). In de top van de Diest Fm werden typische verweringskleimineralen zoals Fe-vermiculiet en zwellende kaoliniet gevonden, die wijzen op een ex-situ verwering. Dit topfacies (Diest D4 eenheid) is echter niet aanwezig in het zuidelijkere deel van het bekken zoals in Olen, Heist-op-den-berg en het Hageland.

De belangrijkste doelstelling van deze studie was echter het gebruik van de kwantitatieve kleimineralenanalyses om zo de stratigrafische grenzen in het Neogeen beter te kunnen bepalen. Het succes hiervan is aangetoond de Diest-Kasterlee en de Kasterlee-Mol stratigrafische grenzen. De kleimineralen data laten toe om betrouwbare grenzen te definieren die bovendien goed correleerbaar zijn. Elke stratigrafische grens werd gedefinieerd op basis van een set van klemineralogische en sedimentpetrologische kenmerken. De Diest-Kasterlee overgang ligt in een transitiezone waarbij mineralogische en sedimentpetrologische kenmerken typisch voor de top Diest gradueel overgaan in kenmerken typisch voor de Kasterlee Fm, zoals fijne korrelgrootte, ca. 5% glauconiet en een kleimineralogie voornamelijk bestaande uit glauconiet-smectiet en een toenemende hoeveelheid kaoliniet.

De basis van de Kasterlee Fm wordt geinterpreteerd aan de basis van deze transitiezone die duidt op een belangrijke herwerking die waarschijnlijk gerelateerd is

aan de emersie van de Diest Fm tijdens het laat-Mioceen. De top van de transitiezone is gedefinieerd op het niveau waar geen invloed meer is van de herwerkt Diest sediment. De Kasterlee-Mol grens werd gedefinieerd op basis van de stijging in kaoliniethoeveelheden en de scherpe daling van de hoeveelheid glauconietbolletjes. Het is belangrijk op te merken dat deze kleimineralogische grenzen een verdere betekenis hebben aangezien ze ook een belangrijke verandering in paleomilieu voorstellen. Bovendien zijn de kleimineralogische grenzen ook gevonden in secties waar de exacte grens Diest-Kasterlee duidelijk gemarkeerd is door de aanwezigheid van een grintlaagje (bv. Olen, Heist-op-den-berg).

Op basis van de systematische kleimineralenanalyse van de verschillende eenheden, is het ook mogelijk om enkele conclusies te trekken omtrent paleogeografie. Kleimineralen in de verschillende eenheden hebben een verschillende oorsprong:

1) Marien detritische klei is aangevoerd vanuit de Noordzee en bestaat typisch uit smectietrijke mineraalassemblages (Berchem Fm, marine Bolderberg Fm, Deurne en Dessel Leden, Diest D2 en D3 eenheden en de Poederlee Fm)

2) Glauconiet-smectiet in de kleifractie van zanden heeft geen detritische oorsprong maar is lokaal gevormd doordat glauconietbolletjes abradeerden of uit elkaar vielen door de intensiteit en/of mate van transport. In de Diest D1 eenheid en in de Kasterlee Fm is dit proces de belangrijkste bron van klei.

3) Kleimineralen aangevoerd van het continent werden aangetroffen in het Opgrimbie facies van de Bolderberg Fm, in de Mol Fm en in top Vlaamse heuvelzanden. Al deze afzettingen hebben een zeer gelijkaardige kleimineralen bestaande uit voornamelijk kaoliniet en illiet. Deze kleimineralen kennen hoogstwaarschijnlijk hun oorsprong door de verwering van het Ardennen-Rijn massief in het zuid tot zuidoosten.

4) Chemische verweringsmineralen zoals Fe-vermiculiet en zwellend kaoliniet werden aangetroffen in de Diest D4 eenheid en zowel in de kleifractie als in glauconieten van de verweerde Fe-zandstenen in de top van de Poederlee Fm. Deze kleimineralenassemblage kent waarschijnlijk zijn oorsprong in geerodeerde bodems.

5) Een belangrijk van de kleimineralen in het Neogeen hebben een herwerkte oorsprong zoals het Deurne en Dessel Lid, the basisafzettingen van de Kasterlee en Poederlee Formation en het glauconiet-smectiet in de Mol Formatie. Bovendien werden ook de glauconietbolletjes, behalve in het Antwerpen Lid, massaal herwerkt voorafgaand aan afzetting.

In de tweede case study van dit werk werd de kwantitatieve kleimineralenanalyse gebruikt om de herkomst te bepalen van recent slib aanwezig op het Belgisch Continentaal Plat (BCP). Door de kwalitatieve en kwantitatieve samenstelling van het slib te vergelijken met dat van verschillende bronnen, is gebleken dat de Schelde riviersysteem de enige bron is met een overeenkomstige kleimineralen-samenstelling. Deze hypothese werd bovendien bewezen door de systematische analyse van de verschillende zijrivieren in het Scheldebekken. Uit de resultaten blijkt dat wanneer de kleimineralensamenstelling van de verschillende rivieren gecombineerd volgens hun relatieve belangrijkheid qua debiet en suspensieconcentratie, de resulterende samenstelling bijna identiek is aan die van het slib in de Noordzee. Het Schelde riviersysteem is bijgevolg de belangrijkste bron van het slib.

Hoewel uit hydrodynamische modelleringen blijkt dat de Schelde momenteel geen fluviatiel materiaal uit het estuarium voert, tonen de vorige resultaten aan dat de Schelde dit in het verleden wel massaal moet hebben gedaan, hoogstwaarschijnlijk in de periode voor antropogene invloeden. De kleimineralensamenstelling van het slib kan terug in de tijd worden getraceerd tot vroeg-Holocene tidale afzettingen in de kustvlakte, maar ook tot Weichsel (MIS-5d), Eem (MIS-5e) en Saale (MIS-7) afzettingen van fluviatiele origine. Logischerwijs werd de samenstelling van de Schelde voor het eerst gevormd toen de verschillende zijrivieren in plaats van in een individuele loop afwaterden, allemaal samenvloeiden tot één rivierstelsel dat afwaterde naar het westen doorheen de Vlaamse Vallei. Hoogstwaarschijnlijk gebeurde dit tijdens het Elster (MIS-12), ongeveer 450000 jaar geleden, na de eerste proglaciale doorbraak in de Noordzee waardoor het Scheldesysteem afwaterde richting het westen.

List of abbreviations & symbols

01E001	Borehole code of the Geological Survey of Belgium
AIPEA	Association International pour l'Etude des Argiles
BCS	Belgian Continental Shelf
BP	Before Present
CEC	Cation exchange capacity
Clay lam.	Clay lamina
d_{060}	d-spacing in Å of 060 reflection of clay minerals
Di-smectite	Dioctahedral smectite
DN	Dinoflagellate cyst biozone
Fe/h.u.c.	Iron content per half unit cell
Fm	Formation
GSB	Geological Survey of Belgium
GL	Glauconite
ICS	International Commission on Stratigraphy
ISS R0	Randomly interstratified illite-smectite-smectite
ka	kiloannus (thousand years)
km	kilometer
m	meter (when referred to depths, m below ground level)
Ma	megaannus (million years)
Mb	Member
MIF	Mineral Intensity Factor
MIS	Marine Isotope Stage
MLM	Mixed layered minerals
Mm	Millimeter
MMU	Mid-Miocene Unconformity
NCS	National Stratigraphic Commission Belgium
RC	Reynolds Cup
RT01	Sample number (also RU, RS and RN)
SPM	Suspended Particulate Matter
Tri-smectite	Trioctahedral smectite
XRD	X-ray diffraction
XRPD	X-ray powder diffraction
ZnO	Zinc oxide
2:1 Al-clays	Al-rich clay minerals one tetrahedral sheet in between 2 octahedral sheets
Å	Angstrom
µm	Micrometer
σ*	Sigma star: orientation function describing the orientation of clay minerals

TABLE OF CONTENTS

Introduction

The full potential of clay mineralogical analyses in geological and sedimentological studies has never been fully exploited in the past due to the poor reliability of the analyses. Primarily methodological limitations and the lack of highly-specialized interpretation software led clay mineralogical research to produce at most semi-quantitative results which strongly reduced their power for interpretations. However, with the introduction of standardized preparation procedures (e.g. Środoń et al., 2001), the awareness that changing exchangeable cations does not modify clay minerals from a quantitative point of view but instead allows to objectively compare clay compositions of different samples, and the development of highly-specialized software packages, systematical clay mineralogical analyses have become a reliable tool in the qualitative and quantitative characterization studies.

The application of such standardized clay procedures has proven to be successful in the Eocene-Oligocene stratigraphic interval of the Campine basin in Belgium (Zeelmaekers, 2011) and allowed for interpretations towards facies, provenance and climatic conditions. The present study builds further on this successful approach for the younger Neogene glauconitic sand deposits in the same sedimentary basin. In addition, clay mineralogical analyses were used to further unravel the provenance of the recent North Sea muds, a problem also tackled already by Zeelmaekers (2011).

The clay mineralogy of the Neogene stratigraphic interval in the Campine basin was not yet studied, although important paleogeographic (influence of the Rhine graben), climatic (mid-Miocene climatic optimum) and tectonic (mid-Miocene unconformity) events took place which also influenced sediment dynamics of the Campine basin. It is most likely that the impact of such important events is reflected in the clay mineralogical stratigraphy of the Campine basin sediments as the clay mineral assemblage of the different possible provenance areas is likely to be very different. Furthermore, clay minerals and their type of weathering are reported as sensitive indictors for climatic conditions and change (Chamley, 1989; Vanderaveroet et al., 1999; Ruffel et al., 2002). The main reason however to study the Neogene clay mineral stratigraphy of the Campine basin is for pure lithostratigraphic purposes.

Internationally, the International Commission on Stratigraphy (ICS) prescribes guidelines for stratigraphy which are mainly concentrated on chronostratigraphy in order to construct a global International Geological Time Scale (e.g. Gradstein et al., 2012). Lithostratigraphic classification however, is mainly a regional and even local matter, composed within sedimentary basins. Although lithostratigraphy is not much internationally controlled, the ICS does prescribe some rules for its classification. The “formation” is the primary lithostratigraphic unit which is defined based on a certain contrast in lithology with other formations, depending on the complexity of the regional geology. Furthermore, formations are considered justifiable when they can be delineated at the scale of geologic mapping practiced in the region (website ICS, www.stratigraphy.org, last consulted 01-2015). Formations can be further subdivided into “members”, “beds”, etc. but also adjoined with other formations into “groups”. Additionally, for each format lithostratigraphic unit, it is essential to define a stratotype which act as a standard of reference of the lithostratigraphic unit. This stratotype can be a “unit stratotype” (standard or reference for a unit), a “boundary stratotype” (standard of reference for the boundary between two units) and a “”composite stratotype” (a unit stratotype formed by the combination of several specified intervals of strata). In the Neogene succession of the Campine basin, formations, with stratotypes, and members have been defined by the National Commission of Stratigraphy Belgium (website NCS http://www.natstratcommbelgium.drupalgardens.com, last consulted 01-2015) following key publications of De Meuter and Laga (1976) and Laga et al. (2001).
All marine formations in the Neogene succession consist of glauconitic sand and look much alike which often makes a macroscopic stratigraphical distinction difficult. Stratigraphic differentiation is nevertheless often relatively straight-forward when only bulk units are considered. However, the lithological heterogeneity within units and certainly

towards formation boundaries makes it very complex to define robust criteria to interpret formation boundaries and make geometrical correlations. Therefore, macroscopic outcrop and core descriptions are regularly complemented with classical sediment analyses such as grain-size analysis and carbonate content analysis. For correlation purposes also other techniques are presently very commonly used, such as well-logging tools, mainly gamma-ray and resistivity, and cone penetration tests (Labat et al., 2011; Wouters and Schiltz, 2011).

Based on the different characteristics and analyses all together, the interpretation of formation boundaries remains however very complex (see for instance Berckmans and Wouters, 2003).

Clay mineralogy has already shown to have a large potential to be a successful lithostratigraphic parameter in order to better define the stratigraphic boundaries. This was demonstrated for the Diest-Kasterlee Formation transition in the Dessel-2 borehole (Louwye et al., 2007) by a preliminary and semi-quantitative analysis. The clay mineralogy and pelletal glauconite in these units were never studied in a systematic way.

In this work, the quantitative clay mineralogical composition of the different litho-units was therefore studied across formation boundaries following a systematic approach. Clay mineral analyses were performed on a selection of both reference and less well-documented outcrop and borehole sections. The final selection of studied material was also based on the availability of dinoflagellate cyst biostratigraphy, which was much refined by Louwye and co-workers and form the biostratigraphical and chronostratigraphical fundament of this study (e.g. Louwye, 2000; 2005; Louwye and De Schepper, 2010; Louwye et al., 1999; 2007).

The dominant lithology in the Neogene succession is glauconitic sand often with very high pelletal glauconite contents (>50%). Clay occurs dispersed in the sand matrix and as well as locally concentrated in clay intercalations. The relation between both occurrences of clay and their mineralogical relation with the massive occurrence of pelletal glauconite is however unclear and will be studied in this work. An important challenge is furthermore to develop a standard procedure to investigate the clay mineralogy of such pelletal glauconite-rich deposits. The possible disintegration of pelletal glauconite during preparation treatments hereby needs to be assessed or preferably even prevented.

The main objective for the Neogene succession remains however the lithostratigraphic use of quantitative clay mineralogy in order to characterize formation units and especially to better define formations boundaries. Additionally, without being a main objective, the significance of the found clay mineral assemblages in the different units is discussed and interpreted towards paleogeographic evolution. A second important objective is to study the mineralogy of glauconite pellets and their relation with the mineralogy of the sedimentary clay fraction.

A second stratigraphic application of quantitative clay mineralogy demonstrated in this work is a provenance study of recent mud deposits on the Belgian Continental Shelf (BCS). The occurrence of fine-grained mud in a high-energetic depositional environment such as the BCS is rather unusual. In this work, it is attempted to better understand this situation by discovering the origin, the provenance of these muds, which were deposited at most several hundreds of years ago. The research approach followed by Fontaine (2004), Gregoir (2005) and Zeelmaekers (2011) was to first characterize the clay mineralogical composition of the BCS muds after which this composition is compared with that of different provenance sources, such as the English Channel, the northern North Sea, the Scheldt estuary, erosion from the sea floor, the Rhine-Meuse system,… This approach is considered justified as the geological background and clay mineralogy of the different provenance sources is estimated sufficiently different in order to discriminate between sources. Quantitative clay mineralogy was proven to be a very useful provenance indicator as visually comparing diffraction patterns already allows a quick interpretation towards provenance potential (Zeelmaekers, 2011). This successful approach was also continued in the present study as after the study of Zeelmaekers (2011) several questions remained unsolved.

The study of Zeelmaekers (2011) revealed that the English Channel area, the most probable source area according to published data (e.g. Fettweis and Van den Eynde, 2003; Irion and Zöllmer, 1999), had a significantly different clay mineralogical composition compared to the BCS muds and which could therefore almost certainly excluded as the main clay source. In contrast, clay minerals in the estuary of the river Scheldt were found nearly identical to the BCS muds. Because estuaries are however influenced by both marine as well as fluvial

suspension waters, it is unclear whether estuarine clay minerals reflect primarily the discharge of fluvial clay or, are essentially the result of marine clay being transported into the estuary.
A second crucial point is that the BCS mud clay composition was also traced back to early-Holocene and late-Pleistocene deposits (Zeelmaekers, 2011) which has shifted the provenance issue back in time. The provenance source responsible for the recent BCS muds deposition was therefore probably already active during Holocene and late-Pleistocene times. A clay mineralogical study of the Holocene and late-Pleistocene deposits in and around the Belgian coastal area would consequently also aid to the original, present-day, provenance issue.
The present study aims to continue the clay mineralogical provenance study by analyzing strategically chosen and stratigraphically well-known samples to solve the remaining issues and prove the provenance of the BCS muds. A major objective is to unravel how clay minerals are discharged from upstream rivers to estuaries where they are mixed with marine-derived clay minerals. For this purpose, bottom mud and suspension material of the different tributaries of the Scheldt river system was collected and their clay mineralogical composition characterized. Furthermore, in order to reconstruct the clay mineralogical evolution during the Pleistocene and Holocene, an extensive sampling of this Quaternary succession in the coastal plain is required. A particular problem in this part of the study is the lack of deposits reliably assigned to the Pleistocene in the Belgian coastal plain which makes such systematic sampling impossible. Sampling was therefore concentrated on late-Pleistocene deposits characterized by reliable stratigraphic and sedimentary facies interpretation.

The structure of this thesis is built up according to the outline explained above. The first part focuses on the methodological aspects of mineralogical, clay mineralogical and sediment petrological analyses. Essential features of the used methods are explained and a standard procedure when working with deposits containing pelletal glauconite is defined ("*Chapter I"*). In "*Chapter II"*, the identification and quantification of clay minerals in clay-sized fractions <2µm is discussed.
A second part of the research deals with the Neogene stratigraphy of the Campine basin with the aid of quantitative clay mineralogy. Firstly, the characteristics and origin of glauconite minerals in the different deposits are reported and discussed ("*Chapter III"*), after which the Burdigalian and Langhian clay mineralogy ("*Chapter IV"*), the Tortonian-Messinian Diest sand case ("*Chapter V"*), the stratigraphy of the Mol-Kasterlee-Diest sand ("*Chapter VI"*) and the Poederlee Formation ("*Chapter VII"*) are discussed. Discussion and conclusions are formulated in *"Chapter VIII*".
The provenance of the North sea muds forms the third part of the thesis. In "*Chapter IX*", "the BCS muds: the state of the art" , the characteristics of the muds are discussed followed by a summary of earlier results after which the most important discrepancies and remaining issues in the research are highlighted. The analyses on new samples of selected potential provenance sources is demonstrated in "*Chapter X*", followed by a discussion ("Chapter XI") in which the main provenance source of the BCS muds will be identified.

PART I.

Methodology

Chapter I

Methods

I.1 SAMPLING AND INITIAL RAW SAMPLE MANAGEMENT

I.1.1 Sampling strategy

A complete clay mineralogical investigation requires a substantially large investment of time and resources for sample preparation and data analysis. It is therefore necessary to adjust the sampling strategy and in comparison reduce when possible the number of samples to be analyzed (Zeelmaekers, 2011). The main strategy followed in this work is to first analyze high quality reference materials (e.g. stratigraphically known sections or horizons from published articles, well-preserved core material or fresh outcrop material,…) before proceeding to unknown or undescribed outcrops or core materials. Likewise in a sample set or stratigraphical core, important "key-samples" at certain intervals were analyzed first. Based on the results of these samples, sampling resolution was increased where necessary and whenever possible.

I.1.2 Sample types & origin

In this work different types of samples were collected:

- ***Core material***. Cores were sampled at the Belgian Geological Survey in Brussels under the supervision of Marleen De Ceuckelaire and Frans Moorkens and at the NIRAS core facility in Dessel under the supervision of Serge Labat. Core material was collected for both the Neogene stratigraphy and the North Sea muds topics. Before sampling the core surface was cleaned or removed as oxidation processes (pyrite oxidation, oversaturated pore water precipitation, contamination) influence the material and its properties. Therefore, samples were taken at fresh surfaces as much as possible. Sample depths were systematically measured from the top of the core on downwards. Specific depths for borehole samples in this work are listed as single depth samples with reference to the local topography (e.g. sample x was taken at 1.24m depth). This single depth number always refers to the middle of the sample.

- ***Outcrop material***. Outcrop samples were collected at existing permanent outcrops, at temporary outcrops or at new cross sections. Each time, a fresh surface was created before sampling.

- ***Fresh material***. For the North sea muds research, both bottom and suspension samples were collected from the rivers of the Scheldt basin and from the Belgian and Dutch part of the North Sea and the English Channel. In the Scheldt basin, bottom samples from the rivers of the Scheldt basin were collected using a Van Veen-grab, thrown out either from the shore or from a small boat. Occasionally, also the riverbank material was collected. Suspended sediment was collected using a flow-through centrifuge of Flanders Hydraulics under supervision of Hans Vereecken and Ivo Mielants. Fresh bottom and suspended sediment samples in the North sea and the English Channel were collected with the oceanographic research vessel BELGICA with the help of Michael Fettweis (MUMM) and under the supervision of André Pollentier and Lieven Naudts. Bottom samples were collected using a Van Veen grab controlled from the ship while suspended sediment was collected by a flow-through centrifuge (Alfa Laval sea water purifier MMB 304 S – 11). In this work also additional samples from Zeelmaekers (2011) were incorporated in the research study. These were already sampled in 2006, left unprocessed and incorporated in this research.

I.2 RAW SAMPLE HANDLING FOR NON-GLAUCONITE PELLET BEARING SEDIMENTS (TEXT OF THIS PART ENTIRELY TAKEN FROM ZEELMAEKERS, 2011)

I.2.1 Sample assessment

After samples are acquired from outcrops or cores, the next step is sample assessment and potential subsampling for further processing in such a way that the (sub)sample is representative for the studied problem and the scale at which it is being considered. In practice this means checking for and removing any large nodules (e.g. pyrite) or obvious oxidation crusts, removing potential traces of drilling mud from core samples by scraping off the outer layer of the sample and taking the potential layered nature of the sample in consideration when subsampling.

I.2.2 Non-routine: Sieving

Unconsolidated samples contain often large fragments that should not be processed with the rest of the sample, this is especially the case for many of the fresh sediments studied in this work . These fragments can be shells, pebbles, vegetation, etc… and should be removed by (preferably wet) sieving the sample at about 1mm.

I.2.3 Drying

Many of the samples analyzed in this study contained high percentages of water and needed to be dried before further processing. Also outcrop and core samples were found to contain some excess water. For this reason and to standardize the treatments as much as possible all samples were systematically dried before further processing. This was done by (manually) disaggregating or spreading out the samples and drying them overnight in a ceramic bowl lined with heat resistant plastic foil in an oven at 60°C. After drying, the samples were re-equilibrated with the ambient conditions and these are the reference conditions for the weights used in the bulk mineral analysis.

I.2.4 Grinding

The further processing steps require the samples to be sufficiently reduced in size to be properly handled. Therefore all samples need to be ground to pass a 0.5mm sieve (an arbitrary selected sieve size, close to the 0.4mm proposed by Środoń et al. (2001). It is important to avoid excessive grinding as it can lead to crystal structure damage or even the production of X-ray amorphous material (Moore and Reynolds, 1997). It also needs to be avoided to prevent reducing non-clays to a clay size fraction, as this will negatively impact the quality of the diffraction patterns of the oriented slides. For these reasons grinding needs to be done by hand using mortar and pestle and only by impact, not by a “smearing” motion.

I.2.5 Splitting

When using portions of a sample mass for different analyses that will be compared, preferentially this sample mass should be splitted using a sample splitter in order to obtain representative portions (e.g. Środoń et al., 2001). This is a time-consuming process and was deemed not feasible for the large number of samples processed in this study. For routine samples it was opted instead to thoroughly homogenize by hand the samples after grinding, followed by splitting into equal parts by hand. Repeatability tests showed that this approach was sufficiently precise for the purpose of the analyses.

I.3 RAW SAMPLE HANDLING FOR SEDIMENTS CONTAINING GLAUCONITE PELLETS

As demonstrated in the previous section, samples are routinely preprocessed by oven drying at 60°C, manual grinding <500µm and finally homogenized prior to any further preparations. Such a strategy is systematic, practical and probably scientifically the optimal working procedure. However, when sand or clay deposits contain significant amounts of glauconite pellets, it is obvious that manual grinding and possibly also other treatments will cause glauconite pellets to disintegrate. By this process, glauconite particles <2µm can be produced and introduce contamination in the clay fraction of samples. In the following section, some experiments were performed to assess the glauconite pellet disintegration behavior to different treatments. After, an optimal working procedure for glauconite pellet-bearing sediments will be described.

I.3.1 Glauconite pellet disintegration behavior

As opposed to other clay minerals, glauconite most often does not occur as individual clay-sized flakes but as aggregate-pellets of sand-size. When these clay pellets experience burial and diagenesis effects, internal chemical and mineralogical characteristics are modified and simultaneously, the physical strength of the pellet strongly improves. The best evidence hereof is the relatively undamaged survival of glauconitic globular particles in Paleozoïc and even Precambrian rocks (Auden, 1933; Gulbrandsen et al. 1963; Odom, 1976; Zaitseva et al, 2005; Cecil and Ducea, 2011). Newly formed or diagenetically unaltered pellets however might be susceptible to physical disaggregation when exposed to natural or laboratory-induced high-energy processes. In order to verify such artificial production of clay-sized glauconite, the effect of different preparation processes was experimentally evaluated on a selection of 12 samples from different Neogene formations. During each of the experiments described below, the amount of clay-sized glauconite was measured before and after the performed experiment.

- <u>Low-risk sediment treatments (washing, sieving, soft stirring)</u>

A first experiment was set up to investigate the effect of commonly applied geological lab procedures. Purified glauconite pellets >32µm were subjected to several normal treatments such as washing, shaking, stirring, wet sieving and oven drying. Afterwards, the clay fraction <2µm was centrifugated and weighed. Results indicate that that this type of preparation procedure causes minimal disintegration of glauconites as amounts of clay material <2µm were always found to be non-existing or <0.1%. Nevertheless, suspension material of samples which were subjected to high speed shaking for >24h demonstrate a noticeable greener coloration, illustrating that glauconite grains actively disintegrate during this latter procedure.

- <u>Clay mineralogical preparations on purified glauconite pellets >32µm</u>

In a second experiment, purified glauconite pellets >32µm were subjected to the standard clay preparation treatment for aggregate-removal, the so called “Jackson-treatment” (modified after Jackson, 1975). The purpose of the Jackson-treatment, the international excepted standard procedure in chemical pretreatment for clay minerals, is to break-up and remove aggregate-forming particles, such as carbonate cements, organic material and iron-coatings. This procedure is essential to acquire successful quantitative clay mineralogical data from samples. The nature of this procedure however, which involves the addition of chemical reagents combined with heating, stirring, shaking and ultrasonic treatments, presents a risk for glauconite pellet disaggregation. To estimate the influence of such procedures, isolated pelletal glauconite >32µm were subjected to the different steps of the Jackson procedure, which involves heating in Na-acetate-buffer solution, H_2O_2 and Na-dithionite in a Na-citrate+$NaHCO_3$-solution (modified after Jackson, 1975, Zeelmaekers, 2011). The clay fraction <2µm was separated by centrifugation combined with periodic ultrasonic treatments. The amount of decomposed grains <2µm was quantitatively determined by weight. Based on 12 samples, the amount of clay produced from decomposed

grains averages between 15-25%. However this experiment was performed on purified glauconite grains, and therefore is not fully representative, it clearly shows that important errors are induced when glauconite pellet-bearing samples are subjected to standard treatments such as the “Jackson treatment”.

- Clay mineralogical preparations on glauconite particles <32µm in host sediment

A third experiment was set up to study contaminations from glauconite particles in the size class 2-32µm, which is more difficult to assess. The amount of glauconite particles in this size class is generally very low (Amorosi, 1997; Adriaens, 2009) but can still be important because these glauconite particles often are broken remnants of larger pellets and are therefore might be susceptible to further break up. As it was practically impossible to work with purified glauconite particles 2-32µm, it was chosen to work with the total sample.

Untreated samples were split in 2 parts and soaked in water. A first part was centrifuged <2µm without any treatment and the amount of glauconite minerals in the <2m and >2µm size fractions was determined. To the second split, the standard clay treatments were applied. After, size fractions <2µm and >2µm were separated by centrifugation and again the amount of glauconite minerals was determined in both size fractions by X-ray diffraction methods.

Two main observations can be made from this experiment. Firstly, large amounts of glauconite already occur in the <2µm size fraction of untreated samples (Figure 1.1). As samples were not treated prior to size separation, this must mean that glauconite was already present in the clay fraction of these samples. Secondly, the increase of glauconite minerals <2µm after treatment is limited to 15-20% (Figure 1.1), indicating that glauconite particles which were originally >2µm have shifted to the smaller size fraction <2µm. This 20% must be an absolute maximum value because it can be expected that due to the applied treatment, clay aggregates have shifted to the <2µm size fraction. The large majority of glauconite particles retains even after the treatment in the >2µm size class.

- Physical mistreatment of sediments

During another experiment, a fresh clay outcrop sample of the Bande Noir horizon at the base of the Asse clay (Maréchal, 1993) containing large amounts of pelletal glauconite were subjected to several destructive actions such as shovel cutting, pushing and shearing. The clay suspension immediately colored much greener compared with the untreated sample. The clay fraction <2µm was centrifuged before and after the destructive actions and measured with powder diffraction methods. Results indicate that while the clay fraction of the untreated sample contains 20% glauconite, the processed sample has 30% glauconite in its clay fraction.

- Conclusion

From the above described experiments it can be concluded that certain applied laboratory procedures (e.g. grinding, Jackson-treatment, physical mistreatment) can affect glauconite particles in these sediments to such a degree that glauconite pellets are broken up into pieces resulting in the artificial production of clay-sized glauconite. However, the experiments also demonstrate that the majority of glauconite minerals <2µm already occur naturally in the clay fraction before any treatments. After destructive treatments, only 20% of glauconite minerals is artificially added as clay-sized material. It is however questionable if these particles were originally larger than >2µm or simply occurred as aggregates of particles individually smaller than 2µm before the treatments. Normal sediment treatments, such as sieving, stirring, shaking, etc. on the contrary, induce no glauconite pellet disintegration and can be safely used.

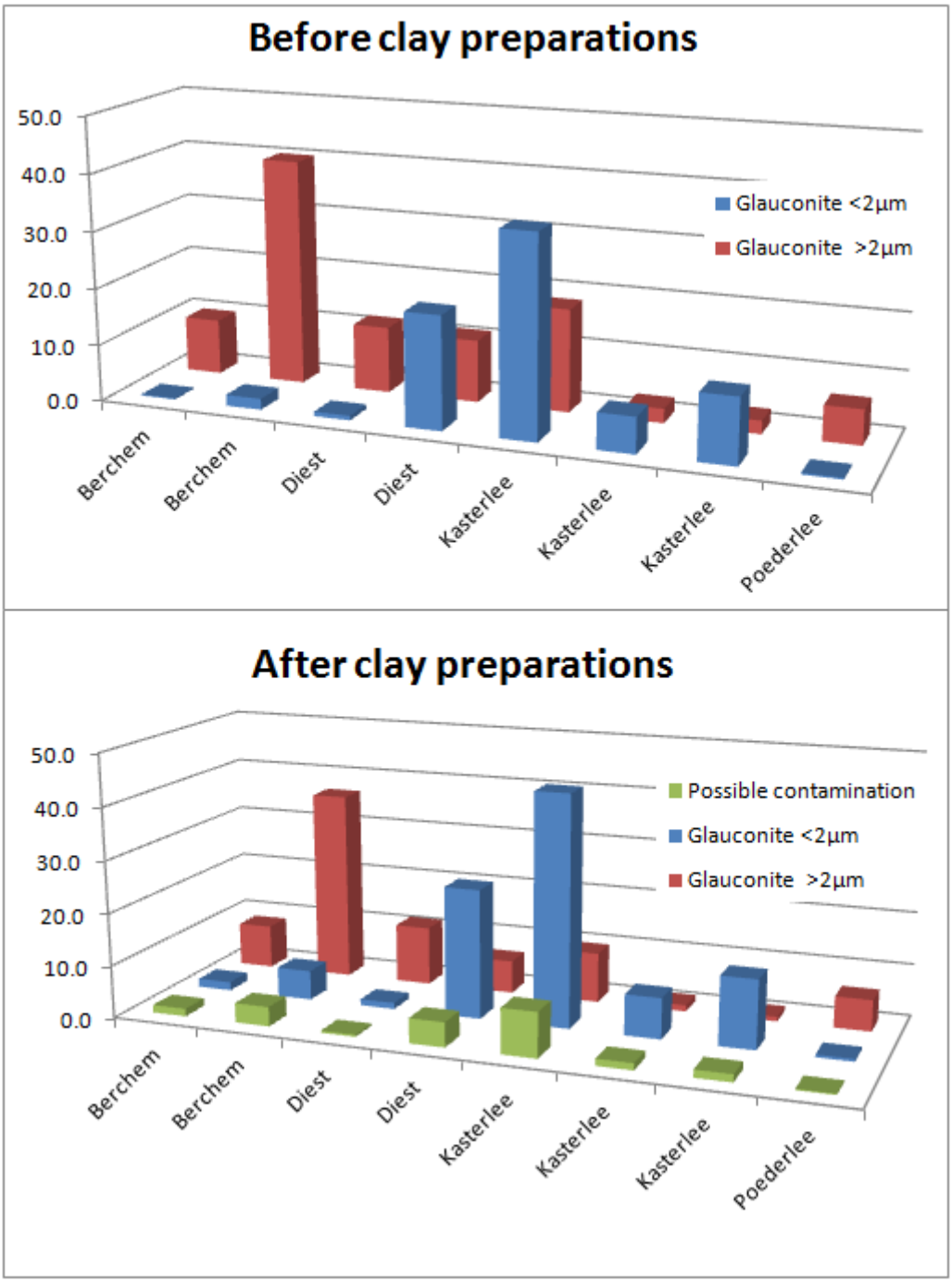

Figure 1.1: Results of the glauconite grain disintegration experiment. Untreated samples were centrifuged <2µm to quantify the amount of glauconite minerals present in the finer and coarser size fractions. This procedure was repeated after applying the standard clay preparation procedures. The columns in green correspond to the maximum amount of possible contamination of glauconite material >2µm which ends up in the clay fraction <2µm.

I.3.2 Towards a standard pretreatment for glauconite pellet-bearing sediments

In the previous section it was demonstrated that when samples containing glauconite pellets are treated according to the standardized procedure set up by Zeelmaekers (2011), non-negligble errors can be induced in the clay fraction <2µm. This is certainly an important issue for the glauconitic sands of the Neogene in Belgium which can contain up to 60-70% glauconite pellets. According to the experiments in the previous section, approximately 20% of the total glauconite particles <32µm and >32µm will end up in the clay fraction <2µm after standard procedures as applied by Zeelmaekers (2011). In order to minimize this type of contamination, raw samples containing glauconite pellets should be subjected to a treatment before clay preparations. The optimal way is to separate raw samples in a fraction >32µm and a fraction <32µm. Hereby the smaller size fraction <32µm is used for bulk mineralogical analysis and detailed clay mineralogical analysis (Figure 1.2). The fraction >32µm is used to study pelletal glauconite but can also be interesting for bulk mineralogical analysis, and in particular the amount of feldspars and mica. Because the large majority of glauconite particles is situated in the >32µm fraction (Amorosi, 1997; Adriaens, 2009), such an operation already excludes important contaminations. This working method furthermore provides extra benefits and is also the preferred method when working with non-glauconitic sands with very low clay contents.

1) ***Clay concentration*.** Because the main lithology in the Neogene deposits is sand, often with relatively low clay contents, very low amounts of clay material is extracted during the standard clay separation method (Zeelmaekers, 2011). Often clay recoveries are too small to produce sedimentation slides for XRD analysis. When the starting material for the clay separation is already <32µm, large clay proportions are extracted which is beneficial for further processing.

2) ***Bulk mineralogy*.** Similar to the previous argument, the quartz-rich nature of many sand deposits will strongly decrease the value of a bulk mineralogical investigation. Because these type of samples often contain dominantly quartz, glauconite and minor feldspar and mica in their fraction >32µm, the detection limit of other minerals, like clays, oxides, sulfides and carbonates is greatly reduced and sometimes they even are completely obscured. When working with concentrated fractions <32µm, lower abundant minerals can be readily detected and thus much more information can be withdrawn from XRD-analyses on random oriented powders.

3) ***Pelletal glauconite extraction*.** Experience has learned that the success and correctness of magnetic separation procedures strongly depends on the preparation of samples (Adriaens, 2009). When untreated samples are processed with the Frantz isodynamic magnetic separator to extract glauconite pellets, this leads to incomplete separations which are moreover contaminated with important amounts of quartz, clay and other mineral impurities. Because particles <100µm easily obtain an electrostatic charge which change the magnetic properties of the particle, a successful magnetic separation is much harder to perform in the presence of such small-sized particles (Rosenblum and Brownfield, 2000). In practice, particles <30-40µm are too small for high-quality separations using dry magnetic separation (Adriaens, 2009). Using washed fractions >32µm therefore strongly improves the effectiveness of the separation.

4) ***Shape analysis*.** Fully automated, dynamic image analysis with a Camsizer was performed on a selection of samples. Particles <32µm are currently not measured correctly with the Camsizer but still have a large effect on the final results. Also this method benefits from analyzing washed samples >32µm rather than bulk samples.

5) ***Mica analysis.*** Experience has learned that the quantification of mica, separately from illite, by normal bulk X-ray powder diffraction analysis is problematic. Mica's often weather to illitic minerals (Moore & Reynolds, 1997) and therefore very often occur together in samples but rarely in the same size fractions. Working with size fractions larger then 32µm therefore allows an unambiguous quantification of the mica content.

6) ***Non-glauconitic sands with very low clay content***. In certain research cases, coarser quartz-rich sand samples occur with very low clay contents. According to standardized treatment of Zeelmaekers (2011), these samples should be ground <500µm before further processing. Experience has shown that even manual grinding in this case leads to quartz fragmentation in pieces <2µm. In this

case, the clay fraction <2µm contains important amounts of quartz, which will disrupt clay orientation at oriented slides and hereby rendering the clay mineralogical analysis less reliable. Instead it is better to “wash out” the finest fraction and continue the analyses with this concentrate.

The most important disadvantage of this working method is the work load. Processing hundreds of samples even before starting clay preparation procedures, demands loads of time but clearly holds very important advantages. Another disadvantage is that bulk mineralogical powder analyses are not any more performed on total samples by which crucial information about the nature of the sample is lost. The importance of this extra information is however only relative as, after pelletal glauconite extraction, the mineralogy of the size fraction >32µm consists of more than 90% or even 95% of quartz. This is easily checked under binocular microscope or using bulk mineralogical analysis of the >32µm fraction. The relative weights of the <32µm and >32µm fractions of processed samples are furthermore systematically included in appendix 1.

In practice, the optimal working method to separate size fractions from sand samples is a wet sieving cycle using a 32µm sieve. This method is also perfectly applicable for clay sediments containing glauconite pellets. The required amount of material depends on 2 factors: the clay content and the glauconite pellet content of the sample. In this work following procedure was applied:

- Soak 200-300g of sand (50g of clay), mix with demineralised water (“AD”) and let it stir on medium intensity for 30min. A peptizing agent can be added (Na-polyphosphate) in clay-rich samples.
- Pour the mixture through a 1mm sieve to remove shells, plant or wood material and gravel >1mm.
- Pour the mixture through the 32µm sieve and collect the passing suspension in a large 2l or 3l beaker. As this operation is often very time consuming, experience showed that it was more convenient to pass everything first through a 63µm sieve and afterwards pour the <63µm through the <32µm sieve.
- Collect the >32µm fraction, mix with AD and let it stir again on medium intensity for 15min.
- Repeat the above procedure until the suspended water <32µm is clear.
- Collect the suspension water <32µm in large bowls covered with plastic foil and collect the >32µm fraction in porcelain cups covered with plastic foil. Both fractions are subsequently oven-dried at 60°C and recuperated afterwards.
- Afterwards, check the quality of the separation for the >32µm fraction under binocular microscope or by a bulk mineralogical analysis.

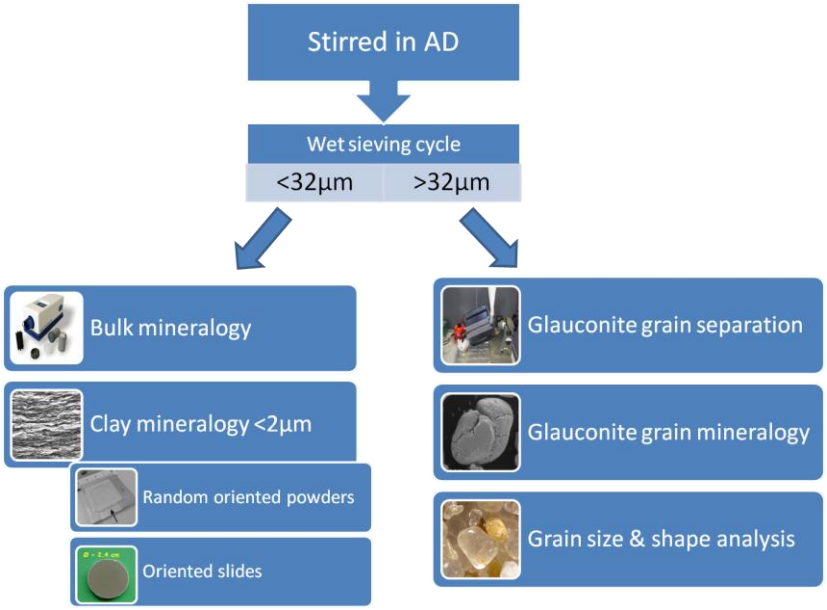

Figure 1.2: Schematic overview of workflow of glauconite grain bearing samples. First a sieving cycle at 32µm is performed after which both fractions are used for several analyses.

I.4 QUANTITATIVE XRD ANALYSIS ON RANDOM ORIENTED POWDERS

I.4.1 Preparation and measurement procedure

way to investigate the mineralogy of samples is scanning random oriented powders by X-ray diffraction. However, although X-ray powder diffraction is relatively simple and basic technique, huge errors exist in the quantification of clay mineral powders (see for example Laenen et al. 1997; Środoń et al. 2001. ; Omotoso et al. 2006)

The success of quantitative X-ray powder diffraction analyses depends in the first place on the type and standardization of sample preparation as this enhances the reproducibility, repeatability and accuracy of the measurements. As described earlier, powder measurements are performed on total bulk samples when pelletal glauconite is absent and the clay content is sufficiently high. In the case of glauconitic samples however, powder scans are recorded from sieved material <32µm.
The preparation procedures which were standardly used in this work rely on the work of Środoń et al. (2001), in which all the considerations and comparisons that have led to the establishment of these techniques are reported in detail. All samples for X-ray powder diffraction analysis (XRPD) were mixed with 10% ZnO, which is used as an internal standard. The mixture of sample and internal standard is then mixed with ethanol and subsequently wet grinded for 5 minutes using zirconia grinding elements in a McCrone micronizing mill. Aluminum sample holders are filled using a side-load technique, to ensure that crystallites are exposed to the X-rays as random as possible.
Additional techniques (use of Vertrel XF, spray drying) for an even better random orientation were investigated and installed at the KULeuven laboratory but were not routinely applied on the samples studied in this work. More detailed theoretical and practical considerations, and explanations of these other techniques, can be found in the laboratory manual provided as an extra document with this thesis.

All bulk powder measurements were performed using a PW1050/37 173mm circle goniometer connected with a PW1830 generator and equipped with Cu-Kα-radiation. The detector is proportional detector type PW3011/00. The diffractometer has a Bragg-Brentano theta-2theta setup for the source and detector respectively.

Standard diffractometer settings for powder measurements are:

- Goniometer circle 173 mm
- Divergency slit: 1°
- Receiving slit 0.1°
- Soller slit 2.3°
- Graphite crystal monochromator
- range: 5 to 65° 2theta
- step size: 0.02° 2theta
- counting time per step: 2 seconds
- measurement duration: 1h40

In many samples of this work, Fe-rich minerals occur in significant proportions. Because Cu-radiation causes Fe fluorescence, the quality of powder diffractograms is often lowered and the choice for Co-radiation might have been more appropriate. However, because of the current diffractometers' superior quality measurement (high intensity) necessary in the study of clay minerals and to stay consistent with the data of Zeelmaekers (2011), no other than Cu-radiation was used.

I.4.2 Interpretation and quantification

For data interpretation and quantitative analysis, the pattern summation software QUANTA was used.

This highly specialized software is designed to fit experimental patterns with a summation of natural, pure mineral, standards. The quantification of this whole-pattern fitting technique is based on the Mineral Intensity Factor (MIF) - concept, which states that diverse series of reflection are characterized by a different sensitivity towards relative abundance but also towards structural crystal defects and isomorphic substitutions, which both are very common for clays. In this MIF-concept, the quantification of a mineral phase

is based on the integrated intensity of a stable, reliable, reflection and its relation to the stable reflection ("MIF-peak") of the internal standard, ZnO. For clay minerals, the 060-reflection is typically chosen as MIF-peak. The drawback of this method is however that clay minerals with similar 060-positions (such as illite, dioctahedral smectite, illite-smectite) are grouped and quantified all together and not separately. In order to quantify each clay species on its own, an additional study on oriented clay slides in required (section I.5). Although this seems a big disadvantage at first hand, an accurate single-species powder quantification of a mixture of e.g. 2:1 Al-clays (illite, smectite, illite-smectite) is extremely difficult as such, also with the more conventional Rietveld refinement techniques. Therefore this disadvantage might be relative, as the MIF-concept prevents any errors which are common when clay minerals are quantified down to species level in bulk powders. The quantification in clay groups can be further subdivided in individual clay species by the identification and quantification of oriented clay slides.

This type of data analysis for XRPD has proven to be very successful in (clay) mineral quantification. To test the accuracy of their methods, mineralogical laboratories can compete in an international biannual round robin organized by the Clay Mineral Society, called the Reynolds Cup. In this contest, each lab receives three highly complex, artificially produced, mineral mixtures which they need to quantify as accurate as possible. During the last three editions, 2010, 2012 and 2014, the KULeuven claylab finished in 10^{th}, 6^{th} and 5^{th} place out of 60, 77 and 81 competitors respectively. Also in the 2008 Reynolds Cup contest, the KULeuven clay lab, in cooperation with the Polish Clay lab of Jan Środoń, finished in 4^{th} place. The complexity of the mineral mixtures and required detail of reporting becomes greater with every edition and the positioning since 2008 amongst the world's most specialized clay mineralogists and laboratories, means that the this technique is able to produce high-quality quantitative data using the methodology described above (Omotoso et al., 2004; Kleeberg et al., 2008).

The concept itself also makes it much better suited for clay-rich samples compared to the more conventional Rietveld refinement methods and furthermore can be operated much faster. Nevertheless, Rietveld refinement in general is more powerful as it combines structure refinement with mineral quantification, which is not possible using QUANTA. The extended theoretical explanations, working formulas, newly imported mineral standards, basics for mineral identification and current possibilities with Rietveld refinement software can be consulted in the laboratory manual.

I.4.3 Quantification of muscovite

It was discussed in the previous section how clays are quantified in groups. The group 2:1 Al-clay comprises smectite, illite-smectite, illite and muscovite. During clay modeling on oriented slides, the individual species of this 2:1 Al-clay group can be identified and quantified down to species level. Muscovite is hardly ever quantified in this way because muscovite <2µm occurs only in very specific geological environments. In certain case studies, the determination of muscovite is however required.

Muscovite typically has more and sharper reflections compared to the broad diffraction bumps of illite, smectite or mixed-layer illite-smectite (compare reference patterns in Figure 1.3). Particularly in the 25-33° 2θ region, muscovite has 4 distinct reflections, which can be used for muscovite quantification. In practice, the reflections at 3.2Å, 2.98Å, 2.85Å and 2.79Å are fitted as best as possible using the muscovite reference pattern, while still maintaining good fitting of the 060-reflection. As discussed in the previous section, the contribution of each mineral of the 2:1 Al-clay group is simply summed up to calculate the total % 2:1 Al-clay. Whereas previously the particular contribution of each mineral of the group is estimated rather unreliable, the contribution of muscovite can now be reliably determined.

The experience gained in the Reynolds Cup 2008, 2010 and 2012 editions has shown that this approach for muscovite determination in a mixture with other 2:1 Al-clays results in very reliable results with low bias values.

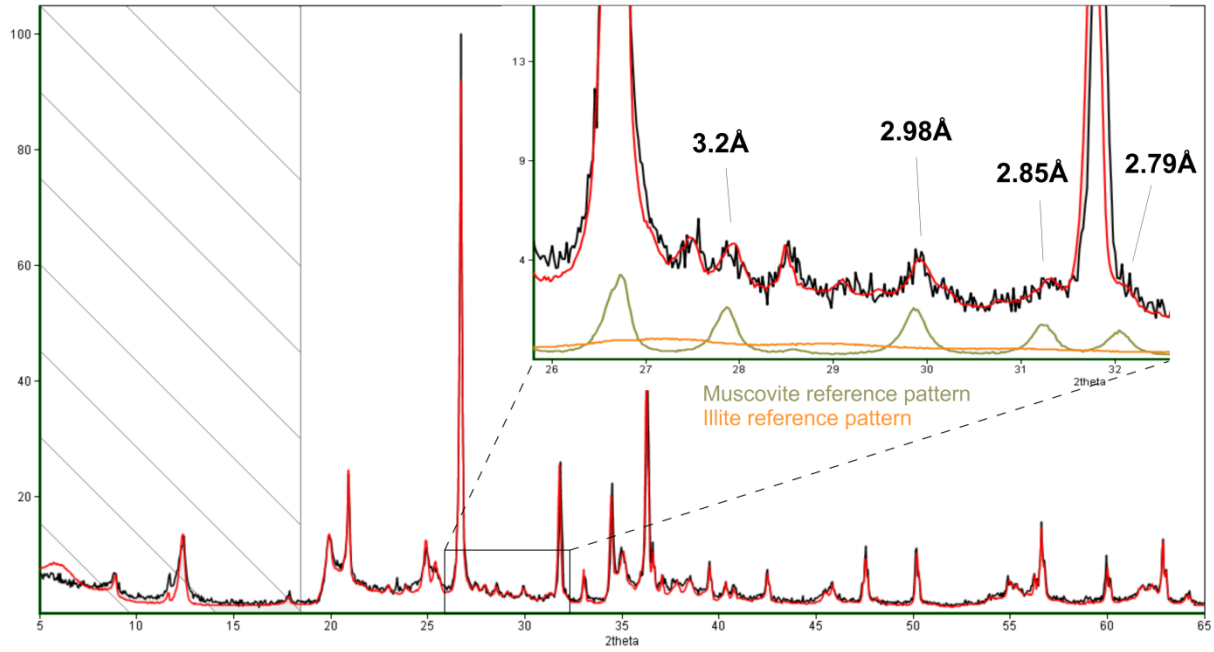

Figure 1.3: X-ray diffractogram showing the quantification fit in red of an experimental pattern in black. In the zoomed rectangle, the diffraction traces are indicated which are used to quantify muscovite.

I.4.3 Precision, detection limit and accuracy

The precision of a XRD measurement refers to the reproducibility and repeatability of the measurement. Whereas the diffractometer itself in normal conditions produces a relatively constant error (signal-to-noise ratio), the processing of the sample and preparing the sample holder will result in significant precision errors when neglected. The total amount of error will furthermore be highly variable when a sample is processed multiple times hereby yielding poor repeatability and reproducibility of the measurements. By following as much as possible standardized preparation procedures and optimally loading the sample as random as possible into the sample holder, such errors are minimized and the precision of the measurement itself is probably less than 1%.

It is important to note however that aside from the measurement precision also the detection limit of a XRD analysis is crucial. The detection limit depends on the inherent background of the diffractometer but also depends strongly on the sample composition and the interpreter. The detection limit is not identical for all minerals because of the differential scattering power of minerals (e.g. tourmaline will only be detected in a mixture in percentages higher than 1.5-2% whereas the detection limit of pyrite is below 0.5%). Furthermore, depending on the experience of the interpreter, it is much more difficult to correctly identify all minerals of a complex mineral mixture causing an important increase of the detection limit of a certain mineral or even a misidentification. Peak overlap for instance will increase the chance of failing to detect low abundant mineral phases.

The accuracy of an analysis can be best checked through round robin contests such as the Reynolds Cup. The results of the contest show that the procedure for XRPD data analysis described in the sections above allows to quantify non-clay minerals accurately to ~ 1% whereas the accuracy for clay mineral is around 2-3%.

I.5: QUANTITATIVE XRD ANALYSIS ON ORIENTED CLAY SLIDES

In the previous section it was demonstrated how clay minerals are accurately quantified on random oriented powders. Individual clay species are however only quantified in groups which means that three of the most common dioctahedral clay minerals (smectite, illite and mixed-layer illite-smectite) cannot be distinguished in a quantitative way. When clays are however concentrated in small size fractions, they can be better studied without the interference of non-clay minerals. The current chapter describes how this process takes place and how clays are identified, characterized and quantified by profile modeling using XRD analysis on oriented clay slides. Chemical procedures, detailed laboratory procedures and instrumental parameters are only briefly discussed as a complete and detailed overview can be consulted in the laboratory manual, provided as an extra document with this thesis.

I.5.1 Preparation and measurement procedure

Because of their small size, clay minerals could be simply isolated from bulk sediments by size separation procedures. Organic material however often glues clay and other mineral particles together to form aggregates. Moreover, different post-depositional processes, such as carbonate cementation and limonitic coatings cause additional aggregation and change the surface properties of the clay minerals. All these aggregate-forming particles need to be removed prior to size separation. The procedure followed in this work is based on the work of Jackson (1975). This “Jackson-treatment” is a time-consuming but very effective chemical pretreatment during which carbonate cements, organic matter and free Fe-(hydr)oxides are efficiently removed from the sediment with oxalic acid buffer, H_2O_2 and Na-dithionite respectively. During the pretreatments exchangeable cations are all systematically exchanged to the Na-form because the used chemicals are soluble Na-salts. This furthermore enhances clay dispersion and the formation of stable suspensions, hereby facilitating the operational steps (Zeelmaekers, 2011).

Next, clays are separated by centrifugation from the remainder of the sediment. Traditionally, 2µm is chosen as the cut-off size. During this separation, ultrasonic treatments are frequently applied to enhance dispersion of the clay particles. After the size separation, the clays are converted to their Ca-form, which is most beneficial for the modeling of the oriented slides as in this state, clays are the least susceptible to ambient humidity variations (Eberl et al., 1987; Sakharov et al., 1999). The Ca-saturation procedure requires an additional dialysis procedure to remove excessive electrolytes after which the clay powder is dried.

Oriented slides are prepared by sedimenting a slurry of clay on glass slides. Subsequently, different XRD scans are recorded as for proper identification XRD measurement in air dry, glycolated and heated (550°C/1h) environments is required. Additionally, extra cation saturations can be performed when necessary. Similarly to the bulk powders, XRD scans of oriented clay slides were performed using a PW1050/37 goniometer connected with a PW1830 generator and equipped with Cu-Kα-radiation. The detector is proportional detector type PW3011/00. The diffractometer has a Bragg-Brentano theta-2theta setup for the source and detector respectively.

Standard diffractometer settings for powder measurements are:

- Divergency slit: 1°
- Receiving slit 0.1°
- Soller slit 2.3°
- Graphite crystal monochromator
- range: 5 to 65° 2theta
- step size: 0.02° 2theta
- counting time per step: 2 seconds
- measurement duration: 1h40

I.5.2 Interpretation and quantification

Structure characterization and quantification of oriented clay slides is obtained by the detailed modeling of each clay mineral present in the clay mixture using the Sybilla software (© Chevron ETC). This type of X-ray profile modeling has proven to produce very detailed as well as accurate results when used properly (Drits et al., 1997; Sakharov et al.; 1999; Aplin

et al. 2006; Hubert et al., 2009; Hubert et al. 2012).

During modeling, clay minerals are represented by theoretical diffraction patterns of basal reflections with several characteristic parameters of which the initial default values can be manually adjusted, within realistic boundaries, according to the characteristics of the clays in the experimental pattern. The contribution of diffraction intensity from each clay mineral is combined to a calculated diffraction pattern which is matched with the experiment pattern. The algorithms and calculations in the Sybilla software were originally developed by Drits and Sakharov (1976). More detailed information about this clay mineral quantification can be found in Chapter II of this work and in the laboratory manual, dealing with clay mineral identification and quantification <2µm in oriented clay slides.

I.5.2 Precision, detection limit, accuracy

The precision of XRD for oriented slides is similar to that of random oriented powders, although the perfect orientation of the clay slides is more difficult to control than the random orientation of powders. This parameter is controlled by the σ* function of which the values were determined by trial-and-error procedures (see further) The precision is therefore estimated at 1-1.5%. The detection limit is, depending on the complexity of the clay mineral mixture <2µm, estimated lower than 1%. The accuracy of Sybilla clay modeling is estimated around 2-3% based on independent checks with XRD powder measurements (see Chapter II) or on independent checks with CEC- and chemical methods (Zeelmaekers, 2011).

I.6 PELLETAL GLAUCONITE CHARACTERIZATION

1.6.1 Pellet separation from bulk sediment

As described in Adriaens (2009), pelletal glauconite is most effectively separated from the rest sediment by magnetic separation methods. The specific paramagnetic nature of pelletal glauconite (Odin, 1982) allows them to be separated from non-magnetic minerals or minerals with other magnetic properties. Magnetic separations are performed using a Frantz isodynamic magnetic separator (Svoboda, 2009) by which a non-destructive and high quality separation can be obtained.

Sample preparation

As described in Adriaens (2009), the success and effectiveness of magnetic pelletal glauconite separation strongly depends on the preparation of samples. When samples are processed without any pretreatment, separations are incomplete and are contaminated with important amounts of quartz, clay and other mineral impurities. Moreover, particles <30-40µm are virtually impossible to separate using dry magnetic separation methods because strong electrostatic forces on these particles restrain the magnetic forces (Rosenblum and Brownfield, 2000). Therefore samples are best washed and wet sieved at 32µm to create optimal separation conditions. In this work, this routine was already performed in glauconite bearing samples to avoid disaggregation of pelletal glauconite during clay preparations. This procedure is consequently also beneficial for separating pelletal glauconite.

Instrumental parameters

The magnetic separation process itself is mainly influenced by 4 adjustable parameters: the supply power, the front and side angle and the flux rate by which particles flow through the device. Optimal parameters for all types of magnetic minerals were listed by Rosenblum and Brownfield (2000). Optimal glauconite separation is obtained using following parameters (Adriaens, 2009):

- Supply power: 0.5 ± 0.1 A
- Front angle: fixed at 20°

- Side angle: between 15-20°, sloping away from the operator
- Flux rate: to be adjusted according to the separation result
- Number of runs: at least 3 times (more if required)

Quality of separation

The success of the glauconite separation also depends on the presence of other paramagnetic minerals with similar paramagnetic properties, like goethite, siderite and ilmenite. As these minerals have very similar paramagnetic properties compared to glauconite minerals, they will be included in the magnetic separate together with pelletal glauconite. However, also the non-magnetic fraction, dominantly consisting of quartz, can still contain minor pelletal glauconite as a 100% effective separation is rarely achieved. Quality control of both separates is performed by binocular microscope or by X-ray diffraction methods. Pelletal glauconite >32µm is extracted from the non-magnetic quartz fraction until this fraction contains at most 2% of pelletal glauconite grains. Generally >10g is extracted to anticipate on the required amounts of material needed during size distribution analysis and mineralogical characterization.

I.6.2 Grain size distribution

The size distribution of isolated glauconite pellets was determined using laser diffraction. After a representative sample part is obtained using a laboratory splitter, the pelletal glauconite is rinsed in the laser diffraction measurement chamber without any additional pretreatments. The use of ultrasonic disintegration tools, which are standard used to maintain optimal sample dispersion, were kept to an absolute minimum because of the obvious risk towards pelletal glauconite disintegration. More detailed information about grain-size analyses and possible pretreatments can be found in the laboratory manual.

I.6.3 Mineralogical characterization

characterization of the size distribution, the detailed mineralogical composition is a fundamental attribute of glauconite pellets. The mineralogy of authigenic glauconite minerals is less-evolved with high amounts of swelling (=expandable) layers and furthermore low amounts of K_2O (<5%) and relatively low amounts of total Fe (Odin and Matter, 1981). The latter is reflected in the 5Å of glauconite minerals but also by the position of the *060* reflection, as the b cell parameter is sensitive to the cation size and site occupancy (Moore and Reynolds, 1997; Środoń et al., 2001). The exact mineralogy of the glauconite particles and the amount of expandable layers can be studied by clay modeling of oriented glauconite slides. Glauconite grains are after magnetic separation reduced in size by wet grinding using the McCrone micronizing mill, equivalent to the pretreatment for bulk mineralogical analyses.

I.6.2.1 Characterization of 060-position

Glauconite powder is mixed with a small amount of zincite (<5%) in order to calibrate the angular positions of the diffraction pattern. The mixture is side-loaded into a XRD measurement holder and recorded from 55°-65°, with 4 seconds counting time per step. The peak position of the *060*-reflection is determined using the X-ray Viewer software (© Chevron ETC).

I.6.2.2 Clay modeling on oriented slides

Oriented slides of glauconite powder are prepared similarly to those of normal sedimentary clay fractions. Because glauconite grains in the Neogene are free from important cementing agents, the Jackson pretreatment and size separation are not included in the procedure. Nevertheless, the glauconite powder is Ca-saturated, with subsequent dialysis, to facilitate clay modeling. Sedimentation slides are prepared and measured similarly to normal clay slides. Clay modeling is performed using Sybilla software (©Chevron ETC).

I.7 BULK SEDIMENT SIZE AND SHAPE ANALYSIS

The grain size distribution of bulk samples is determined using laser diffraction methods and provides insights to the sedimentary conditions of deposition. For the Neogene deposits of the Campine basin, also shape analysis was performed on a selection of samples. The technique of automated dynamic image analysis is currently being installed (Vos et al., in prep). This technique is innovative at the current resolution and provides an renewed tool for characterization and subsequently also for stratigraphical differentiation. Size and shape measurement were performed on a non-routine basis.

I.7.1 Grain size analysis

A grain-size analysis can be performed for several reasons. The ultimate goal of the analysis also determines the strategy for preparation. If for example one wants to evaluate effects of long-distance transport of a sediment, the optimal strategy would be to analyze the sample without removing any cementing agents as these will have a crucial effect on the application. In the current case however, size distribution analysis is performed to characterize the original, uncemented particle distribution during deposition. For this purpose cementing agents need to be removed prior to analysis.

Sample preparation

The procedure to remove cementing agents from a sample for size distribution analysis is very similar to the Jackson treatment used in clay mineralogical preparations. Because structural modification of clay minerals is of less importance in this case, the used chemical reagents are somewhat stronger compared to their counterparts of the Jackson treatment:

- Carbonates are removed using **HCL**, 1.5M
- Fe-(hydr)oxides are mobilized using **oxalic-acid solution** (5%) and resedimented on a Al-plate
- Organic material is removed after boiling in $\mathbf{H_2O_2}$ (30%)

To ensure sufficient dispersal of clays and stabilize the suspension, peptiser (Na-polyphosphate) is added to the sample and boiled. Samples are washed when the suspension does not remain stable. Because particles <900µm cannot be measuring with the Mastersizer-S, they are sieved off before measurement.

Measurement

The stable suspension is splitted into equivalent parts and measured using a Malvern Mastersizer S, which uses laser diffraction to calculate the size of particles. Laser diffraction calculates particle size distributions by measuring the angular variation in light scattering produced when a laser beam passes through a dispersed sample. A mathematical deconvolution process, based on the Mie theory or the Fraunhofer approximation, decomposes the total scatter pattern and converts it into a volumetric particle size distribution which fits best the measured pattern. Hereby each measured particle is transformed into a perfect sphere with exactly the same volume ("volume equivalent spherical diameter"). The final result of the analysis is reported by a probability graph illustrating the volume% in function of the particle size in µm.

I.7.2 Grain shape analysis

Measuring the shape of grains is classical tool for sediment characterization studies and stratigraphic correlation (Folk, 1980). The time and labor intensive nature of such a study however limits the value and the potential of the technique because (1) only a very limited amount of particles, typically 30, is measured and (2) particles are compared to standard charts by an interpreter. Results therefore suffer from low reproducibility and are very susceptible to subjectivity .

Dynamic image analysis

The introduction of automated dynamic image analysis by means of a Camsizer (Retsch Technology) restores the objectivity of the technique and furthermore can be applied on thousands of grains (typically 50000 grains are measured). The developments made by Vos et al. (in prep.) allow for an accurate and reproducible measurement of two diagnostic shape parameters: grain sphericity and grain roundness. Results are reported as an average value for both parameters. The sphericity-

parameter describes to how close a particle approximates a perfect sphere while roundness describes the angularity of a particle. Sphericity differences mainly relate to differences in provenance and source rock and, to a lesser degree, the amount of transport. Rounding of sediment particles however indicate the distance and time of transportation.

Sample preparation & measurement

Reliability tests have performed by Vos et al. (in prep) indicating sphericity measurements remain accurate over the size range 30µm – 30mm while roundness measurements suffer from significant accuracy loss for particles <150µm. Moreover, both parameters are also mineral-specific because quartz grains will demonstrate different results compared to glauconite grains. For this purpose, the starting material for this analysis is the sieved sand material >32µm, which has been separated from glauconite grains. In this way, the detrital sand fraction (dominantly quartz and feldspars) is not influenced by the natural difference in glauconite grain contents between samples. Grain shapes are therefore measured only on detrital sand fractions. As the Camsizer produces only one value for sphericity and roundness as output result, there is no size-dependent measurement of the shape parameters. It was therefore chosen to split the >32µm detrital fraction by sieving into 5 size classes: <90µm; 90-180µm; 180-250µm; 250-500µm; >500µm. This procedure allows for size-dependent shape data and furthermore a certain shape-trend can be characterized through these 4 or 5 data points (Figure 1.4). In this way, 2 samples with similar bulk sample values might still be differentiated based on their size-dependent shape-trends.

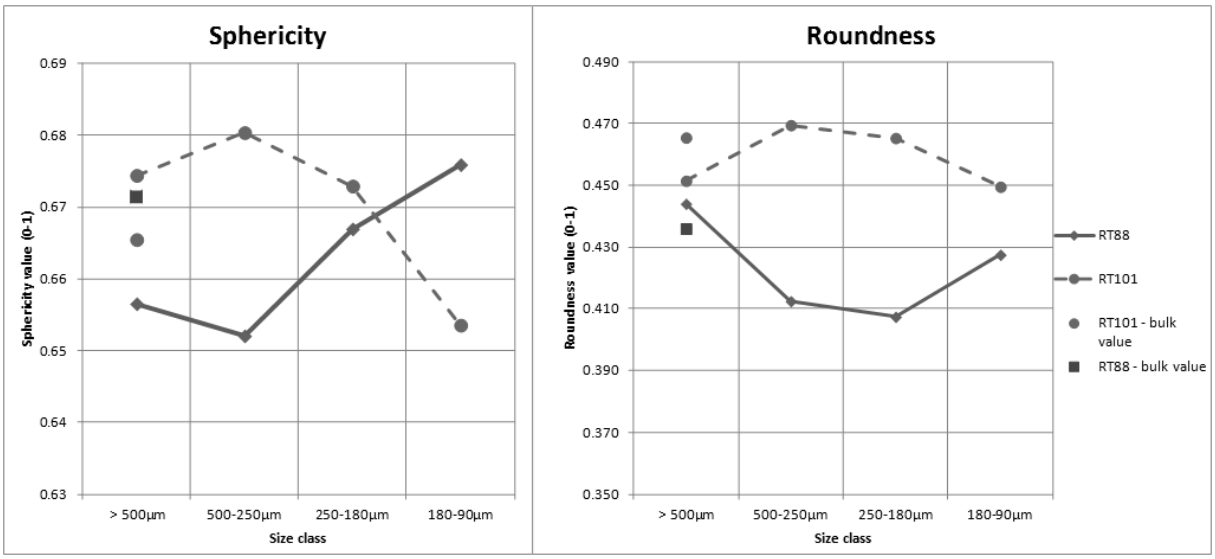

Figure 1.4: Illustration of shape parameters of two samples with bulk values (points) and shape trends (lines) indicating the surplus on information which can be derived from size-dependent shape-trend.

Chapter II

Identification and quantification of clay minerals <2µm

In order to enhance the understanding and highlight the significance of the figured diffraction patterns of oriented clay slides, this chapter will give an overview of the clays minerals which are found in this work. The discussion is limited to the mineral phases identified in this work but the principles discussed are valid also for other clay mineral species and their basic identification criteria can be found in reference literature (e.g. Moore and Reynolds, 1997). More specifically, the discriminating features for each clay phase will be shown by discussing exact positioning and intensity on diffraction patterns. As described in Chapter I, oriented clay slides are produced in such a way that diffraction intensity from the (00l)-planes is selectively enhanced at the expense of other crystallographic planes. There are five main layer types which form the clay minerals encountered in this work: illite, kaolinite, chlorite, smectite and vermiculite layers. The examples illustrated below are theoretical oriented clay patterns produced by the SYBILLA software (© Chevron ETC), which is also used during clay modeling of clay mixtures. Although several parameters can be adapted in the SYBILLA software (mean crystal thickness, interlayer cation content, octahedral Fe-content, water and glycol content, d-spacing,…) it is chosen here to demonstrate theoretical minerals with parameter values which match the mineral characteristics in the experimental patterns presented in this work.

II.1 IDENTIFICATION

The identification of clay minerals is traditionally only based on the position and intensity of (00l)-reflection planes measured on oriented clay slides (Moore and Reynolds, 1997). Studying the diffraction pattern of random oriented powders <2µm however allows a more precise identification (e.g. differentiation dioctahedral – trioctahedral) and discriminate between different clay species which have a very similar appearance on diffraction patterns of oriented slides (e.g. glauconite and illite). In this work, the most common regular clay minerals, such as smectite, illite, kaolinite, chlorite and mixed-layer illite-smectite were found but also vermiculite and glauconite-smectite will be reported in this work. Below, an overview is given of each of those minerals, their particularities and discriminating features for identification.

II.1.1 The expandable phases: smectite and vermiculite

The group of expandables are those layer types which are expand upon intercalation with water or organic molecules such as ethylene glycol and glycerol. The primary structural unit of smectite consist of two tetrahedral sheets with a central octahedral sheet. The bonds between layers are weak which allows water and other molecules to enter the interlayer space (Figure 2.1). This causes expansion of the structure in the c-direction (Grim, 1962).

The difficulty about expandable phases is however their heterogeneity in these swelling capacities. Some species are able to incorporate a single-layer complex while others incorporate a double-layer complex. In general, the former group is considered as vermiculites and the latter group as smectites, which are more expandable than the former group. The

AIPEA nomenclature committee (Bailey, 1980) decided that the layer charge is the decisive criterion to distinguish smectites from vermiculites. Whereas expandable species with a layer charge lower than 0.6 are termed smectites; those with a layer charge higher than 0.6 are vermiculites (Bailey, 1980). Some authors subdivide both smectites and vermiculites into low charge (=high expandable) and high charge (=low expandable) species. Measurements of layer charge are however only achievable when working with mono-mineral samples which in natural conditions is almost never the case. Therefore, several authors have proposed an operational definition to positively identify vermiculite, mostly based on the differential swelling behavior.

In practice however, the identification of vermiculite and its differentiation from smectite is not readily achieved. Both minerals exhibit a range of layer charges which makes that smectites and vermiculites probably constitute a continuous series of swelling clay minerals with variable layer charges. Mosser-Ruck et al., (2005) for instance have demonstrated that the use of liquid ethylene glycol makes both low charge and high charge smectite, as well as low charge vermiculites (<1.2/unit cell), fully expand to 17Å. The use of ethylene glycol is therefore strongly discouraged to differentiate between smectite and vermiculite. Instead, the use of liquid glycerol and Mg-saturation for dioctahedral and trioctahedral smectites will expand those phases to 17.8-17.9Å, whereas vermiculite, in any cation state, will not expand beyond 14.5Å (Walker, 1957, 1958; Harward and Brindley, 1965; Suquet et al., 1975; Viani et al., 1985; Mosser-Ruck et al., 2005). Robert and Barshad (1972) proposed a two-fold operational definition for vermiculite.

1) *Expansion to 14.5Å after Mg-saturation and glycerol solvation treatment*. In contrast to vermiculite, smectite layers will expand to ca. 18Å because it accepts two layers of glycerol instead of 1 glycerol layer for vermiculite which will remain at ca. 14.5Å.
2) *Collapse to 10Å after K-saturation +1h/300°C treatment*. As opposed to chlorite, vermiculitic and smectitic layers will incorporate K-cations in the interlayer space preventing glycerol to enter the interlayer space upon heating. Therefore, smectitic and vermiculitic layers will collapse to 10 Å.

This operational definition allows a distinction between vermiculite and other similar clay species. In cases where it is unclear whether smectite or vermiculite is present, the term “expandable phase” is used.

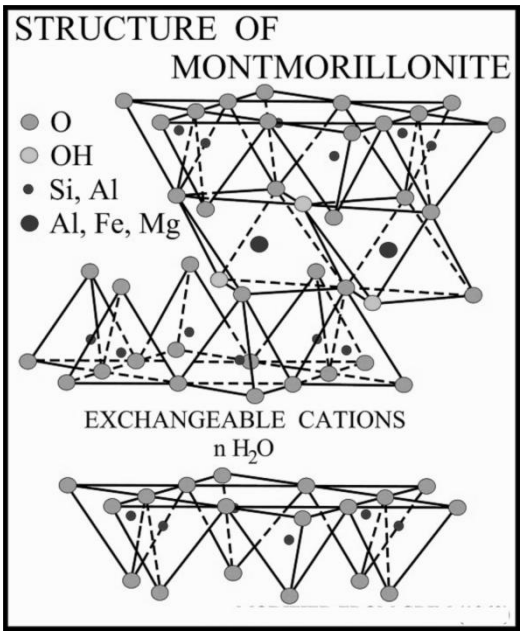

Figure 2.1. Structure of smectite (modified from Grim, 1962).

II.1.1.1 Smectite

The oriented diffraction pattern of smectite (Figure 2.2) is characterized by rational series of reflections starting from ca. 15Å. This (001)-reflection will shift to ca. 17Å in response to ethylene glycol and also the lower order reflections shift to lower angles (Table 2.1). In response to heating (550°/1h), the smectite structure will collapse to ca. 10Å, the equivalent d-spacing for non-expanding 2:1 illite. During clay modeling, it is observed that for most natural smectites, not all layers adopt 2 ethylene glycol complexes ("low-charge smectite"). A small part of the smectite layers only adopt 1 ethylene glycol layer ("higher-charge expandable"). The Sybilla clay modeling software is designed based on this assumption, as it is possible to differentiate between expandable layers based on the amount of EG or water complexes (1 or 2) which are incorporated during swelling. The modeling software is however not yet able to produce clay models with glycerol intercalations molecules which means that although vermiculite is best identified using glycerol, it can only be modeled and quantified in the Sybilla software when intercalated with ethylene glycol. In the example displayed in Figure 2.2, a 80:20 low/high-charge ratio was used, which is a typical ratio in natural Ca-saturated smectites (Zeelmaekers, 2011). In air dry state, the modeled amount of "high-charge smectite" typically is somewhat higher, because of the difference between water and ethylene glycol molecules.

II.1.1.2 Vermiculite

As discussed above, the use of ethylene glycol intercalation in vermiculite produces ambiguous results as those with lower charge can fully expand to 17Å whereas those with higher charge only have limited swelling capacities. Instead, a Mg-saturation combined with glycerol intercalation should allow positive identification. The vermiculitic mineral identified in this work (see Chapters IV, V and VI) belongs to the former group, i.e. almost complete swelling capacities with respect to ethylene glycol. The air dried and glycolated pattern of the vermiculitic mineral is shown in Figure 2.3. In ethylene glycolated condition, 80% of the expandable layers adopts 2 EG-complexes in the interlayer space whereas 20% only adopts one. These numbers are mainly based on the position of the vermiculite (002)-reflection in the experimental patterns which is approximately positioned at 8.28Å. In the example shown in Figure 2.3, this reflection is furthermore relatively intense, which indicates the vermiculite mineral is Fe-rich. Upon glycerol treatment, the vermiculite does not expand further than 14.5Å (Table 2.1).

Table 2.1. Identification criteria for most common sedimentary discrete clay minerals.

	001 in air dry (in Å)	001 in EG (in Å)	001 after heating 550°C (in Å)	001 after Mg-sat + glycerol (in Å)	001 after K-sat+ 300°C (in Å)	Diagnostic characteristics
Smectite	15	17	collapse to 10	18	collapse to 10	Ethylene glycol
Illite	10	10	10	10	10	Strong 002 reflection
Glauconite	10	10	10	10	10	Weak 002 reflection
Kaolinite	7.16	7.16	7.16	7.16	7.16	Heating at 550°C
Chlorite	14.2	14.2	14.2	14.2	14.2	peak at 4.73Å
Vermiculite	14-15	14-15	collapse to 10	14-15	collapse to 10	Mg-saturation

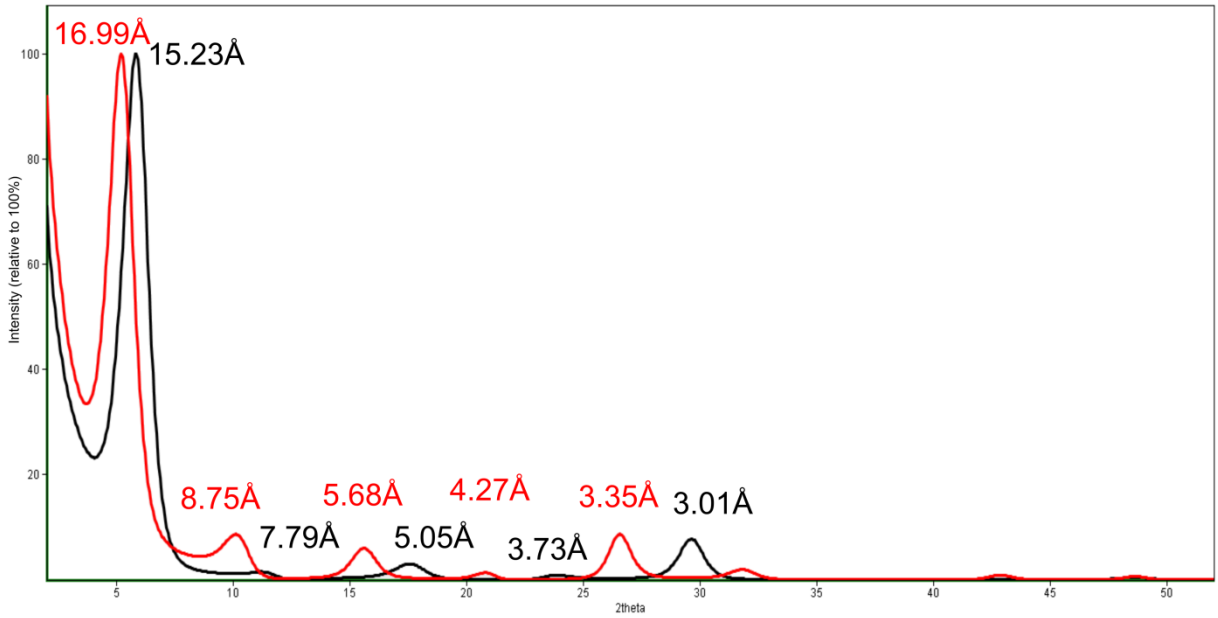

Figure 2.2. Air dried (in black) and glycolated (in red) oriented diffraction patterns of a smectite with 80% of low charge layers (i.e. including two ethylene glycol layer) and 20% high charge layers (i.e. including one ethylene glycol layer).

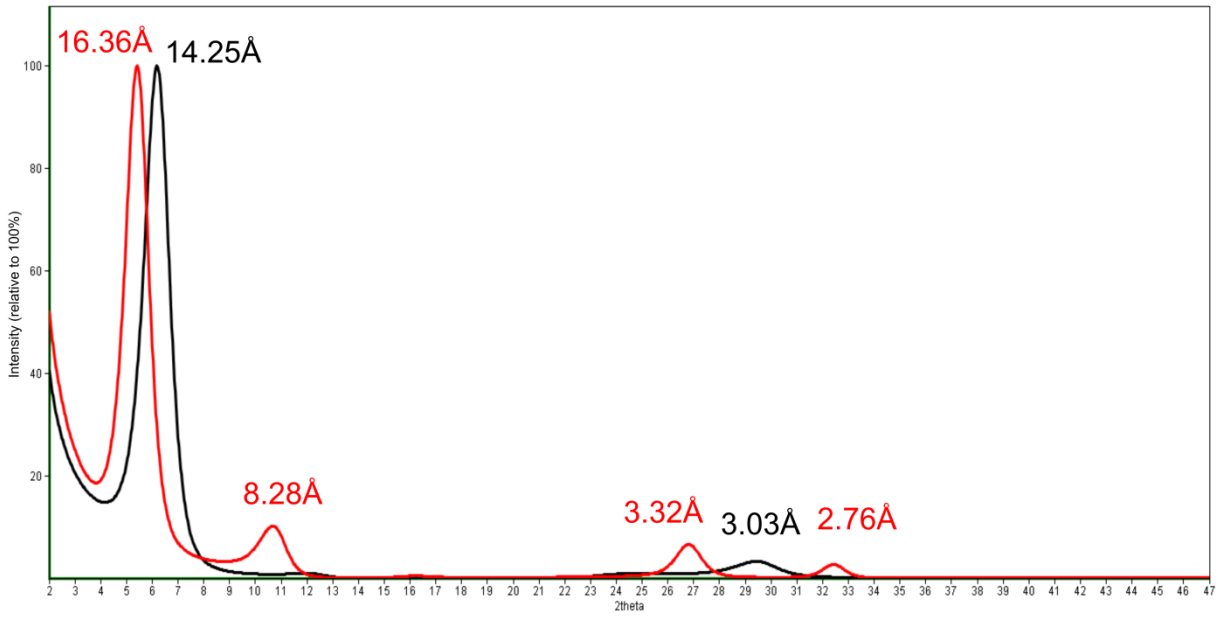

Figure 2.3. Air dried (in black) and glycolated (in red) oriented diffraction pattern for lower charged vermiculite. The relatively strong 8.28A reflection points to the Fe-rich nature of the mineral species.

II.1.2 The 10Å – minerals

This group comprises the dioctahedral layer types which are characterized by a c-cell dimension of 10Å: illite and glauconite. The structure of mica is very similar but contains slightly more potassium and aluminum and is therefore characterized by stronger interlayer forces. In sediments, muscovites and eventually other mica's, occur in size fractions larger than the clay fraction and only in exceptional cases in the clay fraction. The sharp shape of the 10 Å peak , distinguishly sharper than illite, is the indication in that case for the presence of mica but is not further discussed here. The fewer interlayer cations in illite and glauconite allow for more variability in the manner of layer stacking resulting in stacking disorder (Grim, 1962). Typical for these layer types is that the interlayer space is mainly occupied by potassium rather than other monovalent or divalent cations (Figure 2.4). The presence of potassium ensures a strong bonding between adjacent tetrahedral sheets which prevents the intercalation of organic molecules such as ethylene glycol or glycerol. Illite and glauconite therefore are not expandable and also resist a standard heating treatment (550°C/1h) (see Table 2.1).

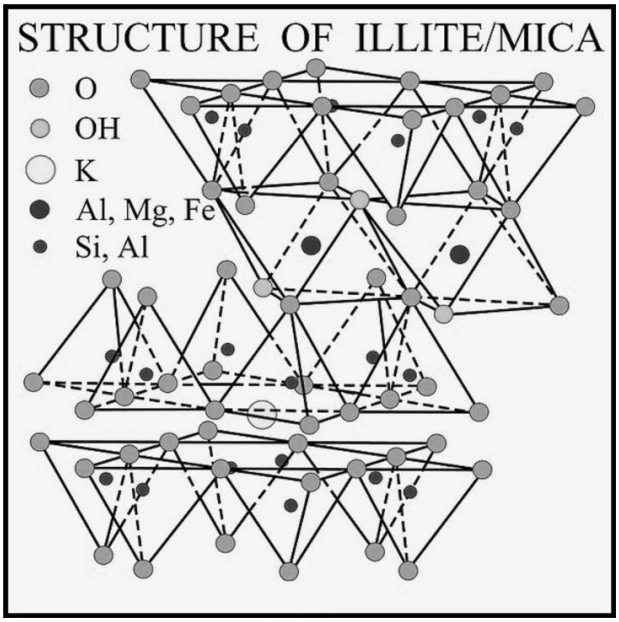

Figure 2.4. Crystallographic structure and unit cell along the c- cell dimension of illite and glauconite. The main distinction between illite and glauconite layers is the octahedral occupancy of iron cations. Modified from Grim (1962).

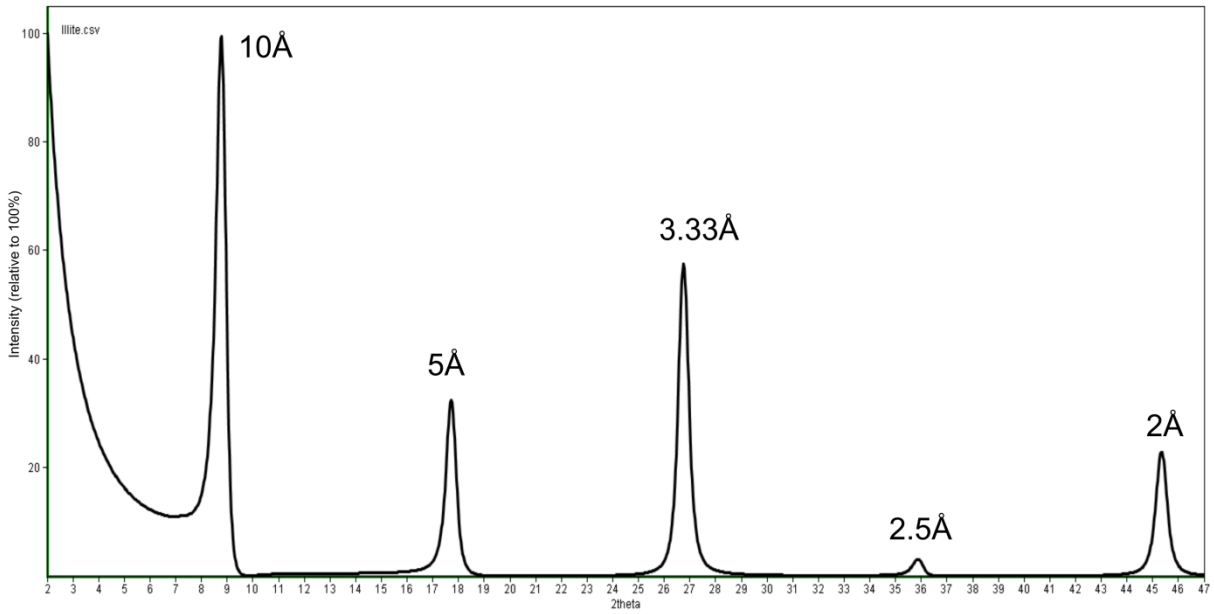

Figure 2.5. The oriented diffraction pattern of illite. Used parameters in SYBILLA: mean crystal thickness Tmean 13.48; octahedral iron content 0; d-spacing 9.98; interlayer cation content 1.8).

II.1.2.1 Illite

In oriented clay slides, illite can be recognized by its rational series of reflections: 10Å - 5Å – 3.33Å,…(Figure 2.5). The mineral illite consists predominantly of non-expandable illite layers. Nevertheless, in sediments and sedimentary rocks, the structure of this minerals is almost systematically characterized by few expandable layers. Currently, illite is defined as a dioctahedral 10Å-mineral containing less than 5% of expandable layers (Meunier, 2005). Less than 5% expandable layers are hardly detectable by glycolation, certainly in clay mineral mixtures.

II.1.2.2 Illite-smectite R0

Randomly interstratified mixed-layer minerals (R0) probably are the most underestimated clay group in quantitative clay mineralogy <2µm. Unlike the regular interstratified types (R1, R3), their identification is not straight-forward. Because they are the product of two end-member clay minerals, in this case illite and smectite, and because their occurrence is often concentrated in the smallest size fractions, the diffraction pattern of randomly interstratified clays merely consist of broad maxima rather than sharp peaks.

The diffraction pattern of R0 illite-smectite used in the examples below is a compromise of the end member illite and smectite (80:20 low charge/high charge) reflections. Figure 2.6 illustrates the diffraction pattern of illite-smectite 70:30 with the ratio low charge/high charge smectite 80:20. This type of illite-smectite, or with slightly modified ratios, is commonly encountered in the clay fraction studied in this work. The reflection at 9.71Å in glycolated conditions is produced by the (001)-reflection of illite and the (002)-reflection of smectite and is now called the illite-smectite mixed-layer (001/002)-reflection. A similar reasoning can be followed for the other reflections. In the example used here, mixed-layer reflections are closer to the end member illite reflections because of the 70:30 illite-smectite ratio. Note that in air dry conditions, the first noticeable peak at 12Å is caused by the interference of the smectite (001) and the illite (001) whereas in glycolated conditions this mixed-layer reflection is decomposed as the illite (001) now interferes with (002) reflection of smectite, hereby forming the glycolated (001/002) illite-smectite reflection (Figure 2.6). The bump at 16-17Å is caused by the diffraction of smectite 17Å-layers only. In this research only randomly (=R0) interstratified illite-smectite was encountered.

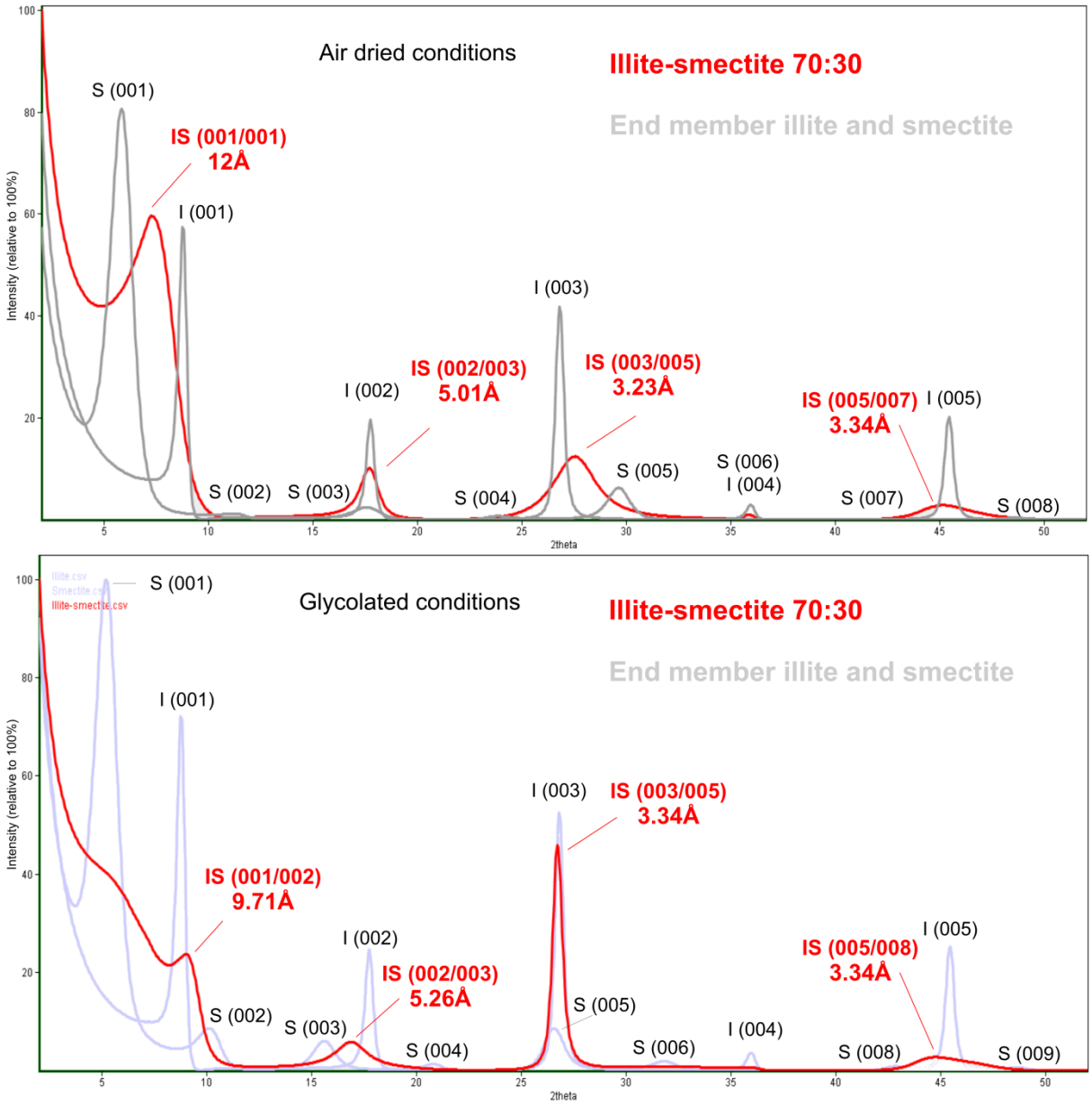

Figure 2.6. Air dried (above) and glycolated (below) oriented diffraction pattern of illite-smectite (70:30) with the low/high charge smectite 80:20, shown in red. The diffraction patterns and indices of the end member illite and smectite are shown in grey.

II.1.2.3 Glauconite minerals

Glauconite layers have exactly the same characteristics than illite layers, except that the amount of octahedral iron is many times higher in glauconite. In oriented slides, the characteristics of glauconite are therefore identical to illite, except for the much less intense (002)-reflection caused by the enhanced scattering of Fe-atoms (Figure 2.7). A positive identification for glauconitic minerals in a clay mixture on oriented slides can therefore be very difficult. The mineralogy and chemistry of glauconite minerals, being glauconite mica and mixed-layer glauconite-smectite, is very similar to that of illite and more specific, Fe-rich illite. It is therefore often difficult to decide in samples whether an Fe-rich 10Å-species is the mineral glauconite or Fe-rich illite. According to published data in literature (Velde, 1985; Meunier, 2005) and the AIPEA nomenclature committee (Bailey, 1980; Bailey, 1988), the distinction can made based on the octahedral iron content with glauconite

minerals typically containing more than 15wt% of total Fe ($FeO+Fe_2O_3$). Nevertheless, a continuous solid solution between glauconite and Fe-illite was suggested by Odin and Matter (1981) and Velde (1985). Meunier and El Albani (2007) however concluded this to be restricted to glauconite minerals which are characterized by (1) a very Al-rich glauconite mineralogy or (2) a highly expandable glauconite-smectite mineralogy (Berg-Madsen, 1983; Weaver and Pollard, 1973), both of which are very rarely reported and only occur in specific environments. Most often glauconite minerals are very Fe-rich, low expandable glauconite-smectites (Buckley et al. 1978; Baldermann et al., 2012). Such characteristics are also typical for pelletal glauconite encountered in the Campine basin in Belgium (Figure 2.8) (Adriaens, 2009).

The compositional domain of Fe-illites is very narrowly defined (Figure 2.8) and their occurrence seems to be restricted to non-marine environments (Meunier, 2005). Glauconite minerals on the contrary are typical marine constituents. It is therefore very unlikely that glauconite minerals and Fe-illites occur together in the same environment.

Consequently, glauconite minerals can be positively identified when occurring in marine deposits and if containing more than 15wt% total Fe (Velde, 1985; Meunier, 2005). In practice, the amount of iron is difficult to assess based on XRD pattern observations only. In the past, creditable attempts were made by Esquivin (1969) who introduced a parameter based on the proportion *001*-intensity vs. *002*-intensity of illites. This type of approach is however restricted to pure minerals as the presence of mixed-layer minerals will have a strong influence on the *002*-intensity of illite and glauconite. Instead, the iron content of clay species can be assessed during clay modeling where the full contribution of each mineral species is taken into account.

An easier and generally also less ambiguous method is the detailed characterization and decomposition of the *060*-clay region performed on clay-sized powder measurements. Clay powders are hereby prepared in a similar way as the powders for bulk mineralogy. This relatively simple tool probably provides the best working method to positively identify glauconite minerals (Figure 2.9) because of the clear distinction of dioctahedral Al-rich and Fe-rich clays in the *060* area. In the case of glauconite minerals, d_{060} should be higher than 1.510Å (Bailey, 1988), while common sedimentary dioctahedral Al-rich clays are characterized by d(*060*)-values close to 1.50Å (Środoń et al., 2001). The decomposition can be made manually as well as automated through the decomposition tool included in the X-RAY VIEWER software (© Chevron ETC).

In nature, clay mineral species consisting exclusively of glauconite layers are very scarce and only are reported in Paleozoic globular pellets. In all other cases, glauconite layers systematically occur interlayered with expandable layers. In this work, two types of glauconite-smectite are necessary to fit the diffraction pattern of glauconitic minerals in pelletal and clay-sized habits (Figure 2.10). The first is a low-expandable glauconite-smectite with 10% of expandable layers, which consist of 80% of regular low-charge (=high expandable) smectite and 20% of high-charge smectite (=low expandable). The second glauconite-smectite phase is characterized by 27% of expandable layers with the low charge/high charge smectite ratio equally at 80:20. During clay modeling, a typical octahedral iron content of 1.52 atoms/half unit cell is used, based on the observed d_{060} value of approximately 1.515Å.

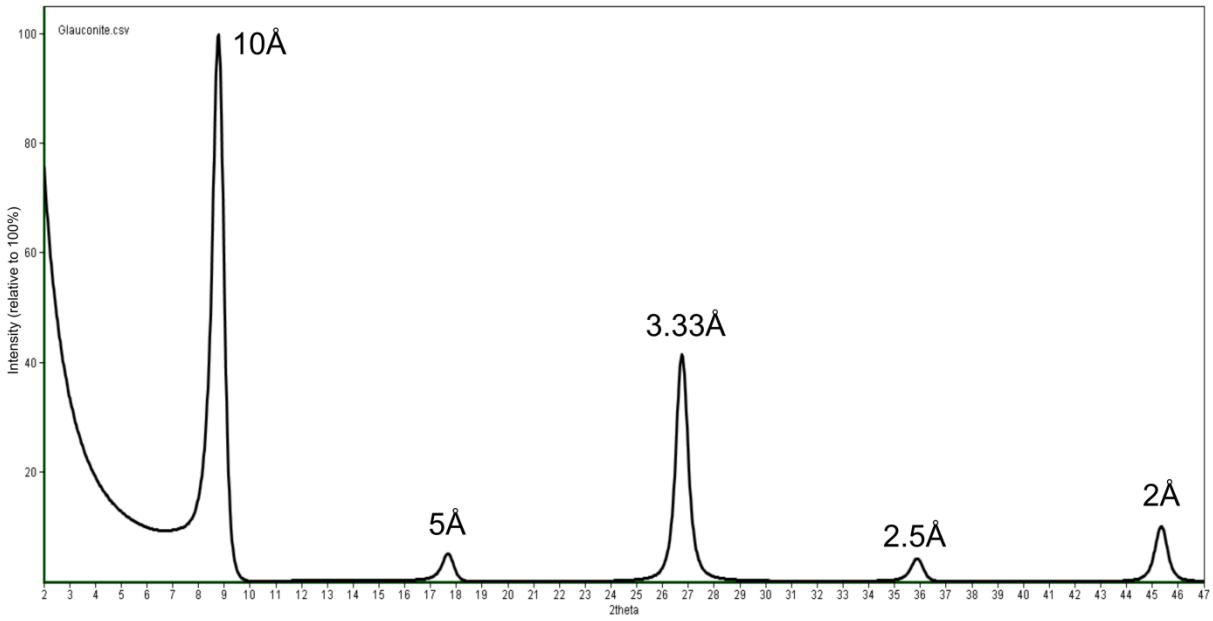

Figure 2.7. The oriented diffraction pattern of glauconite. Used parameters in SYBILLA: mean crystal thickness Tmean 10.75; octahedral iron content 1.52; d-spacing 9.98; interlayer cation content 1.8). Notice the much weaker 5Å reflection compared to illite.

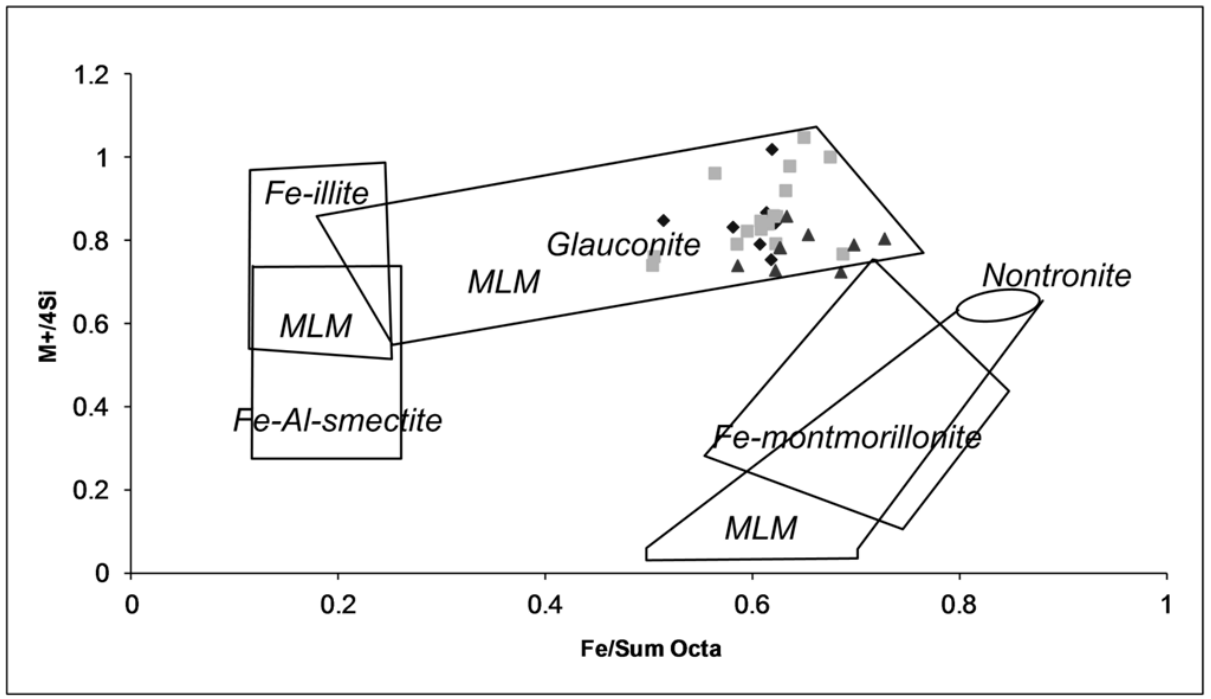

Figure 2.8. Position of Cenozoic glauconite pellets of Belgium in compositional diagram. “MLM” stands for mixed-layer minerals, “M+ corresponds to the interlayer charge while “Sum octa” corresponds to the sum of octahedral cations in the structure. Figure modified from Meunier and El Albani (2007).

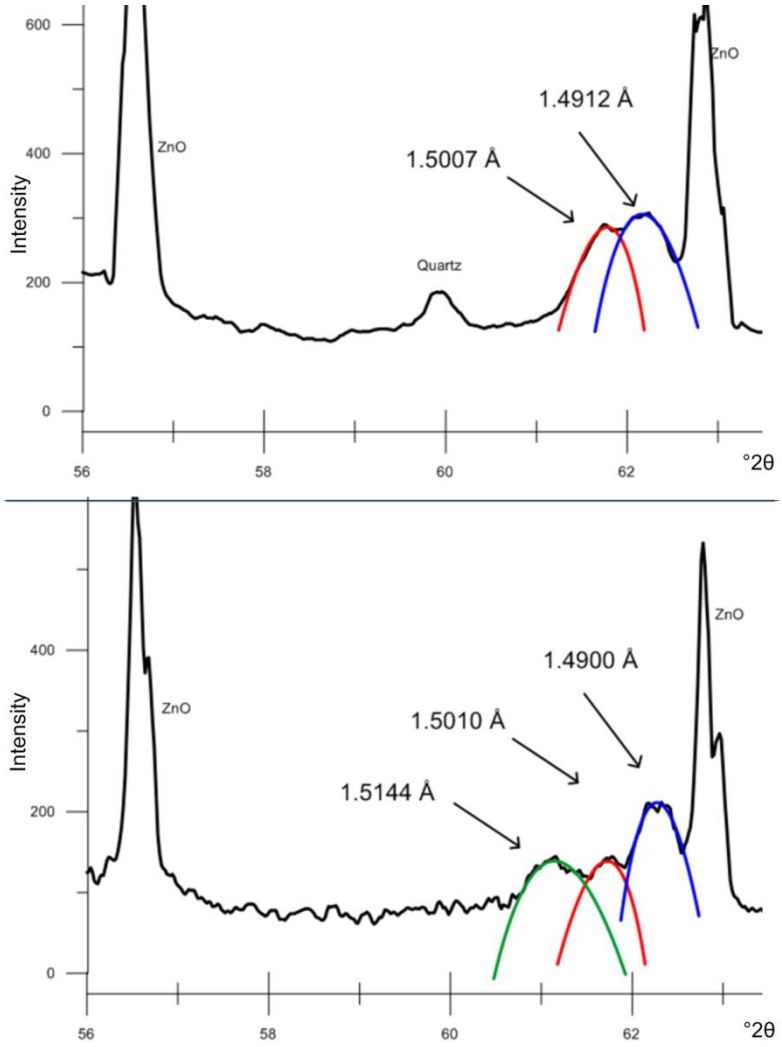

Figure 2.9. Decomposition of 060-area of a powder sample without glauconite minerals (upper) and a sample containing glauconite minerals (lower). The blue curve represents the contribution from kaolinite; the red curve represents the contribution from all dioctahedral Al-clays (smectite, illite, illite-smectite) while the green curve corresponds to the contribution of 2:1 Fe-clay and thus glauconite-smectite. XRD patterns were recorded with ZnO as reference material.

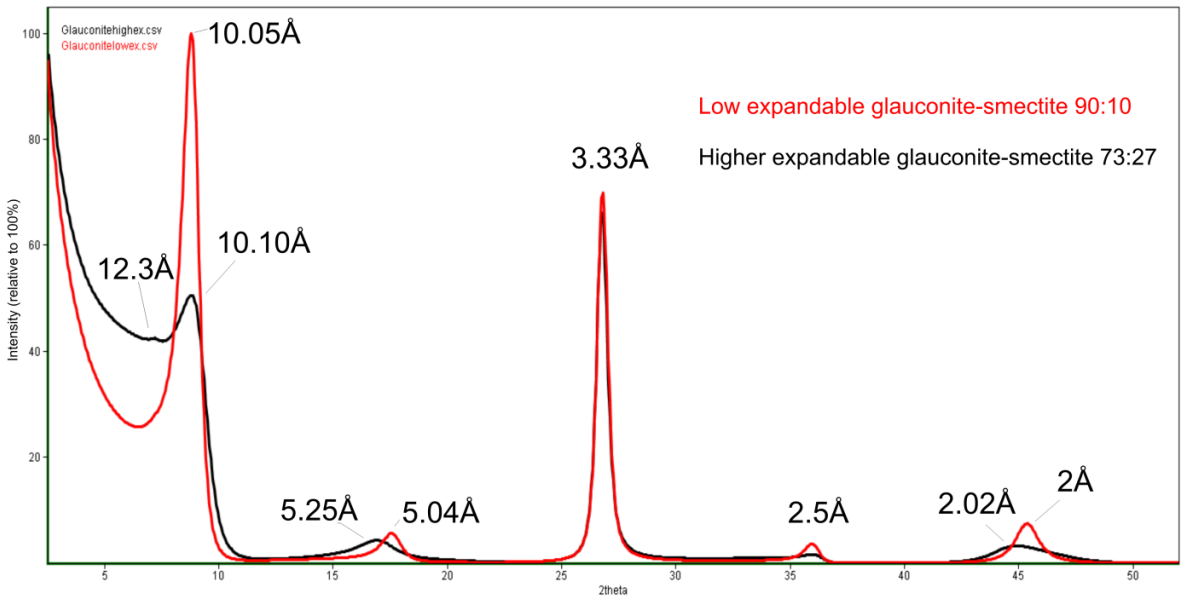

Figure 2.10. Glycolated oriented diffraction patterns of glauconite-smectite. Low expandable glauconite-smectite is shown in red whereas higher expandable glauconite-smectite is shown in black.

II.1.3 The 7Å and 14Å – minerals

Minerals of the kaolinite and chlorite groups both have a recurrent 7Å dimension in the c-direction. The primary structural unit of both minerals is however significantly different. Although both groups include various members which are differentiated based on chemistry or layer stacking, only regular dioctahedral kaolinite and trioctahedral Fe-rich chlorite are considered as no other species were found in this work.

II.1.3.1 Kaolinite

Kaolinite is a 1:1 dioctahedral clay mineral which means its primary structural unit is made up by 1 tetrahedral and 1 octahedral sheet and the c-cell dimension is about 7.16Å (Figure 2.11). The diffraction pattern of kaolinite is therefore relatively easy recognized on oriented slides with rational series of reflections: ca. 7.16Å; 3.58Å,…(Figure 2.12). Glycolation will not alter the diffraction pattern of kaolinite but heating to 550°C will destroy the structure and make it amorphous in response to X-rays (Table 2.1).

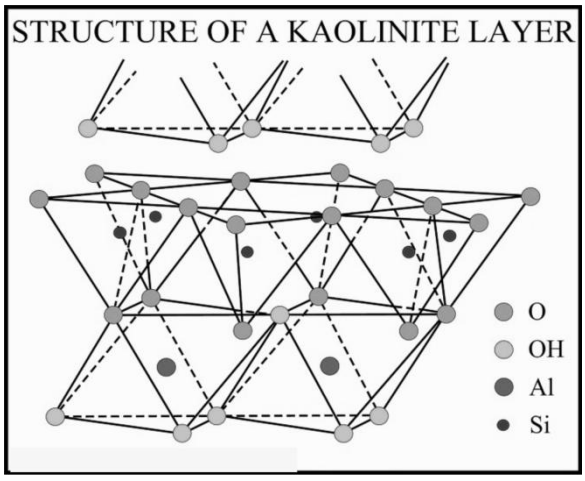

Figure 2.11. Structure of kaolinite (modified from Grim, 1962).

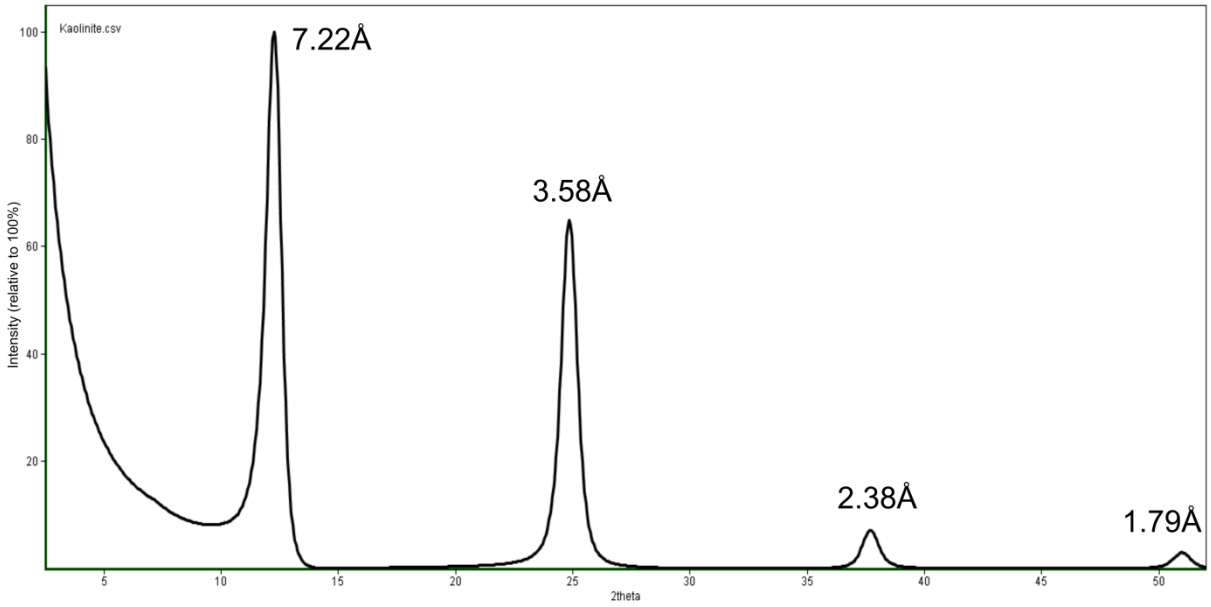

Figure 2.12. The oriented diffraction pattern of kaolinite. Used parameters in SYBILLA: mean crystal thickness Tmean 12.31; d-spacing 7.16).

II.1.3.2 Chlorite

Chlorite is a 2:1 clay mineral with a brucite-like layer occupying the interlayer space (Figure 2.13). As the octahedral cation most often is divalent (Mg, Fe), the large majority of chlorites are trioctahedral. Nevertheless, also dioctahedral chlorites exist, but they are less frequently reported. Chlorites have their (001) reflection at 14 to 14.4Å; depending on the individual species (Moore and Reynolds, 1997) and again with a rational series of reflections (Figure 2.14). This makes that, apart from the 14Å-reflection, the chlorite peaks largely coincide with the reflections of kaolinite. However, the (001)-chlorite reflection resists heating treatment of 550°C/1h and its intensity increases greatly whereas the intensity of the 002,003 and 004 reflections are much weakened (Moore and Reynolds, 1997). At 550°C, kaolinite becomes amorphous to X-rays which should allow a distinction with chlorite. In low abundance mixtures of chlorite and kaolinite however, the heating treatment will not give a complete answer if either kaolinite or chlorite are present, or both. In practice, close inspection of the 002- peak positions almost allows positive distinction, as the kaolinite 001 is present at 7.16Å compared to ca. 7.08Å for the chlorite 001. It has to be noted however that such distinction is only well-visible when the resolution of the used diffractometer is sufficiently high.

Glycolation or cation saturation has no effect on the peak positions of chlorite. Chlorite is scarce in the clay fraction of the sediments studied in this work but is found, based on modeled parameters, to be trioctahedral and Fe-rich rather than Mg-rich. Most diagnostic reflections are the 14.3Å and 4.72Å peaks (Table 2.1).

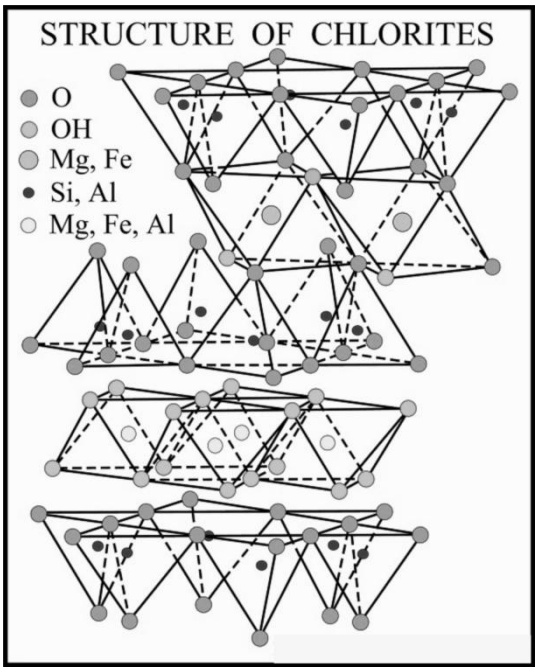

Figure 2.13 Structure of chlorite (modified from Grim, 1962).

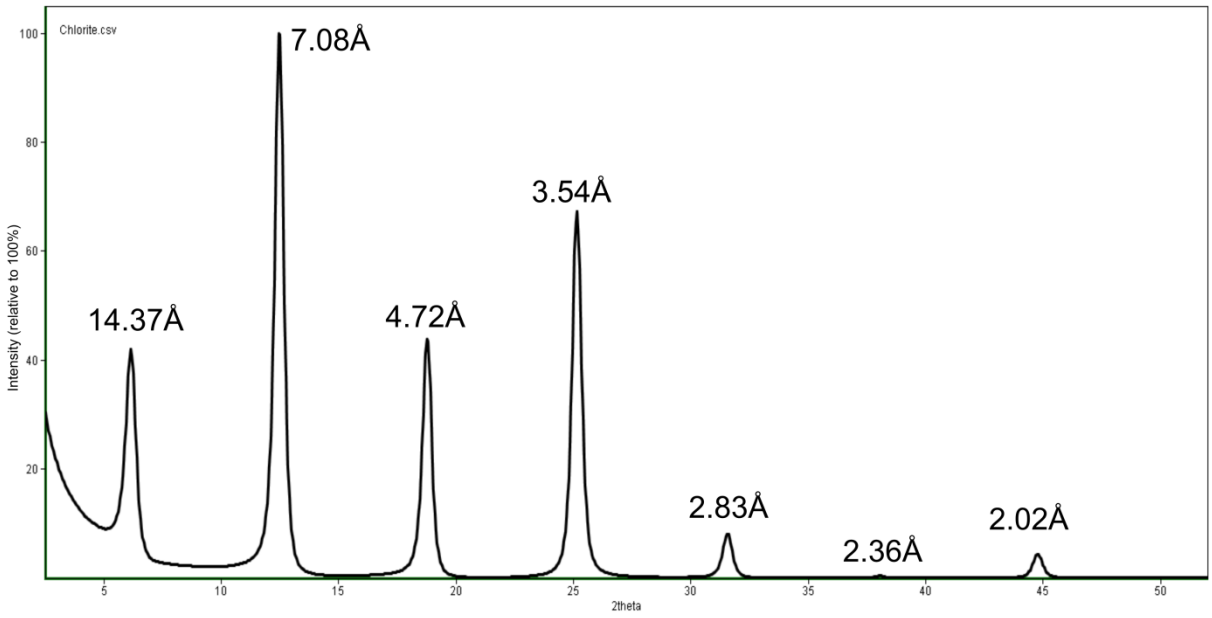

Figure 2.14. The oriented diffraction pattern of chlorite. Used parameters in SYBILLA: mean crystal thickness Tmean 8.8; octahedral iron content 1.72; d-spacing: 14.17Å; interlayer content: 0.79; interlayer iron content 3.42).

III.1.3.3 Kaolinite-expandable and chlorite-expandable

Also kaolinite and chlorite can occur interlayered with expandable minerals. These minerals are far less common than illite-smectite mixed layering but do occur in soils and weathering environments. Similar to illite-smectite, the reflections of kaolinite- or chlorite-expandable are positioned in between the reflections of the end member minerals. Figure 2.15 illustrates this for kaolinite-smectite 85:15, a mineral encountered in this work. The ratio low charge/high charge smectite was set at 80:20 as this seems to be a stable expandable layer ratio often encountered in sedimentary samples. In response to glycolation, the kaolinite-smectite pattern will therefore shift, the 7Å-peak will shift to low angles whereas the 3.5Å peak shifts to higher angles. This is

caused by the fact that in air dry conditions, the (002)-kaolinite peak interferes with the (004)-smectite peak to form the (002/004)-kaolinite-smectite mixed layer reflection. In glycolated conditions however, the smectite (005)-reflection has shifted to 3.35Å, and interferes with the (002)-kaolinite peak to form the (002/005) kaolinite-smectite mixed layer reflection (Figure 2.15).

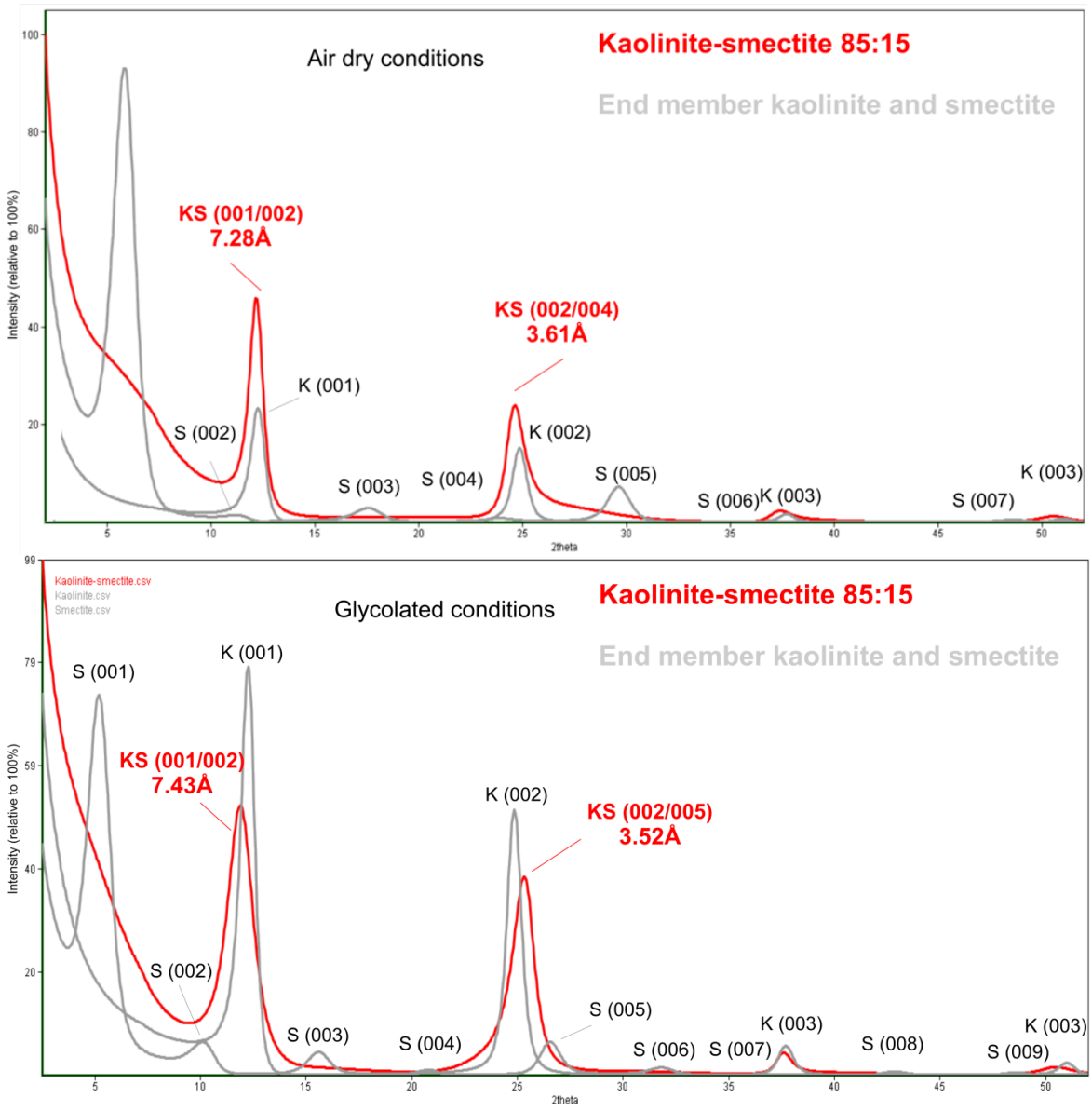

Figure 2.15. Air-dry (above) and glycolated (below) oriented diffraction pattern of kaolinite-smectite (85:15) with the low/high charge smectite 80:20, shown in red. The diffraction patterns and indices of the end member illite and smectite are shown in grey.

II.2 QUANTIFICATION

The quantification of clay mixtures in oriented clay slides is performed using the software SYBILLA (© Chevron). The main operation in this program consists of manually changing the adjustable parameters of the chosen phases, including probability parameters for mixed-layered minerals, until a satisfactory fit between the experimental and the calculated pattern is achieved. In response to the changing of a certain parameter the program automatically adjusts the overall proportions of all the phases using a least squares calculation (Zeelmaekers, 2011). Table 2.2 gives an overview of the adjustable parameters of each layer type. For kaolinite and illite, only one layer type is available while chlorite can be di- or trioctahedral. There are several possibilities for expandable layers. Smectite layers can be di- or trioctahedral and with one or two molecules of either water or ethylene glycol. Some smectite layers are highly expandable and can incorporate 2 glycol or water molecules in their interlayer space ("low-charge smectite layers"). Others are low expandable and are able to only incorporate 1 glycol or water molecule ("high-charge smectite layers"). This "high charge" component sometimes is also referred to as "vermiculitic" (Lindgreen *et al.*,2002 and Claret *et al.*, 2004). In practice, best modeling results for swelling minerals are achieved when both layer types (low and high expandable) are combined, in fact being a mixed-layer mineral. The sigma star value is in fact a function which describes how well each clay mineral is oriented to the flat surface of the clay slide. The crystal thickness of a mineral is expressed as the mean value of a thickness distribution and determines the sharpness of the reflection of that mineral. Additional parameters are the "reichweite", which describes the order in the mixed-layered mineral, and the "layer proportion" which are only adjustable for mixed-layer minerals.

The Sybilla software supports consequently smectite layers in both water- as ethylene glycol saturated state which means that both air dry and glycolated measurement can be modeled. This greatly improves reliability of quantification and structure characterization. Furthermore, to maximize the likelihood of a unique solution, the multispecimen method (Sakharov et al., 1999) requires that a model should produce satisfactory fits to the experimental patterns in at least two states with comparable quantifications. Several additional criteria were depicted by Zeelmaekers (2011) to evaluate the quality of the fit and the model and which were also used in this work:

- Acceptable matching of peak positions
- Acceptable matching of peak ratios for each phase
- Acceptable matching of peak shapes
- The use of realistic parameter values
- Gaps in matching diffracted intensity are acceptable only when reasonably justified (e.g. quartz interference with illite 003-reflection)

Table 2.2 Adjustable parameters of the most common layer types in the Sybilla program.

	Kaolinite	Illite	Chlorite	Smectite 2Gly	Smectite 1Gly	Smectite 2wat	Smectite 1Wat
Dioctahedral/Trioctahedral			x	x	x	x	x
Sigma star	x	x	x	x	x	x	x
Crystal thickness distribution	x	x	x	x	x	x	x
Octahedral Fe-content		x	x	x	x	x	x
d-spacing	x	x	x	x	x	x	x
Delta d-spacing	x	x	x	x	x	x	x
Interlayer cation content		x	x	x	x	x	x
Interlayer iron content			x				
Glycol content				x	x		
Water content				x		x	x
Reichweite				Only mixed-layered minerals			
Layer proportions				Only mixed-layered minerals			

II.2.1 Sigma star values of common sedimentary clay minerals

In the section above the working of the Sybilla program was briefly introduced together with the different adjustable parameters for each layer type. Of these parameters, the sigma star value is the only one which is not directly related to internal characteristics of the layer type but still has a large impact on quantification. The sigma star parameter describes to which degree clay minerals are oriented perfectly parallel to the glass slide. Most often the tilt angles of the clay plates are distributed following a Gaussian function around this ideal orientation (Dohrmann et al., 2009). The standard deviation of this distribution is called "sigma star" (σ*) and is used as a measure for the degree of preferred orientation of a clay mineral in an oriented slide, with higher σ* values indicating lower success in achieving perfect preferred orientation (Zeelmaekers, 2011). Reynolds (1986) concluded 12° is a good sigma star for all clay minerals. It was however demonstrated in Dohrmann et al., (2009) that the σ* values of uncemented samples show important deviations from the default value of 12°.
Based on orientation measurements and independent mineral quantification checks, fixed σ* values were chosen in Zeelmaekers (2011) for both sedimentation and smear slides. These are values of the σ* -parameter originally implemented in the Sybilla software. The σ* value can only be changed stepwise with increments of 0.78°.

- Kaolinite 6.68° (7.46° for fresh marine or river sediments)
- Illite 6.68°
- Smectite 11.36°
- Chlorite 6.68°
- Illite-smectite 6.68° (for illitic illite-smectite phases)

These are values of the σ* -parameter originally implemented in the Sybilla software. The σ* value can only be changed stepwise with increments of 0.78°. Smectites are systematically less well oriented compared to other clay minerals. The study of Zeelmaekers (2011) was performed on very similar samples as those used in this research and fixed values were chosen for each mineral (cfr. fresh muds in the North sea and Eocene-Oligocene interval in the Campine basin). As the use of these parameters resulted in very reliable quantifications, they were also used as standard σ* values in this work. It is important to notice that these values are not necessarily the correct absolute σ* values for each mineral but merely that the relative difference between smectites and other clays is established in such a way that highly accurate results are obtained.

II.2.2 Glauconite-smectite: quantification in clay mixtures and sigma star

In later chapters, it will be illustrated that glauconite-smectite occurs in the clay fraction of Neogene sediments. The appropriate modeling of this phase in the Sybilla model of clay mixtures is however not straight-forward. In addition, the σ* value of this mineral still needed to be established.
Introducing reasonable starting parameter values, other than σ*, for the glauconite-smectite phase model is not an issue as glauconite-smectite can be studied as a mono-phase in sand-sized globular glauconite pellets. Hereby reasonable values and value boundaries can be determined which are applicable for glauconite-smectite occurring in clay-sized fractions. Problems arise however when glauconite-smectite occurs in clay mixtures together with illite-smectite, and this is very often the case. The diffraction patterns of both mixed-layer minerals can be very similar, which makes the modeling much more complex and therefore also the quantification less reliable.
For this purpose, an additional XRD measurement is routinely performed in glauconite-bearing samples by which the glauconite-smectite is independently quantified. As described earlier in this chapter , 2:1 Fe-rich clays can be characterized and quantified separately from 2:1 Al-rich clays using the QUANTA method. A random oriented powder of the clay fraction <2µm is prepared equivalent to powders for bulk mineralogy and measured by X-ray diffractometry. This independent quantification can be used to determine the optimal sigma star value of glauconite-smectite during modeling of oriented clay slides. For a set of samples of the Dessel-3 borehole (see Chapter V), clay-sized glauconite-smectite was quantified on random oriented powders using the QUANTA software and on oriented clay slides using the SYBILLA software in function of different sigma star values for glauconite-smectite while keeping all other parameters fixed. In the range from 5-

80% glauconite-smectite, the optimal sigma star value seems to be 6.68 , which is identical to that of illite (Figure 2.16). This value was consequently used in all clay models.

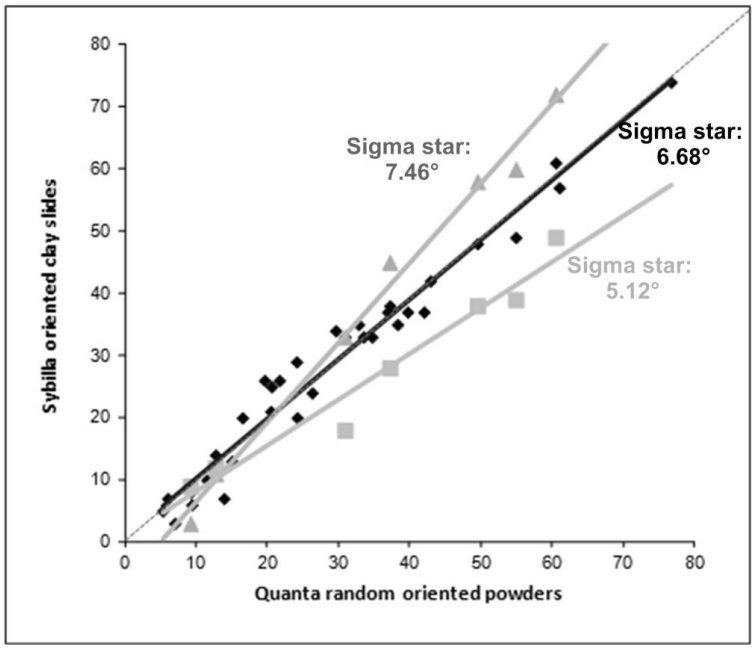

Figure 2.16. Quantification of glauconite-smectite in random oriented powders using the Quanta software and in oriented slides using the Sybilla software in function of different sigma star values.

II.2.3 Quantifying a clay mixture of 10Å-minerals

When combining the four minerals species discussed above (illite, illite-smectite, low expandable glauconite-smectite and high-expandable glauconite-smectite), it is difficult to correctly identify and quantify all four components in the mixture because of the very similar diffraction positions. For example, in a mixture of 20% illite, 30% illite-smectite, 25% glauconite-smectite low and 25% glauconite-smectite high (Figure 2.17), the diffraction positions of all species are so similar that it seems almost impossible to make an accurate decomposition. The exact intensity ratio's of the 10Å and 5Å peaks and their respectively low angle shoulders, as defined by the Fe-content, however will define the amount of each species in such a mixture. The intensity of the true 5Å peak is defined by relatively intensity of the Fe-poor illite 5Å and, by the relative intensity of the Fe-rich, low expandable glauconite-smectite phase (shown in green and red in Figure 2.17). Similarly, the intensity of the low angle shoulder at the left hand side of the 5Å-peak is defined by the intensity of the (002/003) illite-smectite mixed layer reflection and the high expandable glauconite-smectite (002/003) reflection (shown in blue and black in Figure 2.17). A high quality fitting of the 5Å and 10Å regions therefore yields an accurate quantification result, as demonstrated in Figure 2.18, where the experimental pattern is shown in black and resulting fit in red with the 4 different clay species with the SYBILLA clay modeling program. The experimental pattern was created as an artificial mixture of diffraction patterns of idealized clay minerals and its main purpose is to show crucial features in the diffraction pattern of clay mixtures, rather than pointing to the accurate quantification of this artificial mixture.

II.2.4 Quantifying a clay mixture of 7Å and 14Å-mixture

The theoretical glycolated diffraction patterns of kaolinite, chlorite and kaolinite-smectite (85-15) were combined in a mixture with 20% kaolinite, 10% chlorite and 70% kaolinite-smectite. The identification of such a mixture can be made by the typical 14.37Å and 4.72Å reflections of chlorite, the (001)-peak of

kaolinite between 7.10 and 7.20Å and the low angle shoulder of the kaolinite (001)-reflection combined with the reaction of the 7Å-pattern to glycolation treatment (Figure 2.19). Modelling using Sybilla, without previous knowledge of the original quantities of minerals mixed in this XRD trace, can determine the quantities of minerals present in this XRD trace as shown by the good fit in Figure 2.19.

II.2.5 Quantifying a combination mixture

An idealized clay mixture of standard clay diffraction patterns was prepared consisting of 10% illite, 10% kaolinite, 3% chlorite, 25% smectite, 20% illite-smectite, 12% glauconite-smectite high expandable and 20% glauconite-smectite low expandable. The clay modeling of this experimental pattern was performed using SYBILLA resulting in a very accurate quantification (Figure 2.21). Figure 2.21 also illustrates how the separate mineral phases can be identified in such a complex clay mineralogical pattern and where they contribute important intensity to the total pattern. This type of clay mineralogical pattern is commonly observed in the clay fraction of Neogene glauconitic sands.

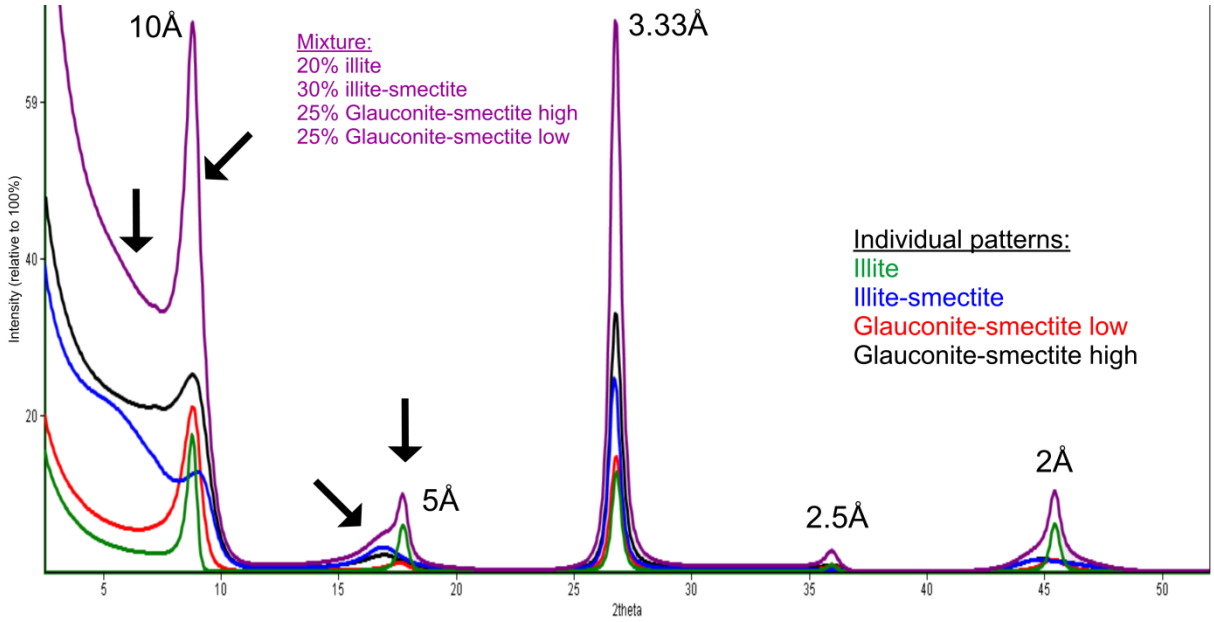

Figure 2.17. Glycolated oriented diffraction pattern of clay mineral mixture composed of different 10Å-minerals. The arrows indicate diagnostic features in the diffraction patterns.

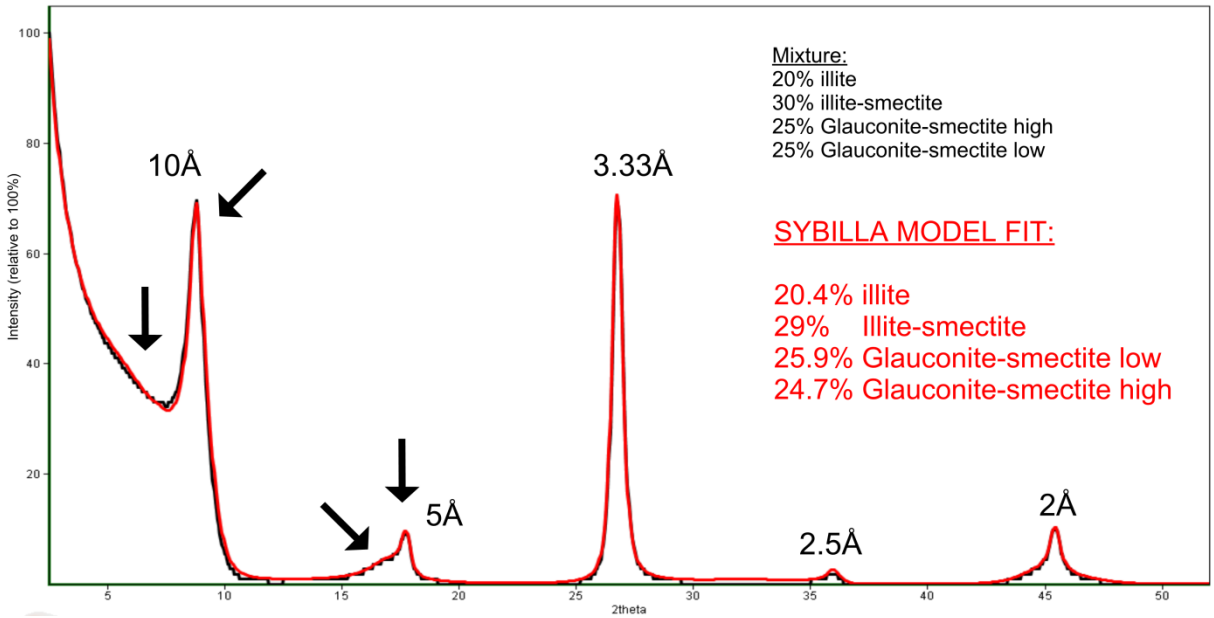

Figure 2.18. Glycolated diffraction pattern of an artificial 10Å-mixture (20% illite, 30% illite-smectite, 25% glauconite-smectite low and 25% glauconite-smectite high) in black and SYBILLA model fit shown in red. The arrows indicate diagnostic features in the diffraction patterns.

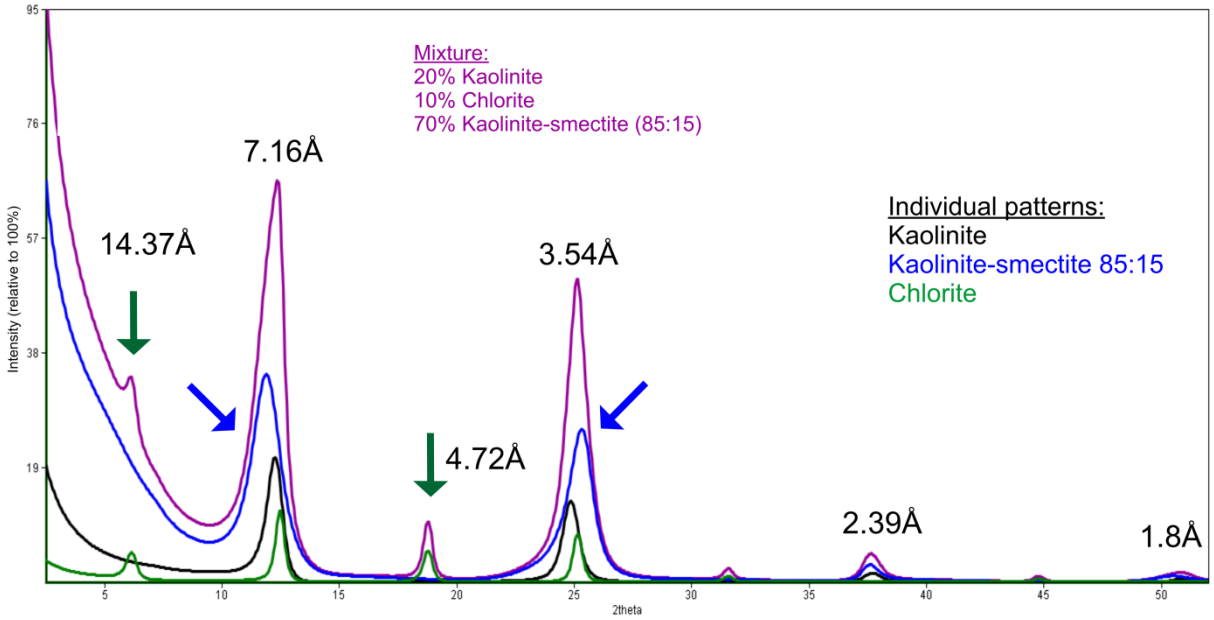

Figure 2.19. Glycolated oriented diffraction pattern of clay mineral mixture composed of different 7Å and 14Å-minerals. The arrows indicate diagnostic features in the diffraction patterns.

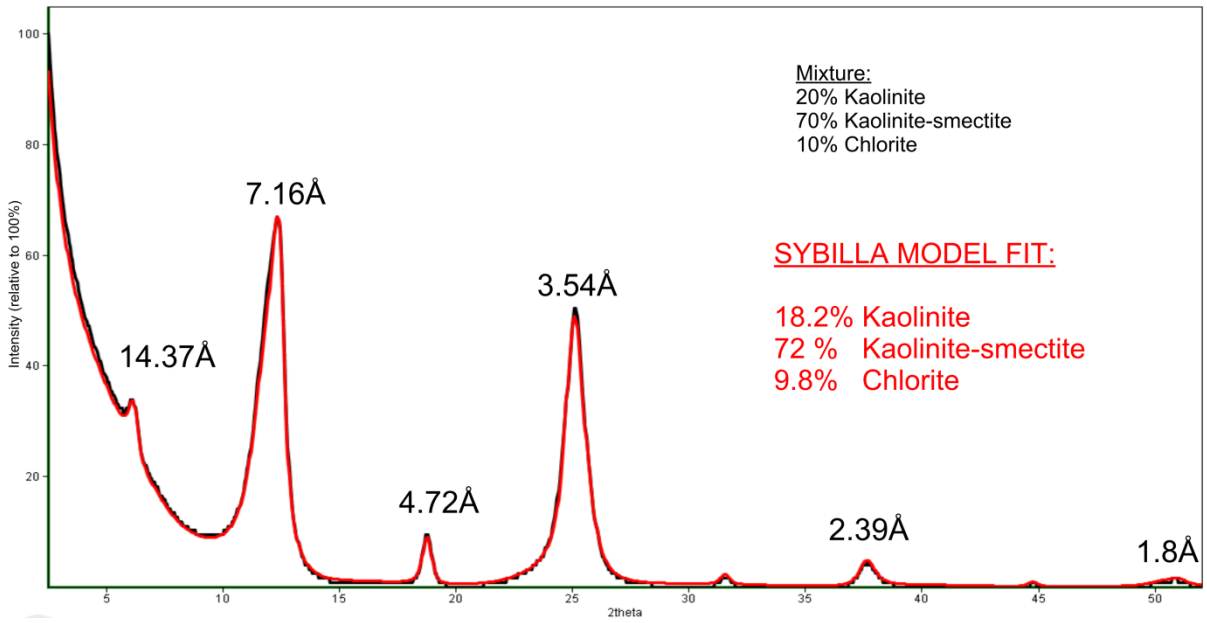

Figure 2.20. Glycolated diffraction pattern of the 7Å and 14Å-mixture (20% kaolinite, 70% kaolinite-smectite, 10% chlorite) in black and SYIBLLA model fit shown in red.

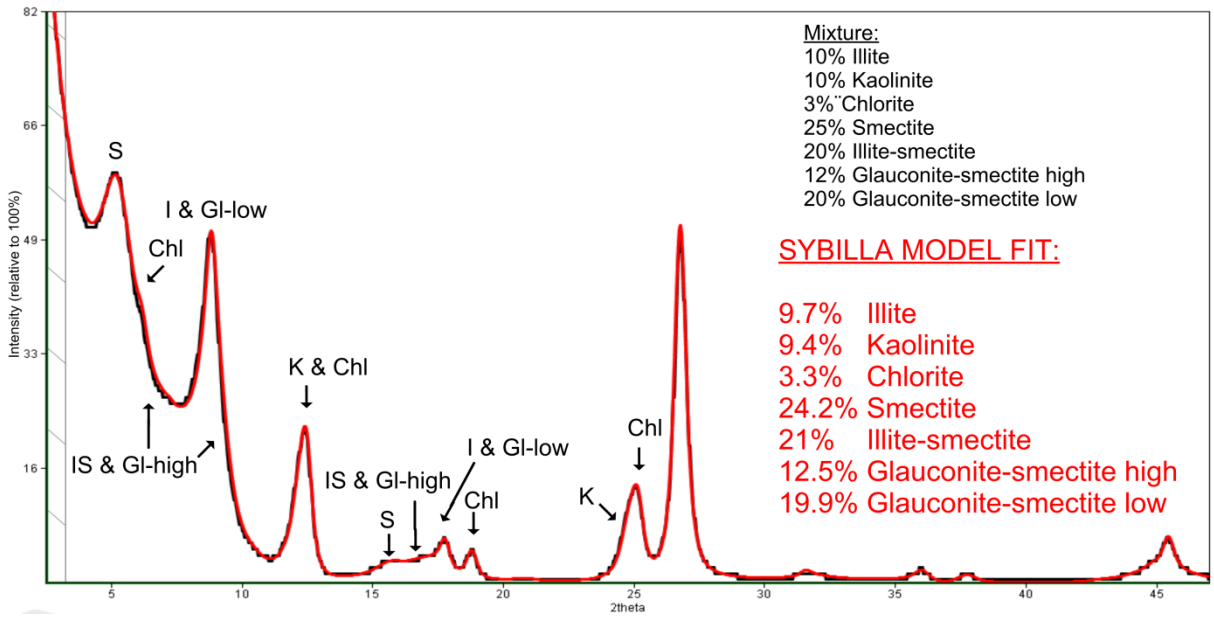

Figure 2.21. Clay mixture with the experimental pattern shown in black and the Sybilla model fit shown in red.

PART II.

Stratigraphic application: Neogene stratigraphy of the Campine basin

Introduction

The Paleogene-Neogene transition is marked by an important glaciation (Mi-1 glaciation on Figure II.1) after the warm period in the Oligocene (De Man and Van Simaeys, 2004). During the Burdigalian to the Langhian however, the climate was again warm, to reach a maximum during the Mid-Miocene Climatic Optimum (17-15Ma) (Zachos *et al.*, 2001). Volcanic activity in the region has been reported in the Upper Rhine graben from the beginning of the Burdigalian, lasting at least until the Serravalian (Blundell *et al.*, 1992). During the Paleogene, a major, widespread, tectonic uplift has been identified in areas around the North Atlantic ocean (Figure II.2), resulting in several large depocentres. These uplifted areas were reactivated at the Oligocene-Miocene transition (Jaspen and Chalmers, 2000; Ziegler and Dèzes, 2005), influencing the sediment dynamics of the northwestern part of the European continent. The uplift of the Wealden-Artois axis furthermore prevented a marine connection between the North Sea Basin and the English Channel area (Ziegler, 1990). During the early Miocene, the North Sea constituted a semi-closed basin with an open marine connection to the Norwegian sea (Louwye and Laga, 2007). In the east, the continuous subsidence of the Roer Valley graben during the Neogene created accommodation space available for sedimentation. The Roer Valley graben has therefore a crucial influence on the sediment dynamics in the eastern part of the Southern North Sea Basin where sediments typically are much thicker compared to northwestern part of the basin. In the Campine Basin in Belgium, the coastline migrated further north compared to the Paleogene resulting in sedimentation being restricted to the northeastern part of Belgium (Figure II.3). Deposition in the Campine Basin consists therefore of very shallow marine sand units with high pelletal glauconite content and separated by important intervals of non-sedimentation. In the eastern part of the Campine Basin, towards the graben area, also estuarine and continental quartz-rich deposits occur (Figure II.4).

The reconstruction of the stratigraphical framework of the different Neogene glauconitic sands is a classical debate in the Cenozoic geology of Belgium (Vandenbroek, 1882; Halet, 1935; de Heinzelin, 1964, Gulinck et al., 1963; De Meuter and Laga, 1976; Vandenberghe et al., 2014; Verhaegen et al., 2014). The macroscopic similarity between different units, gradually transitioning one to another at formation or member boundaries, makes the interpretation of boundaries and lithological correlations, and therefore also the interpretation of bulk-units itself, very difficult

For every defined Neogene formation, lithological characteristics are well described and the definition of stratotypes seems to allow clear-cut differentiations (De Meuter and Laga, 1976; website National Stratigraphic Commission Belgium, www.natstratcommbelgium.drupalgardens.com , last consulted 01-2015). The issue is however that these stratotypes are only representative for a very small part of the total formation, which often is characterized by a high degree of lithological and sediment petrological heterogeneity. Certainly at formation boundaries, the typical stratotype characteristics are not recognized anymore and transitional changes are often so gradual that defining formation boundaries based on macroscopic lithological properties only is practically impossible.

The introduction of biostratigraphic data was therefore required to bring the necessary order in the different strata. The refined dinoflagellate cyst biostratigraphy established by Louwye and co-workers in the last 20 years (Louwye (2001; 2002; 2005); Louwye and Laga (1998; 2008); Louwye and De Schepper (2010); Louwye et al. (1999; 2000; 2007; 2010)) in addition to the traditional Neogene stratigraphy as established by Laga and co-workers based on benthic foraminifera (Laga, 1970; Laga and De Meuter, 1972; De Meuter and Laga, 1976) and the sequence stratigraphy of Vandenberghe et al. (1999; 2004) have resulted in a detailed and reliable timeframe for the large majority of the deposits. Nevertheless, several units, such as the Hageland occurrence of the Diest Formation, do not contain any stratigraphical meaningful fossils.

Although biostratigraphy has been much refined, lithostratigraphic differentiation and correlation still remain important issues. Whereas in the past, only description of lithology and on-site grain-size interpretations were available in routine stratigraphic interpretations, today borehole well-logging

tools such as gamma-ray and resistivity measurements combined with lithology description of samples, eventually complemented by laboratory analyses, are the most important tools for lithostratigraphic characterization and correlations. However, the interpretation of stratigraphic boundaries and correlations remains an issue.

Previous studies (Berckmans and Wouters, 2003; Louwye et al., 2007) have shown, based on preliminary results, that quantitative clay mineralogy is a promising tool to discriminate different litho-units, even towards formation boundaries. Nevertheless, no systematic studies were performed on the mineralogy and clay mineralogical composition of these Neogene deposits whereas reliable pelletal glauconite characterization studies are rather scarce (Labat et al., 2011). Furthermore, as shown by the study of Paleogene deposits in the Campine Basin by Zeelmaekers (2011), a quantitative clay mineralogical characterization is not limited to simple sediment characterization but also allows further interpretation towards provenance, facies analysis and possibly also climatic conditions.

This work therefore attempts a systematic clay mineral analysis of specific Neogene deposits, such as the Berchem Fm and Bolderberg Formations (Chapter IV), the Diest Formation (Chapter V), the Diest, Kasterlee and Mol Formations (Chapter VI) and the Poederlee Formation (Chapter VII). The well-calibrated Neogene dinoflagellate cyst biostratigraphy allowed to select reference sections and boreholes to study in detail the lithological specifications of the different stratigraphic units and their transition zones. Samples are studied for mineralogy, clay mineralogy <2µm, pelletal glauconite content and grain-size distribution. Before the systematic analysis of the different deposits is discussed, the occurrence and origin of glauconite minerals in the Neogene sand deposits is documented and discussed because this information is crucial for the understanding of the results presented in the chapters IV to VII, further in this stratigraphic application part.

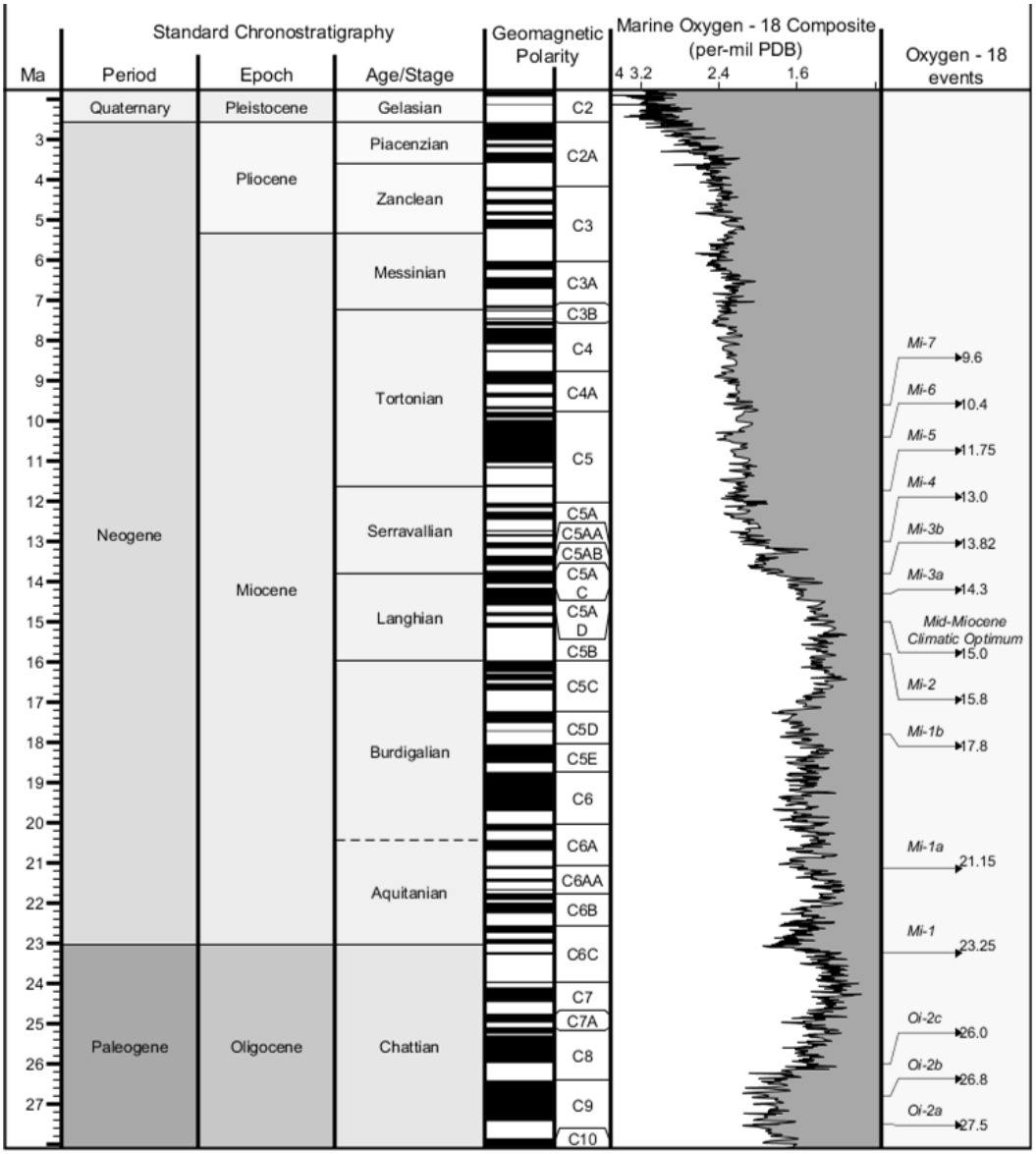

Figure II.1. Chronostratigraphical chart from Oligocene till present showing geomagnetic polarity, marine oxygen isotopes and related events. This chart was created using the software TS Creator (www.tscreator.org) and all data and ages are calibrated to The Geological Time Scale 2012 (Gradstein et al., 2012).

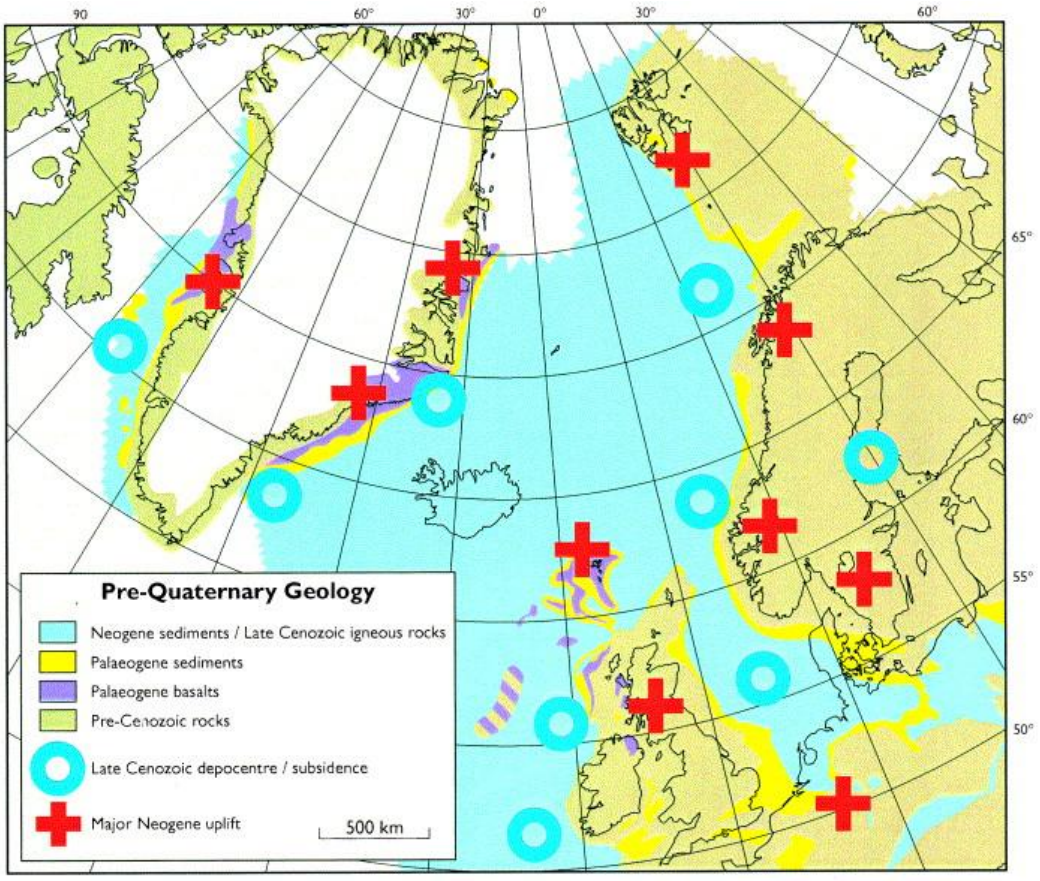

Figure II.2. Pre-Quaternary geology around the North Atlantic ocean showing areas of Neogene uplift/ erosion and of accelerated subsidence/ deposition (Japsen and Chalmers, 2000).

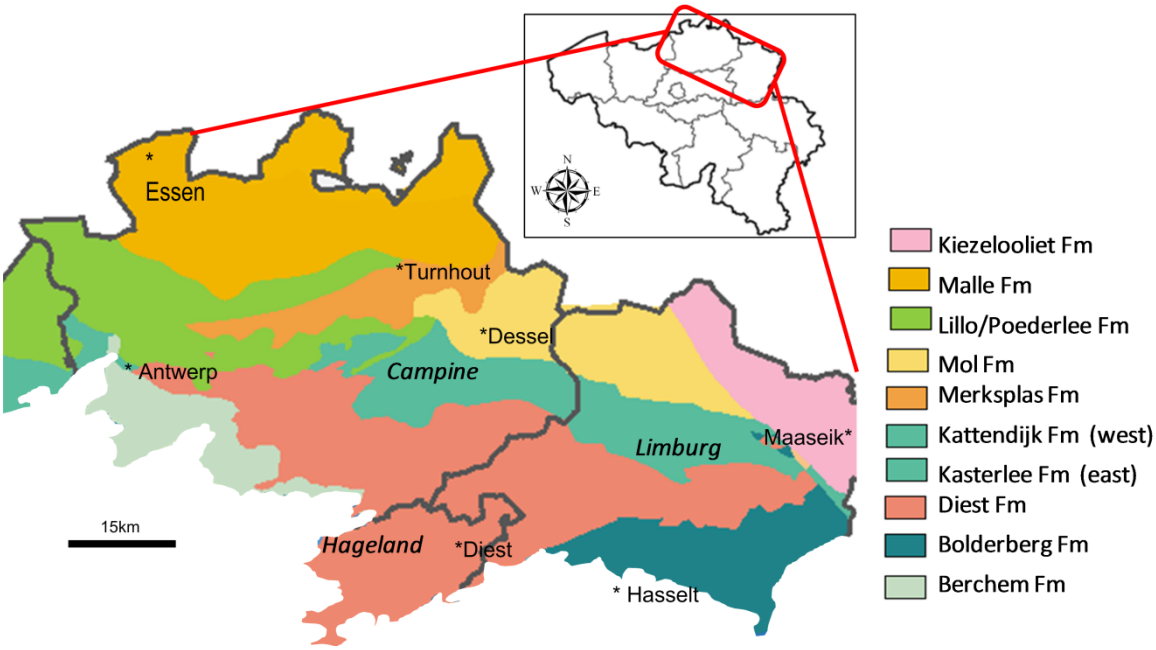

Figure II.3. Geological map of Neogene deposits in Belgium. Different colors represent different formations. Note that according to the decisions of the National Stratigraphical Committee Belgium, the previously defined Brasschaat Fm does not exist anymore. Instead the Malle Fm has been defined with a Brasschaat Member but in areas where both the Brasschaat Member and Merksplas Formation occur, no distinction is made between both and the term Merksplas Fm is used (modified after ALBON, 2009).

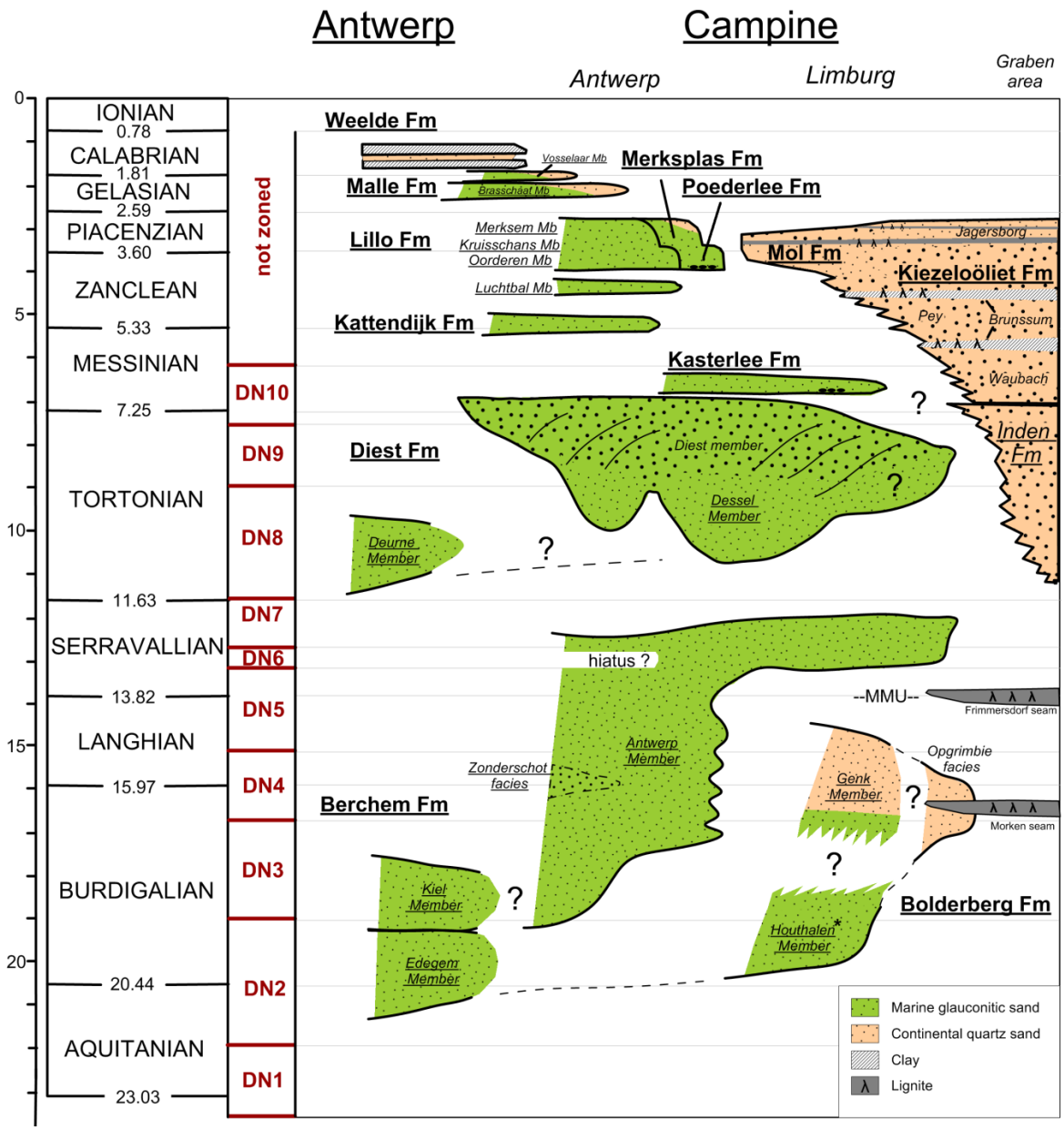

Figure II.4. Sequence stratigraphical architecture of Neogene deposits in the Campine Basin. Note that this chart does not reflect thicknesses of unit but is a chronostratigraphic chart. The position of the different units within Berchem Fm was drawn based on dinoflagellate cyst data of Louwye and Laga (1998); Louwye (2000; 2005), Louwye et al. (1999; 2000; 2007) and Vandenberghe et al. (2005). The Houthalen Member, which also occurs in Brabant *, of the Bolderberg Fm was drawn based on nannoplankton zonations (Martini and Müller, 1973) and benthic foraminifera (De Meuter and Laga, 1976). The position of the Genk Member was drawn based on dinoflagellate cyst data of Louwye and Laga (2008). The lignite layer found in the Opgrimbie facies was interpreted as the Morken seam (Utescher et al., 2012 ; Schäfer and Utescher, 2014) based on the occurrence of white sands below and above the lignite. The Morken and Frimmersdorf lignite seam and the estimated position of the Mid-Miocene Unconformity (MMU) were positioned following Utescher et al.(2012) and Schäfer and Utescher (2014). The position of the Opgrimbie facies was drawn accordingly. Dinoflagellate cyst data allowed to correlate the Deurne Member with DN8 biozone (Louwye, 2002) and the Dessel Member as DN8 to DN9 biozone (Louwye et al., 1999). The Diest member was positioned correlating with DN8-DN9 biozonations in Limburg (Louwye et al., 1999 and Vandenberghe et al., 2005), with DN9 to DN10 biozonations in the Campine (Louwye and Laga, 1998; Louwye et al., 1999) and with latest DN9 and DN10 in the western part of the Campine (Louwye et al., 1999). The Kasterlee Fm was positioned following dinoflagellate cyst data of Louwye et al. (2007) and Louwye and De Schepper (2010). The Kattendijk Fm was positioned following Dinoflagellate cyst data were used to position the Kattendijk Fm and the Lillo Fm (De Schepper et al., 2009; Louwye and De Schepper, 2010); the Poederlee Fm and the Mol Fm (Louwye and De Schepper, 2010). The position of the Merksplas Fm, Malle Fm and Weelde Fm was drawn according to the proposal of the National Committee of Stratigraphy Belgium, approved 04/2014, www.natstratcommbelgium.drupalgardens.com). The sands occurring in Limburg and towards the graben are mainly drawn based on their occurrence in the Maaseik well (Vandenberghe et al., 2005).

Chapter III.

Glauconite minerals: characteristics, occurrence and origin

The intention of this chapter is to provide an overview of the different occurrences, mineralogical and crystal-chemical characteristics of glauconite minerals present throughout the Neogene strata of the Campine Basin. The main goal is, moreover, to interpret these data and finally discuss the origin of the glauconite minerals, either authigenic or transported. This knowledge is essential for understanding the results provided in the following chapters which will clarify the occurrence and significance of glauconite minerals in these particular Neogene deposits. Consequently, in this chapter the focus is neither on glauconite contents or characteristics linked to stratigraphy, nor on the potential of glauconite as stratigraphical parameters because this is provided into detail in the chapters IV, V, VI and VII. Further in this work, the term “glauconite minerals” will be used for all sediment particles of which the mineralogy consists dominantly of mineral glauconite. However, the distinction between glauconite minerals occurring in pelletal form (“pelletal glauconite”) or in clay-sized <2µm form (“clay-sized glauconite”) will be made as much as possible.

III.1 AUTHIGENIC OR REWORKED ?

The occurrence of glauconitic minerals is often linked to specific geological environments. The presence of newly-formed (“authigenic”) glauconitic minerals is for instance a very reliable marker for a marine, calm and stable sedimentary environment with very low sedimentation rates (Odin and Giresse, 1972; Meunier and El Albani, 2007). If pelletal glauconite is however reworked from other sedimentary deposits, such a facies interpretation is of course invalid. The crucial question is whether the presence of glauconite in a sediment is due to authigenic growth or reworking. Note that authigenesis sensu stricto implies that glauconite is buried at exactly the same position as it was formed, such as often reported from main flooding surfaces (Ketzer et al., 2003). Nevertheless, glauconites are often also termed authigenic in the context of basal green sands, consisting of abundant pelletal glauconite and occurring at the base of transgressive sediment packages. The presence of such high glauconite concentrations in the transgressive greensands also requires a phase of new formation of glauconite; however the transgressive movement has swept these authigenic glauconite over the shelf to form the greensands. Therefore glauconite formed slightly before the increased rate of sea-level rise and was concentrated by short-distance transport into a greensand. Consequently, the term “authigenic” in this work is designated to such short-distance transported transgressive glauconites. By the terms “transported” or “reworked”, further distance transport or the actual reworking from older deposits is implied.

The origin and history of pelletal glauconite reveals important information for facies

reconstruction and depositional history of the sediment. Table 3.1 lists a number of parameters indicating either authigenic growth or transportation of glauconite.

Physical transport will affect the relatively weak glauconite grains leading to enhanced pelletal roundness and polishing by abrasion (Amorosi, 1997; Udgata, 2007), but also to possible fragmentation of pelletal glauconite and the production of small-sized glauconite particles. Also the spatial distribution of glauconite in the host sediment is significant as transported grains will occur concentrated in certain horizons and depleted in others, leading to highly variable glauconite contents (Amorosi, 1997). Another excellent decisive factor is comparing the size distribution of glauconite and the detrital fraction (Bornhold and Giresse, 1985; Odin and Lamboy, 1988) . Hereby the similarity between the distribution of transported, mainly detrital, components and the glauconite population indicates the amount of mutual transport (Figure 3.1). Because of the slight difference in density (2.6 for quartz; 2.6-2.9 for glauconite), the distribution of glauconite particles should be slightly finer-sized in the case of proper sedimentary sorting (Figure 3.1). When the size distribution of the glauconite population is totally different from the distribution of the detrital fraction, this points to glauconite authigenesis or very short-distance transport. It has to be noted however that such a relation also strongly depends on the original size of quartz and pelletal glauconite particles in their source area.

Table 3.1: Sedimentary parameters indicating possible diagnostic differences between authigenic and transported glauconite (modified after Amorosi, 1997)

Parameter	Glauconite authigenesis	Transported glauconite
Grain roundness	Variable	Enhanced roundness
Grain polishing	Low polishing	Enhanced polishing
Fragmented particles	Low	High
Glauconite habit	Film and granular habit	Granular habit
Sedimentary environment	Restricted to marine deposits	Occurrence in non-marine deposits
Size distribution	Mainly between 100-500µm	Important population <100µm
Glauconite size distribution relative to detrital components	Independent	Very similar shaped distribution
Sorting of glauconite distribution	Generally poor	Generally well
	Well when formed on uniform substrate	Poor sorting when short distance transport
Spatial distribution	Homogeneous distribution	Concentrated in horizons or zonations
Glauconite contents	Low variability	High variability
Thickness of glauconite-bearing interval	Low (few meters)	Variable
Association with phospate grains	Commonly	Rarely
Mineralogical maturity	High amount of expandable layers	depends on original host formation
K2O-content	< 4-5%	depends on original host formation

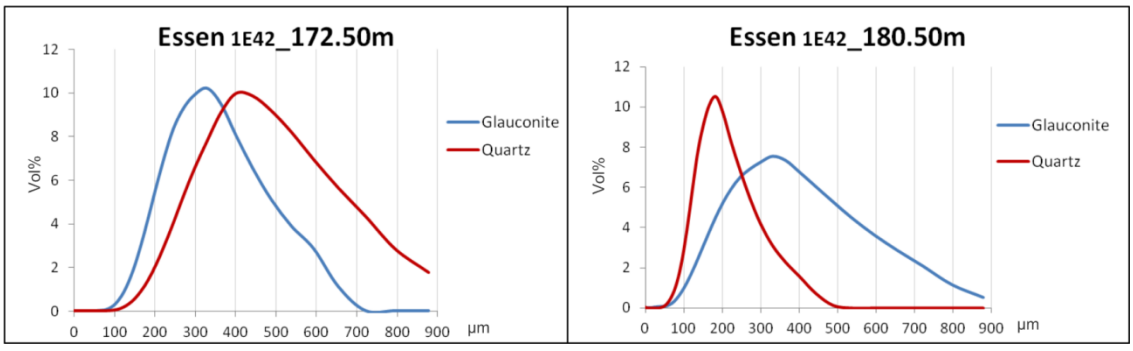

Figure 3.1. Size distribution of glauconite and detrital (quartz) fraction indicating mutual transport between both fraction (left) and independent transport of glauconite population with respect to the detrital quartz (right).

III.2 PELLETAL GLAUCONITE IN NEOGENE STRATA OF THE CAMPINE BASIN: AN INVENTORY

As described above, a comparison of the size distribution curves of glauconite pellets and the remainder of the sediment (=rest fraction) provides a good estimation whether glauconite pellets were formed authigenically, or, were transported prior to deposition. Furthermore, other characteristics such as morphology, spatial distribution, mineralogy, and, chemistry can provide additional arguments to assess whether glauconite was authigenically precipitated or transported before deposition in its current setting. It has to be noted, mainly for practical reasons, that analyses of glauconite pellets are systematically performed on >32µm fractions (see PART I Methodology). However, pelletal glauconitic particles <32µm are scarce and manual checks under the binocular microscope did not reveal important pelletal glauconite amounts in these smaller size fractions (see also Figure 3.1).

III.2.1 Occurrence

Glauconite pellets are omnipresent in marine Cenozoic deposits of the Campine Basin. Highest concentrations are found in the sand matrix of the Neogene marine deposits, which have a distinct green to dark green coloration. Pellets are, however, absent in intercalated clay layers which have brown to purple coloration (Figure 3.2). Furthermore, glauconite pellets are also absent in estuarine and continental quartz-sand deposits (Continental Genk Member of Bolderberg Fm; Mol Fm) which seems to confine the presence of glauconite pellets to the sand matrix of marine deposits in the Campine Basin.

III.2.2 Morphological characteristics

Sand- and silt-sized glauconite in the Neogene deposits of the Campine Basin occurs as pale to dark green colored granular pellets. Glauconite films as shell infillings or coatings, often mentioned as indicative for glauconite authigenesis (Odin, 1982), are never observed. Pellets are characterized by a well-rounded and polished surface, leading to a dominantly spheroïdal habit. Irregular shapes occur, however, quite frequently (Adriaens, 2009) which is partly explained by the large amount of broken fragments (Figure 3.3). Certainly in size fractions <180µm, the pellets consist dominantly of broken fragments.

III.2.3 Spatial distribution

Macroscopically, glauconite pellets seem to occur randomly dispersed in the sand matrix but in reality the spatial distribution is quite irregular. Within the same formation unit, but also downscale to outcrop level, glauconite contents differ significantly from one horizon to another. Glauconite pellets occur concentrated in sand laminae, separated from laminae enriched in quartz, in cross beds transgressive surfaces and concentrated in basal green sands and basal transgressive sediments in general. Moreover, they apparently are never incorporated in sedimentary clay intercalations in the Campine Basin (Figure 3.2).

III.2.4 Size distribution curves

In Adriaens (2009), it was demonstrated that while pelletal glauconite in Cretaceous deposits of the Campine Basin are likely to be authigenic, Cenozoic glauconite pellets show no narrow size distribution independent of quartz distribution but on the contrary seem closely related to the quartz size distribution (Figure 3.4). This observation is made for the majority of Neogene litho-units, suggesting common transport history of both fractions. Nevertheless, also pelletal glauconite size distributions independent of the quartz size distribution are observed (Table 3.2 and Figure 3.4a-g-h-i). The graphs shown in Figure 3.4were carefully chosen as representative examples. In general, glauconite pellets of the Edegem and Kiel Members of the Berchem Formation, of the Dessel and Deurne Members, and, the Diest sand member itself, of the Kasterlee sand, and, of non-oxidized samples of the Poederlee sands show very similar size distribution curves as the detrital rest fraction. For the Antwerp Member of the Berchem Formation and oxidized samples of the Poederlee sands, however, the majority of glauconite pellet distributions are much coarser

compared to the detrital quartz fraction and have, moreover, totally different shapes. (Figure 3.4a-g-h-i). This indicates either that no common transport of glauconite and quartz particles occurred and pelletal glauconite was formed authigenically or that the pelletal glauconite size distribution was altered after deposition, e.g. during weathering. The different size distribution curves of glauconite and quartz particles are nevertheless not systematic for the Antwerp and Poederlee sand, as for some samples also similar distribution shapes are observed (Figure 3.4b).

Figure 3.2. (Left) Glauconitic sands of the Diest Formation intercalated with thin irregular clay layers. (Right) Slightly glauconitic sands of the Kasterlee Formation with thin clay intercalations.

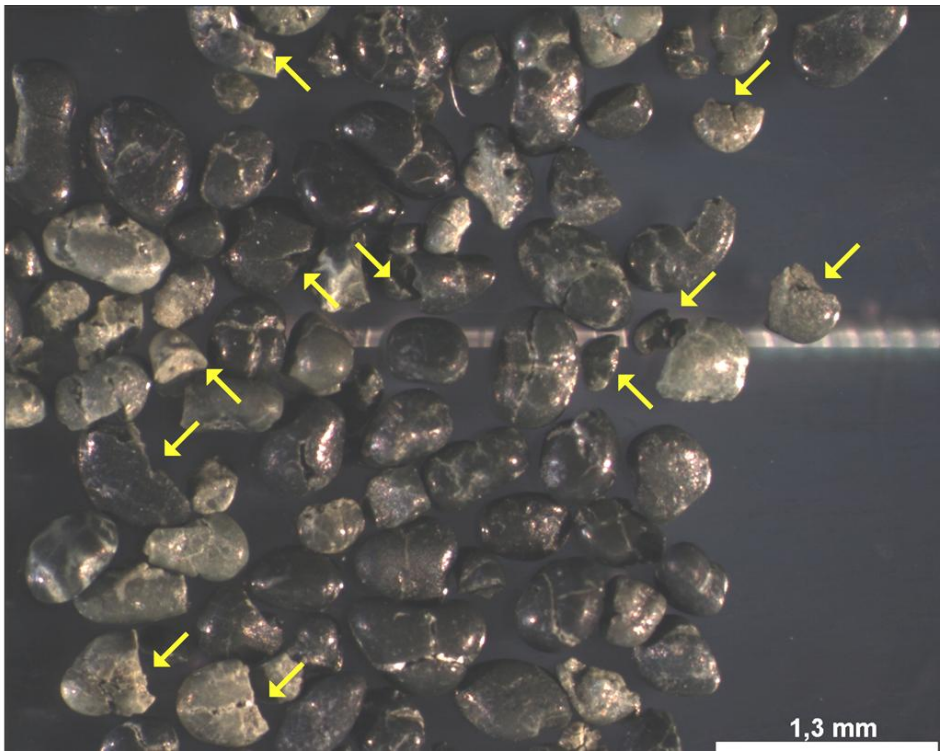

Figure 3.3. Pelletal glauconite of the Diest Formation under the binocular microscope. Yellow arrows indicate some broken glauconite fragments.

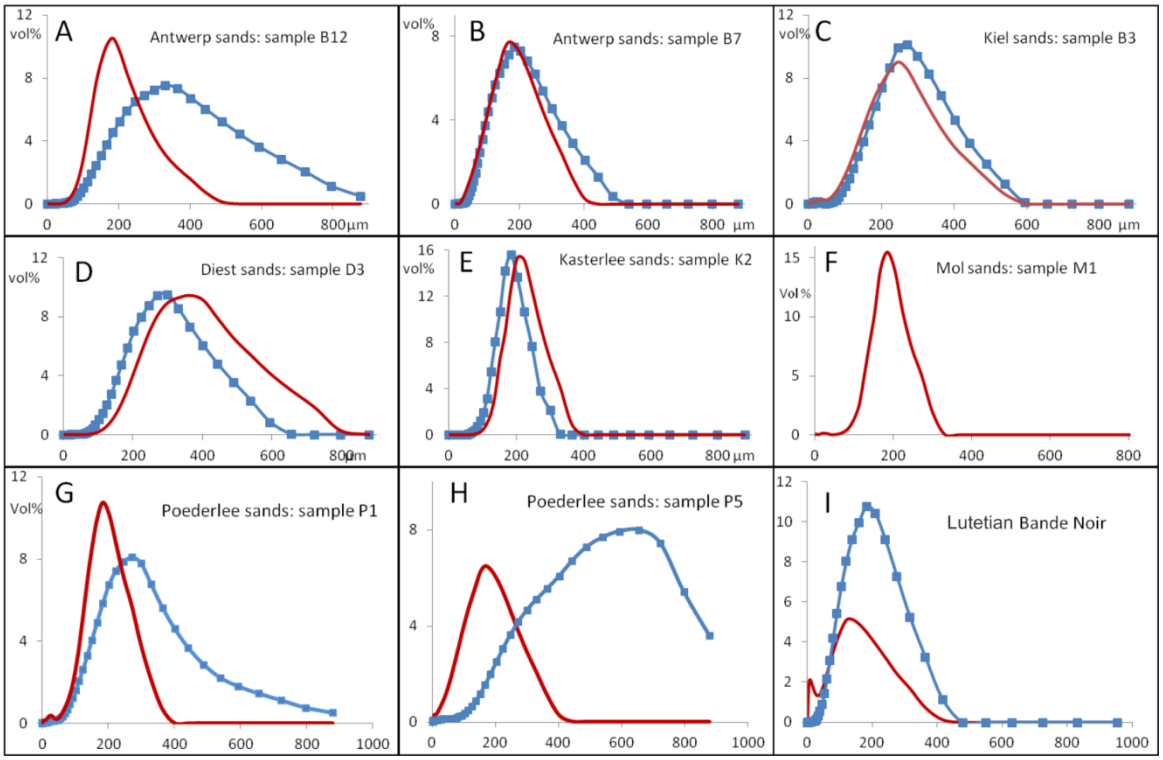

Figure 3.4. Comparison of the particle size distribution comparison between the glauconite fraction >32 µm (dotted blue) and rest fraction (red). The Poederlee (G and H) and Antwerp sands (A and B) typically hold large glauconite pellets with a particular size distribution suggesting potential authigenic glauconitisation. The pellet size is however less well sorted than could be expected for authigenic minerals; e.g. the Lutetian Bande Noir horizon (I) (Odin, 1982; Maréchal, 1993). Some samples of the Antwerp and Poederlee sand (B and G) have similar particle size distributions for quartz and glauconite suggesting a common transport history.

Table 3.2: Overview of the glauconite pellet size distribution vs. detrital size distribution for each Neogene litho-unit of the Campine area. Only for specific samples of the Antwerp sands and the Poederlee sands, both comparable as well as similar size distributions of pelletal glauconite and the quartz-dominated rest fraction were observed.

Formation	member	Pelletal size distribution vs. detrital rest fraction	
		Comparable shapes	Different shapes
Poederlee		x	x
Kasterlee		x	
Diest	Diest sand	x	
	Deurne	x	
	Dessel	x	
Berchem	Antwerp	x	x
	Kiel	x	
	Edegem	x	

III.2.5 Mineralogy

The mineralogical characteristics and chemical compositions of the glauconite-pellet bearing horizons in the Upper-Cretaceous and Cenozoic in Belgium were analyzed by Adriaens (2009). In this inventory study, Cretaceous glauconite-bearing horizons are characterized by a 1*M* to 1*Md* polytype glauconite-smectite R1 phase with expandable layers ranging between 6-8%. Throughout the Cenozoic record, glauconite pellet mineralogy displays low variability, consisting of one or two Fe-rich 1*Md*-polytype glauconite-smectite R1 phases. Neogene glauconite pellets typically contain between 6 and 20% expandable layers in total. The position of the 060 reflection of these pellets varies between 1.515Å and 1.519Å.

The majority of Neogene glauconite pellets analyzed in this work consists of two separate phases: a glauconite-smectite R1 phase with 5-10% expandable layers and a glauconite-expandable R1 phase with in total 25-35% expandable layers of two types. The expandable minerals in the former phase are smectites of the low-charge type while in the latter they consist of both low-charge and high-charge smectite with a 60:40 to 70:30 ratio respectively. Furthermore, during modeling, the octahedral iron content of the glauconite pellets is assessed. This parameters shows low variability for all investigated glauconite pellets, ranging from 0.75 to 0.9 /half unit cell. Traces of clay precipitation are often found intimately fixed in the fine rims between the lobes of the pellets (Figure 3.5).

Although mineralogical variability between different formations seems rather low, there seem to exist some systematic differences in pelletal expandability between different formations. Glauconite pellets of the Berchem Formation typically display a 75:25 ratio between the low expandable and higher expandable glauconite-smectite phase respectively. Glauconite pellets of the Diest, Kasterlee and Poederlee Formations generally have a lower amount of expandable layers which is reflected in their 90:10 low expandable-high expandable ratio (Figure 3.5). Nevertheless, also higher expandable glauconite pellets are found in certain parts of the Diest and Kasterlee Formations and in certain parts of the Poederlee Formation, also Fe-rich expandable minerals are found, coexisting with the two R1 glauconite-smectite phases (Figure 3.5. The nature and stratigraphic significance of the pelletal glauconite mineralogy in these particular formations will be further elaborated in Chapters IV, V, VI and VII of this work.

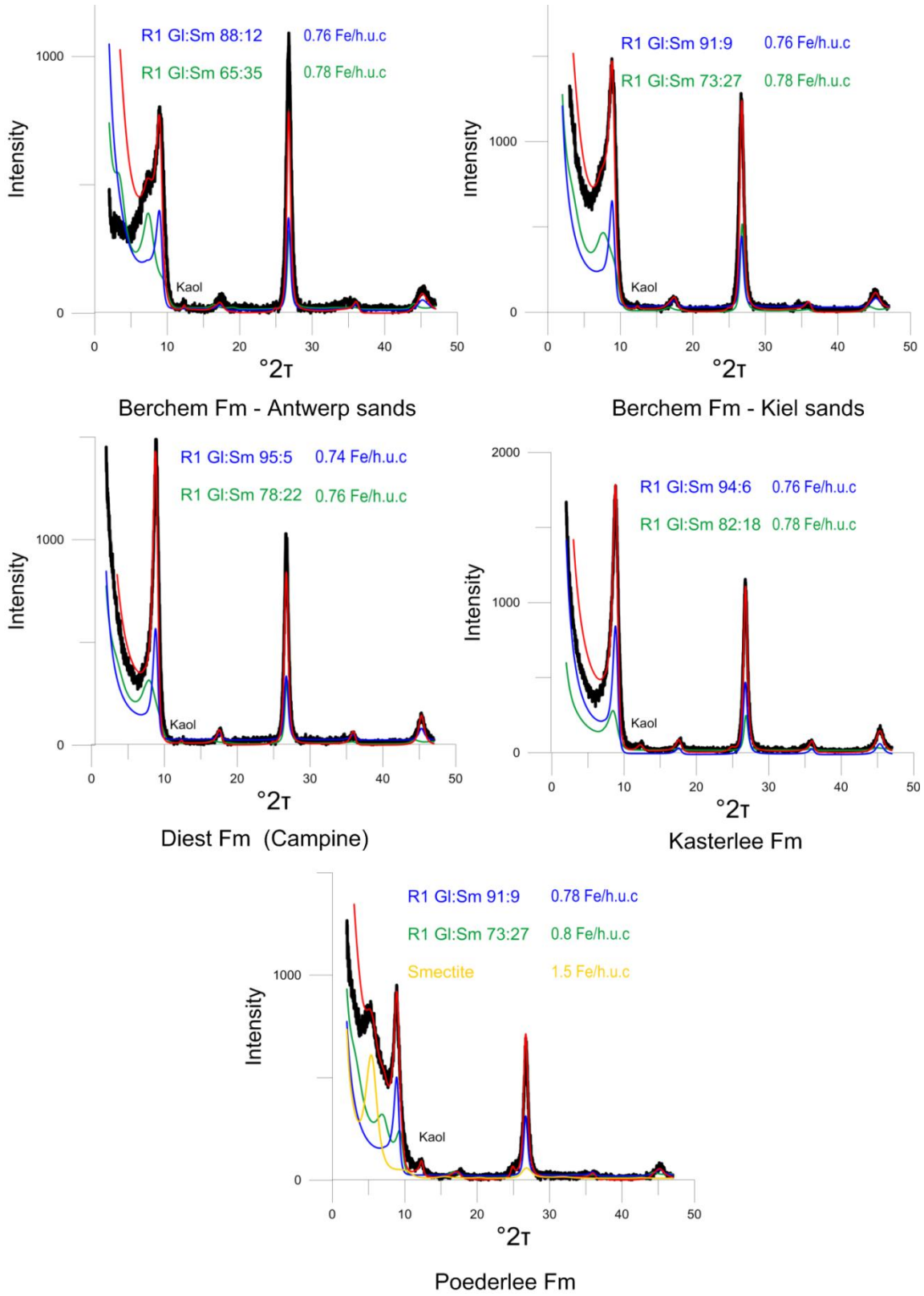

Figure 3.5. Glycolated XRD recordings (black) and Sybilla model fit (red) from glauconite pellets on oriented slides after Ca-saturation. The glauconite-smectite R1 phases used in the clay modeling are shown in blue and green for each formation and are representative for all studies samples. “Kaol” indicates low amounts of kaolinite.

Table 3.3: Bulk chemical data of Cenozoic glauconite pellets, analyzed with ICP-OES. Loss on ignition was not determined due to the low amount of available material.

Chronostratigraphy	Chemical phase / Detection / Lithostratigraphy	SiO2	Al2O3	Fe2O3	FeO	MgO	CaO	Na2O	K2O	MnO	TiO2	P2O5
		%	%	%	%	%	%	%	%	%	%	%
		0.01	0.01	0.01	0.01	0.01	0.01	0.01	0.01	0.001	0.001	0.01
Turonian	Dièves marls	43.00	6.88	5.73	0.00	3.46	1.21	0.12	6.63	0.01	0.07	0.35
Coniacian	Craies de Maisières	46.84	9.45	16.57	0.00	3.77	0.07	0.19	7.40	0.01	0.07	2.15
Santonian	Chalky sandstone	49.40	7.40	19.22	2.56	3.98	0.76	0.31	8.14	0.01	0.06	0.42
Campanian	Vaals sands	48.09	7.46	24.35	1.30	2.45	0.76	0.14	6.10	0.01	0.12	0.18
Thanetian	Tuffeau de Lincent	47.27	7.32	20.15	0.76	3.29	0.85	0.11	6.23	0.14	0.20	0.11
Ypresian	Egem sandstone	47.56	6.95	22.19	2.73	3.36	0.56	0.14	6.23	0.03	0.36	0.11
	Bierbeek sands	44.57	12.44	15.25	2.20	2.83	1.08	0.23	3.71	0.08	2.17	0.11
	Vlierzele sands	49.69	7.86	21.11	1.13	3.13	1.28	0.18	5.95	0.03	0.16	0.06
	Vlierzele sands	49.53	9.51	19.91	1.12	3.02	0.77	0.18	5.62	0.02	0.21	0.05
	Vlierzele sands	44.11	9.41	11.76	0.76	2.67	0.63	0.14	4.57	0.03	0.19	0.11
	Vlierzele sands	47.46	8.52	21.18	1.12	3.49	0.72	0.16	5.85	0.03	0.26	0.07
	Aalter sands	49.42	8.86	21.43	1.48	3.67	0.66	0.14	5.65	0.05	0.79	0.14
Lutetian	Brussel sands (Gobertange	46.02	8.25	11.68	1.49	4.01	0.44	0.10	6.49	0.02	0.12	0.04
	Brussel sands (Gobertange	48.84	8.38	20.93	1.66	4.26	0.69	0.13	6.96	0.02	0.11	0.06
	Brussel sands (Gobertange	47.72	8.53	19.23	1.66	4.30	0.44	0.14	6.85	0.01	0.12	0.07
	Lede sands	42.69	8.91	12.27	0.00	2.94	0.67	0.11	4.99	0.13	0.00	0.03
	Wemmel sands	43.06	8.86	21.02	0.00	3.66	0.04	0.13	5.86	0.09	0.00	0.05
	Wemmel sands	42.30	8.07	19.53	1.84	3.70	1.45	0.13	6.07	0.23	0.44	0.06
	Bande Noir	38.88	5.44	8.35	1.31	3.18	0.68	0.21	5.56	0.02	0.24	0.02
	Bande Noir	45.16	8.89	21.97	1.30	3.54	0.53	0.11	6.16	0.05	0.41	0.06
	base Asse-Ursel	43.06	8.77	16.30	3.27	2.74	0.41	0.22	6.13	0.01	0.15	0.05
	base Asse-Ursel	43.04	6.65	14.03	3.48	2.45	0.48	0.19	5.85	0.01	0.15	0.05
Rupelian	Eigenbilzen sands	46.19	9.76	20.81	0.00	3.08	0.48	0.11	6.12	0.06	0.00	0.45
Burdigalian	Kiel sands	46.98	9.58	17.71	3.09	3.45	0.30	0.13	6.60	0.01	0.15	0.16
	Kiel sands	45.58	9.84	18.27	2.19	3.02	3.29	0.13	5.96	0.01	0.22	0.26
	Kiel sands	47.35	9.99	20.37	2.20	3.07	0.37	0.13	6.55	0.01	0.22	0.26
	Kiel sands	45.16	9.68	13.55	2.55	3.17	2.55	0.20	6.09	0.01	0.16	0.07
Burdigalian-	Antwerp sands	46.06	10.22	19.67	2.55	3.16	0.50	0.29	6.50	0.01	0.23	0.30
Langhian-	Antwerp sands	44.11	9.51	18.80	0.00	3.05	0.85	0.15	6.32	0.01	0.17	1.27
	Antwerp sands	50.34	12.56	18.59	3.09	3.35	1.63	0.22	6.43	0.03	0.54	0.15
Serravallian	Zonderschot sands	45.44	8.67	20.27	3.27	3.19	1.32	0.21	6.40	0.02	0.29	0.17
Tortonian	Deurne sandstone	45.81	9.87	14.58	2.37	3.42	0.24	0.14	6.23	0.02	0.23	0.32
	Deurne sand	46.85	9.77	20.28	1.84	3.37	0.50	0.11	6.72	0.02	0.13	0.26
	Diest sand	46.23	10.51	19.92	2.56	3.05	0.41	0.09	6.96	0.01	0.21	0.12
	Diest sand	46.89	9.49	19.77	2.21	3.12	0.39	0.13	6.95	0.01	0.16	0.11
	Diest sand	45.11	10.69	18.62	2.74	2.79	0.40	0.10	6.19	0.02	0.50	0.17
Messinian	Kasterlee sand	49.15	10.20	21.57	1.30	2.95	0.48	0.14	6.26	0.01	0.32	0.10
	Kasterlee sand	44.08	12.81	15.63	1.48	2.45	0.40	0.14	5.52	0.02	0.49	0.12
Zanclean	Kattendijk sand	44.25	9.86	20.29	1.48	3.03	1.10	0.14	6.45	0.02	0.35	0.20
	Luchtbal sand	43.99	9.94	19.10	1.66	3.01	0.36	0.13	6.34	0.05	0.86	0.19

III.2.6 Chemistry

Major element analysis by ICP-OES reveals that glauconite chemistry generally shows low variability with K_2O-contents ranging from 5.5 to 7 wt%, pointing to well-evolved pelletal maturity (Table 3.3). Total Fe contents, expressed as the sum of Fe_2O_3 and FeO, range between 17-22%, with a typical ferric:ferrous-ratio of 9:1.

III.2.7 Age dating

Radiometric K-Ar and Rb/Sr isotopic dating were performed by Odin et al., (1974) on glauconite pellets of the Berchem Formation. The authors concluded an authigenic nature for the Antwerp sands since glauconite dates (~16-20.5 Ma) correspond relatively well to the biostratigraphically accepted ages of the sediment (Louwye, 2001; Louwye *et al. 2000*, ~11-19Ma). One sample of the Zonderschot facies even showed a 15Ma pelletal glauconite date.
However, the Edegem and Kiel sands are considered to contain reworked glauconites because glauconite dates were systematically of Aquitanian, and thus Oligocene, age (~20-32Ma), instead of their biostratigraphically determined Burdigalian age (Louwye, 2001; Louwye *et al.*, 2000). Odin *et al.*, (1974) also determined the K-Ar age of one glauconite pellet sample of the Diest sands resulting in an estimated age of 14Ma. K-Ar analyses performed on a sample set of 13 Diest sand samples indicate that glauconite pellets in the Diest Formation are massively reworked from older deposits. All pelletal glauconite K-Ar dates indicate an early-Miocene age, except for an authigenic glauconite date for a basal green sand in the Campine area (Dessel Member (Vandenberghe *et al.* ,2014).

III.2.8 Conclusion: authigenic or transported ?

In the previous sections, it was shown that the main mass of glauconite pellets in Neogene strata of the Campine Basin were not authigenically formed but transported through pelletal reworking from older deposits.

Authigenic glauconite pellets occur in the Antwerp sand. The main arguments are the radiometric dating corresponding to the biostratigraphic age and the size distribution of the pellets compared to the quartz size distribution. It should be noted that de biostratigraphic range established by dinoflagellate investigations in what is described as lithostratigraphic Antwerp sand is very large, i.e. Burdigalian to Serravallian (Vandenberghe et al., 2014). Therefore not all glauconite pellets in deposits described as Antwerp sand need to be authigenic as the Antwerp sand unit most likely consists of several individual subunits.

In the Poederlee Formation, the relative size distributions of quartz and glauconite suggest a possible authigenesis and the expandable phase content in the pellets could also be interpreted as an early glauconitisation phenomenon. However, the latter could also be due to weathering and the large spread in pellet sizes could also point to erosion and transport. Besides, no radiometric ages are available from the Poederlee sand. Therefore authigenesis of glauconite in the Poederlee sand is not excluded but will be discussed more in detail in Chapter VII.

In the case of authigenesis, glauconitisation probably occurred at a site nearby the depositional area during which transport only had minimal effect to sort the pelletal glauconite. For all other Neogene glauconitic deposits, no indications were found other than pointing to transported pellets. Nevertheless, in isolated cases, such as for instance in basal green sand horizons (base of the Dessel Member sample in Vandenberghe et al., 2014), such nearby glauconitization cannot be excluded.

III.3 CLAY-SIZED GLAUCONITE

Neogene glauconite minerals in the Campine Basin occur not only in granular pellets but also as clay-sized particles. Whereas the characteristics of glauconite pellets can be easily investigated through isolation from the rest sediment, identifying and assessing specifications of glauconite minerals occurring in clay-sized fractions needs to be done in mixtures instead of the pure mineral. As shown in chapter II, such identification can be made based on the 001/002 intensity ratio in oriented slides but even better based on the d060 of random oriented powders <2µm. Mineral species consisting dominantly of the mineral glauconite have d060 >1.51Å.

III.3.1 Mineralogical specifications

The quantitative mineralogical composition of the clay fractions <2 µm of sands, as determined by clay modeling (Figure 3.6), illustrates the systematical presence of clay-sized glauconite-smectite, which is defined by its unique d_{060}-value and modeled octahedral iron content (Table 3.4). Optimal modeling results were only obtained after introducing glauconite-smectite R1 phases similar to those phases which make up the mineralogy of the associated sand-sized glauconite pellets. Furthermore, also d_{060}-values of both pelletal and clay-sized glauconite are very similar (Table 3.4). The modeled octahedral Fe/half unit cell of the clay-sized glauconite ranges between 0.74- 0.82, which is an expected value for glauconite minerals and comparable to values obtained from the pellets (see section III.2.5). Although the glauconite-smectite R1 phases are identical for pelletal and clay-sized glauconite, clay-sized glauconite seems to be systematically more expandable compared to pelletal glauconite (Figure 3.8).

Other common clay minerals in the clay fraction of sand samples are smectite, illite, mixed-layer illite-smectite, kaolinite and chlorite. These are exactly the minerals, with very similar modeled characteristics, which make up the clay fraction of clay intercalations (Figure 3.6 and Table 3.4), demonstrating that clay-sized glauconite has no detrital origin.

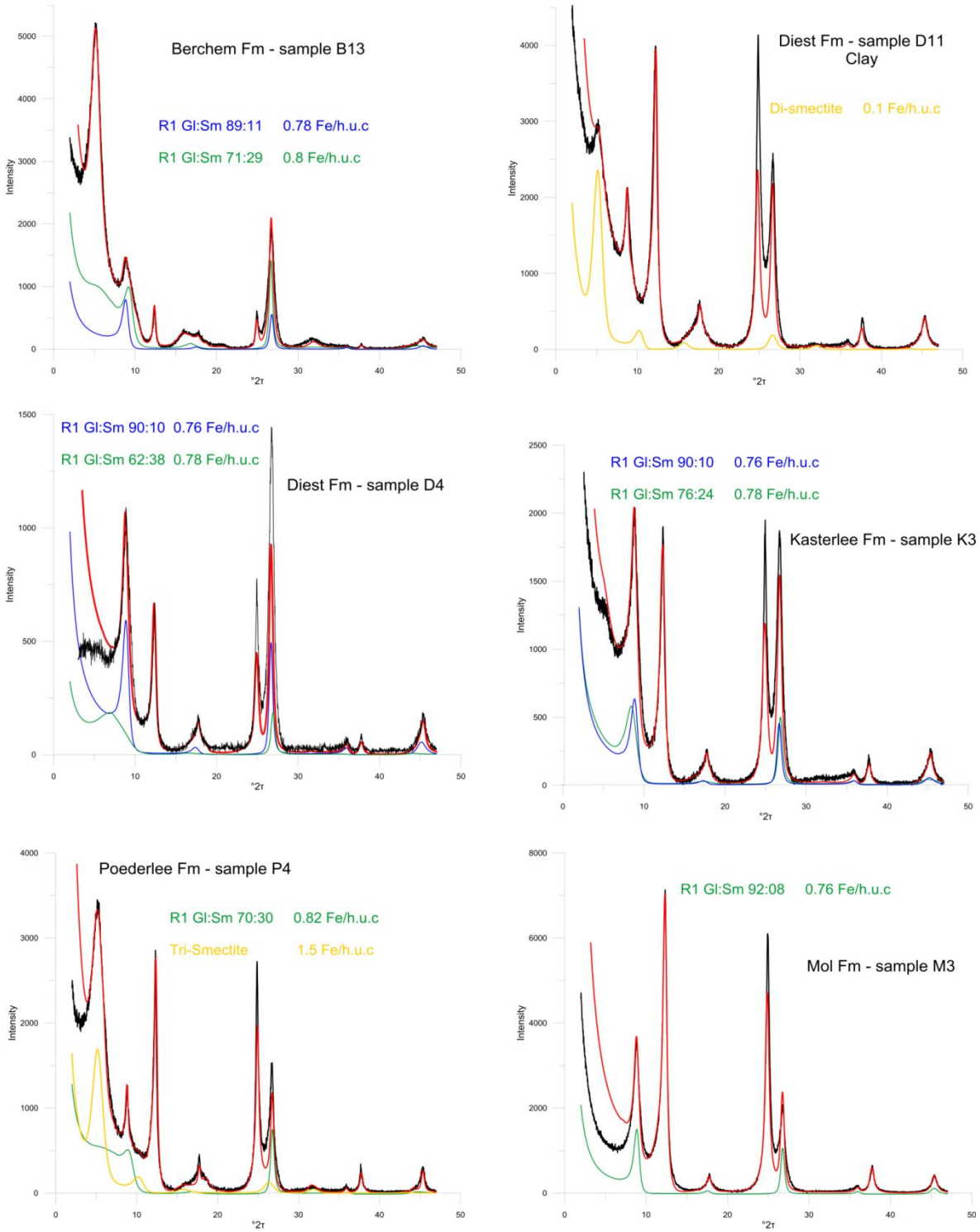

Figure 3.6. Glycolated XRD recordings of Ca-saturated clay fractions <2 µm on oriented slides (black). Sybilla clay model fit is shown in red. The glauconite-smectite R1 phases used in the clay modeling are shown in blue and green for each formation. Smectite contributions are shown in yellow where mentioned in the text.

Table 3.4: Quantitative clay mineralogy of each analyzed sample. Glauconite contents are given for sand samples together with d_{060}-values of pelletal and clay-sized glauconite. Question marks indicate that the exact 060-position could not be determined due to low amounts present in the sample.

					Clay mineralogy <2µm							
Sample	Formation	Glauconite grains 060 (Å)	Glauconite clay 060 (Å)	% Glauconite grains in >32µm fraction	Kaolinite	Illite	Mixed layer illite-smectite	Clay-sized Glauconite (low expandable)	Clay-sized Glauconite (high expandable)	Di-smectite	Tri-smectite	Chlorite
B1	Berchem	1.5139	1.5144	40%	4	8	22	3	13	50	0	1
B2	Berchem	1.5139	1.5139	32%	5	14	13	2	13	51	0	1
B3	Berchem	1.5144	1.5139	29%	2	4	29	3	7	55	0	1
B4	Berchem	1.5148	1.5135	34%	4	4	36	7	11	37	0	1
B5	Berchem	1.5148	1.5144	36%	1	5	32	3	14	44	0	1
B6	Berchem	1.5139	1.5131	39%	5	5	17	1	18	54	0	1
B7	Berchem	1.5128	1.5153	43%	1	7	26	10	13	42	0	1
B8	Berchem	\	\	\	10	14	48	0	0	27	0	1
B9	Berchem	\	\	\	10	13	48	0	0	29	0	1
B10	Berchem	1.5139	1.5135	35%	3	3	38	6	15	35	0	1
B11	Berchem	1.5144	1.5131	43%	5	5	33	0	2	54	0	1
B12	Berchem	1.5148	1.5144	48%	7	17	33	4	10	28	0	1
B13	Berchem	1.5139	?	55%	1	5	34	5	12	42	0	1
							0					
D1	Diest	1.5153	1.5157	20.20%	6	17	25	27	17	7	0	1
D2	Diest	1.5148	1.5162	26.70%	5	10	30	32	13	9	0	1
D3	Diest	1.5148	1.5157	20.20%	5	10	27	34	15	7	0	2
D4	Diest	1.5162	1.5171	19%	15	18	26	30	8	2	0	1
D5	Diest	1.5180	1.5175	38%	5	4	33	4	18	15	21	0
D6	Diest	\	\	\	28	14	26	0	0	31	0	1
D7	Diest	1.5189	1.5189	31%	2	3	5	90	0	0	0	0
D8	Diest	1.518	1.5189	32%	1	6	10	84	0	0	0	0
D9	Diest	1.518	1.518	36%	2	2	22	72	0	1	0	1
D10	Diest	1.5189	1.5184	35%	1	0	3	96	0	0	0	0
D11	Diest	\	\	\	19	18	29	0	0	34	0	1
D12	Diest	\	\	\	21	12	35	0	0	31	0	1
							0					
K1	Kasterlee	1.5166	1.5162	5.50%	18	4	16	51	10	0	0	1
K2	Kasterlee	1.5166	1.5166	6%	24	5	44	17	5	4	0	1
K3	Kasterlee	1.5171	1.518	4.50%	25	10	17	34	9	4	0	1
K4	Kasterlee	1.5162	1.5166	4.50%	20	8	19	20	26	6	0	1
K5	Kasterlee	1.5166	1.5171	4.90%	18	6	19	28	23	5	0	1
K6	Kasterlee	\	\	\	34	19	39	0	0	7	0	1
K7	Kasterlee	\	\	\	30	15	42	0	0	12	0	1
M1	Mol	\	1.5135	0	45	7	14	34	0	0	0	0
M2	Mol	\	1.5144	0	48	8	13	31	0	0	0	0
M3	Mol	\	1.5148	0	49	8	12	31	0	0	0	0
M4	Mol	\	1.5139	0	48	12	10	30	0	0	0	0
M5	Mol	\	1.5135	0	47	11	12	30	0	0	0	0
P1	Poederlee	1.5222	1.5238	19.50%	14	15	18	4	12	18	17	2
P2	Poederlee	1.5211	1.522	24%	16	18	16	5	9	15	19	2
P3	Poederlee	1.522	?	21.50%	16	17	22	2	4	20	17	2
P4	Poederlee	1.5211	?	20.50%	17	14	21	2	2	28	16	0
P5	Poederlee	1.5202	?	23.50%	11	6	16	0	0	32	33	2
P6	Poederlee	1.5202	?	22%	9	5	12	0	3	38	33	1

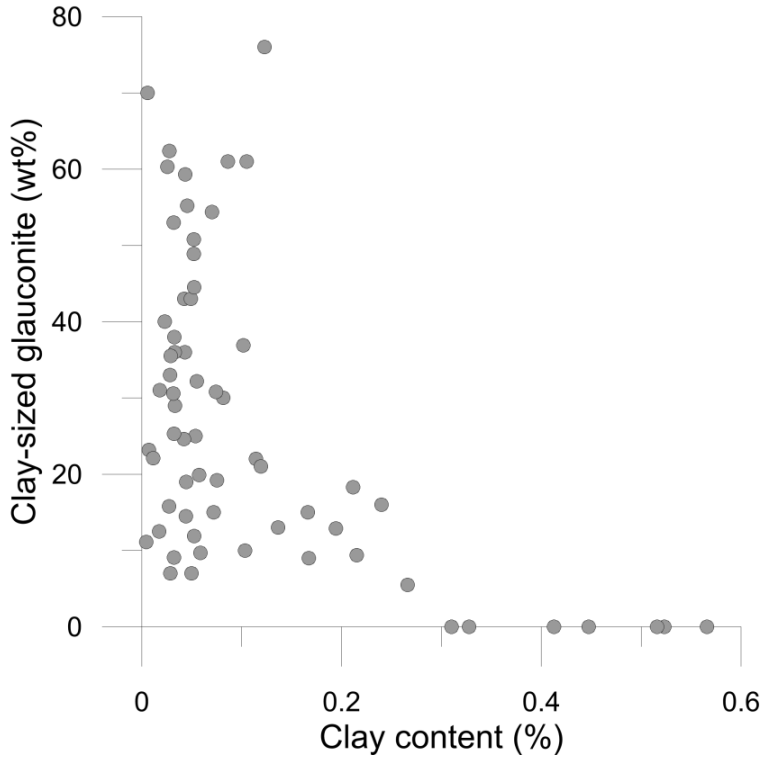

Figure 3.7. Clay content <2 µm plotted against the amount of clay-sized glauconite in the clay fraction <2 µm showing no linear relation.

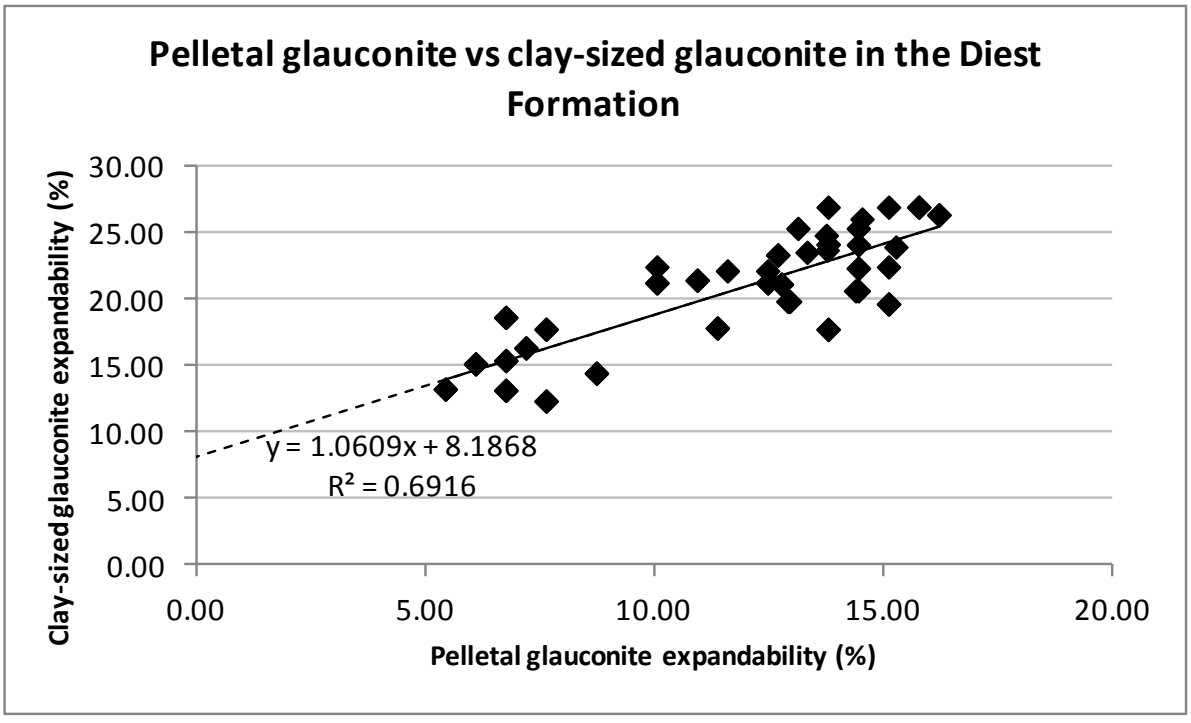

Figure 3.8. Pelletal glauconite vs. clay-sized glauconite expandability demonstrated for samples of the Diest Formation. Clay-sized glauconite is systematically more expandable compared to pelletal glauconite.

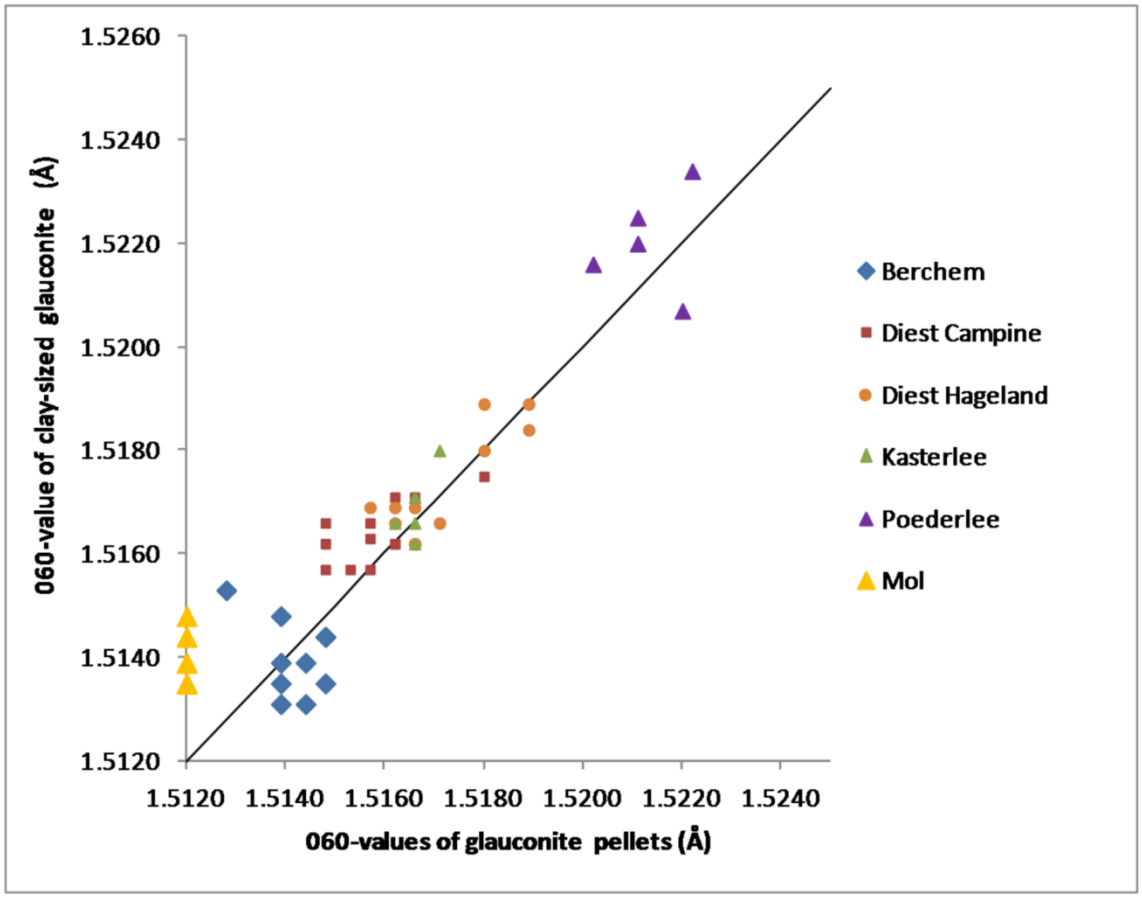

Figure 3.9. 060 peak position (in Å) for pelletal and clay-sized glauconite showing an intimate relationship. Furthermore, this 060-position seems to be an important characteristic for lithostratigraphic distinction. See also Chapters IV, V, VI and VII.

III.3.2 Occurrence

Natural clay-sized glauconite occurs systematically in all <2µm fraction of marine sand samples of the Neogene. Moreover, the presence is confirmed in clay fractions <2µm of the estuarine Mol sands, which contain hardly any pelletal glauconite but clay-sized glauconite is absent in the continental Opgrimbie facies of the Bolderberg Formation. In marine units, clay-sized glauconite occurs together with the "normal" sedimentary clay dispersed in the sediment. Besides this dispersed occurrence, several silt layers are observed where clay-sized glauconite is concentrated in these silt horizons. Clay intercalations embedded in the sand matrix, however, never appear to hold clay-sized glauconite in their clay fractions.

III.3.3 Origin of clay-sized glauconite in marine units

The occurrence of clay-sized glauconite was reported by Tedrow (1986; 2002) who claims that the origin of clay-sized glauconite is the disintegration of pelletal glauconite during soil weathering processes. Baioumy and Boulis (2012), however, suggested clay-sized glauconite represents a pre-pelletal stage in the glauconitisation process. When both glauconite occurrences are part of the same system, this most probably means that either pellet disaggregation or pelletization of clay-sized glauconite is the controlling process.

The occurrence of fine-grained glauconite is indeed expected in areas where new glauconite pellets are being formed (Odin, 1982). Clay-sized glauconite is, however, hardly ever reported coexisting with sand-sized

glauconite pellets. If reported, the clay fraction of early-stage or more evolved glauconitic sediments typically consists of Al-rich clay minerals (Bell and Goodell, 1967; Seed, 1968; Baldermann *et al.*, 2012) and rarely of Fe-rich clays. El Albani (2005) and Banerjee *et al.,*(2012) have furthermore demonstrated that glauconite authigenesis results in distinct mineralogical and crystal-chemical differences between different glauconite habits, which is clearly not observed in the present setting. Baioumy and Boulis (2012) suggested that clay-sized glauconite can form pellets in a later stage due to reworking or circulation processes. This seems rather unlikely in the current situation because clay-sized and pelletal glauconite systematically occur together in the same system. Based on d_{060}-values, and thus Fe-contents, and K_2O-values of the glauconite pellets (Table 3.4), both types of glauconite represent well-evolved glauconitisation stages which already contradicts an early-stage origin. Considering that the main mass of pelletal glauconites were actively transported, and that both pelletal and clay-sized glauconite are probably part of the same system, a true authigenic nature of the clay-sized glauconite is therefore very unlikely. The only environment where clay-sized glauconite has been reported coexisting with glauconite pellets are soils and weathering profiles where pedogenesis causes disintegration of pelletal glauconite (Van Ranst and De Coninck, 1983; Tedrow, 1986; 2002; Velde and Meunier, 2008). In the current setting, however, soil environments are excluded. Considering the limited depth of burial and the fact that glauconite pellets are not deformed, compaction is also to be excluded. Most likely, the origin of the clay-sized glauconite is therefore related to the abrasion and breaking up of glauconite pellets during physical transport.

A key observation confirming this proposed origin is that clay-sized glauconite is incorporated in the clay fraction of sands but never in the intercalated clay layers (Figure 3.2). The type and relative proportions of clay minerals in clay laminae and of clay minerals other than glauconite in sands are very similar, indicating that Al-smectite, Al-rich illite-smectite, illite -smectite, kaolinite, and, chlorite mainly originate from a detrital source area. This clay assemblage most likely constitutes the “sedimentary background”-clay mineralogy in sands and clays but apparently does not include clay-sized glauconite as no linear relation exists between the clay-sized glauconite content and the detrital sedimentary clay content (Figure 3.7). This indicates that a distant source area is excluded as main source for clay-sized glauconite and instead points to a more local origin. Most likely, a physically weaker population of incomplete or broken glauconite pellets of older deposits are abraded on short range transport or disintegrated on impact. It is systematically observed that expandability increases after the production of clay-sized glauconite (Figure 3.8) indicating the enhanced reactivity of the clay-sized glauconite in the sedimentary environment. Also the 060-position confirms the relation between pelletal and clay-sized glauconite (Figure 3.9).

This process of pelletal glauconite abrasion into a clay-sized glauconite fraction is most logic in glauconite pellet-bearing sediments for which there is indication that the glauconite pellets are transported or mixed with the detrital, mainly quartz, fraction. Although the Antwerp sands, and possibly also the Poederlee sands, favor glauconite pellet authigenesis based on size distribution and age-dating results (Figure 3.4), clay-sized glauconite is also present in these samples, which seems in conflict with an authigenesis, and therefore lack of transport, of the pellets (Table 3.4). The heterogeneity in pelletal size distribution, however, suggests a variety of depositional processes played an important role, indicating that glauconite pellets are not exclusively authigenic. Glauconite pellets in these units were only transported over short distances which is apparently sufficient to produce clay-sized glauconite, although in lower amounts compared to abrasion from truly reworked glauconite pellets (compare Berchem Fm samples with Diest Fm samples in Table 3.4). It is therefore likely that, depending on the amount of detrital clay input, the amount of clay-sized glauconite can be used as a proxy for the amount and/or intensity of pelletal transport.

III.3.4 Origin of clay-sized glauconite in estuarine units

The estuarine sands of the Mol Fm are mineralogically and texturally mature sands and contain lignite horizons. The sand unit holds hardly any pelletal glauconite but contains up to 30% clay-sized glauconite in its clay fraction (Table 3.4). The clay-sized glauconite in these sands can therefore not be derived from pre-existing pelletal glauconite in the Mol Formation. Nevertheless, clay-sized

glauconite produced in slightly older deposits can be further taken up in subsequent erosion and sedimentation cycles together with clays from other sources. The clay-sized glauconite in the estuarine Mol Formation must therefore be reworked from the locally outcropping glauconitic sands occurring around the estuary. The 060-position of the Mol sands is, however, slightly different compared to the slightly older Kasterlee and Poederlee Formations, suggesting that Fe is lost from the clay mineral structure during transport or as the result of acid percolation, leading to a more Al-rich glauconite mineralogy.

III.4 GLAUCONITE MINERALS IN NEOGENE DEPOSITS : AUTHIGENIC OR REWORKED ?

It was demonstrated that the main mass of pelletal glauconite was transported by reworking from older deposits. Although the area of glauconitisation for the Antwerp, and possibly even Poederlee, sands occurred nearby the depositional area, transported pelletal glauconite remains important in these deposits. Pelletal glauconite in these units most likely consists of a mixture of less transported and more intensively transported pellets.

Clay-sized glauconite is formed during transport of pelletal glauconite due to abrasion or physically breaking-up of pelletal glauconite. The relation between pelletal and clay-sized glauconite is clearly demonstrated in their detailed mineralogical characteristics, such as expandability (Figure 3.8) and 060-position (Figure 3.9).The source area is not detrital as neither pelletal nor clay-sized glauconite is incorporated in intercalated clay layers. The origin is therefore local, within the same depositional basin. Even short-distance transport, e.g. the sweep over the transgressive surface at the start of transgressive sequences, is sufficient to produce clay-sized glauconite. The occurrence of clay-sized glauconite is therefore a proxy for the amount and/or intensity of pelletal transport.

The presence of clay-sized glauconite in the estuarine deposits proves that glauconite minerals are not restricted to marine deposits. The clay-sized glauconite in these units is, however, derived from the erosion and subsequent resedimentation of clay-sized glauconite present in the marine formations around the estuary.

CHAPTER IV.

BURDIGALIAN AND LANGHIAN CLAY MINERALOGY

IV.1 PALEOGEOGRAPHY AND CLIMATE-TECTONIC EVENTS

During the Aquitanian, the uplift of the Rhenish Massif, the Savic pulse of the Alpine Orogen, introduced an important period of erosion, leaving no deposits in the Campine Basin. Sedimentation restarted in the Burdigalian and Langhian with different transgressive pulses from northwestern direction resulting in shallow marine glauconitic sands in the Antwerp area and Limburg. The regressional phase afterwards resulted in continental quartz-rich deposits in the southern and eastern part of the basin. Sedimentation is discontinuous with important breaks pointing to the continued uplift of the region competing with a rising sea level (Vandenberghe *et al.*, 1998; Louwye, 2005). The favorable climate and subsidence tectonics of the graben system in the east allowed the formation of peat and browncoal in the graben area, which already started in the Oligocene but bloomed during the mid-Miocene. The most extensive peat layer extended till east Limburg in the Opgrimbie glass sand facies of the Bolderberg Formation.

The marine glauconitic sands deposited in the Antwerp area are grouped under the Berchem Formation and are subdivided into three members: Edegem, Kiel and Antwerp. Burdigalian and Langhian deposits in Limburg are grouped under the Bolderberg Formation. These deposits are approximately time-equivalent to those of the Berchem Formation and are subdivided into the marine glauconitic Houthalen sand Member, and the Genk Member, which groups the continental deposits in the eastern part of Limburg, including the Opgrimbie glass sand facies.

IV.2 THE MARINE BERCHEM FORMATION

IV.2.1 Stratigraphy and sedimentology

The Berchem Formation (Figure 4.1) is subdivided into the Edegem, Kiel and Antwerp Members which are interpreted as incomplete sequences separated by hiatal intervals as a result of the deposition in a marginal marine environment with fluctuating sea level and affected by tectonic uplift (Vandenberghe et al., 1998; 2004). The main lithology is highly glauconitic sands, although clay intercalations are common. The lowermost Edegem Member is a clayey, glauconitic, fine- to medium-grained sand unit with locally a basal gravel and reworked septaria from the underlying Boom Fm and is correlated with dinoflagellate biozone DN2 (Louwye et al., 2000). The Burdigalian Kiel Member is defined as a glauconitic, medium- to coarse-grained sandy unit, largely devoid of fossils due to post-depositional decalcification (Louwye *et al.*, 2000; 2010). The Kiel Member is correlated with the DN2 and mainly DN3 biozones (Louwye *et al.*, 2000). Whereas both the Edegem and Kiel Members are geographically restricted to the Antwerp area, the youngest Antwerp Member of the formation occurs more widespread in the Campine area. Locally, the Zonderschot sands are a distinct facies of the Antwerp Member characterized by a slightly younger K-Ar glauconite age and different microfossil content (Odin et al., 1974; De Meuter and Laga, 1976; Huyghebaert and Nolf, 1979). Lithologically, the Antwerp Member

consists of a very glauconitic, medium-grained sand unit with disperse clay and variable shell layers, phosphate nodules, bones and shark teeth. According to Louwye *et al.* (2000) and Louwye and Laga (2008), the Antwerp Member was deposited mainly during the Langhian, correlating with the dinoflagellate cysts DN4 and DN5 biozones. Nevertheless, deposits assigned to the Antwerp Member were reported with varying biozonations within the Burdigalian, the entire Langhian and sometimes even in the Aquitanian and the Serravalian, covering the entire span from DN2 to possible even DN7 biozonations (reviews by Vandenberghe et al., 1998; Louwye and Laga, 2008; Vandenberghe et al., 2014). It seems unlikely for one sedimentation pulse to be active during such a long period of time. Instead, it seems very likely that all deposits presently reported as Antwerp sand Member represent a series of individual sedimentation pulses with highly similar lithological characteristics. The different defined units of the Berchem Formation are particularly enriched in pelletal glauconite, up to 60-70% according to Bastin (1966). Pelletal glauconite in the Edegem and Kiel Members are considered to be reworked, whereas age dating of pelletal glauconite in the Antwerp Member suggests an authigenic nature (Odin *et al.*, 1974). The mineralogy and clay mineralogy of these different members has nevertheless never been characterized in detail before.

IV.2.2 Samples

A set of 32 samples was selected on stratigraphically interpreted (Piet Laga, pers. comm.) sections in boreholes and outcrops available from the stratigraphical collections of the Geological Survey of Belgium (GSB) and the KULeuven. The sample set contains 4 Edegem Member, 7 Kiel Member and 21 Antwerp Member samples. Of the Antwerp Member samples, three non-glauconitic clay laminae are studied, whereas all other Antwerp, Kiel and Edegem Member samples are glauconitic sand samples. Three samples of the base of the Antwerp Member and of the Kiel Member originally collected from the Nachtegalenpark outcrop were used in this work. One additional Kiel Member sample was originally collected at the ring road of Antwerp during construction works. A sample of the Edegem Member was collected from the Argex quarry in Kruibeke. Other samples were collected from various boreholes: Mol 31W237, Essen 1E42, Turnhout 17E329, Schilde 29W283, Herentals 45W337, Oostmalle 16E153. The Dessel-5 31W370 borehole was sampled from the collection of NIRAS/ONDRAF and both Antwerp Member samples as well as three samples from the underlying glauconitic Voort Formation (Oligocene) were studied (Figure 4.1). Sampling depths from boreholes and descriptions can be found in. Sand samples were investigated for bulk mineralogy <32µm, clay mineralogy <2µm and pelletal glauconite content and mineralogy and pelletal glauconite size distribution with respect to the quartz population. Clay samples were characterized for bulk mineralogy (on total samples) and clay mineralogy <2µm (see Chapter I and Chapter II).

IV.2.3 Results

IV.2.3.1 Bulk mineralogy

Bulk mineralogical analyses on random oriented powders are performed on fractions <32µm for sand samples but on total samples for clays. In this way, the quartz, and sometimes also pelletal glauconite, dominated mineralogy of these sands does not obscure the presence of less abundant mineral phases as illustrated in Figure 4.2. The mineralogical results of the sand samples are dominated by dioctahedral clays, both Al- and Fe-rich. Feldspars are both K-feldspars as plagioclase. Carbonate minerals show large variation both in a qualitative as quantitative way. The results in Figure 4.2 are arranged by their occurrence in the different boreholes as well as grouped by stratigraphic member.

Samples of the Edegem Member typically contain relatively large amounts of carbonates consisting of mainly calcite, aragonite and minor siderite. On the contrary, Kiel Member samples contain no, or very low amounts of calcite (Figure 4.2). The carbonate content of the Antwerp Member is highly variable and mainly calcitic with traces of siderite but when macroscopic shells are present, also aragonite is found. In general, amounts of quartz and clays show large variability depending on the disperse clay content of each sample. Note that the composition of the three clay samples is more homogeneous and that no glauconitic minerals (=2:1 Fe-clays) are present in these samples (Figure 4.2).
Three samples of the Voort Formation in the Dessel-5 borehole have a very similar mineralogical bulk composition compared to the Berchem Fm samples.

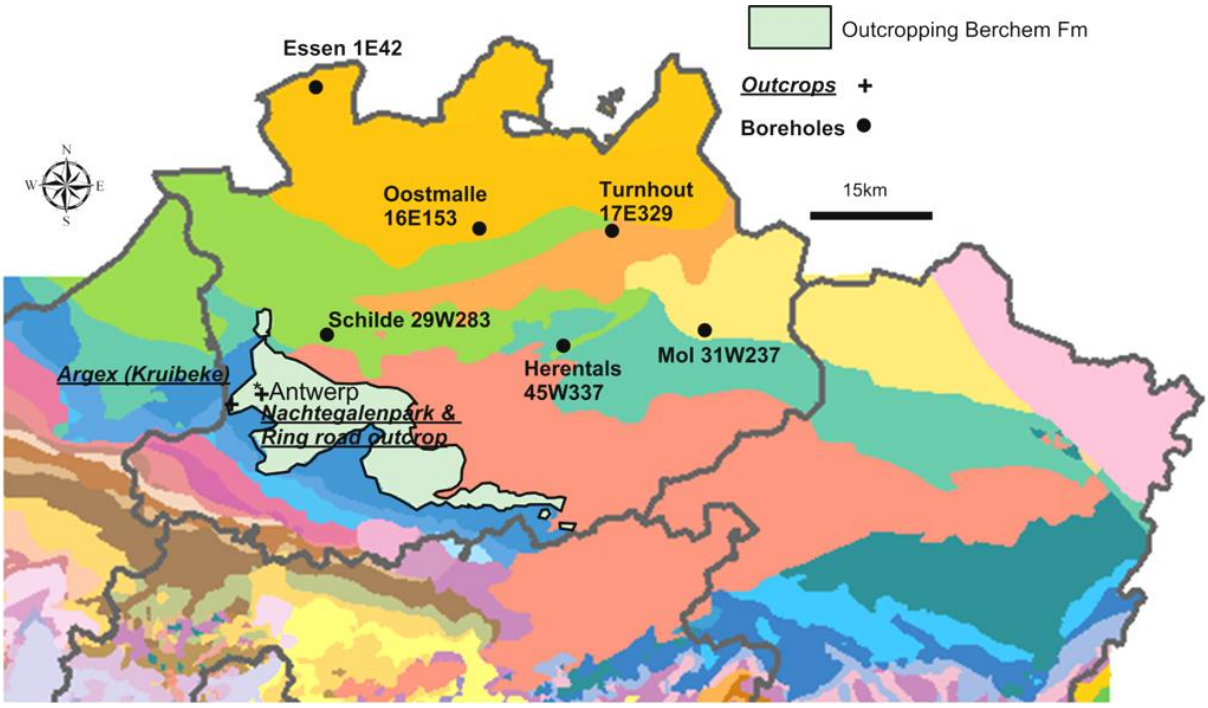

Figure 4.1. Cenozoic geological map of the Campine Basin indicating the Berchem Formation in pale green and dipping to the northeast. The geographical position of Berchem Formation samples studied in this work are indicated on the map. Geological map modified after ALBON (2009).

Table 4.1: Overview of samples studied from the Berchem Formation. The stratigraphic interpretation of each sample (P. Laga, pers. comm.), the borehole/outcrop and depth information and lithology is given.

Litho-unit	Sample code	Borehole		Outcrop		Lithology
Member		Code	Depth (m)	Place	Depth (m)	
Antwerp	**RT92**	Mol 31W237	140.90			Clay lam.
Antwerp	**RT93**		141.50			Gl sand
Antwerp	**RT94**		143.70			Gl sand
Antwerp	**RT95**		144.65			Gl sand
Antwerp	**RT97**		147.20			Clay lam.
Antwerp	**RT105**	Essen 1E42	177.30			Gl sand
Antwerp	**RT106**		177.70			Gl sand
Antwerp	**RT107**		179.30			Gl sand
Antwerp	**RT108**		180.50			Gl sand
Kiel	**RT109**		182.80			Gl sand
Kiel	**RT110**		183.80			Gl sand
Kiel	**RT111**		184.80			Gl sand
Antwerp	**RT120**	Turnhout 17E329	165.70			Gl sand
Antwerp	**RT121**		167.30			Gl sand
Antwerp	**RT122**		168.10			Gl sand
Antwerp	**RT125**	Schilde 29W283	60.80			Gl sand
Antwerp	**RT126**		62.80			Gl sand
Kiel	**RT127**		64.80			Gl sand
Kiel	**RT128**		66.30			Gl sand
Edegem	**RT129**		68.30			Gl sand
Edegem	**RT130**		70.30			Gl sand
Antwerp	**RT132**	Herentals 45W337	75.50			Gl sand
Antwerp	**RT133**		79.00			Gl sand
Antwerp	**RT134**		85.50			Gl sand
Antwerp	**RT135**		88.50			Gl sand
Antwerp	**RT136**		91.70			Clay lam.
Antwerp	**RT140**	Oostmalle 16E153	138.30			Gl sand
Antwerp	**RT141**		140.80			Gl sand
Antwerp	**RT142**		142.30			Gl sand
Antwerp	**RT143**		144.30			Gl sand
Antwerp	**RT144**		146.30			Gl sand
Edegem	**RT146**		152.30			Gl sand
Antwerp	**RT221**	Dessel 5	147.00			Gl sand
Antwerp	**RT222**		153.00			Gl sand
Antwerp	**RT223**		165.50			Gl sand
Antwerp	**RT237**		165.60			Gl sand
Antwerp	**RT238**		165.90			Gl sand
Edegem	**RTarg**			Argex quarry	2m	Gl sand
Kiel	**RG49**			Nachtegalenpark	?	Gl sand
Antwerpen	**RT308**			Nachtegalenpark	base	Gl sand
Antwerpen	**RT309**			Nachtegalenpark	base	Gl sand
Antwerpen	**RT310**			Nachtegalenpark	base	Gl sand
Kiel	**RG51**			Ring road Antwerp	?	Gl sand

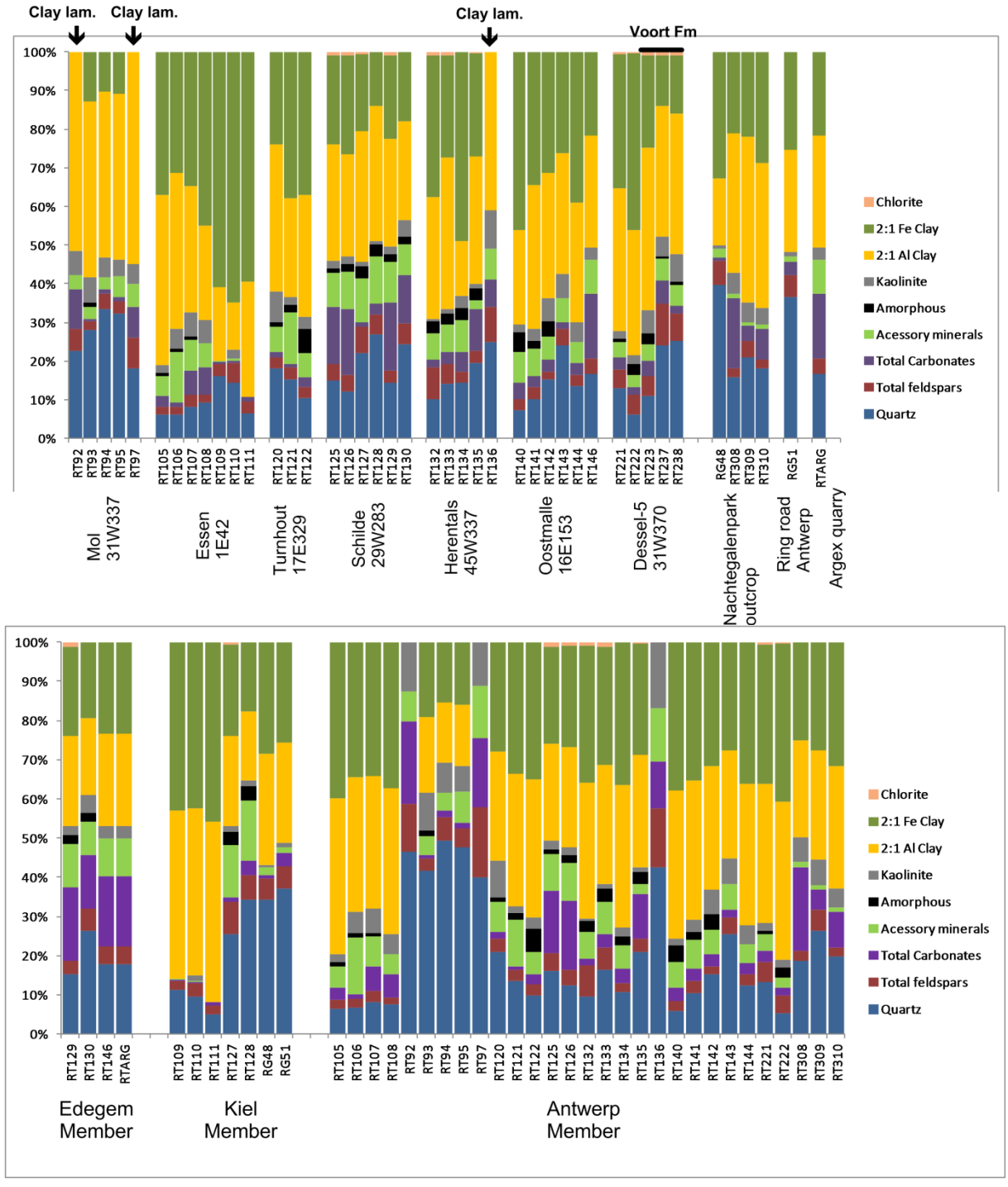

Figure 4.2: Berchem Formation: quantitative mineralogy of the fraction <32µm (in wt%) of individual samples. Three samples of the Dessel-5 borehole belong to the Oligocene Voort Formation. Clay laminae samples are indicated with an arrow and contain no glauconitic minerals. Above: Samples arranged per borehole / outcrop with increasing depth. Below: Samples arranged per stratigraphic Member

IV.2.3.2 Clay mineralogy 2µm

When studying the diffraction patterns <2µm of sand and clay samples (Figure 4.3), the 10Å/5Å-intensity ratio is significantly different between clay samples and sand samples. For sand samples, the 5Å-intensity is much lower, which suggests that Fe-bearing clays, such as glauconitic minerals, are present in the <2µm fraction. As discussed in chapter II, the presence of glauconite minerals can be relatively easily detected by studying the diffraction pattern of random oriented powders <2µm. When the 060-regions of both sands and clays are compared (Figure 4.4), it is unambiguous that glauconite-smectite is systematically present in sand samples, as documented by the unique d_{060}-position >1.51Å. In clay samples on the contrary, glauconite-smectite is systematically absent and mainly Al-rich clays, such as smectite, mixed-layer illite-smectite, illite and kaolinite are observed (Figure 4.4). Clay modeling of diffraction patterns of oriented clay slides allows for quantification of the different clay species present in the mixtures. The clay assemblage of the three clays typically consist of high amounts of smectite (40-50%), mixed-layer minerals (15-20%) and minor amounts (<15%) of illite, kaolinite and chlorite (Figure 4.5). This composition is quite constant in the three clay samples (Figure 4.6).

Although the general clay composition of sands, of all members, is somewhat more variable, the same type and characteristics of Al-rich clay minerals are encountered compared to the clay samples. Both air dry and glycolated patterns could be fitted with high quality and close matching quantifications (Figure 4.7). The relative proportions of the Al-rich phases are relatively constant but the main variability is caused by the presence of glauconite-smectite which occurs in both higher expandable form (27-30% expandable layers) and low expandable form (9-11% expandable layers), with the former type clearly predominating (Figure 4.6). Diffraction patterns of random oriented powders reveal that the d_{060} values of the Berchem glauconite-smectite range between 1.513Å and 1.5155Å (Adriaens et al., 2014).

The amount of glauconite-smectite is generally <25% in sands but in some samples, all belonging to the Antwerp Member, substantial higher amounts of glauconite-smectite occur (Figure 4.6). Apart from the latter observation, samples of the three members of the Berchem Formation are not very different and are virtually impossible to differentiate one from another based on clay mineralogy only (Figure 4.6).

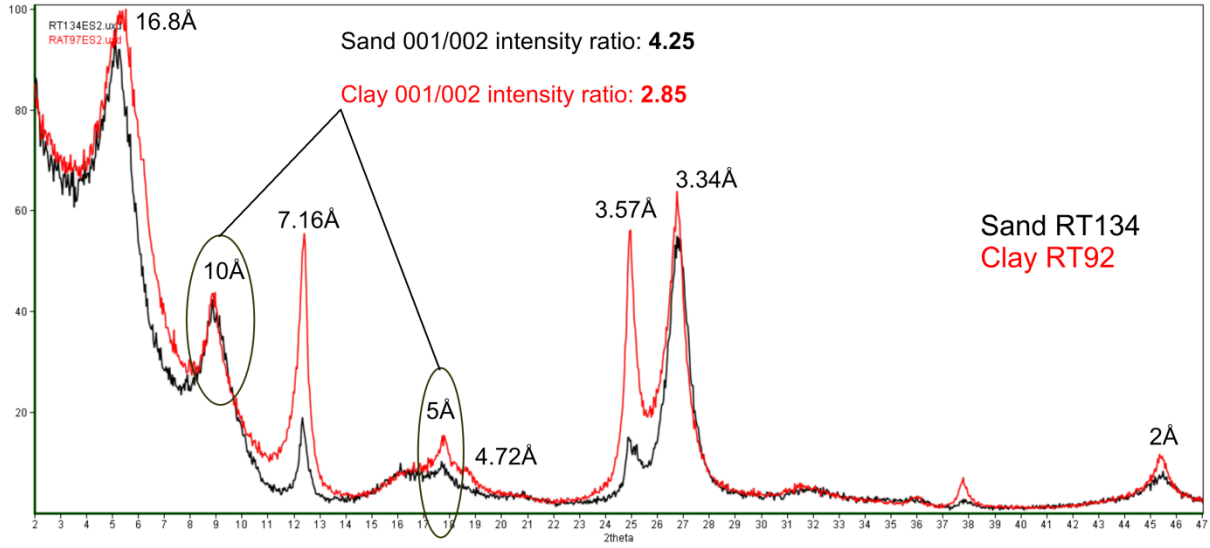

Figure 4.3: Berchem Fm: diffraction patterns of oriented clay slides <2µm recorded in glycolated conditions of sand sample RT134 and clay sample RT92. The diffraction patterns were scaled to match the intensities of the 10A-reflections. Note the significant difference in 5A-intensity between the sand sample (black) and the clay sample (red), resulting in very different 001/002 intensity ratios caused by the presence of Fe-bearing clays in the sand sample.

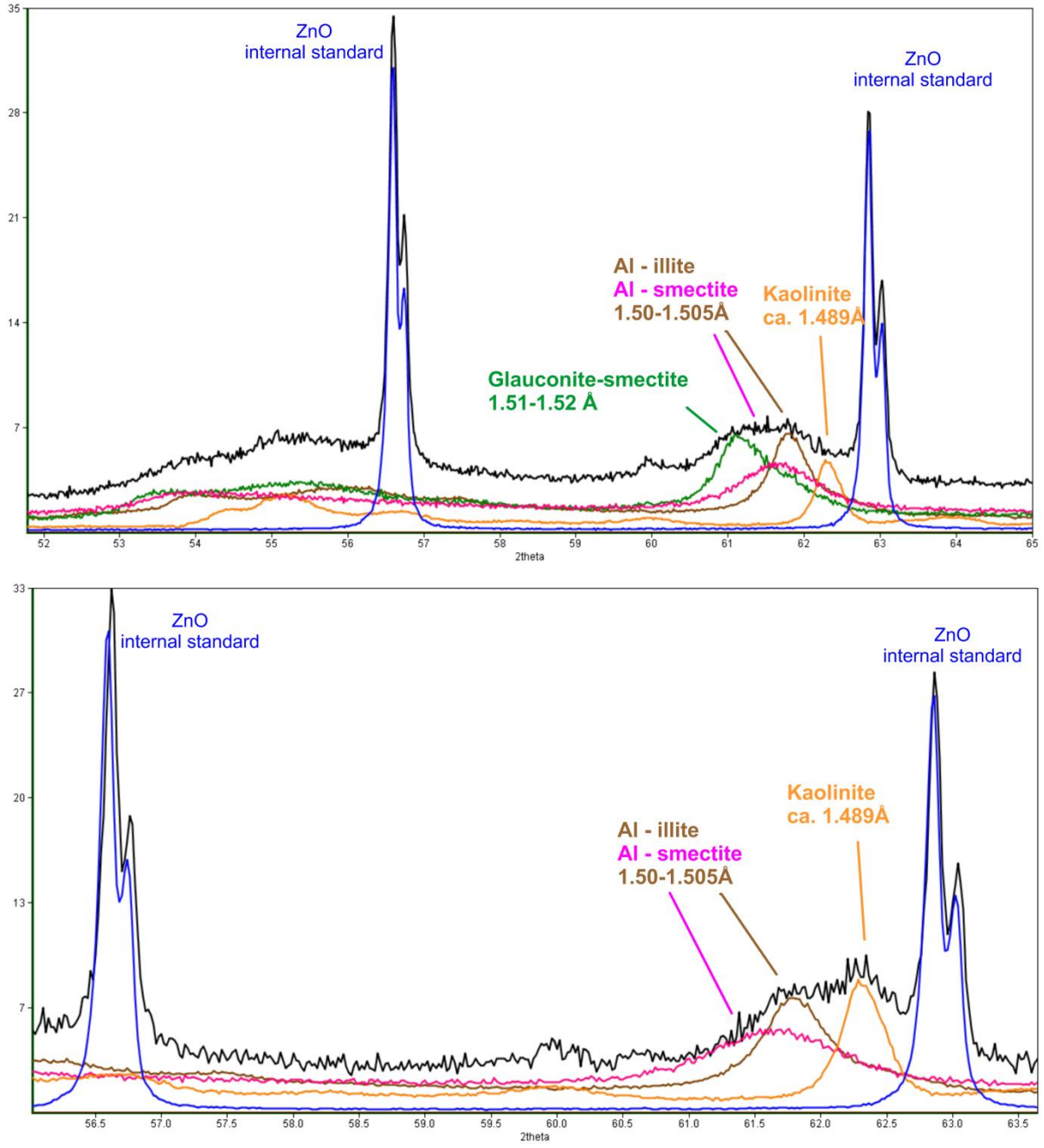

Figure 4.4: TOP : Antwerp Member sand sample RT134: diffraction pattern of random oriented powder <2µm, zoomed in on the 060-region. In color, reference patterns of glauconite-smectite, illite, Al-smectite and kaolinite are shown, with ZnO in blue as the internal standard. It is apparent from the 060-region that there is a significant contribution from Fe-bearing clays, with a d060 >1.51Å (glauconite-smectite), aside from the regular Al-rich clays such as illite, smectite, illite-smectite and kaolinite, which all have a d060 < 1.51Å. BOTTOM: Antwerp Member clay sample RT92: diffraction pattern of random oriented powder <2µm illustrating the absence of glauconite-smectite.

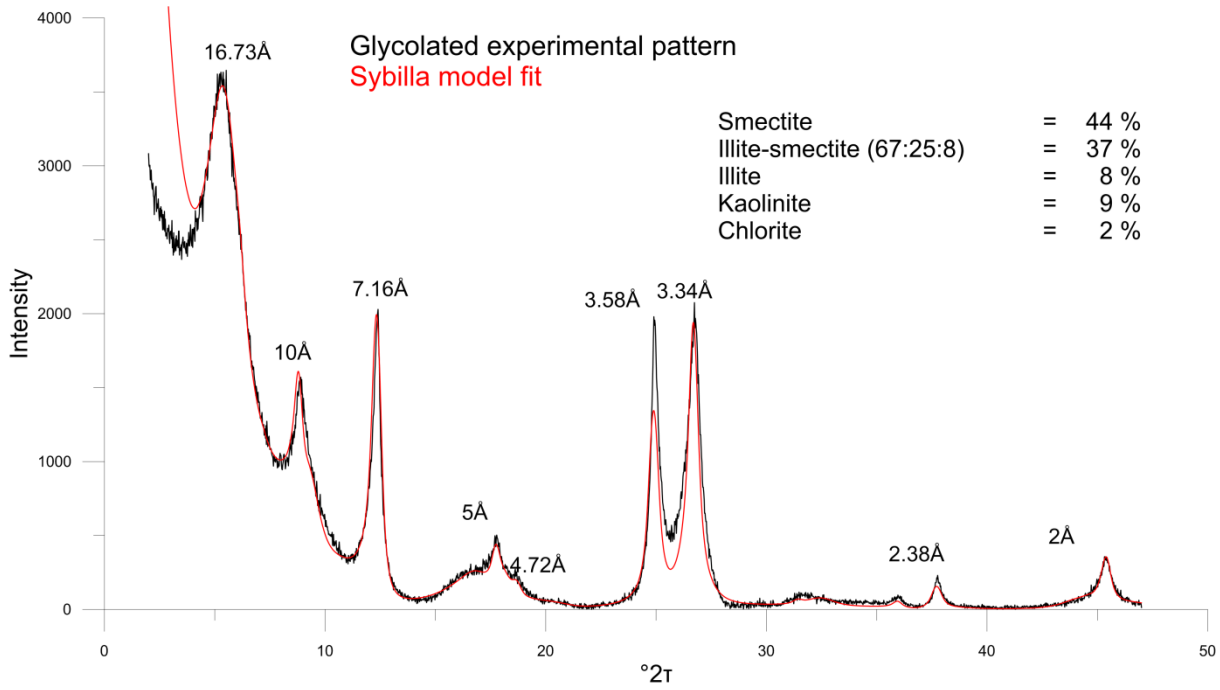

Figure 4.5: Berchem clay sample RT97: Ca-saturated glycolated diffraction pattern (black) and Sybilla clay model fit (red) with indication of quantitative figures for each clay mineral phase.

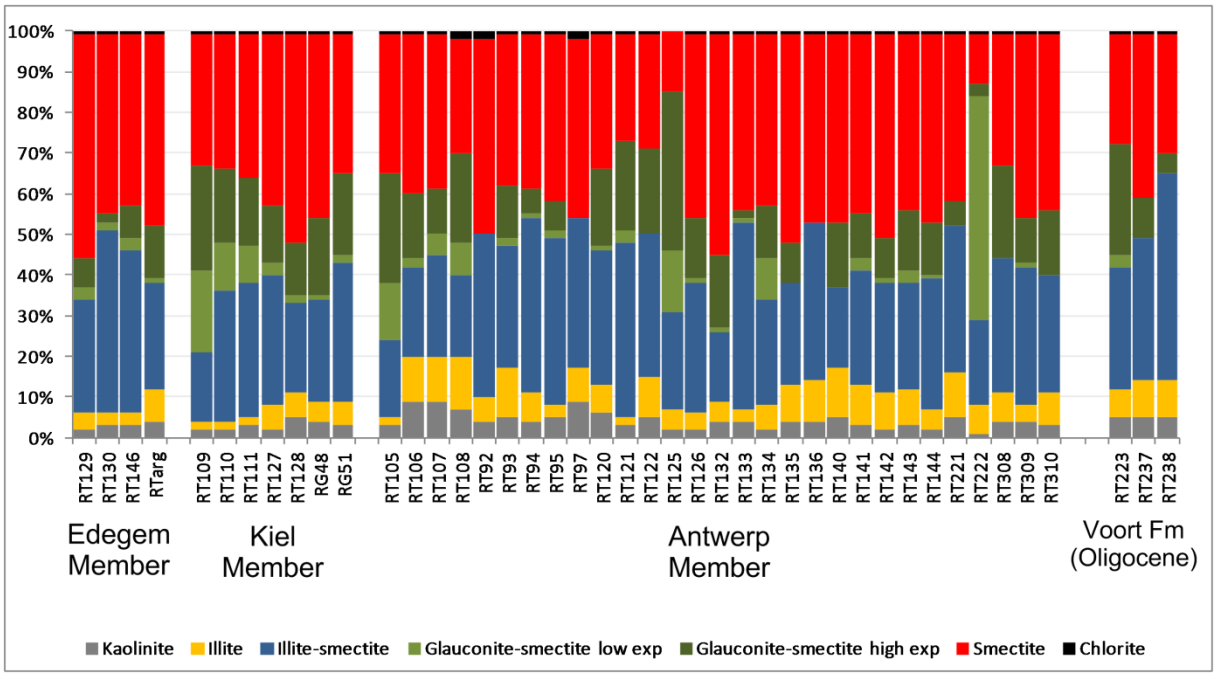

Figure 4.6: Quantitative clay mineralogy <2µm of the Berchem Fm: illustration of the quantitative proportions of individual mineral phases arranged by member. The three samples of the Voort Formation are shown on the right.

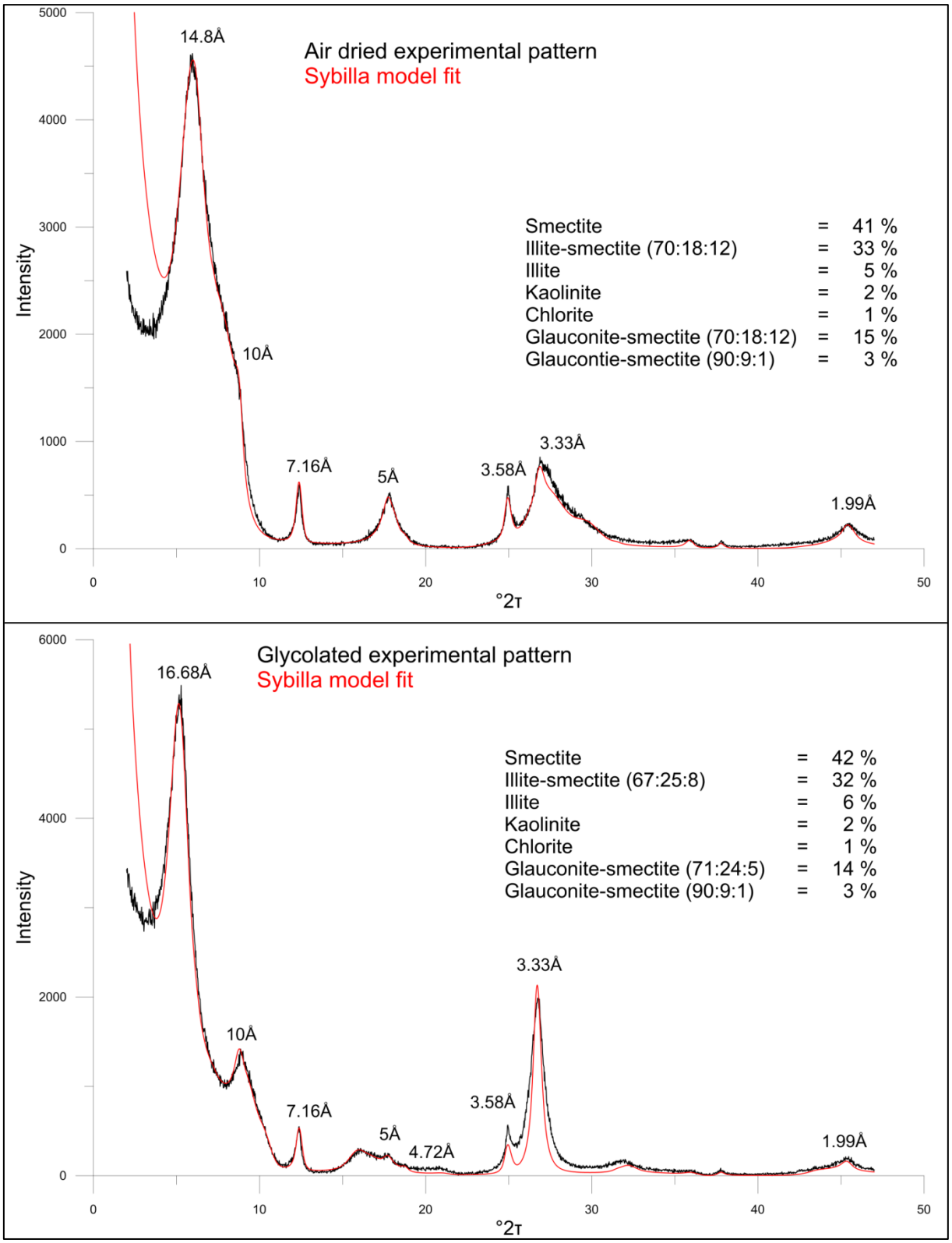

Figure 4.7: Ca-saturated air dry (TOP) and glycolated (BOTTOM) diffraction patterns of sand sample RT127 accompanied with the Sybilla clay model fit and the quantitative figures for each mineral phase. Both criteria for a reliable clay model are achieved: well pattern fitting and comparable phase quantification.

IV.2.3.3 Pelletal glauconite

Contents

Whereas pelletal glauconite is absent in clay intercalations, the sands of the Berchem Formation are known to be very rich in pelletal glauconite, with most likely the highest concentrations in the entire Campine Basin (Bastin, 1966; Adriaens, 2009). Typically the Edegem (on average 37 ± 5%) and Kiel sands (on average 33 ± 8%) display lower amounts compared to the Antwerp sands (on average 47 ± 11%). One particular Antwerp Member sample in the Dessel-5 borehole was found to contain a staggering amount of 87% (Figure 4.8).

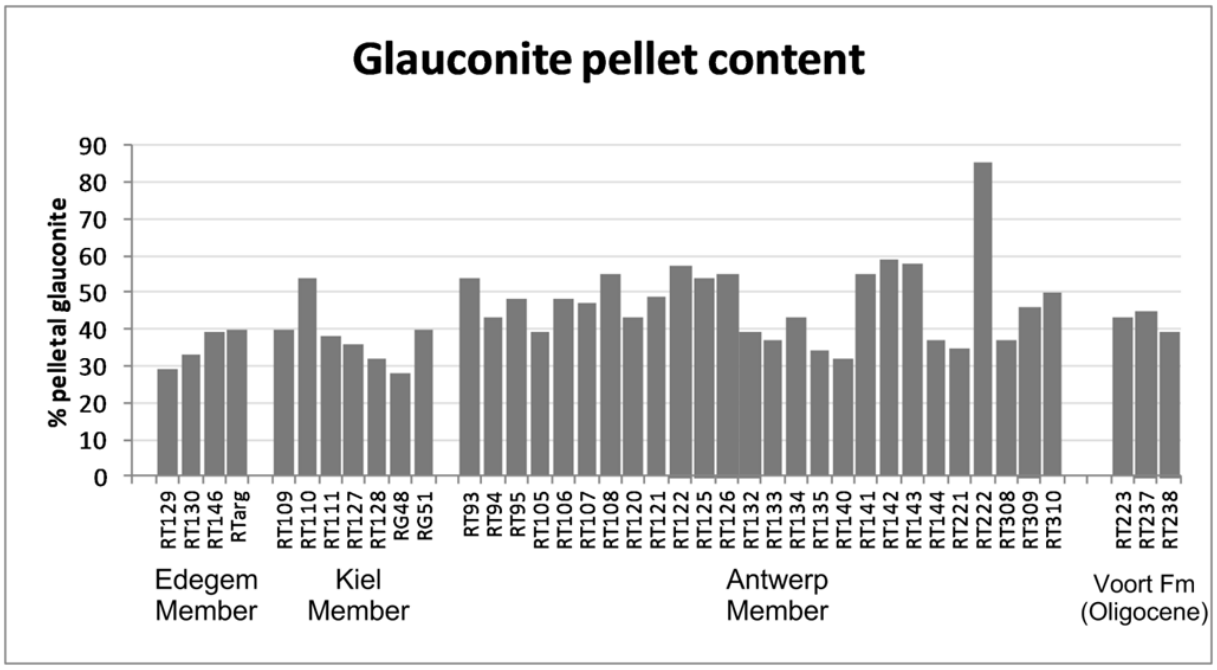

Figure 4.8: Glauconite pellet content of the different members of the Berchem Fm and comparison with the Oligocene Voort Fm.

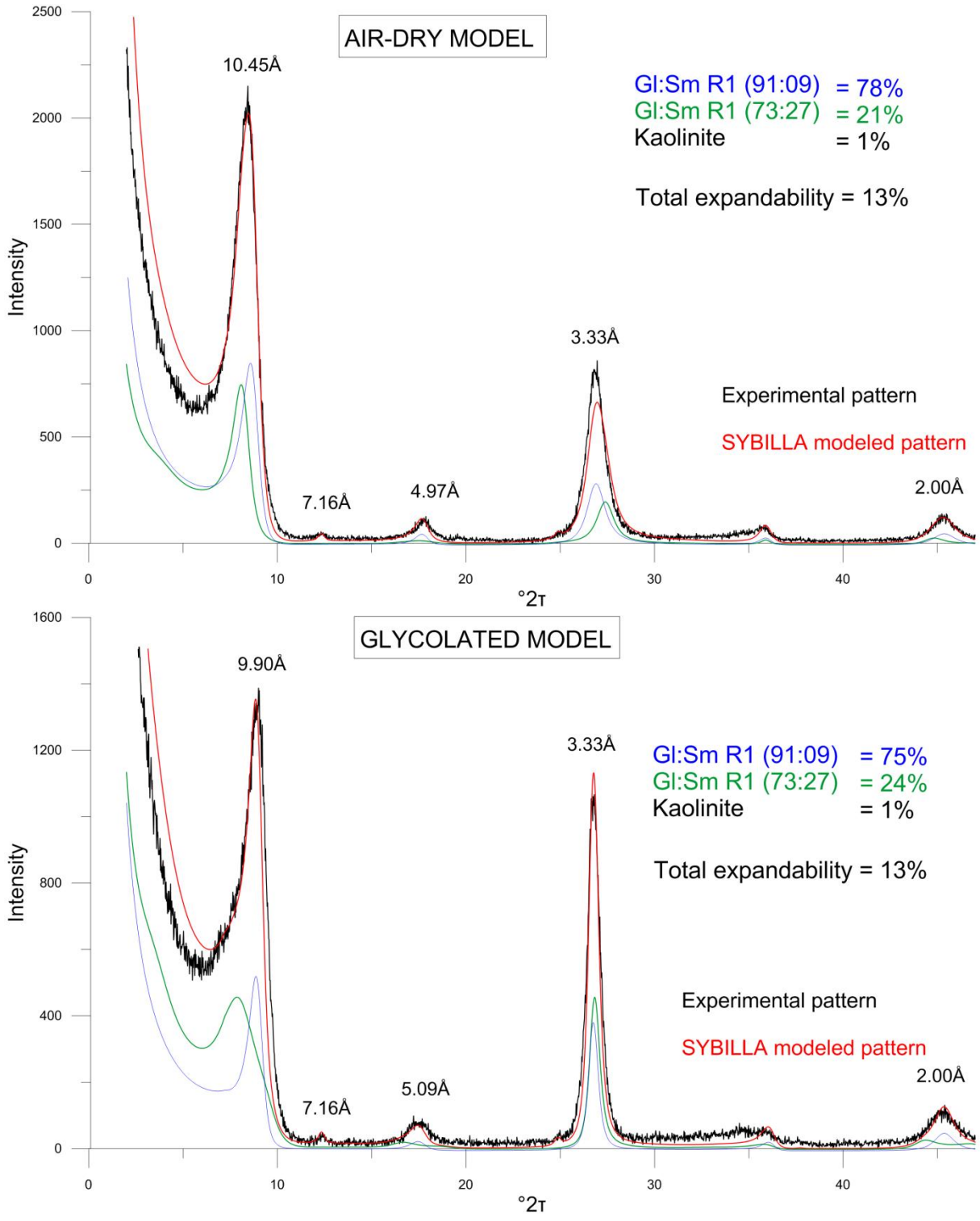

Figure 4.9: Sybilla model fits of pelletal glauconite in air dried conditions (top) and glycolated conditions (bottom) of sample RT126. For modeling two separate glauconite-smectite R1 phases were used. Kaolinite is present as a trace mineral.

Mineralogy

The internal mineralogical characteristics of the pelletal glauconite in the Berchem Fm (Table 4.3) are very constant throughout the formation. Typically, the d_{060} position is positioned between 1.513Å and 1.5153Å. Modeling of oriented slides reveals two glauconite-smectite R1 phases (Figure 4.9), which are exactly the same two phases (relatively high expandable and low expandable glauconite-smectite) found in clay fractions <2µm. The total amount of expandable layers derived from clay modeling is relatively stable ranging between 13 to 16% of smectite layers. Nevertheless, the proportions in which both phases occur are slightly different compared to the occurrence of glauconite-smectite in the clay fraction. Glauconite-smectite in the clay fraction seems to contain slightly more expandable layers. The mineralogy of the pelletal glauconite also contains traces of kaolinite as the result of clay precipitation in pelletal rims. Logically, also other clay minerals such as illite and illite-smectite are present as impurities but which cannot be separated from glauconite by XRD in such low amounts.

Size distribution in relation to quartz

The relation of the size distribution of pelletal glauconite and quartz grains was already briefly discussed in chapter III. This relation is useful to interpret the depositional history of pelletal glauconite in sediments. The results for the Antwerp Member samples can be split in two groups. The first type of samples show a similar distribution compared to Edegem and Kiel Member samples (Figure 4.10). For the majority of Antwerp samples however, the pelletal glauconite distribution is not only much coarser than the quartz grains but also characterized by a significantly different shape (Figure 4.10). Although some pelletal glauconite samples of the Kiel and Edegem Members also have slightly differing distribution curves (see for instance sample Kiel-RG49 in Figure 4.10), the majority of Kiel and Edegem pelletal glauconite size distribution curves are equally shaped compared to the quartz fraction (Figure 4.10). It seems a typical characteristics that glauconite pellets of the Berchem Fm have a coarser mode of the distribution (Table 4.2). It can be concluded that pelletal glauconite in the Edegem and Kiel Members were, probably shortly after authigenesis, dominantly transported together with the quartz fraction whereas this mutual transport was less effective for the Antwerp Member pelletal glauconite in most samples. Consequently, pelletal glauconite in the Antwerp Member is authigenic and underwent a minimum of transport.

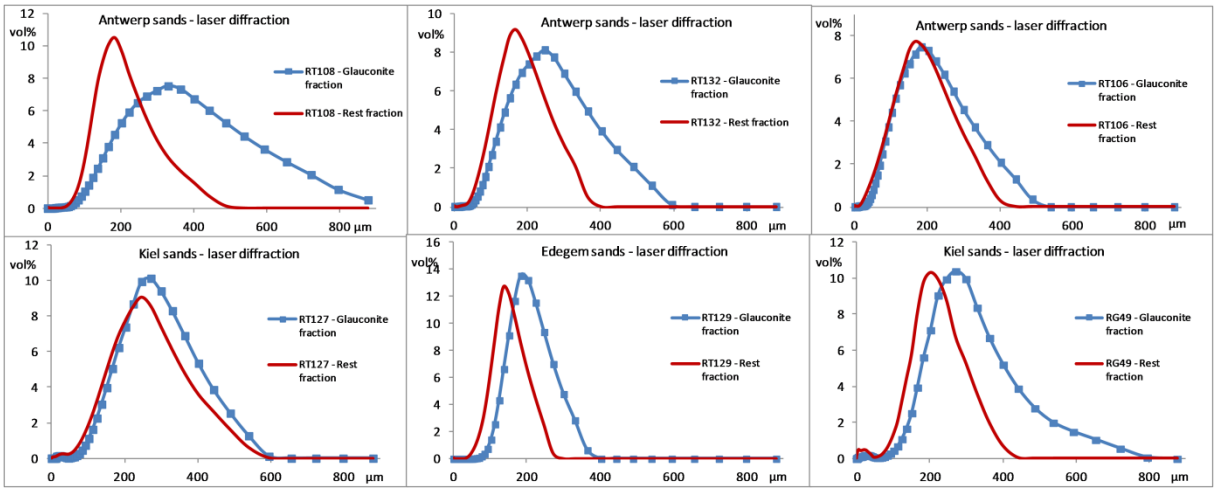

Figure 4.10: Pelletal glauconite and quartz fraction: comparing size distributions of the different members of the Berchem Formation.

Table 4.2: Pelletal glauconite in the Berchem Formation: mode and standard deviation (stdev) of glauconite pellet size distribution compared with the mode of the quartz size distribution.

Sample	Member	Mode Gl fraction (µm)	Stdev (µm)	Mode Quartz fraction (µm)	Stdev (µm)
RT108	Antwerp	330.6	*157.0*	183.9	*73.7*
RT132	Antwerp	246.6	*88.8*	166.8	*61.2*
RT106	Antwerp	185.9	*76.0*	172.8	*87.9*
RT127	Kiel	246.6	*68.8*	223.6	*67.5*
RG49	Kiel	271.9	*121.0*	202.8	*71.2*
RT129	Edegem	181.6	*83.5*	142.2	*55.7*

Table 4.3: Mineralogical characteristics of pelletal glauconite of the Berchem Fm. Note that the 060 position and amount of expandable smectite layers are relatively constant for all analyzed samples ranging from 13-16% expandable layers in total.

Sample	Member	Content	*d 060*	*Higher expandable* Glauconite-smectite (73:27)	*Low expandable* Glauconite-smectite (91:09)	Glauconite layers (total)	Smectite layers (total)
RT93	Antwerp	54%	1.5139	37	63	84	16
RT94	Antwerp	43%	1.5131	35	65	85	15
RT95	Antwerp	48%	1.5139	30	70	86	14
RT105	Antwerp	39%	1.5135	21	79	87	13
RT124	Antwerp	54%	1.5144	21	79	87	13
RT126	Antwerp	55%	1.5144	22	78	87	13
RT127	Antwerp	34%	1.5153	34	66	85	15
RT132	Antwerp	39%	1.5131	31	69	85	15
RT134	Antwerp	43%	1.5153	26	74	86	14
RT128	Kiel	32%	1.5139	32	68	85	15
RG49	Kiel	29%	1.5139	34	66	85	15
RT130	Edegem	33%	1.5131	32	68	85	15
RTARG	Edegem	39%	1.5144	33	67	85	15

IV.3 THE BOLDERBERG FORMATION

IV.3.1 Stratigraphy and sedimentology

The Bolderberg Formation outcrops east to southeast from the Berchem Fm (Figure 4.11) and is at least 100m thick (Sels et al., 2001). In the Limburg area, this Miocene succession is a classical marine-continental sedimentary and stratigraphic cycle (Vandenberghe *et al.*, 1998) with the marine Houthalen Member and the continental Genk Member (Figure 4.1). The Opgrimbie unit is in this work considered as a facies of the Genk Member because of its distinct characteristics. Although Louwye and Laga (2008) also consider the yellow, highly oxidized and glauconite-poor sands occurring on top of the green glauconitic sands as part of the marine Houthalen Member, such a reasoning is not followed in this work because of the obvious lithological difference between both units. In this work, the marine Houthalen Member is used only for the lower green-grey glauconitic sands. The Genk Member comprises the yellow to brown oxidized sands whereas the Opgrimbie facies consists of high-quality quartz sands.

The base of the Miocene in Limburg is marked by a transgressive basal gravel with reworked Oligocene components and phosphate pebbles (Elsoo gravel). It is overlain by almost 50m of dark green, medium to fine-grained, micaceous, glauconitic and very slightly lignitic

sands of the marine Houthalen Member (De Meuter and Laga, 1976; Louwye and Laga, 2007). Benthic foraminifera (De Meuter and Laga, 1976) and nannoplankton associations (Martini and Müller, 1973) correlate the Houthalen Member with the Edegem Member of the Berchem Fm. Louwye and Laga (2008) correlated the Bolderberg Fm occurrence in the Wijshagen borehole with the DN4 biozone and the top part even with the lowermost part of the DN5 biozone, which points to a Burdigalian – Langhian age.

Above the glauconitic sands, yellow to brown sands occur which seem to have undergone intensive oxidation. The sands are medium coarse and lignitic fragments have been reported (Sels et al., 2001). The quartz sands of the Opgrimbie facies, also referred to as "silver sands", is subdivided into two subunits which are separated by a gravel layer (Sels et al., 2001). The Opgrimbie facies consists of white, medium-sized, high-quality quartz sands, which are locally cemented. Locally, also a lignite layer occurs in the sand. The exact chronostratigraphical position of the Opgrimbie facies remains unknown but logically, the lignite layer present in this unit most likely correlates with the middle Miocene extension of lignite in the Rhine graben (Figure II.4), the Burdigalian Morken seam (described in Utescher et al., 2012; Schäfer and Utescher, 2014)

.

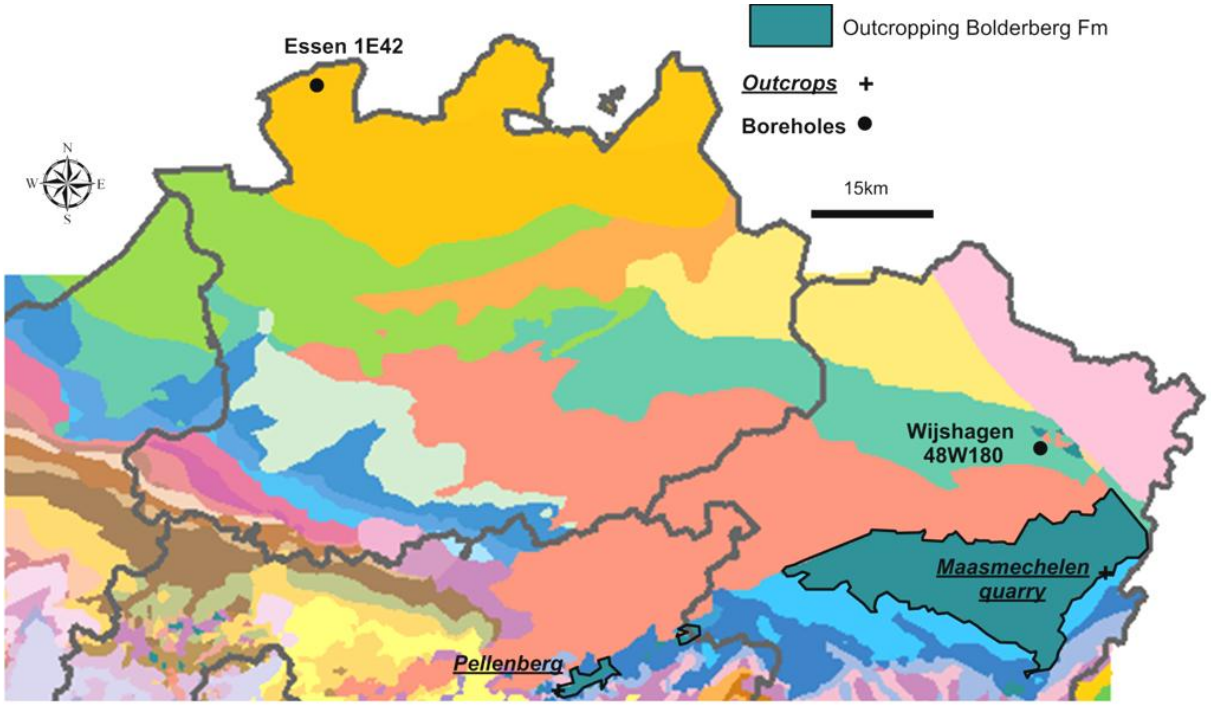

Figure 4.11: Geological map of the Neogene strata in the Campine basin. The outcrop area of the Bolderberg Fm has been highlighted and sample locations are also shown. Geological map modified after ALBON (2009).

IV.3.2 Samples

Clay-rich glauconitic sand samples of the Houthalen Member were collected in outcrop in the Pellenberg sand pit, roughly 5km east from Leuven (Figure 4.11). One additional glauconitic sand sample was collected from the Wijshagen $48^{W}180$ borehole at 160m depth. Six samples of the Genk Member were also sampled in the Wijshagen borehole which all appear very poor in glauconite. Four additional samples (RU36-39) were collected from the Opgrimbie facies, sampled in the Maasmechelen quarry of Sibelco SCR. One sample, RU36, was taken below the distinct lignite horizon present in the quarry while samples RU37-38-39 were all taken a few meters above this lignite layer. All samples are sand samples which are characterized for bulk mineralogy (<32µm), clay mineralogy <2µm and pelletal glauconite contents and pelletal glauconite size distributions with respect to quartz.

IV.3.3 Results

IV.3.3.1 Bulk mineralogy

The results of the bulk mineralogical analysis are presented in a sample-by-sample overview in Figure 4.12. In general, samples of the marine Houthalen Member are similar to the Berchem Fm samples with also significant amounts of glauconite minerals (2:1 Fe-clay). The amount of carbonate minerals (siderite) is however very low or non-existent.
The Genk unit, however, contains substantially less clays, and no glauconite minerals. These samples are particularly enriched in sulphate minerals: jarosite, alunite, hexahydrite, gypsum but also contain slightly more amorphous components (Figure 4.12). Traces of siderite also occur. Samples of the Opgrimbie facies are similar to the Genk Member but without the sulphates and with higher kaolinite amounts.

IV.3.3.2 Clay mineralogy 2µm

Air dried and glycolated patterns <2µm of the Houthalen Member indicate a smectite-dominated clay mineralogy with low variability between different samples. The diffraction pattern and the individual clay species are moreover very similar as identified for the Berchem Fm (Figure 4.13). During Sybilla clay modeling (Figure 4.14), identical clay mineral characteristics could be used and very similar quantifications as in the Berchem Fm samples were obtained (Figure 4.15). The glauconite-smectite is again dominantly of the higher expandable type and is characterized by d_{060}-values of 1.515Å.

The clay mineralogy of the continental Genk Member is very similar to that of the Houthalen Member, apart from the total absence of glauconite-smectite (Figure 4.15). The clay mineralogy of the Opgrimbie facies is nevertheless quite different and is dominated by kaolinite and illite minerals with only minor contributions from smectite minerals (Figure 4.15). In total, kaolinitic and illitic layers make up 80 – 90% of clay layers in these samples. Furthermore, there is no distinct difference between the clay mineralogy of the quartz sand occurring above or below the lignite horizon.

IV.3.3.3 Pelletal glauconite

Contents
While mineralogical and clay mineralogical characteristics of the Bolderberg and Berchem Formations are similar, the amount of glauconite pellets is clearly lower in the Bolderberg Fm with percentages being <20%. The amount of pelletal glauconite in the Genk Member samples is <1% and virtually no pelletal glauconite was found in the Opgrimbie facies samples.

Mineralogy
The mineralogy of the glauconite pellets is very similar to the pelletal glauconite in the Berchem Formation, with 13-14% expandable layers in total and d060-values of 1.5151 – 1.5157Å (Table 4.4). Typically, the low expandable glauconite-smectite type dominates the higher expandable type.

Size distribution in relation to quartz
The size distribution of pelletal glauconite in the Houthalen Member shows an identical relation with the quartz distribution as in the Berchem Formation. Pelletal glauconite and quartz distributions are equally shaped, demonstrating their common transport history (Figure 4.16). Nevertheless, mode values for pelletal glauconite are systematically higher, as was also the case in the Berchem Formation samples.

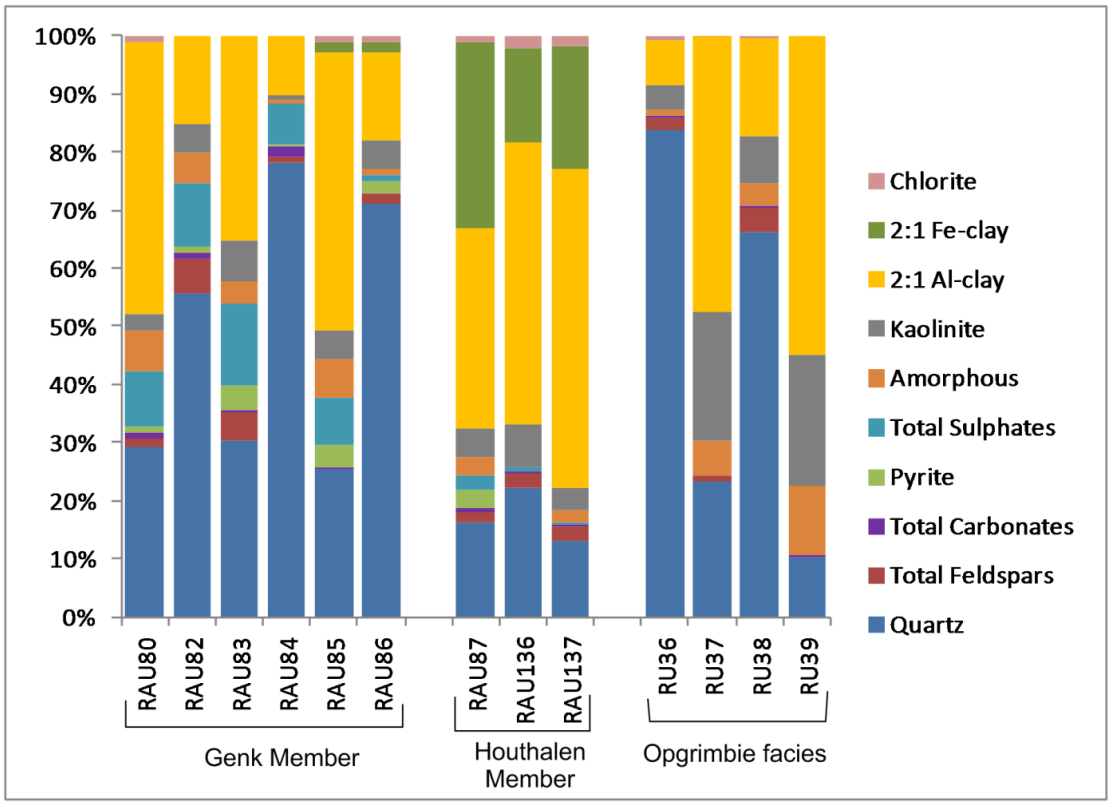

Figure 4.12: Quantitative bulk mineralogical results <32µm (in wt%) of samples of the Bolderberg Fm.

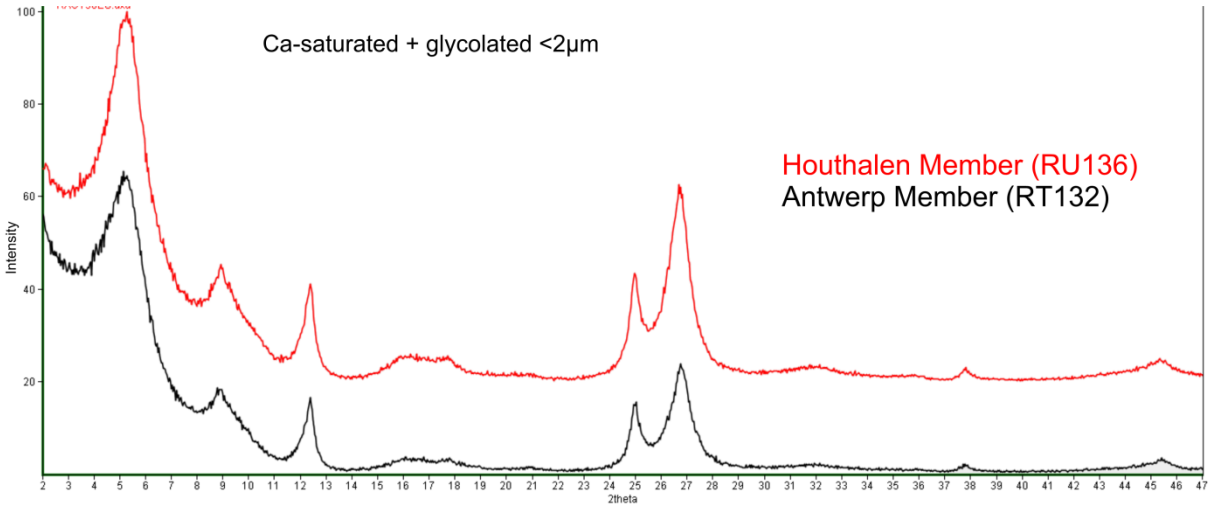

Figure 4.13: Diffraction patterns of oriented clay slides <2µm in glycolated condition: comparison between Antwerp Member and Houthalen Member sample showing an almost perfect match.

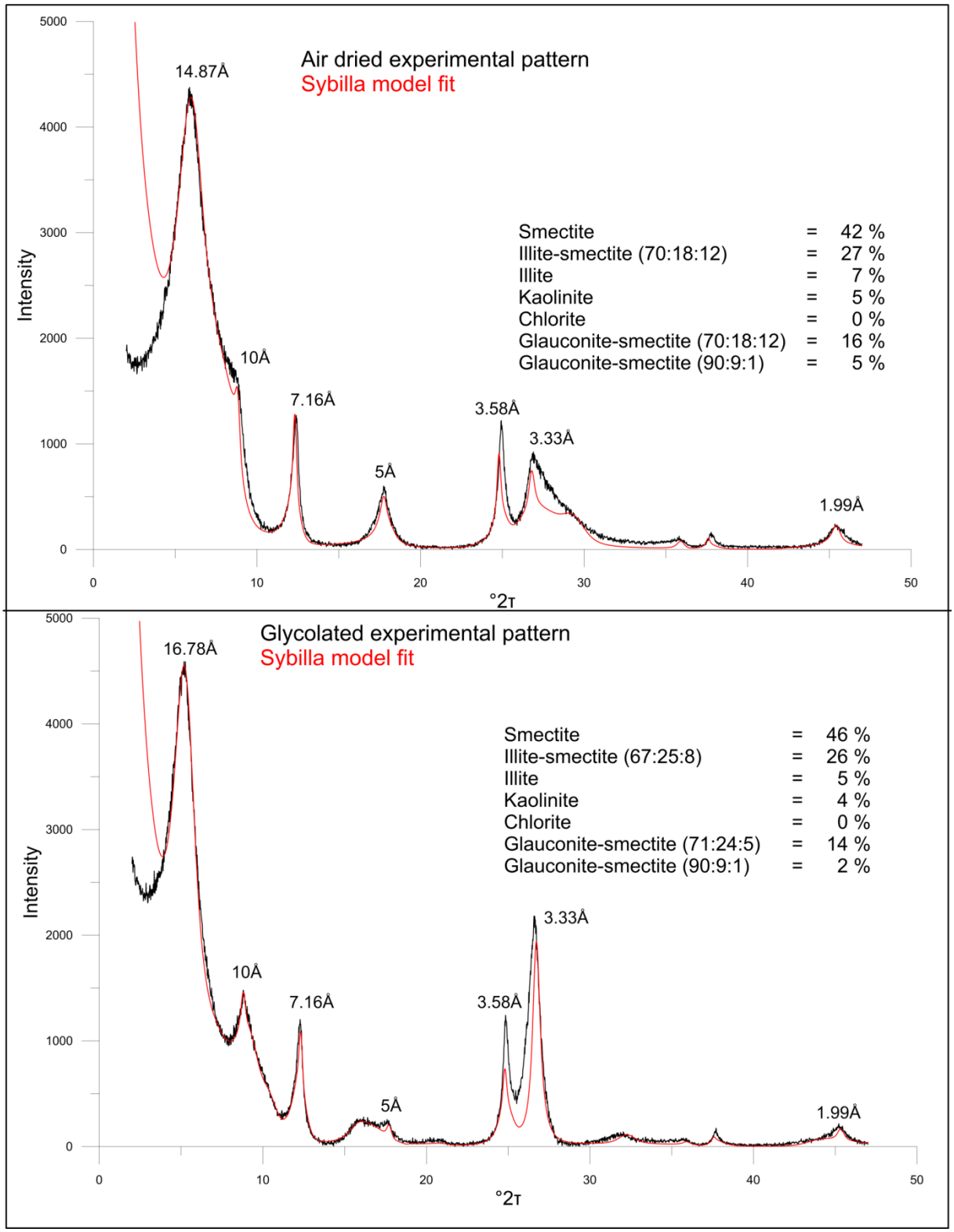

Figure 4.14: Ca-saturated air dry (above) and glycolated (below) diffraction patterns of sand sample RU136 accompanied with the Sybilla clay model fit and the quantitative figures for each mineral phase.

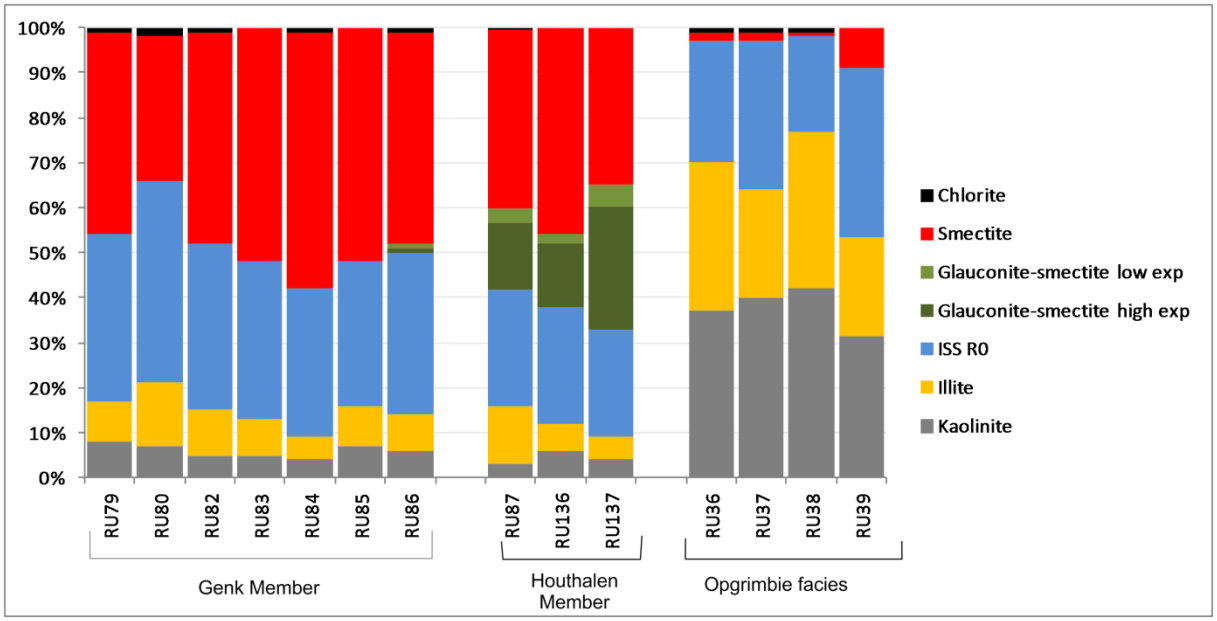

Figure 4.15: Clay mineralogy <2µm of the Bolderberg Formation: quantitative figures of individual samples.

Table 4.4: Mineralogical characteristics of pelletal glauconite of the Houthalen Member of the Bolderberg Fm. These mineralogical characteristics are identical to glauconite pellets of the Berchem Formation.

Sample	Member	Content	*d 060*	*Higher expandable* Glauconite-smectite (73:27)	*Low expandable* Glauconite-smectite (91:09)	Glauconite layers (total)	Smectite layers (total)
RU87	Houthalen	18%	1.5151	21	79	87	13
RU136	Houthalen	13%	1.5157	21	79	87	13
RU137	Houthalen	17%	1.5157	25	75	86	14

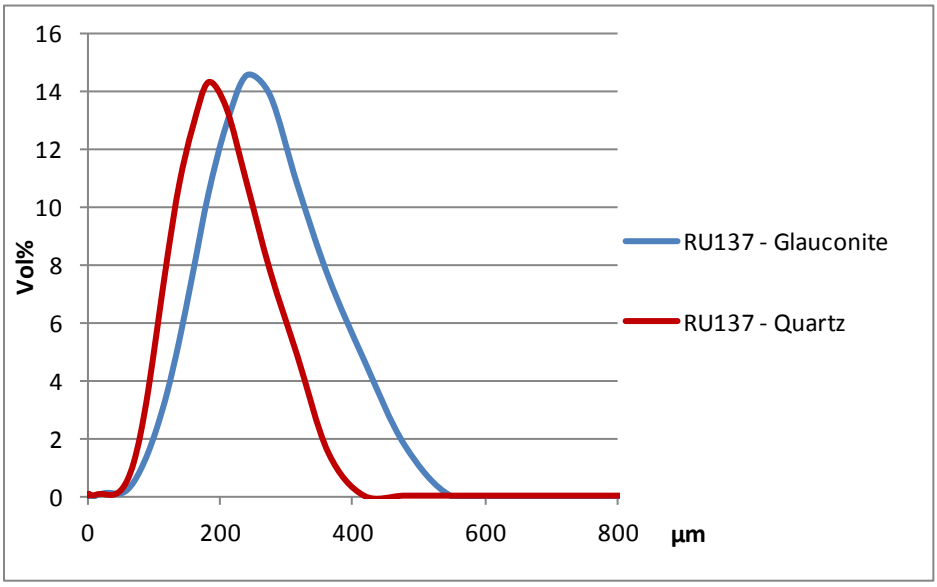

Figure 4.16: Comparison of size distributions of pelletal glauconite vs. quartz fraction of the Houthalen Member sample RU137 (Pellenberg). The glauconite fraction distribution is similarly shaped to the quartz fraction distribution but has a larger mode value.

IV.4. INTERPRETATION AND DISCUSSION

IV.4.1 Stratigraphy

The lithostratigraphic subdivision of the glauconitic Berchem Formation in three members is based on the recognition of the consistent geometric position of a lower fine-grained, clay containing and calcareous sand (Edegem Member), a middle sand unit without carbonates (Kiel Member) and an upper very glauconitic and calcareous fossil-bearing sand (Antwerp Member). Further differentiation can be made using microfossils such as benthic foraminifera and dinoflagellate biozonations (see De Meuter and Laga, 1976; Louwye and Laga, 1998; Louwye et al., 2000; Louwye, 2001; and Vandenberghe *et al.*, 2004). Bastin (1966) and Louwye (2005) reported differences in glauconite content with the highest contents occurring in the Antwerp sands. Our results confirm that the highest pelletal glauconite amounts indeed occur in the Antwerp Member. The size distribution of Antwerp glauconite pellets seems almost unrelated to the quartz fraction in most samples, in contrast with the Edegem and Kiel glauconite pellets. The difference in amount as well as in size distribution of pelletal glauconite between Antwerp and Kiel-Edegem is however not absolute. In addition, the quantitative (clay) mineralogy and pelletal glauconite mineralogy have shown that no stratigraphically meaningful differences exist in these Miocene deposits. Even the marine deposits of the Bolderberg Formation, geographically located to the east of the Berchem Formation but with about similar chronostratigraphy, have a similar bulk and clay mineralogy compared to the Berchem Formation.

The clay mineralogy of the Opgrimbie quartz sands was found to be particular rich in kaolinite, in contrast with the smectite-dominated clay mineralogy of the other Bolderberg deposits. Although glauconite pellets are more abundant in the Berchem Formation, the mineralogy of the pelletal glauconite in both formations is very similar. The difference in Berchem and Houthalen pelletal glauconite amounts might be explained by an increased continental input in the Houthalen deposits. If so, the pelletal glauconite content of the marine transported sediment was diluted through the mixing with continental quartz sands resulting in the dilution of the pelletal glauconite content in the Houthalen deposit.

IV.4.2 Relation between clay-sized and pelletal glauconite

It was illustrated for the different units of the Berchem Formation that the occurrence of glauconite-smectite in the clay fraction of sand samples seems conditioned by the presence of glauconite pellets. As discussed in chapter III, clay-sized glauconite originates from pelletal disintegration during short-distance transport. Therefore ideally all characteristics of both glauconite habits should be exactly the same. This is confirmed for the d_{060} of glauconite-smectite in both the clay-sized and pelletal glauconite. Also the mineralogical characteristics of both occurrences are similar. A higher-expandable glauconite-smectite and a low-expandable glauconite-smectite type were required to model the diffraction pattern of glauconite-smectite in both clay-sized and pelletal glauconite. The results however also demonstrated that, clay-sized glauconite is more expandable compared to pelletal glauconite.

The mineralogy of clay-sized and pelletal glauconite is however so similar that it can be concluded that there is no doubt that clay-sized glauconite originates from pelletal glauconite according to the mechanism proposed in chapter III. The slightly higher amount of expandables in clay-sized glauconite is therefore most likely due to the more intense weathering compared to pelletal glauconite before, during and after deposition.

IV.4.3 Sediment sources

The relatively high kaolinite and illitic (illite + illite-smectite) contents of the Opgrimbie facies clearly contrasts with the smectite-dominated clay mineralogy of the underlying continental Genk Member, the marine Houthalen Member, and, more to the west, the marine Berchem Formation. This strongly suggests that during Burdigalian and Langhian times, the main proportion of smectite minerals

has a marine provenance and is not derived from a continental source, either via the Rhine delta sediments situated in the Roer Valley graben in the northeast or via direct denudation of the landmass in the south. Smectite has been dominantly present in marine clay suspensions since the deposition of the smectite-rich Chattian Voort sands and this clay mineral assemblage remains intact during the Early and Middle Miocene times.
The kaolinite- and illite- rich clay mineralogy of the Opgrimbie facies reflects a continental provenance. Possibly it represents the denudation of the Ardennes-Rhenish Massif consisting for a large part of illite-rich pelites and having an kaolinite-rich paleo-alteration cover (Yans, 2003). Hermanns (1992) furthermore identified kaolinite-illite clay in the continent-sourced Lower Miocene deposits of the Lower Rhine Basin. Nevertheless, it has to be noted that the Opgrimbie quartz-sands were purified by post-depositional leaching processes (Van Loon, 2009), which probably also affected clay minerals. In such conditions, kaolinite is expected to occur relatively enriched in the leached sediment as all other clays are more easily dissolved and removed from the sediment (Chamley, 1989).

IV.5 CONCLUSIONS

Smectite is the dominant clay mineral in marine deposits of the Berchem and Bolderberg Formations. The bulk and clay mineralogy of all these units is so similar that no use of it can be made for stratigraphic differentiation. Pelletal glauconite content in the Houthalen Member (on average 16%) is nonetheless significantly lower compared to Berchem Members (37% for Edegem, 33% for Kiel and 47% for Antwerp). The mineralogy of clay-sized and pelletal glauconite are so similar that they must be related, although clay-sized glauconite appears to be slightly more expandable compared to pelletal glauconite. This is most likely related to increased weathering of clay-sized glauconite during or after abrasion. The clay mineralogy <2µm of the Genk Member contains no trace of glauconite-smectite, but the clay mineralogical assemblage found in the Houthalen Member and Berchem Members, remains largely the same.

In contrast, the clay mineralogy of the Opgrimbie facies is kaolinite- and illite-dominated. This composition is interpreted as the signal of continental denudation whilst the smectite-dominated glauconitic sand deposits have a marine sediment provenance area. In this scheme, the Genk Member lacks the abundance of glauconite pellets but still has a marine provenance signature. Therefore it is considered as a marginal coastal sand deposit whilst the Opgrimbie sand is deposited under full continental conditions.

CHAPTER V

THE TORTONIAN AND MESSINIAN DIEST SAND CASE

V.1 THE MID-MIOCENE UNCONFORMITY & CLIMATE-TECTONIC EVENTS

Seismic profiles in the central and northern part of the North Sea indicate that Tortonian and Messinian sediments in the North Sea area rest unconformably on early and middle Miocene deposits, which is named the mid-Miocene Unconformity (MMU) (intensely studied for southern North Sea basin by Kuhlmann, 2004). Although the exact age of this MMU is still under discussion, most authors report this event during the Langhian or at the Langhian-Serravalian transition (ca. 15-13Ma), which places it during the hiatus between the Berchem-Bolderberg Fm and the Diest Fm (Utescher et al., 2012; Schäfer and Utescher, 2014; Rasmussen and Dybkjaer, 2014). The exact cause of the MMU however, remains a point of discussion. Nevertheless, important tectonic events occurred during Langhian and Serravallian times as evidenced by the inversion of the Weald Basin in England (King, 2006), the closing of the eastern passage way of the Mediterranean Sea (Rögl, 1999) and gas expulsions in the North Sea (Andresen *et al.*, 2009). Also paleoclimatic conditions changed drastically (Figure 26) during the Mid-Miocene Climatic Optimum with a strong cooling and eustatic sea-level drop (Zachos *et al*., 2001). Furthermore, during the middle Miocene, an important paleogeographic development of the Rhine system occurred with clastic material from the uplifting Ardennes and northeastern France actively being transported to the Lower Rhine graben (Sissingh, 2003, 2006). These changes ended the major peat deposition in the Lower Rhine area and introduced a new period of, coarse, clastics prograding over the peat deposits in Rhine graben area in Germany and the Netherlands during the Tortonian (Schäfer *et al.*, 2004; Wong *et al.*, 2007; Schäfer and Utescher, 2014). In Belgium, differential tectonic movements between a subsiding Campine and an uplifting border have been documented by De Man et al.,(2010) and Vandenberghe and Mertens (2013) at the end of the Rupelian and the renewed subsidence of the Roer Valley Graben during the Chattian is well documented by its thick deposits (a.o. Voort Fm). It is most likely that the tectonic and sedimentary evolution of the Lower Rhine Graben area during the middle and late Miocene also influenced the sediment dynamics and provenance of the Tortonian-Messinian Diest Formation in the Campine Basin as discussed by Vandenberghe et al. (2014).

According to Wouters and Vandenberghe (1994), the regressive character of the continental part of the Bolderberg Formation introduced a period of non-sedimentation during the Serravallian. A large and deep erosional valley was formed, locally eroding more than 100m Rupelian Boom Clay (Figure 5.2 and Figure 5.3). The SW-NE orientation of this valley extends from the Hageland area to Limburg (Demyttenaere, 1989), crosscuts the formations of Berchem and Bolderberg and was filled by the Diest Formation (Figure 5.1, Figure 5.2 and Figure 5.3). Vandenberghe et al. (1998) considered that the valley erosion was related to a period of combined low sea level and tectonic uplift in central Belgium. Recent mapping of the base of the Diest Fm (Matthijs *et al.*, 2013) shows that erosional incisions also occur outside the main valley, even in the western Campine area (Figure 5.4). Today, the sediments of the valley fill crop out in the central part of Belgium where its top is cemented with limonite leading to the typical NE-SW oriented hilly morphology in the Hageland region.

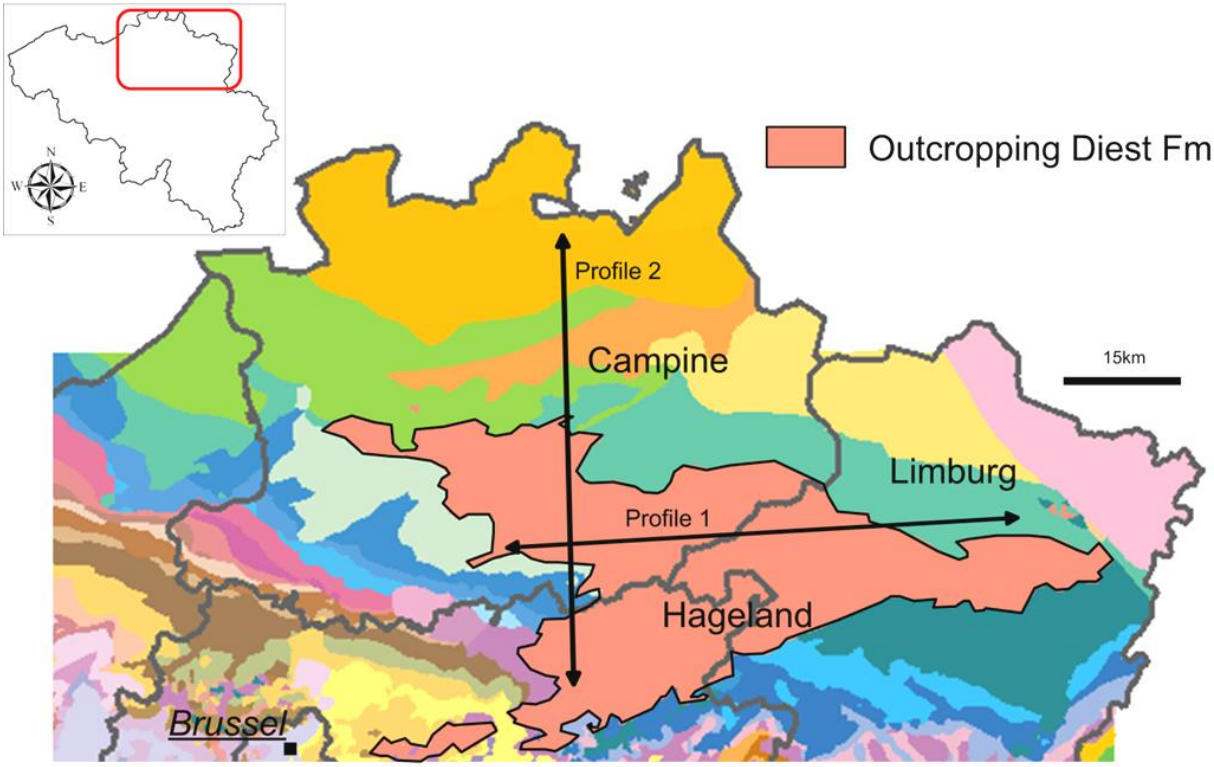

Figure 5.1. Cenozoïc geological map of northeast Belgium with indication of the geographic regions Campine, Hageland and Limburg and the capital city of Belgium, Brussels. The position of the two profiles (Figure 5.2 and Figure 5.3) lines are indicated. Map modified after ALBON (2009).

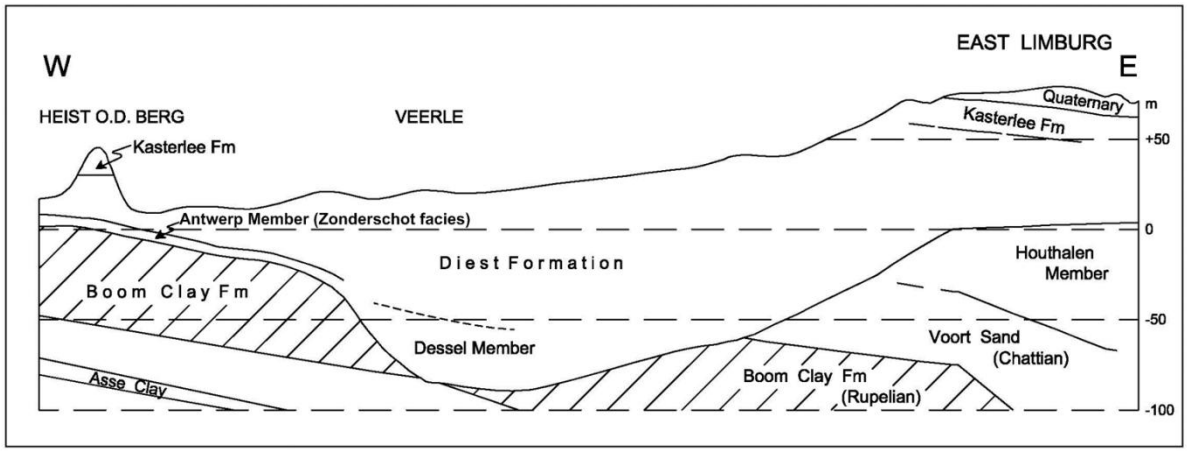

Figure 5.2. East-west profile from Heist-op-den-Berg, across the Veerle borehole to eastern Limburg showing the the Diest Formation valley (Veerle borehole) eroding Houthalen Sands and Voort Sands in the east and Antwerp Sands (Zonderschot facies) in the west. In the centre of the erosion, almost the entire Boom Clay is removed (after Vandenberghe et al., 2014). For location see “profile 1” on Figure 5.1.

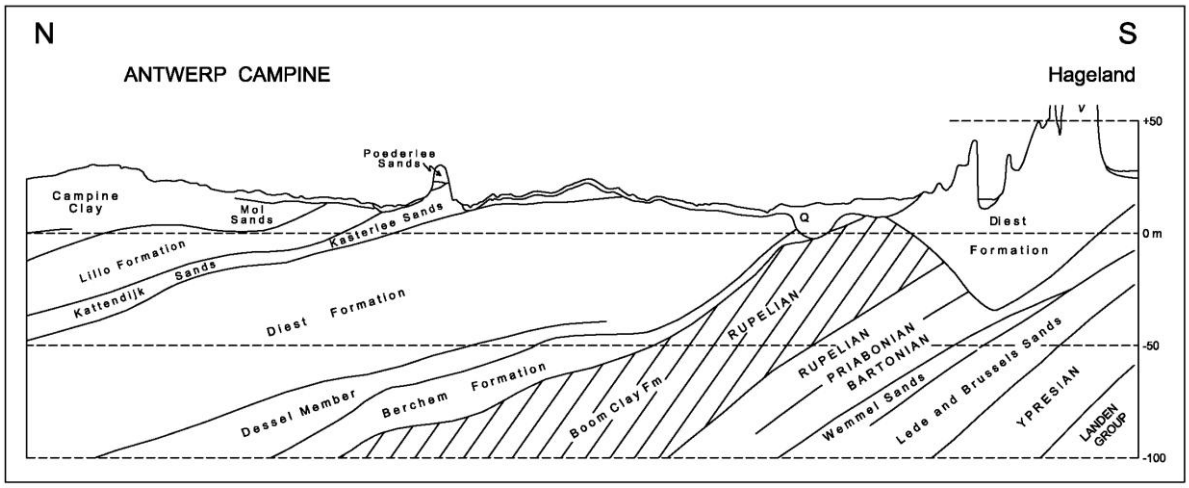

Figure 5.3. North-south profile from the Antwerp Campine extending to the Hageland area showing the position of the north-dipping Diest Formation in the Campine and the Hageland. Furthermore, it illustrates the intensive erosion and hilly nature of the Diest Formation in the Hageland region (simplified from Laga, 1975). For location see “profile 2” on Figure 5.1.

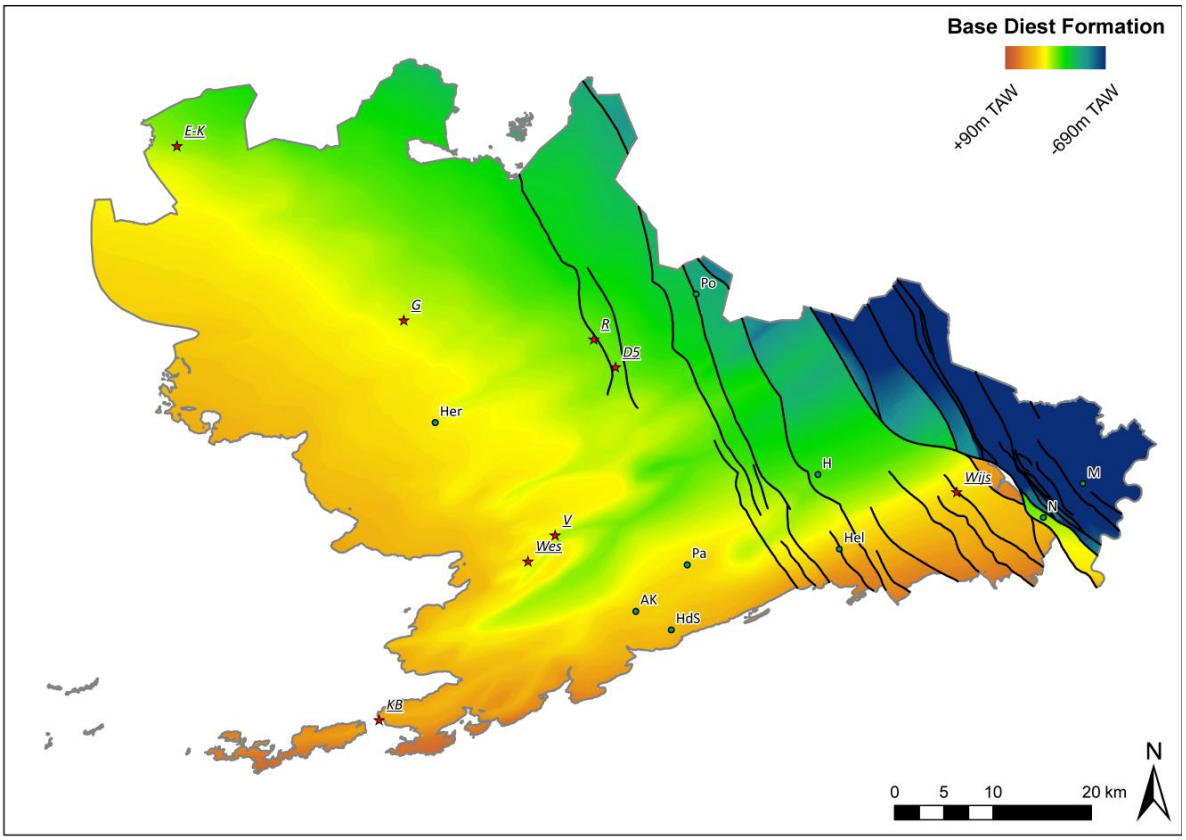

Figure 5.4. Map showing the base of the Diest Formation. Note the existence of multiple southwest-northeast oriented gullies, not only in the Hageland but also in the Campine area above (modified after Matthijs *et al.*, 2013).

V.2 STRATIGRAPHY

The stratigraphy of the Diest Formation is mainly based on biostratigraphy of dinoflagellate cyst assemblages. Louwye et al. (1999; 2007) report DN8, DN9 and DN10 as dinoflagellate cyst biozones in the Diest Formation, which means the Diest Formation was deposited mainly during the Tortonian, and extending into the Messinian. At present, two members have been assigned to the Diest Formation which both are glauconitic, relatively fine-grained sand units and contain calcareous fossils: the Dessel Member in the Campine and the Deurne Member in the Antwerp area (Laga et al., 2001; website National Stratigraphic Commission Belgium www.natstratcommbelgium.drupalgardens.com , last consulted 01-2015). Both defined members are, at least partially, time-equivalent as the Deurne Member contains the DN8 dinoflagellate cyst biozone, while in the Dessel Member both DN8 and DN9 dinoflagellate cyst biozones are found (Louwye, 2002). The main mass of glauconitic sand in the Diest Formation however, has not been given a specific stratigraphic status or name. This is an unsatisfactory situation and in this work the term Diest sand member is used for these sands. This follows the description used by Vandenberghe et al. (2014), who distinguished a Campine Diest member overlying the Dessel Member and a Hageland Diest member, as subdivisions of the Diest Formation. This Diest sand member consists of poorly sorted, coarse, very glauconitic sands with low clay contents. Additionally, some specific facies of the Diest sand member have been reported (Figure 5.5): the glauconite-poor Poppel facies in the top of the Diest Sands in northern part of the Campine (Laga and Notebaert, 1981), the fine- to medium-grained Gruitrode facies with occasionally calcareous macrofossils (Sels *et al.*, 2001) and the quartz-rich Opoeteren facies in Limburg (Gulinck, 1964). Also the glauconitic sand on top of residual hills in the western part of Flanders have been argued to belong to the Diest Formation.

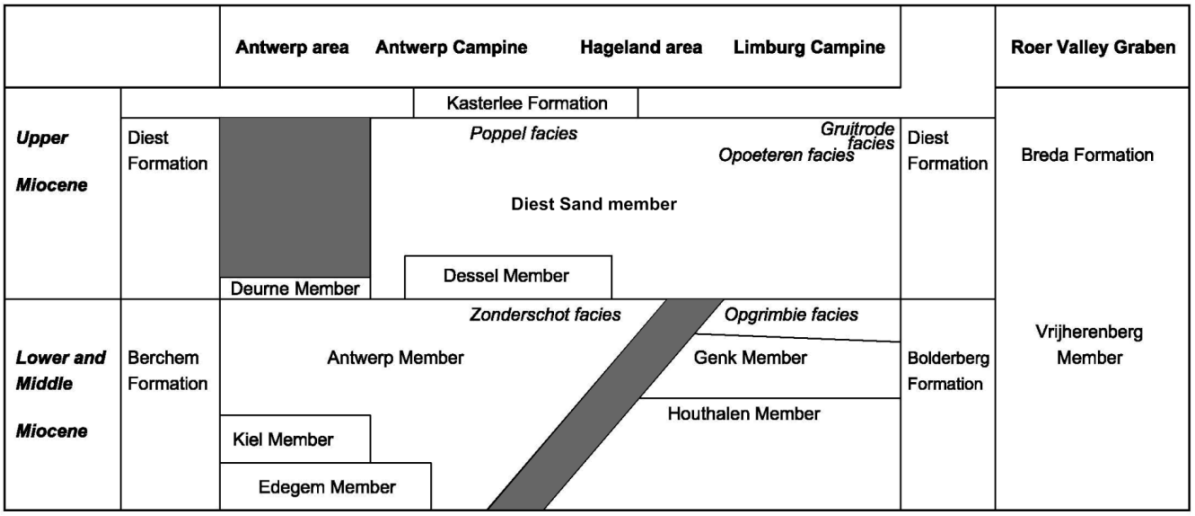

Figure 5.5. Stratigraphy of the Miocene deposits in central and northern Belgium, in the Roer Valley Graben and in the southern Netherlands. The dark area above the Deurne Member indicates the absence of Miocene deposits older than the Deurne Member in the Antwerp area. The dark area between the Bolderberg and Berchem Formation is drawn because both formations never occur in close contact because of the deep erosion gully separating both.The term facies is used when a particular name has been given in descriptions without formally identifying this sand unit as a separate lithostratigraphic unit (after Vandenberghe et al., 2014).

V.3 THE RELATIONSHIPS BETWEEN REGIONAL DIEST UNITS IN THE CAMPINE AND THE HAGELAND AREA AND ON TOP OF THE FLEMISH HILLS.

There are several indications suggesting that the occurrence of the Diest Formation in the Hageland region and the Campine occurrence of the Diest sand member could be stratigraphically different (Vandenberghe *et al.*, 2014):

1) **Biostratigraphic content**. Whereas the Campine Diest sand member contains dinoflagellate cyst biozones DN8, DN9 and DN10, neither calcareous nor organic-walled fossils are found in the Hageland (Figure 5.6). Since stratigraphically meaningful fossils are lacking, the exact stratigraphical position of the Diest sand member in the Hageland area remains debatable.
2) **Heavy minerals**. Although a systematic study for this specific purpose is lacking, published heavy mineral data for the Campine Diest occurrence are different compared to those of the Diest sand in the Hageland. The main difference is the high garnet content (ca. 30%) and relatively low ubiquist content (ca. 45%) in the Campine compared to relatively high ubiquist content (ca. 60%) and almost absence of garnet (ca. 3%) in the Hageland. Garnets are also abundant in samples of the Dessel and Deurne Members while heavy minerals of Diest sand member samples in Limburg seem to match the results of the Hageland area (Geets and De Breuck, 1991; Gullentops, 1963; Gullentops and Huyghebaert, 1999).
3) **Sediment transport directions**. Van Calster (1960) and Gullentops (1963,1988) have reported in the Hageland outcrops the systematic presence of oblique stratifications showing sediment transport to the northeast (Figure 5.4). In the Campine area however, large-scale clinoforms are observed with progradational directions to the northwest and to the southwest close to the graben area (Demyttenaere, 1989) and to the northwest in the centre of the Campine (De Batist and Versteeg, 1999; Vandenberghe et al., 2014). It is likely that the latter progradation directions are part of the same clastic delta system that progressively filled the Roer Valley Graben during the Miocene as described by Schäfer *et al*. (2004) and Wong *et al*.(2007).

The stratigraphic position of the limonitic and slightly glauconitic sand at the top of the residual Flemish hills in southwest Flanders and Northern France (Figure 5.7) can be disputed as the sand contains no stratigraphically meaningful fossils. Based on the lithological resemblance and the geometric position with respect to the Hageland hills, Gullentops (1957) and Tavernier and de Heinzelin (1962) have assigned these deposits to the Diest Fm, which is also their stratigraphic position on the old 1:40 000 and the new 1:50 000 maps of the area. Houthuys (2014) has reinvestigated the outcrops in the area. Based on lithostratigraphic subdivisions and correlations, facies analysis and regional geometrical considerations this author has concluded that the top sand of the hills does not belong to the Diest Formation and he proposes a Late Eocene age for these deposits.

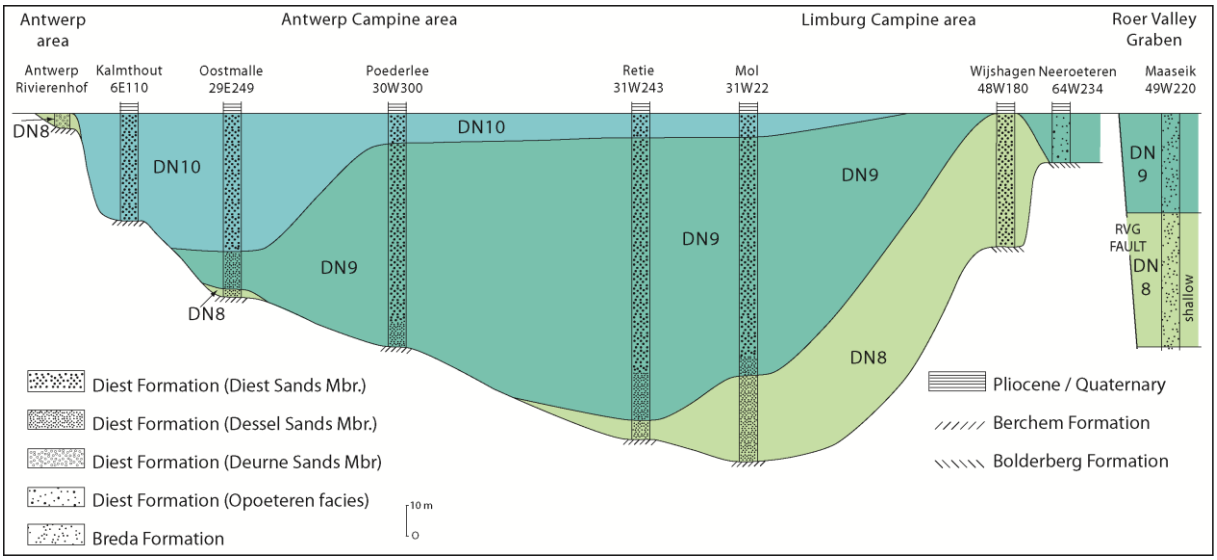

Figure 5.6. Northwest-southeast profile based on boreholes through the Campine Basin indicating the dinoflagellate cyst biozones DN8, DN9 and DN10 (after Vandenberghe et al., 2014).

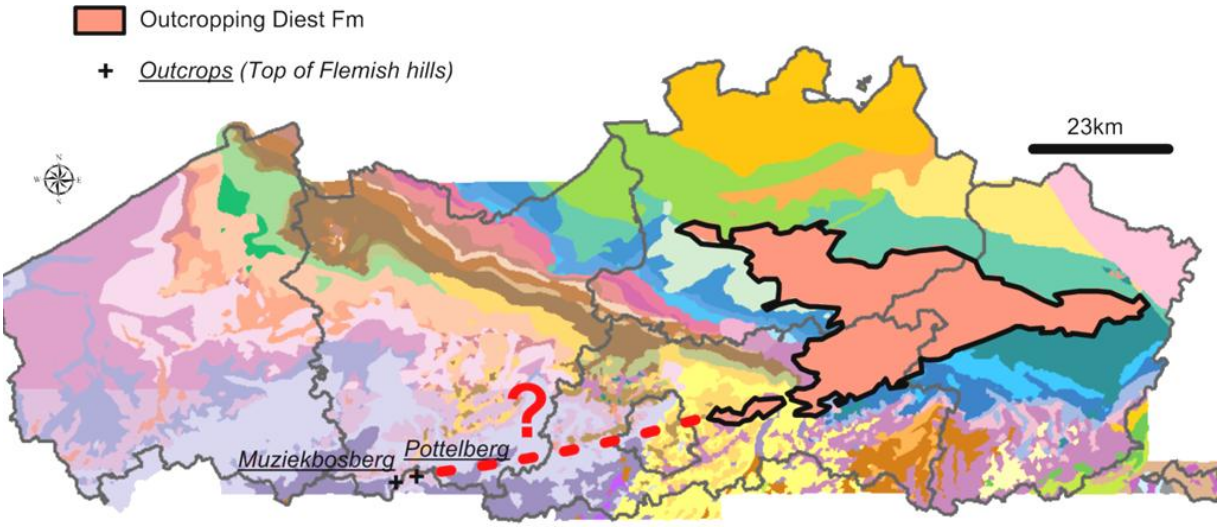

Figure 5.7. Geological map of Flanders with the outcrop area of the Diest Fm highlighted. In the western part of Flanders, at the top of the Flemish hills such as Muziekbosberg and Pottelberg, the Diest Fm also occurs. The dotted line in red shows the possible extension of the NE-SW orientation of the Diest Formation in the Hageland area towards the western part of Flanders (modified after ALBON, 2009).

V.4 A MODERN PALEOGEOGRAPHIC MODEL

In the previous section it was demonstrated that there are indications that the Hageland and Campine Diest Sands do not belong to the same stratigraphical system and might have, at least in part, different provenance areas. Furthermore, as the sand on top of the Flemish hills could very well be unrelated to the Diest Formation, the area of southwest Flanders and Northern France is left out of the paleogeographical discussion.
Paleogeographic sketches were produced by Vandenberghe et al., (2014) based on the different available data and maps supplemented by radiometric K-Ar dating on glauconite pellets (Figure 5.8). Glauconite dates for the Hageland area and the base of the Diest Fm in the Campine were found to be of Langhian age while a Burdigalian age was given to glauconite pellets from the middle to top Diest sands in the Campine. Given the overall thickness and high glauconite content of the Diest Formation and considering the intense erosion prior to deposition (e.g. Figure 5.2 and Figure 5.3), the pelletal glauconite of the Diest Formation is most likely massively reworked from older Miocene deposits. The paleogeographic model proposed by Vandenberghe et al.(2014) implies that glauconite in the northern to northwestern Campine Diest is derived from the Antwerp sands and lateral time-equivalents (Burdigalian to Serravalian) while pelletal glauconite in the Hageland and incised valley fill Diest sand was reworked from the Langhian Houthalen sands or more probably from the Zonderschot facies of the Antwerp sands. Vandenberghe et al. (2014) estimate the volume of reworked pelletal glauconite around 50%.

The Late Serravallian (Figure 5.8) is characterized by a time of uplift in northern France and southwest Belgium (Van Vliet-Lanoë et al., 2002, 2010). Sedimentation was restricted to the Rhine Graben area with peat deposits being relayed by estuarine Neurath Sands to the north and further in that direction, by marine argillaceous green sands of the Breda Formation (Wong et al., 2007). In the Campine area, the land surface was incised by a river system eroding mainly early to middle Miocene deposits of the Berchem Fm (Antwerp Sands). The eroded Antwerp sands and their lateral time equivalent sediments were then redeposited in submarine fans at the fault boundary marine area. During the Early Tortonian (Figure 5.8), a low-energy marine transgressive pulse from the north delivers shallow marine, relatively fine-grained, deposits in the Campine Basin which are characterized by the DN8 dinoflagellate cyst biozone. These deposits comprise the Deurne sands in Antwerp, the Dessel sands and part of the Diest Sands in the Campine and in east Limburg.

Vandenberghe et al.,(2014) and Houthuys (2014) propose that the Hageland Diest sands were formed in a semi-enclosed tidal embayment and that deep incisions were formed by flow constriction, as already inferred for the Brussels sands by Houthuys (2011). This model comprises a lateral fill of the NE-SW oriented tidal embayment immediately after deep channel erosion, which was caused by strongly enhanced ebb currents in narrowing channels. The NW-SE transgression, depositing the DN8 Deurne, Dessel and basal Diest sediments might have played the role of the lateral fill causing sand pressure and flow constriction. The main argument of Vandenberghe et al. (2014) to suggest a DN8 age for the Hageland Diest sand member is the correlation of the Hageland Diest sand in the Veerle borehole with the DN8 Diest found in the Wijshagen borehole (Figure 5.6). The NE-progradational direction of oblique stratifications in the Hageland area furthermore indicates that this unit is a Highstand System Tract deposit (HST).

The DN9 biochron is characterized by an important renewed transgressive pulse from the north depositing coarser Campine Diest sand over the DN8 Deurne, Dessel and basal Diest sand (Figure 5.8). Simultaneously, the Rhine delta in the east produced massive amounts of coarse-grained quartz-rich sands after the rearrangement of the Rhine river system. These quartz-rich deposits are grouped in the Kiezeloöliet Fm, a coarse braided river facies (Schäfer et al., 2004). Vandenberghe et al. (2014) imply that the prograding Rhine delta front causes the introduction of a new sediment type, a mixing of coarse quartz sands with the redeposited Antwerp and time equivalent sand sediments which are then swept over the Central Campine area and form the main mass of the coarser Diest Formation in the central Campine area during biochron DN9. During the DN10 biochron, the Kiezeloöliet Fm prograded further to the northwest, and the coarse quartz-sand – reworked Antwerp sand mixture was shifted to the western part of the Campine area (Figure 5.8).

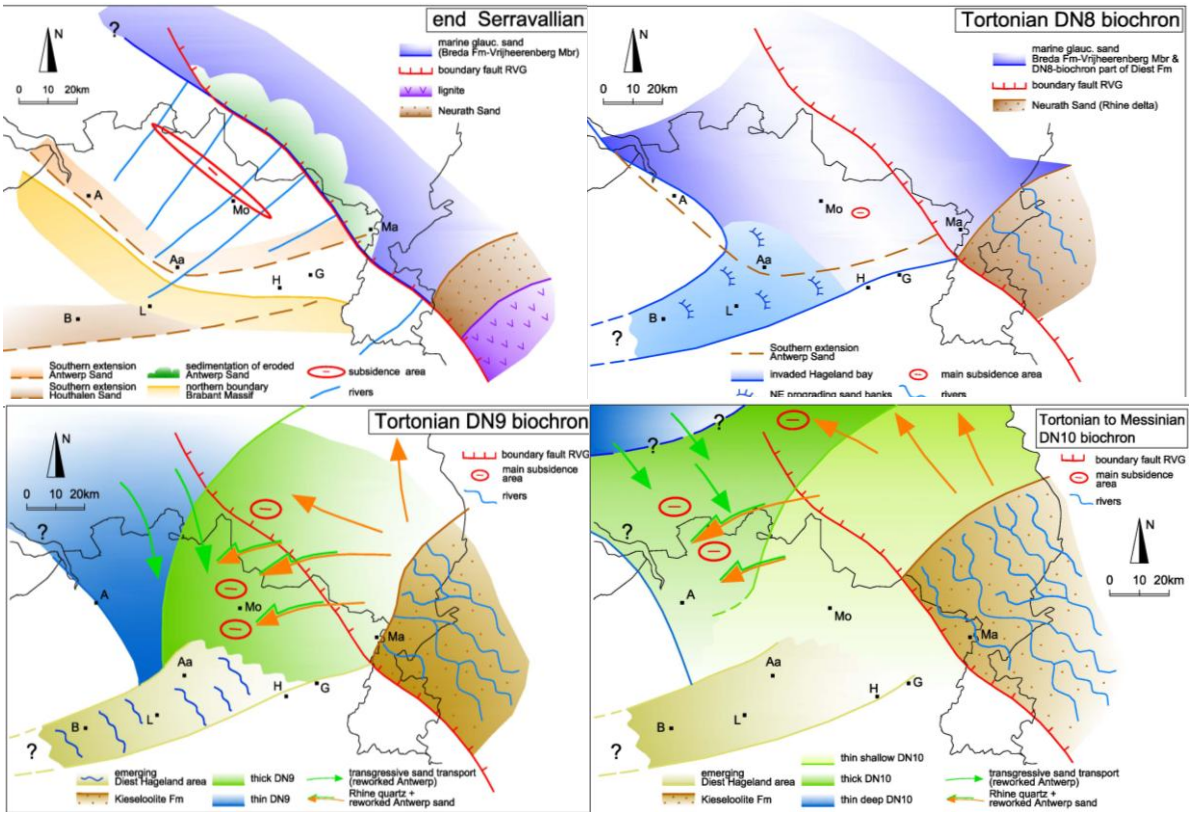

Figure 5.8. Paleogeographic maps of the Campine Basin during the Middle to Late Miocene (Vandenberghe et al., 2014). A=Antwerp; Aa=Aarschot; B=Brussel; H=Hasselt; G=Genk; L=Leuven; M=Mol; Ma=Maaseik.

V.4 SAMPLES FOR MINERALOGICAL AND SEDIMENTPETROLOGICAL ANALYSIS

Paleogeographical studies of the Diest Formation as outlined above suffer from the absence of systematic sediment petrographical data. In particular such data in relationship with the recently available biostratigraphic characterisation are lacking. Grain-size distributions and pelletal glauconite contents have been analysed in several boreholes (Broothaers, 2000; Wouters and Schiltz, 2011; Labat et al., 2011). Heavy mineral analyses are published by Gullentops (1963) and Geets and De Breuck (1991) but bulk mineralogical and clay mineralogical data are very scarce (Berckmans and Wouters, 2003). The objective of this chapter is to provide such mineralogical and petrographic reference data (bulk mineralogy, clay mineralogy <2µm, glauconite content and mineralogy, grain-size distribution) for the different stratigraphic units distinguished in the Diest Formation and to understand their areal variability.

Sampling of the Diest Formation was performed in boreholes in the Campine subsurface and from outcrops in and around Antwerp and in the Hageland (Figure 5.9). Additionally, outcrop samples were collected from the top Flemish hills, west from Brussels on the Muziekbos- and Pottelberg (Figure 5.7). For sand samples, bulk mineralogy <32µm, clay mineralogy <2µm, pelletal glauconite content and mineralogy and the total grain-size distribution was systematically analyzed. Additionally, particle shapes for quartz grains were analyzed from a selection of Campine and Hageland Diest sand member samples. For clay lamina samples, the bulk mineralogy (on total samples), clay mineralogy <2µm and grain-size distribution was determined (see Chapter I).

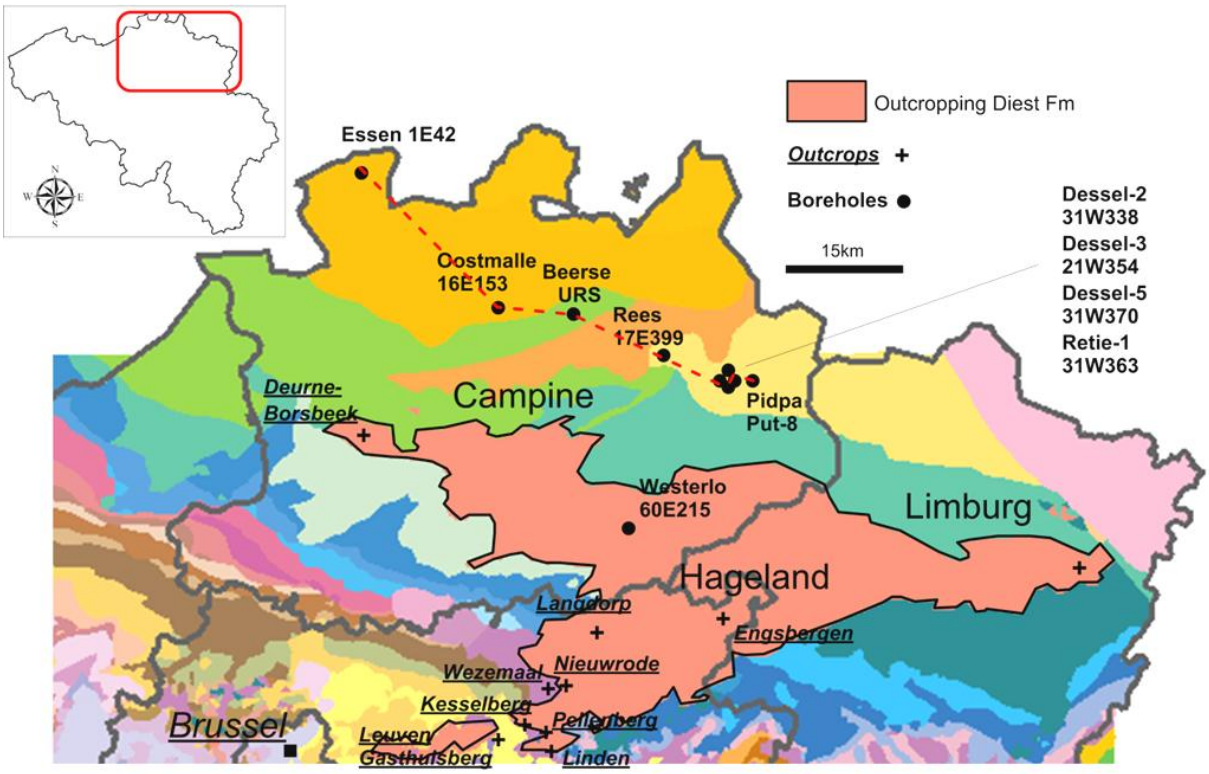

Figure 5.9. Geographical spread of samples in outcrop and borehole cores. The red dotted line indicates a profile line illustrated later in this work. Outcrop sections are underlined. Boreholes numbers refer to codes of the Geological Survey of Belgium (GSB). Map modified after ALBON (2009).

V.5 RESULTS

In this section, the results of all investigated boreholes and outcrop sections are discussed. For each borehole and outcrop, if present, the elements on which the current stratigraphic interpretation is based are discussed. Then, the results of the current research are presented. The final end-product of each borehole is a comprehensive log containing most relevant mineralogical and petrological data with depth for all samples and the existing interpreted stratigraphic subdivisions within the Diest Fm and of underlying units. Different subdivisions within the Diest Fm will be made based on the new data. For this subdivision, clay mineralogy is an important factor but also other sediment petrological criteria such grain-size, non-clay minerals, pelletal glauconite content and mineralogy and occurrence of carbonates are decisive criteria:

- **Published stratigraphy:** Deurne Member, Dessel Member, Diest sand member (based on grain-size properties and fossil content)
- **Geographical occurrence:** Campine, Hageland, Limburg, Flemish hills
- **Sediment petrological parameters:**
  - Grain size
  - Mineralogy
  - Clay mineralogy
  - Pelletal glauconite content and mineralogy
  - Occurrence of carbonate minerals: calcite, aragonite, siderite

The litho-units defined are identified in the different outcrops/boreholes presented below and are further discussed in the section following the results. A NW-SE oriented profile is drawn afterwards (see Figure 5.9). In this results section, all results of samples belonging to the Diest Formation are discussed. This means that the results of the Rees, Dessel-2, Dessel-3 and Retie-1 boreholes, which were essentially sampled to unravel the Mol-Kasterlee-Diest stratigraphic issue (see

Chapter VI), are only discussed as far as the analyses are relevant for the Diest Fm. Criteria marking the Diest-Kasterlee transition and boundary, and the crucial analyses used for this purpose are therefore discussed in Chapter VI. The results for the Essen 1E42 borehole are not included in this section because of the stratigraphic uncertainty of the interval which has been interpreted as "Diest Formation". All results of the Essen 1E42 borehole are therefore incorporated in appendix.

V.5.1 MINERALOGY, CLAY MINERALOGY AND SIZE DISTRIBUTION

V.5.1.1 Deurne-Borsbeek outcrops

Three samples were collected at the base of the Deurne Member in a temporary outcrop in Borsbeek, near the Deurne airport. The first two samples were collected in an intensely bioturbated facies less than 1m from the base of the Deurne Member, marked by a basal gravel. A third sample was collected somewhat higher up in the section, in a less bioturbated part with cross stratification (Table 5.1). This last sample was collected in the foresets.

Bulk mineralogy <32µm
The bulk mineralogical composition <32µm consists mainly of 2:1 Al-clays (24-36%) and 2:1 Fe-clays (27-45%). All three samples contain carbonate minerals, both calcite and aragonite and traces of siderite. In sample RU209, a particularly large amount of gypsum was quantified (18%) as well as high amounts of pyrite (8%). Sample RU210, collected in the foresets, seems to be enriched in both quartz and 2:1 Fe-clays compared to the two bioturbated samples (Figure 5.10).

Clay mineralogy <2µm
The clay composition <2µm of the two bioturbated Deurne samples (Figure 5.11) is almost identical with mainly smectite (35-37%), illite-smectite mixed-layers (38%). Illite occurs between 12-14% whereas kaolinite is less frequent (7-8%) and chlorite only occurs in traces. Higher expandable glauconite-smectite with 27% expandable layers, occurs only around 4-5%.
In the foreset sand sample (RU210), glauconite-smectite is much more abundant (25%) with higher-expandable glauconite-smectite (22%) clearly predominating the low-expandable type (3%). Note that this clay mineral composition is very similar to the composition encountered in the Berchem and Houthalen Member deposits (Figure 5.12).

Pelletal glauconite content
The pelletal glauconite of the three Deurne Member samples, as determined by magnetic separation, is 46%, 39% and 40% (Table 5.1). Pelletal glauconite mineralogy is dominantly of the higher-expandable type, with 27% expandable layers) (Table 5.2).

Size distribution
The three Deurne Member samples have a very similar grain-size distribution (Figure 5.13) with distribution modes ranging from 270-280µm and around 12% of grains >355µm.

Table 5.1. Position and lithology and pelletal glauconite content of the Borsbeek Deurne Member samples.

Sample	Position	Lithology	Pelletal glauconite content
RU208	10 cm above basal gravel	Bioturbated sand	46%
RU209	40 cm above basal gravel	Bioturbated sand	39%
RU210	1.5m above basal gravel	Sand with cross stratification	40%

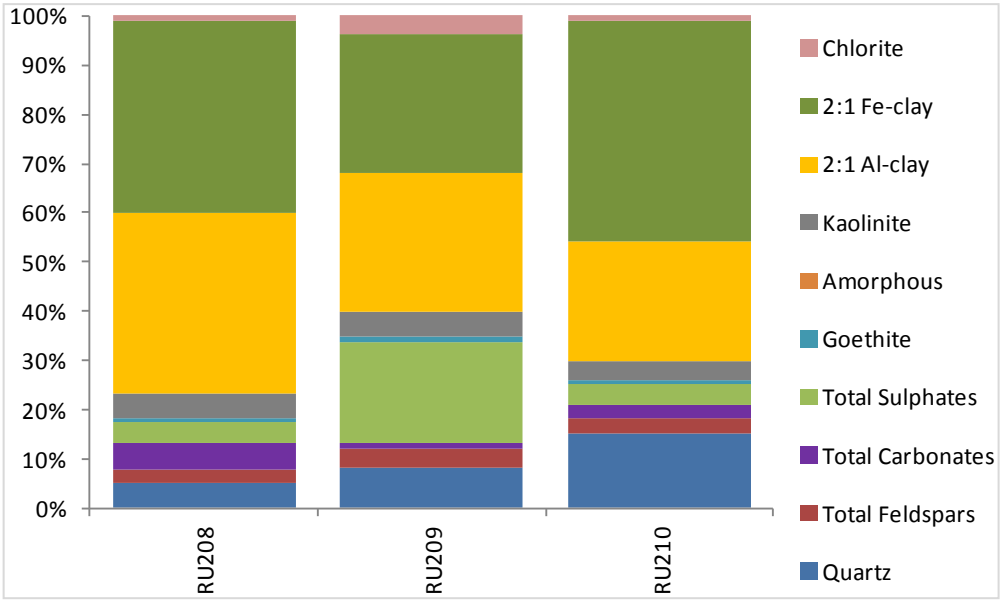

Figure 5.10. Deurne Member samples from the Borsbeek temporary outcrop: bulk mineralogical composition <32µm.

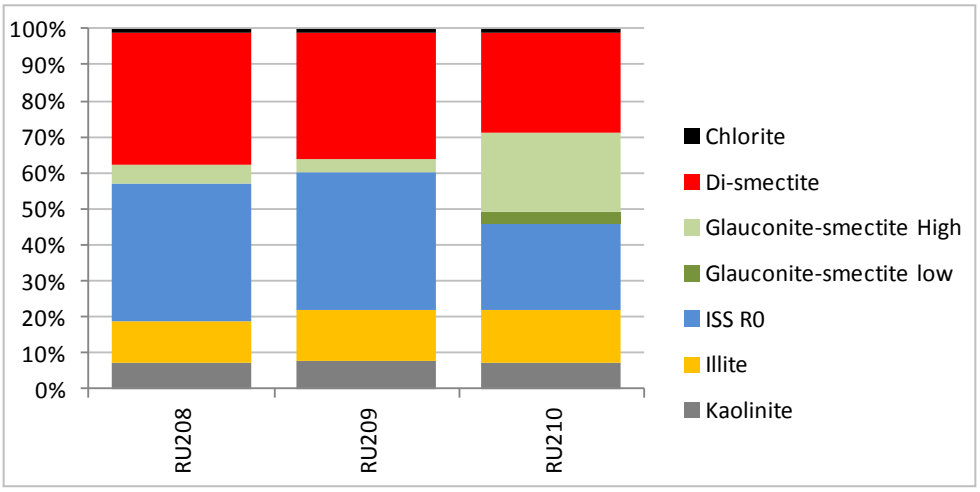

Figure 5.11. Clay mineralogical composition <2µm of the Deurne Member samples collected at the Borsbeek temporary outcrop.

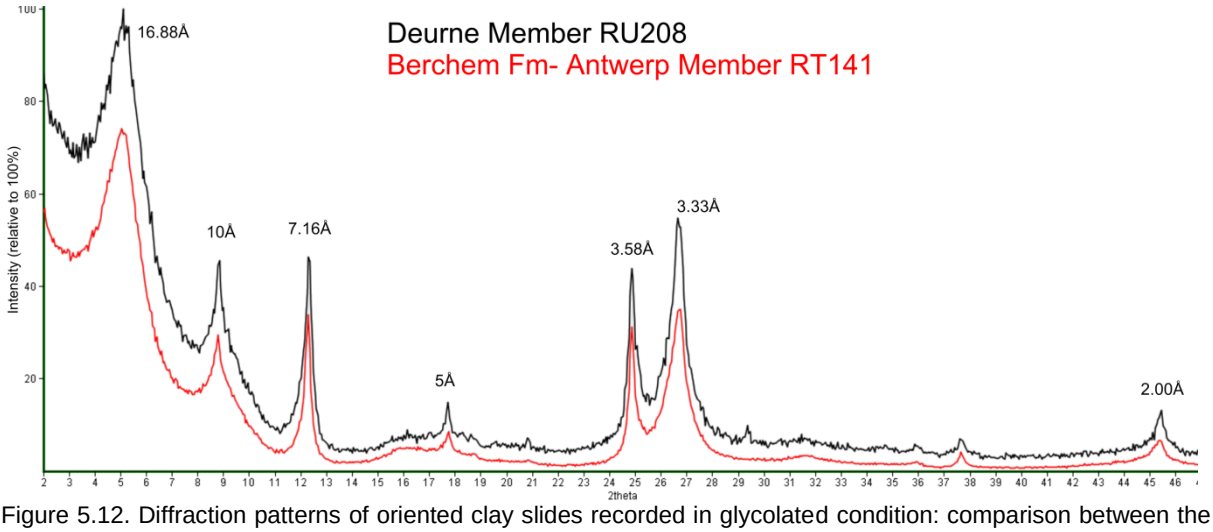

Figure 5.12. Diffraction patterns of oriented clay slides recorded in glycolated condition: comparison between the Deurne Member RU208 sample and Antwerp Member sample RT141.

Table 5.2. Pelletal glauconite content and expandability of the Deurne Member samples from the Deurne-Borsbeek outcrop.

Sample	Member	Content (%)	d060	Higher expandable G-S (27% expandable)	Low expandable G-S (5% expandable)	Total amount Glauconite layers	Total amount Expandable layers
RGU208	Deurne	46	1.5153	41	59	86	14
RGU209	Deurne	39	1.5153	45	55	85	15
RGU210	Deurne	40	1.5153	40	60	86	14

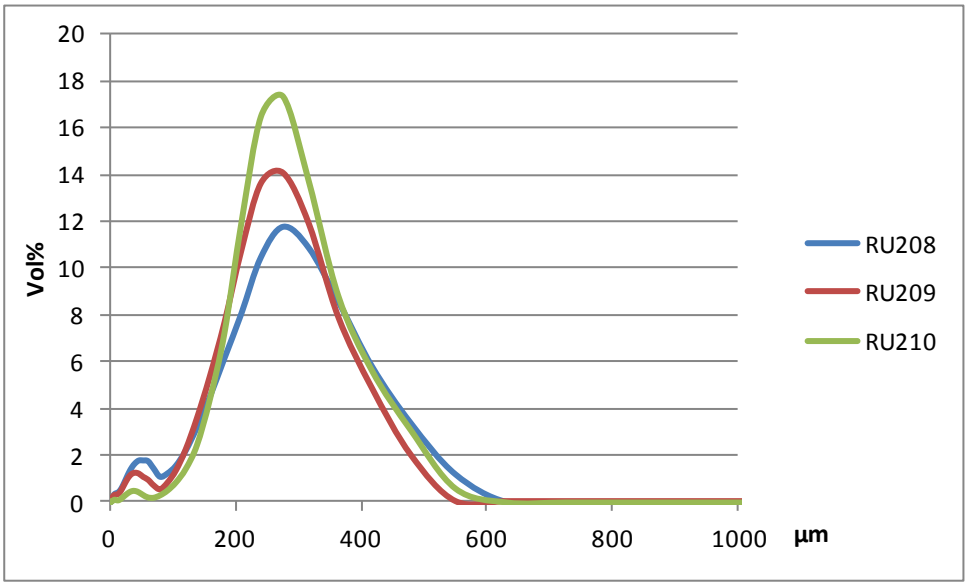

Figure 5.13. Size distribution of Deurne Member samples.

V.5.1.2 The Oostmalle-Rijkevorsel 16E153 borehole (Figure 5.14)

Stratigraphic description by Gulinck and Laga (1975a)

The original description of the Oostmalle-Rijkevorsel borehole is given by Gulinck and Laga (1975a). Based on calcareous foraminifera assemblages, they interpreted the base of the Diest Formation at 138.10m depth, on top of the Berchem Fm. The 135.90 - 138.10m interval is glauconite-rich and slightly calcareous with also shell fragments dispersed in the sand matrix. This 135.90 - 138.10m interval contains the typical foraminifera assemblage of the Dessel Member. Above 135.90m, the glauconitic sediment is often bioturbated and becomes non-calcareous. Nevertheless, based on grain-size properties and local shell debris in the 124-125m interval, the total 111-138.10m interval was assigned to the Dessel Member by Gulinck and Laga (1975a) (Figure 5.14). The Berchem Formation below (138.1-154m) is a green to black glauconitic fine and calcareous sand with shells and variable clay content which occurs dispersed in the sediment but also as brown laminae or lenses in the sand matrix.

Samples

In total, 9 sand samples were collected from the 16E153 Oostmalle-Rijkevorsel borehole in order to document the transition between the Berchem and Diest Formation (Dessel Member) and explore the variability within the Dessel Member (Table 5.3).

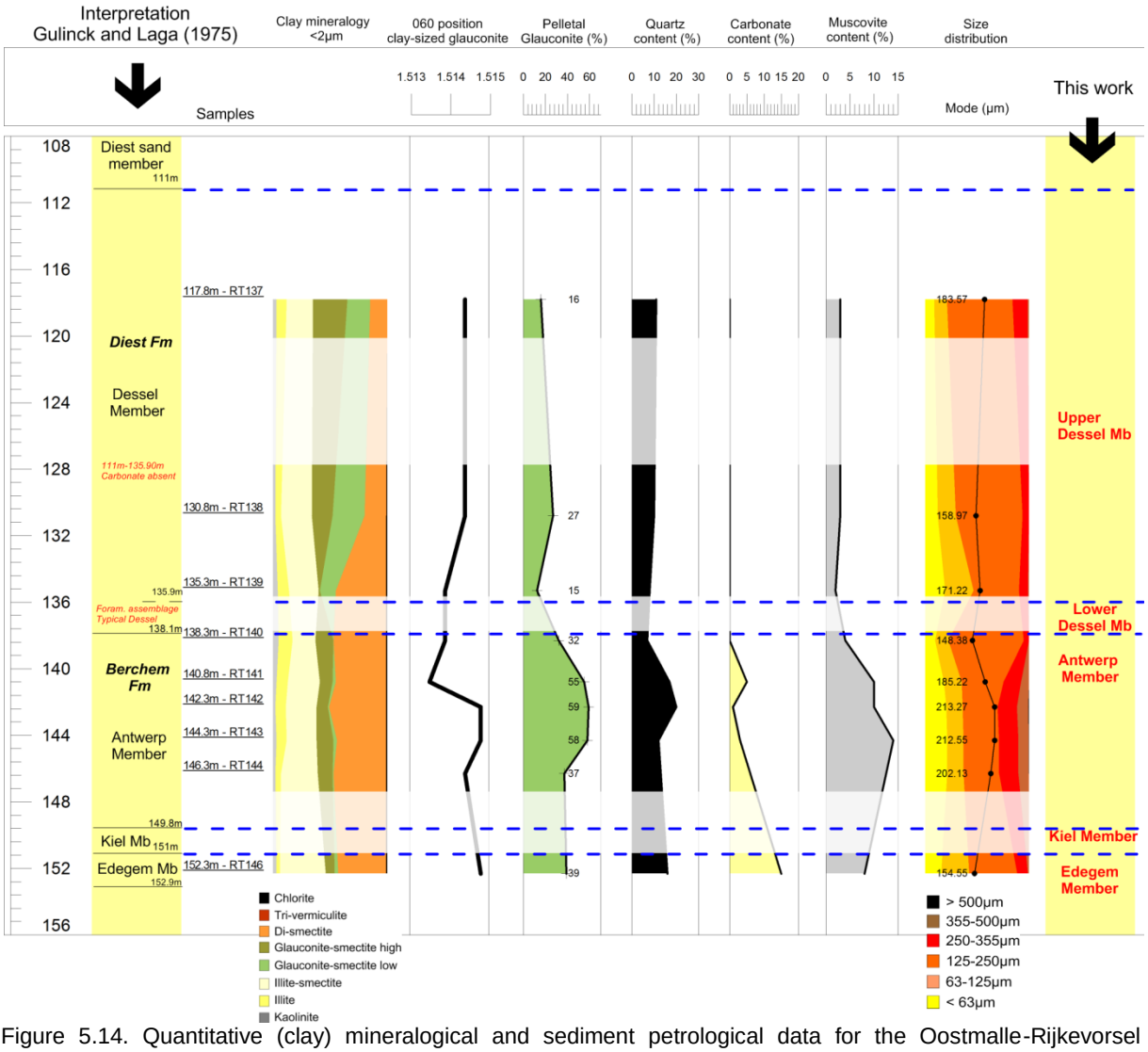

Figure 5.14. Quantitative (clay) mineralogical and sediment petrological data for the Oostmalle-Rijkevorsel borehole. Geophysical well log data are given on the left with the original interpretation of Gulinck and Laga (1975a). Sample levels are indicated as underlined text right of the geophysical well log data. The different columns in the middle part summarize (clay) mineralogical data and size distribution with indication of the distribution modes. On the right side, the lithostratigraphic interpretation of this work is presented. Blurred transparent zones indicate a range from which no samples were analyzed. Data points in these 'no-sample" ranges may therefore be not continuous, as is suggested on the figure. While Gulinck and Laga (1975a) named the entire 111-138.10m interval as the Dessel Member, the current research makes the difference between an upper Dessel Member without carbonates and a lower Dessel Member with the typical foraminifera assemblage of the Dessel Member Gulinck and Laga (1975a). The distinction Antwerp – Kiel – Edegem Members was kept from the original interpretation.

Table 5.3. Samples of the Rijkevorsel-Oostmalle borehole. "Gl sand" indicates "glauconitic sand".

Sample code	Depth (below ground level)	Stratigraphy	Lithology
RT137	117.8m	Diest Fm	Gl sand
RT138	130.8m	Diest Fm	Gl sand
RT139	135.3m	Diest Fm	Gl sand
RT140	138.3m	Antwerp Mb	Gl sand
RT141	140.8m	Antwerp Mb	Gl sand
RT142	142.3m	Antwerp Mb	Gl sand
RT143	144.3m	Antwerp Mb	Gl sand
RT144	146.3m	Antwerp Mb	Gl sand
RT145	152.3m	Edegem Mb	Gl sand

Bulk mineralogy <32µm
The mineralogy <32µm of the three analyzed Dessel Member samples is quite similar. Glauconitic minerals make up almost 50% of the samples, while 2:1 Al-clays account for ca. 20%. Quartz contents are around 10%, while both K-feldspars and plagioclase occur in amounts <5%. Typically, these samples contain between 5-10% gypsum and only minor amounts of Fe-oxides (0-2%). Calcite is only present in the 135.3m sample, however only in very small amounts (1%). Compared with the underlying sediments of the Berchem Formation, the Diest Formation (Dessel Member) sediments in the Rijkevorsel borehole contain less muscovite, less carbonate minerals and are slightly less quartz-rich (Figure 5.14).

Clay mineralogy <2µm
The clay mineralogical composition of the 135.3m sample is almost identical to the relatively stable composition encountered in the Berchem Fm below. In the two uppermost samples, however, the amount of smectite minerals is significantly lower, <20% compared to >40% below. Although the amount of kaolinite, illite and illite-smectite remain unchanged, the amount of glauconite-smectite increases sharply from 15% to ca. 50% in the Dessel interval. Moreover, both high and low expandable glauconite-smectite are present in these samples, whereas the Berchem Fm typically only contains high expandable glauconite-smectite. The 060-position of the clay-sized glauconite does not change significantly with a typical value of 1.514Å (Figure 5.14).

Pelletal glauconite
Glauconite pellets are, in general, less common above 138m depth, compared to the underlying sediments. Whereas the Berchem Fm on average contains 40-55%, the 138.3m sample contains only 32% and the 135.3m only 15% of glauconite pellets. The two uppermost samples contain 27% and 16% glauconite pellets respectively (Figure 5.14).

Size distribution
The results of analyzed samples show that the size distribution of the Antwerp Member interval contains samples which are relatively coarse. The uppermost Antwerp sample (135.3m) as well as the Edegem sample (152.3m) below are finer-grained, which is documented by the distribution modes (Figure 5.14). Above 138m, the distribution is slightly better sorted but in general the size distribution remains relatively constant in the Dessel Member.

Interpretation
The original boundary between Berchem and Dessel is interpreted by Gulinck and Laga (1975) at 138.1m, based on the occurrence of foraminifera assemblages and the well-sorted, fine-grained size distribution typical for the Dessel unit (Figure 5.14). Based on carbonate content, muscovite content and pelletal glauconite content, this boundary seems justified (Figure 5.14). Clay mineralogy and also size distribution data analyzed in this work however, show a more complex signature as a marked change only occurs upwards from the 130.8m sample. Because the clay minerals might represent a basal reworking effect and because the Gulinck and Laga (1975) have successfully identified the typical Dessel foraminifera assemblage between 138.1m and 135.3m, the original boundary of Gulinck and Laga (1975) at 138.1m is retained here.
Size distribution data in the 111-135.3m interval point to a relatively fine-grained sand, typical for the Dessel Member. Clay mineralogy, i.e. the smectite content, and carbonate content however allow an internal subdivision. A “Lower Dessel Member”, from 135.3m-138.1m is defined containing the typical foraminifera assemblage, reported by Gulinck and Laga (1975), and with relatively high smectite content (Figure 5.14). Above, an “Upper Dessel Member” is defined which is principally devoid of carbonates and contains much less smectite and more glauconite-smectite in the clay fraction (Figure 5.14). This internal subdivision does however not encompass a clear difference in grain-size.
It has to be noted that, looking back at the different results after analyses, the sampling positions density of this borehole were not optimally chosen.

V.5.1.3 The Dessel-5 31w370 borehole

Stratigraphic description

The Dessel-5 borehole was drilled at the research centre in Mol-Dessel and was interpreted by ONDRAF-NIRAS with the aid of P. Laga and N. Vandenberghe based on geophysical well log data combined with lithology descriptions and size distribution data (Labat et al., 2011; Wouters and Schiltz, 2011). In this work only the 108-166m stratigraphic interval is considered. From 108 to 128m a glauconitic fine sand is present with relatively low clay content, intensively bioturbated but not calcareous. The sediment also seems to contain more angular grains. This interval was interpreted as the Diest sand member of the Diest Formation based on a slight increase in grain-size at 128m although the boundary could also be drawn around 130m based on a lower gamma-ray signal (Figure 5.15). From 128m to 139.5m, the sediment is similar to the sediment above but this interval is slightly calcareous, somewhat more fine-grained and was therefore interpreted as the Dessel Member. Pelletal glauconite at the base of the Dessel Member (139.1m) was interpreted as authigenic based on K-Ar dating (11.4 ± 0.4 Ma) by Vandenberghe et al. (2014). The boundary with the underlying Berchem Fm was based on an important trend change on the gamma-ray curve and change in grain-size (Figure 5.15). From 139.5m to 159.3m, the sediment is a green to black glauconitic fine and calcareous sand with elevated clay content which occurs dispersed in the sediment but also as brown-grey laminae or lenses in the sand matrix. Within the Antwerp Member of the Berchem Fm, important excursions exist in the gamma-ray curve indicating the heterogeneity of this unit (Figure 5.15). Below 159.3m, the sediment was interpreted as the Voort Formation, mainly based on a finer grain-size compared to the Berchem Formation.

Samples

In total seven samples were collected of the 110-166m interval across the Berchem – Diest Fm transition in order to characterize the different litho-units present, the Voort Fm, the Berchem Fm and the Diest Formation. Four samples of the Diest Formation were sampled, two of the calcareous lower part and two of the non-calcareous upper part. Two samples of the Berchem Formation and one of the Voort Fm were collected (Table 5.4).

Bulk mineralogy <32µm

Bulk mineralogical results <32µm of the two lowermost Diest (Dessel Member) samples (134.25m and 138.25m) are particularly rich in clays with the total amount of Al- and Fe-rich dioctahedral clays around 65% and kaolinite between 5 and 10%. Quartz and feldspars make up 15%, with also 5-10% of sulphur-bearing minerals (pyrite and gypsum). Calcite is present in amounts <1% which contrasts with the amount of carbonate minerals encountered in the Berchem Formation below (Figure 5.15). The two uppermost Diest Formation samples, at 110.30m and 120.35m, are very similar to the lower Diest samples but however do not contain calcite. Compared with the samples of the underlying Antwerp Member of the Berchem Fm, the difference in calcite and muscovite content stand out. The sample of the Voort Fm seems very similar to those of the Antwerp Member of the Berchem Fm.

Clay mineralogy <2µm

The clay mineralogy of four uppermost samples of the borehole is smectite-rich (ca. 40%) with low kaolinite and illite contents (<10%), which remain relatively stable. Illite-smectite occurs in amounts from 17-31% while glauconite-smectite is 11% in the 138.25m sample but increases to 23% in the 134.25m sample and even to 36% in the 110.3m sample. Although high expandable glauconite-smectite remains the dominant clay-sized glauconite type, the low expandable form gradually becomes more important and gradually increases from 1% to 10% in the 138.25m to 110.3m interval. The lower- and uppermost Berchem samples only contain high expandable glauconite-smectite. The 153m sample however, contains 50% of the low expandable glauconite-smectite form. The d_{060} does not show important variation throughout the sampled interval (Figure 5.15).

Table 5.4. Samples of the Dessel-5 borehole. “Gl sand” indicates “glauconitic sand”.

Sample code	Depth (below ground level)	Stratigraphy	Lithology
RT217	110.3m	Diest Fm	Gl sand
RT218	120.35m	Diest Fm	Gl sand
RT219	134.25m	Diest Fm	Gl sand
RT220	138.25m	Diest Fm	Gl sand
RT221	147m	Antwerp Mb	Gl sand
RT222	153m	Antwerp Mb	Gl sand
RT223	165.5m	Voort Fm	Gl sand

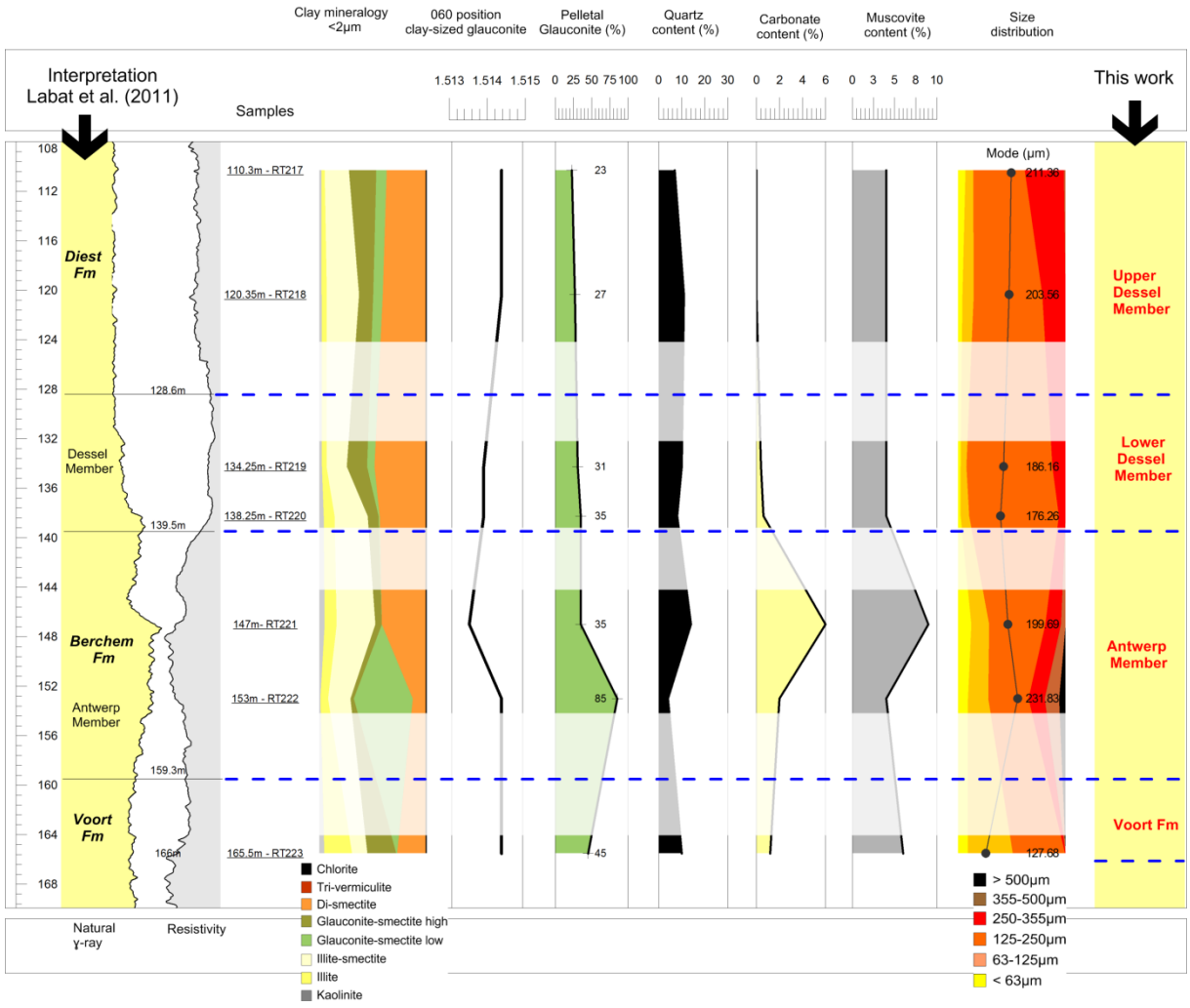

Figure 5.15. Quantitative (clay) mineralogical and sediment petrological data for the Dessel-5 borehole. Geophysical well log data are given on the left with the original interpretation of ONDRAF-NIRAS. Samples levels are indicated as underlined text right of the geophysical well log data. The different columns in the middle part summarize (clay) mineralogical data and size distribution with indication of the distribution mode . On the right side, the lithostratigraphic interpretation of this work is presented. Blurred transparent zones indicate a range from which no samples were analyzed. Data points in these ‘no-sample” ranges may therefore be not continuous, as is suggested on the figure.

Table 5.5. Pelletal glauconite mineralogy evolution in the Dessel-5 borehole indicating stratigraphy, pelletal glauconite content in %, the d060 position and the modeled amounts of higher expandable and low expandable glauconite-smectite with 27% and 5% expandable layers respectively. The final two columns indicate the total amount of glauconite and expandable layers in the sample.

Sample	Member	Content (%)	d060	Higher expandable G-S (27% expandable)	Low expandable G-S (5% expandable)	Total amount Glauconite layers	Total amount Expandable layers
RGT217	Diest	23	1.5153	30	70	88	12
RGT219	Dessel	31	1.5148	46	54	85	15
RGT220	Dessel	35	1.5148	37	63	87	13
RGT221	Berchem	35	1.5144	40	60	86	14

Pelletal glauconite

Pelletal glauconite in the four Diest Fm samples occurs in the highest amounts in the most basal 138.25m sample (35%) but gradually decreases upwards to 23% in the uppermost 110.30m sample level. The 153m sample of the Berchem Fm, which also contained increased amounts of low-expandable glauconite in the clay fraction, contains large amounts of glauconite pellets, with a content of 85% and almost no macroscopically visible quartz grains. The lowermost Berchem sample contains 35% glauconite pellets, whereas the Voort Fm sample contains 45% glauconite pellets. The mineralogy of the pelletal glauconite in this vertical succession is prone to only little variation (Table 5.5). Glauconite pellets of the Dessel Member have very similar, or even identical, characteristics to the Berchem pelletal glauconite below with >13% expandable layers and the d_{060} around 1.5148Å. The Diest sand member sample is characterized by a d_{060} of 1.5153Å but contains somewhat less expandable layers, 11.6% in total (Table 5.5).

Size distribution

The granulometry of the lowermost part typically contains elevated amounts of grains <63µm and <125µm: ca. 50% in the 165.5m samples and 30% in the 147m sample. The 153m sample moreover also contains important amounts of grains >355µm and >500µm, which are identified, after mineralogical analysis, as coarse-sized quartz grains. In the 138.25m sample, the amount of grains <125µm decreases sharply with a dominant size distribution between 125 and 250µm. In the 120.35m sample, the distribution contains slightly more fines and coarse grains but the difference is very small. Note that in the Dessel-5 borehole, unlike the general definition of a coarse Diest sand member, the interpreted Dessel Member and Diest sand member by Wouters and Schiltz (2011) both demonstrate a similar size distribution and that the coarsening in the 108-128m interval is only limited.

Interpretation

Although Labat et al., (2011) interpret both the Dessel Member and the Diest sand member in the 139.5m-110.3m interval, there are very little, or even no, arguments for this distinction to be found in lithological parameters and certainly not in grain-size which is the main argument to distinguish the finer-grained Dessel Member from the coarser-grained Diest sand member (P. Laga, pers. com.).

The main difference in the 139.5m-110.3m is the absence of carbonates in the upper part (110.3-128m) compared to the lower part. This leads us, similar to the Rijkevorsel borehole, to subdivide the 110.3-139.5m interval in a Lower calcareous Dessel Member (128-139.5m) and a Upper non-calcareous Dessel Member (110.3-128m) instead of interpreting the presence of the Diest sand member which should be coarser-sized compared to the Dessel Member (Figure 5.15). Grain-sizes of samples upwards from 105m, reported in Labat et al. (2011), but not analyzed in this work, become significantly coarser, with clearly > 50% grains >250µm. At the uppermost analyzed level in this work (110.3m), 37% of the particles is larger than 250µm, while at the 120.35m level this percentage is 22%. This suggests that Dessel Member to Diest sand member transition occurs at ca. 105m depth. This interpretation honours the original practical distinction of the Dessel sand and the overlying Diest sand member applied by Laga and Gulinck in borehole description and is based on the grain-size difference (Laga,pers. com.). This new interpretation also implies that bioturbations are not only typical for the Diest sand member but can also occur abundantly in the finer-grained sediments belonging to the Dessel Member.

Similar to the Rijkevorsel borehole, the Berchem-Dessel transition is marked by a subtle change in clay mineralogy but also

carbonate (and possibly also muscovite) contents allow a distinction (Figure 5.15). Glauconite pellet amounts are the highest in the Antwerp Member but the uppermost analyzed Antwerp sample is not different from the lower Dessel Member samples. The increased amount of clay-sized glauconite in the 153m sample could be related to the very high pelletal glauconite amount (85%) in this sample through increased pelletal disintegration.

V.5.1.4 The Westerlo 60E215 borehole (Figure 5.16)

Three samples were collected from the Westerlo 60E215 borehole, which belongs to the stratigraphic collection of the Geological Survey of Belgium (GSB). The original interpretation was made by Gulinck (1964a) based on lithology. The author interpreted the Diest Fm between 4m and 68m. From 31m to 58m, the author describes a quite homogeneous sediment consisting of coarse-sized, very glauconitic and heteromorphic sand with very low to extremely low dispersed clay content, although locally also brownish clay lenses do occur. Within the 56-58m range, bioturbations occur abundantly in the sand matrix.
Only three samples were collected from this borehole, at 33.50m, 37.50m and 57.50m (Figure 5.16), as it was not the objective for this borehole to unravel the entire vertical stratigraphy but to analyze and characterize the coarse-sized, very glauconitic and loose sands most often associated with the Diest sand member.

Bulk mineralogy of sands <32µm
The mineralogical composition of the three investigated samples is quite similar. All three samples contain dominantly glauconitic minerals: 34% at the 57.5m level ; 54% at the 37.5m level and 69% at the 33.5m level. The remainder of the mineral fraction is composed of 2:1 Al-clays and more abundant quartz in the lowermost 57.5m level. K-feldspars, plagioclase, sulphur-bearing minerals (pyrite – gypsum), siderite, kaolinite and chlorite make up fractions smaller than 5% (Figure 5.16).

Clay mineralogy <2µm
Glauconite-smectite is the dominant clay species in all three samples of the 33-58m interval with 55% in the lowest 57.5m sample but increasing to 62% and 72% in the 37.5m to 33.5m interval respectively. Simultaneously, the proportion of dioctahedral smectite is gradually lower in this interval (Figure 5.16). The dominant glauconite-smectite type is the low expandable species which becomes more important upwards. The d_{060} of the clay-sized glauconite minerals is relatively constant between 1.5166 and 1.5171Å.

Pelletal glauconite
The amount of glauconite pellets in the Westerlo borehole between 33 and 58m is continuously elevated. In all three investigated sample depths, the pelletal glauconite amount is higher than 45% (Figure 5.16). The mineralogy of the uppermost 33m glauconite pellet sample shows a d_{060} of 1.5157Å. The total amount of expandable layers is low, 7% .

Size distribution
The size distribution of the three samples of the Westerlo borehole shows a coarse and poorly sorted size distribution. In the lowermost samples the amount of grains >355µm is constrained to 10%. In the 37.5 and 33.5m samples however, this amount is higher than 25% and 35% respectively (Figure 5.16).

Interpretation
The Diest sand member sediment analyzed in the three samples of the Westerlo borehole is undoubtedly quite different from the Dessel and Deurne Member sediments. The Diest sand member in this borehole is coarse-sized, very poorly sorted and contains high amounts of pelletal glauconite (>40%). The clay mineralogy <2µm is characterized by a relatively low smectite content, with 32% in the basal 57.5m sample, 22% in the 37.5m sample and only 10% in the 33.5m sample. In contrast, clay-sized glauconite is very abundant (55%-72%) with low-expandable glauconite-smectite (10% expandable layers) being dominant over higher-expandable glauconite-smectite (30% expandable layers). This type of characteristic sediment will be termed the Diest D1 facies further in this work (Figure 5.16).

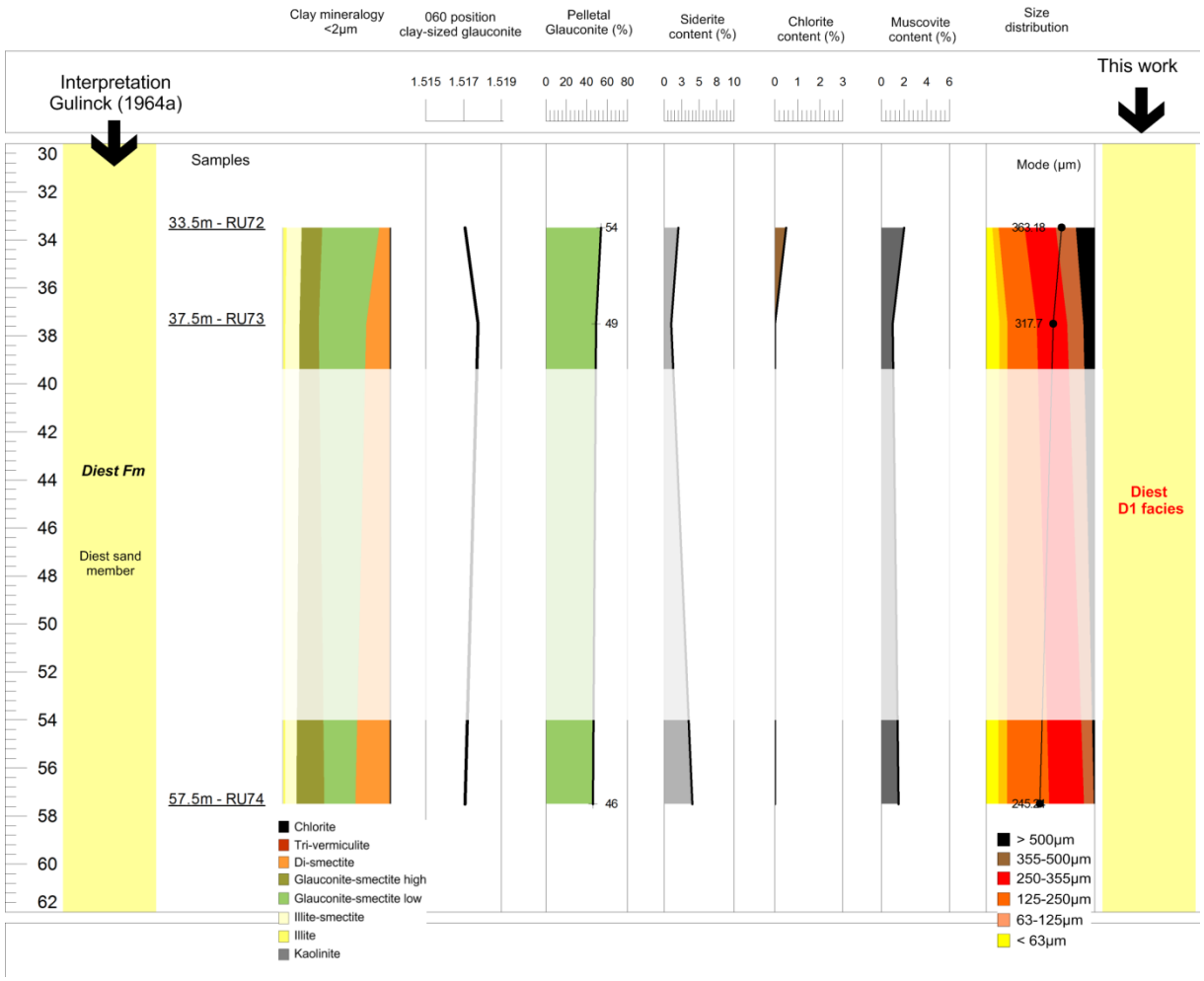

Figure 5.16. Quantitative (clay) mineralogical and sediment petrological data for the Westerlo 60e215 borehole. The most left column gives the initial interpretation of Gulinck (1964a) which is based on borehole lithology descriptions. Sample levels are indicated as underlined text in the second column. The different columns in the middle part summarize (clay) mineralogical data and size distribution with indication of the distribution mode . On the right side, the lithostratigraphic interpretation of this work is presented. Blurred transparent zones indicate a range from which no samples were analyzed. Data points in these 'no-sample" ranges may therefore be not continuous, as is suggested on the figure.

V.5.1.5 The Dessel-3 borehole (31W354)

The Dessel-3 borehole is a 50m deep cored borehole in Dessel. Sampling was carried out from cores which are stored under vacuum conditions at the SCK – ONDRAF-NIRAS site in Dessel. The upper part of the borehole consists of the formations of Mol and Kasterlee. The stratigraphic boundary between the Diest and Kasterlee Formations is debatable and will be the subject of the next chapter. In this section, only the interval below 35m will be discussed, which can safely be termed the Diest sand member of the Diest Formation. The original description and interpretation was performed by ONDRAF-NIRAS based on lithology, grain-size characteristics, cone penetration tests and geophysical well log interpretations. Wouters and Schiltz (2011) interpreted the Diest Formation to be present below 34m. The sediment oxidizes very quickly (timespan of hours) after sampling. Vivianite concretions (>1mm) are present in the 35.17m and 38.72m samples (Figure 5.17). The Diest sediment below 35m is described as a dark green, medium to coarse-sized, very glauconitic sand with elevated clay content. According to Wouters and Schiltz (2011), this clayey sediment forms the top of the Diest Fm in the Mol-Dessel region and is systematically identified as a “Clayey Diest” facies within the Diest sand member.

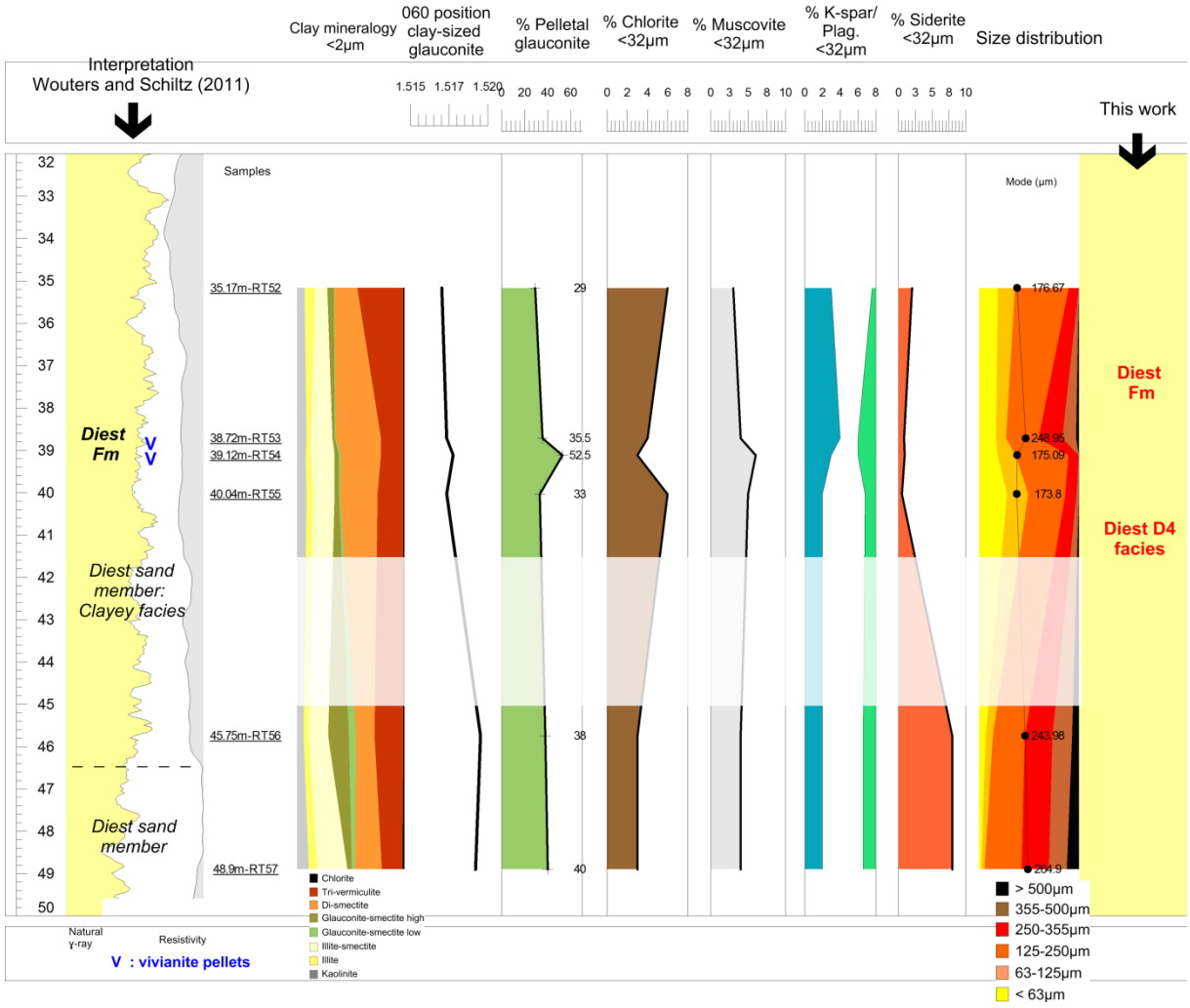

Figure 5.17. Quantitative (clay) mineralogical and sediment petrological data for the Diest Fm in the Dessel-3 borehole. The most left column shows the initial interpretation based on borehole lithology descriptions and geophysical well log data (Wouters and Schiltz, 2011)). Samples levels are indicated as underlined text in the second column. The different columns in the middle part summarize (clay) mineralogical data and size distribution with indication of the distribution modes. On the right side, the lithostratigraphic interpretation of this work is presented. Blurred transparent zones indicate a range from which no samples were analyzed. Data points in these ‘no-sample” ranges may therefore be not continuous, as is suggested on the figure.

Size distribution
The grain-size distribution of the 35-45m is coarse-sized characterized by poor sorting. At the base of the interval the amount of finer-grained particles <125µm is very small, but a fining upward trend is observed (Figure 5.17).

Pelletal glauconite
Glauconite pellets in the 35-45m interval vary between 30-50%. The pelletal glauconite content shows a gradual decreasing upward trend. In contrast with the relatively low d_{060}-value of Dessel Member samples, the d_{060} of the pelletal glauconite in the Dessel-3 borehole are higher than 1.517Å. Similarly, also the amount of expandable layers is larger, varying between 10 and 15% (Table 5.6).

Bulk mineralogy of sands <32µm
The mineralogy of the analyzed samples between 35-45m is characterized by high amounts of 2:1 Al-clays (>30%), quartz (5-22%) and glauconitic minerals (7-25%). Chlorite proportions are moreover also elevated (3-7%). Additionally, aside from chlorite, another trioctahedral clay species was identified in random oriented powders. The d_{060} of this species is ca. 1.535Å. These samples also contain both K-feldspars and albitic plagioclase, low amounts of mica, and, detectable amounts of siderite (Figure 5.17).

Clay mineralogy <2µm: the nature of the trioctahedral expandable phase
The clay mineralogy of the samples in the 35-45m interval are characterized by relatively high amounts of expandable minerals and mixed-layer minerals. Glauconite-smectite, illite, kaolinitic and chloritic minerals are less important. In the results of the bulk mineralogy, a trioctahedral clay species was found which is suspected to have an expandable nature with a d_{060}-value of 1.535Å (Figure 5.18). Its nature will be discussed separately because trioctahedral minerals are only rarely reported in the clay mineralogy of sediments, in contrast to their dioctahedral counterparts.

Table 5.6. Pelletal glauconite mineralogy evolution in the Dessel-3 borehole indicating stratigraphy, pelletal glauconite content in %, the d060 position and the modeled amounts of higher expandable and low expandable glauconite-smectite with 27% and 5% expandable layers respectively. The final two columns indicate the total amount of glauconite and expandable layers in the sample.

Sample	Member	Content (%)	d060	Higher expandable G-S (27% expandable)	Low expandable G-S (5% expandable)	Total amount Glauconite layers	Total amount Expandable layers
RT53	Diest	53	1.518	34	66	88	12
RT54	Diest	29	1.5175	23	77	90	10
RT56	Diest	53	1.5189	43	57	86	14
RT57	Diest	33	1.5189	34	66	85	15

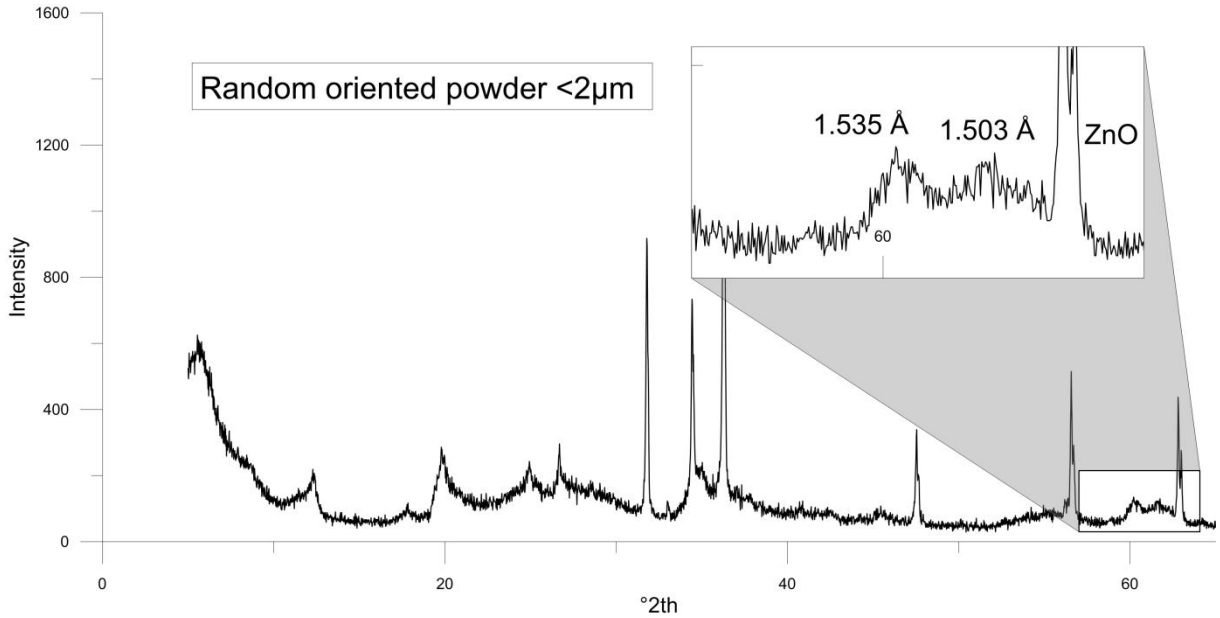

Figure 5.18. Random oriented powder measurement of sample RT52 illustrating a high d060 value which indicates the presence of a trioctahedral clay species.

Cation saturations and treatments

The group of trioctahedral expandable minerals does not consist exclusively of smectites but also of vermiculites. As already discussed in chapter II, the identification of vermiculite is difficult because of its variable characteristics. The AIPEA nomenclature committee (Bailey, 1980) decided that the layer charge is the decisive criterion to distinguish smectites from vermiculites. This definition however needs a translation to the practice of XRD analysis of sediments and therefore several authors have proposed an operational definition to positively identify vermiculite. We repeat here the twofold operational definition for the identification of vermiculite with respect to smectite and chlorite by Robert and Barshad (1972):

1) *Expansion to 14.5Å after Mg-saturation and glycerol solvation treatment*. In contrast to vermiculite, smectite layers will expand to ca. 18Å because it accepts two layers of glycerol instead of 1 glycerol layer for vermiculite which will remain at ca. 14.5Å.
2) *Collapse to 10Å after K-saturation + glycerol + 300°C/1h treatment*. As opposed to chlorite, vermiculitic and smectitic layers will incorporate K-cations in the interlayer space. Therefore, smectitic and vermiculitic layers will collapse to 10Å, whereas chlorite will remain its 001-spacing at ca. 14Å.

To make the distinction with smectite, it is essential that glycerol is used instead of ethylene glycol because all types of vermiculites (low- or high-charged) will not swell with respect to glycerol. Low-charged vermiculites were however reported to swell to almost 17Å as a response to ethylene glycol treatment, whereas high-charged vermiculites retained their initial basal spacing (Mosser-Ruck et al., (2005). The use of glycerol, combined with different cation saturations, is therefore necessary to confirm or reject the presence of vermiculite in clay mineral mixtures. The standard clay identification procedures (air dry, ethylene glycol + heating 550°C) supplemented with the vermiculite-discriminating tests prescribed by Robert and Barshad (1972) were applied on the uppermost 35.18m sample in the Dessel-3 borehole (RT52) and the results of these treatments are discussed below.

Air-dry and glycolated 2µm fraction measurements of the 35.18m sample demonstrate a clay assemblage consisting of minor illite, illite-smectite, kaolinite and chlorite but mainly of expandable layers with visible swelling in response to ethylene glycol (see peak at 16.92 Å), indicating the presence of expandable layers, presumably smectite (Figure 5.19). In addition, there is also the appearance of an unusual intense 002 reflection at 8.25Å after ethylene glycol treatment and a weak reflection at 4.72Å. Heating to 550°C causes the expandable layers to collapse to 10Å and shows the appearance of a marginal increase of intensity at 13.55Å, which suggests the presence of chlorite. However, this 13.55Å reflection has a high angle shoulder that transitions into the 10Å reflection, suggesting this diffraction intensity is caused by traces of chlorite-expandable, rather than true chlorite. Because the reflection is extremely weak, it is however difficult to determine if it is chlorite, chlorite-expandable or both.

Mg-saturation followed by glycerol treatment (Figure 5.20) shows only a very limited shift of the 001-reflection from 16.92Å to 17.3Å. The reflection is however remarkably broad and peak traces can be observed at 14.5Å and at 14.3Å. The 4.72Å reflection remains visible after this treatment. K-saturation followed by heating treatment at 300°C furthermore shows a general collapse of the expandable layers with the almost complete disappearance of the 14.5Å, the 14.3Å and the 4.72Å reflections. Although the 14.3Å and 4.72Å are normal diffraction intensity positions for chlorite, both reflections seem to disappear after the Mg-saturation + glycerol procedure. A possible explanation would be that the chlorite-layers are heat-defective as described by Renngarten et al. (1978), Varentsov et al. (1983), Sakharov et al. (2004) and Zeelmaekers (2011). This is however unlikely because chlorite reflections are present in the heated 550°C/1h diffraction pattern (Figure 5.19). It is therefore most likely that the 14Å-region of the K-saturated pattern in Figure 5.20 has been elevated to such a degree, due to the collapse of expandable layers, that the observation of trace peaks of chlorite or chlorite-expandable has become impossible.

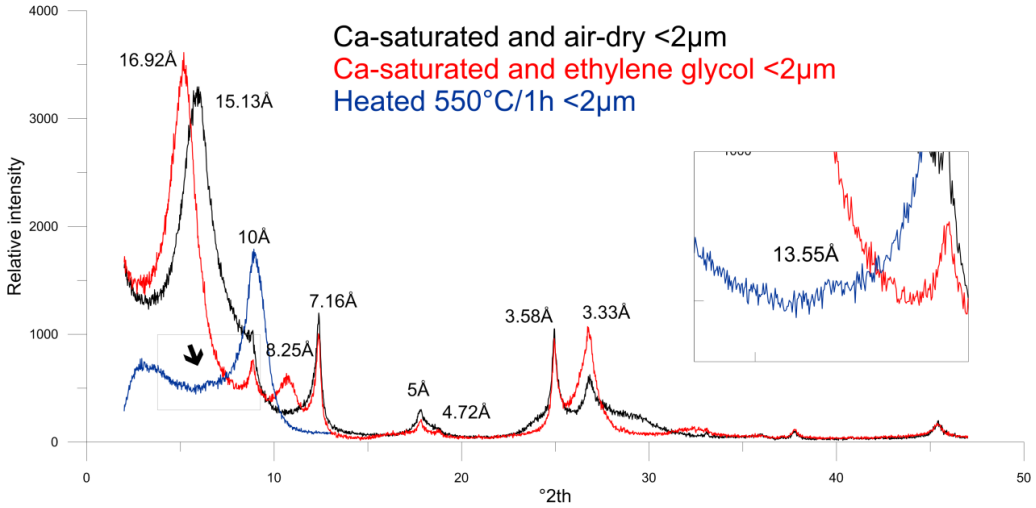

Figure 5.19. Comparison of air-dried, ethylene glycolated and heated XRD scans of the 2µm fraction of sample RT52.

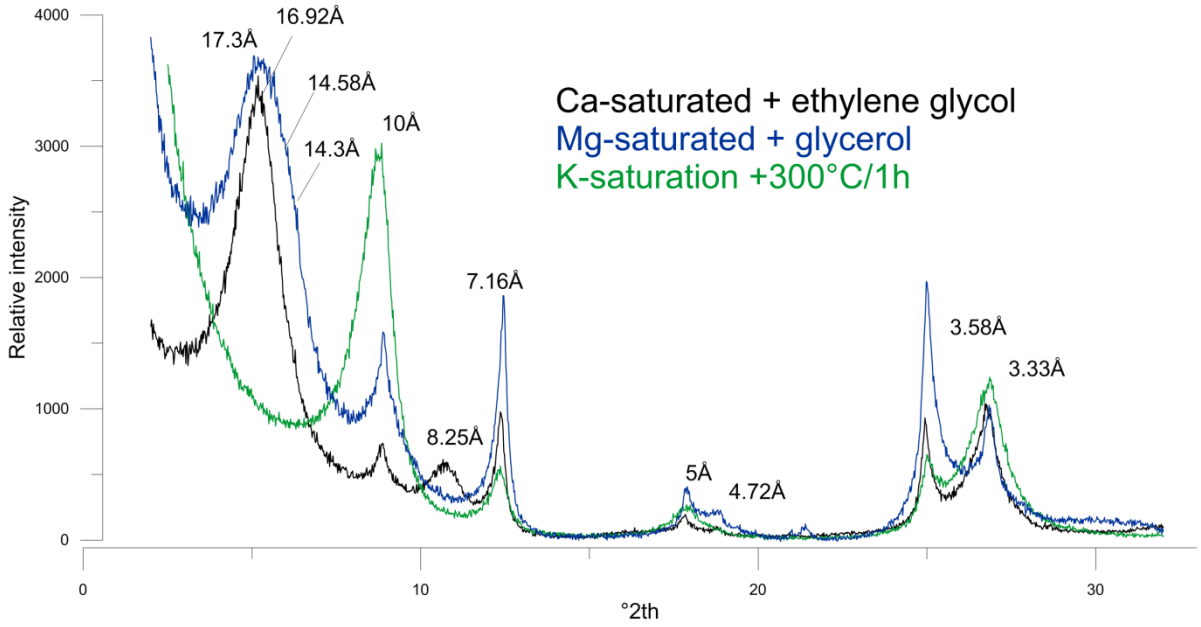

Figure 5.20. Comparison of Ca-saturated and glycolated, Mg-saturated and glycerol solvated, and, K-saturated and heated XRD scans of the 2µm fraction of sample RT52.

Expandable minerals: the limited shift

The ethylene glycol and glycerol behavior showed the unmistakable presence of smectite (Figure 5.19 and Figure 5.20). In random powder measurements of the clay fraction <2µm, the 060-peak shows, in addition to the dioctahedral signal, also a large contribution of trioctahedral 2:1 minerals (Figure 5.18). As the chlorite is only a minor component , part of the larger amount of swelling minerals present must be trioctahedral (saponite, vermiculite,…).

As shown above, parts of the oriented diffraction patterns show unusual behavior with a very intense 002 reflection at 8.25Å after ethylene glycol treatment and a very limited swelling as a reaction on the Mg-saturation followed by glycerol treatment (Figure 5.19 and Figure 5.20). The latter phenomenon is quite odd because the Mg-saturation + glycerol treatment generally causes significant extra swelling to ca. 18Å in the case of regular smectites. The strong 002 intensity can correspond to higher bivalent iron content in the octahedral position and the limited swelling could be explained by the admixture of

dioctahedral smectite and vermiculite, which in sediments is often trioctahedral.

This interpretation can be tested by a modified application of the Greene-Kelly test. This treatment combines Li-saturation with glycerol treatment and heating 300°C for 12h and is used to distinguish between different dioctahedral smectite species. The test is usually designated to neutralize octahedral charge through Li-diffusion entering vacant octahedral sites. As dioctahedral montmorillonite has no tetrahedral charge, the 001 of montmorillonite will collapse during the Green-Kelly test and therefore can be distinguished from beidillite or nontronite. Because trioctahedral smectites lack vacant octahedral sites, such treatment is per definition inoperative and not useful for trioctahedral minerals. In our case however, the presence of trioctahedral swelling minerals will keep their swelling capacity after the Li-test, whereas the dioctahedral smectite, if montmorillonite, will collapse.
The modified application of this Li-treatment procedure reveals quite remarkable results for the 0.2µm fraction of the 35.18m sample (Figure 5.21). The diffraction pattern illustrates that part of the expandable layers have collapsed as evidenced by the appearance of a 9.6Å "shoulder" at the right, high angle side of the 10Å, confirming the presence of dioctahedral montmorillonite (Moore and Reynolds, 1997). The collapse of the montmorillonite phase reveals the presence of a second expandable phase in the 14-18Å region which did not react to the treatment and retained its initial d_{001} basal position at 14.5Å (Figure 5.21). This 14.5Å-position was already observed in the Mg-saturated XRD scan (Figure 5.20) and must be the trioctahedral expandable mineral. The d_{001}-value of this mineral, 14.5Å, is far too low for regular low-charge smectites (e.g. saponite) in glycerol conditions and indicates the expandable phase is trioctahedral vermiculite. This vermiculite does not expand with glycerol, neither when Mg-saturated, nor when Li-saturated. Expansion is however observed when ethylene glycol vapor is used after Ca-saturation, which suggests a relatively high-charge vermiculite.

The presence of vermiculite explains the unusual limited swelling after Mg-saturation + glycerol treatment because only the montmorillonite expanded. The very intense 002-reflection moreover indicates that this trioctahedral vermiculite is Fe-rich. This is confirmed by chemical analysis of the 2µm and 0.2µm fractions of several samples. The total amount of Fe (ferric and ferrous) measured by ICP-OES correlates very well with the quantified amount of trioctahedral vermiculite by QXRD. A positive correlation also exists for MgO while Al_2O_3 is negatively correlated (Figure 5.22). During clay modeling, almost 2 Fe atoms/half unit cell are required to fit the expandable phase.

The nature of the kaolinitic minerals
Apart from the smectite, vermiculite and chlorite or chlorite-expandable, also kaolinitic minerals are present in the clay fraction. Air-dried and glycolated measurement of the 2µm fraction (Figure 5.19) confirm the presence of kaolinitic minerals at 7.16Å and 3.58Å. The same measurements on the 0.2µm fraction however (Figure 5.23), show that the 3.58Å peak clearly shifts to higher angles demonstrating the swelling nature of the kaolinite. During clay modeling, both regular, non-expandable kaolinite and kaolinite-expandable (82:18) are necessary for optimal fitting results.

It can be concluded after different cation saturations and treatments that the 35.18m (RT52) sample is characterized by a unique clay assemblage with trioctahedral Fe-vermiculite, dioctahedral montmorillonite, illite-smectite, illite, glauconite-smectite, kaolinite, kaolinite-expandable and traces of chlorite or chlorite-expandable. This particular composition was found in the Dessel-3 borehole in all samples between 35m and 49m. In the upper part, smectite and vermiculite together account for 50% of the total mineral content <2µm, which gradually decreases to 40% deeper in the borehole. Glauconitic minerals are scarce and are only found in amounts higher than 10% in the 45.75m sample (Figure 5.17).

Interpretation
The 35-49m interval of the Dessel-3 borehole was interpreted as a separate facies of the Diest sand member because the clayey character contrasts with the generally coarse and clay-poor appearance of the Diest sand member. The size distribution analyzed in this work confirms the clayey nature of the sediment, certainly in the 35-40m interval. The two samples below 45m are coarser (Figure 5.17). The most important characteristics of the Diest sand member in the Dessel-3 borehole is nevertheless the unique clay mineralogical composition with trioctahedral Fe-vermiculite and kaolinite-expandable (and possible also chlorite-expandable). The implication of this specific clay mineral assemblage will be discussed further in section "*II.6.7 Discussion"*

of this chapter but the presence of such clay minerals is so specific that a new lithofacies, Diest D4, can be defined. In the Dessel-3 borehole, this Diest D4 facies is present from at least 35.17m to 48.9m (Figure 5.17) and thus bridges the grain-size shift between 40.04m and 45.75m.

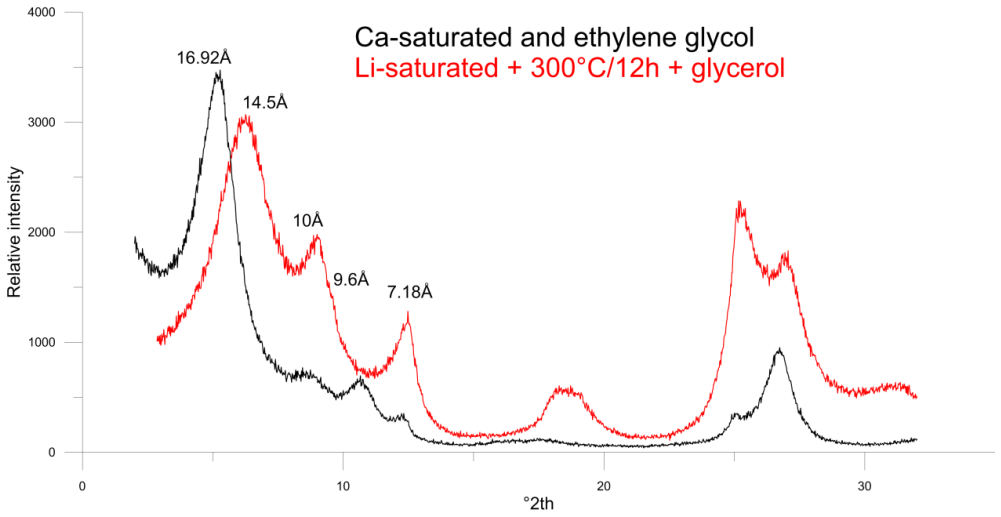

Figure 5.21. Comparison of Ca-saturated and ethylene glycolated, and, Li-saturated and heated XRD scans of the 0.2µm fraction of sample RT52.

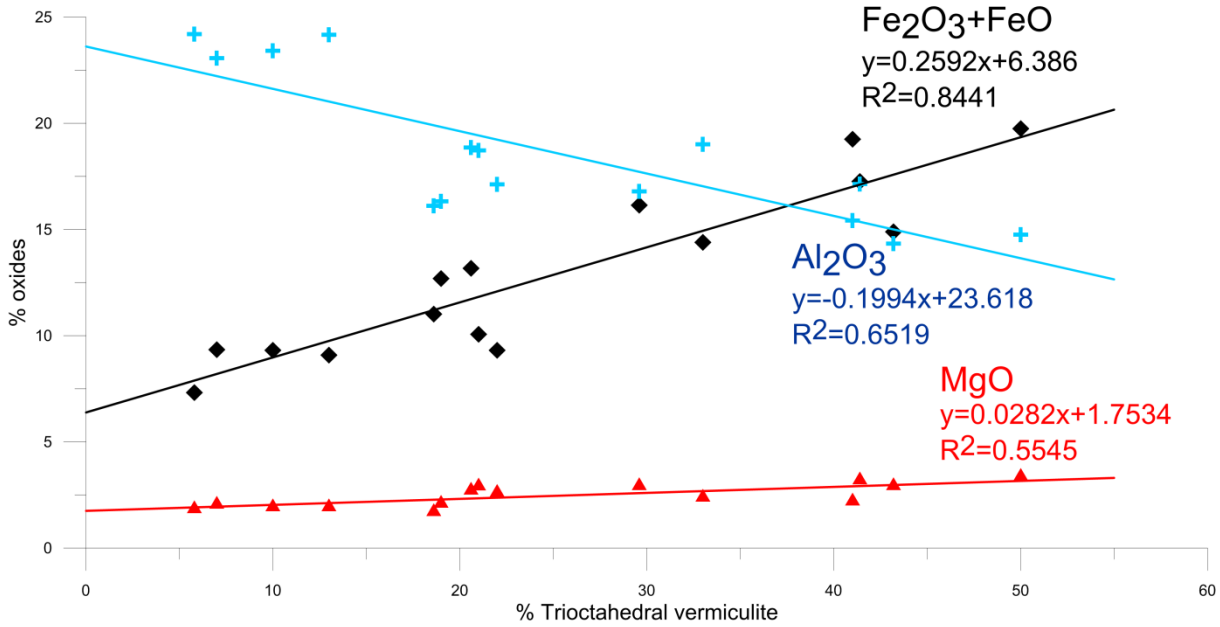

Figure 5.22. Correlation of Fe (squares), Al_2O_3 (crosses) and MgO (triangles) measured with ICP-OES with quantified amounts of trioctahedral vermiculite in the 2µm fraction (XRD quantification).

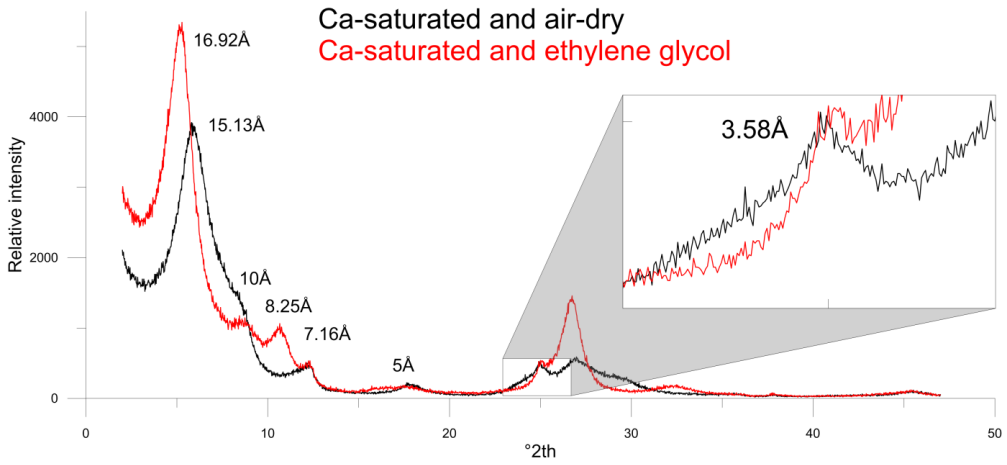

Figure 5.23. Comparison of Ca-saturated air-dried and ethylene glycolated XRD scans of the 0.2µm fraction of sample RT52.

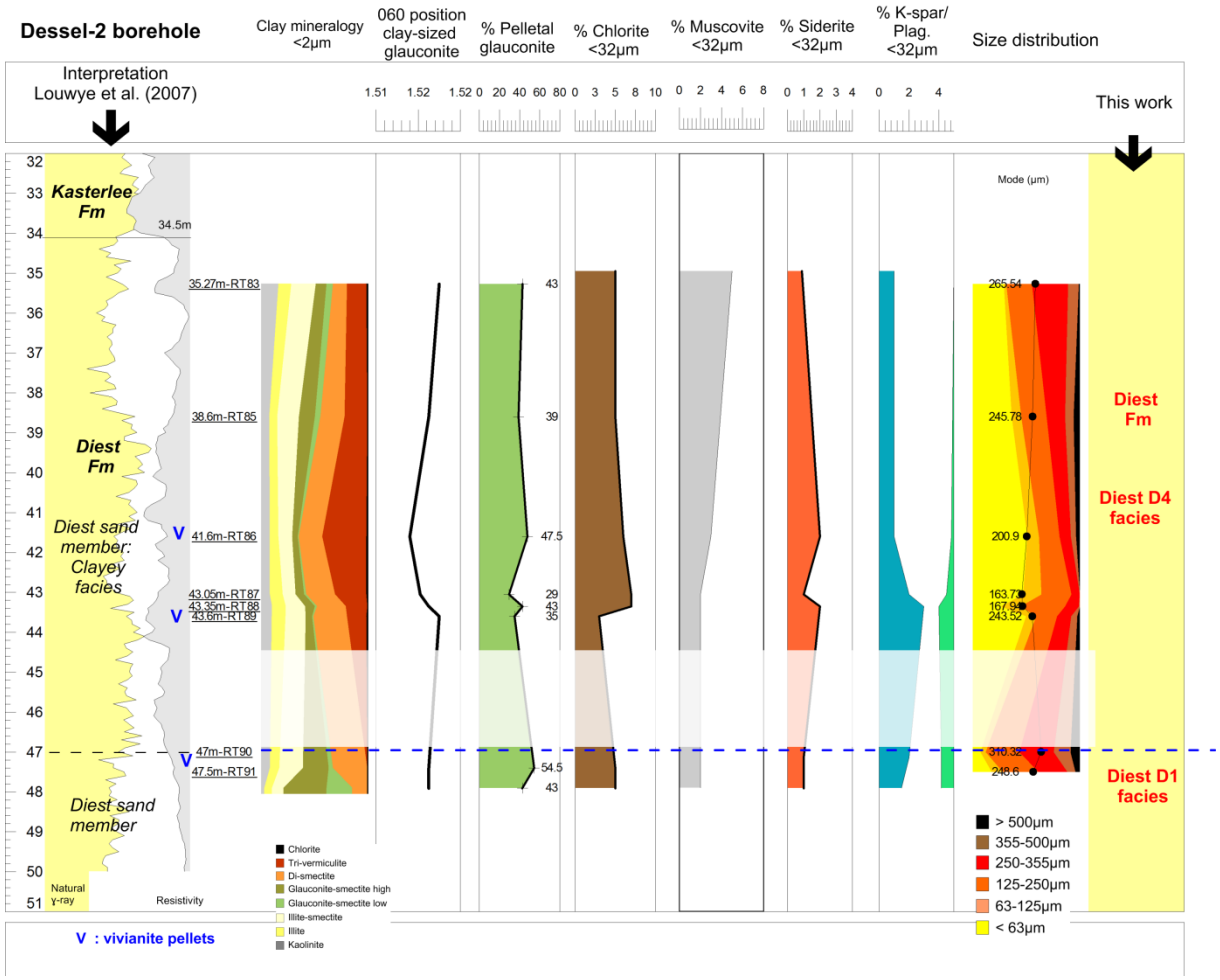

Figure 5.24. Quantitative (clay) mineralogical and sediment petrological data for the Diest Fm in the Dessel-2 borehole. The most left column shows the initial interpretation based on borehole lithology descriptions, cone penetration tests and geophysical well log data (Wouters and Schiltz, 2011). Samples levels are indicated as underlined text in the second column. The different columns in the middle part summarize (clay) mineralogical data and size distribution with indication of the distribution mode . On the right side, the lithostratigraphic interpretation of this work is presented. Blurred transparent zones indicate a range from which no samples were analyzed. Data points in these 'no-sample" ranges may therefore be not continuous, as is suggested on the figure. The Diest D4 facies was identified based on the presence of trioctahedral vermiculite.

V.5.1.6 The Dessel-2 borehole (31W338)

The Dessel-2 borehole is a 50m deep cored borehole in Dessel. Sampling was performed from cores stored under vacuum conditions at the SCK–ONDRAF-NIRAS site in Dessel. The original description and interpretation was performed by ONDRAF-NIRAS who interpreted the boundary of the Kasterlee Fm and the underlying Diest Fm at 34m based on lithology, grain-size, cone penetration tests, geophysical well log data and dinoflagellate cysts biozones (Louwye et al., 2007; Wouters and Schiltz, 2011). An internal stratigraphic boundary within the Diest Fm was set at 47.1m to distinguish the clayey top facies which covers the typical coarse Diest sand member (Figure 5.24). The stratigraphic boundaries of this borehole are discussed in detail in chapter VI and in this section only the Diest part below 35m is discussed. The 35m-50m interval consists of a dark green, medium to coarse-sized, very glauconitic sand with elevated clay content without clay intercalations. The sediment oxidizes very quickly to a brown sediment, within hours after sampling. Vivianite pellets (>1mm) are present in the 41.6m, 43.05m and 47.4m samples. The entire 35-50m interval was interpreted as the clayey facies forming the top of the Diest sand member (Louwye et al., 2007). In total 8 samples were collected from the Dessel-2 borehole of the top of the Diest Fm (Figure 5.24).

Bulk mineralogy of sands <32µm

The mineralogical results of the Dessel-2 borehole are very similar to those of the Dessel-3 borehole. 2:1 Al-clays are the main phase, but also 2:1 Fe-clays and quartz occurs in proportions higher than 10%. Glauconitic minerals are less abundant (<10%) while chlorite and a trioctahedral phase, which might be the Fe-vermiculite also in the Dessel-3 borehole (see section Clay mineralogy <2µm), are present in proportions higher than 5%. K-feldspars, plagioclase and siderite occur in proportions <5% (Figure 5.24). Below 47m, the amount of glauconitic minerals increases while trioctahedral expandable clays are absent. The kaolinite content is relatively constant below 5% except in the uppermost 34.95m sample, where it is 10%.

Clay mineralogy <2µm

The clay mineralogy <2µm of the sands in the 35-45m interval systematically contain the Fe-vermiculite already identified in the Dessel-3 borehole and diffraction patterns of samples are nearly identical in both boreholes (Figure 5.25). The remainder of the clay composition is formed by dioctahedral montmorillonite and lower amounts of illite-smectite, glauconitic minerals, illite, kaolinite and kaolinite-expandable minerals and traces of chlorite and/or chlorite-expandable. The nature of the different minerals is identical to the ones of the Dessel-3 borehole. Below 47m, Fe-vermiculite is absent as well as the kaolinite-expandable phase. Glauconite-smectite becomes more important with both high and low expandable glauconite-smectite types occurring. The d_{060} of the glauconite minerals varies around 1.517Å over the vertical interval (Figure 5.24).

Pelletal glauconite

Glauconite pellets occur in proportions higher than 30% in the 35-45m interval. In the two samples below 47m, the pelletal glauconite content increases to values higher than 40% (Figure 5.24).

Size distribution

The size distribution of samples in the 35-45m interval is characterized by a clayey but very poorly sorted distribution which still contains between 5-10% of grains >355µm. Two samples at 43.05m and 43.35m are better sorted with less than 2% grains >355µm. The two lowermost samples, below 47m, have a coarse grain-size distribution with less clay compared to the samples above (Figure 5.24).

Interpretation

Similar to the Dessel-3 borehole, also the top of the Diest Fm in the Dessel-2 borehole (35-45m) is characterized by the presence of trioctahedral Fe-vermiculite and kaolinite-expandable which is correlated to lithofacies Diest D4. Furthermore, the sediment in the 35-45m is very clayey which confirms the presence of a clayey top facies in the Diest sand member (Louwye et al., 2007). The clay mineralogy below 47m however, consists of significantly less expandable layers and no Fe-vermiculite or kaolinite-expandable could be identified. Their grain-size distribution is also coarser which strongly suggest the presence of the Diest D1 facies. This stratigraphic boundary was also interpreted by Wouters and Schiltz (2011) to separate the clayey top facies covering the coarse Diest sand member. In contrast to the Dessel-3 borehole, Fe-vermiculite is only present in the clay-rich sediments (“Clayey top facies” of Wouters and Schiltz, 2011) and not in the coarser-sized sediments (“Typical coarse Diest sand” of Wouters and Schiltz, 2011) present below 47m in the Dessel-2 borehole.

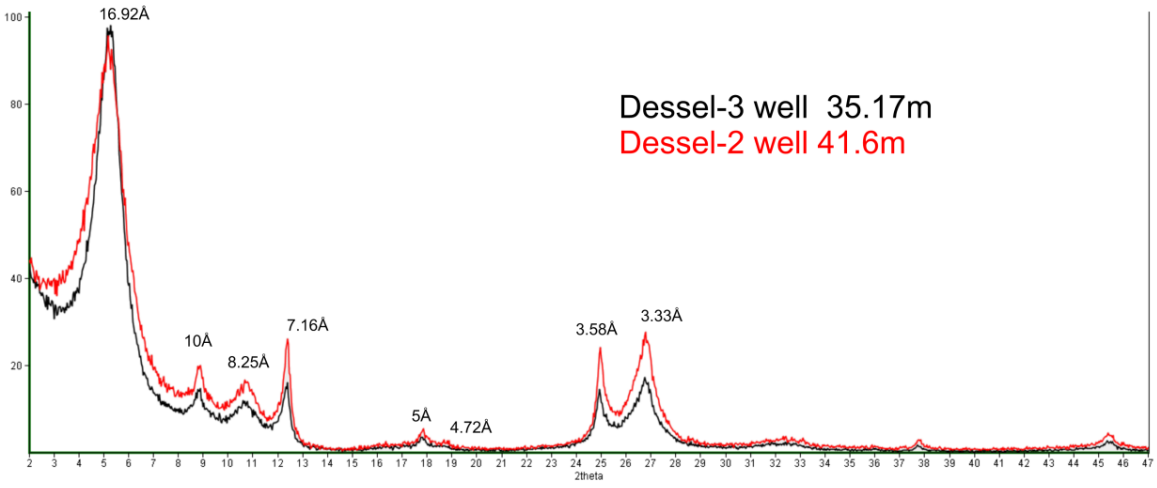

Figure 5.25. Comparison of diffraction patterns (Ca-saturated + glycolated) of Dessel-2 well and Dessel-3 well showing almost identical diffraction effects.

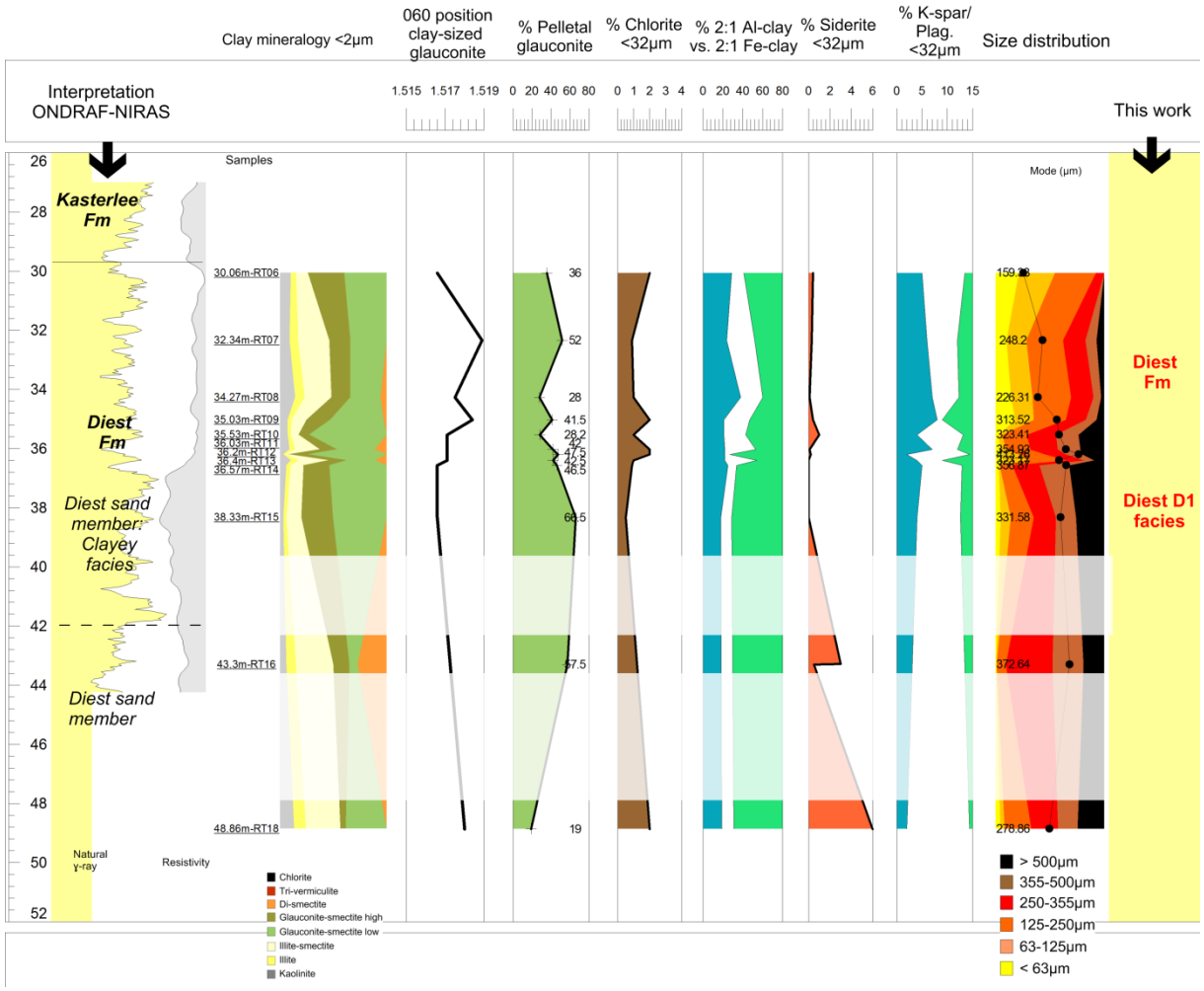

Figure 5.26. Quantitative (clay) mineralogical and sediment petrological data for the Diest Fm in the Retie-1 borehole. The most left column shows the initial interpretation based on borehole lithology descriptions, cone penetration tests and geophysical well log data (Wouters and Schiltz, 2011). Samples levels are indicated as underlined text in the second column. The different columns in the middle part summarize (clay) mineralogical data and size distribution with indication of the distribution mode . On the right side, the lithostratigraphic interpretation of this work is presented. Blurred transparent zones indicate a range from which no samples were analyzed. Data points in these 'no-sample" ranges may therefore be not continuous, as is suggested on the figure.

V.5.1.7 The Retie-1 borehole (31W363)

The Retie-1 is another 50m deep cored borehole of ONDRAF-NIRAS (Figure 5.9). Its location is approximately 2km northwest of the Dessel-3 borehole. The original interpretation by ONDRAF-NIRAS (Wouters and Schiltz, 2011) is based on lithology, grain-size characteristics, geophysical well log data and cone penetration tests. The boundary of the Diest Fm with the overlying Kasterlee Fm was interpreted at ca. 29.5m (Wouters and Schiltz, 2011). Below this boundary, until ca. 34m, the sediment consists of brown-green poorly sorted sand with slightly elevated clay content.
From 34-49m a brown coarse-sized sand with low clay content is present. This sediment was already completely oxidized. Wouters and Schiltz (2011) interpreted the 34-42m interval as the clayey top facies whereas the typical coarse Diest sand member is interpreted below 42m.
Like the Dessel-3 and Dessel-2 boreholes, the sampling of the Retie-1 borehole was intended to document the Kasterlee – Diest transition which is why a more narrow sampling was performed in the top 8m (30-38m) and less samples were collected (only 3) from the 38-50m interval (Figure 5.26).

Bulk mineralogy of sands <32µm
The mineralogy of the 30-49m interval is mainly composed of glauconitic minerals (20-50%), 2:1 Al-clays (20-38%) and quartz (11-25%). Feldspars typically constitute another 5-20%. Carbonate minerals occur only in the form of siderite (<6%). Chlorite occurs in proportions lower than 4% while kaolinite varies between 0.5% and 10%. Limonite alteration minerals (goethite and minor ferrihydrite) are systematically present in amounts between 3 and 7%. The uppermost samples (30-35m) seem to be slightly enriched in kaolinite compared to the lower 35-49m interval (Figure 5.26).

Clay mineralogy <2µm
The clay mineralogical composition of the 30-49m interval of the Retie-1 borehole displays low variability. Glauconite-smectite occurs in proportions between 50-85% in the 30-43m interval. Below, its proportion decreases to 25-40% as illite-smectite is more abundant. No trioctahedral vermiculite is present in these samples (Figure 5.26).

Pelletal glauconite
Glauconite pellets are most abundant in the 30m until 43.3m samples, varying between 28-66%. In the two lowermost samples, in the 48-50m interval, the pelletal glauconite content is clearly lower with values between 15-20%. The mineralogy of pelletal glauconite at 36.2m and 36.57m (RT12 and RT14) was analyzed resulting in very low amounts of expandable layers (<7%) and the d_{060}-values around 1.5162Å (Table 5.7).

Size distribution
The granulometry of the 30-49m interval can be subdivided in two parts. The part from 30 to 34m is relatively clay-rich with the distribution mode often <250µm. The lower 34-49m interval is however very coarse with modes >300µm (Figure 5.26).

Interpretation
Wouters and Schiltz (2011) interpreted the Diest sand member over the ca. 30-50m interval and a clayey top facies from ca. 30m until ca. 42m. The results of this work confirm a clay-rich top in the Retie-1 borehole from 30-35m and show that below 35m, the sediment becomes significantly coarser with the mode shifting from <250µm above to >300µm below 35m (Figure 5.26). However, unlike the clayey top sediments of the Dessel-2 and Dessel-3 boreholes, which are geographically only a few kilometers apart, the clayey top Diest in the Retie-1 borehole shows no traces of Fe-vermiculite or kaolinite-expandable in the clay mineralogy <2µm. Instead, clay-sized glauconite-smectite is the dominant clay mineral. Because the interpretation of the Diest D4 unit is mainly based on the presence of Fe-vermiculite, and not on grain-size, the entire 30-49m interval was consequently interpreted as the Diest D1 lithofacies ("typical coarse Diest sand" of Wouters and Schiltz, 2011) which has a clayey top part in the Retie-1 borehole. The top of the Diest Formation in the Retie-1 borehole can therefore not be simply correlated to the top Diest in the Dessel-2 and Dessel-3 boreholes. Biostratigraphy also indicates that such correlation indeed is problematic as the top Diest in Dessel is correlated with the DN9 biozone (Louwye et al., 2007) whereas in Retie, and also more to the east and west, the top Diest is correlated with the DN10 biozone (Louwye et al., 1999).

Table 5.7. Pelletal glauconite mineralogy in the Retie-1 borehole indicating pelletal glauconite content in %, the d060 position and the modeled amounts of higher expandable and low expandable glauconite-smectite with 27% and 5% expandable layers respectively. The final two columns indicate the total amount of glauconite and expandable layers in the sample.

Sample	Member	Content (%)	d060	Higher expandable G-S (27% expandable)	Low expandable G-S (5% expandable)	Total amount Glauconite layers	Total amount Expandable layers
RT12	Diest	48	1.5162	2	98	95	5
RT14	Diest	46	1.5162	5	95	94	6

V.5.1.8 The Beerse URS borehole

The Beerse borehole (location see Figure 5.9) is a 160m deep borehole cored at intervals 25-60m, 80-100m and 120-130m. The original interpretation was made by the company URS (URS, 2002) who interpreted the Diest Fm to be present from 48m till 130m based on lithology descriptions. Throughout the entire stratigraphic interval of the Diest Fm, large lithological heterogeneity is found (URS, 2002). In total 20 samples were collected in the different cored intervals to characterize the entire stratigraphic interval of the Diest Fm (Figure 5.27). The sediment description is shown below.

48-50m: Medium-sized to coarse glauconitic sand with black traces
50-60m: Medium-sized to coarse sand with smaller glauconite content, locally containing shells.
60-78m: Medium to finer sized sand, slightly glauconitic.
78-83m: Clayey glauconite-poor sand with brown colored clay and often bioturbated (Figure 5.28)
83-88m: Medium-fine sand; clayey sand to medium sand transition with brown clay and occasional bioturbations (Figure 5.29)
88-130m: Coarse, heteromorphic glauconitic sand with low clay content (Figure 5.29).

Bulk mineralogy of sands <32µm
The mineralogical results of the analyzed sand samples allow to subdivide the Diest Fm in the Beerse URS borehole in 3 parts. The lowermost part, from 88-130m depth contains a relatively stable mineralogy. Glauconitic minerals account for 40% to 65%, while dioctahedral Al-clays are present from 14-36%. The main anomaly in this lowermost part is caused by the important siderite contribution (12-18%) in the 96-99m interval. Under the binocular microscope, this siderite appears as needle-shaped crystals. Above 88m, until 60m, the mineralogy changes sharply as dioctahedral Al-clays are present in proportions >50%, kaolinite in proportions from 5 till 10% and glauconitic minerals in proportions less than 10%. As part of the dioctahedral Al-clays, also the amount of muscovite increases while the amount of siderite is relatively less important. In the upper 48-60m interval, the presence of a trioctahedral clay mineral is observed, possibly the Fe-vermiculite also identified in the Dessel-3 borehole, while also increased amounts of glauconitic minerals, chlorite and siderite, and lower amounts of 2:1 Al-clays and kaolinite compared to the 60-88m interval are found. The sample at 56.4m is furthermore very glauconitic (55%).

Clay mineralogy <2µm
Similar to the bulk mineralogical results, also the clay mineralogy <2µm allows a threefold subdivision. The lowermost 88-130m is characterized by a glauconite-smectite content >60% with the lower expandable type predominating the higher expandable type. In the 60-88m interval however, glauconite-smectite completely disappears in the clay mineralogical assemblage <2µm. Instead, the proportion of dioctahedral smectite reaches 40-45% in the 85-88m interval, and increases to >65% in the 78-85m interval. In the uppermost 48-60m, trioctahedral Fe-vermiculite is the most characteristic clay mineral while also the amount of dioctahedral smectite remains high (>40%). In contrast, the 56.4m sample is characterized by >60% glauconite-smectite.

Pelletal glauconite
Contrary to the existing general idea that the Diest Formation has a fairly constant glauconite content, glauconite pellets in the Beerse borehole show important variability. Whereas the pelletal glauconite amount is 30-37% in the 93-130m interval, it gradually decreases towards 88m. Between 85 and 86m, only 10% of pelletal glauconite is present, which decreases even further to less than 5% in the 78-85m interval. Above 60m, the pelletal

glauconite amount increases again slightly to percentages higher than 10%.
The mineralogical composition of pelletal glauconite in the lowermost part below 92m (samples RU188, RU192 and RU195) is characterized by very low expandable layers (<8%) and d_{060}-values between 1.5153 and 1.5171Å. Pelletal glauconite in the clayey, glauconite-poor interval between 60-87m has similar characteristics as indicated by the analysis of the 85.45m RU185 sample (Table 5.8).

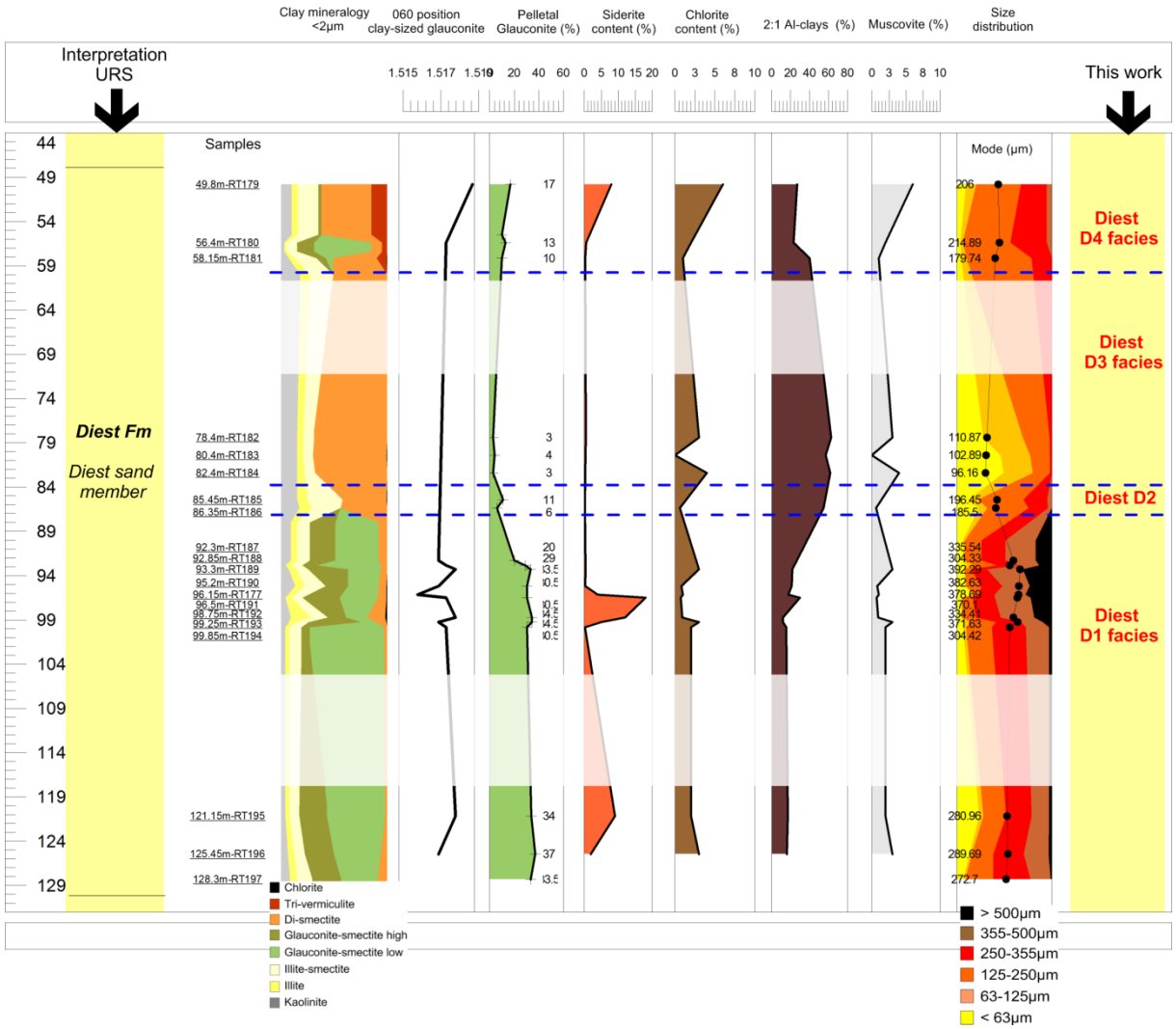

Figure 5.27. Quantitative (clay) mineralogical and sediment petrological data for the Diest Fm in the Beerse borehole. The most left column shows the initial interpretation based on borehole lithology descriptions URS (2002). Samples levels are indicated as underlined text in the second column. The different columns in the middle part summarize (clay) mineralogical data and size distribution with indication of the distribution mode . On the right side, the lithostratigraphic interpretation of this work is presented. Blurred transparent zones indicate a range from which no samples were analyzed. Data points in these 'no-sample" ranges may therefore be not continuous, as is suggested on the figure. The entire range of the Diest Fm was sampled in this borehole leading to the interpretation of 4 facies within the Diest Fm in the Beerse borehole.

Figure 5.28. Brown glauconite-poor and bioturbated clayey facies D3 in the Beerse URS in the 78-79m interval.

Figure 5.29. (Above): Intensively bioturbated glauconitic sand of the Diest D1 facies in the Beerse URS borehole in the 100-101m interval. (Below): The coarse glauconitic sand of the Diest D1 facies, with coarser sized, quartz-rich, 1cm-thick levels in the 95-96m interval.

Size distribution
The size distribution of the Beerse URS borehole displays little variation in the 100-130m interval resulting into a poorly sorted and relatively coarse distribution. The 88-100m interval is clearly coarser sized with more than 50% of grains >355µm. Above 88m however, the distribution becomes much finer and in the most clayey part between 78m and 83m, more than 50% of particles are smaller than 125µm while grains >250µm are scarce. Finally, the upper 48-60m interval is slightly coarser, with mainly grains in the 125-250µm interval and only 5% of the grains being larger than 355µm.

Interpretation
In the Beerse URS, the entire span of the Diest Fm was sampled and analyzed. The basal part (ca. 90-130m) consists of relatively coarse-sized sands with clay-sized glauconite-smectite the dominant clay mineral <2µm, which are the decisive criteria to interpret the Diest D1 facies, defined in the Westerlo borehole. Above 87m however, the coarse sandy facies gradually transitions into a clayey facies with much less pelletal glauconite. The clay mineralogy contains no clay-sized glauconite but instead is very smectite-rich, ca. 40% (Figure 5.27). Above 83m, the sediment becomes even more clay-rich with almost no pelletal glauconite and ca. 68% smectite in the clay fraction <2µm. This glauconite-poor and clay-rich facies is definitely a new lithofacies. We define the Diest D2 facies as the transitional sand-clay facies from 83-87m and the clay-rich and glauconite-poor Diest D3 facies above 83m (Figure 5.27). The upper boundary of this Diest D3 facies is difficult to assess as no samples were available from 60-75m but following the clay-rich description of the sediment in this interval (URS, 2002), the clay-rich facies between 60-83m is interpreted as Diest D3 subdivision. The uppermost three samples, between 45-60m, are again much more sandy and contain Fe-vermiculite and kaolinite-expandable. This part is therefore interpreted as the Diest D4 facies.

Table 5.8. Pelletal glauconite mineralogy evolution in the Beerse borehole indicating stratigraphy, pelletal glauconite content in %, the d060 position and the modeled amounts of higher expandable and low expandable glauconite-smectite with 27% and 5% expandable layers respectively. The final two columns indicate the total amount of glauconite and expandable layers in the sample.

Sample	Member	Content (%)	d060	Higher expandable G-S (27% expandable)	Low expandable G-S (5% expandable)	Total amount Glauconite layers	Total amount Expandable layers
RGU185	Diest	11	1.5162	15	85	92	8
RGU188	Diest	29	1.5153	8	92	93	7
RGU192	Diest	34	1.5171	12	88	92	8
RGU195	Diest	34	1.5157	8	92	93	7

V.5.1.9 The PIDPA Put-8 borehole

The Put-8 borehole in Dessel is a suction, pure water drilling without clay-rich drilling muds, of the drinking water company PIDPA (Figure 5.9). During the drilling process, a sample was collected from the drilling fluid every 4m and sampled for analyses. The stratigraphic description on site of the sediment allowed to identify the Diest Fm below 40-44m until at least 108m (bottom drilling). The sediment from 44-56m is a dark green glauconitic sand, medium-sized and slightly clayey. The sediment oxidized to a brown color within hours after exposure to air-dry conditions. Below 56m to 108m, the sediment is much coarser-sized and loose, is green colored and retains its color after exposure. As the objective of the current chapter is to document the mineralogy and sediment petrology of the Diest Fm, samples were collected every 4m from 44-108m. Although the nature of the drilling method only allows taking samples that consist of sediment mixed over 4m, this is also an advantage because in this way almost the entire stratigraphic interval of the Diest Fm can be studied. Samples were collected every 4m from 44m until 108m (Figure 5.30).

Bulk mineralogy of sands <32µm
The mineralogical composition of the sampled interval is mainly controlled by the ratio of dioctahedral Al-clays vs. Fe-clays. In the upper part (44-56m), dioctahedral Al-clays are present in amounts of 26-48%, with relatively less glauconitic minerals (12-26%). Most characteristic for this interval is however the presence of trioctahedral clay, presumably the Fe-vermiculite, also identified in the Dessel-2, Dessel-3 and Beerse URS boreholes. In the

lower 56-108m interval, the proportion of glauconitic minerals is much higher (systematically >60%) while 2:1 Al-clays are less abundant (<20%). Carbonates are only present in the form of siderite, which is found in proportions <2.5% throughout the entire interval. The same observation is made for feldspars (microcline and albite) and sulphur-bearing minerals (pyrite-gypsum). Fe-(oxy)hydroxide minerals, mainly goethite and ferrihydrite, occur in considerable amounts (2-13%) throughout the interval.

Clay mineralogy <2µm
Clay mineralogical results support the results from the bulk analysis since in the upper 44-56m interval, 20% of smectite is present with 20-35% of illite-smectite minerals. Trioctahedral vermiculite is identified (5-15%) together with kaolinite-expandable. Furthermore, the amount of glauconite-smectite gradually increases downwards, less than 10% in the 44m sample while almost 50% is present in the 56m sample. Below 56m, the amount of glauconite-smectite increases further to 80-90% with the high expandable glauconite phase being more abundant than the low expandable phase (Figure 5.30).

Pelletal glauconite content
Glauconite pellets occur in very regular proportions in the sediment, with amounts varying between 40 and 47% (Figure 5.30). One sample, at 56m, contains up to 58% of pelletal glauconite.

Size distribution
Grain size distributions of the Pidpa Put-8 borehole demonstrate that in the upper part, until 52m, the distribution is medium-sized with a slightly elevated clay content. Below, the amount of grains >355µm reaches 20% at the 60m level, and increases to a constant 50% in the 64-108m interval. The distribution mode is low in the upper interval (>250µm) whereas below 56m, the mode is systematically very coarse >300µm (Figure 5.30).

Interpretation
The results presented above allow to subdivide the stratigraphic 44-108m interval of the Diest Fm into two lithofacies. From ca. 44-56m, the presence of Fe-vermiculite and kaolinite-expandable point to the Diest D4 lithofacies whereas below, from 56-108m, the coarse and clay-poor grain-size, high pelletal glauconite content and clay-sized glauconite content indicate the occurrence of the general lithofacies of the Diest sand member: the Diest D1 lithofacies (Figure 5.30).

V.5.1.10 The Rees 17E399 borehole

The uppermost 40m of the Rees borehole was sampled from the stratigraphical collection of the Geological Survey of Belgium (GSB). Buffel et al. (2001) interpreted the Diest Formation below 33m based on granulometry and regional correlations. In this chapter, only the 33-40m Diest Fm interval will be discussed as the upper part of this borehole with the occurrence of the Kasterlee and Poederlee Formation is discussed in further chapters. The sediment in the 33-40m interval underwent prolonged exposure to air-dry conditions resulting in intense oxidation and rusty appearance of the sediment. The sediment is generally coarse-sized and loosely packed although a clay lense of 0.5cm thickness was observed at 35.9m. Locally in the sediment, red staining is observed at 35.70m, 36.60m, 37.25m and 39.5m. In total, 12 samples were collected spread over the 7m interval.

Bulk mineralogy of sands <32µm
The mineralogy of the 33-39.5m interval of the Rees borehole consists of 28-51% 2:1 Al-clays, 4-22% glauconitic mineral, 5-13% trioctahedral clays (chlorite excluded) and 2-5% of limonitic minerals. Siderite typically occurs dispersed in the sediment in concentrations <1% but also occurs concentrated in the red-stained levels from 4 to even 13% in the 37.4m sample (Figure 5.31). Chlorite occurs in proportions from 1-8%. Also apatite is found in proportions <2%.

Clay mineralogy <2µm
The clay mineralogy of the 33-39.5m interval consists of 35-60% of expandable minerals, of which the majority is smectite and 6-16% of trioctahedral Fe-vermiculite. Illite and illite-smectite show relatively low variability of 5-15% and 16-30% respectively while glauconite-smectite is scarce (<10%), except in the 35.7-36.6m interval. Kaolinite percentages are more variable, 4-26%. Part of the kaolinite is again mixed-layered with expandable minerals (Figure 5.31).

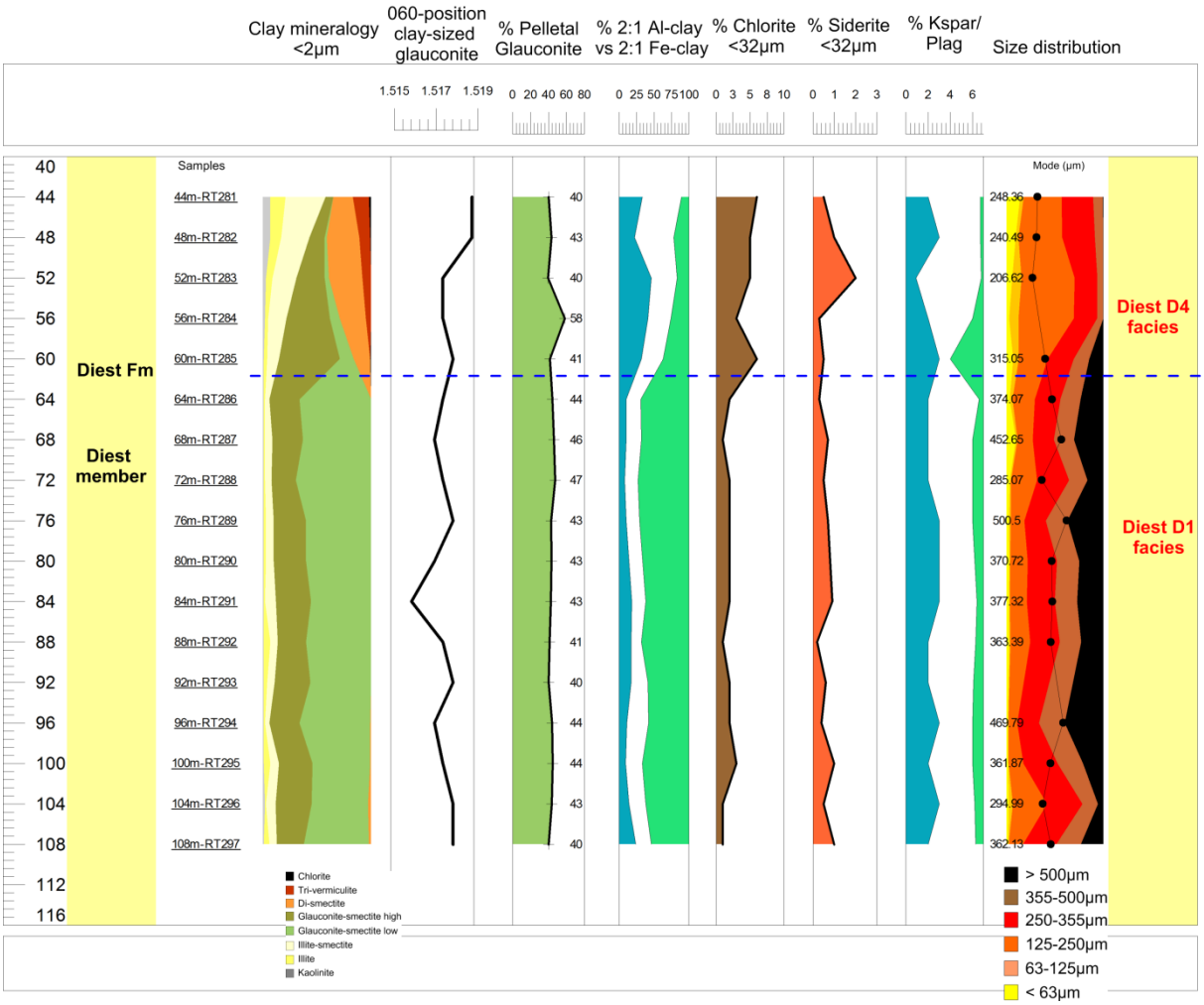

Figure 5.30. Quantitative (clay) mineralogical and sediment petrological data for the Diest Fm in the PIDPA-Put-8 borehole. The most left column shows the initial interpretation based on borehole lithology descriptions. Samples levels are indicated as underlined text in the second column. The different columns in the middle part summarize (clay) mineralogical data and size distribution with indication of the distribution mode. On the right side, the lithostratigraphic interpretation of this work is presented. Blurred transparent zones indicate a range from which no samples were analyzed. Data points in these 'no-sample" ranges may therefore be not continuous, as is suggested on the figure.

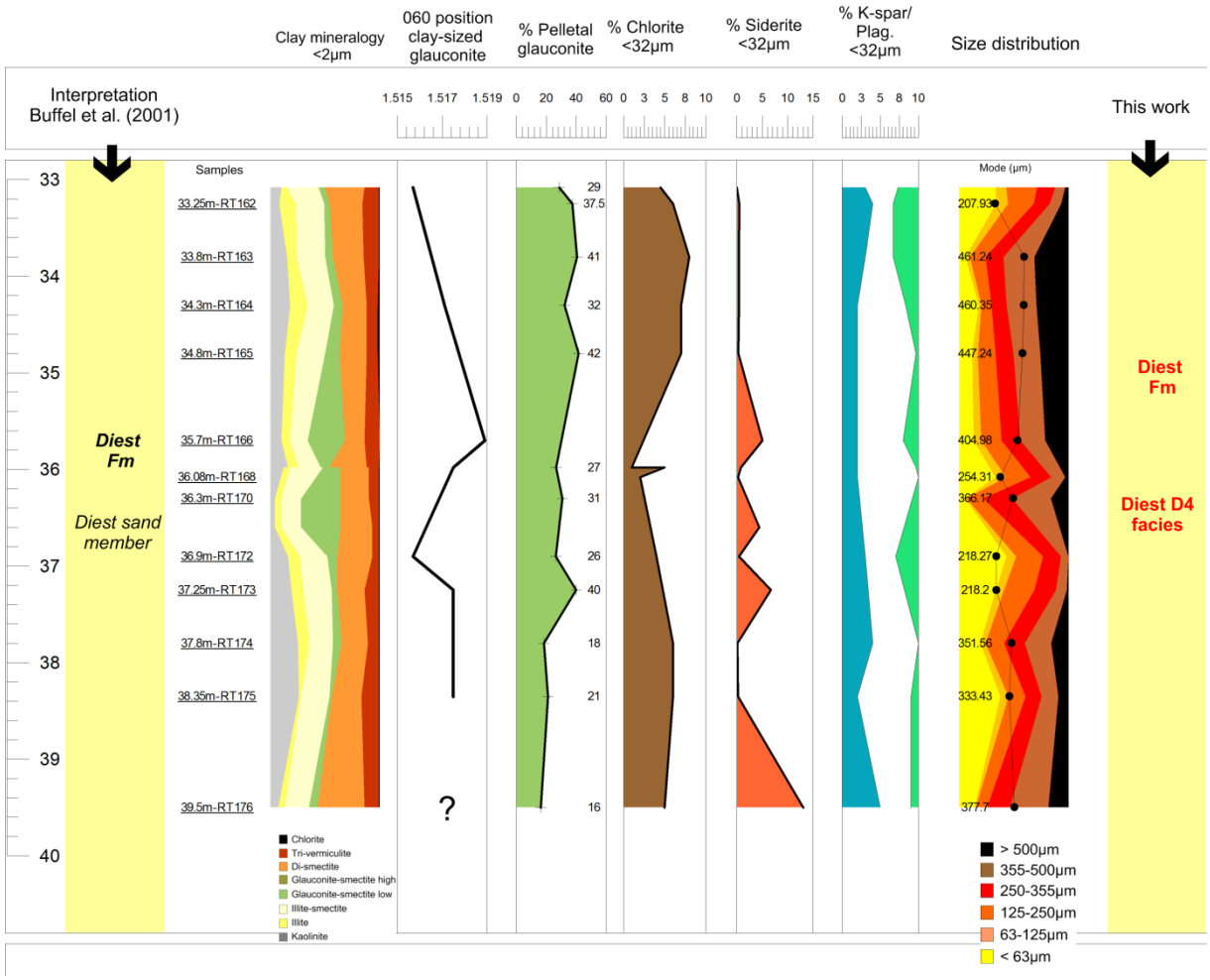

Figure 5.31. Quantitative (clay) mineralogical and sediment petrological data for the Diest Fm in the Rees 17E399 borehole. The most left column shows the initial interpretation based on grain-size and regional correlations (Buffel et al., 2001). Samples levels are indicated as underlined text in the second column. The different columns in the middle part summarize (clay) mineralogical data and size distribution with indication of the distribution mode . On the right side, the lithostratigraphic interpretation of this work is presented.

Pelletal glauconite

The amount of glauconite pellets in the upper 3m of the interval is ca. 30%, but slightly decreases below 37.5m, with values of ca. 20%. The mineralogical composition of the pelletal glauconite is characterized with substantial amounts of expandable layers (>12%) and d_{060} values around 1.5171Å (Table 5.9).

Size distribution

Granulometry of the Rees 33-39.5m interval demonstrates a poorly sorted distribution with the mode of the distribution almost systematically >250µm but often higher than 350µm resulting in a very coarse-sized sediment (Figure 5.31).

Interpretation

Since Fe-vermiculite and kaolinite-expandable was systematically found in the 33-40m Diest Fm interval, the entire interval is interpreted as the Diest D4 facies (Figure 5.31). The occurrence of the Diest D4 lithofacies seems not restricted to clay-rich sediments such as identified in the top of the Dessel-2 and Dessel-3 boreholes but also occurs in coarser-sized sediments such as in the Rees borehole.

Table 5.9. Pelletal glauconite mineralogy evolution in the Rees borehole indicating stratigraphy, pelletal glauconite content in %, the d060 position and the modeled amounts of higher expandable and low expandable glauconite-smectite with 27% and 5% expandable layers respectively. The final two columns indicate the total amount of glauconite and expandable layers in the sample.

Sample	Member	Content (%)	d060	Higher expandable G-S (27% expandable)	Low expandable G-S (5% expandable)	Total amount Glauconite layers	Total amount Expandable layers
RGU166	Diest	37	1.5153	51	49	84	16
RGU168	Diest	22	1.5171	49	51	84	16
RGU172	Diest	21	1.5175	40	60	86	14
RGU175	Diest	16	1.5171	35	65	87	13

V.5.1.11 Outcrops in the Hageland area

Samples of the Diest sand member were not only collected in the subsurface of the Campine Basin but from the outcropping area in the Hageland region (Figure 5.9). The outcrops often are characterized by some form of Fe-cementation or encrustation, resulting into meter-thick banks of Fe-sandstone or cm-thin Fe-crusts consisting of limonitic minerals and even metallic Fe. Non-cemented and non-oxidized glauconitic sand can occur closely related in space to iron-cemented sandstone banks, e.g. as alternating cm thick layers. Whereas cemented iron layers generally follow the sedimentary structuring , Fe-crusts can also cross cut the sedimentary structure and even display typical liesegang shapes (Figure 5.32).

Typically, an iron-cemented stone bank occurs associated with thin clay layers, which also commonly are intercalated in the sand matrix in the Hageland outcrops. Samples were collected from the loose glauconitic coarse sand, from the red or brown clay layers, and additional samples from the Fe-sandstone in various outcrops in the Hageland area (Table 5.10; see for locations Figure 5.9).

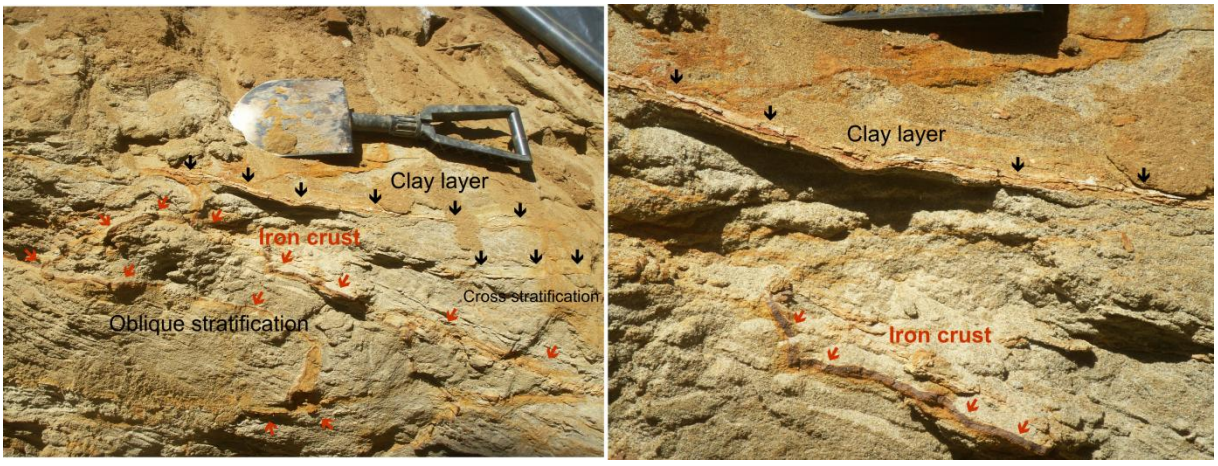

Figure 5.32. The Hageland Diest sand with typical oblique stratification, thin bedding-parallel clay layers, iron encrustations and liesegang banding structures indicated by red arrows.

Table 5.10. Samples collected from outcrops in the Hageland. In total , 19 samples were collected among which 5 clay layers and 14 sand matrix samples.

Sample code	Outcrop	Description	Pelletal glauconite (%)
RT224	Gasthuisberg	Grey clay layer	0
RT239	Gasthuisberg	Grey clay layer	0
RT241	Gasthuisberg	Grey clay layer	0
RT242	Gasthuisberg	Purple-Red clay layer	0
RU139	Beninksberg	Brown-red clay layer	0
RT229	Gasthuisberg	Coarse glauconitic sand	32
RT236	Kesselberg	Coarse glauconitic sand	45
RT231	Gasthuisberg	Coarse glauconitic sand	36
RT232	Gasthuisberg	Coarse glauconitic sand	31
RT233	Gasthuisberg	Coarse glauconitic sand	38
RT234	Gasthuisberg	Coarse glauconitic sand	33
RU140	Wijngaardberg	Coarse glauconitic sand	36
RU141	Wijngaardberg	Coarse glauconitic sand	31
RU142	Wijngaardberg	Coarse glauconitic sand	34
RU143	Beninksberg	Medium-sized glauconitic sand	26
RU144	Beninksberg	Medium-sized glauconitic sand	48
RU145	Beninksberg	Coarse glauconitic sand	30
RU146	Beninksberg	Coarse glauconitic sand	32
RU147	Pellenberg	Coarse glauconitic sand	58
RU148	Pellenberg	Coarse glauconitic sand	58

Bulk mineralogy

The mineralogical composition of sand samples consists predominantly of glauconitic minerals (40-80%), limonitic alteration minerals (mainly goethite), quartz and 2:1 Al-clays. Kaolinite and both feldspar groups are minor constituents. Carbonate minerals, also siderite, are absent. White powdery and very coarse grains to pebbles, typically a few mm in diameter, were found in the Wijngaardberg outcrop and occur randomly dispersed in the sediment and consist of poorly crystalline quartz (90%) and amorphous opal (10%).

Clay samples on the contrary do not contain any glauconitic minerals but are instead composed of 40-50% 2:1 Al-clays and 25-40% quartz. Kaolinite and feldspars are minor constituents whereas anatase and gypsum occur in traces.

Clay mineralogy

The clay mineralogical composition of sand samples <2µm consists in all outcrop samples of high amounts of glauconite-smectite (>80%) with low expandable glauconite-smectite more abundant than the high expandable type (Figure 5.33). This composition is also systematically encountered in Fe-sandstone samples. In contrast with sand samples however, the clay mineralogy of clays contains no glauconite-smectite but instead consists of 30-35% smectite, 35-40% illite-smectite, 15% illite and ca. 10% kaolinite (Figure 5.34).

Pelletal glauconite

Glauconite pellets in the Hageland occur in proportions between 26% and 58% with an average of 39%. In contrast to other intervals of the Diest Formation, pelletal glauconite in the Hageland Diest deposits is not only green colored but also brown, altered glauconite pellets are common. The mineralogical composition of the glauconite pellets is variable in expandable layer amount (Table 5.11). The amount of expandable layers is never found lower than 9% but can be higher. Such higher expandable layer contents seem restricted to

samples with elevated amounts of brown, weathered glauconite pellets.
In Fe-sandstone samples, most pelletal glauconite has been altered by goethitization, preserving the outer pelletal shape but changing the mineralogy. Some parts of the Fe-sandstone have however not been altered and green pelletal glauconite is still present. Clay layers contain no pelletal glauconite.

Size distribution
The grain size distribution of the sand samples demonstrates a coarse-sized distribution with low clay contents. Such coarse granulometry is typical for Diest Fm sands in the Hageland, with the mode of the distribution in the 250-355µm interval. Nevertheless, also finer-sized sands occur, e.g. the Beninksberg samples, with distribution modes <250µm (Figure 5.35).

Table 5.11. Pelletal glauconite mineralogy of outcrop Diest samples in the Hageland area indicating stratigraphy, pelletal glauconite content in %, the d060 position and the modeled amounts of higher expandable and low expandable glauconite-smectite with 27% and 5% expandable layers respectively. The final two columns indicate the total amount of glauconite and expandable layers in the sample.

Sample	Member	Content (%)	d060	Higher expandable G-S (27% expandable)	Low expandable G-S (5% expandable)	Total amount Glauconite layers	Total amount Expandable layers
RGU141	Diest	31	1.5153	27	73	89	11
RGU144	Diest	48	1.5157	40	60	86	14
RT230	Diest	55	1.5153	7	93	93	7
RT232	Diest	31	1.518	30	70	86	14
RT235	Diest	32	1.5175	22	78	87	13

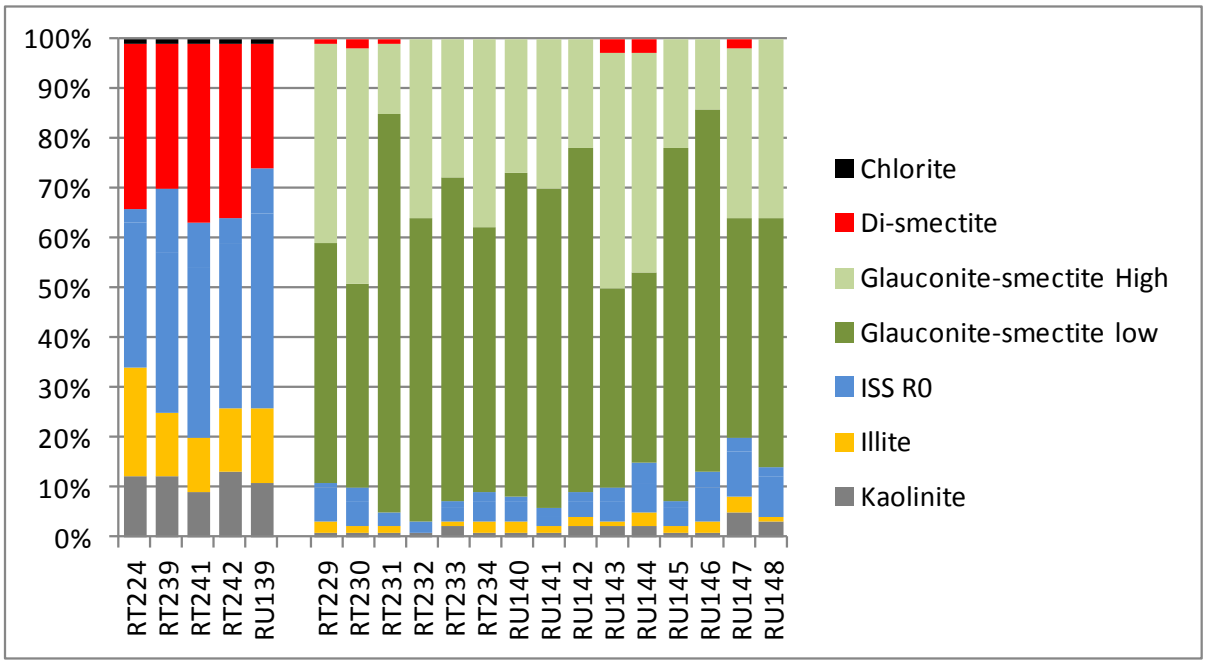

Figure 5.33. Graphical representation of quantitative clay mineralogical data of 5 clay samples (left) and 14 sand samples (right) from various outcrops in the Hageland area.

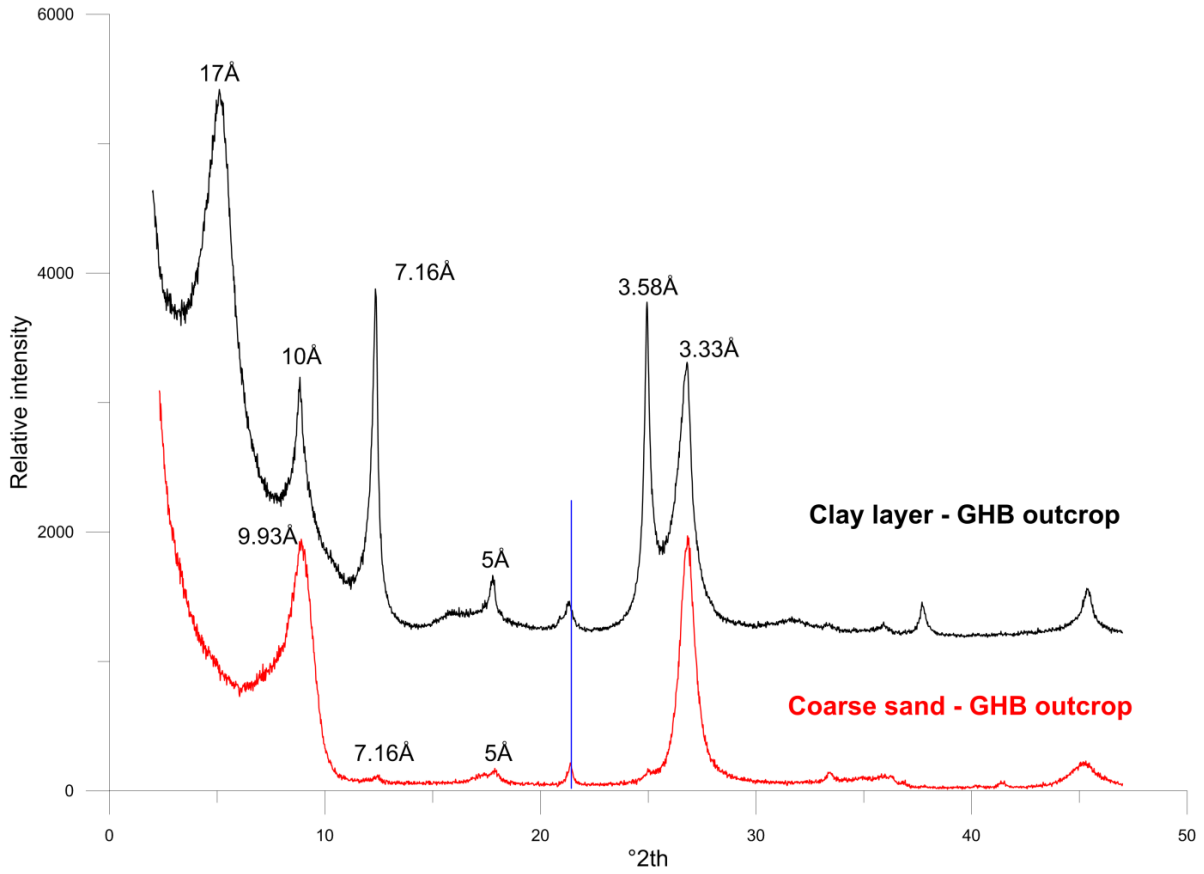

Figure 5.34. Comparison of glycolated diffraction patterns of 2µm fractions of sands and clays occurring in close contact in the Gasthuisberg outcrop in the Hageland region. Blue lines indicate the presence of goethite.

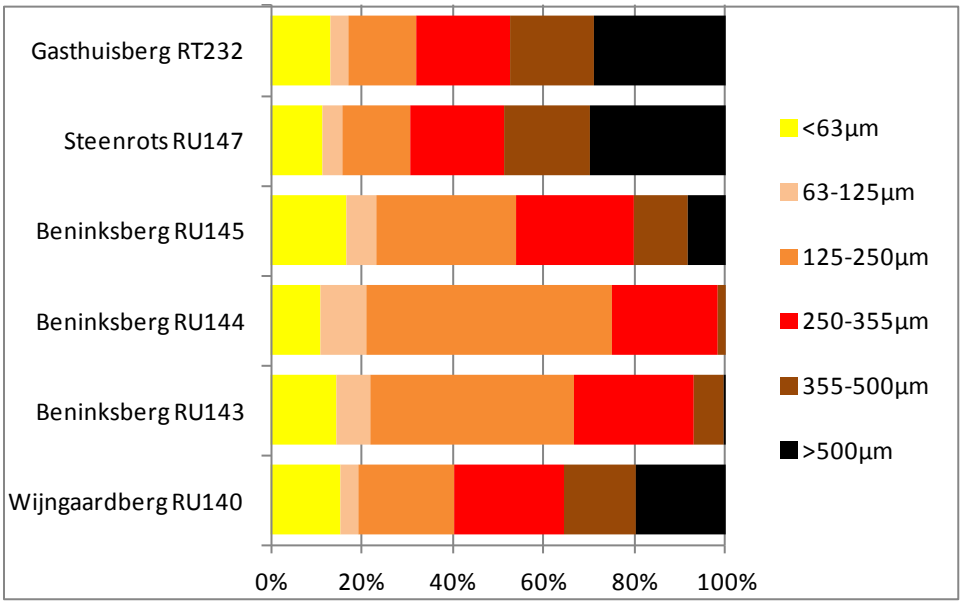

Figure 5.35. Size distribution data of 6 samples from the outcrops Gasthuisberg, Steenrots, Beninksberg and Wijngaardberg in the Hageland. Distributions systematically are coarse-sized, although also finer-sized sands were found at certain levels at the Beninksberg.

Detrital grain shapes of the Hageland Diest sand and the Campine Diest D1 sand

Although the assessment of particle shape parameters has always been a classical sediment-petrological characterization technique, measurements are very labor intensive and furthermore prone to an important factor of subjectivity, causing this technique to become neglected in clastic sedimentological studies. With the development of dynamic image analysis using a Camsizer (Vos et al., in preparation), millions of particles can be scanned within a short time span. The great advantage by using such equipments is their objectivity, improved particle statistics and it is furthermore less labor intensive. In order to explore the possibilities of this renewed technique applied on the Diest Formation case, a set of 21 samples of the Diest D1 lithofacies in the Campine (the coarse, loosely packed Diest sand member) was compared to 12 samples of the Diest sand member in the Hageland.
As the objective was to compare mainly quartz shapes, samples were wet sieved >32µm, and glauconite pellets removed by magnetic separation. Next, each sample was subdivided by sieving in 5 sieve classes: [>500µm]; [500-250µm]; [250-180µm]; [180-90µm] and [<90µm]. This resulted in fractions consisting of >95% of quartz. In this way, 5 Camsizer measurements were performed on each sample. The selected shape parameters are the sphericity and the roundness parameters. Whereas sphericity is a measure of how close a particle approaches the shape of a sphere and generally relates to the host rock of particles, roundness is a measure of the irregularity of the grain outline and is an estimate for the amount of transport (ISO, 2006). Particles subjected to analysis are evaluated by a score between 0 and 1, with higher values indicating particles are more spherical and have a better curved, or less irregular, particle outline. The value scores are made comparable to the shape characterization table proposed by Krumbein and Sloss (1963).

The size-dependant results of the Diest sand member(Figure 5.36), displayed by the average and the standard deviation between brackets, show that for both sphericity and roundness, values are systematically higher for larger particle classes. Furthermore, the pattern for both the Campine and Hageland samples is very similarly shaped and the average values for each size class is equivalent for Campine and Hageland.

It is presently still unclear if grain-shape is a suitable parameter to find differences between sand units which were deposited in similar energetic environments. Even if the provenance areas of those sand masses would be different, the shape characteristics could be significantly changed in the depositional environment. Nevertheless, it can be concluded that quartz shapes in the Diest D1 facies and the Hageland are characterized by very low variability. Although the value of this technique for such stratigraphic distinction is still to be further explored, it can be concluded that quartz grain-shapes do not distinguish the Diest D1 lithofacies from the Hageland Diest sand member.

Interpretation
It has been demonstrated that the glauconitic Diest sand in the Hageland has some typical lithological characteristics: coarse-sized, on average 38% pelletal glauconite and a clay fraction, at least in sands, consisting predominantly of glauconite-smectite. These characteristics were also found in the Campine Diest D1 unit defined earlier in this work and therefore could represent the same sand mass. However, clear differences between Diest Campine and Diest Hageland in heavy mineral content, pelletal glauconite radiometric dating and sediment transport directions still suggest that both can be considered as different sand units. Therefore, although clay mineralogy and sediment petrology do not allow a distinction, the occurrence of the Diest sand member in the Hageland is treated separate from the Campine Diest D1 facies.

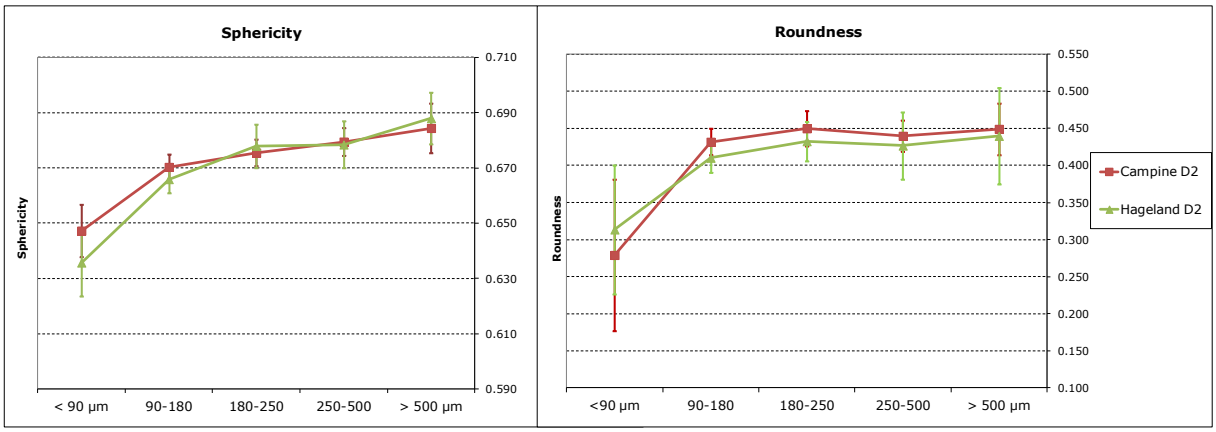

Figure 5.36. Sphericity and roundness values for 21 Campine D2 and 13 Hageland D2 samples. The average value is pointed out with the negative and positive standard deviation indicated by the vertical lines.

V.5.1.12 The Flemish hills: Muziekbosberg and Pottelberg

A set of 8 samples originating from the top parts of the Pottelberg and Muziekbosberg, positioned west of Brussels, were analyzed (Figure 5.7 and Figure 5.37). The sand deposits on the top of these hills have traditionally being attributed to the Diest Formation, as a lateral westward continuation of the Diest sand member deposits in the Hageland (see old geological map 1:40000 and more recent 1:50000 geological map Geraardsbergen). The stratigraphic position of these deposits is however controversial because there are very few elements, e.g. the presence of glauconite and ironstones, supporting the hypothesis. The deposits are furthermore devoid of any fossils. Houthuys (2014) has reinvestigated the stratigraphic position of the sands in the top of these hills. During his study, samples from the outcrops were analysed for comparison with genuine Hageland Diest Formation mineralogy and size distribution. Houthuys (op.cit.) identified 3 subunits in these outcrops and samples of all three subunits were examined for mineralogical content and size distribution.

Samples RU124, RU125 are from the lowermost bioturbated sand of which the base is formed by bluish egg-shaped pebbles (several cm's thick) which are very similar to those reported at the base of the Houthalen Member of the Bolderberg Fm (De Meuter and Laga, 1976). Samples RU121, RU122, RU128 and RU129 were collected in the middle section characterized by a low-angle parallel lamination with high amounts of silicified pebbles. Whereas these two lower parts typically are whitish to grey colored with limited limonitization, the uppermost part has a red-brown color with more intensive limonitization. Samples RU126 and RU127 at the Pottelberg originate from this uppermost section which is characterized by parallel lamination and higher pelletal glauconite contents (Figure 5.37).

Results

All the samples investigated show a clay mineralogy dominated by kaolinite with smaller contributions from illite, illite-smectite and glauconite-smectite and traces of smectite (Figure 5.38). Sample RU121 is a clay layer and does not contain any glauconite-smectite. In sand samples however, glauconite-smectite is systematically present with the low-expandable glauconite-smectite type predominating the higher expandable type.

The grain-size distribution of the samples in the lower and middle units is relatively fine-grained with modes of the distribution between 200 and 250 µm which is rather unusual for the generally coarse Diest sand member in the Hageland, with the exception of a finer-sized sample at the Beninksberg (Figure 5.39). The size distribution of samples in the upper units is however slightly coarser with distribution modes around 300µm (Figure 5.39). It can be seen in Figure 5.39 that samples are progressively coarser upwards. In comparison with the typical grain-size distribution of Hageland Diest sands, the top Flemish hills are much better sorted and generally finer-sized.

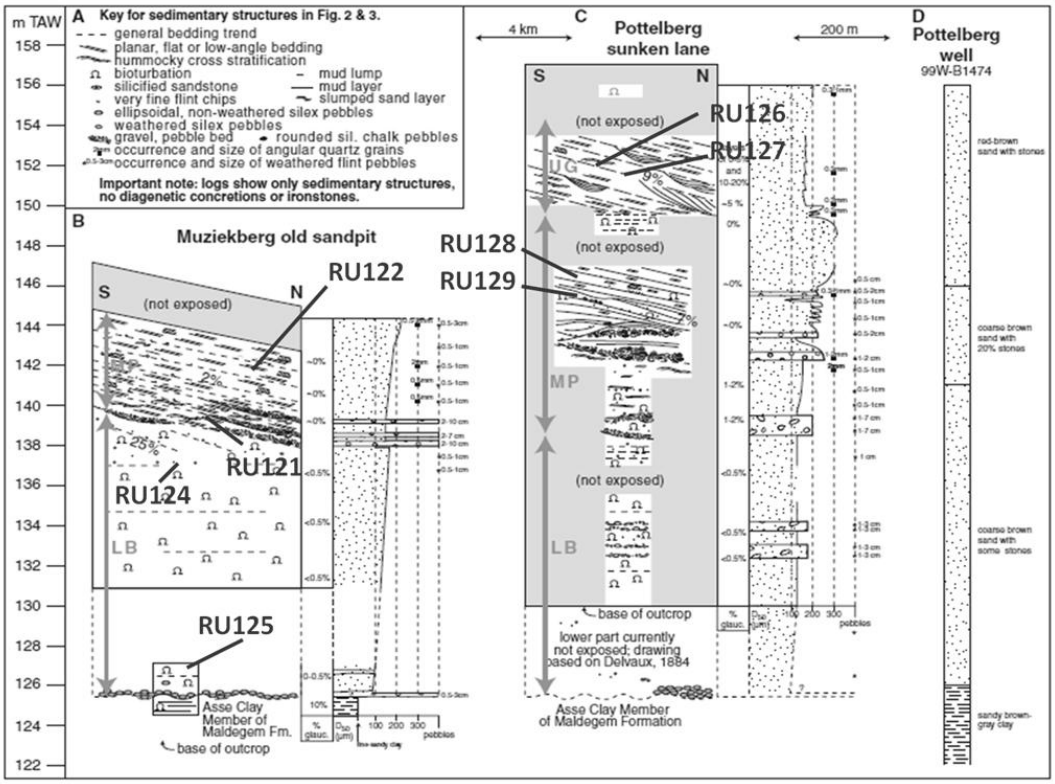

Figure 5.37. Vertical succession and grain size log of the sedimentary facies of the Flemish Hills Sands on the Muziekbosberg and Pottelberg indicating the samples investigated in this study (modified after Houthuys, 2014).

Pelletal glauconite is scarce in the lowermost bioturbated sand and the middle section, with amounts systematically lower than 1%. The uppermost section contains up to 5% pellets consisting of glauconite minerals. Many of the glauconite pellets have however been altered by goethitization which preserved the original grain shapes but not the mineralogy. When also taking the goethitic pellets into account, the two lowermost sections contain less than 2% pellets. The sample of the uppermost section of the Muziekbosberg contains 5.3% pellets, while those at the Pottelberg were found to contain 13% and 45% of pelletal material. In comparison, the pelletal glauconite content in the Hageland Diest sand is on average 39%. This means that only in the uppermost part of Flemish hills pelletal glauconite is found in quantities comparable to the Hageland.

It is repeated here that in the Hageland sediment small (<0.5cm) white powdery pebbles sporadically occur dispersed in the sediment consisting of poorly crystalline quartz and opal. Houthuys (2014) reported on the frequent occurrence of white silicified chalk pebbles in the middle section of the Flemish hills which are much larger (up to 1-3cm) but have an identical mineralogical composition to the small powdery coarse grains/pebbles occurring in the Hageland (poorly crystalline quartz and minor opal).

Interpretation

Based on sedimentary facies analysis, Houthuys (2014) concluded that the deposits on top of the Flemish hills do not belong to the Diest Fm but instead proposes an Eocene age for these deposits. The contribution from the present mineralogical and grain-size study is a confirmation that the samples of the top Flemish hills are significantly different from the Hageland Diest samples. A first important difference is the kaolinite-dominated clay mineralogy in contrast to the glauconite-smectite dominated clay mineralogy of the Hageland Diest sands. Secondly, the grain-size distribution of the top Flemish hill sands is finer-sized and much better sorted compared to the Hageland Diest sands. Also the pelletal glauconite content is considerably lower compared to the Hageland Diest sands. Nevertheless, the mineralogical similarity between the large silicified chalk pebbles in the Flemish hills and fine powdery pebbles in the Hageland is remarkable, which still suggests some kind of relation between both.

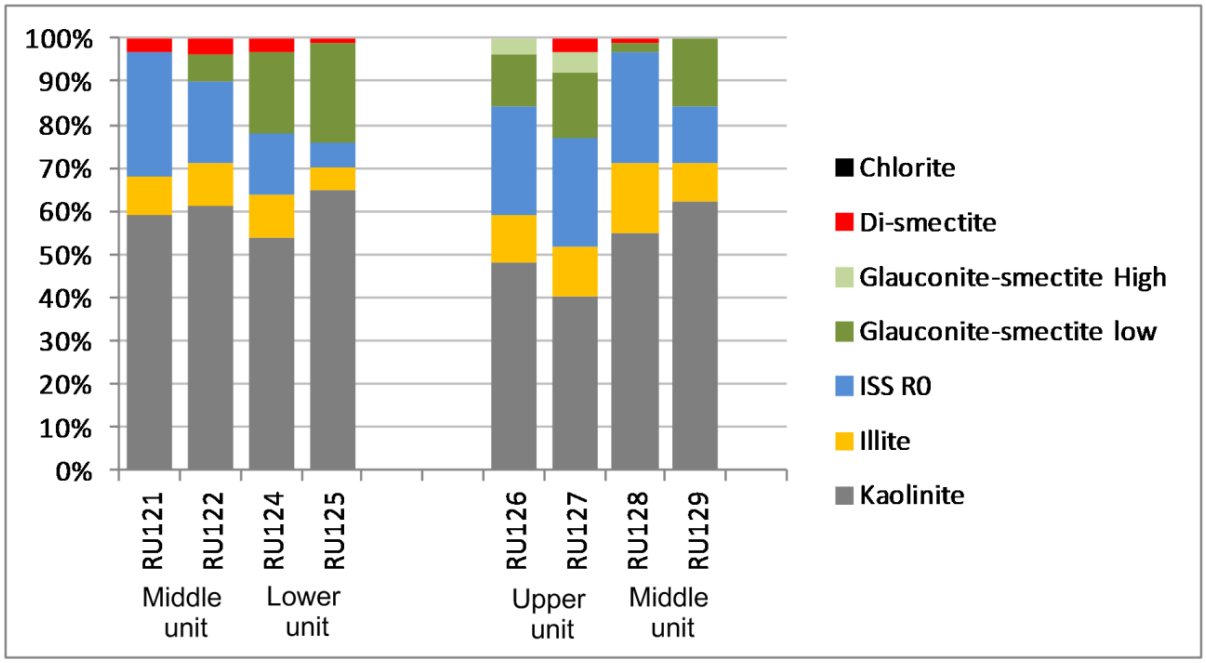

Figure 5.38: Quantitative clay mineralogical results of 2µm fraction of samples of the Muziekbosberg (left) and the Pottelberg (right).

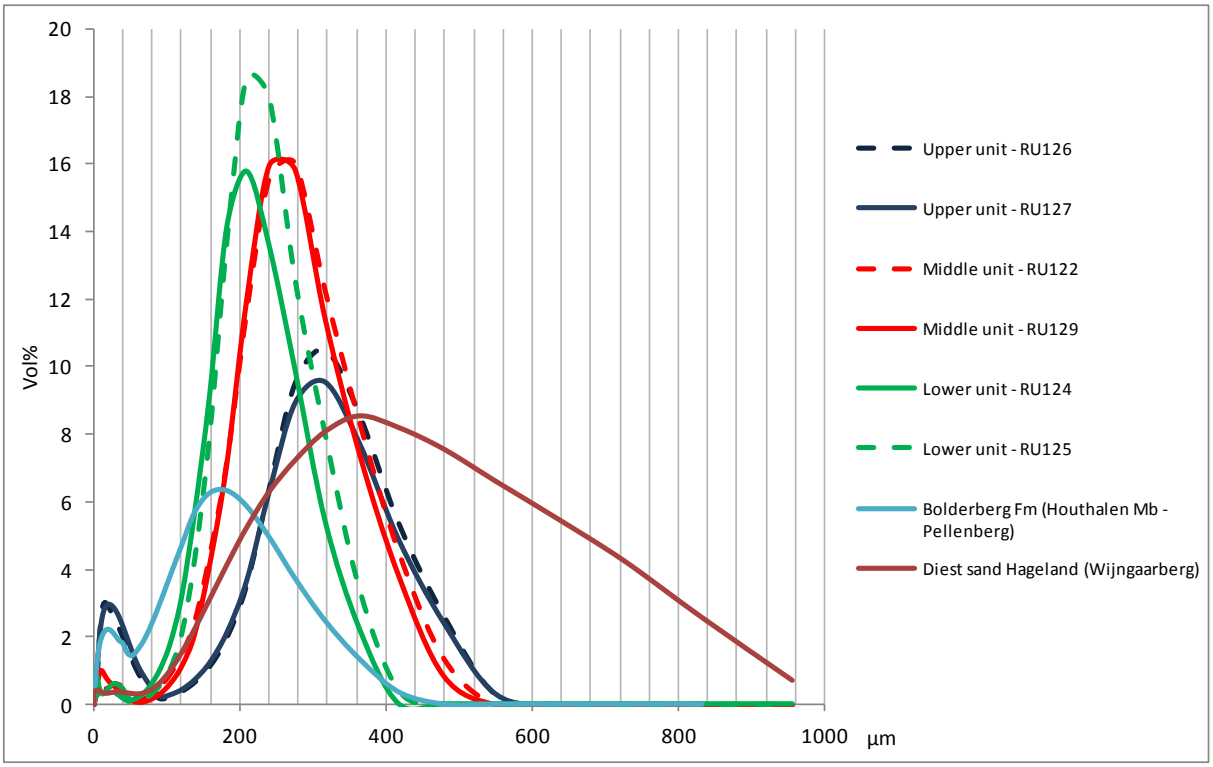

Figure 5.39. Grain-size distribution of samples of the lower unit (green), the middle unit (red) and the upper unit (blue) of the top Flemish hills showing a coarsening upward trend. In comparison, the grain-size distribution of a typical sample of the Diest sand in the Hageland (brown) and one of the Houthalen Member of the Bolderberg Fm (light blue) is shown.

V.6 DISCUSSION

V.6.1 Definition of different lithofacies and relation with dinoflagellate cyst biostratigraphy

In the previous section, mineralogical and sediment petrological data were presented for different stratigraphic intervals and different geographical locations of the Diest Formation. These results demonstrate a large amount of variability and heterogeneity in the Diest Formation. However, at one location the variable mineralogical and sediment petrological properties seem to occur grouped in certain stratigraphic depth intervals that also can be recognised in sections at other locations. This allowed to discriminate several lithofacies within the formation based on characteristic features. Apart from the already defined Deurne and Dessel Members, specific numbers have been assigned to the different lithofacies identified in the Diest sand member, namely Diest D1 to Diest D4 facies. These numbers simply have a discriminating function and are not necessarily in the correct stratigraphic order. In this section, the characteristics of each defined lithofacies will be listed. Furthermore, the lithostratigraphic subdivision will be correlated with dinoflagellate cyst biostratigraphy of nearby boreholes , i.e. the DN8, DN9 and DN10 biozones reported for the Diest Formation by Louwye et al., (1999), Louwye (2002), Louwye et al., (2007). A northwest-southeast oriented profile through the Campine area was constructed (see Figure 5.40 and location in Figure 5.9) indicating reference biozones and the different litho-facies defined in this work. Below, the specific characteristics of every defined facies is summarized.

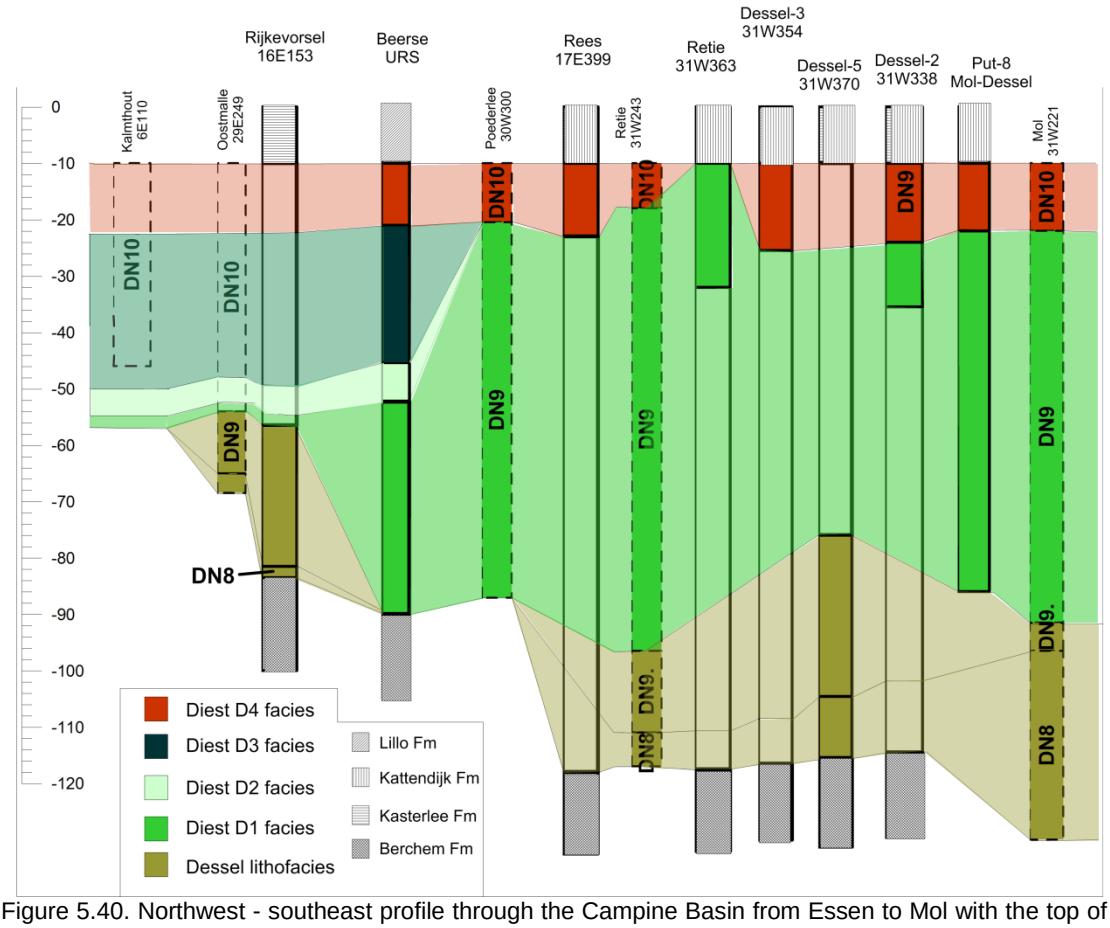

Figure 5.40. Northwest - southeast profile through the Campine Basin from Essen to Mol with the top of the Diest Fm represented as a flat surface. The different litho-units defined in this work are shown over the different borehole sections and interpolated in brighter color. Dinoflagellate cyst biozones of nearby reference boreholes are also drawn in stripes and marked with "DN" annotations (after Louwye et al., 1999; Louwye et al., 2007). Profile line location can be found in Figure 5.9.

V.6.1.1 The Deurne lithofacies

The Deurne Member is an official member of the Diest Formation and is defined as a fine-grained glauconitic and calcareous sand unit at the base of the Diest Formation. Its occurrence is restricted to the Antwerp area. Deurne Member samples typically contain abundant bivalves and bryozoans. Dinoflagellate cysts of the Deurne Member point to a DN8 biozone (Louwye, 2002). Only three samples of the Deurne Member were investigated. The clay mineralogy of these samples is relatively smectite-rich and resembles the clay mineralogy found in samples belonging to the Berchem Formation. The mineralogy of the clay-sized glauconite consists of mainly higher-expandable glauconite-smectite, which is also found in the clay-sized fraction of the Berchem Fm samples. This mineralogical sharply contrast with the generally glauconite-smectite dominated clay mineralogy and the mainly low-expandable clay-sized glauconite of the Diest sand member. The pelletal glauconite content in these samples ranges, in contrast with the slightly less pelletal glauconite-rich Dessel Member, between 39% and 46% (Figure 5.41).

V.6.1.2 The Dessel lithofacies

The Dessel Member is another official member of the Diest Formation and is, similarly to the Deurne Member, fine-grained but occurs only in the subsurface of the Campine at the base of the Diest Formation. Samples of the Dessel Member are reported rich in calcareous microfossils (Laga and De Meuter, 1972). In this work, the Dessel lithofacies was assigned to all Campine sediments at the base of the Diest Formation with a relatively fine-grained grain-size (mode of the distribution <200µm) clearly contrasting with the coarse grain-size of the typical Diest sand member covering the Dessel Member. This means that sediments of the Dessel lithofacies not necessarily need to be calcareous. Grain-size has traditionally been the main argument to identify the Dessel Member in borehole descriptions whereas calcareous content was only of minor importance (P. Laga, pers. comm.). In this work, we have made the distinction between a lower calcareous Dessel Member and an upper Dessel Member devoid of calcareous content, see for instance Rijkevorsel (Figure 5.14) and Dessel-5 boreholes (Figure 5.15).

This interpretation implicates the fine-grained Dessel Member reaches a thickness of almost 30m both in Rijkevorsel as well as in the Dessel area. Labat et al. (2011) only reported 11m Dessel Member sediments in the Dessel-5 well based on grain-size properties as they only considered the “Lower Dessel lithofacies” defined in this work. The grain-size indeed becomes slightly coarser in the Upper Dessel lithofacies of the Dessel-5 well (Figure 5.15) but the size distribution mode is <210µm, which is still significantly finer compared to the coarse Diest sand member sands (Diest D1 lithofacies).
Another argument to unite the Lower and Upper Dessel lithofacies is the smectite-rich clay mineralogy in these sediments which is similar to the Deurne Member clay mineralogy but contrasts with the glauconite-smectite clay mineralogy of the Diest sand member (Diest D1 facies) above. Pelletal glauconite content is on average 26% and the mineralogy of the pelletal glauconite is very similar to the Berchem glauconite pellets, with >11% expandable layers (Figure 5.41) (Table 5.5).
It has to be noted that this new interpretation also implies that bioturbations are not restricted to the Diest sand member but also can occur massively in the Dessel Member, as can be clearly observed in the Dessel-5 borehole.

Dinoflagellate cyst biozones of reference boreholes, such as the Oostmalle 29E249 and the Retie 31W243 boreholes (Louwye et al., 1999) show that both DN8 and DN9 occur in the Dessel Member The DN8 is relatively thin, and seems to coincide with the thin Lower calcareous Dessel facies defined in this work. The largely decalcified Upper Dessel facies is correlated with the DN9 biozone (Figure 5.40). There seems to be a relation between the DN9 occurrence of the Dessel Member and decalcification, not only observed in the Oostmalle 29E249 and the Retie 31W243 boreholes, but is also confirmed in the lithological descriptions of samples in the borehole reports of the Poederlee 30W300 and Mol 31W221 boreholes (Louwye et al., 1999).

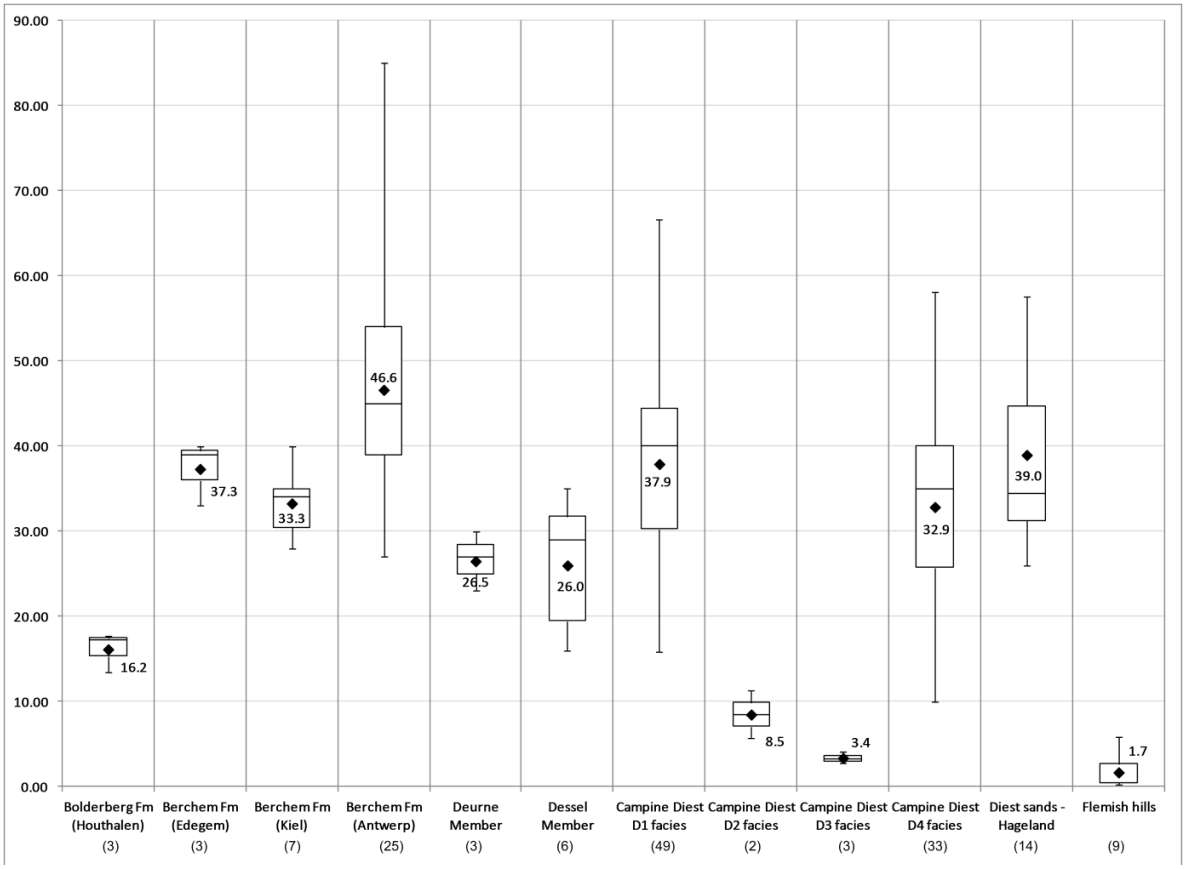

Figure 5.41. Boxplot representation of pelletal glauconite content of each defined lithofacies of the Diest Fm and comparison with the Berchem and Bolderberg Formations. Numbers indicate the average value for each subclass. The amount of samples per unit is listed between brackets at the bottom.

V.6.1.3 Lithofacies Diest D1 Campine

The Diest sand member contains the main mass of sediments in the Diest Formation. The Campine Diest D1 lithofacies corresponds to the typical description of Diest sand in borehole reports: a coarse, poorly-sorted and loosely-packed ("heteromorphic" as described by Laga and Gulinck in the Archives of the Geological Survey of Belgium) sand, sometimes intensely bioturbated, with very low clay content and relatively enriched in pelletal glauconite. Sedimentary structures such as oblique stratifications have never been observed or reported from this part of the Diest member. Often the sand is so loosely packed that it is hard to recover in cores without losing material.

Characteristic for this facies is the coarse grain size with significant amounts of particles >500µm. The mode of the distribution typically lies in the 300-400 µm interval but occasionally also in the 250-300µm interval. The low amount of dispersed clay mainly consists of clay-sized glauconite with hardly any smectite. Glauconite pellet contents are on average 40% but range from 20 to 60% (Figure 5.41). Typically, the lowest contents occur in the least coarse samples while glauconite pellets are the most abundant in the very coarse-sized samples. The mineralogy of pelletal glauconite consists of low amounts of expandable layers (<8%), which is very characteristic for this facies. The d_{060}-values have, compared to Dessel Member samples, shifted to slightly lower angles with 1.5171Å as an average value. The Campine Diest D1 lithofacies was identified in:

- *Mol Put-8 PIDPA 68-112m (*Figure 5.30*)*
- *Beerse URS 88-130m (*Figure 5.27*)*
- *Westerlo 33-57m (*Figure 5.16*)*
- *Dessel-2 47-48m (*Figure 5.24*)*
- *Retie-1 30-50m (*Figure 5.26*)*

The Diest sand member contains no calcareous microfossils but dinoflagellate cysts biozones DN9 and DN10 were reported for the Diest sand member in the Campine by Louwye et al. (1999), Louwye and Laga (1998), Louwye and De Schepper (2010) and Louwye et al., (2007). Louwye and Laga (2008) found DN8 Diest sand member deposits in the Wijshagen well in Limburg, southeast of the

Campine Basin but no such samples were investigated in this work. Dinoflagellate cyst biostratigraphy by Louwye et al. (1999) of the Poederlee 30W300, the Retie 31W243 and the Mol 31W221 indicates that Diest sand member mainly correlates with the DN9 biozone. The upper part of the Diest Formation in the Retie 31W243 well (close to the Retie-1 borehole studied in this work) however is interpreted as the DN10 biozone. Consequently, the Diest D1 facies is mainly DN9 (Late-Tortonian) but the occurrence in the Retie-1 borehole might also be DN10 (Tortonian-Messinian) (Figure 5.40).

V.6.1.4 Lithofacies Diest Hageland

This lithofacies has very similar mineralogical and sediment petrological characteristics as lithofacies D1 Campine, but occurs in outcrops in the Hageland area. Mineralogical and sediment petrological characteristics (bulk mineralogy, clay mineralogy, pelletal glauconite content, low clay contents) of the D1 Campine and the Diest Hageland are almost identical. The sedimentology of the deposits is however somewhat different. Whereas clay intercalations are rare in the Campine Diest D1 facies, they occur quite commonly in the Hageland outcrops in the form of discontinuous clay laminae or thin clay layers with were originally grey but often altered to a typical brown to even red color. The clay mineralogical composition of the clay layer samples is very different from that encountered in sands, as no glauconite-smectite is present and smectite and illite-smectite both occur in proportions of ca. 30%. This clay composition furthermore is not so different from the composition encountered in the Dessel Member and the Deurne Member (Figure 5.33).

Due to the prolonged exposure to intensive oxidation, the glauconitic sands have locally been altered from green to a brown colored sand with iron staining, widespread limonitization, and even the development of metallic iron-encrustation, emphasizing the iron-rich nature of the pore waters in these deposits. In many cases, the precipitation of limonitic agents has initiated cementation and the development of Fe-sandstone banks, consisting almost entirely out of quartz and low crystalline Fe-(hydr)oxides. Possibly, also the presence of siderite has played a role in the cementation process, as already reported by Laga (1972). Furthermore, dispersed in the sand(stone) matrix of the Hageland facies, powdery white pebbles (<0.5cm) occur, consisting of poorly crystalline quartz and opal. These pebbles are not found in samples of the Campine D1 facies. This Diest Hageland facies was found in the different sampled outcrops in the Hageland: Kesselberg, Gasthuisberg, Wijngaardberg, Beninksberg, Steenrots, Linden Houwaertstraat.

Because any stratigraphical meaningful fossils are lacking in the Hageland occurrence of the Diest sand member, its biostratigraphical age, and stratigraphical position in general, remains uncertain. Vandenberghe et al., (2014) have suggested a DN8 age for the Hageland Diest sands based on the DN8 age of the Dessel sand underlying the Hageland facies in the Veerle well and the similar DN8 biochron in the Diest sand of the Wijshagen borehole which lies in the direction of the Hageland Diest sand transport and contains also comparable heavy minerals.

V.6.1.5 Lithofacies Diest D2 and D3

Lithofacies Diest D2 was found as a 4m thick unit in the Beerse URS borehole (Figure 5.27) where it covers the coarse D1 facies. The D2 facies is a transitional unit which lies in between the coarse sands of the Diest D1 facies and the clayey glauconite-poor Diest D3 facies.The size distribution mode ranges between 180-200µm and contrasts with the mode of the underlying Diest D1 unit sediments, which is systematically >300µm. The uppermost coarse Diest D1 sample was collected at 92.3m and the lowermost Diest D2 sample at 86.35m (Figure 5.27). This leaves almost 6m without sample information, so the boundary between both units could be a more gradual transition instead of a sharp boundary. Furthermore, the clay mineralogy also changes from glauconite-dominated to smectite-dominated with 40% smectite in the 2µm fraction. Pelletal glauconite contents are low ranging from 6-11% (Figure 5.41).

Lithofacies Diest D3 covers the D2 facies in the Beerse URS borehole (Figure 5.27) and is a very clayey facies with the size distribution mode varying around 100µm. The facies is furthermore glauconite-poor, less than 5% (Figure 5.41), which makes this facies rather unusual for the Diest sand member. The smectite content is even higher in this facies compared to the D3 facies, with 60% smectite in the 2µm fraction.

Louwye et al., (1999) reported a DN10 biozone for the entire Diest sand member above the

Dessel Member (DN8 and DN9) in the Oostmalle 29E249 well and Kalmthout 6E110 well. Considering the thickness of the clayey and glauconite-poor D2 and D3facies in the Beerse borehole, it is very likely that these facies are linked to the dinoflagellate DN10 biozone.

V.6.1.6 Lithofacies Diest D4

Lithofacies D4 is, similar to the D3 facies, very rich in expandable minerals. The important difference however is that the D3 facies only contains dioctahedral smectite whereas the D4 facies is characterized by both dioctahedral smectite and trioctahedral Fe-rich vermiculite. Although siderite and phosphate minerals (vivianite but also fluorapatite) can occur in all of the defined Diest lithofacies, the highest concentration occurs at levels within the Diest D4 unit. The size distribution of D4-samples is typically poorly sorted with an elevated clay content ("Clayey top facies" of Wouters and Schiltz, 2011) with distribution modes ranging between 170-250µm. Nevertheless, as Diest D4 facies is mainly defined based on the presence of Fe-vermiculite and less based on grain-size characteristics, also coarser-sized D4 sediments occur, such as in the Rees borehole (Figure 5.31). Pelletal glauconite amounts are relatively high (32.9%) but on average slightly lower compared to the Diest D1 facies (37.9%) (Figure 5.41).

The Diest D4 unit is identified in:

- Beerse URS (49-60m) (Figure 5.27)

- Rees (33-39.5m) (Figure 5.31)

- Dessel-3 (34.5-49m) (Figure 5.17)

- Dessel-2 (34.5-47m) (Figure 5.24)

- Put-8 Pidpa (44-56m) (Figure 5.30)

Louwye et al. (1999) reported a 10-15m thick dinoflagellate cyst biozone DN10 in the Poederlee 30w300, the Retie 31w243 and the Mol 31w221 wells. The geometry of these DN10 biozone seems to coincide with the occurrence of the Diest D4 lithofacies, which is therefore most likely of Late Tortonian to Messinian age. Nevertheless, Louwye et al., (2007) reported a DN9 to DN10 biozone for the top 5m of the Diest Fm in the Dessel-2 borehole, which could indicate a local DN9 age for the top Diest Fm in the Dessel area (Figure 5.40). The D4 facies seems to form the top of the Diest Formation in the entire Campine Basin (Figure 5.40), with the exception of the Retie-1 (31W363) borehole. In this borehole, the top 5m was found to be more clay-rich compared to the underlying sediments but no Fe-vermiculite was found in the clay fraction of these sediments and were therefore interpreted as Diest D1 sediments.

V.6.1.7 Flemish hills

Samples of the Pottelberg and Muziekbosberg, east from Brussels, were subdivided in a different category: the Flemish hills facies. Although these quartz-rich samples with common limonite coatings are described as glauconitic, the pelletal glauconite is rather low (≤ 5%) in comparison with the Diest facies described above (Figure 5.41). The size is medium-grained with distribution modes ranging from 200 to 300µm. The clay mineralogy is significantly different compared to all other facies of the Diest Formation. The top Flemish hill deposits systematically display a very characteristic kaolinite-rich mineralogy with smaller contributions of glauconite-smectite and illitic and smectite minerals. No biostratigraphical information is available from these deposits.

V.6.2 The difference between clay minerals in sands and clays explained

In the previous sections, the bulk mineralogy and clay mineralogy <2µm of the different identified lithofacies was determined. Clay fractions were found to be rich in either smectite (Deurne, Dessel, Diest D2, D3, and D4) or glauconite-smectite (Diest D1). However, glauconite-smectite in the Diest D2 facies is only predominant in sandy sediments, as the < 2µm fraction of clay laminae intercalations is more smectite-rich and resembles the clay assemblage of the other Diest subunits. This result is remarkable as two very different detrital sources for the clays in a marine sediment, one in the clay laminae and one for the dispersed clay in the sandy intervals of the sediments, is very unlikely. As the clay mineralogy of the clay laminae is comparable to the dispersed clay mineralogy of the Dessel member and of the D2 and D3 Diest units, it is interpreted to represent the normal detrital clay mineralogy during the

Tortonian to Messinian in the Campine area. The dispersed clay-sized glauconite in the D1 unit of the Diest sand member is produced during the sedimentation process of the coarse glauconitic sands which was a turbulent process preventing the sedimentation of other clay-sized detrital minerals. The process of the production of clay-sized glauconite by the abrasion or even disintegration of pelletal glauconite during turbulence is described in Chapter III. The amount of glauconite-smectite in the clay fraction of sediments is therefore related to the intensity and distance of pelletal transport and the energy of the depositional environment. As such, pelletal glauconite disintegration is the dominant process for supply of clay material in sediments enriched in clay-sized glauconite. In the energetic environment of the Diest D1 sands, as indicated by the coarse size distributions and low clay contents, clay-sized glauconite is massively produced resulting in >70-80% of glauconite-smectite in the <2µm fraction. Some detrital clay is probably deposited together with the abraded/disintegrated pelletal glauconite material but the amount of detrital clay is significantly lower compared to the massive production of clay-sized glauconite, which has caused dilution of the detrital clay. In the more smectitic lithofacies, the detrital input of clay material is relatively more important and clay-sized glauconite production less prominent, which results in lower clay-sized glauconite-smectite amounts and higher detrital clay amounts.

V.6.3 Glauconite mineralogy in pelletal and clay-sized habits

Pelletal glauconite mineralogy in the different facies of the Diest Formation is relatively variable. Whereas the pelletal glauconite mineralogy (expandability) of the Deurne and Dessel Members is very similar to that of the Berchem Fm, pelletal glauconite in the Diest D1 to D3 facies contain significantly less expandable layers (Figure 5.42). Glauconite pellets of the Diest D4 top-facies are again more expandable (Figure 5.42 and Figure 5.43).

Glauconitic minerals in the Diest Formation are not only encountered in pelletal habit but also, often in substantial amounts, in the clay fraction of the different Diest litho-facies units. In chapter III, it was demonstrated that clay-sized glauconite is the result of pelletal glauconite abrasion and disintegration. When comparing the mineralogical characteristics of pelletal and clay-sized glauconite (lower part on Figure 5.44), it can be stated that the d_{060} crossplot reveals roughly a 1:1 relation. Berchem glauconitic minerals are characterized by relatively low values, which are also found in the Bolderberg and Dessel glauconitic minerals. In the Diest D1 to Diest D4 units however, the d_{060} shift to slightly higher values.

The d060-value of glauconite minerals is strongly influenced by the octahedral iron content. As the mobility of Fe is enhanced in reducing environments, the d060 is mainly determined based on the specific redox conditions and the availability of Fe in the sedimentary environment (see also El Albani, 2005). Nevertheless, also post-depositional alteration, such as oxidation after an emersion phase, influences the pelletal mineralogy. Oxidation causes K_2O-depletion hereby increasing expandability and eventually leading to a complete goethitization. Most of the iron probably remains immobile during such oxidation but also the increase in expandability might alter the d060.

Also the expandability in both glauconite habits illustrates a relation (upper part in Figure 5.44), although the 1:1 relation has been obscured. Typically, clay-sized glauconite minerals have 5-10% more expandable layers compared to their pelletal counterparts. This might be related to enhanced reactivity of the clay-sized glauconite after pelletal abrasion/disintegration, transport and re-deposition during which weathering process cause glauconite layers to be transformed to expandable layers. The expandability crossplot illustrated in Figure 5.44 moreover allows partial discrimination of the different Diest lithofacies. Glauconitic minerals in the Diest D1 unit are substantially less expandable compared to for instance the Hageland or the Diest D4 unit (upper part in Figure 5.44). This might be due to post-depositional alteration. The current position of glauconitic minerals of the Diest Hageland and Diest D4 units in the expandability crossplot diagram (Figure 5.44) is therefore most likely not their original position, equivalent to the current Diest D1 glauconites, but has shifted due to post-depositional weathering processes. The mineralogical nature of glauconitic minerals before the Diest D1 (Berchem, Houthalen, Deurne, Dessel) and after, changes significantly which strongly suggests that during the deposition of the Diest D1 facies, during DN9, pelletal glauconite has a different source area compared to before or, more likely, that pelletal glauconite has gained in K_2O-content and therefore also has become less expandable.

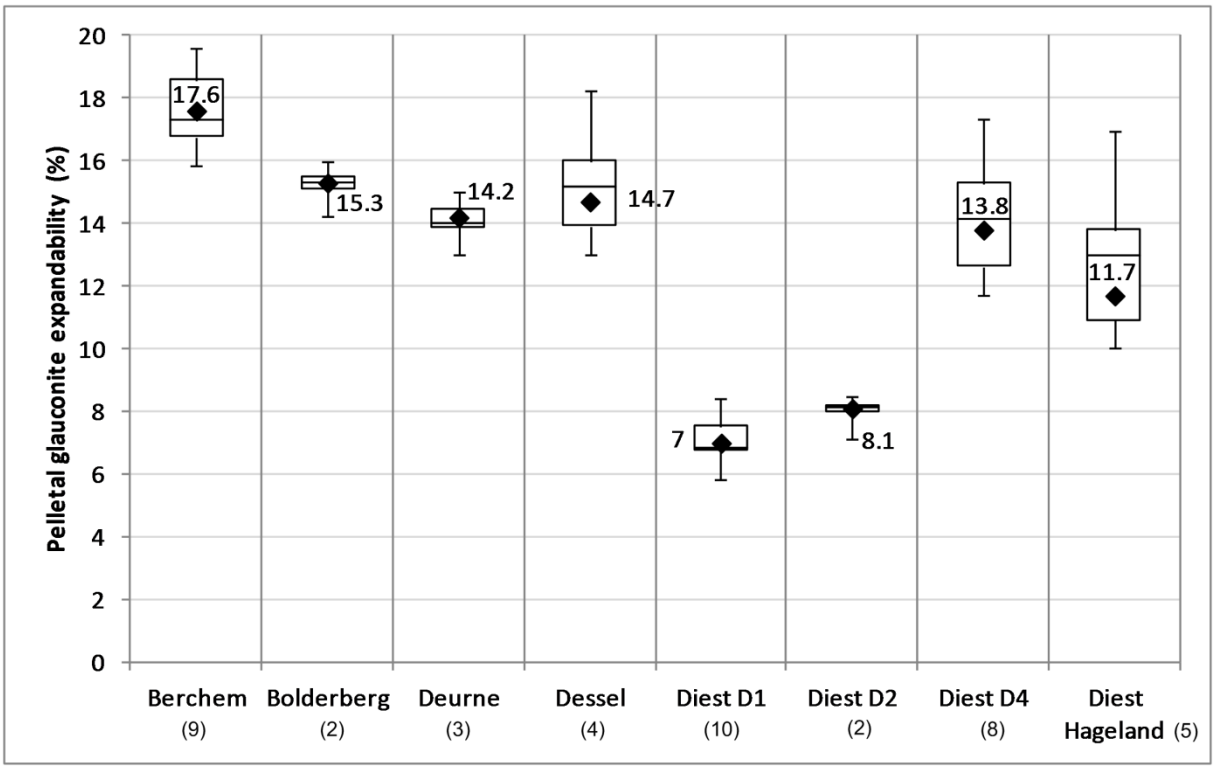

Figure 5.42. Pelletal glauconite expandability of different Diest facies compared with the Berchem and Bolderberg Formations. Note the similarity between Dessel and Berchem/Bolderberg and the contrast with the Diest D1 and D2 pelletal glauconite mineralogy. The amount of samples per unit is shown between brackets at the bottom.

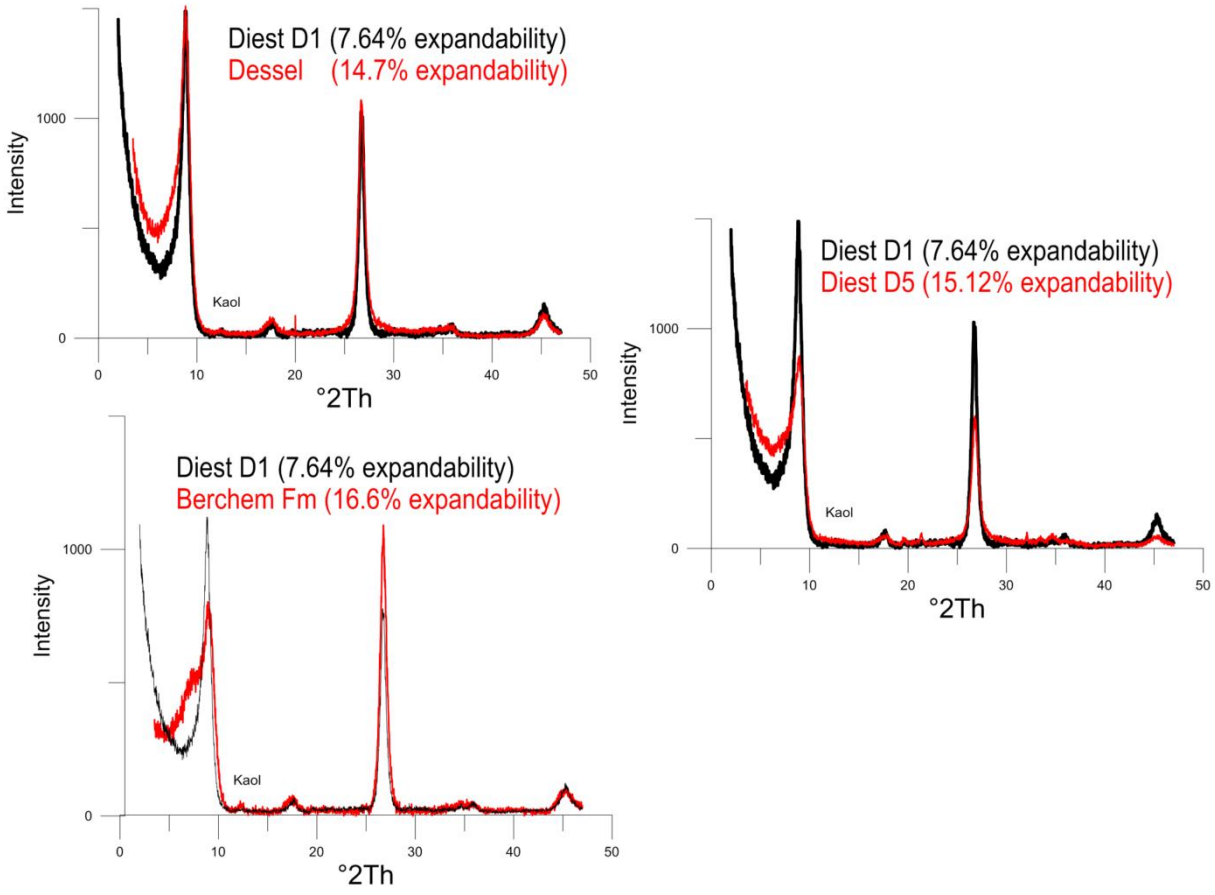

Figure 5.43. Glycolated diffraction pattern of glauconite pellets of the Diest D1 facies compared with the Berchem pelletal glauconite, Dessel pelletal glauconite and Diest D5 pelletal glauconite.

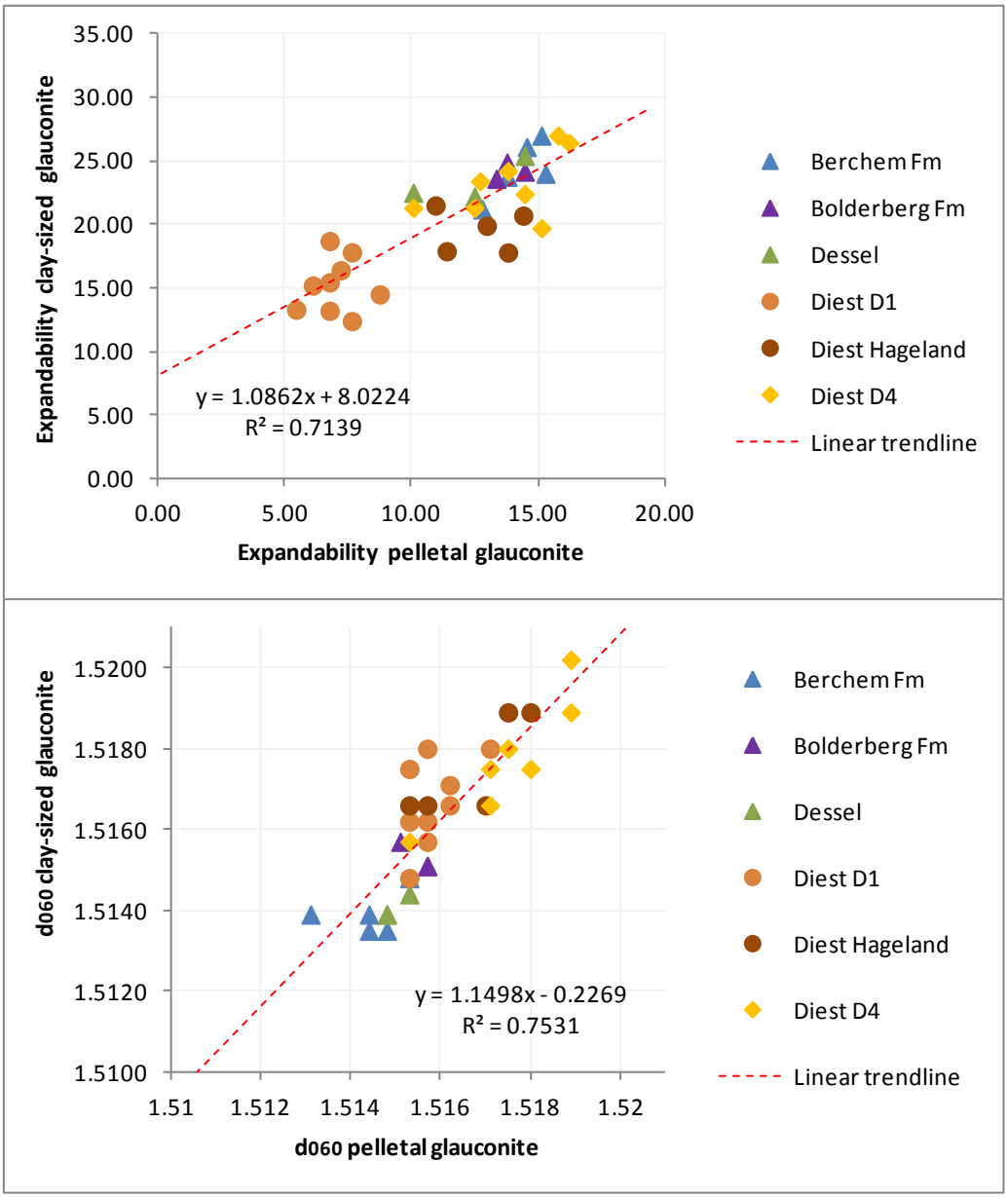

Figure 5.44. Comparison between the expandability (above) and d060 (below) of pelletal and clay-sized glauconite of the Berchem and Bolderberg Formations and the different identified lithofacies of the Diest Formation.

V.6.4 Is the Diest Formation reworked from the Berchem/Bolderberg Fm ?

Vandenberghe et al. (2014) have proposed that more than 50% of the sediment of the Diest Formation is reworked from the Early to Middle Miocene Berchem and Bolderberg Formations. Indeed, the intense and deep erosion prior to the deposition of the Diest Formation has eroded large volumes of these deposits and also sediments from the same age can have been swept in from the north (Figure 5.2 and Figure 5.3).

The clay mineralogical and sediment petrological data of parts of the Diest Formation are comparable to those of the Bolderberg and Berchem Formations. Particularly the Deurne and Dessel litho-units display very similar characteristics: a similar clay mineralogy, fine-grained size distribution, clay-sized glauconite mainly of the higher expandable type and with d_{060}-values similar to the Berchem and Bolderberg d_{060} values. Also

the mineralogy and size distribution of pelletal glauconite are very similar. The pelletal glauconite content is slightly lower than 30% for the Deurne and Dessel deposits as opposed to an average of 47% for the Antwerp Member and 16% in the samples investigated of the Houthalen Member (Figure 5.41). Based on lithological grounds, it is therefore reasonable to assume that the Deurne and Dessel material is almost entirely reworked from the older Miocene deposits in the Campine Basin.

The transition of the Deurne/Dessel Members to the Diest D1 to D4 units is however marked by an important change in grain-size, clay mineralogical and glauconite mineralogical characteristics (see Figure 5.44). This change suggests the influence of reworked Berchem/Bolderberg sediments drastically decreased with the deposition of the Diest D1 facies. This is clearly indicated by the occurrence of coarser-sized pelletal glauconites, which are not present in the Berchem and Bolderberg deposits. The change in mineralogical characteristics of the pelletal glauconite confirms this. Whereas the Deurne and Dessel Members as well as the Berchem and Bolderberg pelletal glauconites are characterized by more expandable layers (>11%) and d_{060} values between 1.513 and 1.515Å, the mineralogy becomes much less expandable in the Diest D1 facies (<10%) and the d_{060} shifts to values higher than 1.5166Å.

Although the mineralogy of glauconite pellets is sensitive to alteration, this would involve important weathering and oxidation effects. Such processes would definitely induce an increase of expandable layers rather than a decrease, as explained in the previous section. The supply of potassium towards the glauconite grains creating non-expandable layers is only described to occur at the sea bottom in a micro-reducing environment during the original glauconitisation process, or, during diagenesis. Both options are excluded in this case which indicates that the glauconite minerals in the Diest D1 to D4 deposits are not reworked from the older Miocene deposits in the Campine Basin, such as the Berchem, Bolderberg Formations, Deurne and Dessel Members. Instead, the changing mineralogy indicates the introduction of sediment from a new provenance area probably during a new transgressive pulse in DN9 as suggested by Vandenberghe et al. (2014)

Logically this new glauconite provenance area is located in the North Sea Basin (see green arrows in Figure 5.8). From radiometric age dating it is known that the glauconites in the Diest D1 facies have ages of Burdigalian (Campine) to Langhian (Hageland-East Limburg) age and consequently marine glauconite-rich deposits of that age interval in the North Sea can be candidate sources for the Diest D1 facies. Major marine Neogene deposits in the North Sea of that age range are located in the central North Sea (Neo 1 23-15 Ma) reaching up to over 1km thickness (Anell et al. 2012). In a previous study (Adriaens, 2009), an authigenic pelletal glauconite from a main flooding surface from the Danish Måde Group, provided by GEUS (courtesy E. Rasmussen), was analysed and had similar to identical mineralogical properties with 8 % expandables as the Diest D1 unit. The Måde Group is made up of the middle Miocene Hodde Fm, the ØrnhØj condensed section and the upper Miocene Gram Fm. (Rasmussen et al., 2010). The sample analyzed in Adriaens (2009) originates from the late Serravalian ØrnhØj Fm condensed section. Although the central North Sea is positioned relatively far away from the Campine basin, the mineralogical similarity between both pelletal glauconite occurrences suggests a relation. Furthermore, pelletal glauconite contents in these deposits are very high (>60%) and when only considering the sand fraction, pelletal glauconite contents are higher than 90%. The pelletal glauconite source area however remains an open question and more extensive analyses are needed from North Sea borehole samples to further explore the origin.

V.6.5 Carbonate minerals in the Diest Formation

Calcite and aragonite are absent in the Diest sand member and only in a few localities in the Hageland macrofossil casts are reported. In contrast, calcite and aragonite occur in substantial amounts in the Deurne and Dessel Members. Siderite ($FeCO_3$) however, seems to be constantly present in the Diest Formation sediments occurring in almost all defined units. Remarkably, elevated siderite contents occur in Diest sand intervals where quick sediment oxidation after sampling is observed (see descriptions of Dessel-2, Dessel-3 and Retie-1 boreholes).

Under binocular microscope, siderite systematically consists of strongly elongated and angular particles, showing that these particles are not transported and can only have grown in the sediment after deposition.

Siderites are regularly reported coexisting with Fe-phosphate vivianite, also present in the Diest Formation, as precipitates during early diagenesis (Mozley, 1989; Curtis, 1995; Tebbens, 2000). The precipitation of these mineral products is controlled by the availability and Fe/Ca- ratio in the pore water. This Fe/Ca-ratio must be very high for the precipitation of both minerals. Remarkably, siderite is often concentrated in certain layers, such as observed for four centimeter-thick siderite-rich intervals in the Rees borehole (Figure 5.31). The occurrence of concentrated siderite, such as a siderite cemented sandstone layer in the Diest sand member at Olmen (Laga, 1972), in contrast to the common small dispersed siderite crystal aggregates, could represent transformed original calcium carbonate cemented layers. The processes causing the iron concentration in the Diest Formation and the sometimes coupled occurrence of vivianite were not further investigated in this research.

The systematic presence of siderite most likely indicates that Ca-carbonates were initially present in the Diest sand member but were later dissolved.

V.6.6 The significance of the Diest D4 facies

The top of the Diest Formation in the Campine is marked by the distinctive Diest D4 unit. This facies is characterized by the presence of Fe-rich trioctahedral vermiculite but also mixed-layer kaolinite-expandable and chlorite-expandable mixed-layers. The nature of all these minerals is very specific indicating an important weathering stage took place. This weathering is also confirmed in the mineralogy of glauconite, with clearly more expandable layers compared to the other Diest subunits (Figure 5.43 and Figure 5.44). The chlorite-vermiculite alteration is a common weathering process in soil profiles (Moore and Reynolds, 1997). The Fe-vermiculite is therefore most likely the alteration product of trioctahedral Fe-chlorite, which occurs in elevated amounts in the bulk mineralogy <32µm of the D4 unit. The presence of these specific clay mineralogical assemblage indicates an important influx of weathered/ soil material in the Campine Basin during the Latest Tortonian to Messinian. The Diest D4 unit is the youngest litho-unit of the Diest Formation in the Campine and reflects the mineralogy of weathered marine glauconitic sands. Vandenberghe et al. (2014) and Verhaegen et al. (2014) have suggested, based on rounded and weathered iron crusts in the basal gravel of the Kasterlee Fm, that certainly parts of the Diest Fm were exposed during the late Miocene. Louwye et al., (2007) reported unambiguous freshwater influences in the Kasterlee Fm covering the Diest Fm which also indicates a shallowing of the sedimentary environment compared to the depositional environment of the Diest sands. The weathered glauconitic sands at the top Diest Fm are therefore probably related to soil weathering as a result of an emerging Campine.

V.6.7 The significance of the sands on top of the Flemish hills

Historically, the Flemish hill top sands were regarded as part of the Diest Formation. Houthuys (2014) however claims that the sedimentological features of the Flemish hill sands and the Hageland Diest Sands are significantly different and instead suggested the top Flemish hills belong to the Eocene Zelzate Fm. The dissimilarity between Hageland and Flemish hills sands is confirmed by the sedimentpetrological and mineralogical data presented in this work. However, there are also indisputable mineralogical similarities. Small whitish powdery pebbles are sporadically found dispersed in the sand matrix in the Hageland whereas larger white pebbles are reported by Houthuys (2014) in the top Flemish hill deposits. Both pebble occurrences consist of poorly crystalline quartz and opal. This mineralogy is also found in larger pebbles present in the middle section of the Muziekbosberg outcrop (Figure 5.37). Most likely, these represent silicified limestone fragments of Mesozoic age.

A second similarity is the nature of the glauconite minerals which are predominantly of the low expandable type in the top Flemish hill deposits. This type of glauconite mineralogy is typical for the Hageland Diest sand and, furthermore, this low expandable glauconite minerals are in the Neogene stratigraphy of Belgium only found in the Diest Sand and in a particular glauconitic facies of the Eocene Brussels Fm (Adriaens, 2009). This could point to a connection with the Hageland area. The marine glauconitic sands found in the Hageland are however not an important sediment source for these deposits, as evidenced by the grain-size and clay mineralogical differences (Figure 5.38 and Figure 5.39).

The clay mineralogy of the top Flemish sand consists of 40-65% of kaolinite while smectite contents are lower than 5%. Such high kaolinite contents are very specific and are neither found in Neogene marine nor in Eocene deposits in Belgium.

A kaolinite-rich clay mineralogy <2µm is however found in estuarine quartz sands of the Pliocene Mol and Merksplas Formations in the Campine and, in the continental Opgrimbie facies of the Bolderberg Fm in Limburg (Figure 5.45). As kaolinite is the result of strong weathering, the sediments in these deposits are probably largely derived from the continent. Kaolinite-rich deposits are known from the weathering of Paleozoïc rocks in the southern part of Belgium (Yans, 2003). Hermanns (1992) furthermore identified kaolinite-illite clay assemblages in the continent-sourced Lower Miocene deposits of the Lower Rhine Basin. This makes it probable that these kaolinite–illite clays are eroded from the source areas of the Rhine Basin, including the Ardennes, and are transported with the prograding Rhine delta in estuarine deposits in the Campine Basin. The top Flemish hill deposits could be similar erosional products of kaolinite-rich clay assemblages covering Paleozoïc deposits in the Ardennes in the south. The timing of deposition remains debatable. The grey egg-shaped pebbles at the base of the deposit look identical to the typical base gravel of the Miocene Bolderberg Fm, which would suggest a Miocene age.

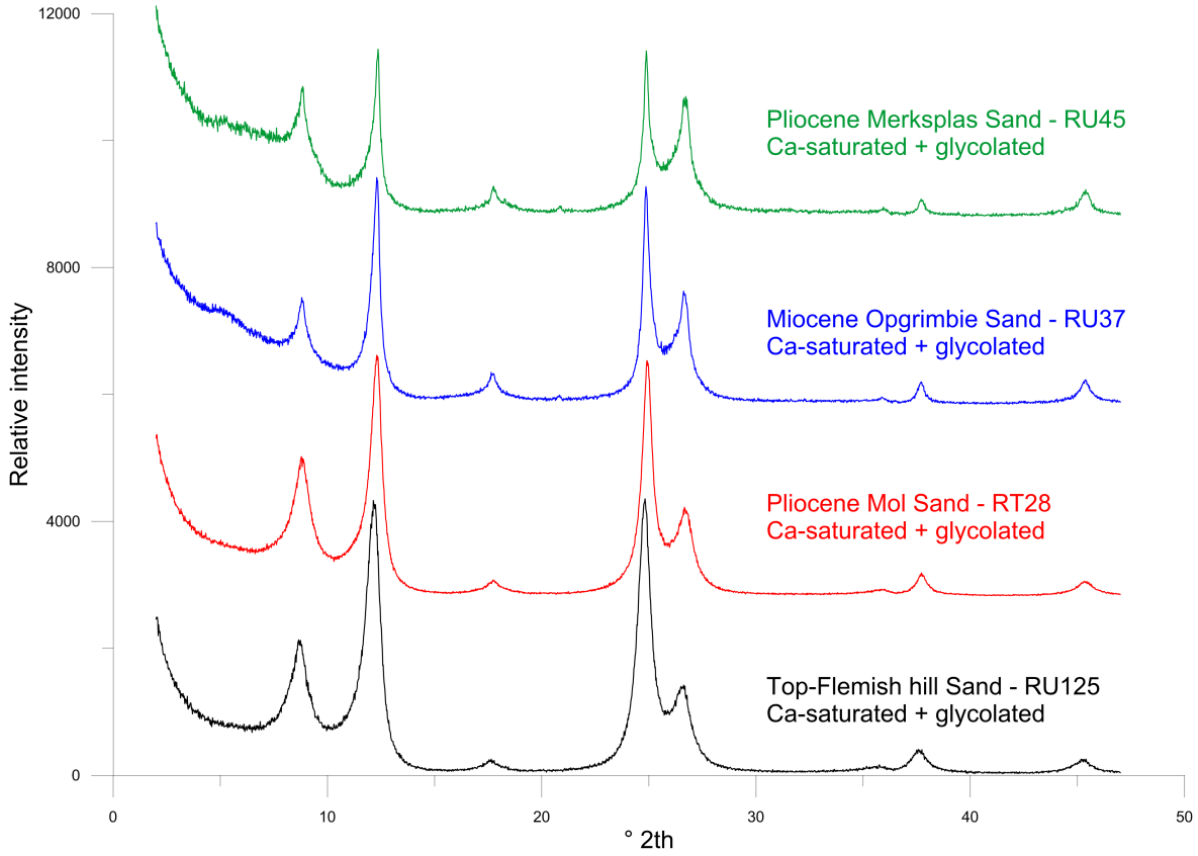

Figure 5.45. Glycolated diffraction patterns <2µm of Top Flemish Sand and typical estuarine to continental sand deposits in the Miocene and Pliocene in Flanders.

V.7 CONCLUSIONS

The Diest Formation is subdivided in the Deurne and Dessel Members whereas the majority of Diest sediments have been grouped in the non-official Diest sand member. The mineralogical and sediment petrological data provided in this chapter indicate important heterogeneity within the Diest Formation allowing for further subdivision. The lowermost Deurne and Dessel Members are fine-grained glauconitic units with very similar characteristics as the Berchem Fm. The Dessel Member was interpreted up to 30-40m in the Dessel-5 borehole with also abundant bioturbations present in the sediment. The occurrence of the Diest sand covering the Dessel Member in the Campine subsurface however introduces an important break in grain-size, clay mineralogy and pelletal glauconite content and mineralogy pointing to a shift in source material. This Diest sand member was subdivided in 4 litho-units, termed the Diest D1 to Diest D4 facies. The Diest D1 facies is the typical Diest sand member consisting of coarse-sized, poorly-sorted and loosely-packed sands with the highest pelletal glauconite contents of the Diest Fm. The mineralogy of the pelletal glauconite is characterized by less than 10% expandable layers. In contrast with the Deurne and Dessel Members, the clay mineralogy of Diest D1 is predominated by glauconite-smectite, indicating that pelletal glauconite abrasion/disintegration instead of detrital clay supply is the main clay production process. Although heavy minerals, radiometric age dating, dinoflagellate biozones in Limburg and their correlation with the Hageland and the paleogeographic-sequence model of Vandenberghe et al. (2014) suggest an important difference between the Hageland Diest sands and the Campine Diest sand member (Diest D1 facies), both occurrences have very similar mineralogical and sediment petrological characteristics. Pelletal glauconite expandability however seems to allow for distinction (<10% for Diest D1; >10% for Diest Hageland) but this difference could be related to post-depositional alteration.

In the northwestern part of the Campine, the Diest D1 facies is covered by glauconite-poor (<10%) clayey sediments with relatively high smectite contents (>40%). These deposits are grouped in the most clayey Diest D3 unit which is covering a transitional Diest D2 facies. The top of the Diest Fm in the Campine is formed by a 10 to 15m-thick sand to clayey sand facies (Diest D4 unit) of which the presence of Fe-vermiculite indicates that these glauconitic sediments underwent important weathering before being deposited at their present location as there are no indications for in-situ soil formation.

The occurrence of dinoflagellate cyst biozones in the Diest Formation is associated to the occurrence of different lithofacies defined in this work. The DN8 biochron (early-mid Tortonian) comprises the Deurne Member and the lower, calcareous part of the Dessel Member. The upper, non-calcareous part of the Dessel Member is related to the DN9 biochron (late-Tortonian) as well as the massive Diest D1 facies. The fine-grained D2, D3 and weathered Diest D4 facies are mainly of DN10 age (Tortonian-Messinian).

The fine-grained nature, the occurrence of large pebbles, contrasting sedimentology (Houthuys, 2014) and kaolinite-rich clay mineralogy of the top Flemish hill sands clearly distinguishes these deposits from any of the Diest Formation facies. The kaolinite-rich clay mineralogy implies an estuarine to continental origin. Although pelletal glauconite mineralogy and the occurrence of opaline pebbles suggest some mineralogical relation with the Hageland Diest sands, the top Flemish hill deposits should probably not be included in the Diest Fm. It can however not be excluded that these deposits are time-equivalent to the Diest Formation deposits.

The present-day stratigraphy of the Diest Formation only includes the Dessel and Deurne Members (see website National Stratigraphic Commission Belgium) leaving out the majority of sediments, now grouped in an informal Diest sand member, but which are not grouped as such in official stratigraphy. This situation causes confusion. The Diest sand member should therefore be promoted to an official Diest sand Member. The International Commission on Stratigraphy however discourages to use identical geographical names for Formation and Member which is probably why the Diest sand member never has evolved to an official status. The term "*Diest sand*" is however so well established amongst Belgian geologists and engineers to designate the coarse, loosely packed glauconitic sands (termed Diest D1 facies in this work) that the term "Diest sand" should be promoted to an official Member status ("Diest sand Member"). Since in that case Deurne, Dessel and Diest would be official Member

names, the geographic name for the formation should be changed.

Here, the Veerle Formation is suggested as the town Veerle has a central geographic position in the outcrop area of the formation connecting the Campine and Hageland areas. The Veerle Formation should be assigned three members: the Deurne Member, the Dessel Member and the Diest sand Member. The Diest sand Member is subdivided in a Campine and Hageland facies whereas in the western part of the Campine, the clay-rich Diest D3 unit is defined as a clay-rich facies occurring in the western part of the basin. The weathered top facies Diest D4 should not yet be assigned an official status because the lateral distribution and complexity of this unit is not yet fully understood.

CHAPTER VI

STRATIGRAPHY OF THE DIEST-KASTERLEE-MOL SANDS

VI.1 STRATIGRAPHICAL ISSUE

In the area Mol-Dessel in the Campine, the Diest Formation is covered by the slightly glauconitic Kasterlee Formation which itself is overlain by the non-glauconitic Mol Formation. These three formations are well-known and well-characterized sand units with well-established stratotypes which should allow for a straight-forward distinction. The Diest Formation is typically a heteromorphous, bioturbated, coarse-sized sand with high glauconite contents. The Upper Miocene Kasterlee Formation was also deposited in shallow marine conditions and is also slightly glauconiferous but with a distinctly better sorting and smaller mode of the size distribution. The Kasterlee Formation contains no calcareous fossils, but dinoflagellate cysts in the Kasterlee Fm were reported by Louwye et al. (2007). Finally, the Pliocene estuarine to continental Mol Formation consists of white, quartz-sands with no or very little amounts of pelletal glauconite and with lignitic horizons (NCS website, www.natstratcommbelgium.drupalgardens.com , last consulted 01/2015). The Mol Formation has traditionally been subdivided in a lower finer-grained unit ("*Mol Inférieur*" – Mol Donk Member) and an upper medium to coarse-sized unit ("*Mol Supérieur*" – Mol Maatheide), which are separated by the Maat lignite (De Meuter and Laga, 1976).

In practice, a positive differentiation between these formations is only achievable when comparing their typical occurrences in the middle part of stratigraphical intervals. Towards formation boundaries however, typical lithological characteristics seem to change gradually and furthermore vary from one place to another which makes that at formation boundaries, these formations are often barely distinguishable.

Drilling a cored and geophysically logged well in 2002 at the future site for low level radioactive waste storage in Dessel (Dessel-2 borehole) showed the problem even more clearly when, even with cores, geophysical logs and sediment analyses, still the lithostratigraphical subdivisions Mol-Kasterlee-Diest remained problematic and very difficult to reconcile with the very nearby formerly well studied borehole at Belchim (Gulinck et al., 1963). During a workshop the stratigraphical division of the Dessel-2 borehole was discussed (Berckmans and Wouters, 2003). Up to 8 different interpretations were proposed for the exact position of the Kasterlee Fm (Figure 6.1). To conclude this workshop, a stratigraphic proposal was synthesized differentiating between a sandy top part and a clayey basal part of the Kasterlee Fm (Figure 6.1). This synthesis was mainly based on geophysical well log data, which presently is, combined with cone penetration tests, still the main tool for stratigraphic interpretation and correlation of boreholes in the area Mol – Dessel – Kasterlee (Wouters and Schiltz, 2011). Louwye et al.,(2007) confirmed these stratigraphic boundaries and added an extra argument for the Diest-Kasterlee boundary by reporting the dinoflagellate cysts species *Grammocysta verricuta* only in the Kasterlee Fm and not in the underlying Diest Fm. Dinoflagellate cysts however do not allow to distinct to the Kasterlee Fm and the Mol Fm as *Grammocysta verricuta* occurs also at the bottom of the Mol Fm indicating very little or no paleoenvironmental change at the Kasterlee-Mol transition.

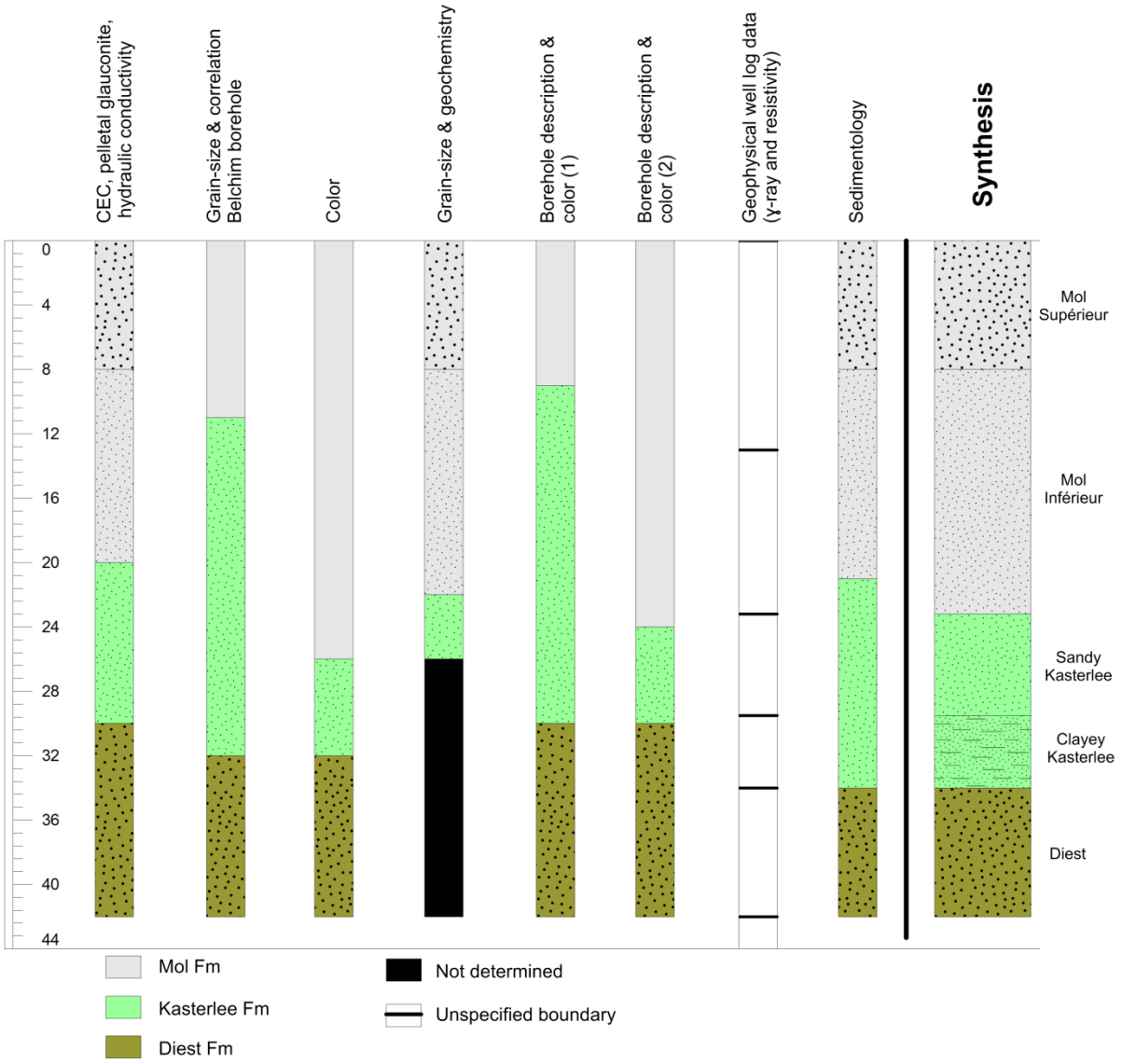

Figure 6.1. Stratigraphic interpretation of the Dessel-2 borehole based on different parameters (after Berckmans and Wouters, 2003). A synthesis of the different stratigraphic interpretations is shown on the far right, which is mainly based on the geophysical well log data.

The comparison of the Dessel-2 borehole interpretation (Berckmans and Wouters, 2003; Louwye et al., 2007) with the BELCHIM borehole interpretation of Gulinck et al., (1964) and data of the Mol-Donk Sibelco SCR exploitation is shown in Figure 6.2. These three stratigraphic intervals all occur less than 1.5 km apart in east-west direction, at about the same topographic height. Whereas Gulinck et al., (1964) place the Kasterlee-Mol transition on the change of the drilling mud colour (Figure 6.2), the criterion used by Sibelco SCR in Mol Donk is an increase of K, Al and Na with 0.3% K_2O as transition value. Such interpretation implies that a large part of what was called “Kasterlee sands” by Gulinck et al., (1964) is interpreted as Mol Donk sands by Sibelco SCR and Louwye et al., (2007) (Figure 6.2). In borehole descriptions (Mol Rauw 031E287, Mol Sas 031E288 and Overpelt 032E128 wells, Gulinck, archives Geological Survey of Belgium), pelletal glauconite is reported in the base Mol sands while the top Kasterlee sands are often reported to be bleached to white or white-green, adding complexity and confusion to the problem. Changes in grain size distribution are subtle and the boundary Mol-Kasterlee in boreholes was consistently placed by Gulinck at the change in drilling mud color from grey to green (P. Laga, oral communication), which suggests an influence of pelletal and/or clay-sized glauconite. The % K_2O (criterion Sibelco SCR) indicates a change in mineralogy, through

either pelletal and clay-sized glauconite minerals or, mica or K-feldspar contents.

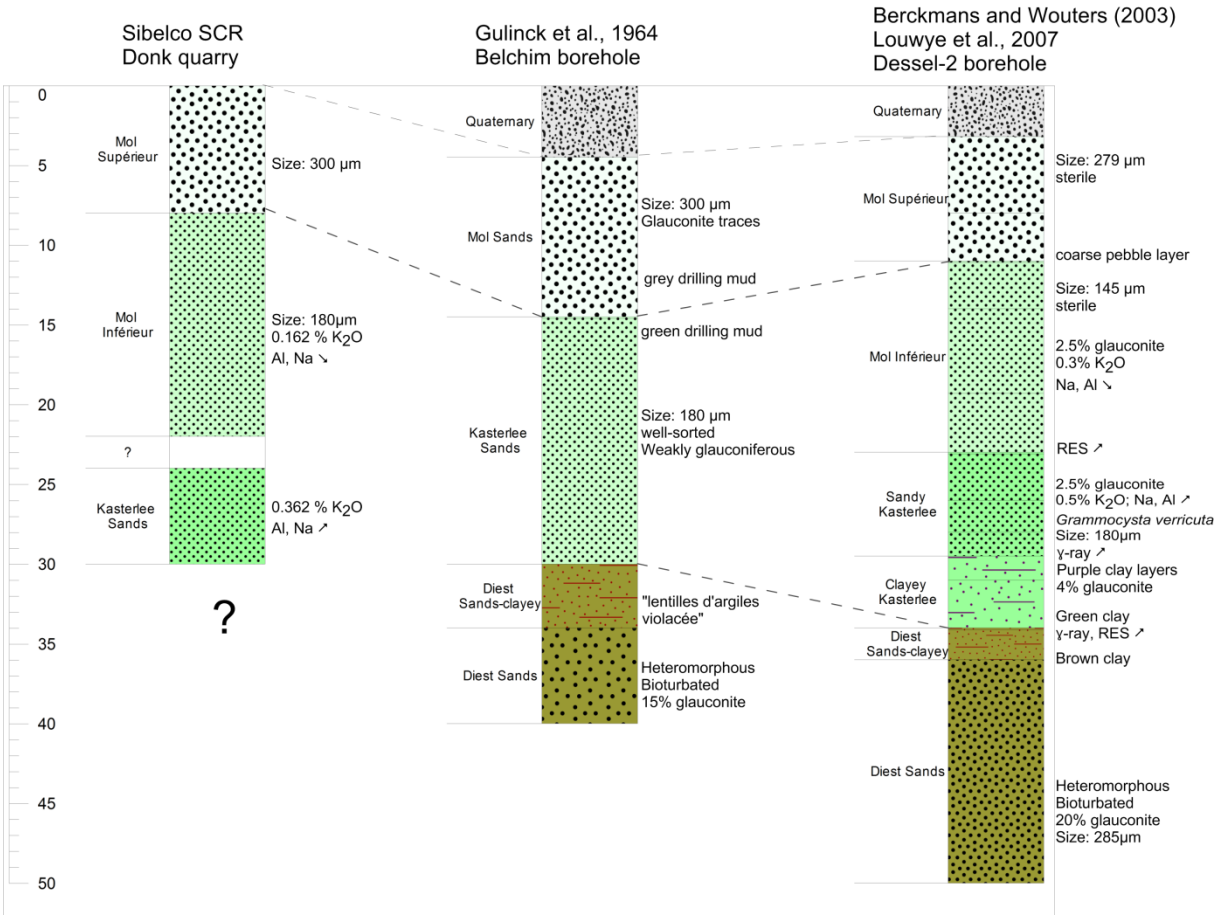

Figure 6.2. Schematic illustration of the different interpretation made on the Diest-Kasterlee-Mol transition zones by Sibelco SCR at the Mol Donk exploitation, Gulinck et al., 1964 for the BELCHIM borehole and Berckmans and Wouters (2003) and Louwye et al. (2007) for the Dessel-2 borehole.

Also the base of the Kasterlee Fm remains a point of discussion. Similarly to the Kasterlee-Mol transition, the use of different parameters has led to several stratigraphic interpretations for the Diest-Kasterlee transition. Gulinck et al. (1964) based their interpretation on the difference in grain-size between “Kasterlee” with a mean grain size of 180µm, and “Diest”, with a mean grain size of 280µm. Furthermore, the presence of purple to salmon-colored clay intercalations (“lentilles d’argiles violacée” on Figure 6.2) was systematically assigned to the top Diest Fm by Gulinck (P. Laga, oral communication). In the Dessel-2 borehole, this transition is found at 34.8m depth, which coincides with a clear excursion in resistivity, self potential and also the gamma-ray drops at this level. Preliminary clay mineralogical analyses furthermore indicate a shift of illite-dominated “Kasterlee sands” towards smectite-dominated “Diest sands” around 34m (Berckmans and Wouters, 2003). The color of the clay seems to evolve from green clay above 34m to brown below 34m depth. This level furthermore is also characterized by a paleoenvironmental event since almost 30% of the dinoflagellates at this level are reworked forms whereas the total number of in-situ marine dinoflagellates decreases drastically. Furthermore, above 34.8m, the amount of terrestrial palynomorphs increases significantly compared to the amount of in situ marine dinoflagellate cysts which points to freshwater influences for the interval above 34m, the “Kasterlee Formation” (Louwye *et al.*, 2007).

A sharp gamma-ray increase however also occurs at 29.5m in the Dessel-2 borehole (Figure 6.2) which suggests an internal stratigraphic boundary within the Kasterlee Fm (Berckmans and Wouters, 2003). Berckmans and Wouters (2003) assigned this level to the

transition of a sandy Kasterlee part and the clayey basal part of the Kasterlee Formation (Figure 6.2). At this level, also an important palynological changeover occurs (Louwye et al., 2007). Above 29.5m, the total amount of pollen and dinoflagellate cysts decreases while the relative amount of *Gramocysta verricula* increases, as a result of an important shoaling of the environment compared to the already marginal marine clayey zone below (Louwye et al., 2007).

Louwye et al. (2007) correlated the 34.8m level in the Dessel-2 borehole with the gravel layer at the base of the Kasterlee Fm in the Olen sluice. The Olen sluice exposure was a temporary outcrop in 1972 and the only location showing a gravel layer marking the base of the Kasterlee Formation. Recently the same type of gravels have been found at the base, and confirming the presence of the Kasterlee Fm, at the hills of Heist-op-den-Berg and Beerzel (Verhaegen et al. , 2014).

In the past, based on geometrical grounds, the Kasterlee Fm was considered to be the lateral equivalent of the fossiliferous and well-dated Pliocene Kattendijk Formation (Gulinck, 1963; De Meuter and Laga, 1976). Louwye et al. (2007) however, concluded a Miocene age for the Kasterlee Fm which only occurs in the Campine, as opposed to the Pliocene Kattendijk Fm, which only occurs in the Antwerp area. The Kattendijk Formation will not be further dealt with in this study.

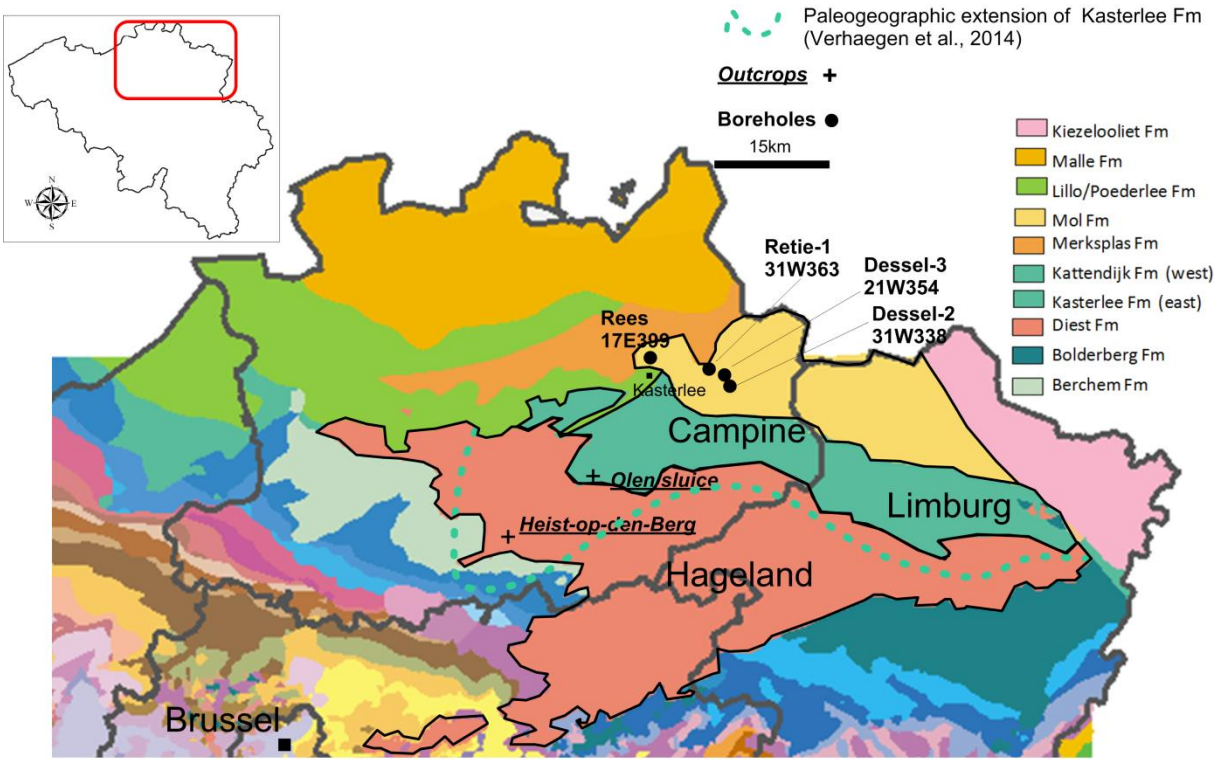

Figure 6.3. Geographical position of the Dessel-2, Dessel-3, Retie-1 and Rees boreholes and the Olen sluice outcrop (modified after geological map of ALBON, 2009).

VI.2 SAMPLES FOR MINERALOGICAL AND SEDIMENT PETROGRAPHICAL ANALYSIS

As described and illustrated above, the Diest-Kasterlee-Mol stratigraphical distinction is not yet fully understood. Whereas each unit as such has been intensively studied and characterized in its type area, the transition zones between formations are probably more heterogeneous, causing problematic interpretations. Many of the tools today used for borehole interpretations and correlations, such as geophysical well log data, are directly related to mineralogy, clay mineralogy and the occurrence of pelletal glauconite. For instance, the % K_2O in these sediments originates from either glauconitic minerals, mica and/or K-feldspars whereas the green color of sediment and drilling mud relates to the pelletal glauconite and the clay-sized glauconite amount. Geophysical well log data, probably the most important tool for correlations, often reflect grain-size variations in the sediment but also the occurrence of pelletal glauconite has an important effect on ɣ-ray and resistivity data. Although (clay) mineralogy and pelletal glauconite have such a fundamental impact, systematic mineralogical and clay mineralogical data in reference sections are scarce. Pelletal glauconite content measurements are reported by Labat et al. (2009) and Wouters and Schiltz (2011).

The aim of this chapter is to unravel mineralogical and sediment petrological data of the three formations, and their transition zones, in reference boreholes. Based on these new results and elements of previous investigations, stratigraphic boundaries will be defined in three reference boreholes in the Mol-Dessel area are used in this study: the Dessel-2, Dessel-3 and the Retie-1 borehole (Figure 6.3). These three boreholes are core drillings currently being investigated by ONDRAF-NIRAS. The samples are therefore of the highest quality, as the drilling core are stored under vacuum conditions which strongly limits oxidative processes. Additionally, reference material for the Diest-Kasterlee transition zone was also collected from the Rees reference borehole (Buffel et al., 2001), and at the Olen sluice outcrop (samples from KULeuven stratigraphic collection). Finally, samples were also collected at the top of residual hills in Heist-Op-den-Berg (Verhaegen et al., 2014) (Figure 6.3). Both in the Olen outcrop and the Heist-op-den-berg outcrop, a gravel layer marking the Diest-Kasterlee boundary was reported (Louwye et al., 2007; Verhaegen et al., 2014). All samples were analyzed for bulk mineralogical and clay mineralogical <2µm content, pelletal glauconite content and mineralogy and grain-size distribution (see Part I. Chapter I).

VI.3 RESULTS

VI.3.1 The Dessel-3 borehole

VI.3.1.1 Borehole description

The stratigraphic succession and lithological characteristics of the Diest-Kasterlee-Mol transition were already introduced in section VI.1. A photographic representation of the succession in the Dessel-3 borehole (Figure 6.4), from 6-50m depth below surface, shows that the upper part of the borehole is characterized by whitish to pale grey fine sands which locally display intense surface oxidation. The limonitic crusts at the surface of the cores clearly demonstrate the iron-rich nature of the pore waters in these sediments. Beneath this iron skin, the sediment is fresh. The grayish color of the sediment is in fact most prominent in wet conditions and is mainly caused by the color of the fines. When separating size fractions at a 32µm sieve, it can be observed that the <32µm fraction has a distinct green color while the >32µm sand fraction is white to pale grey. Around 26m depth, the grey patina of the sand units locally starts to display green coloration and the sediment becomes relatively more clayey. At 26.80m to ca. 28.5m, a transition to an intense green-colored sediment is observed, which is even more prominent in the coloration of the fines (<32µm). Also sand-sized glauconite pellets appear in higher proportions downwards from this 26.80m boundary. Below the intense green colored zone, pale green,

slightly glauconitic clayey sands occur which are sporadically intercalated with brown to sometimes even salmon-colored clay laminae. The clay intercalations often have an irregular shape (Figure 6.4), at the base most likely caused by clay draping over an irregular sand surface and, at the top, caused by erosion. The frequency of occurrence increases in the 32-34m interval. Some of the clay laminae in this interval are also slightly green colored and, the glauconite pellet content of the interstitial sand increases. In the 33-34.5m interval, the type of sediment gradually changes from dark green glauconitic sands and clay intercalations with sharp boundaries to a more dispersed clayey glauconitic sand sediment with high glauconite pellet contents and only few or no intercalated clay laminae. This type of sediment oxidizes very quickly, in a time-span of hours, which results in iron crusts on the surface of the sediment. Downwards, the sediment becomes gradually coarser in size and the structure-less character of the sediment remains intact to at least 50m of depth. Samples were collected from sands and clay laminae (Figure 6.6).

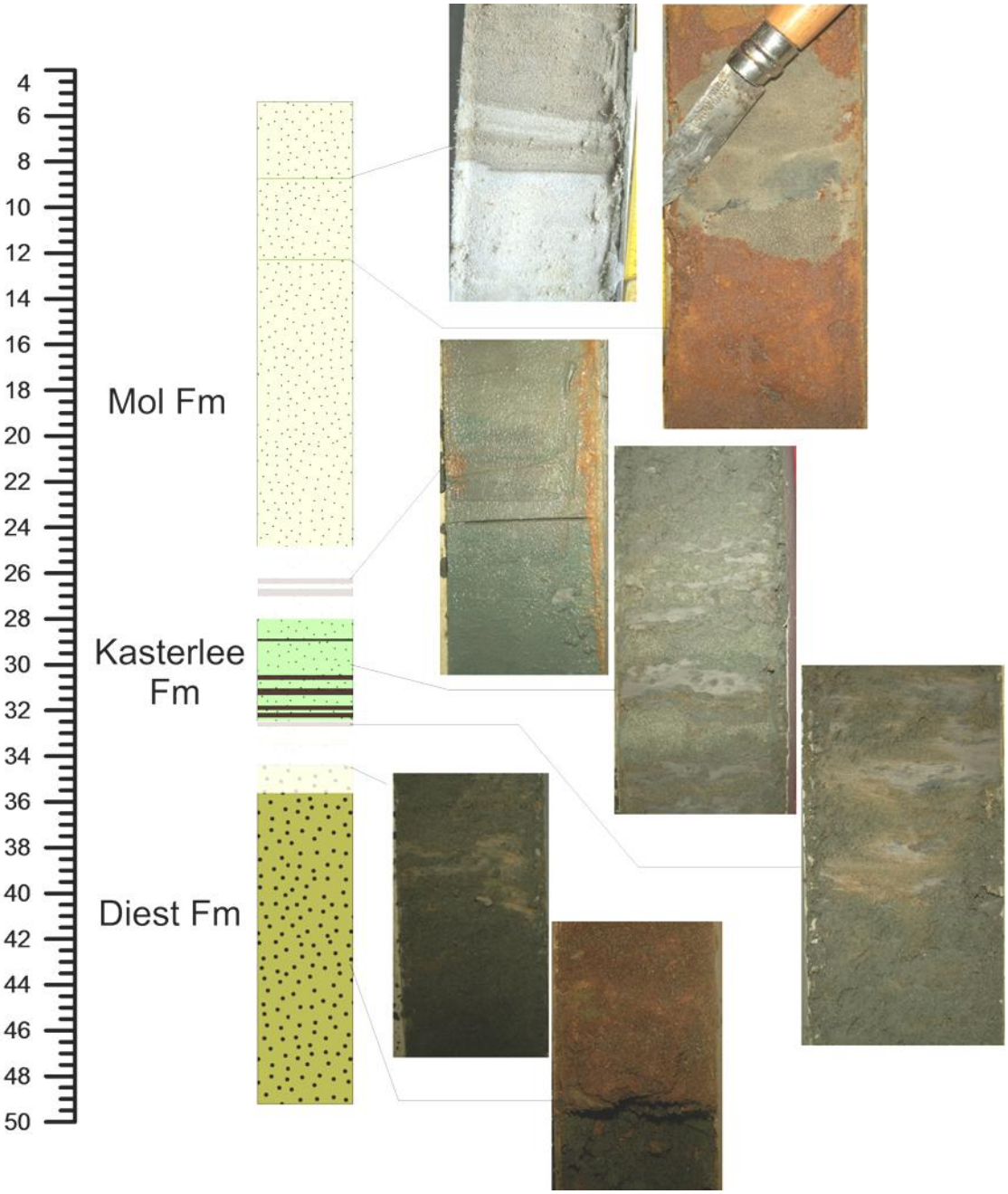

Figure 6.4. Photographic representation of the stratigraphic succession of the Diest-Kasterlee-Mol Formations in the Dessel-3 borehole. Vertical scale shows depth in meters below topography. Transition zones were blurred.

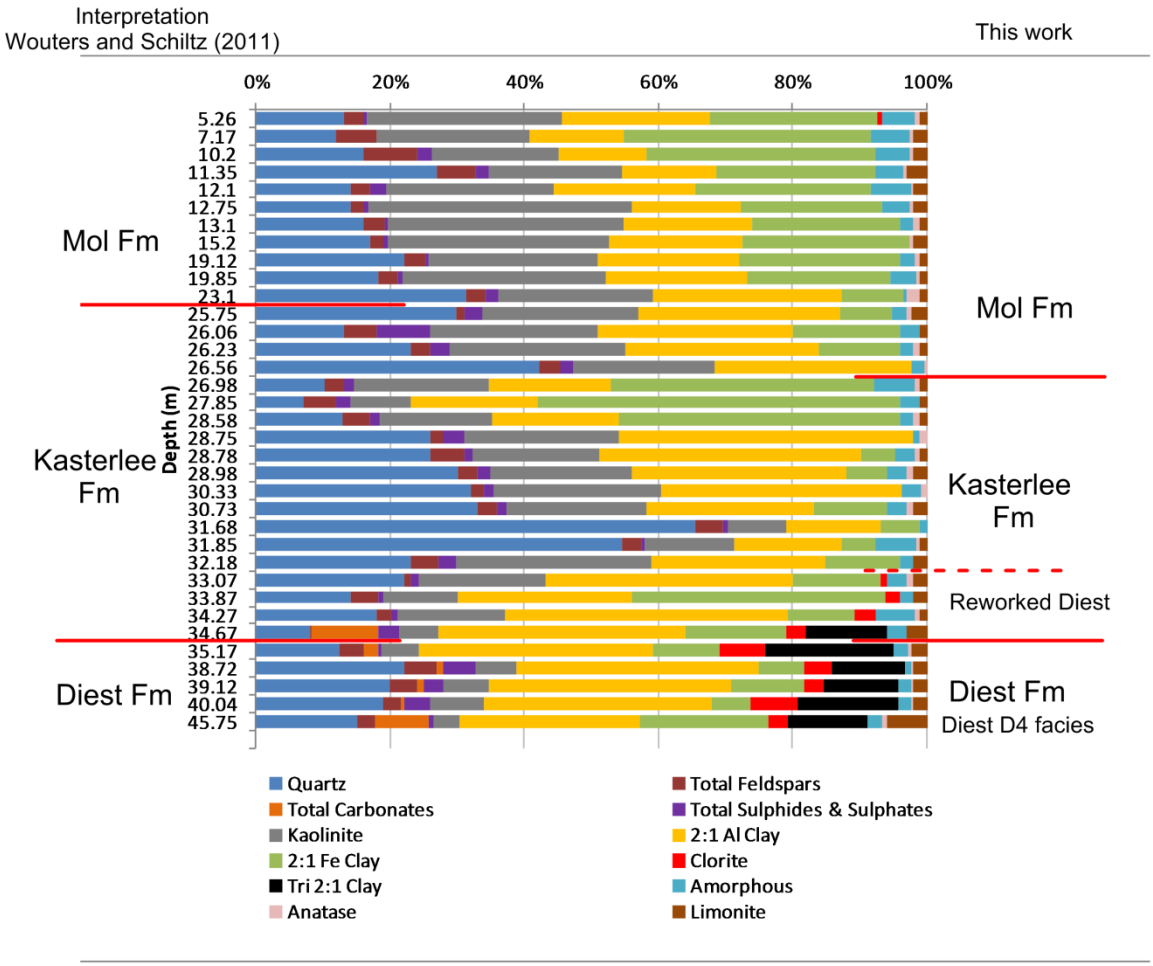

Figure 6.5. Bulk mineralogical results <32µm for the Dessel-3 borehole. On the left, the interpretation of Wouters and Schiltz (2011), based on geophysical well data and cone penetration tests is shown whereas on the far right, the stratigraphic interpretation of this work is shown.

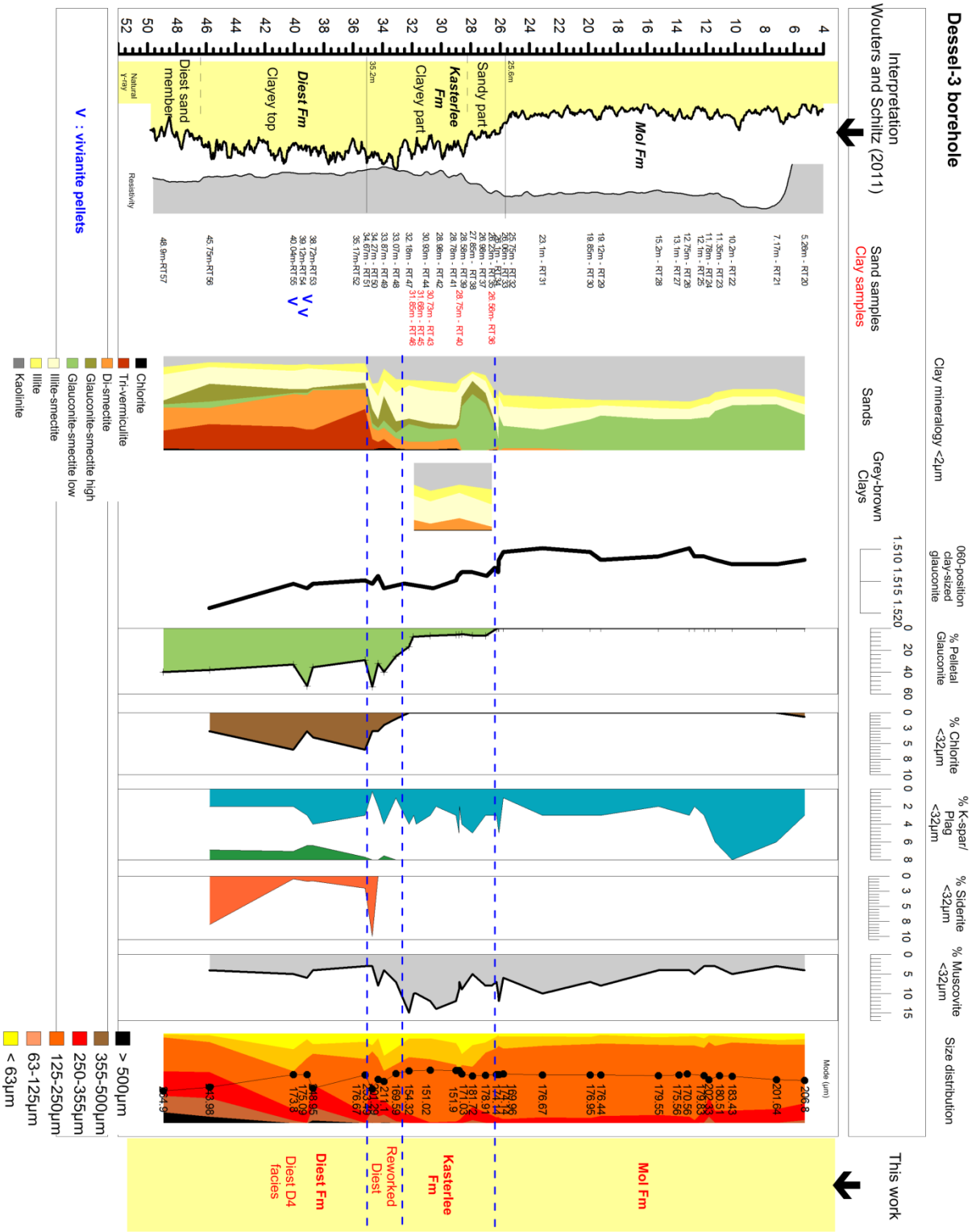

Figure 6.6. Combined mineralogical, clay mineralogical and size distribution results for the Dessel-3 borehole. On the left, the interpretation of Wouters and Schiltz (2011) is shown, mainly based on gamma-ray (yellow on figure), resistivity (grey on figure) and cone penetration tests. In the second column, sample depths and codes have been listed for sands (in black) and clay laminae (in red). Clay mineralogy was analyzed from sands, grey and brown clays and green clays. Pelletal glauconite was measured from samples >32µm, while mineralogical results for chlorite, K-feldspars vs. plagioclase, siderite and muscovite contents were analyzed on fractions <32µm. Size distributions were derived from total samples. The stratigraphic interpretation of this work is shown in the far right column.

VI.3.1.2 Bulk mineralogy of clays and mineralogy <32µm of sands

The mineralogy of the analyzed samples (Figure 6.5) demonstrates that in the upper part of the section, i.e. the Mol Formation, 60-75% is constituted by kaolinite and Al-rich and Fe-rich dioctahedral clays. The remaining part is made up by quartz, K-feldspars, pyrite and gypsum, and traces of amorphous components, limonite and Ti-oxides. The first break in mineralogy downwards is noticeable in the 26.98m sample where the proportion of dioctahedral Fe-clays sharply increases. At the same level, the proportion of kaolinite is lowered and keeps diminishing further downwards. Just above this distinct level a clay-rich and glauconite-poor level occurs at 26.1m. Below 28.5m however, the amount of glauconite minerals drops again to relatively lower levels but micaceous minerals become relatively more important (see Figure 6.6). In the zone 30-34m, the sand matrix is more intensively disrupted by intercalated clay layers of cm-thickness. In the brown and grey clay laminae and intercalations, glauconite minerals, pelletal or clay-sized, are absent. However also green-colored clays occur, such as at level 31.68m, which is caused by the presence of clay-sized glauconite minerals.

The second break in mineralogy occurs in the interval between 33.5 and 34.67m. In this interval, important mineralogical changes occur: (1) muscovite becomes less abundant and reaches a constant lower value at 34.27m, (2) downwards from 34.27m, needle-shaped siderite crystals are present in significant amounts while siderite is absent in the upper part, (3) the nature of the feldspars changes as below 33.87m, plagioclase (albite) feldspars are present as opposed to only K-feldspars (microcline) in the upper part of the borehole, (4) chlorite is present in trace amount in the bulk mineralogy <32µm at 33.87m and becomes gradually more important towards 34.67m depth, (5) trioctahedral swelling clays are observed in large amounts downwards from 34.27m.

VI.3.1.3 Clay mineralogy

The clay mineralogy <2µm of the Dessel-3 borehole (Figure 6.6) can, equivalent to the bulk mineralogy, be subdivided in three parts. The top part is characterized by mainly kaolinite and low expandable glauconite-smectite and minor amounts of illite and mixed-layer illite-smectite. The clay mineralogy reflects a strong increase in glauconite-smectite at 26.98m. Downwards from this level, kaolinite gradually decreases, the glauconite-smectite also contains higher expandable glauconite-smectite and smectite and illite-smectite becomes significant. The clay mineralogy of clay intercalations in the 26-32m interval is relatively constant and equivalent to the clay mineralogy of the sands, except the absence of glauconite-smectite. In clay intercalations with green coloration, glauconite-smectite is however present in significant amounts. The d060 of clay-sized glauconite is characterized by a sharp increase below 26.33m. The second break in clay mineralogy occurs between 33 and 34.5m. In this interval, kaolinite contents further decrease (lower than 10%) simultaneously with glauconite-smectite. The most striking feature is however the sharp increase of swelling minerals at the 34.67m level, which comprises both dioctahedral smectite and trioctahedral vermiculite, characteristic for the Diest D4 unit defined in the previous chapter. This characteristic mineralogy remains important from 34.67m until 49m. Throughout the investigated interval, the expandability of the clay-sized glauconite-smectite (Figure 6.7) significantly changes from high expandable in the Diest Fm to lower in the Kasterlee Fm and very low in the Mol Fm.

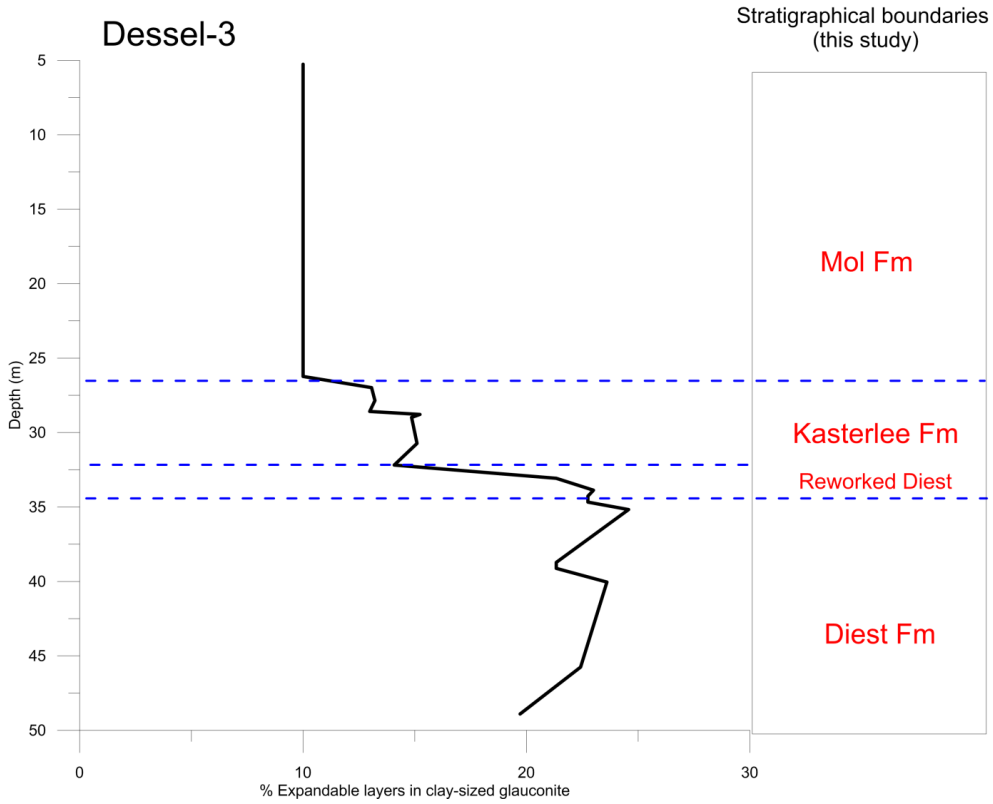

Figure 6.7. Expandability of clay-sized glauconite in relation to the depth and stratigraphical boundaries in the Dessel-3 borehole.

Table 6.1. Pelletal glauconite mineralogy evolution in the Dessel-3 borehole indicating stratigraphy, pelletal glauconite content in %, the d060 position and the amount of expandable layers in pelletal and clay-sized glauconite. Red lines indicates stratigraphic boundaries, as defined in this work.

				Pelletal glauconite		Clay-sized glauconite
Sample	Depth	Content (%)	d060	Total amount Glauconite layers	Total amount Expandable layers	Total amount Expandable layers
RT37	26.98	6.83	1.5166	93	**7**	13
RT38	27.85	6.51	1.5166	92	**8**	13
RT39	28.58	5.5	1.5162	92	**8**	13
RT48	33.07	25	1.5171	84	**13**	19
RT49	33.87	40	1.5175	83	**16**	20
RT51	34.67	40	1.5175	83	**18**	20
RT53	38.72	53	1.518	87	**13**	21
RT54	39.12	29	1.5175	85	**15**	21
RT56	45.75	53	1.5189	86	**15**	22
RT57	48.9	33	1.5189	85	**16**	20

VI.3.1.4 Pelletal glauconite

Glauconite pellets only occur in detectable amounts below 26m. Above this level glauconite pellets are very scarce, in amounts lower than 0.001%. Below the 26.1m level, the amount gradually increases from 0.5% to 7% at the 30.73m level. At 32.18m, the glauconite pellet content increases to 17%. From 33m downwards, the glauconite pellet content remains higher than 30% with 53% at the 34.67m level and the 39.12m level. The mineralogical composition of pelletal glauconite displays important variations throughout the vertical stratigraphic succession. Although the d_{060} only changes slightly, the amount of expandable layers significantly increases with depth (Table 6.1). A significant break is observed between the samples below 33m, characterized by high amounts of expandable layers in both pelletal and clay-sized glauconite, and samples of shallower depth of which pelletal and clay-sized glauconite are clearly less expandable. Clay-sized glauconite is systematically more expandable compared to the pelletal glauconite (Table 6.1).

VI.3.1.5 Grain size distribution

The grain size distribution of the Dessel-3 borehole (Figure 6.6) displays a very stable and well-sorted size distribution for the 5-26.1m section with 80% of the particles in the 125-250µm interval. Below 26.1m, the distribution is clearly somewhat finer with important amounts of particles <125µm and <63µm. The trend towards a finer grain size in the sand between 26-34 m is accompanied by more abundant clay laminae. At 34.27m, the distribution is characterized by important amounts of particles >355m, a few meters lower also particles >500µm occur frequently and the distribution becomes poorly sorted.

VI.3.1.6 Stratigraphic boundaries

The results presented in the previous sections demonstrate important variations in sediment petrological parameters that can be used as lithostratigraphic boundaries. The first break is noted around 26-27m. The distinct color change from grey above to green below is linked to the first significant appearance of pelletal glauconite and the sharp increase of clay-sized glauconite-smectite at 26.80m. It is most likely that this increase of glauconitic minerals is linked to a stratigraphic boundary but it is however unclear whether the zone between 26.80-28.5m is the glauconitic base of the Mol Formation, or the glauconitic top of the Kasterlee Formation. The sudden increase in clay-sized glauconite minerals indisputably indicates an important event causing massive pelletal glauconite disintegration. This event could be (1) pedogenesis, (2) a basal transgressive surface resulting in a *green sand followed by massive disintegration*, (3) a high energetic near-shore environment at the end of the deposition of the Kasterlee Formation. As the sediment does not resemble the present-day highly oxidized soils on glauconitic substrates and no other indications for glauconitic soil weathering were found, such as the Fe-vermiculite and increased expandability of pelletal glauconite in the Diest D5 unit (see Chapter V), in-situ pedogenesis seems rather unlikely. The basal green sand of the Mol Fm hypothesis is possible but seems rather incompatible with the general non-glauconitic nature of the Mol Fm. The third option seems therefore the most probable: a very shallow depositional environment at the end of the already near-shore Kasterlee Formation by which pelletal glauconite is massively abraded and/or disintegrated to produce clay-sized glauconite. Additionally, the mineralogy of clay-sized glauconite also drastically changes around the 26.33m level, with much lower d060-values above 26.33m compared to below this level. Because the d060 in glauconite minerals is sensitive to changes in the sedimentary environment, the 26.33m level most likely indicates an important sedimentological change. Because the Mol Formation lacks pelletal glauconite, the clay-sized glauconite in this unit cannot be derived directly by pelletal abrasion. Instead, clay-sized glauconite in the estuarine Mol Fm is, as discussed in Chapter III, reworked from slightly older glauconitic units, such as the Kasterlee Fm. The lower d060-values in the estuarine Mol Fm suggest that Fe is lost during transport.

Based on the occurrence and mineralogy of clay-sized glauconite, it is proposed to set the stratigraphic boundary between the Mol Formation above, and the Kasterlee Formation below, between 26.33m and 26.80m (Figure 6.6).

The boundary between the Kasterlee and the Diest Formation is clearly marked by numerous changes at the 32-34m interval. Whereas in the top of the Kasterlee Fm, pelletal glauconite is rather poor, it becomes much more prominent below 32m. In this lower zone, clay intercalations occur more frequently but also

the sands have a higher dispersed clay content. The concept of a sandy part and clayey part of the Kasterlee Fm (e.g. Berckmans and Wouters, 2003) seems to be confirmed by these observations. The most logic stratigraphical boundary is at 34.67m which marks the top of the Diest D4 unit with very high Fe-vermiculite contents, the presence of siderite, albitic feldspars and lowered mica contents. Similarly, also pelletal glauconite, elevated chlorite contents and an increased amount of grains >355µm are typical for the Diest D4 unit. Although such coarse grain size, higher chlorite and pelletal glauconite content also occur between 32 and 34,67 m depth, this last interval is interpreted as the reworking of the Diest Sand at the base of the Kasterlee Fm transgression. The reason for this interpretation is the gradual change in these parameters from the base of the interval towards normal Kasterlee Fm values at the top of the interval at 32 m. Also muscovite gradually increases in this interval towards normal Kasterlee Fm values at 32 m. In addition the change in clay mineralogy, siderite and feldspar type is abrupt at 34,67 m. Therefore this depth is interpreted as the boundary between the Diest and Kasterlee Formations. The basal 2m of the Kasterlee Fm is termed “reworked Diest”, occurring at the base of the Formation (Figure 6.6).

VI.3.2 The Dessel-2 borehole

VI.3.2.1 Borehole description

The lithological succession of the Dessel-2 borehole is very comparable to the Dessel-3 borehole (Figure 6.8 and Figure 6.9). In general, the sediment in the cores was relatively fresh with less surface alteration compared to the Dessel-3 sediment. Quickly after sampling however, limonitic alteration is observed in many samples, particularly in the clayey sands between 36-46m.

The uppermost part consists of grayish fine sands, which at a depth between 23 and 25.5m becomes somewhat more clayey and the sediment <32µm has a more grey color when mixed with water compared to the green color of the <32µm sediment mixed with water in the 4-23m interval. At a depth of 26.2m however, the sediment displays an intense green coloration with also the appearance of low amounts of pelletal glauconite. The intense green color becomes somewhat less pronounced below 28m, from where on pale green glauconitic sands are intercalated with brownish to salmon-colored, and sometimes also distinct green, clay laminae. From 32m pelletal glauconite content increases together with the frequency and thickness of the salmon colored clay laminae. Also the disperse clay content of the interstitial sand is relatively high in these samples. As observed in the Dessel-3 borehole, the top of the clay laminae shows eroded surfaces which are filled up with glauconitic sands. While clay intercalations are very prominent in the 33-34m core, they are almost absent downwards from the 34-35m interval, from where on only clayey glauconitic sand occurs till the total depth at 50m.

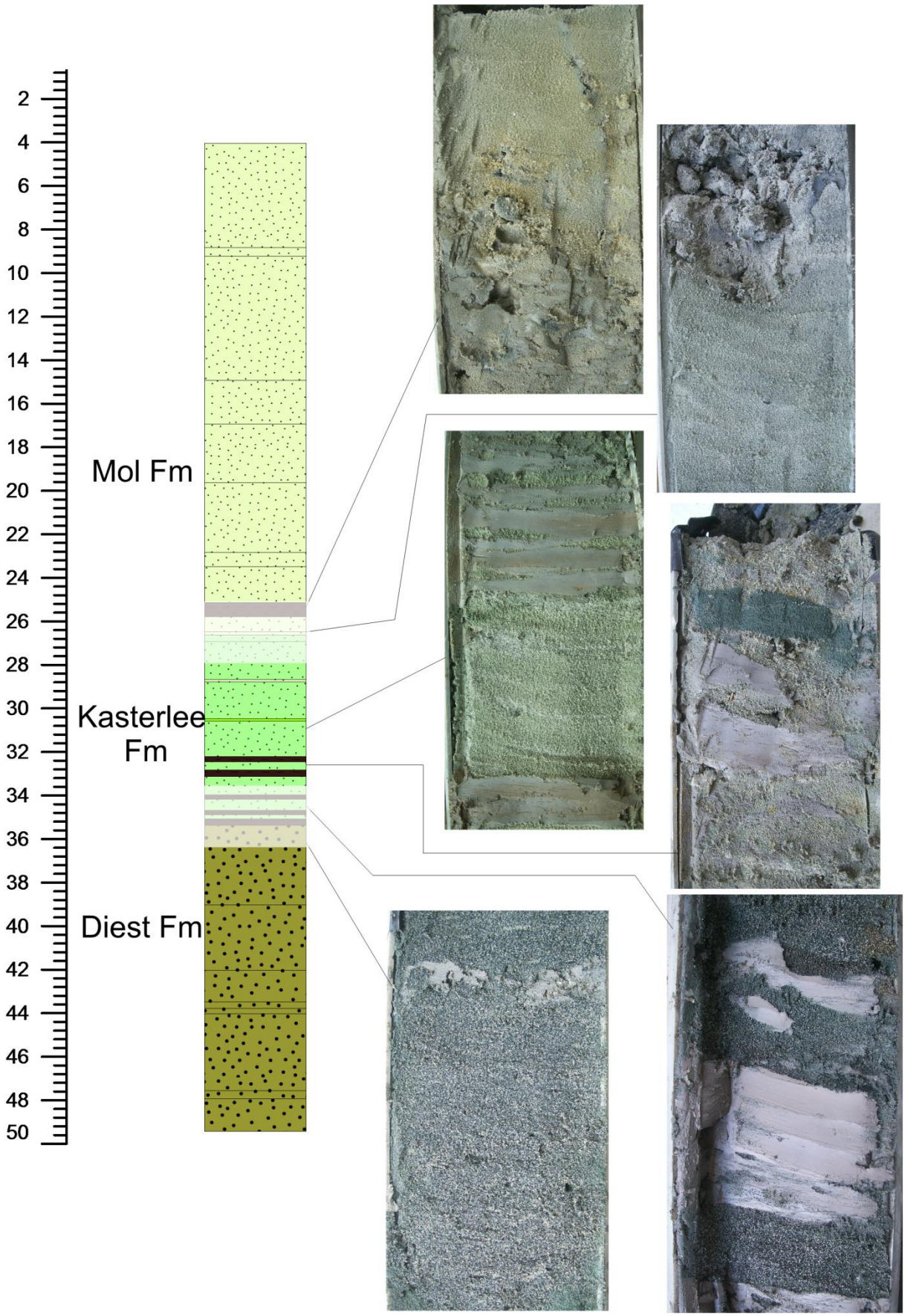

Figure 6.8. Photographic representation of the stratigraphic sequence of the Diest-Kasterlee-Mol Formations in the Dessel-2 borehole. Vertical scale indicates depth in m below topography. Transition zones were blurred.

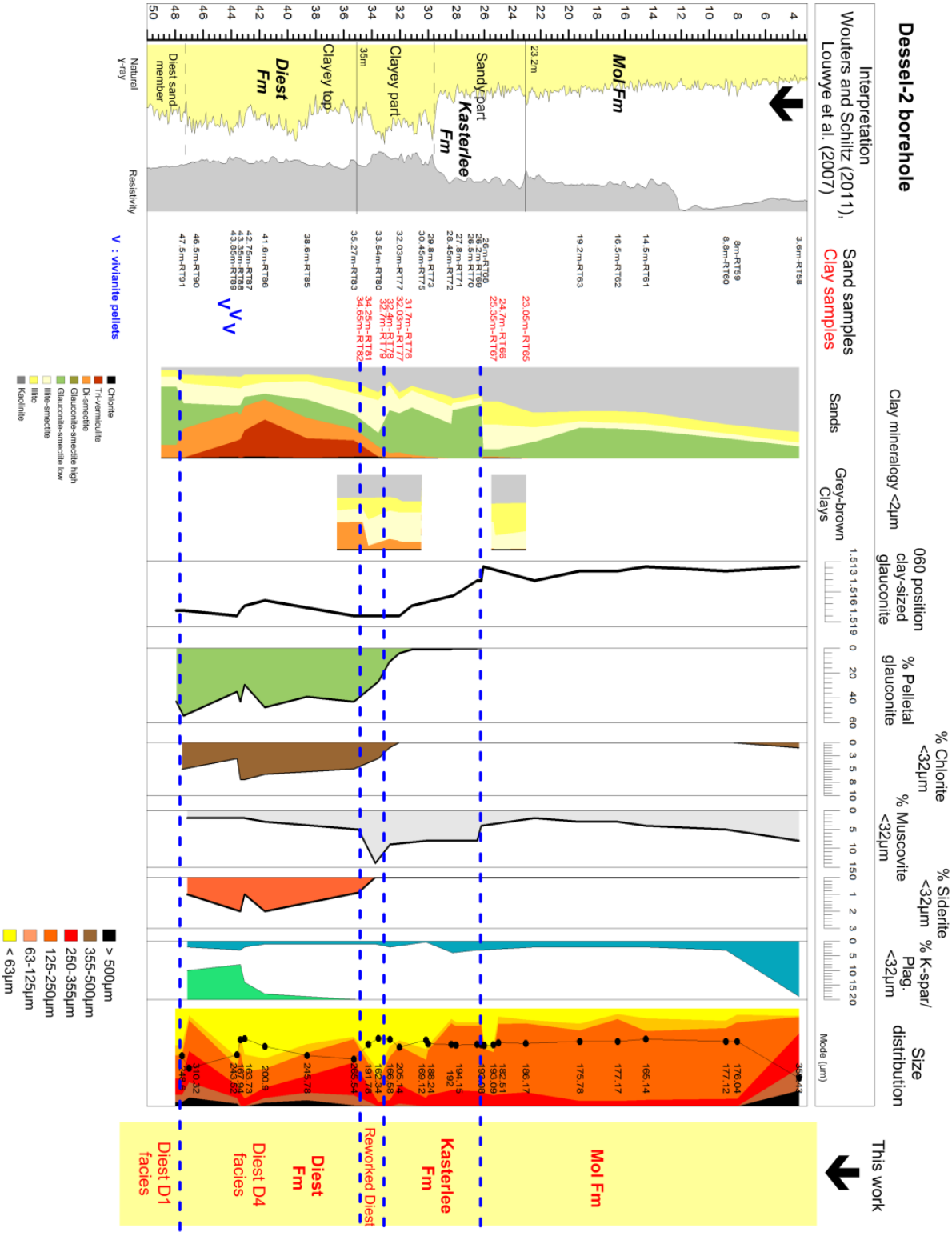

Figure 6.9. Combined mineralogical, clay mineralogical and size distribution results for the Dessel-2 borehole. On the left, the interpretation of Wouters and Schiltz (2011) and is shown, mainly based on gamma-ray (yellow on figure), resistivity (grey on figure) and cone penetration tests. In the second column, sample depths and codes have been listed for sands (in black) and clay laminae (in red). Clay mineralogy was analyzed from sands, grey and brown clays and green clays. Pelletal glauconite was measured from samples >32µm, while mineralogical results for chlorite, K-feldspars vs. plagioclase, siderite and muscovite contents were analyzed on fractions <32µm. Size distributions were derived from total samples. The stratigraphic interpretation of this work is shown in the far right column.

VI.3.2.2 Bulk mineralogy

The mineralogical composition of sand and clay samples of the Dessel-2 borehole are illustrated in Figure 6.10. Along the vertical succession for sand samples, it can be observed that kaolinite is the main mineralogical constituent above 20m in sand samples. Below, clay-sized and pelletal glauconite become more abundant and the amount of kaolinite decreases gradually. In sand samples below 32m, the amount of chlorite slightly increases. This trend continues at the 34.95m samples, and below, with also the first appearance of trioctahedral clay (Figure 6.10). In the same interval, the amount of glauconitic minerals is drastically lowered. Although substantial amounts of macroscopic vivianite concretions (spherical, <0.5cm) were identified in the 43.05m and 46m samples, no vivianite traces are present in their respective <32µm size fractions.

In the right part of Figure 6.10, the total mineralogical composition of clay intercalations is illustrated. The green clay samples are identified at 30.3m and at 32.03m. The mineralogical results illustrate clearly that the green color of these clay intercalations is caused by the presence of non-pelletal but clay-sized glauconite minerals. Kaolinite contents are very low in these green clays. The composition of the brown to grey clay laminae is composed of mainly quartz, kaolinite and 2:1 Al-clays. Clay laminae above 31m seem to be slightly more quartz-rich compared to clay laminae below this depth level.

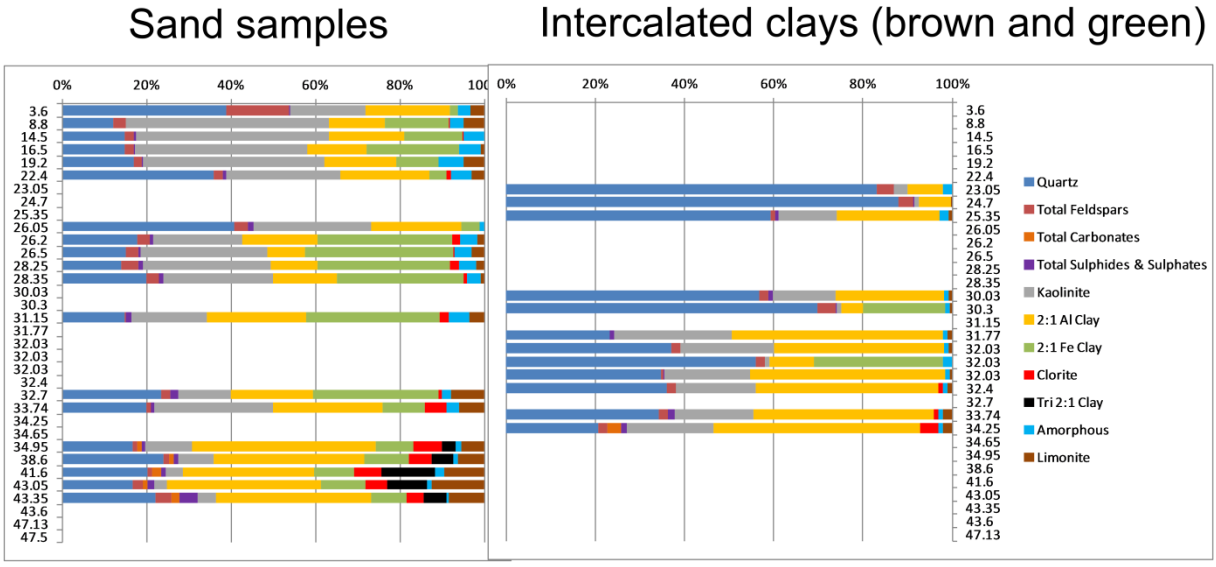

Figure 6.10. Dessel-2 borehole: Bulk mineralogical composition of sands (<323µm) and both green and brown clays (total sample). Green clays are characterized by elevated amounts of glauconitic (2:1 Fe-clays) minerals. Depth levels are shown at the left and right in m.

VI.3.2.3 Clay mineralogy

The clay mineralogy of the upper part of the Dessel-2 borehole is mainly dominated by kaolinite with illite, illite-smectite and glauconite-smectite as less abundant clays. The amount of kaolinite gradually decreases downwards in favor of the other clay minerals. The greyish clayey interval between 23 and 25m contains no or little clay-sized glauconite. The distinct intense green color of the sediment at 26.2m is clearly reflected in the clay mineralogy by almost 60% of clay-sized glauconite minerals and the appearance of pelletal glauconite (see section VI.3.2.4 Pelletal glauconite). This level represents the first break in clay mineralogy. In sand samples, the abundance of glauconite-smectite in the clay fraction remains very high until 32.70m, while the kaolinite percentage continuously decreases and the smectite and illite-smectite content increases with depth. In the salmon colored clays, no glauconite-smectite is present and their clay mineral composition shows little variation. In green clays however, the proportion of glauconite-

smectite is as high as 70% and the clay composition differs clearly from sand and clay samples in the same interval (Figure 6.9 and Figure 6.11). In the 32-34m interval, pelletal glauconite and chlorite contents start to increase while clay-sized glauconite-smectite and kaolinite further decrease. At 34.67m, the clay mineralogy of the salmon-colored clays drastically changes to a dioctahedral smectite-rich composition (Figure 6.12). Below this level, the amount of clay laminae drastically decreases and the clay mineralogy of the sands also contains more expandable minerals, in the form of Fe-vermiculite, less kaolinite and low amounts of glauconite-smectite, which correlates to the Diest D4 unit defined in Chapter V. At 47.5m, the clay mineralogy is again dominated by glauconite-smectite and Fe-vermiculite is absent, matching the typical clay mineralogical assemblage of the Diest D1 lithofacies.

Similar to the Dessel-3 borehole, the expandability of clay-sized glauconite varies significantly in the investigated interval, changing from relatively high-expandable Diest to lower Kasterlee and Mol expandability (Figure 6.13).

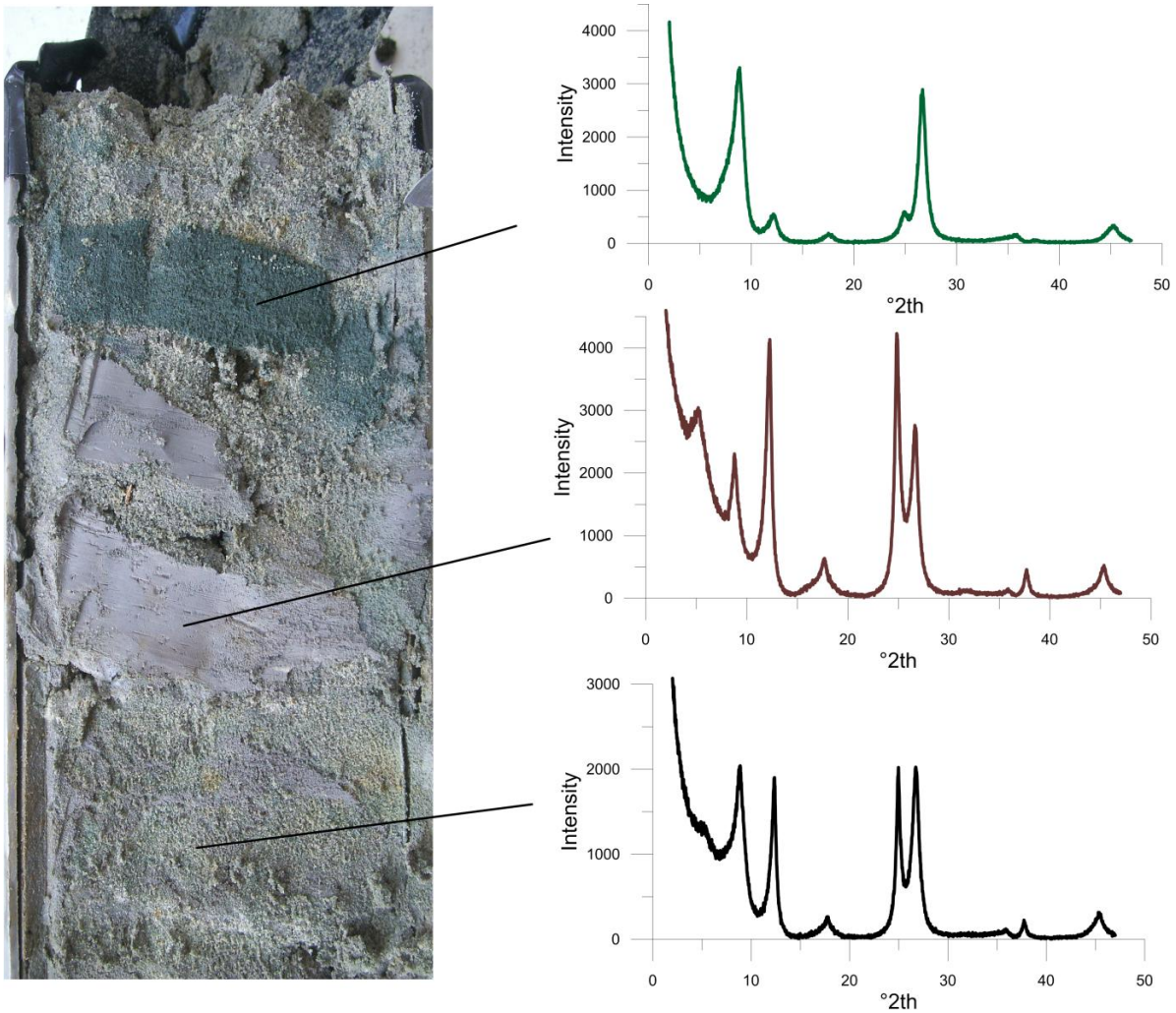

Figure 6.11. Glycolated XRD patterns <2µm of the different lithologies of RT77 at 32.03m. The green clay is characterized by high amounts glauconite-smectite; the salmon colored clays contains more smectite and kaolinite while the sand matrix typically consists of elevated amounts glauconite-smectite and kaolinite and minor smectite amounts.

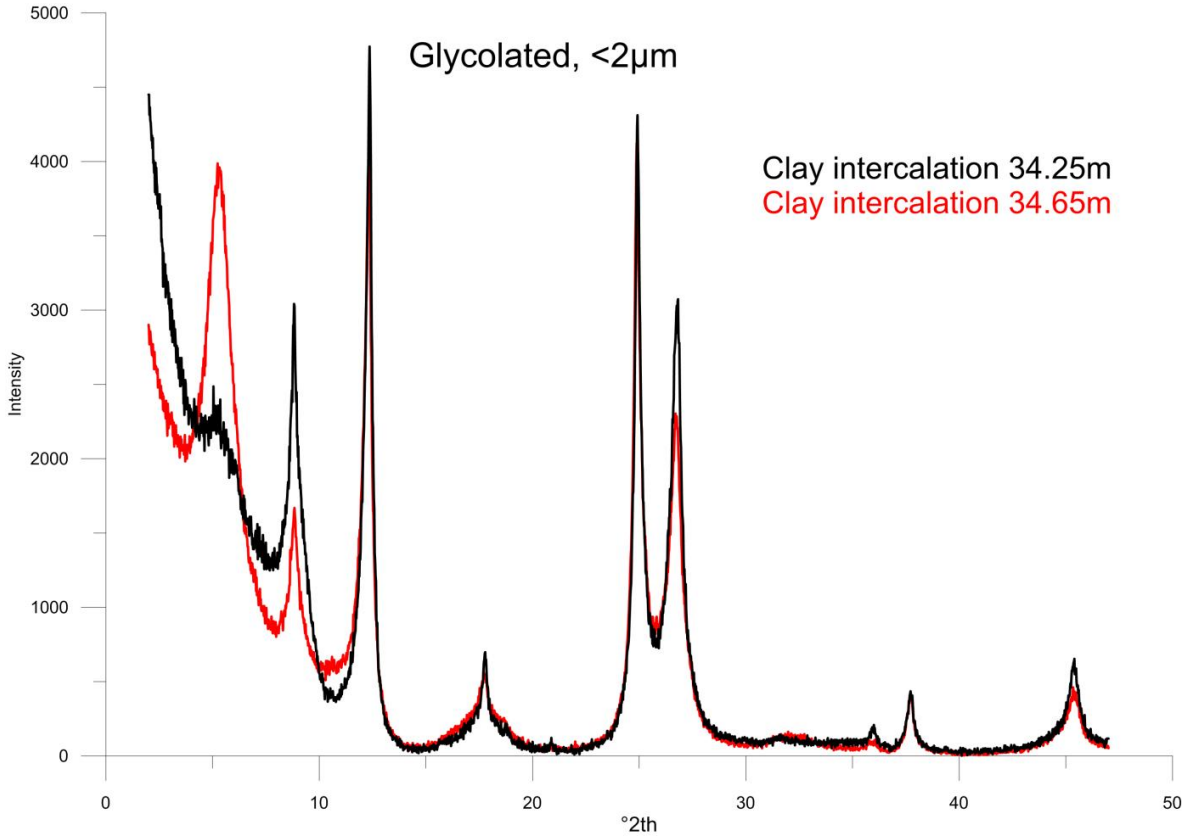

Figure 6.12. Glycolated XRD patterns <2µm of intercalated clay at 34.25m (black) and 34.65m (red) illustrating the sudden increase in dioctahedral smectite and marking the Kasterlee-Diest transition.

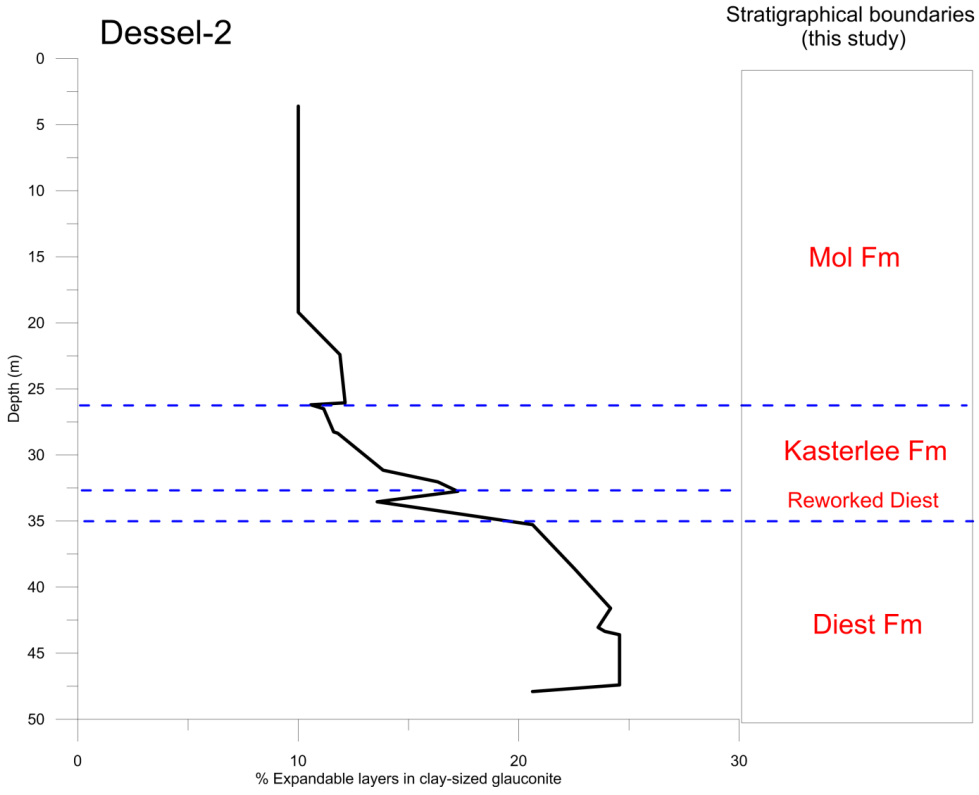

Figure 6.13. Expandability of clay-sized glauconite in relation to the depth and stratigraphical boundaries in the Dessel-2 borehole.

Table 6.2. Pelletal glauconite mineralogy evolution in the Dessel-2 borehole indicating stratigraphy, pelletal glauconite content in %, the d060 position and the modeled amounts of higher expandable and low expandable glauconite-smectite with 27% and 5% expandable layers respectively. The final two columns indicate the total amount of glauconite and expandable layers in each sample.

				Pelletal glauconite		Clay-sized glauconite	
Sample	Depth	Content (%)	d060	Total amount Glauconite layers	Total amount Expandable layers	Total amount Expandable layers	
RGT71	28.25	0.5	1.5162	92	**8**	7	Kasterlee Fm
RGT79	33.2	4	1.5171	92	**8**	13	
RGT80	33.54	27	1.5175	87	**13**	17	Reworked Diest
RGT83	35.27	43	1.518	86	**14**	19	
RGT85	41.6	48	1.5189	85	**15**	23	Diest D4 facies
RGT86	43.05	29	1.5175	85	**15**	23	
RGT88	43.6	35	1.518	84	**16**	24	

VI.3.2.4 Pelletal glauconite

As in the Dessel-3 borehole, pelletal glauconite does not occur in the upper 4-26m in amounts higher than 0.001%. At 26.2m, the glauconite content rapidly increases to 0.1% and further increases downwards to reach 4% at the 32.03m depth level. Below 32.75m, the amount of pelletal glauconite again increases sharply to 11% and further increases to 40%-50% at the 38-41m interval. Below 35m, the pelletal glauconite content never drops below 30% until 50m.

Similar to the Dessel-3 borehole, the mineralogical composition of the pelletal glauconite is subject to substantial variation. Pelletal glauconite in upper 28.25m and 33.2m samples are characterized by low amounts of expandable layers, typically around 8%. Below from the 33.54m sample however, expandability has increased to values above 10% (Table 6.2). Furthermore, the d_{060} seems slightly lower in the two uppermost samples. Expandability in clay-sized glauconite is systematically somewhat increased compared to pelletal glauconite.

VI.3.2.5 Grain size distribution

The size distribution from 4-26m is fine-sized (mode: 165-175µm) and well-sorted displaying little heterogeneity (Figure 6.9). The greyish interval between 23-25.5m, lacking glauconite-smectite, is however somewhat more clay-rich. The size distribution is also finer downwards from 28m with the mode of the distribution ranging from 160-205µm. An important break is noted at 35m, the distribution becomes poorly sorted with important amounts of particles >355µm and >500µm while still yielding a relatively high amount of particles <62µm (ca.30%).

VI.3.2.6 Stratigraphic boundaries

The Dessel-2 borehole is probably one of the most intensely studied boreholes to unravel the Diest-Kasterlee-Mol stratigraphy (see Berckmans and Wouters, 2003; Louwye et al., 2007 and Wouters and Schiltz, 2011). Wouters and Schiltz (2011) interpreted the Mol-Kasterlee boundary at 23.2m based on clear excursions in the gamma-ray and resistivity logs and cone penetration tests (Figure 6.9) which coincides with the top of the clay-rich facies between 23.2m and 25.5m. Based on the (clay) mineralogical results of this work however, the Kasterlee-Mol transition is most logically placed at 26.10m based on changes in pelletal glauconite content, the intense green coloration of the sediment, the sharp change in clay mineralogical composition (increase of glauconite-smectite and decrease of kaolinite) and the change in muscovite content. The 26.10m level is not only a clay mineralogical boundary but also paleoenvironmental conditions change drastically at this level as evidenced by the sharp decrease of the total amount and diversity of dinoflagellate cysts and in particular the species *Gramocysta verricula* which is strongly environmentally controlled (Louwye et al., 2007). In contrast, the amount of green algae, genus *Pediastrum*, becomes relatively more important (Louwye et al., 2007) which strongly suggests that the paleoenvironment shifted towards more brackish, estuarine waters with an important river influx.

The Diest-Kasterlee boundary is most logically chosen between 34.25 and 34.65m because of the numerous changes in clay mineralogy in

clays and sands (Figure 6.9 and Figure 6.12), the coarser and poorly sorted grain size distribution and the appearance of siderite and albitic plagioclase. As in the Dessel-3 borehole, the pelletal glauconite content and chlorite content is already elevated in the 33.54m sample and keeps increasing rapidly until 35m where a more stable value is reached (ca. 40%). Pelletal and clay-sized glauconite are considerably less expandable above the 33.54m sample. As such, the 33.54m-34.25m interval is therefore similarly interpreted as reworked Diest Sands as the basal 2m of the Kasterlee Formation. The sediment below 34.65m is interpreted as the Diest D4 facies of the Diest Formation. The 34.25-34.65m boundary was also proposed as the stratigraphic boundary between Diest and Kasterlee Formations by Louwye et al. (2007) based on dinoflagellate cysts assemblages whereas geophysical well log data show a boundary between 34m and 35m (Wouters and Schiltz, 2011).

VI.3.3 The Retie-1 borehole

VI.3.3.1 Borehole description

The Retie-1 borehole was studied and sampled from 24m to 50m in order to characterize the Diest-Kasterlee transition (Figure 6.14). Wouters and Schiltz (2011) interpreted the Diest-Kasterlee boundary at 29.5m depth (Figure 6.15). The upper boundary of the Kasterlee Fm was not determined in this borehole. When opening the vacuum-wrapped cores, the sediment clearly suffered strong and rapid surface oxidation in the store house (Figure 6.14). Underneath the hard iron crust skin, a fresh glauconitic sediment is observed. Quickly after sampling however, samples oxidize again and display a rusty brown color. From 24m to 26m, the sediment has a grey patina, is slightly glauconitic and contains grey clay intercalations. One sand sample and two clay laminae were collected for analysis. Between 26 and 28m, the glauconite pellet content in the glauconitic sand matrix increases rapidly and clay intercalations seem to be absent. In addition to the 3 samples above 26m, 14 sand samples were collected from the sediment present from 26m to 48m (Figure 6.15).

VI.3.3.2 Bulk mineralogy <32µm

Bulk mineralogical results <32µm of the Retie-1 borehole (Figure 6.16) show that in the uppermost samples quartz is present in amounts from 20-40% while below 28.16m, only 15% is present and below 36m it is only 10%. This is mainly caused by the increasing amount of dioctahedral Fe-clays, i.e. glauconite minerals in pelletal and clay-sized habits. The two clay samples at 25.51m and 25.93m contain however no glauconite minerals. Important changes in mineralogy occur at the 28.16m sample, with the appearance of chlorite, siderite and albitic plagioclase (Figure 6.15). The amount of kaolinite is >20% above 28.16m but sharply decreases below to less than 10%. Also the total amount of feldspars increases in the 28.16m sample compared to uppermost samples. The proportion of muscovite drops significantly at the 30.06m level (Figure 6.15). Siderite is the only carbonate minerals found in the Retie-1 samples.

VI.3.3.3 Clay mineralogy

The clay mineralogical composition of the uppermost analyzed sample of the Retie-1 borehole (Figure 6.15) is characterized by relatively higher kaolinite contents compared to the samples below, of which the clay composition is mainly made up by glauconite-smectite. The kaolinite percentage further decreases and the proportion of mixed-layer minerals (illite-smectite) slightly increases below 30m. In the 30-50m depth interval, dioctahedral smectite occurs at certain levels. Trioctahedral Fe-vermiculite, as found in the top Diest in the Dessel-2 and Dessel-3 boreholes, is however absent in all samples.

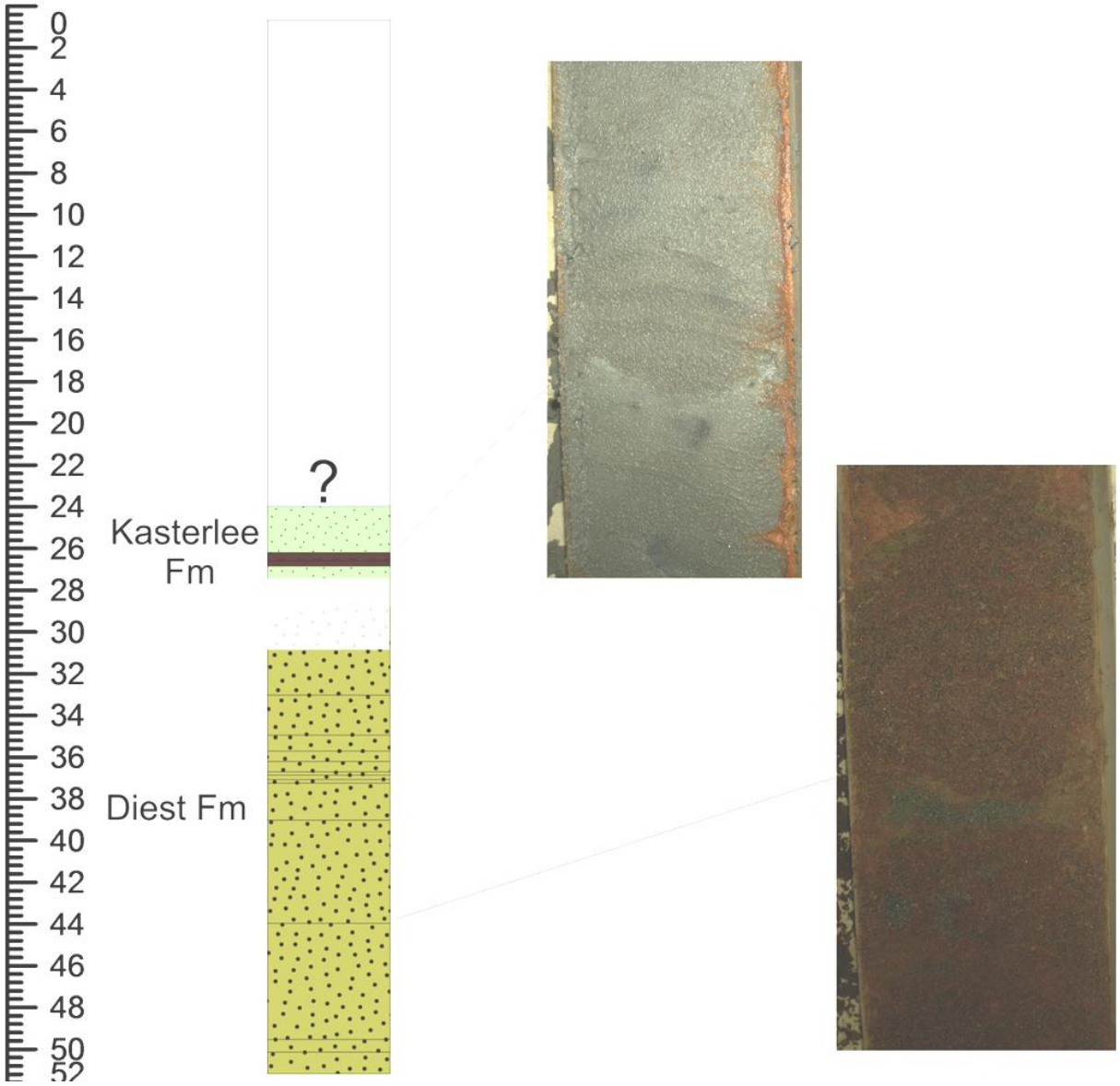

Figure 6.14. Photographical representation of the sampled stratigraphic succession of the Kasterlee and Diest Formations in the Retie-1 borehole. Vertical scale shows depth in m below topography. In the uppermost picture (25-26m) a lithological boundary is shown from sand, to clayey interacted sand. The lower photograph (44-45m) shows the rusty brown surface alteration layer.

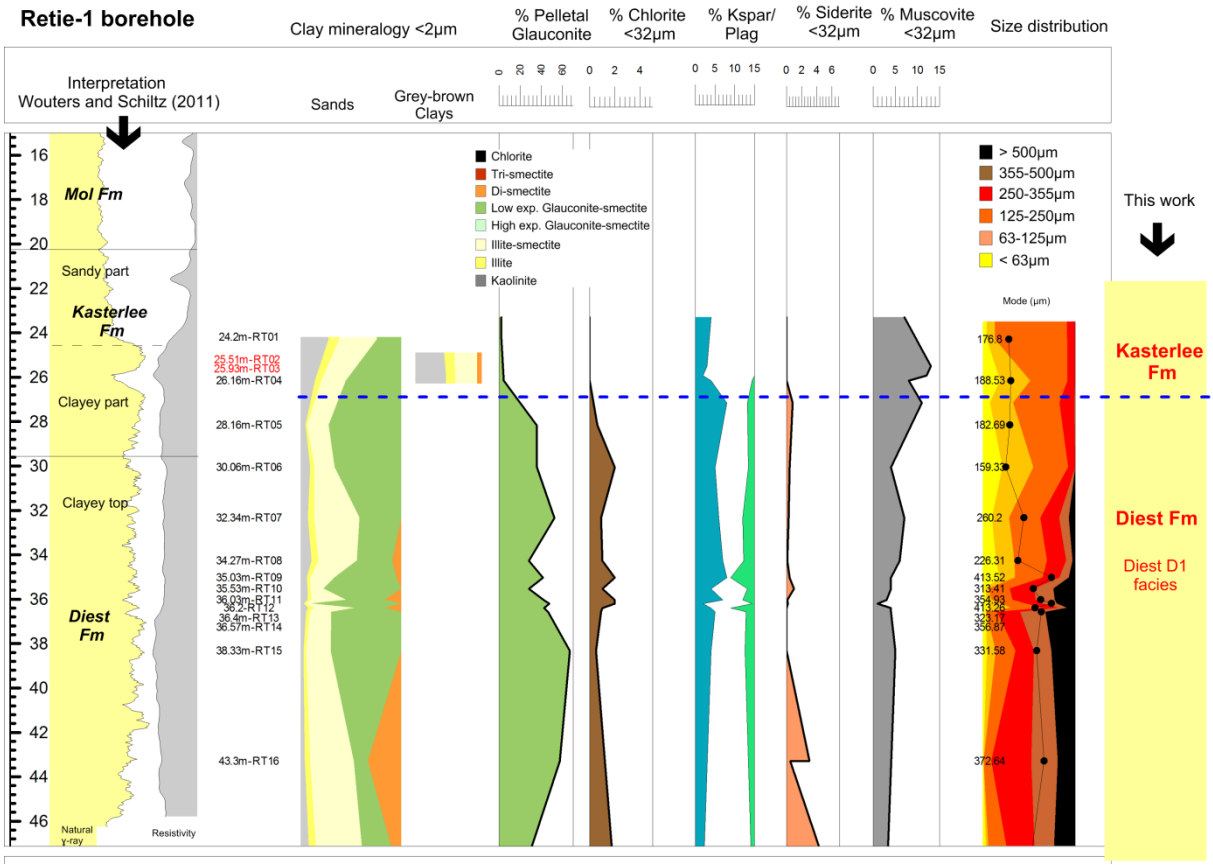

Figure 6.15. Combined mineralogical, clay mineralogical and size distribution results for the Retie-1 borehole. On the left, the interpretation of Wouters and Schiltz (2011) and is shown, mainly based on gamma-ray (yellow on figure), resistivity (grey on figure) and cone penetration tests. In the second column, sample depths and codes have been listed for sands (in black) and clay laminae (in red). Clay mineralogy was analyzed from sands, grey and brown clays and green clays. Pelletal glauconite was measured from samples >32µm, while mineralogical results for chlorite, K-feldspars vs. plagioclase, siderite and muscovite contents were analyzed on fractions <32µm. Size distributions were derived from total samples. The stratigraphic interpretation of this work is shown in the far right column.

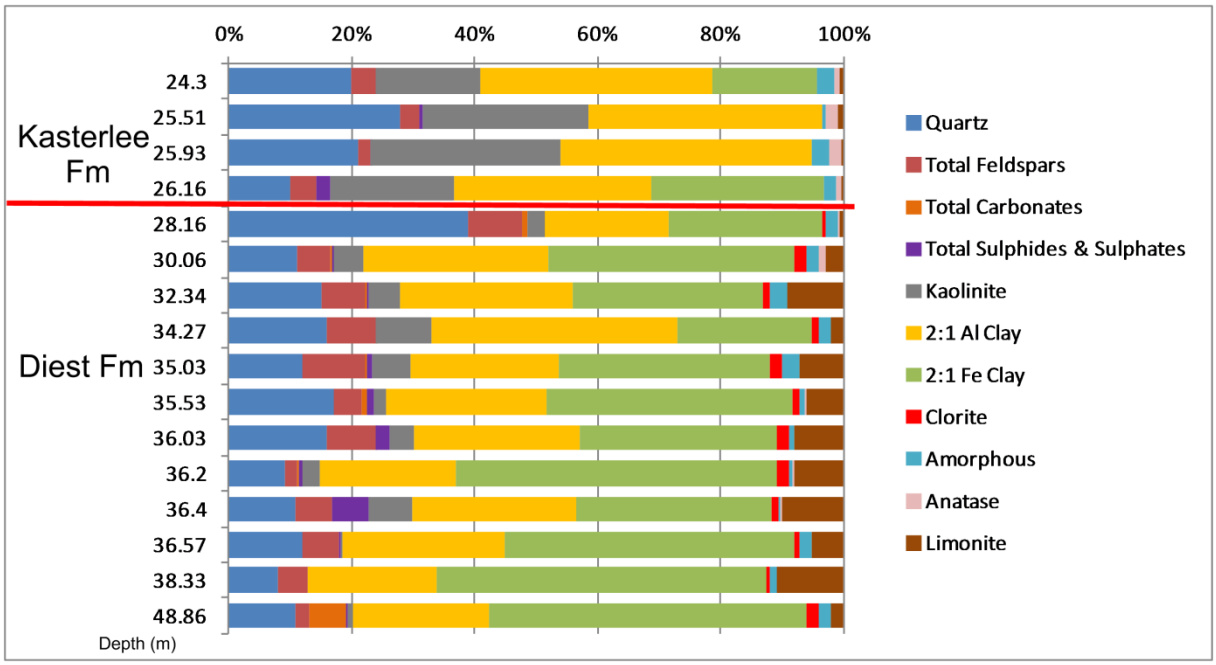

Figure 6.16. Bulk mineralogical results <32µm for the Retie-1 borehole. The vertical scale shows depth in m below topography.

VI.3.3.4 Pelletal glauconite

Whereas pelletal glauconite is less abundant in the 26.16m an the 24.2m samples (less than 5%), amounts are systematically >28% in 28-45m depth interval, with a concentration of >60% around the 38m level (Figure 6.15). The two bottommost samples at 48.86m and 49.46m are slightly less glauconitic with percentages of 19% and 16% respectively. At the top of the sampled sequence, there is a clear break in pelletal glauconite content between the 26.16m sample (4.4%) and the 28.16m sample (35%). In the uppermost sample, 2.3% of glauconite pellets are present in the sand matrix. The mineralogical composition of the pelletal glauconite in the entire section, based on 4 analyzed samples, is characterized by low amounts of expandable layers (<10%). The expandability increases slightly in the 28.16m sample but remains, relatively low (Table 6.3). The uppermost 24.2m sample contains 7.86 % expandable layers, which again is very low.

VI.3.3.5 Grain size distribution

The size distribution of the analyzed samples can be subdivided in a part above and below 30m. Above 30m, the grain-size is relatively fine-grained with elevated amounts of particles <125µm and modes <200µm (Figure 6.15). Below the 30.06m sample, the amount of particles <125µm gradually decreases, ,whereas the particle population >250µm becomes more important and distribution modes increase to >225µm. Below 35m, the grain-size is even coarser and the distribution mode is systematically higher than 300µm.

VI.3.3.6 Stratigraphic boundaries

In the Dessel-2 and Dessel-3 boreholes the Kasterlee-Diest transition was relatively clearly marked by the presence of trioctahedral Fe-vermiculite typical for the Diest D4 litho-unit. It was already discussed in Chapter V that the 10-15m thick Diest D4 facies is absent in the Retie-1 borehole, although the Retie-1 and Dessel boreholes are only a few kilometers apart. The top Diest in the Retie-1 borehole is more clay-rich compared to lower levels (see also Figure 6.15) but the (clay) mineralogical characteristics are almost identical compared to the more coarser-sized Diest sand sediment below 30m. Both the fine-grained top part and the coarser part below were therefore interpreted as the Diest D1 facies. The transition to the Kasterlee Formation is consequently also less clear to interpret from the mineralogical data in the Retie-1 borehole. Wouters and Schiltz (2011) also stated that the Kasterlee-Diest transition, based on geophysical well log data and cone penetration tests, is much less straight-forward to interpret compared to the Dessel-2 and Dessel-3 boreholes.

Nevertheless, the Kasterlee-Diest transition is also in the Retie-1 borehole marked by some distinct mineralogical changes. The 28.16m is the highest level containing siderite, chlorite and plagioclase minerals. Furthermore, also pelletal glauconite contents increase sharply between 26m and 28m. It is therefore most logically to interpret the Diest-Kasterlee boundary between the 26.16m and 28.16m samples (Figure 6.15). In contrast to the Dessel-2 and Dessel-3 boreholes, no reworked Diest interval is interpreted. It has to be noted however that the mineralogical criteria are not as strong as in the Dessel-2 and Dessel-3 borehole. Based on the grain-size distribution only, a stratigraphic break could also be interpreted around 35m but there are no additional arguments to interpret this level as an important boundary (Figure 6.15).

Table 6.3. Pelletal glauconite mineralogy evolution in the Retie-1 borehole indicating stratigraphy, pelletal glauconite content in %, the d060 position and the amount of expandable layers in both pelletal and clay-sized glauconite.

				Pelletal glauconite		Clay-sized glauconite
Sample	Depth	Content (%)	d060	Total amount Glauconite layers	Total amount Expandable layers	Total amount Expandable layers
RGT01	24.2	2.3	1.5162	92	**8**	14
RGT05	28.16	36	1.5166	91	**9**	10
RGT12	36.2	48	1.5162	95	**5**	13
RGT14	36.57	46	1.5162	94	**6**	15

VI.3.4 The Rees borehole

The Kasterlee-Diest transition has been described in Buffel et al. (2001) in the Rees 17E399 borehole which is located ca. 10km northwest from the Dessel-2, Dessel-3, and Retie-1 boreholes. Buffel et al. (2001) interpreted the Kasterlee Fm between 25.3m and at 33.25m based on the change from a fine-grained Kasterlee to a poorly-sorted Diest part below ca. 33.25m, with a considerable increase of particles >250µm. The Diest part of the Rees borehole was interpreted as the Diest D4 facies in Chapter V.

VI.3.4.1 Borehole description

The top of the Rees borehole consists of quartz-sand of the Quaternary Merksplas Formation (previously termed Vosselaar Member of the Brasschaat Formation by Buffel et al.,2001)) and the local coarse Rees facies of the Pliocene Mol Formation. Below, the Poederlee Formation was interpreted with a well-sorted Heieinde facies at the top underlain by ferruginous glauconitic sands to iron-cemented sandstones. The base of the Poederlee Formation is marked by a fine shell debris layer at 24m and, gravel and ferruginous sandstone levels between 24.90m and 25.30m (Figure 6.17). From 25.30m until 33.10m, fine glauconitic clayey sands occur which have been altered by intense limonitization. This part was interpreted as the Kasterlee Fm by Buffel et al. (2001). The Diest-Kasterlee transition occurs at 33.10m according to Buffel et al., (2001) based on grain-size. This level is marked by a thin clay layer, and below and the grain-size indeed is coarser but all other macroscopic characteristics of the sediment seem to remain unchanged. Locally, less limonitization is observed and at three levels, 35.70m, 36.60m and 37.25m the sediment is characterized by red staining.

VI.3.4.2 Bulk mineralogy of sands <32µm

Mineralogical results of the Rees borehole (Figure 6.19) show a relatively stable composition in the 26-40m interval. Dioctahedral Al-clays and quartz are the most important mineral constituents. Also elevated amounts of chlorite and trioctahedral swelling clays occur with relatively lower amounts of glauconitic and kaolinite minerals. A remarkable trend is the decreasing content of sulphur-bearing minerals with depth. Although pyrite is also present in small amounts, the majority are sulphates, mainly as gypsum and, less common, jarosite. Carbonates, always in the form of siderite, are systematically present in trace amounts (<1%) but also occur concentrated in reddish stained samples (35.7m, 36.6m, 37.4m and 39.5m). Apatite is absent in most samples but does occur in low amounts in a few samples (26.76m, 33.8m, 36.9m, 37.95m and 39.3m). Both K-feldspars and plagioclase are present throughout the entire interval. Muscovite remains relatively constant around 5%. It can be concluded that the proposed 33.25m boundary by Buffel et al. (2001) does not include a clear mineralogical change. Even more, the specific composition of the Diest D4 unit (interpreted in chapter V) seems to remain identical above 33.25m.

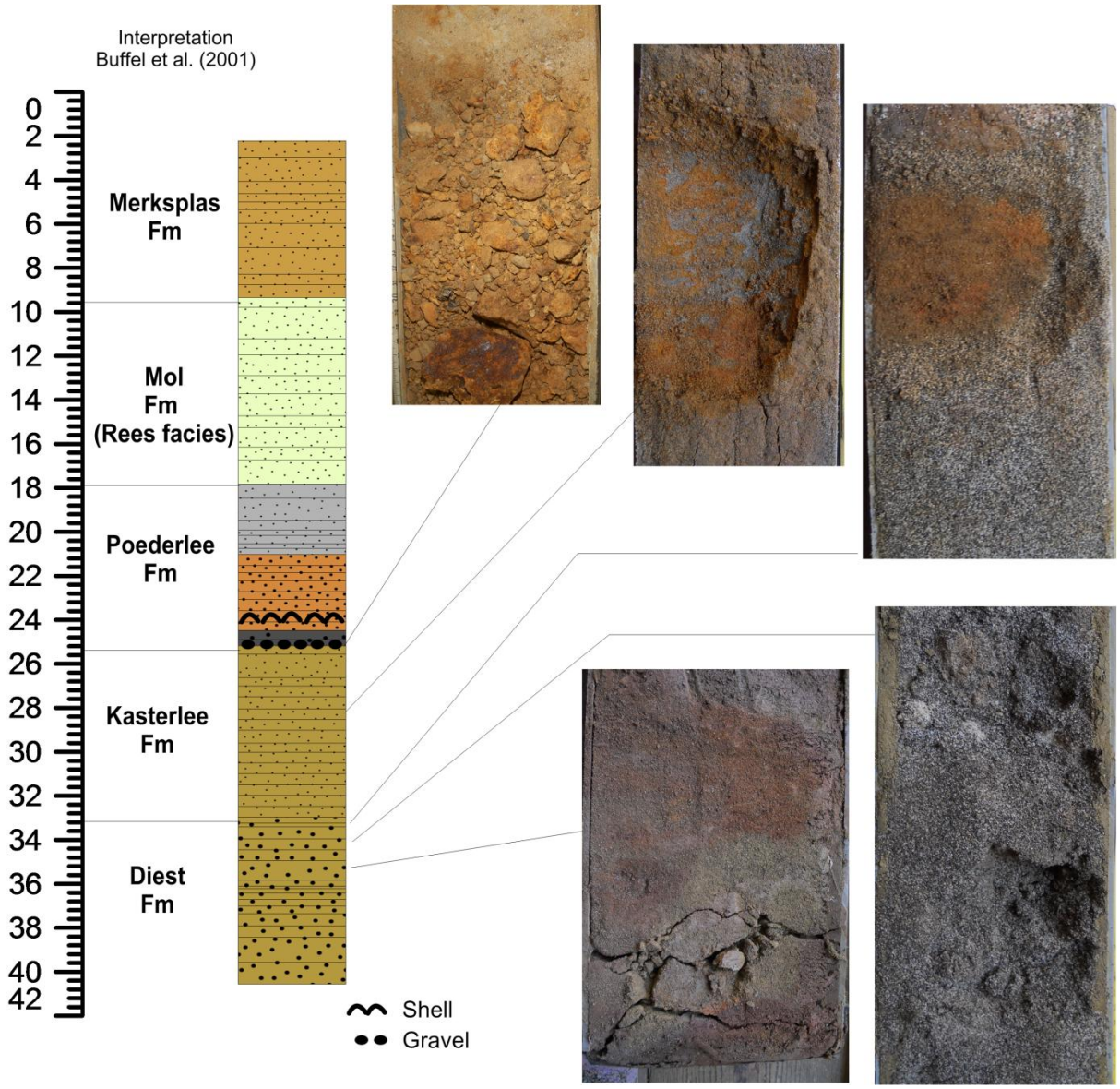

Figure 6.17. Photographic representation of the vertical succession from 26-40m in the Rees borehole. Vertical scale shows depth in m below topography. The photo at 26m displays the fossiliferous and iron cemented base of the Poederlee Fm. The photo at 29.3m shows iron oxidation of glauconitic sand samples, which even is spread throughout the whole depth of the borehole. The photo at 33.08m shows a clayey intercalations marking the boundary between finer and coarser sized glauconitic sediments. The photo at 33.70m shows the coarser glauconitic sands. The photo at 35.80m displays reddish zonations in the sediment together with a clay lense.

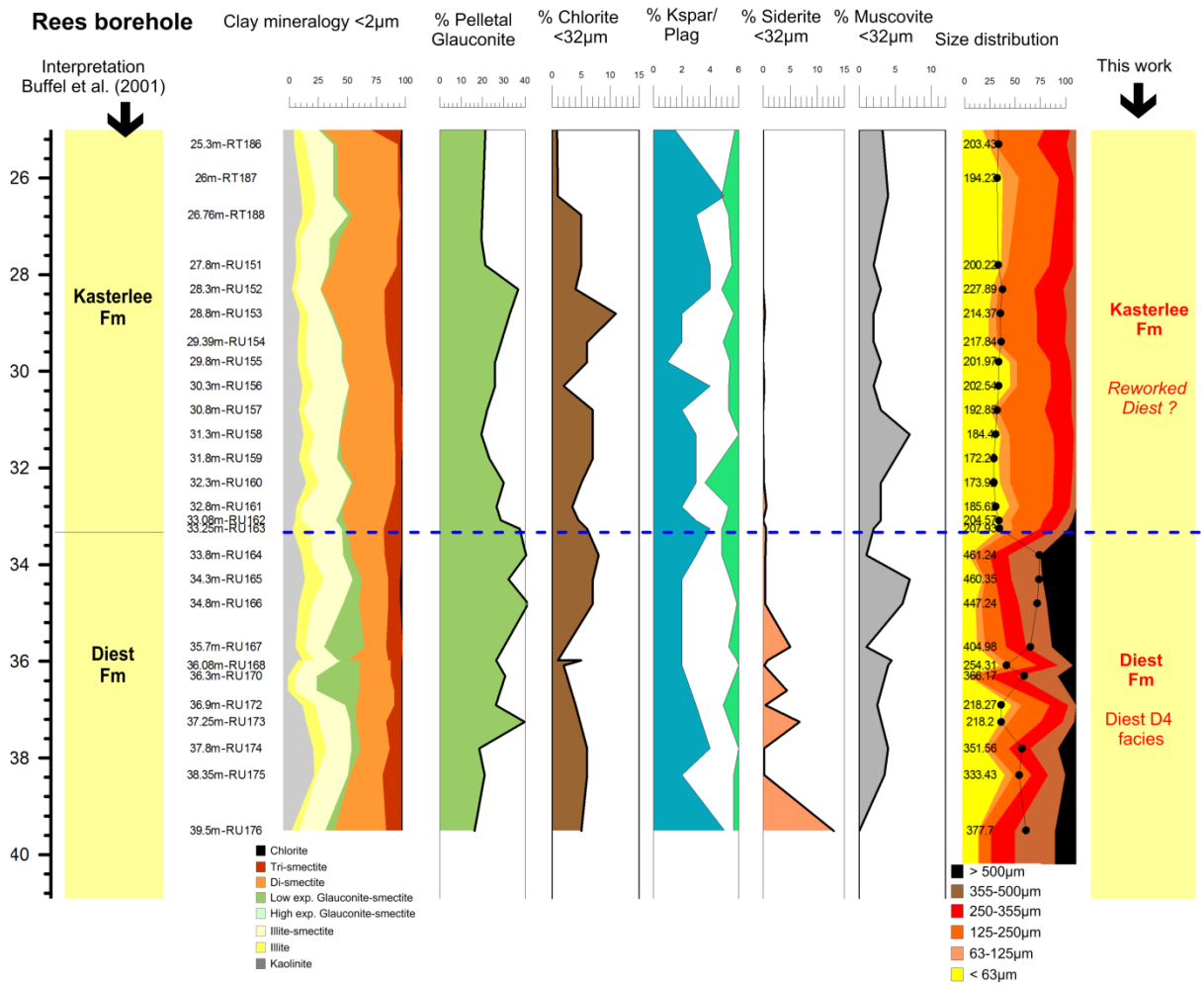

Figure 6.18: Quantitative mineralogical, clay mineralogical and grain size distribution data for the Rees 17E399 borehole. The vertical scale shows depth in meter below topography. X marks on the right side of the litho-column indicate sample levels. Above 18m, no bulk mineralogical analyses was performed due to low sample amounts.

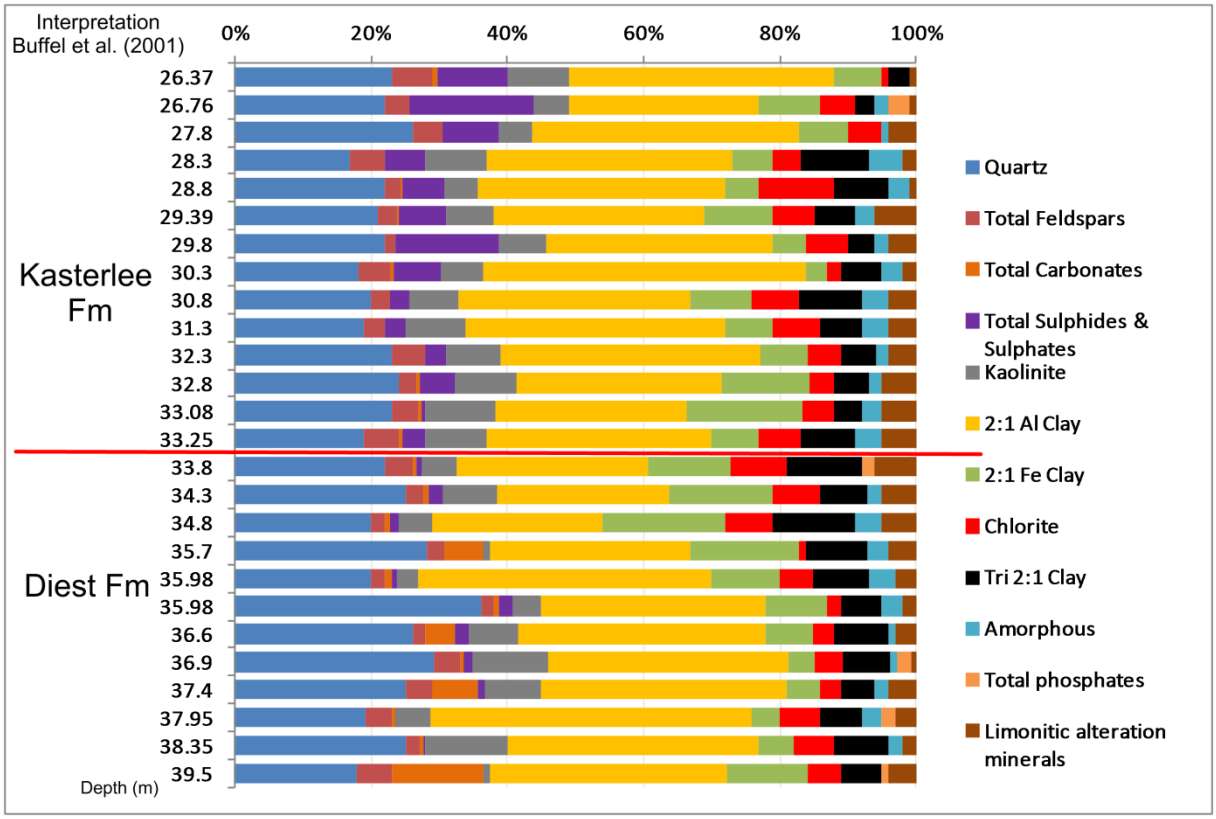

Figure 6.19. Bulk mineralogical results of the Rees 17E399 borehole between 26m and 40m. The vertical scale shows depth in meters below topography.

Table 6.4. Pelletal glauconite mineralogy evolution in the Rees borehole indicating stratigraphy, pelletal glauconite content in %, the d060 position and the total amount of glauconite and expandable layers in each sample. The total amount of expandable layers in clay-sized glauconite is also shown.

				Pelletal glauconite		Clay-sized glauconite
Sample	Depth	Content (%)	d060	Total amount Glauconite layers	Total amount Expandable layers	Total amount Expandable layers
RGU153	28.8	28	1.5171	86.20	**13.8**	24.2
RGU154	29.39	24	1.5157	86.64	**13.36**	23.6
RGU158	31.3	14	1.5171	83.34	**16.66**	25.3
RGU159	31.8	18	1.518	83.34	**16.66**	27
RGU166	34.8	37	1.5153	83.78	**16.22**	26.4
RGU168	36	22	1.5171	84.22	**15.78**	27
RGU172	36.9	21	1.5175	86.20	**13.8**	24.2
RGU175	38.4	16	1.5171	87.30	**12.7**	23.4

VI.3.4.2 Clay mineralogy

The clay mineralogy of the lower sampled part 26-40m of the Rees borehole (Figure 6.18) illustrates that swelling clay minerals make up almost 50% of the <2µm mineralogy. The amount of dioctahedral smectite is slightly higher in the 26-33m interval compared to the 33-40m interval. Remarkable is the continuous presence of trioctahedral Fe-vermiculite over the entire interval and thus also in the presumed Kasterlee Fm between 25-33m. The amount of clay-sized glauconitic minerals is very low and only occurs in elevated amounts in the 35.5-36.5m interval. It can be concluded that, unlike the previous boreholes, there is no clear break in clay mineralogy between 26m and 40m depth.

VI.3.4.3 Pelletal glauconite

The amount of pelletal glauconite in the 26-40m interval (Figure 6.18) is always higher than 20% . Below 33m, the content increases slightly but the order of magnitude remains equal. The high pelletal glauconite amounts for the 25-33m interval is odd for the presumed Kasterlee Formation and furthermore very different than the results for the Kasterlee Formation in the Dessel-2, Dessel-3 and Retie-1 boreholes. Consequently, pelletal glauconite does not allow a differentiation between the two proposed sections.

The mineralogy of the pelletal glauconite, described by the d_{060} and expandability is prone to little variation throughout the 28-38m interval. The d_{060} remains relatively constant throughout the sampled interval with a typical value of 1.517Å. The amount of expandability is systematically higher than 12% with the highest expandability amounts in the 31.3m and 31.8m samples (Table 6.4). Similar to previous results, the expandability of clay-sized glauconite is higher than pelletal glauconite.

VI.3.4.4 Grain size distribution

The size distribution of the Rees borehole is the only observed parameter indicating a clear and sharp break at 33.25m. Above this boundary, the sediment is relatively clayey with distribution modes ranging from 170-230µm. Below 33.25m however, the sediment is clearly coarser-sized with the distribution mode >400µm. The upper boundary of the 26-33m section is determined by the gravel layer at 25m.

VI.3.4.5 Stratigraphic boundaries

The characteristics of the Kasterlee Formation, as defined by Buffel et al.,(2001), are completely different compared to the sandy or clayey Kasterlee section found in the Dessel area. Pelletal glauconite amounts are systematically higher than 20% and the clay mineralogy <2µm consists of high amounts of dioctahedral smectite but also contains Fe-vermiculite. The mineralogical characteristics of the 25-33.25m interval are furthermore identical compared to the coarse Diest D4 unit below. A stratigraphic boundary can be drawn at 33.25m only based on grain-size properties. Several options remain for a stratigraphic interpretation of the 25-33.25m interval.

A first interpretation implies that the interval indeed belongs to the Kasterlee Formation but represents a new, totally different facies compared to the Kasterlee occurrences in the Dessel area (see Dessel-2,Dessel-3 and Retie-1 boreholes in this chapter) or the Kasterlee area (see Chapter V). As all these geographical locations are less than 10km apart, this option seems rather unlikely.

A second possible interpretation is that the interval was deposited after deposition of the Diest Formation but consists entirely of reworked material of the Diest D4 unit. Such a “reworked Diest” interval was also defined for the Dessel-2 and Dessel-3 borehole to mark the max. 2m-thick transition interval between the Kasterlee and Diest Formations. However, in the Rees borehole, the reworked Diest interval would reach the entire 8m thickness of the Kasterlee Fm as it is not covered by other Kasterlee sediments.

A third possibility is provided by former palynological studies. Louwye and De Schepper (2010) stated that in the Dessel-2 borehole a more shallow marine facies of the Kasterlee Fm is found compared to the Kasterlee Fm occurrence in the more northern situated Oud-Turnhout borehole. As the Oud-Turnhout borehole was correlated with the Rees borehole by Buffel et al.,(2001), it is most likely that also the Kasterlee Fm occurrence in the Rees borehole represents a deeper water facies deposition and is therefore different in mineralogical characteristics and thickness compared to the Kasterlee Fm occurrence in the Dessel-2 borehole, situated southeast from the Rees borehole.

A deeper water facies is the most likely option as it would explain why no shallow marine Kasterlee sand facies, such as encountered in the Dessel-2 and Dessel-3 boreholes, is found in the Rees borehole. Nevertheless, the mineralogical similarity between the “reworked Diest” intervals in Dessel-2, Dessel-3 and Rees suggests that the material comprising the interval is mainly reworked from underlying Diest Fm sediments.

VI.3.5 The Olen sluice outcrop

Construction works at the sluice complex in Olen, 20km southwest from Dessel, in 1972 exposed a temporary outcrop of the Diest-Kasterlee transition (Figure 6.3). The Diest-Kasterlee boundary was marked by coarser quartz grains to gravel, occasional round pebbles and silicified shell fragments. If a distinctive basal lithological boundary layer is present at the base of the Kasterlee Formation it is a somewhat coarser sand which is often hard to observe. The Olen outcrop is the only locality where distinct cm-sized pebbles occur at the base of the Kasterlee Fm. Therefore the Olen outcrop is a reference section for the Diest-Kasterlee Formations boundary, also studied as such by Louwye et al. (2007) in a comparison with the Dessel-2 borehole. Small samples taken in 1972 (Figure 6.20) are available for this study. Four samples were analyzed, two from the Kasterlee Formation (at 3.9m and 4.5m) and two from the Diest Formation below (at 8.5m and 11m) (Figure 6.21). The gravel layer bordering both formations occurs at approximately 5.5m depth. All four samples are glauconitic and sandy, with the two lowermost Diest samples being characterized by a more brown coloration.

VI.3.5.1 Bulk mineralogy <32µm

The mineralogical composition of the lowermost Diest sample (11m) consists of high amounts 2:1 Fe-clays and 2:1 Al-clays but also substantial amounts of gypsum and jarosite, the latter most likely oxidation products. Both K-feldspars and plagioclase occur and siderite is present in small amounts (<2%). Kaolinite percentages are very low. A similar observation is made for the 8.5m Diest sample, but with a higher 2:1 Al-clay proportion and much less sulphates. Also the Kasterlee samples above have a comparable bulk mineralogical assemblage, although the amount of kaolinite clearly increases (Figure 6.22). Siderite disappears in the mineralogical assemblage as opposed to muscovite flakes, which are much more abundant in the upper Kasterlee sample. Whereas small amounts of plagioclase are still present in the 4.5m Kasterlee sample, only K-feldspar is found in the upper 3.9m sample.

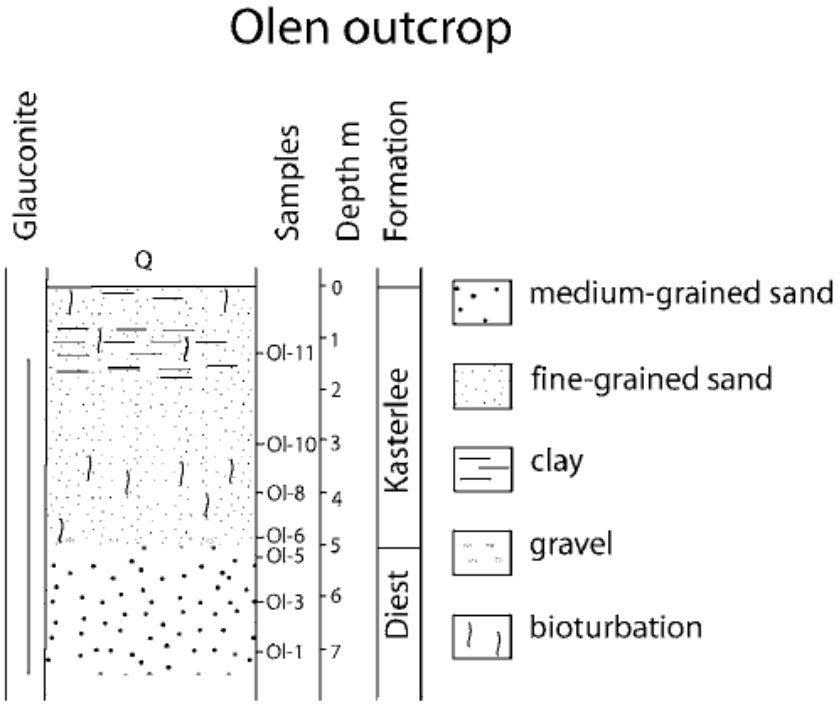

Figure 6.20. Lithology and lithostratigraphic interpretation of the Olen sluice outcrop in 1972 (after Louwye et al., 2007). Note that sample numbers do not refer to sample number used in this study.

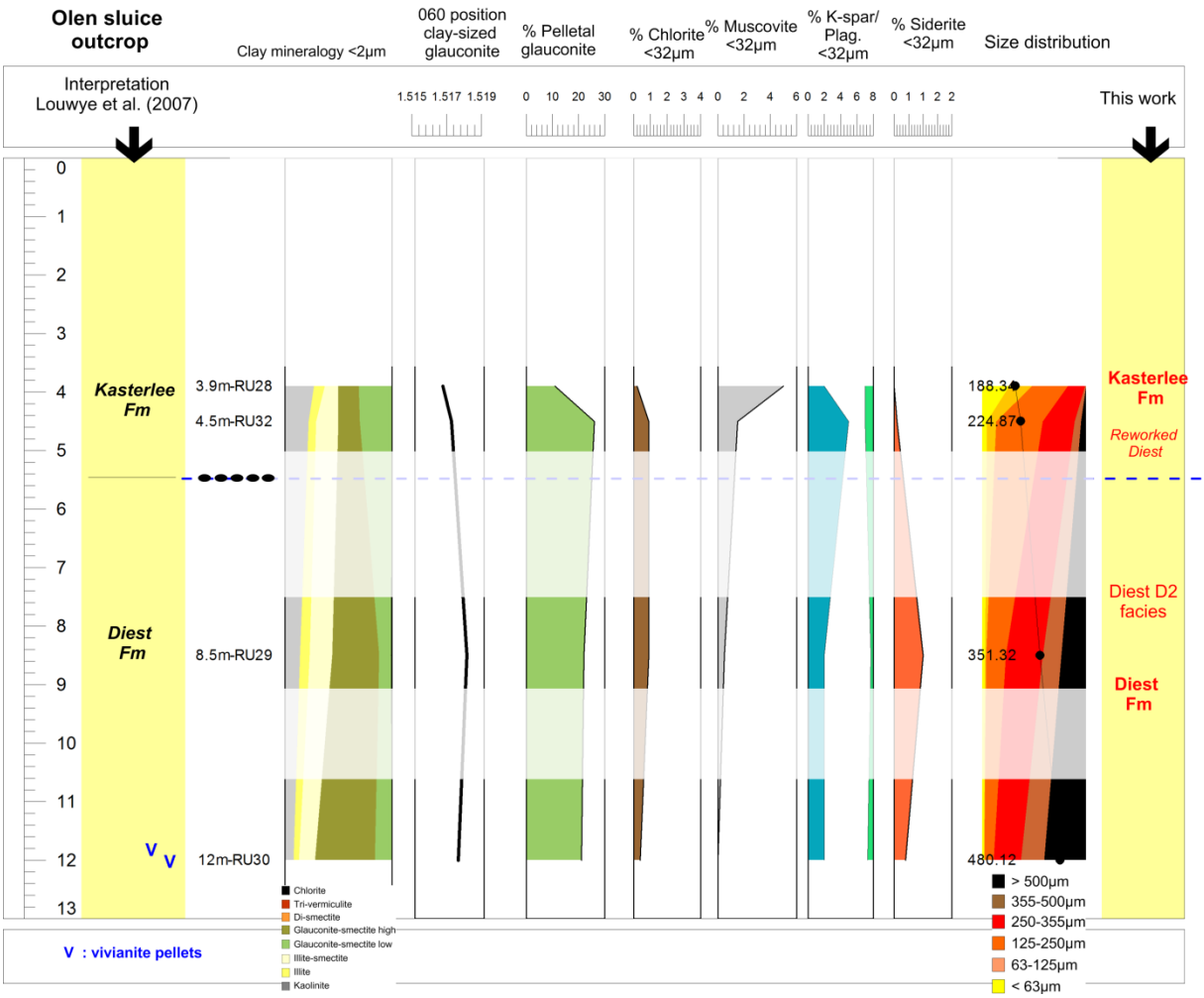

Figure 6.21. Quantitative (clay) mineralogical and sediment petrological data for the Olen sluice outcrop. Samples levels are indicated in the second collumn. In the yellow bar on the left, the stratigraphical interpretation of Louwye et al. (2007) is shown while in the yellow bar on the right, the current interpretation is shown.

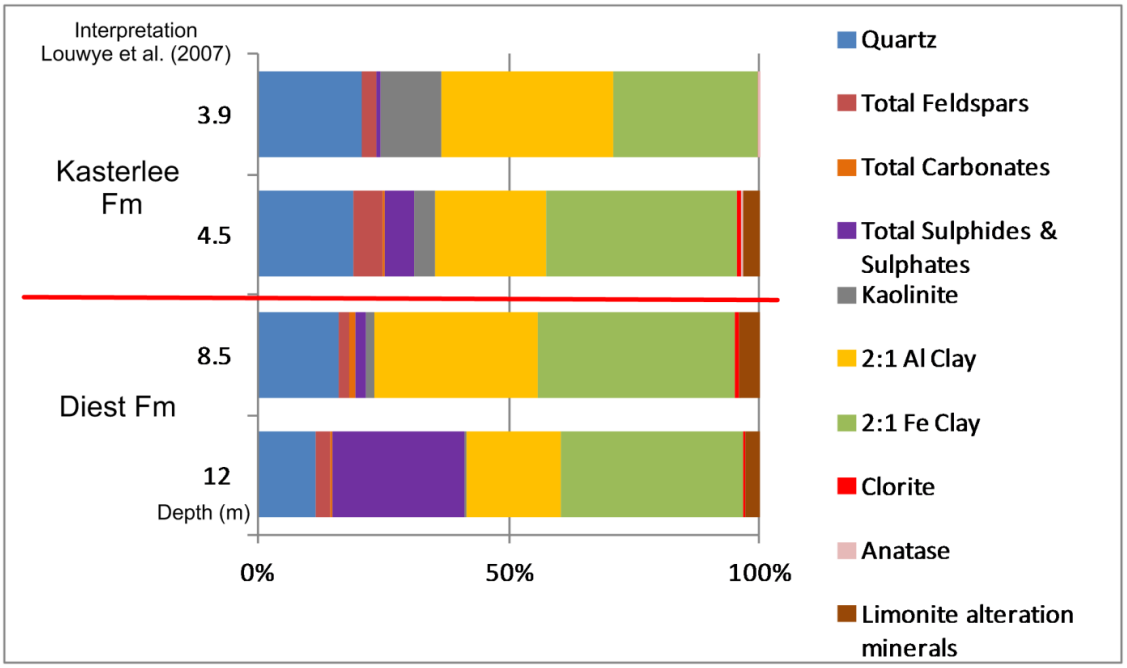

Figure 6.22. Bulk mineralogical composition of the four analyzed samples at the Olen sluice. The gravel layer separating both formations is located at 5.5m.

VI.3.5.2 Clay mineralogy <2µm

The clay composition <2µm of all four samples of the Olen outcrop is dominated by glauconitic minerals (Figure 6.21). Smectite is very scarce and the proportion of illite and illite-smectite mixed-layers remains constant over the entire interval. Kaolinite is scarce in the lower Diest samples but occurs in higher amounts above the gravel layer. The main difference is however the nature of the glauconitic minerals which change from mainly higher expandable glauconite-smectite below the gravel, to mainly low expandable glauconite-smectite above the gravel layer (Figure 6.21). This change is accompanied with a slight d_{060} change of the clay-sized glauconitic minerals from 1.5175 to 1.5166Å. This latter shift is however so small that it might be not significant.

VI.3.5.3 Pelletal glauconite

Glauconite pellets occur through the entire interval. Below the gravel, in the Diest samples, pellet glauconite amounts are 20 and 21%. Just above the gravel, the pelletal glauconite content is 26% but then decreases sharply to 11% at the 3.9m sample (Figure 6.21).

VI.3.5.4 Grain size distribution

The granulometry of the lower Diest samples is the typical coarse-sized distribution with substantial amounts of grains >500µm and distribution modes >300µm. Above the gravel layer however, coarse grains are scarce and the distribution consists of mainly particles occurring in the 125-250µm interval. The distribution mode in 4.5m sample is only 224µm whereas in the uppermost 3.9m sample, it is only 188µm, which is the typical mode value for the Kasterlee Fm (see Dessel-2, Dessel-3 and Retie-1 boreholes) (Figure 6.21).

VI.3.5.5 Stratigraphical boundary

Louwye et al. (2007) correlated the occurrence of the Diest Formation at the Olen outcrop to the Tortonian DN9 biochron. The (clay) mineralogical and petrological characteristics analyzed in this work allow furthermore toidentify this occurrence as the Diest D1 unit. Although pelletal glauconite is slightly less abundant than expected for the Diest D1 facies, the glauconite-dominated mineralogy and clay mineralogy, the very coarse size distribution of the two investigated Diest samples clearly links this Diest occurrence to the Diest D1 facies.

The presence of a basal gravel in the Olen sluice outcrop marks the Diest-Kasterlee boundary. The most important change at this boundary is the grain-size difference. Additionally, other differences also occur but are less outspoken, such as kaolinite content, muscovite and siderite content, pelletal glauconite content and the change of clay-sized glauconite mineralogy.

The pelletal glauconite contents of the 4.5m level (26%) and the 3.9m level (11%) suggest that the two analyzed samples of the Kasterlee Formation are part of a reworked Diest interval at the base of the Kasterlee Fm in which properties gradually evolve from coarse-sized, pelletal glauconite-rich and kaolinite-poor Diest D1 sand towards a finer-sized Kasterlee sand with slightly more kaolinite, more muscovite and less pelletal glauconite (Figure 6.21). Louwye et al.,(2007) concluded for the Kasterlee an important shoaling of the environment compared to the underlying Diest Fm in samples of the Olen outcrop. The dinoflagellate cysts assemblage of the Diest-Kasterlee transition in Olen was furthermore correlated with the Diest-Kasterlee transition in the Dessel-2 borehole (see section VI.3.2).

VI.3.6 The Heist-op-den-Berg outcrop

The stratigraphic succession outcropping on the Heist-op-den-Berg and Beerzelberg hills (Figure 6.3) consists of coarse Diest sands covered by finer-grained Kasterlee sands (Verhaegen et al., 2014) Fobe (1995) proposed a threefold division based on sedimentological characteristics.
The lowermost unit, the Hallaar member, represents a phase of intense reworking of the Diest Fm, which Fobe (1995) supposed stood already in relief. This reworking is explained as erosion by a river system flowing through the Hageland hills formed in Diest sand. The second unit is the Beerzel member, a quartz-rich unit with much less pelletal glauconite compared to the Hallaar member. The deposition of the Beerzel member occurred in a bay after sea level rise invaded the river system. The top unit is the Heist-op-den-Berg member, which contains even less pelletal glauconite (Fobe, 1995) and in which clay intercalations are common. The frequent occurrence of clay intercalations was interpreted as deposition in a restricted environment which was partially disconnected from the marine area (Fobe, 1995). Verhaegen et al., (2014) reported pebbles at the base of the Hallaar member with identical characteristics to the gravel layer at the Diest-Kasterlee boundary in the Olen outcrop. In total 4 sand samples, one of each unit defined by Fobe (1995) (Figure 6.23), were analyzed for mineralogy and clay mineralogy.

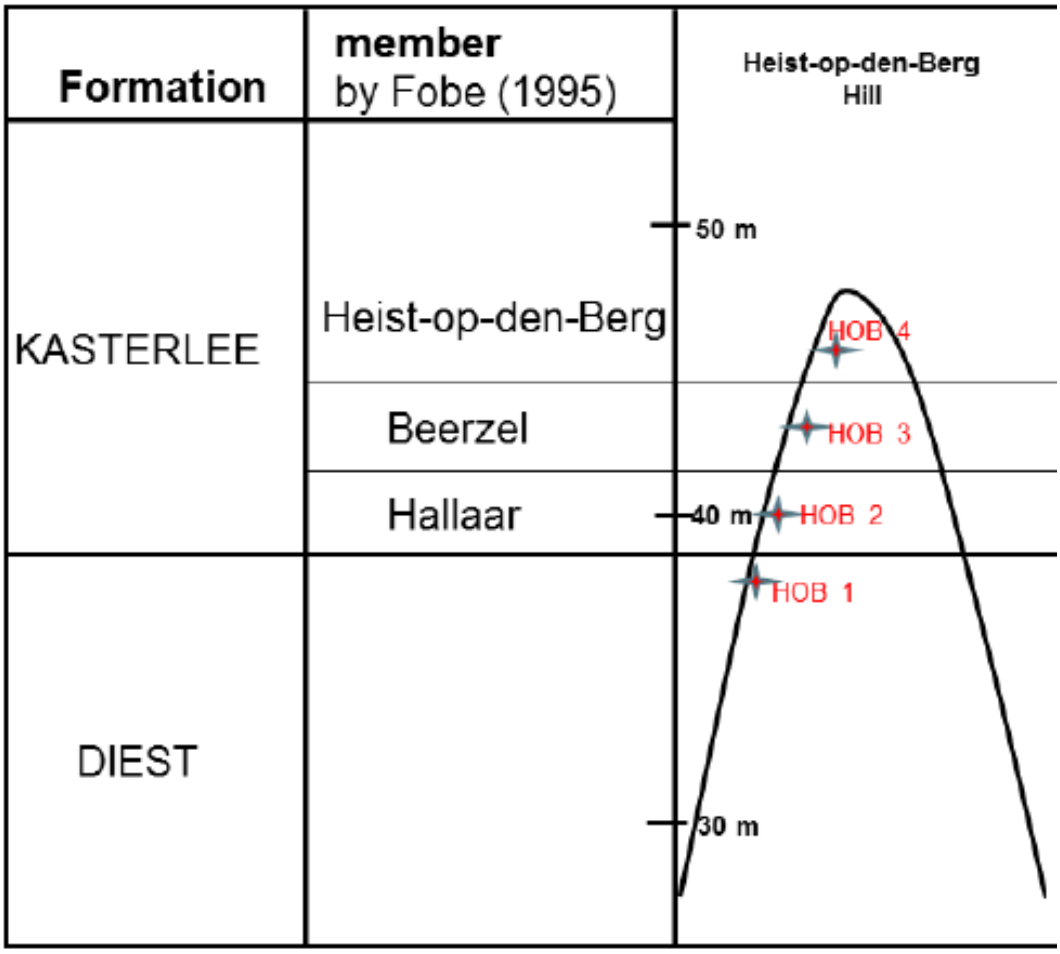

Figure 6.23. Schematic sketch of the sample positioning on the Heist-op-den-Berg hill (after Verhaegen et al., 2014).

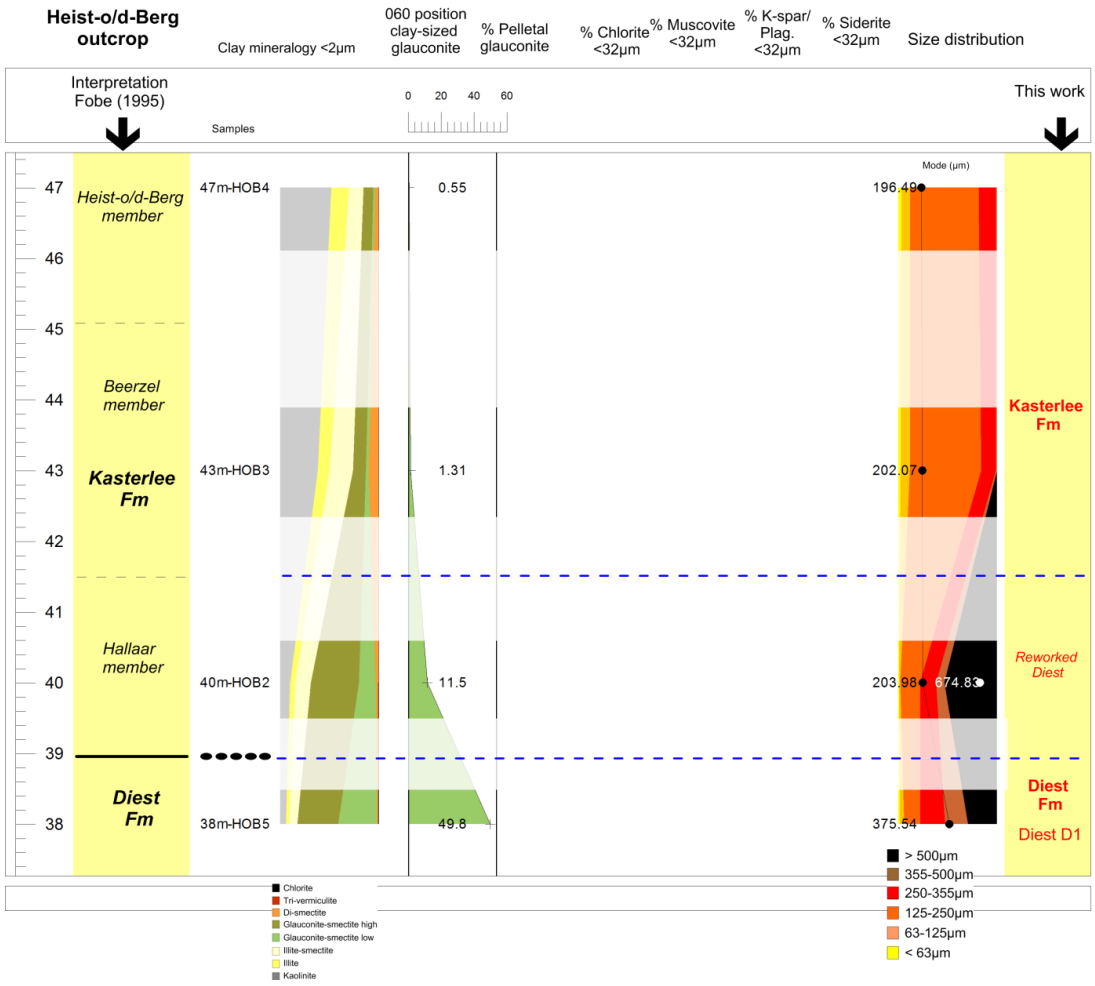

Figure 6.24. Quantitative (clay) mineralogical and sediment petrological data for the Heist-op-den-Berg outcrop. Samples levels are indicated in the second column. In the yellow bar on the left, the stratigraphical interpretation of Fobe(1995) is shown while in the yellow bar on the right, the current interpretation is shown.

VI.3.6.1 Clay mineralogy <2µm

The clay mineral composition <2µm of the lower Diest Fm sample is dominated by glauconite-smectite, ca. 80%. Above the pebble layer, the composition of the Hallaar member sample is very similar although the amount of glauconite-smectite is somewhat lower, 65%. In the two uppermost samples however, the amount of glauconite-smectite is much lower, <15%, whereas kaolinite contents have increased to 38% in the Beerzel member sample and 51.5% in the Heist-op-den-Berg member sample (Figure 6.24).

VI.3.6.3 Pelletal glauconite

Pelletal glauconite is the most abundant in the lower Diest Fm sample (49.6%). In the Hallaar member sample, the content has decreased to 11%. In the two uppermost members, pelletal glauconite is scarce, <2% (Figure 6.24).

VI.3.6.4 Size distribution

The grain-size distribution of the Diest Fm sample is coarse and poorly sorted with 375µm as the distribution mode value (Figure 6.24). The Hallaar member sample is equally coarse but its distribution is bimodal with modes at 203µm and 674µm. In contrast, the grain-size of the uppermost member is significantly finer and much better sorted with distribution modes around 200µm.

VI.3.6.5 Stratigraphic boundaries

Although a limited amount of samples was studied of the Heist-op-den-Berg outcrop, the sedimentological subdivision proposed by Fobe (1995) seems to be justified by the (clay) mineralogical and grain-size analysis results of this work. Verhaegen et al. (2014) reported a basal gravel in the outcrop which marks the Kasterlee-Diest boundary. Despite the gravel, both (clay) mineralogy and grain-size shows great similarity between the Diest Fm, which is interpreted as the Diest D1 facies, and the lowermost Hallaar member. Such intense reworking of the Diest Fm in the Hallaar member confirms the hypothesis of Fobe (1995) and is also as such interpreted in this work (Figure 6.24). The characteristics of the Beerzel and Heist-op-den-Berg members contrast sharply with that of the Hallaar member (pelletal glauconite content, kaolinite content,…) and are therefore interpreted also part of the Kasterlee Fm but not consisting of reworked Diest Fm material. The high kaolinite and low pelletal glauconite contents in the two uppermost units can be interpreted as increased terrestrial run-off in the restricted bay environment with relatively less input from the marine area.

VI.4 DISCUSSION

VI.4.1 The Kasterlee - Mol boundary

The Kasterlee-Mol transition, studied in the Dessel-2 and Dessel-3 boreholes, is characterized by differences in the nature and amounts of glauconite minerals incorporated in sand- and clay-sized fractions, changes in the amount of kaolinite and, slight changes in the total feldspar and muscovite content. In the lower part of the Mol Formation (Donk Member), glauconite-smectite is a common constituent of the clay fraction <2µm (20-30%) while only traces of pelletal glauconite (<0.001%) occur. At the boundary with the Kasterlee Fm however, the amount of pelletal glauconite increases to 0.5-1% whilst also the amount of clay-sized glauconite sharply increases to 50-60%. Additionally, clay-sized glauconite in the Mol Formation is characterized by lower d_{060} –values and less expandable layers (Figure 6.6 and Figure 6.9).

The Kasterlee-Mol boundary is furthermore reflected in both microscopic and macroscopic characteristics of the sediment. At the base of Mol Donk, around 26.10m in the Dessel-2 borehole, a silty to clayey sand interval is present, containing only low amounts of clay-sized glauconite. In the Dessel-3 borehole, this interval seems restricted to less than 1m, while in the Dessel-2 borehole a thickness of several meters is observed. Both in Dessel-2 and Dessel-3, at the base of this interval intercalated clay laminae sporadically occur. The sediment therefore loses its grey-greenish color for a more distinguished darker grey color, which is even more clear when studying the color of the fines after mixing with water. The intense green color of the sediments below, certainly of the fines, therefore creates a sharp contrast which represents the sharp increase of clay-sized, and sand-sized, glauconitic minerals and the start of the Kasterlee Formation.

Whereas in this work the Kasterlee-Mol boundary is interpreted at the base of the clayey interval around 26m in the Dessel-2 borehole (Figure 6.9), Wouters and Schiltz (2011) systematically interpret the Mol-Kasterlee boundary at the top of this clayey interval, based on gamma-ray, resistivity and cone penetration test data (see Figure 6.1, Figure 6.6 and Figure 6.9). Sibelco SCR interprets the base of the Mol Formation whenever the $\%K_2O$ exceeds 0.3%. In the Dessel-2 borehole, this level coincides with the increase of pelletal and clay-sized minerals but also the increase of muscovite. Gulinck et al. (1964) however interpreted the top of the Kasterlee Formation in the Belchim borehole much higher based on the change in drilling mud color to green (Figure 6.2). The presence of clay-sized glauconite in the fine fraction of the Mol Donk Member most likely moved Gulinck to systematically interpret the Mol Donk Member incorrectly as the top of the Kasterlee Fm.

It is important to note that the interpretation of the Kasterlee-Mol boundary is not solely based on mineralogical and clay mineralogical criteria but is supported by important paleoenvironmental changes taking place at this boundary (Louwye et al., 2007). The clay mineral-based Kasterlee-Mol boundary also

corresponds to a noticeable gamma-ray and resistivity excursion in the Dessel-3 borehole (Figure 6.6).

VI.4.2 The Diest - Kasterlee boundary

In the Dessel-2 reference borehole, geophysical logging data, cone penetration tests (Wouters and Schiltz, 2011) and even dinoflagellate cysts assemblages (Louwye et al., 2007) all allowed to place the Diest-Kasterlee boundary between 34m and 35m. The results presented in this work confirm important changes in this interval and the Diest-Kasterlee boundary was defined between 34.25m and 34.65m. Above 34.25m, grain-size is finer, pelletal glauconite, siderite, muscovite, plagioclase and chlorite contents and clay mineralogy becomes less expandable (Figure 6.9). Whenever the Diest D4 unit forms the top of the Diest Formation, the mineralogy of pelletal and clay-sized glauconite also drastically changes at the boundary (Figure 6.7 and Figure 6.13). If the top Diest is composed of the Diest D1 unit, as in the Retie-1 borehole and the Olen and Heist-op-den-Berg outcrops, this is not the case. Also in all other investigated borehole and outcrop sections, mineralogy, clay mineralogy and sediment petrological data allow to define the Diest-Kasterlee boundary following the above stated criteria. Nevertheless, it was systematically observed that sediment properties typical for the top Diest sediments gradually transition, all together in the same interval, into sediment properties typical for the Kasterlee Formation. In the Dessel-2 borehole, but also in other sections, this transition zone reaches its top when no siderite, plagioclase or chlorite contents are detected, pelletal glauconite contents drop below 5% and the mode of grain-size distribution is lowered to values around 200µm. Furthermore, when the Diest D4 unit forms the top of the Diest Formation, Fe-vermiculite is also found in the transition zone gradually decreasing and also pelletal and clay-sized glauconite expandability decreases significantly above the transition zone (Figure 6.7 and Figure 6.13). Most often, this transition zone is ca. 2m thick indicating a general reworking of Diest material at the start of the Kasterlee deposition.

Berckmans and Wouters(2003) and Wouters and Schiltz(2011) proposed a twofold subdivision of the Kasterlee Formation, the Kasterlee sand above, and the Kasterlee clay below, based on geophysical well log data . The “reworked Diest” transition zone at the base of the Kasterlee most likely represents a third unit at the base of the formation. It has to be noted that the significant difference of the top Diest sediments (ca.15m) in Dessel and Retie, which are only a few km apart, is difficult to explain and remains an open question which should be addressed in further research.

The Diest-Kasterlee boundary interpretation as defined by the (clay) mineralogical criteria given above is also an important paleoenvironmental boundary (Louwye et al., 2007) which strongly enhances the reliability of the interpretation. The defined Diest-Kasterlee boundary also corresponds to significant gamma-ray and resistivity excursions, although the strongest gamma-ray and resistivity peaks seem to be located at the top of the reworked transition zone (Figure 6.6 and Figure 6.9).

VI.4.3 Implication of the reworked Diest transition zone

A ca. 2m-thick Diest-Kasterlee transition zone was identified at the base of the Kasterlee Formation in all investigated borehole and outcrop sections. This transition zone was termed the Hallaar member in the Heist-op-den-Berg outcrop by Fobe (1995) who stated that the Diest Formation already stood in relief before deposition of the Kasterlee. This argument was acknowledged by Verhaegen et al., (2014) based on weathered and rounded iron crusts indicating that iron crustation already took place before deposition of the Kasterlee Formation. Furthermore, the occurrence of the Kasterlee Fm in Heist-op-den-Berg indicates considerable thinning of the Diest Formation to the south and implies ongoing subsidence of the Campine Basin and uplift of the Caledonian Brabant Massif during the Late Miocene and Pliocene (Verhaegen et al., 2014) (Figure 6.25). This emersion of the Diets Fm would also explain the relatively high amount of reworking at the base of the Kasterlee Fm and low amount of in-situ dinoflagellates counted at the Diest-Kasterlee boundary (Louwye et al., 2007).

Fobe (1995) suggested that a river system eroded the southern emerging Diest deposits which were transported into a bay environment in Heist-op-den-Berg (see Figure 6.3). The widespread lateral distribution of the transition

zone indicates that sediments are possibly redistributed over the entire Campine area.

In the Rees borehole, the typical Kasterlee sediment, not reworked and occurring above the transition zone in the Dessel area, is completely absent. Instead, the mineralogical characteristics of the underlying Diest D4 unit are integrally taken over in the 7-8m-thick finer-grained sediment lying above. Louwye and De Schepper (2010) have shown that the Kasterlee Fm occurrence northwards from Dessel represents a deeper water facies, which probably explains the absence of the typical Kasterlee sediment in Rees. Because the mineralogical characteristics of this 7-8m interval are identical to the 2m-thick encountered reworked Diest sediment in the Dessel area, the entire "Kasterlee" interval is interpreted as reworked Diest sediment (Figure 6.18). The lateral distribution of this thick interval is unknown and its significance, and the absence of the other Kasterlee units, is not yet fully understood and need further research.

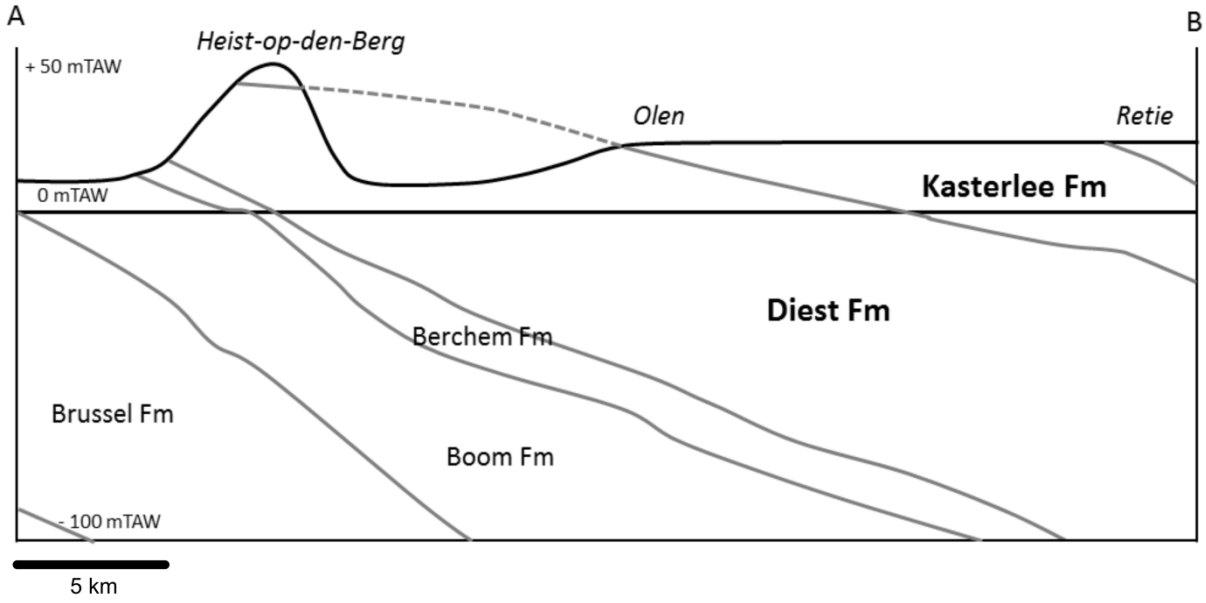

Figure 6.25:SW-NE profile from Heist-op-den-Berg to Retie, showing the curved base of the Kasterlee Formation (modified after Verhaegen et al., 2014).

VI.4.3 Clay and glauconite mineralogy of the Mol Formation

As demonstrated in the Dessel-3 (Figure 6.6) and Dessel-2 boreholes (Figure 6.9), the clay mineralogical assemblage of the Mol Formation is dominated by kaolinite minerals whereas smectite minerals are absent. Such a specific clay composition was also encountered in other estuarine and continental deposits in the Campine Basin, such as in the Opgrimbie sand of the Bolderberg Formation (Figure 26). As already indicated, Hermanns (1992) identified kaolinite-illite clay assemblages in Lower Miocene deposits of the Lower Rhine Basin suggesting that these kaolinite – illite clays are eroded from the source areas of the Rhine Basin, such as the Ardennes, and are transported with the prograding Rhine delta in estuarine deposits into the Campine Basin. The clay mineralogy of the Mol Formation reported in the current work therefore indicates that also during the Pliocene this kaolinite-illite assemblage was still the major clay composition delivered from the graben area. In contrast with the Opgrimbie facies sand samples, in all analyzed samples of the Mol Formation clay-sized glauconitic minerals are present. As earlier demonstrated, clay-sized glauconitic minerals result from pelletal glauconite abrasion and disintegration. Because of the absence of pelletal glauconite however, such an origin is incompatible for the estuarine Mol Formation. The clay-sized glauconite minerals of the Mol Formation must therefore have been reworked from slightly older, laterally or possibly also underlying, deposits such as the Kasterlee Formation. When the expandability of clay-sized glauconite in the Mol Formation is compared

with that of the Kasterlee deposits (for instance in the Dessel-2 borehole Figure 6.13), it can be observed that this expandability gradually decreases in the Kasterlee Formation and at the top, in the sandy Kasterlee unit, is almost equal to the Mol clay-sized glauconite expandability. It has to be noted however that the d_{060} is slightly lower in the Mol Fm (Figure 6.6 and Figure 6.9), which suggests that Fe is lost from the clay mineral structure during transport.

It has to be noted that Louwye et al. (2007) reported marine in-situ dinoflagellate cysts in the 26m to 19m interval of Dessel-2 borehole, which in this work was identified part of the estuarine Mol Formation. Most likely, this paradox exists because the basal part of the Mol Formation was deposited under marine-dominated estuarine, or even very shallow marine conditions. After the deposition of this basal part, fully estuarine to continental conditions prevail as evidenced by the sterile nature of the Dessel-2 samples above 19m (Louwye et al., 2007).

VI.4.4 Clay and glauconite mineralogy of the Kasterlee Formation

The clay mineralogy of the Kasterlee Formation in the Dessel-2, Dessel-3 and Retie-1 boreholes, above the reworked Diest interval, is mainly rich in glauconitic minerals. This indicates that pelletal glauconite disintegration was a relative important process for the clay contribution in this stratigraphic interval. Louwye et al. (2007) have stated that the Kasterlee Formation was deposited in very shallow marine conditions and, with clear influences of the land. The higher energy depositional environment often associated with very shallow marine conditions yields transport, and most likely also local reworking, of pelletal glauconite which in turn yields the production of clay-sized glauconite. The green silt levels identified in the Dessel-2 borehole could represent an important pelletal glauconite abrasion and/or disintegration event preserved in a condensed level. Nevertheless, such green silt levels might also be related to destructive actions during the drilling operation.

The clay mineralogical composition of the Kasterlee Formation seems a transitional composition between the Diest and Mol Formations. Whereas the top of the Diest Fm is characterized by substantial amounts of expandable minerals (in the case of the Diest D4 unit), high pelletal glauconite content and very low kaolinite contents, the Mol Formation contains no pelletal glauconite, has no, or only traces, of expandable minerals but very high kaolinite contents. The composition of the Kasterlee Formation lies in-between, with low pelletal glauconite, low amounts of expandable minerals and elevated kaolinite amounts, but less than the Mol Formation (Figure 6.6 and Figure 6.9). This mineralogical composition correlates with the sedimentological nature of the different formations. The fully marine clay mineralogical assemblage is reflected in the Diest Formation, whereas the composition encountered in the Mol Formation represents the sediment composition eroded from the continent. The Kasterlee Formation was deposited in somewhat more shallow conditions compared to the Diest Formation, with influences from the continent (Louwye et al., 2007) and therefore contains intermediate characteristics.

VI.6 CONCLUSIONS

In general terms, lithostratigraphy attempts to subdivide geological layers into different units, each with its specific characteristics which can be recognized and correlated in different locations. For each unit, a stratotype section is defined which acts a reference section for a particular unit. The most direct method is to only use the macroscopic visible lithology for this purpose as lithological characteristics are in general easily recognized. Also macroscopic fossils are commonly used as correlation tools because it combines geometrical correlation with a certain time estimation. Most often, such an approach yields the recognition of bulk litho-units, as is the case of the Mol, Kasterlee and Diest units which can be straight-forwardly discriminated based on their defined stratotypes (website National Stratigraphic Commission Belgium, www.natstratcommbelgium.drupalgardens.com , last consulted January 2015)

However, the lithostratigraphic differentiation between the Diest-Kasterlee-Mol Formations towards boundaries has proven to be a complex exercise in the past (see Berckmans and Wouters, 2003). The typical stratotype characteristics change towards formation boundaries and defining the exact boundary is difficult. Lithology and color differences was the main tool in the 1960's (Gulinck, archives GSB) often leading to inconsistent interpretations. At the Belchim borehole, Gulinck et al.(1964) even misinterpreted Mol and Kasterlee bulk units pointing to the complexity of the problem using only basic research techniques (see Figure 6.2). The use of geophysical well logging tools improved the way of working but it was only when geophysical logging measurements were combined with lithology and cone penetration tests that an important step forward could be made from assigning bulk units to the traditional Mol, Kasterlee and Diest stratotypes with only a rough estimation of position of the boundary to defining subunits within the bulk units and choosing the appropriate log signal to interpret a formation boundary more accurately (Wouters and Schiltz, 2011).

It was demonstrated in this work that quantitative (clay) mineralogy and sediment petrological data can be used to characterize the bulk units and allow for a relatively precise determination of formation boundaries. The results presented in this work furthermore show that mineralogy and clay mineralogy allow for robust correlations between sections and boreholes, whereas other criteria have failed to define unequivocal boundaries between units. Although sampling density of the investigated sections was not always optimal, stratigraphic boundaries could be systematically placed at a level characterized by a crucial change in certain mineralogical parameters.

The top of the Kasterlee Formation (Kasterlee-Mol boundary) is set at the level downwards from the Mol unit characterized by a sharp increase of clay-sized glauconite (60-70% compared to less than 30% above) and pelletal glauconite content, a slight decrease in kaolinite content whereas the muscovite content increases. The boundary is also well reflected in the mineralogical specifications of the clay-sized glauconite with a sharp increase of the d060 value (from 1.513Å to <1.515Å) and an increase in expandable layers. It is possible that not all parameters individually are discriminating (compare muscovite change in Dessel-2 and Dessel-3 boreholes Figure 6.6 and Figure 6.9). The Kasterlee-Mol boundary is consequently placed below a grey silty to clayey interval, characterized by low amounts of clay-sized glauconite, which was identified in both the Dessel-2 and Dessel-3 boreholes and of which the top is interpreted as the Kasterlee-Mol boundary based on gamma-ray and resistivity measurements by Wouters and Schiltz (2011).

The Diest-Kasterlee transition is characterized by a decrease of kaolinite and muscovite, an increase of siderite, chlorite and plagioclase and pelletal glauconite content whereas grain-size becomes coarse and poorly-sorted. If the Diest D4 unit forms the top of the Diest Fm, the boundary is also characterized by a sharp increase of Fe-vermiculite and expandability in both clay-sized and pelletal glauconite. Although at the boundary itself many parameters change sharply, a transition zone was systematically identified at the base of the Kasterlee Formation. In this transition zone, mostly 2m-thick, sediment properties typical for the top Diest Formation simultaneously and gradually fade out towards the top of the transition zone. This interval therefore represents intensive reworking of the Diest Formation and is defined as third subunit of the Kasterlee Formation, besides the sandy top and clayey middle part (Berckmans and Wouters, 2003; Wouters and Schiltz, 2011). In the Rees borehole, only the transitional reworked Diest unit is the only unit identified in the Kasterlee Formation and is up to 8m thickness. The sandy and clayey Kasterlee units are completely absent in this borehole.

The boundary Diest-Kasterlee is systematically set at the bottom of the transition zone, i.e. whenever sharp changes occur or a constant value is reached (see for instance pelletal glauconite, chlorite, muscovite and siderite in Dessel-2 borehole Figure 6.9). Above the interval, there is no influence of typical Diest sediment properties on the mineralogy.

It must again be emphasized that the clay mineralogical boundaries defined in this work also have an important paleoenvironmental significance and that they can be correlated with gamma-ray and resistivity events.

CHAPTER VII

THE PLIOCENE POEDERLEE FORMATION

VII.1 PALEOGEOGRAPHY AND STRATIGRAPHY

Pliocene deposits are preserved only in the very north of Belgium reflecting continued global sea-level lowering (Vandenberghe et al., 2004). After a period of non-deposition, very shallow deposits in the Campine Basin rest unconformably on the Miocene glauconitic sands. In the eastern part of the Campine Basin, the influence of the westwards prograding Rhine delta system increases with the deposition of the estuarine quartz sand of the Mol Formation which contains two lignite layers. On top of the Kasterlee Formation in the area of Poederlee-Lichtaart and Herentals, a fine glauconitic sand unit occurs, the Poederlee Formation (De Meuter and Laga, 1976; Louwye and De Schepper, 2010) (Figure 7.1).

The Poederlee Formation was described by Gullentops (1963) and later by De Meuter and Laga (1976) as a fine glauconitic sand with rather heterogeneous characteristics. The base of the formation is marked by the presence of a basal gravel (the Hukkelberg gravel) and small lenses of clay occur in the lower part. The upper part is however strongly oxidized, sometimes containing limonitic sandstones with moulds of shells (De Meuter and Laga, 1976). At the top of the formation, the Heieinde facies was defined by Buffel et al., (2001), which is a very well-sorted and fine-grained sand unit. The formation reaches a maximum thickness of 10 m (Schiltz et al., 1993).

Although the sediments of the Poederlee Fm are largely decalcified, a Piacenzian age was proposed by Buffel et al. (2001) based on the correlation of mollusk shells of the Poederlee Fm with members of the Lillo Formation occurring more to the west. The age of the Poederlee Fm was further constrained by Louwye and De Schepper (2010) between 3.21 and 2.76 Ma (Piacenzian), based on dinoflagellate cyst assemblages and sequence stratigraphy.

Although the base of the Poederlee Formation is often clearly marked by the Hukkelberg gravel, the reported lithological heterogeneity of the formation causes confusion in many borehole descriptions. The comparable size distribution and similar macroscopic outlook makes the distinction between the Poederlee and Kasterlee Formations not straight-forward. Therefore, reference sections of the different parts of the Poederlee Fm were analyzed for mineralogy and clay mineralogy, and their relation with the mineralogical and sediment petrological characteristics of the Kasterlee Fm found in the previous chapter, discussed.

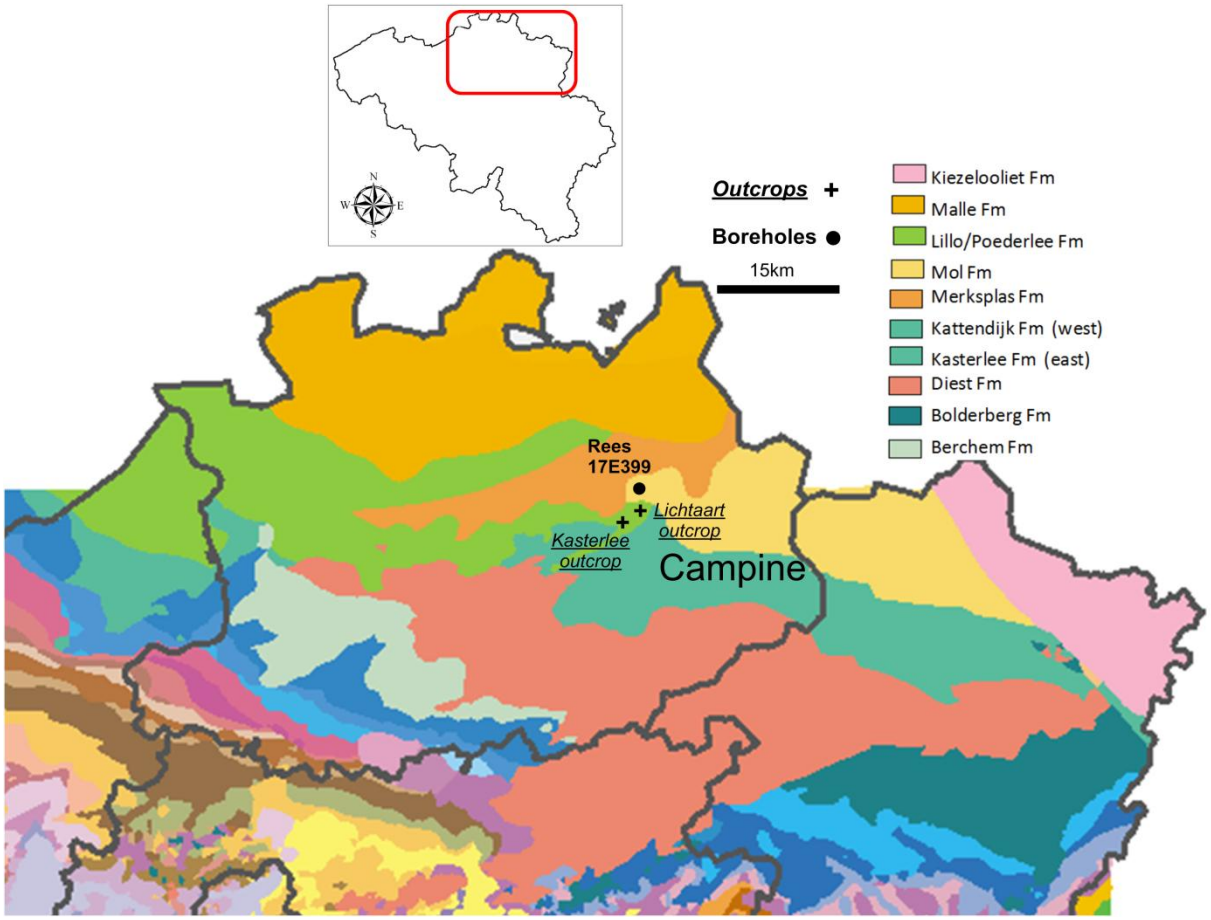

Figure 7.1. Tertiary geological map of the Campine Basin in Belgium showing the three loctaions, one borehole and two outcrops at the Poederlee Formation was sampled. Geological map modified after ALBON (2009).

VII.2 SAMPLES

Sediments of the Poederlee Formation were sampled at 3 locations. In Lichtaart, the Kasterlee-Poederlee transition was refreshed in a temporary outcrop at a former excavation where the Hukkelberg gravel was described exposing the Kasterlee – Poederlee transition (Geets, 1962). A second sampling was performed from discontinuous outcropping Kasterlee and Poederlee sediments during major incised road construction works in Kasterlee. In this section, also the Hukkelberg gravel was exposed. The oxidized stony upper part of the Poederlee Formation was sampled in the Rees borehole. All samples were analyzed for bulk and clay mineralogical composition. The grain-size distribution was only analyzed for samples of the Rees borehole.

VII.3 RESULTS

VII.3.1 The Lichtaart outcrop

In the vicinity of the village of Kasterlee, the Poederlee Formation crops out. Near Lichtaart, a temporary outcrop was dug out, exposing approximately 2m of the basal Poederlee Fm which covers 1m of the underlying Kasterlee Fm. The boundary between both formations is clearly marked by the presence of milky, flat and rounded quartz pebbles, the Hukkelberg gravel. Just above this gravel layer, a 20cm-thick purple clay layer is observed. The sand section above consists of a pale green to green-brown and fine-grained sand which is slightly glauconitic and altered by intense limonitization. The sand of the Kasterlee Formation below the Hukkelberg gravel is equally fine-grained and glauconitic but is somewhat more green-grey colored compared to the brown-green color of the Poederlee sands above. Although the outcrop was freshly dug out, this lower sediment was also altered by limonitization. One sample of the upper Poederlee sand was collected, together with five clay laminae samples. Two additional samples of the underlying Kasterlee sand were collected (Figure 7.2).

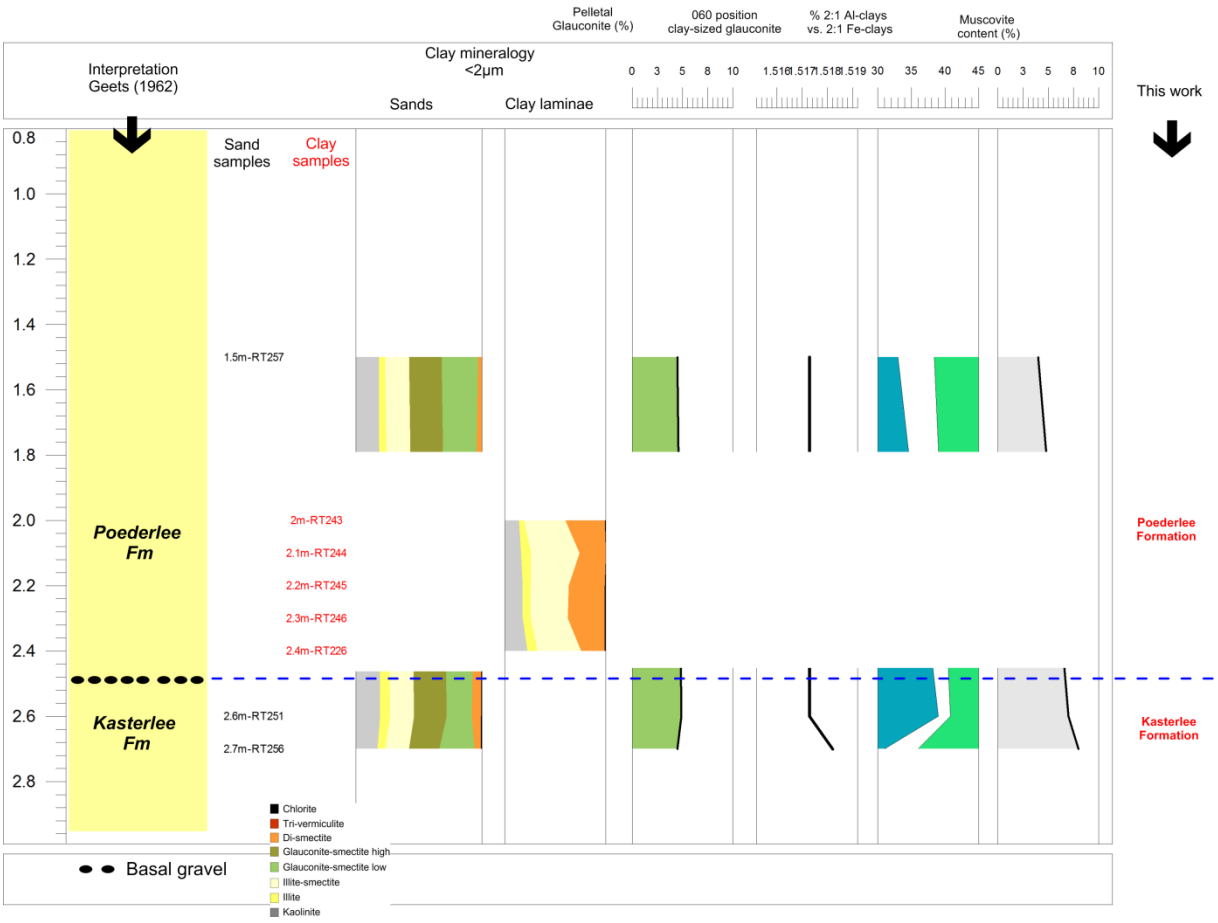

Figure 7.2. Quantitative (clay) mineralogical and sediment petrological data for the Lichtaart outcrop. Samples levels are indicated in the second column.

VII.3.1.1 Bulk mineralogy

The mineralogical composition of the sand sample of the Poederlee Fm and the two Kasterlee sand samples are very similar. The groups 2:1 Al-clays and Fe-clays are present in amounts from 25% to 35%, with also kaolinite amounts >10%. Muscovite seems to be slightly more abundant in the two Kasterlee samples (9% and 10%) compared with the Poederlee sand sample (4%).Carbonates are absent in all samples and only K-feldspars occur, no plagioclase. The bulk mineralogical composition of the clay laminae samples just above the Hukkelberg gravel was not analyzed.

VII.3.1.2 Clay mineralogy <2µm

Similar to the bulk mineralogical results, clay mineralogy <2µm of the Poederlee and Kasterlee sand can barely or not differentiated from one another. Glauconite-smectite is the dominant clay phase occurring in amounts of 45-55% with higher and low expandable glauconite-smectite evenly proportioned. Smectite amounts are lower than 10%. The d_{060} of clay-sized glauconite remains relatively stable in the three samples with a limited range between 1.517Å and 1.518Å. In contrast, the clay mineralogy <2µm of the clay laminae samples consists of high proportions of illite-smectite (>30%) and smectite minerals (>23%). Kaolinite contents range between 14% and 22% whereas illite is the least abundant phase (<10%). Glauconite-smectite is absent in all examined clay laminae samples.

VII.3.1.3 Pelletal glauconite

The pelletal glauconite content of the Poederlee sand sample is 4.5%. The content of the samples of the Kasterlee sand is 4.9% and 5%. Whereas pelletal glauconite of the Kasterlee Formation has a bright green color, Poederlee pelletal glauconite contains green and brown glauconite pellets. However, this might be a post-depositional effect considering the Poederlee sediments occur closer to the top of the outcrop and therefore were subjected to more intense oxidation.

VII.3.1.4 Interpretation

Although only a few samples were investigated, almost no differences were found between the Kasterlee and Poederlee sands. It is suspected that, because the Poederlee samples were collected less than 1m above the basal gravel, the Poederlee sand sample contains reworked Kasterlee material. Clay-sized glauconite in the Poederlee Formation only occurs in the clay fraction <2µm of sand samples and is systematically absent in clay laminae samples. This observation was already made in Miocene deposits (see Chapters IV,V and VI) and seems to remain constant in the Pliocene of the Campine basin, which indicates an identical mechanism for production, i.e. the abrasion and/or disintegration of pelletal glauconite during transport.

VII.3.2 The Kasterlee outcrop

A temporary lateral road section was exposed in Kasterlee during construction works in 2012. The Hukkelberg gravel was recognized by the typical white, flat and well-rounded quartz pebbles. Nevertheless, also blue silex pebbles and white powdery pebbles of ca. 1mm large were observed in the Hukkelberg level. The gravel layer is discontinuous and also the thickness varies from a few centimeters to 10 centimeters. Just above the gravel layer, a more clay-rich sedimentation is present which is associated with limonitization. Above the Hukkelberg gravel, the Poederlee Formation consists of a brownish fine-grained slightly glauconitic sand which are regularly intercalated with bioturbated clay laminae. The sand itself is finely laminated and also commonly bioturbated. The sand below the Hukkelberg gravel belongs to the Kasterlee Formation, which is not characterized by a macroscopic lamination but is equally fine-grained and slightly glauconitic as the Poederlee sand. Whereas the dominant color of the Poederlee sediment is brown, the Kasterlee sediment is green colored. In total, 17 sand samples and 4 clay laminae samples were investigated for bulk and clay mineralogical composition (Figure 7.3).

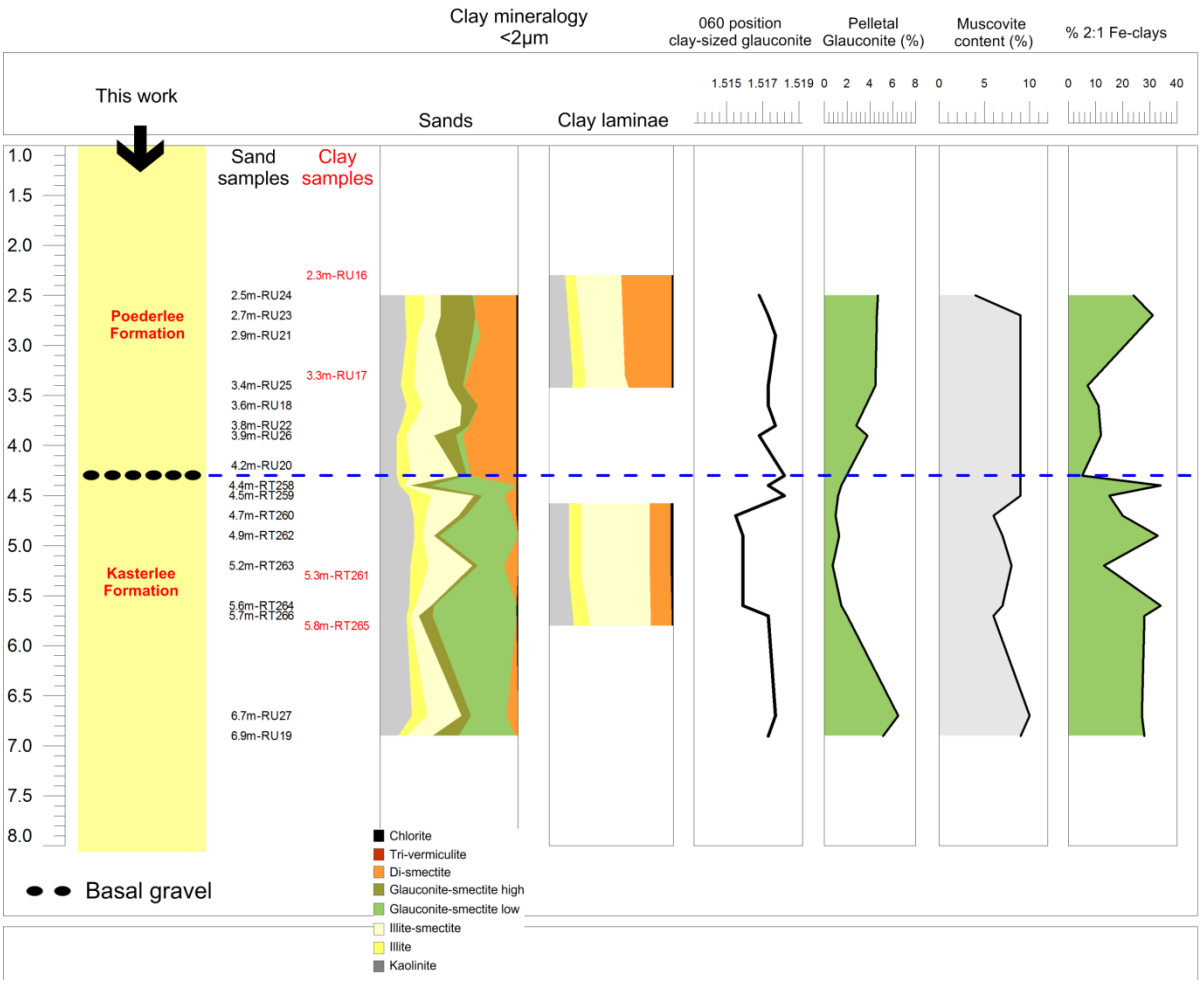

Figure 7.3. Quantitative (clay) mineralogical and sediment petrological data for the Kasterlee outcrop. Samples levels are indicated in the second column. The distinction Kasterlee-Poederlee can be made based on the amount of smectite minerals in sand and clay laminae samples.

VII.3.2.1 Bulk mineralogy

The mineralogy of the sands above the Hukkelberg gravel (Poederlee Fm) consist of mainly quartz and 2:1 Al-clays. Glauconitic minerals (2:1 Fe-clays) are less abundant (<12%) in the basal 1.5m but their amount increases in the two uppermost samples (>20%). Clay samples contain no glauconitic minerals. Below the Hukkelberg gravel, the proportion of glauconitic minerals increases sharply (>30%) with also the amount of 2:1 Al-clays systematically higher than 25%. In several samples, traces of jarosite have been identified. The bulk composition of the clay laminae was not analyzed.

VII.3.2.2 Clay mineralogy <2µm

The clay mineralogy <2µm allows a clear distinction, in sands and clays, between the upper Kasterlee and the lower Poederlee Formation. The clay fraction <2µm of Poederlee sand samples typically are enriched in smectite (25-39%) and have relatively low amounts of glauconite-smectite, <20% in the 3.4m-4m interval. The amount of the latter increases nevertheless in the upper 1.5m to 40%. Typically, higher expandable glauconite-smectite predominates the low expandable glauconite-smectite.

In contrast, Kasterlee sand samples contain less than 10% smectite. In fact, most samples contain less than 5%, and values ranging between 5% and 10% are the clay-rich sand samples which also hold relatively lower amounts of glauconite-smectite. Sand samples

without disperse grey clay, are enriched in glauconite-smectite (>60%). Furthermore, the nature of the glauconite-smectite in these samples is dominantly low expandable which is in strong contrast with the Poederlee sand covering the Kasterlee sand.

Similarly to sands, clay samples of the Poederlee Formation are rich in smectite (38-41%) and illite-smectite (>30%) but in clay samples of the Kasterlee Formation, the smectite content is drastically lower <20% and illite-smectite contents are higher (49-55%).

VII.3.2.3 Pelletal glauconite

Glauconite pellet contents in the Kasterlee outcrop samples are variable. At the bottom part of the sampled outcrop, values of 4-6% are analyzed but this value drops to 1% and lower in the upper part of the formation and close to the Hukkelberg gravel. Pelletal glauconite content in the Poederlee sand samples ranges between 2.8 and 4.7%, with samples closer to the Hukkelberg gravel typically holding less pelletal glauconite.

The pelletal glauconite mineralogy consists entirely of glauconite-smectite with Kasterlee pelletal glauconite characterized by <10% expandable layers in contrast with >11% expandable layers in the Poederlee pelletal glauconite.

VII.3.2.4 Interpretation

In contrast to the Lichtaart outcrop (Figure 7.2), sediment mineralogical and clay mineralogical composition changes considerably at the Hukkelberg gravel level. The clay mineralogy <2µm is more smectite-rich in Poederlee (>25%) compared to the Kasterlee sands (<10%) whereas clay-sized glauconite is much more abundant in the Kasterlee sands. A similar difference in smectite content is also found in clay laminae samples. Clay-sized glauconite is furthermore abundant and less expandable in the Kasterlee Formation whereas the Poederlee sands contain less than 10% clay-sized glauconite-smectite which is relatively more expandable (Figure 7.3). The Kasterlee Fm occurrence in the Kasterlee outcrop is very similar to that found in the Lichtaart outcrop.

Table 7.1. Mineralogical specifications of pelletal glauconite of the Kasterlee and Poederlee Formations in the Kasterlee outcrop. The total amount of expandable layers of pelletal glauconite is compared to that of clay-sized glauconite.

					Pelletal glauconite		Clay-sized glauconite
Sample	Depth	Formation	Content (%)	d060	Total amount Glauconite layers	Total amount Expandable layers	Total amount Expandable layers
RU23	2.7	Poederlee	4.6	1.518	87	13	27
RU21	2.9	Poederlee	2.5	1.5189	88	12	23
RU22	3.8	Poederlee	2.8	1.518	88	12	24
RU20	4.2	Poederlee	3.1	1.518	89	11	20
RT266	5.7	Kasterlee	2	1.5177	92	8	9
RU27	6.7	Kasterlee	6.5	1.5166	92	8	10
RU19	6.9	Kasterlee	5.2	1.5166	91	9	12

VII.3.3 The Rees borehole (Figure 7.5)

In the Rees 17E399 borehole, a vertical succession of Miocene Diest Fm to Quaternary sediments were sampled, of which the Diest and Kasterlee Formations were already discussed in chapters V and VI. The original stratigraphic interpretations was performed by Buffel et al. (2001) based on grain-size and geometrical correlation. The top of the Kasterlee Formation is marked by a gravel layer at ca. 25.5m covered by shell debris which introduces a new sedimentary sequence: the Poederlee Formation. The nature of the Poederlee sediment is however very different from the Lichtaart and Kasterlee outcrops. The basal 24-25.5m consists of a dark grey clayey sand enriched in shell debris. In the 20.5m-24m interval, the sand sediment shows a rusty coloration with intense limonitization and often lithification to Fe-sandstones is observed. Locally, bioturbated sandstones seem to be mineralized (Figure 7.4). In the 17.5-20m interval, the Heieinde facies has been interpreted by Buffel et al. (2001) which is a grey fine-grained and very well-sorted sand facies. At a depth of ca. 17m, the fine-grained sand transitions in a coarser-sized sand: the Rees facies of the Mol Formation. The lower 3m of this unit consists of brown colored sand which transitions into beige and white sand upwards. The upper 8m of the borehole are made up by Quaternary deposits. Below 2m of soil, the Vosselaar unit was interpreted by Buffel et al. (2001), which is part of the Quaternary Malle Formation but is incorporated in the Merksplas Formation where both the Malle and Merksplas Formations are present (National Stratigraphic Commission Belgium website). The entire vertical succession of the Rees borehole was sampled with a relatively high sampling density (Figure 7.5). Only sand samples were collected, because of the absence of well-developed clay intercalations. From the sand samples of the Heieinde facies, the Mol Formation and the Malle Formation, only limited amounts of material were available for analyses. It was chosen to use the limited amount of material for clay mineralogical analysis <2µm rather than for bulk mineralogical analysis. Bulk mineralogical data are consequently only available from samples below 21m (Figure 7.5).

Figure 7.4. Photographic detail of the base of the fossiliferous Fe-sandstone interval at 25.2-25.5m. On the left side black traces can be spotted which is the result of pyrite mineralization of bioturbations.

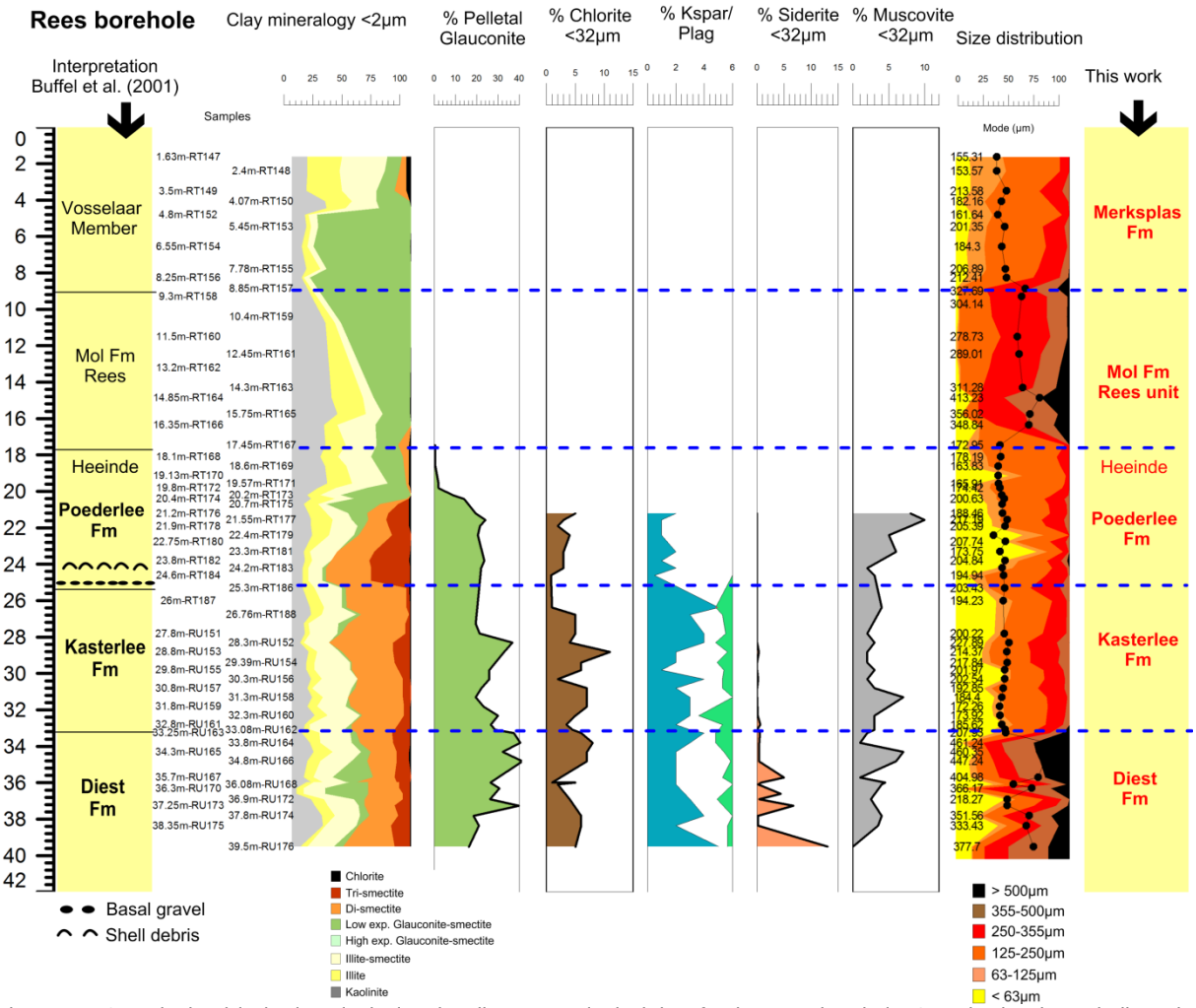

Figure 7.5. Quantitative (clay) mineralogical and sediment petrological data for the Rees borehole. Samples levels are indicated in the second column.

VII.3.3.1 Bulk mineralogy

The mineralogical composition of the 21-25m interval shows a relatively clay-rich composition consisting of mainly 2:1 Al-clays (23-45%), kaolinite (7-17%), trioctahedral expandables (6-19%). Glauconitic minerals are less common (<15%) whereas chlorite contents vary between 1 and 5%. A substantial amount of each sample is however composed of limonite alteration minerals (goethite, ferrihydrite, lepidocrocite) which systematically are present in amounts >5%. In the basal 25.5-24.6m, gypsum is very abundant (>10%) in the iron-sandstones with mineralization although minor amount of jarosite and pyrite are also present. In the 24.2m sample, the amount of gypsum is drastically lowered to 1% and less. This sample is however characterized by elevated amounts of calcite and aragonite (21%) which is related to the shell debris present in this sample. Compared to the underlying Kasterlee sediments, the Fe-sandstone facies of the Poederlee Formation has comparable characteristics, except for the absence of plagioclase traces and the relative abundance of muscovite flakes (Figure 7.5).

VII.3.3.2 Clay mineralogy <2µm

The clay composition of the 20-25m Poederlee samples shows a particular assemblage rich in expandable minerals, which is quite similar to the composition of the units below 25m. The expandable minerals are regular dioctahedral smectite but also comprise trioctahedral Fe-vermiculite, with identical characteristics as found in the Diest D4 litho-unit. Kaolinitic minerals occur in proportions between 10% and 17% of which 2-4% is mixed-layered with expandable minerals. Chloritic minerals are present in trace amounts. Glauconite-smectite is scarce and only becomes more abundant, >10% in the clay fraction, higher than 21.5m depth. In the Heieinde facies, the amount of

expandable minerals decreases sharply and no Fe-vermiculite is identified. Instead, illitic minerals (illite and illite-smectite) and glauconite-smectite become relatively more abundant.

The Mol-Rees unit covering the Poederlee Formation is particularly rich in glauconitic minerals and also contains slightly more kaolinite. Glauconite-smectite is moreover the dominant clay phase in the Quaternary Vosselaar Member.

VII.3.3.3 Pelletal glauconite

The Poederlee Fm in the Rees borehole contains relatively abundant pelletal glauconite, around 20%, being significantly higher compared to the Lichtaart and Kasterlee outcrops. Above 21m, the pelletal glauconite content gradually decreases to 10% at the 20m level and below 2% at 19.5m level. The mineralogical composition of the pelletal glauconite in the Rees borehole consists of both low expandable (9%) and higher expandable (20%) glauconite-smectite but also of an expandable phase (Figure 7.6 and Table 7.2). In air dry conditions, the d_{001} of this expandable phase is 14.25Å and shifts to 16.99Å upon ethylene glycol treatment. Its nature is furthermore very Fe-rich as can be observed by the very low scattering intensity at the 5Å low angle side. This expandable phase is identical to the Fe-vermiculite identified in the associated clay fraction of these Poederlee sediments. This mineralogy is unique for pelletal glauconite in the Campine Basin (Adriaens, 2009).

VII.3.3.4 Size distribution

The grain size distribution of the Poederlee sediments confirm its fine-grained nature with over 75% of the grains being smaller than 250µm. The basal sediments are characterized by 50% of grains being <63µm but this amount gradually decreases towards the top of the formation. The boundary with the Mol-Rees unit above is sharp, as this unit contains over 50% of grains >250µm with very low amounts <63µm and 25% of grains >355µm. The boundary with the Kasterlee Formation below can be made based on the amount of grains <63µm.

VII.3.3.5 Interpretation

The mineralogy and clay mineralogy of the Poederlee Fm occurrence in the Rees borehole is significantly different compared to the Lichtaart and Kasterlee outcrops. The presence of Fe-vermiculite in Poederlee, similar to the Diest D4 unit, points to a weathered origin of the sediments. As this Fe-rich expandable mineral is also encountered in pelletal glauconite, together with glauconite-smectite, a relation between pelletal glauconite and the clay fraction of the sediment is expected.

Table 7.2. Mineralogical characteristics of pelletal glauconite in the Poederlee deposits (Rees borehole). Note that also Fe-rich expandable phase was identified aside from the common R1 glauconite-smectite phases.

Sample	Depth	Member	Content (%)	d060	Fe-expandable	Higher expandable G-S (20% expandable)	Low expandable G-S (9% expandable)	Total amount Glauconite layers	Total amount Expandable layers
RT177	21.55	Poederlee	24	1.5211	2	60	40	82	**18**
RT178	21.9	Poederlee	22	1.522	8	67	25	76	**24**
RT179	22.4	Poederlee	21	1.5211	11	65	24	74	**26**
RT182	23.8	Poederlee	24	1.5202	14	50	33	73	**27**
RT183	24.2	Poederlee	22	1.5202	18	30	45	72	**28**
RT184	24.6	Poederlee	20	1.5222	22	27	46	68	**32**
RT186	25.3	Poederlee	23	1.5211	17	21	61	73	**27**

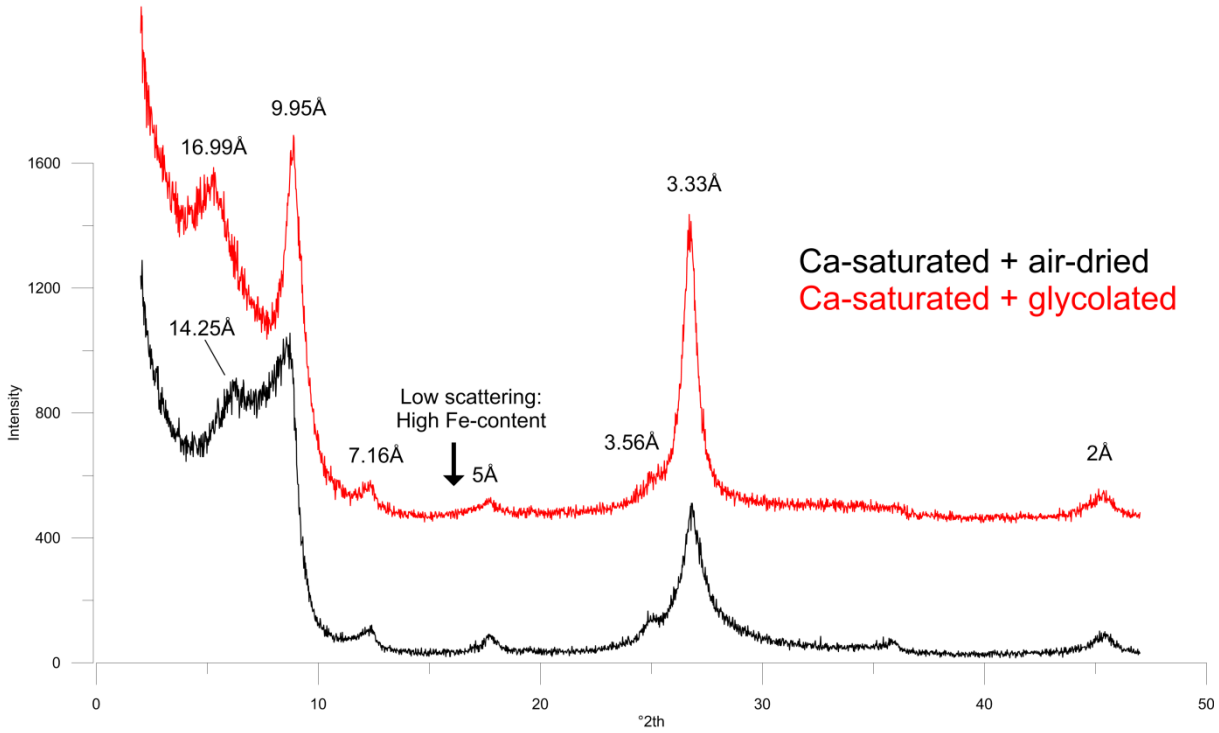

Figure 7.6. Poederlee Fm: air dried and glycolated diffraction patterns of pelletal glauconite at 24.6m depth in the Rees borehole. Note that aside from glauconite-smectite also the presence is confirmed of an expandable phase at 14.25Å which shifts to 16.99Å after ethylene glycol treatment.

VII.4 DISCUSSION

The mineralogical and clay mineralogical characteristics of the Poederlee Formation were studied in the Lichtaart and Kasterlee outcrops and in the Rees borehole, each section with quite heterogeneous lithological characteristics. In the Lichtaart outcrop, the Hukkelberg gravel clearly marks the Kasterlee-Poederlee boundary but no convincing mineralogical or petrological data were obtained to differentiate both formations. The Poederlee occurrence in Lichtaart was consequently interpreted as reworked Kasterlee. In the Kasterlee road section however, the Kasterlee-Poederlee transition is characterized by a sharp increase in smectite, both in sand and clay laminae samples whereas clay-sized glauconite is more abundant but also less expandable in the Kasterlee Formation compared to the Poederlee Formation. Furthermore, the Kasterlee occurrence in the Lichtaart and Kasterlee outcrops is highly similar. In the Rees borehole, the Poederlee Formation consists of weakly lithified Fe-sandstones and contains trioctahedral Fe-vermiculite, similar to the Diest D4 unit and, the underlying Kasterlee Fm. The amount of trioctahedral vermiculite sharply increases in the Poederlee sediment compared to the underlying formations which could indicate a new important weathering stage took place in the source area. Clay-sized glauconitic minerals are of minor, or no, importance indicating that pelletal glauconite disintegration was not an important contributor to the clay fraction of these sediments. In contrast, the Heieinde facies covering the Fe-sandstones in the Rees borehole holds very little pelletal glauconite (<5%) but contains substantial amounts of clay-sized glauconite. Although an important hiatus exist with the Quaternary Vosselaar sand, the clay mineralogy of the latter unit consists of high amounts of clay-sized glauconite, indicating that clay-sized glauconite probably has a local

provenance and is systematically being reworked in Pliocene and Quaternary deposits in the Campine Basin.
The occurrence of Fe-rich expandables (vermiculite) in both the clay fraction and in pelletal glauconite in the Rees borehole is quite uncommon and suggests a mutual relation. This expandable phase could have acted as the precursor of glauconitisation, a mechanism already suggested by Odin (1983) and demonstrated by Buatier et al. (1989) and Jimenez-Millan *et al.*,(1998). Due to the weathered state of the Poederlee sediment and the interpretation of Fe-vermiculite as weathered alteration clay mineral in the Diest and Kasterlee Formations (see chapters V and VI), it is more likely that the presence of Fe-vermiculite in pelletal glauconite is the result of intense weathering rather than being a precursor product for glauconitisation. This pelletal glauconite mineralogy is unique for Cretaceous or Neogene pelletal glauconites in the Campine Basin (Adriaens, 2009). The presence of Fe-vermiculite in pelletal glauconite combined with the clearly increased amount of Fe-vermiculite (>30%) in the clay fraction compared to the Kasterlee and Diest sediments (Figure 7.5), signifies that the ferruginous top part of the Poederlee is a more intensive weathered glauconitic sediment than the underlying deposits.

It can be concluded that in the three investigated Poederlee sections, three different types of Poederlee sediment were found. Reworked Kasterlee sediment was found in Lichtaart, Poederlee sediment characterized by high smectite contents and low amounts of relatively high-expandable clay-sized glauconite in the Kasterlee section and, relatively intensively weathered Fe-sandstones consisting of Fe-vermiculite in the clay fraction as well as in pelletal glauconite in the Rees borehole.

The lateral distribution of these different Poederlee facies is presently unclear based only on the three investigated sections. It is however likely that reworking at the base of the Poederlee Formation is a local feature and that the Poederlee sediment in the Kasterlee outcrop represents new transgressive material of which the clay minerals were differently sourced compared to the Kasterlee Formation. Clay-sized glauconite is scarce and detrital smectite becomes more abundant in the Poederlee Formation suggesting that the sedimentary environment was calmer, possibly also somewhat deeper, compared to the Kasterlee Formation. The upper part of the formation consists of intensively weathered Fe-sandstones characterized by high amounts Fe-vermiculite and weathered pelletal glauconite. Louwye and De Schepper (2010) postulated a distinct shallowing in this upper part of the Poederlee Fm.

CHAPTER VIII

SUMMARIZING SCHEMES & CONCLUSIONS

In this second part of research, the mineralogical, clay mineralogical and sediment petrological properties of the Berchem Fm, the Bolderberg Fm, the Diest Fm, the Kasterlee Fm, the Poederlee Fm and the Mol Fm in the Campine Basin were characterized. The results of this characterization are summarized by means of two profiles through the Campine basin (Figure 8.1), one through the Campine region (Figure 8.2) and one through the Hageland region (Figure 8.3).

In profile 1 through the Campine (Figure 8.2), the clay mineralogical similarity between the different units of the Berchem Formation is shown. Although pelletal glauconite is on average, however not always, the highest in the Antwerp Member (46%) and the Kiel Member is the only decalcified member, clay mineralogy does not allow to distinguish the different members of the Berchem Fm. All members consist of a smectite-rich assemblage with varying contents of relatively high-expandable glauconite-smectite. This exact clay mineral assemblage is also found in the Deurne Member and the Dessel Member of the Diest Fm. This similarity, complemented with important erosion of the Berchem and Bolderberg Fm (see figures 5.2 and 5.3) and the pelletal glauconite ages of Vandenberghe et al. (2014), indicate a significant reworking of Berchem/ Bolderberg material within the Deurne and Dessel Members. Note that it was suggested in this work to restore the traditional definition of the Dessel Member, which is its fine-grained nature and not necessarily its calcareous content.

In the Hageland (Figure 8.3), identical clay mineralogical characteristics are found in the Houthalen and Genk Members of the Bolderberg Formation. Pelletal glauconite in Houthalen is however much lower compared to the Berchem Fm whereas it is absent in the Genk Member. The Opgrimbie facies is characterized by totally different assemblage, which is dominated by kaolinite and illite.

The base of the Diest sand member (Diest D1 – DN9) is marked by a significant break with coarser-sized sand and with a low-expandable glauconite-smectite dominated clay mineralogy (Figure 8.2). The analyses of the Diest Formation occurrence in the Hageland reveal no strong arguments to distinguish it from the Diest D1 unit in the Campine based on the investigated mineralogical, clay mineralogical and sediment petrological parameters. The top Flemish hill deposits, traditionally attributed to the Diest Formation, are kaolinite- and illite-rich and are significantly different from the Diest Fm deposits in the Hageland area (not shown in schemes).

In the western part of the Campine basin, the Diest D1 sand gradually transitions into clayey sand (Diest D2 to Diest D3 facies) which is characterized by a smectite-rich clay mineralogy and only ca. 5% pelletal glauconite.

In the top of the Diest Fm, Fe-vermiculite was found to be an important contributor to the clay fraction of the Diest D4 unit indicating the weathered origin of these sediments. This weathered top facies was however not found in Retie and also not more towards the south in Olen, Heist-op-den-berg and the Hageland area (Figure 8.3).

The litho-units of the Diest Formation defined here based on clay mineralogical composition show a good correlation with the dinoflagellate cyst biostratigraphy (Figure 8.4). Only for the weathered Diest D4 top facies, both DN9 and DN10 biozonations occur. As also grain-sizes within this Diest D4 unit vary from medium-coarse-grained to fine-grained, this most likely indicates that this Diest D4 unit might consist of several subunits. Nevertheless, the weathered origin (Fe-vermiculite and kaolinite-expandable) of all Diest D4 sediments justifies that they are considered as one unit in this work.

At the base of the Kasterlee Formation, a transition zone is found which indicates important reworking. Relatively high amounts of Fe-vermiculite, siderite, plagioclase, chlorite,

pelletal glauconite, typical for the top Diest Formation, gradually transition into typical Kasterlee Fm sediment properties which are pelletal glauconite <5%, fine-grained and well-sorted size distribution, a glauconite-smectite dominated clay mineralogy, higher muscovite contents and only traces or even the complete absence of chlorite, siderite, plagioclase and Fe-vermiculite (Figure 8.2). Where the top Diest is formed by the Diest D1 facies (see Figure 8.3), the transition of characteristics is similar except for Fe-vermiculite which is absent in the Diest D1 unit. In Olen and Heist-op-den-berg, the position of the boundary is confirmed and accentuated by the presence of a gravel layer (Figure 8.3). In Rees, only the transition zone is found, no "new" Kasterlee deposition (Figure 8.2).

In the Dessel-Mol area, the transition zone is covered by a sand facies which is frequently intercalated with clay laminae which disappear towards the top of the formation. The top of the Kasterlee Fm and the boundary with the Pliocene Mol Fm is interpreted whenever the glauconite-smectite-dominated clay mineralogy of the Kasterlee Formation drastically changes to a kaolinite-dominated clay mineralogy of the Mol Fm. Muscovite contents can be significantly lower in the Mol Formation, which at its base is characterized by a relatively clay-rich zone.

Also the Poederlee sediments are quite variable in lithological characteristics. At the base of the formation, sediment are locally reworked from the underlying Kasterlee Fm. The sediment petrological characteristics of the typical brown sands of the Poederlee Fm are quite similar to those of the underlying Kasterlee Fm sands except that the Poederlee sands are relatively enriched in smectite. At the top of the formation, the Poederlee sediment underwent significant weathering which is reflected in the formation of oxidized Fe-sandstones, the presence of high amounts of Fe-vermiculite in the clay fraction and the weathered nature of pelletal glauconite.

The main objective of this part was to study quantitative clay mineralogy in order to better define stratigraphic boundaries. It was extensively demonstrated in this part, and summarized in the schemes explained above that quantitative clay mineralogy with the aid of sediment petrological parameters is very successful in lithostratigraphy and allows to 1) unravel a more concise and detailed stratigraphic positioning, 2) make robust correlations between boreholes and 3) define reliably boundaries between different formations and subunits, even in the most complex cases and unlike any other parameter.

Furthermore, the stratigraphic boundaries defined in this work (e.g. Diest-Kasterlee and Kasterlee-Mol) are not specific levels of which the boundary interpretation is strictly based on the parameter "clay mineralogy". It was demonstrated in the Dessel-2 and Dessel-3 boreholes (Chapter VI) that the clay mineral-based boundaries also have an important paleoenvironmental significance (see for instance Louwye et al., 2007). The defined boundaries can furthermore also be correlated with gamma-ray and/or resistivity excursions (see for instance Diest-Kasterlee boundary on figure 6.6 and figure 6.9). These factors strongly increase the reliability of the defined boundaries and facilitate practical correlations.

Aside from the clay mineral characterization of the different units and their boundaries, it is also possible to draw some preliminary conclusions for paleogeographic evolution. It can be concluded that clay minerals in the investigated Neogene deposits origin from several sources:

1) Marine detrital clay is mainly transported from the northern North Sea and typically results in smectite-rich clay assemblages during the Miocene (e.g. Berchem Fm, marine Bolderberg Fm) and also the Pliocene (Poederlee Fm).
2) Clay-sized glauconite-smectite has no detrital origin but instead is locally derived from pelletal glauconite abrasion or even complete disintegration upon energetic transport. Clay-sized glauconite production can be the dominant clay supplier whenever detrital, marine- or land-derived, clay supply is insignificant, such as in the Diest D1 sand unit.
3) Continentally-derived clays were encountered in the Opgrimbie facies of the Bolderberg Fm, the Mol Fm and in the top Flemish hill sand deposits. The clay composition of all of the former deposits consists dominantly of kaolinite and illite most likely originating from the Ardennes-Rhenish massif in the south to southeast. This specific clay mineral assemblage is consequently also discharged by the Rhine delta in the east of the Campine basin.
4) It seems typical from the Neogene deposits that substantial amounts of the clay has a reworked origin, such as the Deurne and Dessel Member of the Diest Fm and the basal deposits of the Kasterlee and

Poederlee Formations. Glauconite-smectite in the Mol Formation is also considered as reworked. Also Neogene pelletal glauconite is massively reworked from older deposits.

5) Intense weathering of deposits also affects the clay mineralogy. Fe-vermiculite and kaolinite-expandable minerals were found in sediments of the Diest D4 unit, in the reworked part of the Kasterlee Formation and in the Poederlee Formation. These chemical weathering products were not formed in-situ but might origin from the erosion of soils.

Not only clay minerals were reworked in the Neogene but also pelletal glauconite in these deposits is massively reworked from older deposits. Only pelletal glauconite in the Antwerp Member of the Berchem Fm has a probable authigenic origin. Such massive reworking of pelletal glauconite is quite unusual. Glauconite occurrences reported in literature are mainly documentation of authigenic glauconitisation such as recent glauconitisation taking place during sedimentation in the Niger delta (Porrenga, 1966)) or as the result of diagenetic alteration ((Burst, 1958; Ivanovskaya and Geptner, 2004).There are however also some authors reporting small-scale pelletal glauconite reworking, such as the occurrence of pelletal glauconite on tidal flats (McRae, 1972; Odin and Fullagar, 1988; Chafetz and Reid, 2000; Gonzalez et al., 2004). The Neogene interval in the Campine basin is probably the first case in which pelletal glauconite reworking is observed on such a large scale and over such a long time-interval. Due to this reworking, clay-sized glauconite is systematically found in pelletal glauconite-bearing sands as the result of abrasion or even complete disintegration of pelletal glauconite during transport. The mineralogical characteristics of pelletal and clay-sized glauconite are very similar. The mineralogy of clay-sized glauconite is however systematically somewhat more expandable which indicates that clay-sized glauconite has an increased reactivity.

It can be concluded that the intra-formational variability in lithological, clay mineralogical and sediment petrological characteristics reported and discussed in this work suggests that more refinement is required in the Neogene Campine lithostratigraphy. The internal heterogeneity within formations suggests that additional members and facies should be defined and more research is required in order to study the lateral variability of the different units and boundaries. Furthermore, instead of working with unit stratotypes, local stratigraphy would strongly benefit from the use of boundary stratotypes.

Such refinement however will also require that more sytematic sediment petrological analyses are carried out on other borehole and outcrop samples to better define the geographical distribution of the different litho-units identified in the present study. Ideally such lithostratigraphic studies should extend over the boundary with the Netherlands and also Germany.

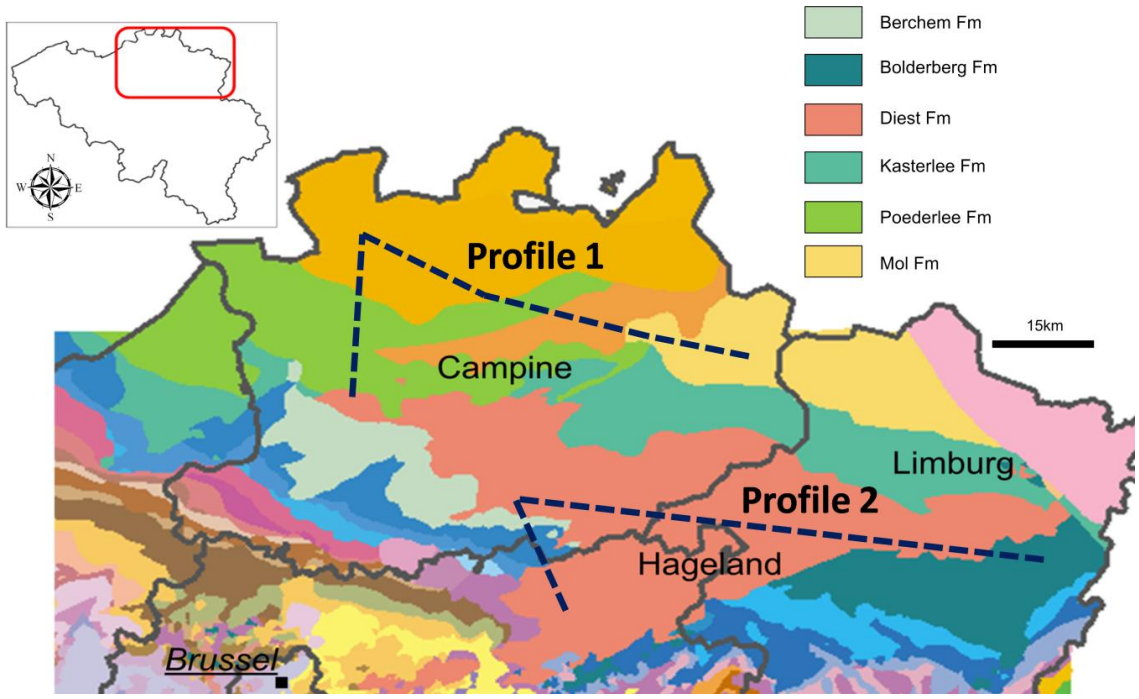

Figure 8.1 . Geological map of the Campine basin indicating the position of two profiles, one across the Campine area, one across the Hageland area. Map modified after ALBON (2009).

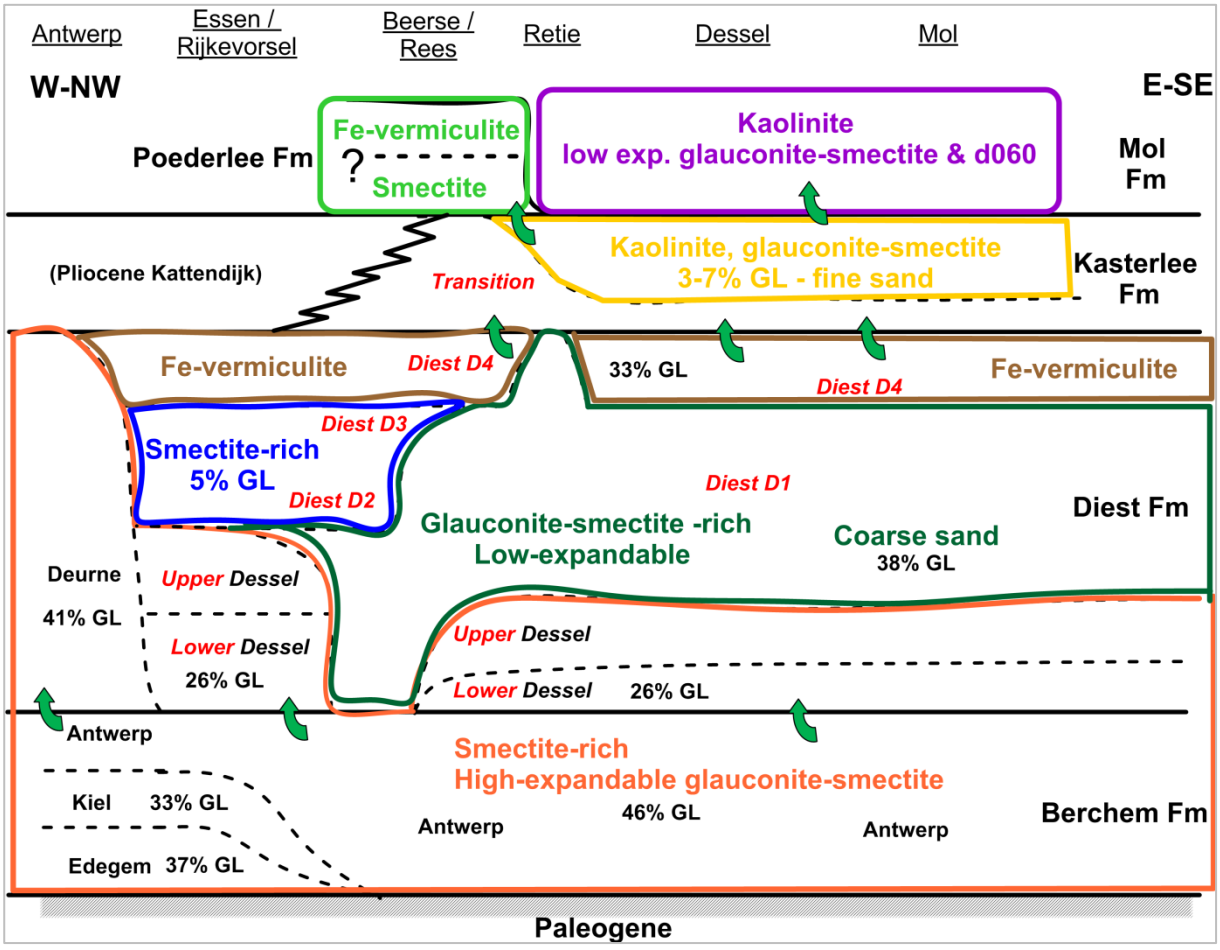

Figure 8.2. Geological profile through the Neogene succession in the Campine region (see Figure 8.1for profile line).

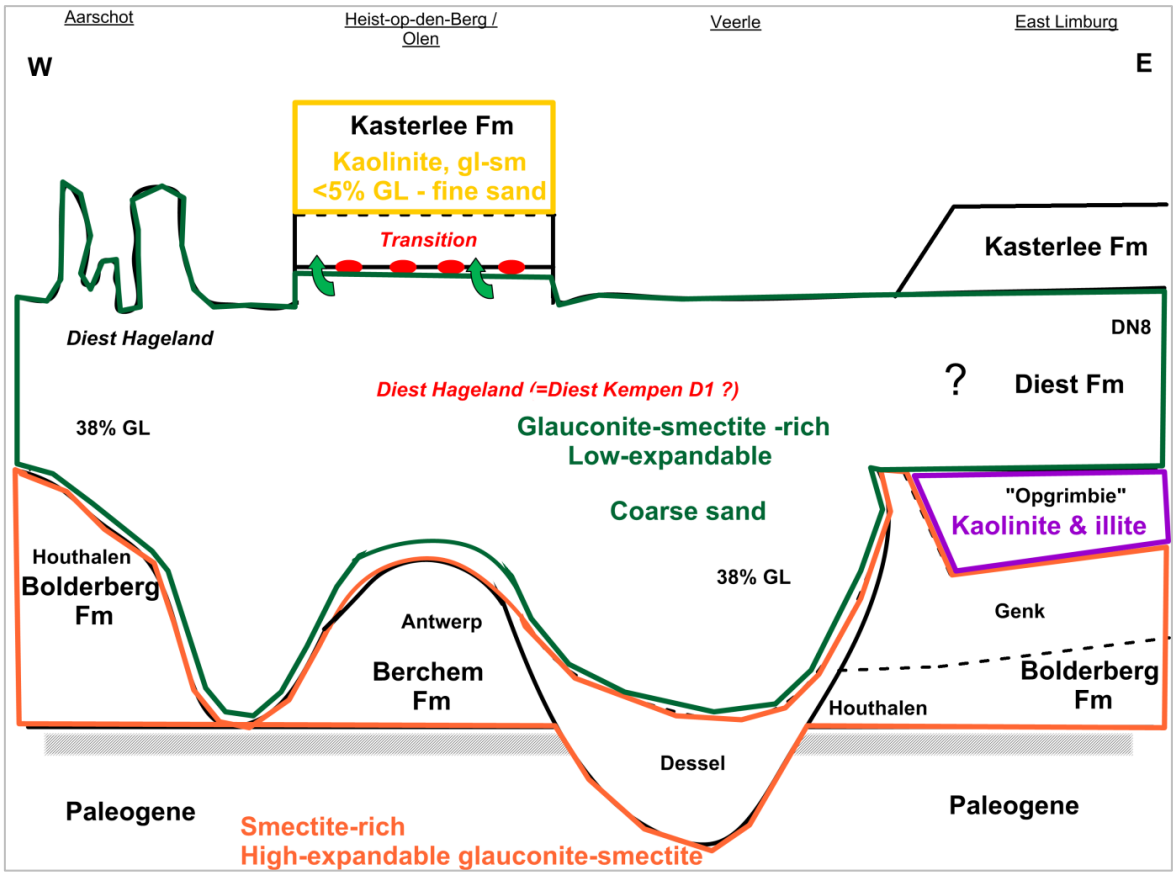

Figure 8.3. Geological profile through the Neogene succession in the Hageland region (see Figure 8.1for profile line).

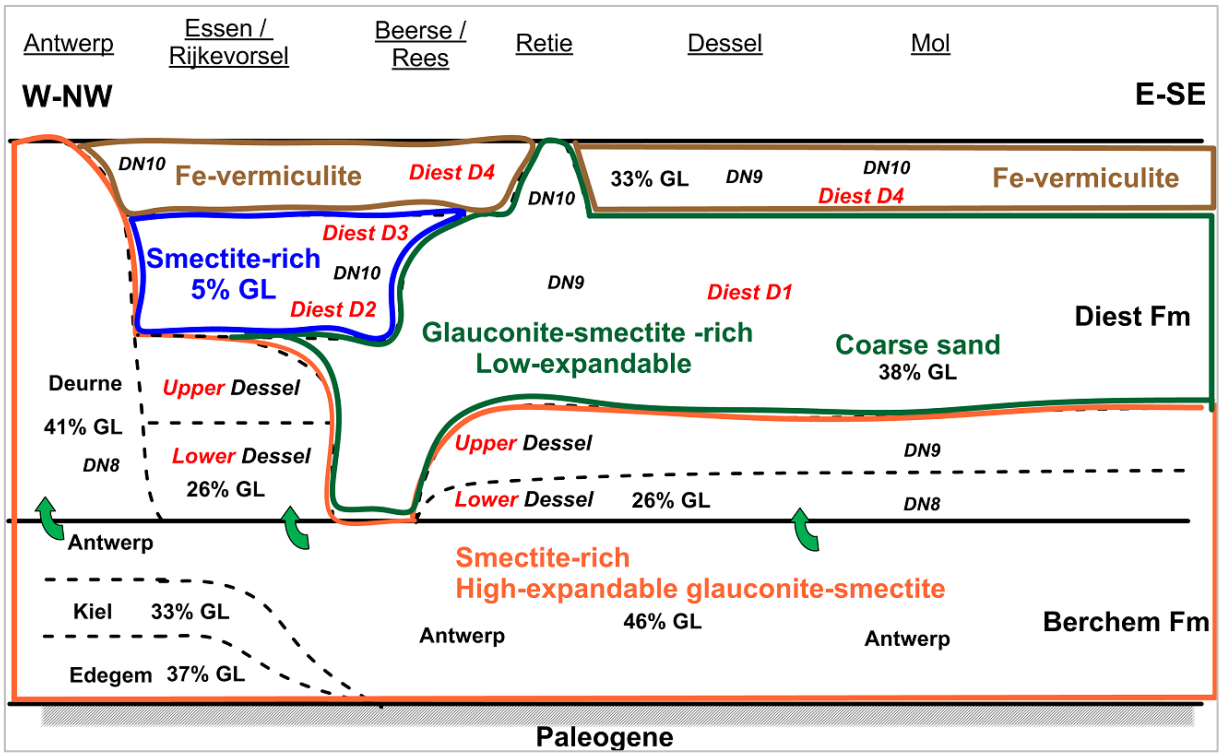

Figure 8.4. Geological profile through the Neogene succession in the Campine region showing the correlation of the defined Diest Fm litho-unit with the dinoflagellate cyst biozonations (see Figure 8.1for profile line).

PART III.

Stratigraphic application: Provenance of the North sea muds

Introduction

The Belgian continental shelf (BCS) is a tidal-controlled, high-energetic depositional environment consisting mainly of coarser-grained sand deposits with low clay content. Along a near-coastal path however, from Oostende to Zeebrugge, fine-grained mud deposits were mapped by Bastin (1974) and high Suspended Particulate Matter (SPM) concentrations occur (Figure III.1, Figure 9.1, Figure 9.2) (Fettweis and Van den Eynde, 2003). The occurrence of muds in such an energetic shelf environment has inspired several researchers to explain this odd hydrodynamic situation (Bastin, 1974; Nihoul, 1975; Gullentops et al., 1976; Van Alphen, 1990; Baeteman, 1999; Fettweis and Van den Eynde, 2003; Van Lancker et al., 2009). Others have attempted to discover the provenance area of the muddy sediments using microfossils (Fontaine, 2004), semi-quantitative clay mineralogy (Irion and Zöllmer, 1999; Grégoir, 2005) and fully quantitative clay mineralogy (Zeelmaekers, 2009). In these studies, several source areas were proposed and both erosion of recent and older marine deposits as well as fluvial discharge of clay was considered (see further). The most significant results were obtained by Zeelmaekers (2011) who analyzed the clay mineralogy <2µm of different potential sources and evaluated their provenance potential. Zeelmaekers (op. cit.) demonstrated that the clay mineralogy of most of the in the literature cited sediment sources are significantly different from that of the BCS muds except of the sediments in the Scheldt estuary which closely resemble the BCS mud clay mineralogy. A major finding by Zeelmaekers (2011) has been the observation that the typical BCS mud clay mineralogy <2µm was also found in older Holocene and Pleistocene deposits of the coastal plain. This shifts the issue of the BCS mud provenance back into time. It could indicate that the provenance source for the coastal mud plate was already actively transporting mud to the North Sea since the late Quaternary. The origin of the mud in the recent coastal mud plate could then be a reworking of previously deposited mud from that same provenance source. Therefore more Holocene and Pleistocene clay-rich deposits from the Belgian coastal plain are analyzed in this study. A particular problem in this part of the study is the lack of deposits reliably assigned to the Pleistocene time periods in the Belgian coastal plain.

This approach of studying both the recent and the Pleistocene deposits is applied in the present work in a reconnaissance study of the Dutch coastal area and the Rhine-Meuse river system, a potential source area contributing to the BCS mud plate but only briefly discussed by Zeelmaekers (2011). Another potential source that needed confirmation with respect to the study of Zeelmaekers (op.cit.) is the contribution by the transport from the English Channel. However the most substantial part of the contribution to the origin of the BCS mud in the present work comes from the analysis of the clay minerals of the Scheldt river system and the simulation of this river-influx clay mineral contribution to the present clay mineral composition in the Scheldt estuary.

In a first chapter the present state of knowledge about the origin of the BCS muds will be given based on the work of Zeelmaekers (2011) and also some basics on the late Quaternary evolution of the coastal plain and the present day Scheldt estuary-North Sea dynamics will be summarized in the first chapter.

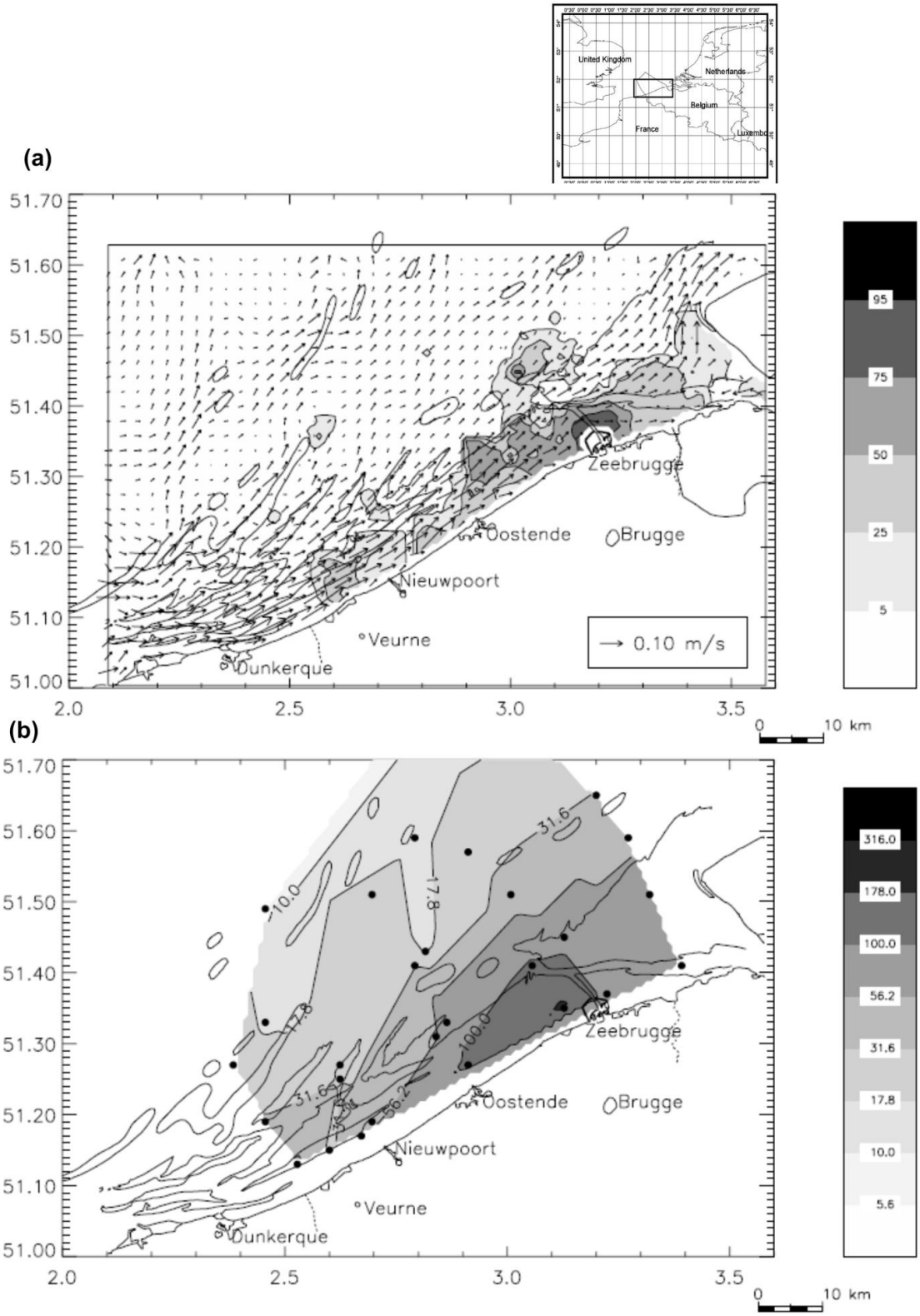

Figure III.1. (a) Mud content (in wt%) in surface sediments of the Belgian Continental Shelf. The vectors indicate the residual water transport pattern, tidal and wind driven, of 1999 and, (b) Mean SPM (suspended particulate matter) concentrations of MUMM monitoring data (modified after Fettweis and Van den Eynde, 2003).

CHAPTER IX
The BCS muds: state of the art

IX.1 THE BCS MUDPLATE

The bottom mud deposits, also referred to as "mudplate", were already recognized in the late-19th century (Stessels, 1866; Van Mierlo, 1899; Gilson, 1900) and later more precisely mapped and documented by Bastin (1974), Missiaen et al., (2002) and Van Lancker et al., (2004). The muds were recognized by Mathys (2009) on seismic images as a rather distinct seismo-stratigraphic unit (unit "U6") of a few meters thickness deposited during the late-Holocene (Figure 9.1). The mudplate itself consists of a surface layer of recent fluid mud, covering weakly to medium consolidated muds of the U6 unit below (Fettweis and Van den Eynde, 2003). Dating by radionuclides ^{210}Pb, ^{226}Ra and ^{137}Cs in Fettweis et al., (2007) showed that the weakly consolidated muds on top of the plate are probably from the second half of the 20th century and the medium consolidated muds slightly deeper in the plate several decades older, confirming a very young age for the BCS mudplate.

The mineralogical composition of the muds is prone to some variation but the large mineral groups are proportioned in 20-40% clays, 20-40% quartz, 20-30% carbonates and 0.5-7% organic material. The clay mineral composition <2µm is quite stable with ca. 40% smectite, 20-25% randomly interstratified illite-smectite, 15-20% illite, 15% kaolinite and 5% or less chlorite (Zeelmaekers, 2009). As clay minerals are often the main mineralogical constituent of the sediment, this makes the mud deposits suitable for provenance analysis using quantitative clay mineralogy, although it is recognised that also other methods can contribute to provenance analysis.

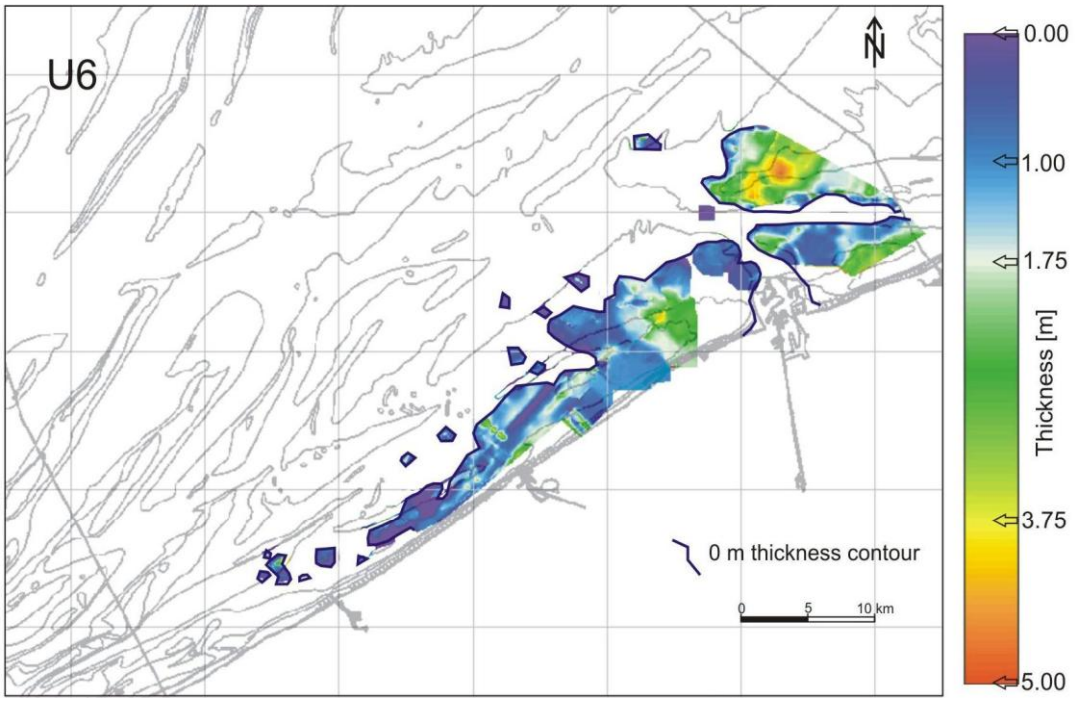

Figure 9.1. Thickness of the U6 mudplate deposits (after Mathys, 2009).

IX.2 THE POTENTIAL PROVENANCE AREAS

The provenance of the mudplate deposits has been discussed intensely (Figure 9.2). Some authors argue that most of the Holocene deposits in the Belgian coastal area, and thus also the BCS U6-muds and recent deposits, are locally derived sediments, reworked from older Holocene or Pleistocene deposits (Baeteman, 1999; Beets and van der Spek, 2000; Matthys, 2009), hereby shifting the provenance problem in time. Hydrodynamic modeling (Fettweis and Van den Eynde, 2003) and clay mineralogy (Irion and Zöllmer, 1999) however suggest transport of sediment through the English Channel either by tidal transport from the Atlantic ocean or by coastal erosion in the Dover Strait. Fontaine (2004) identified reworked microfossils in the muds coming from the erosion of Cretaceous chalk cliffs along the Channel and from the erosion of earliest Oligocene sediments (NP21 biozone) at the Western Scheldt mouth. Others have cited erosion of the Paleogene sea floor as main clay source (Bastin 1974, Gullentops et al. 1976) or input from the Scheldt river system (Gullentops et al., 1976; Nechad et al., 2003; Zeelmaekers, 2011) with possibly also minor contributions (ca. 5%) from the Rhine-Meuse rivers (Lacroix et al., 2004). Other possible sources are the northern North Sea or an important influence of the dredging of navigation channels and subsequent dumping actions in the area (Figure 9.2). A more extensive literature review can be found in Fontaine (2004) and Zeelmaekers (2011).

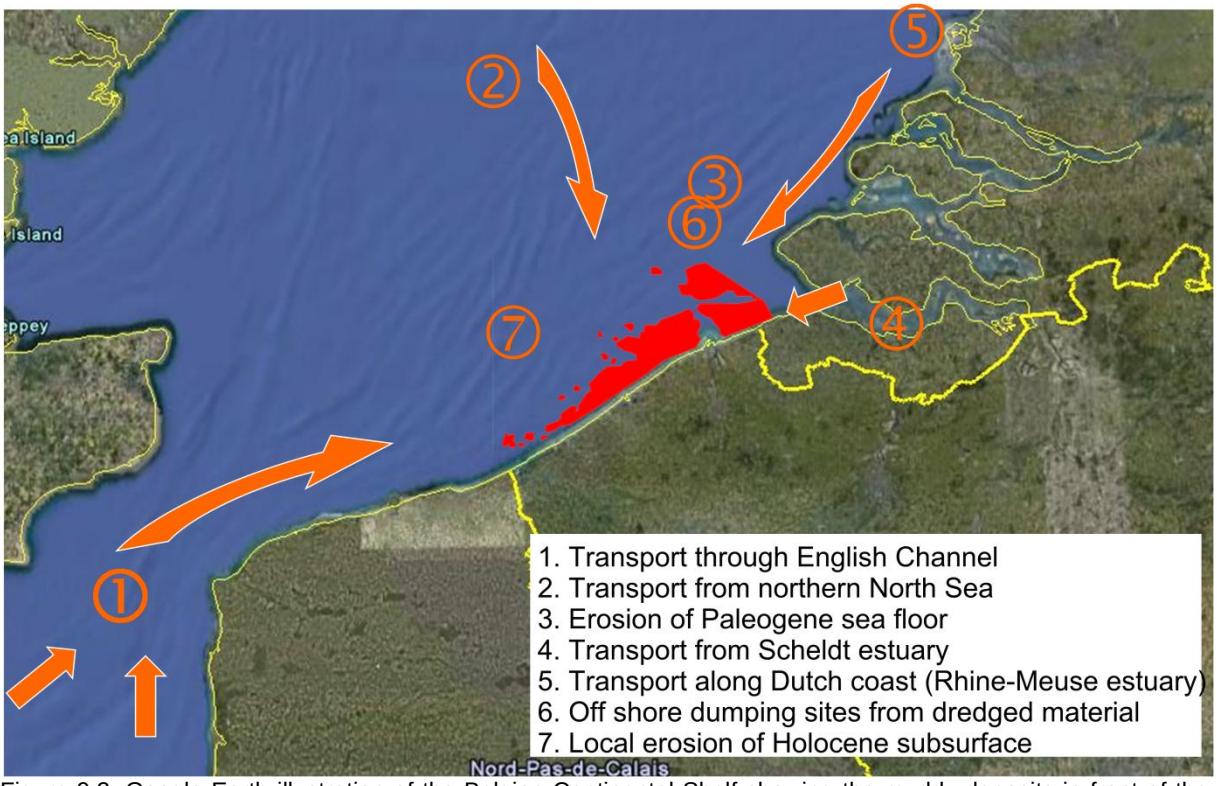

Figure 9.2. Google Earth illustration of the Belgian Continental Shelf showing the muddy deposits in front of the coast in red. The different numbers and arrows indicate cited sediment sources which refer to the text.

IX.3 PRESENT-DAY SCHELDT- NORTH SEA DYNAMICS

Although the net northeastern sediment transport direction in the North Sea indicates that the English Channel is the most logical provenance area for the BCS muds, the clay mineralogical data presented by Zeelmaekers (2011) contradict this and furthermore suggest that one of the sources with good provenance potential is the Scheldt estuary (Figure 9.3). From a sedimentological point of view, it is not so surprising that the clay mineralogy of the Scheldt estuary, even higher upstream, is similar to that of the BCS as estuaries and tide-dominated environments undergo sediment infilling and therefore are not considered as net sediment suppliers to the marine environment. Instead, there is a net import of marine sediment in the estuaries (Reading and Collinson, 1996). The present-day hydrodynamic models of the Scheldt estuary seem to confirm such processes. Van Alphen (2000) for example calculated an annual net input of 0.6 Mt of marine mud into the Westerschelde estuary. The model of Vanlede et al.,(2009) estimated a net export of 2Mt/year.

At Schelle, at 90km from the estuary mouth (Figure 9.3), a strong seaward component of sediment transport still exists, estimated at 400 kT/year according to Van Maldeghem (1993) and varying between 94 and 336 kT/year according to Taverniers (2000). Despite this strong seaward component at Schelle, there seems nowadays to be a consensus amongst fluvial engineers that the fluvial material eroded upstream the river system and transported along the estuary, is massively being deposited in the Antwerp harbor and near the Dutch/Belgian border and is not transported out of the Westerschelde to the sea (Figure 9.3). The tidal waves control where in the estuary material is being deposited, resulting in a dynamic balance between marine waters, and thus suspended sediment, flowing upstream and fluvial SPM flowing downstream. Salden (2000) and Chen et al., (2005) concluded that the import of marine SPM in the Westerschelde has even doubled due to the deepening of navigation channels.

This hydrodynamic situation implies that the Scheldt river system presently cannot be the clay supplier for the North Sea muds as no, or only very little, fluvial sediment is being transported out of the estuary, which in time will result in complete siltation of the estuary. Consequently, suspended sediment transport from the estuary to the sea consists predominantly of material which initially originates from the sea and was imported into the estuary.

Nevertheless, many modern mud-dominated shelves receive their fines from large river systems draining the continent, such as the Amazon and the Yellow river delta, often driven by wind action and strong seasonal variation (Johnson and Baldwin, 2006). Liu et al., (2009) calculated sediment budgets for the major Asian river systems and concluded that for all analyzed rivers 50-70% of their sediment load is discharged to the sea. Therefore, export of fluvial sediment out of the estuary is very normal on a geological time scale but also today. Certainly during special events such as heavy storms, heavy winds and tidal extremes, the dynamic balance between marine inflow and fluvial outflow in the estuary is disturbed, allowing fluvial material being transported out of the estuary.

Although the Belgian Continental Shelf area is a high-energy environment controlled by tidal currents, Bastin (1974) reported the existence of a closed circulation cell characterized by equal ebb and flood currents. Because of this tidal balance, suspended sediment is actively deposited in the cell. The model of closed circulation cells could explain the existence of the mud deposits on the BCS. According to Fettweis and Van den Eynde (2003) however, such closed circulation cell system is actually not present at the BCS.

Figure 9.3. Geographical position of the Scheldt river system, draining the upper part of Belgium and flowing in the Southern North Sea through the Westerschelde. The North Sea mudplate U6 deposits of Matthys (2009) are indicated in red.

IX.4 A SUMMARY OF THE QUATERNARY EVOLUTION OF THE BELGIAN CONTINENTAL SHELF

The shallow subsurface of the Belgian Continental Shelf (BCS) consists of dominantly Holocene and Pleistocene deposits resting unconformably on Paleogene deposits. Locally the Quaternary cover is lacking and Eocene and Oligocene deposits are outcropping at the sea bottom (Fettweis et al., 2007). Intensive erosion and reworking have made the detailed geology and sedimentology of the Quaternary cover very complex (see also Baeteman et al. 2002; Fettweis et al., 2007; Vos and Zeiler, 2008; Mathys, 2009).

The Quaternary geology of Belgium is mainly controlled by the alternating climatic conditions of glacial and interglacial periods affecting the sea-level and therefore also the interplay between deposition and erosion in the coastal plain and on the shelf. The chronostratigraphy of the alternating glacial and interglacial periods is based on the variation of ^{16}O and ^{18}O isotopes in marine sediments, resulting in different stages, Marine Isotope Stages (MIS). Table 9.1 gives a partial overview of the correlation of these MIS-stages with the regional nomenclature (after Zagwijn, 1992) of middle- to late-Pleistocene glacial and interglacial periods (based on Pillans and Gibbard, 2012).

Table 9.1. Correlation of Marine isotope stages with regional stages and series and starting dates (after Zagwijn, 1992 and Pillans and Gibbard, 2012).

MI - stage	Stage / *Series*	Start date
MIS 1	*Holocene*	ca. 14 ka
MIS 2-5d	Weichselian	ca. 112 ka
MIS 5e	Eemian	ca. 130 ka
MIS 6-10	Saalian	ca. 337 ka
MIS 11	Holsteinian	ca. 424 ka
MIS 12	Elsterian	ca. 480 ka

During glacial periods, the erosion base level of rivers on the continent, such as the Scheldt river system in Belgium, is drastically lowered resulting in erosion of the river valleys and in the shift of deposition of fluvial sediments towards the marine realm. During the shorter

interglacial stages, the sea-level rises and allows the sea to invade the incised valleys thereby evolving into estuaries. A clear remnant of such a paleo-drainage system is the Flemish Valley, which is the Pleistocene paleo-valley of the Scheldt river system (Mostaert et al., 1989). This Flemish Valley was formed before the Holsteinian interglacial, most likely during the Elsterian glaciation (MIS12) (Mostaert and De Moor, 1989) when the paleo-Scheldt system started to drain Flanders in west to northwestern direction (Mostaert et al., 1989). Similar to the Elsterian glaciation (Figure 9.4), a proglacial lake formed in the Southern North Sea area during the Saalian maximum ice-sheet extension (MIS6) (Gibbard, 2007). During deglaciation, the proglacial lake overtopped the ridge north of the Dover Strait causing a breakthrough followed by intense erosion (Gibbard, 2007; Mathys, 2009). This breakthrough most likely also caused the connection of the Flemish Valley with the English Channel area after which the Scheldt river system discharged in westward direction towards the English Channel. Equivalent to the Rhine-Meuse system at the Dutch coastal area (Busschers et al., 2007), the westward-flowing paleo-Scheldt system developed a delta close to the coastline (Figure 9.4). At the start of the Holocene , the sea-level was rapidly rising, flooding the previously dry Belgian Continental Shelf and the Dover Strait. In this early Holocene period, an open tidal-flat environment developed with deposition of a tidal flat U4 unit consisting of sand or alternating sand and clay laminae (Mathys, 2009). After, coastal barrier islands with back-barrier basins developed and intertidal mud and peat were deposited behind the barrier (Beets and van der Spek, 2000). After subsequent erosion and reworking, increasing anthropogenic degradation and severe storm surges resulted in the erosion and submersion of these islands, to form the present-day coastline around the 16th century (Mathys, 2009). Sometime during these very last stages of the Holocene evolution of the BCS the U6 mud deposits were formed in the BCS nearshore zone. According to Mathys (2009), the U6 unit origins from redeposition following massive erosion of the Wulpen island in the 15th to early 16th century offshore the Scheldt estuary mouth. After deposition of the U6 mud deposits, the U7 sand ridges developed as a reaction of tidal influence and wave action (Mathys, 2009). The provenance of the U6 mud deposits, which coincide with the mudplate mapped by Bastin (1974), and the younger weaker consolidated mud sediments covering them are the subject of this study.

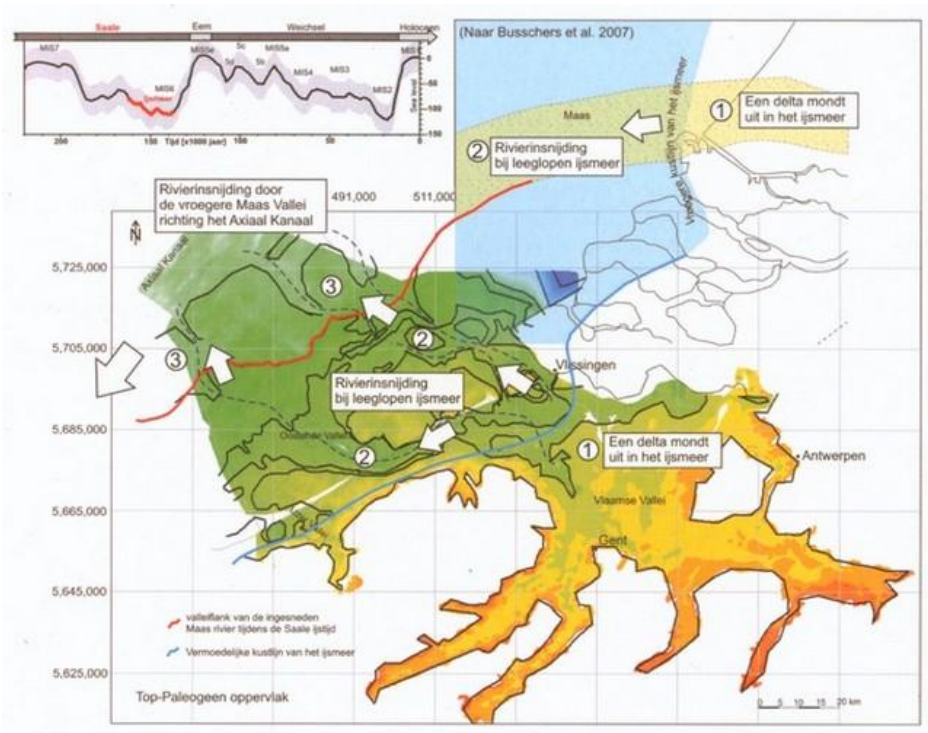

Figure 9.4. Schematic scenario of the river incision after the Saalian proglacial-lake drainage (modified after Busschers, 2007 and Mathys, 2009).

IX.5 MAIN ISSUES LEFT IN THE PROVENANCE DISCUSSION

The most crucial result obtained prior to this research is probably that sediment sources in the English Channel have a significantly different clay mineralogy than the North Sea muds. This is rather surprising because the residual tidal transport direction in the southern North Sea is indeed in northeast direction but apparently this is not reflected in the clay mineralogy of the North sea muds. Nevertheless, Fontaine (1999) identified typical Cretaceous calcareous microfossils in suspension and in bottom sediments of the Belgian North Sea, which suggests that erosion of the Mesozoic deposits outcropping in the English Channel is responsible for at least part of the carbonate fraction of the North sea muds. The different clay mineralogy however proves that the provenance of the clay minerals lies elsewhere.

A second important conclusion is the fact that the clay composition of the muds is equal to the composition of the Suspended Particulate Matter (SPM) floating above the mud area. Gradually further away from the mudplate the clay mineral composition of bottom mud and SPM starts to show more variability. To the southwest, the BCS clay mineral composition remains intact in beach and coastal deposits to Calais whereas the extension of the mudplate to the north is less clear.

A third essential point is that, based on two exploration samples, the clay mineralogy of the mudplate is also found in underlying Holocene deposits. Furthermore, also late-Pleistocene (MIS 5d and MIS-5e, F. Bogemans, pers. comm..) intertidal flats of the Leeuwenhof core in the Belgian coastal area have very similar clay mineralogy compared to the BCS muds. Early Pleistocene deposits however, although not analyzed from samples in the coastal plain, were found to contain a significantly different clay mineralogy. Also outcropping Paleogene deposits in the North Sea are characterized by significantly different clay compositions.

The key conclusion of the previous research is the result obtained for samples at the bottom and in suspension in the Scheldt estuary. The clay mineralogy of these samples is identical to the North Sea muds composition throughout almost the entire estuary. Upstream from Antwerp (Figure 9.3), slightly more variation in clay composition is observed but overall, the North sea muds composition is continuously present from the mouth of estuary until the upper estuary part of the Scheldt river system.

Below, the main unsolved issues of the provenance of the North sea muds are discussed more elaborately. These four remaining issues are the subject of the current study and contributing to their solution forms the main objective of this study by analysing new strategically located samples.

IX.5.1 Clay mineralogy in the English Channel

The results obtained in the research of Fontaine (2004), Grégoir (2005) and Zeelmaekers (2011) point out that the English Channel is not the main sediment source but might contribute an unknown percentage of carbonates to the deposition area. It is however clearly not the main source area for the clays. The analyses of Zeelmaekers (2011) mainly deal with the coastal clay-rich beach sediment in the English Channel but only very few analyses of the suspended material in the Channel itself were carried out. Therefore, additional SPM sampling is required, preferably at different distances from the coast, before any coastal or more off shore transport paths of clay definitely can be ruled out.

IX.5.2 Scheldt river system

The clay mineralogical similarity of the bottom and suspended sediment in the Scheldt estuary and the Belgian North Sea bottom strongly suggests a relation in origin of mud. The sediment dynamics in tidal estuaries are controlled by the interplay of downwards fluvial and upwards marine sediment transport. The clay signal of the Scheldt estuary could therefore indicate either the fluvial sediment component or the marine sediment component. Most likely however, the estuary mud sediment is a mixture of fluvial drainage and marine sediment inflow. A better understanding of such systems is required to evaluate the Scheldt river system as potential main provenance source. The input fluvial clay mineralogical component can be determined by analysing this composition in the different tributary rivers before they join the main river course. In the main course, the minerals combine into the average clay mineral

composition that is delivered by the Scheldt to the estuary.

IX.5.3 Quaternary clay mineralogy and sediment dynamics in the southern North Sea basin

Zeelmaekers (2011) found the typical North Sea clay composition in two samples of the underlying late-Holocene, and even in late-Pleistocene deposits. The preliminary nature of these results demand for confirmation on a broader sample set. If confirmed, such similar clay-mineral composition most likely indicates that the clay source was already active during the Holocene and possibly also during late-Pleistocene times, transporting clay sediment to the Belgian coastal area. Because of the clay-mineral similarity of the Scheldt estuary sediments, the BCS mudplate and possibly the Holocene and late-Pleistocene coastal deposits, it could very well be that the Paleo-Scheldt river is the main provider of clay minerals for mud deposition in the coastal plain during the Holocene and late-Pleistocene. As the flow regime of the Paleo-Scheldt was subjected to drastic changes during the Holocene and Pleistocene, a relation between its evolution and the clay mineralogy in sediments is expected.

The tidal deposits in the Leeuwenhof core sampled and analyzed as Eemian tidal deposits by Zeelmaekers (2011), have recently been re-interpreted as MIS-5d (~early-Weichsel) and only the lowermost analyzed sample has a MIS-5e signal (~Eemian) (Verheyden et al., 2013). This could mean that the same mud mineralogy as now found on the BCS mudplate is consistently incorporated in Holocene, glacial Weichsel and interglacial Eemian deposits of the coastal plain. However, such a conclusion is only preliminary as it is based on only 2 Holocene samples whereas the late-Pleistocene samples originate from one borehole. The sample set of Holocene and Pleistocene deposits is as such very limited and will be expanded in this research. Furthermore, only Holocene and Pleistocene borehole samples with a reliable stratigraphic and facies control are analyzed.

IX.5.4 Influence of the Rhine/Meuse river system and the Dutch coastal area

A previously unexplored provenance area is the Rhine/Meuse river system and the Dutch coastal area. Nevertheless, Lacroix (2001) estimated that presently at least 5% of the water in the Belgian North Sea is transported along the Dutch part of the North Sea by coastal transport. Samples of the Dutch continental shelf can clarify the influence of the area and furthermore indicate how far the mudplate extends northeastwards. A characterization of present-day as well as Holocene/late-Pleistocene Rhine and Meuse river samples will indicate their clay mineralogical signal.

IX.6 CARBONATE DISTRIBUTION IN THE MUD DEPOSITS

Although the main focus of this work is clay provenance, also the carbonate fraction might hold valuable information regarding provenance (Fontaine, 2004).
When comparing the amount of carbonate minerals in the fresh muds, the Holocene U6 and U4 deposits, the Pleistocene fluvial deposits and the present-day Scheldt river, it is apparent that the carbonate amounts are highly variable in these different deposits (Table 9.2). Zeelmaekers (2011) also identified significantly less carbonates in the Scheldt estuary compared to the bottom and suspension BCS muds.
The calcareous fossils (>63µm) present in the >63µm fraction of the analyzed samples displayed in Table 9.2, are almost exclusively in-situ and/or recent forms whereas reworked forms are rare (P.Stassen, pers. comm.). As the percentage of the total carbonate content occurring in the fraction >63µm is relatively high in all samples(Table 9.2), this indicates that a very large part of the carbonates is not provenance-related but was formed in-situ. Using quantitative carbonate contents as provenance indicator for the BCS muds is therefore unreliable.

Note that also in the Scheldt estuary in Schelle, calcareous fossils are dominantly of marine origin (foraminifera, echinoderms, ostracods in Table 9.2). The highest carbonate amounts outside the estuary are found in the Scheldt tributary with max. 10%. The discrepancy in carbonate content between the recent bottom muds and the Scheldt estuary and tributaries is consequently controlled by the inflow of marine carbonates and therefore gradually decreases higher in the estuary.

Table 9.2. Total carbonate content, percentage of this total carbonate content occurring in the >32µm fraction, calcareous fossils and diatoms present in different deposits, with almost exclusively recent in-situ forms.

	Total carbonate content	% of total carbonate content in >32µm fraction	Forams (in situ)	Ostracods (in situ)	Echinoderms (in situ)	Bryozoa	Bivalves	Diatoms
Surface mud (Fontaine, 2004)	24%	41%	++	+				++
Late Holocene U6 (RAN23)	20%	50%	++	+	+	+	+	++
Early Holocene U4 (RAN19)	12%	28%	+		+			+
Fluvial MIS-7 (Saalian) (RAN38)	<1%	18%					+	
Scheldt estuary Schelle (EZN41)	14%	44%	++	+	++	+	+	++

Chapter X

Clay mineralogy of selected potential provenance sources

In order to clarify each of the remaining issues discussed in section VIII.5, new samples were collected for clay mineralogical analysis. In this chapter, the samples and their clay mineralogical composition will be discussed after which the provenance potential of each source is evaluated. As many of the clay mineralogical analyses in this research refer back to, or are compared with, the clay mineral analyses of Zeelmaekers (2011), clay models are kept as consistent as possible with the clay models of Zeelmaekers (2011). All the Marine Isotope Stage – datings referred to in this work were interpreted by Verheyden et al. (2013) and F. Bogemans (pers. comm.) based on work in progress.

X.1 THE ENGLISH CHANNEL

X.1.1 Sampling

Suspended Particulate Matter was collected by a through-flow centrifuge present on board of the research vessel R/V BELGICA along 6 tracks. Each sample is a mixture of SPM collected over the entire track indicated on Figure 10.1. By this sampling configuration, the variability of clay mineralogy as a function of distance from the French Coast can also be evaluated. Bottom load material was collected with a Van Veen grab exactly in the middle of each track. Only the clay mineralogy <2µm was determined from these bottom samples. Details of this sampling campaign (2011/18a) can be consulted in the open-access cruise reports at the website of the Management Unit of the North Sea mathematical models.

X.1.2 Bulk mineralogy

The mineralogy of suspension samples in the English Channel is made up by 4 major mineralogical groups: quartz, carbonates, amorphous and 2:1 Al-clays (Figure 10.2). Carbonate minerals comprise mainly calcite but also aragonite, Mg-calcite and traces of siderite and dolomite. Amorphous material consists of diatoms and organic matter. Additionally, the analysis also reveals <5% feldspars, both K-feldspar and plagioclase, and 3-7% halite, which most likely precipitated from the seawater. In comparison with the typical mudplate composition (Figure 10.2), the amount of carbonates is similar but the mudplate contains less amorphous components.

X.1.3 Clay mineralogy <2µm

The clay mineralogical composition of the SPM samples in the English Channel can be subdivided in two categories. There is first the sample east from Calais (RAN104) of which the composition is similar, but not identical, to the average mudplate clay composition. Secondly, the suspension samples west from Calais contain significantly less smectite, varying between 18% and 31% and increased amounts of illite-smectite (34-47%)(Figure 10.3). The clay composition is furthermore relatively homogeneous over the five west-of-Calais samples and shows little or no relation with distance from the French coast.

The clay mineralogy of the bottom samples matches those of the suspended material very well. Although these samples are very sandy and are poor in the clay fraction, their clay mineralogy is also characterized by less smectite (16-30%) and higher illite-smectite contents (35-44%).

X.1.4 Interpretation

These results presented above confirm the results of Zeelmaekers (2011) who stated that sediment sources in the English Channel, either by coastal erosion or by transport through the English Channel (Atlantic ocean), are not the main clay source for the BCS muds. The results of the bottom and suspended samples in the English Channel of Zeelmaekers (2011) are complemented with the new results and compared in a ternary diagram with the clay mineralogical composition of the mudplate on the Belgian Continental Shelf (Figure 10.4). The ternary diagram in Figure 10.4 illustrates quite well how the different provenance areas in the English Channel, such as the Atlantic Ocean, the French coastal sediments, the English coastal sediments and suspended material at different positions in the English Channel, all are characterized by significantly lower smectite contents compared to bottom and suspended samples of the BCS mudplate. Samples plotting closer to the typical BCS muds composition typically are geographically positioned closer to the BCS and therefore probably reflect influence of suspended BCS material rather than the clay signal of an external source.

It was already noticed by Zeelmaekers (2011) that beach coast sediments have the typical BCS mud clay mineralogy to the southwest until Calais, but that further southwestwards the clay mineralogy changes drastically. The clay mineralogical composition of the SPM samples studied in this work (Figure 10.3) shows that this relation is also confirmed not only in beach and coastal sediment but also in marine suspensions.

Zeelmaekers (2011) stated that the main variability in clay mineralogy is found in sediments at the English coast. Some of the samples analyzed by Zeelmaekers (2011) indeed plot very close the BCS surface muds composition (Figure 10.4). The qualitative composition of the clay minerals in these samples was however found to be different to those of the mudplate, which excludes them as major sediment source. It can therefore be concluded that none of bottom and suspended samples analyzed from the English Channel, the coasts or the ocean have a qualitative or quantitative clay mineralogical composition which closely matches the typical mudplate composition on the Belgian Continental Shelf. These sediment sources are therefore not the main clay source of the recent BCS muds. The typical BCS clay mineral composition is not transported from the English Channel but instead that the BCS clay composition extends to Calais and must have a different clay provenance.

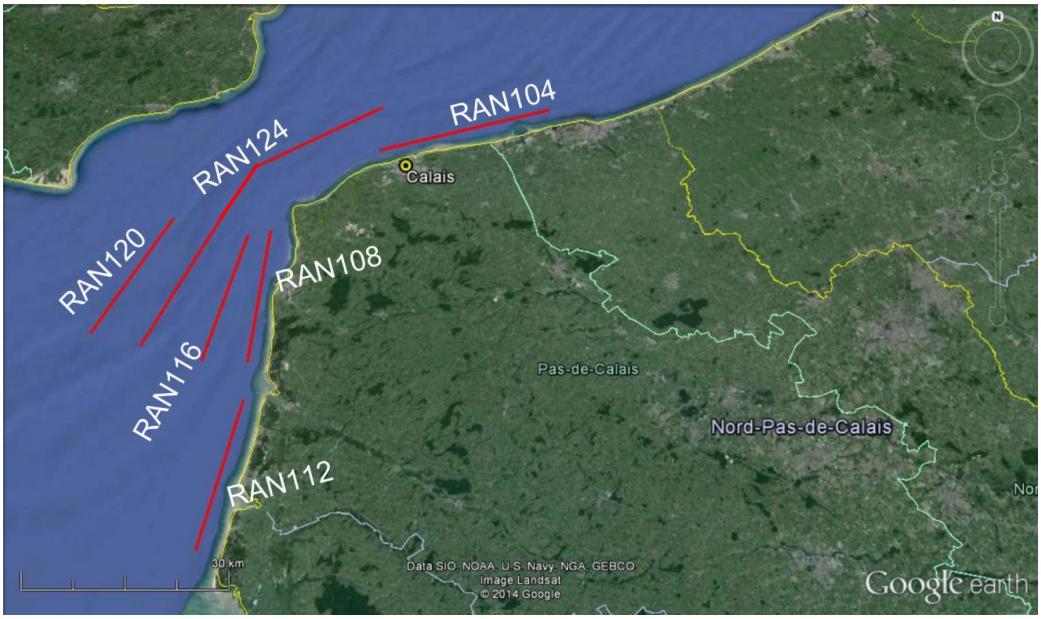

Figure 10.1. Sampling locations in the English Channel and off shore the French coast. Red lines indicate centrifugation tracks on which SPM was collected. At the middle of each track, a bottom load sample was collected with a Van Veen grab.

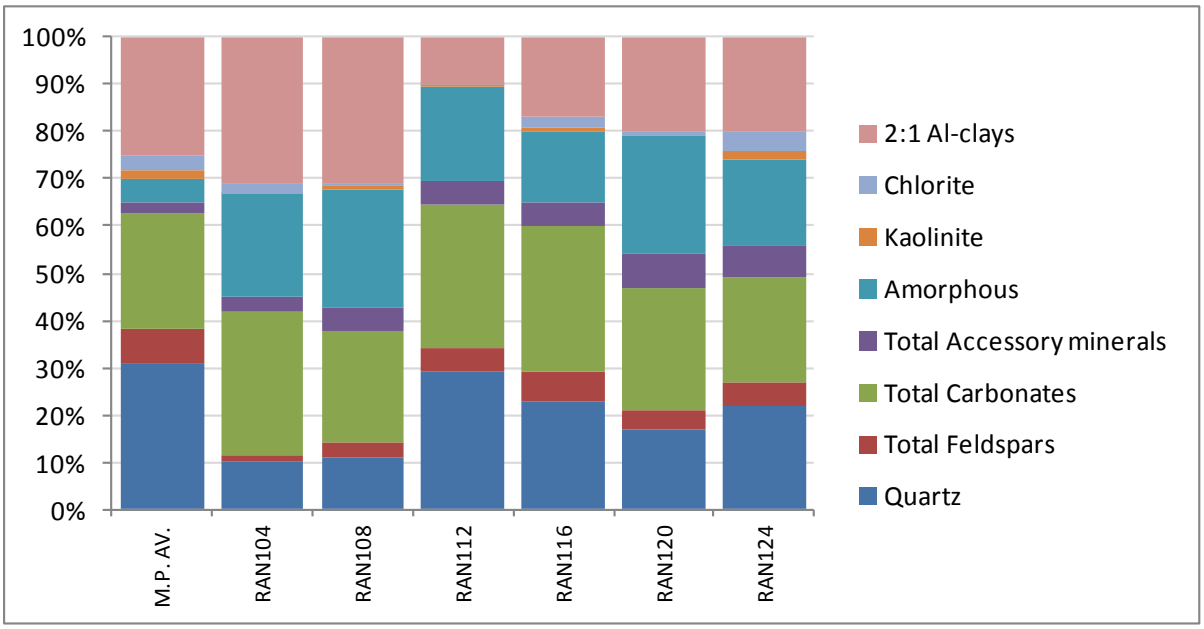

Figure 10.2. Suspension tracks on the French side of the English Channel: quantitative bulk results (in wt%) of individual samples. MP. AV. Indicates the average bulk mineralogical composition of the mudplate on the Belgian Continental Shelf.

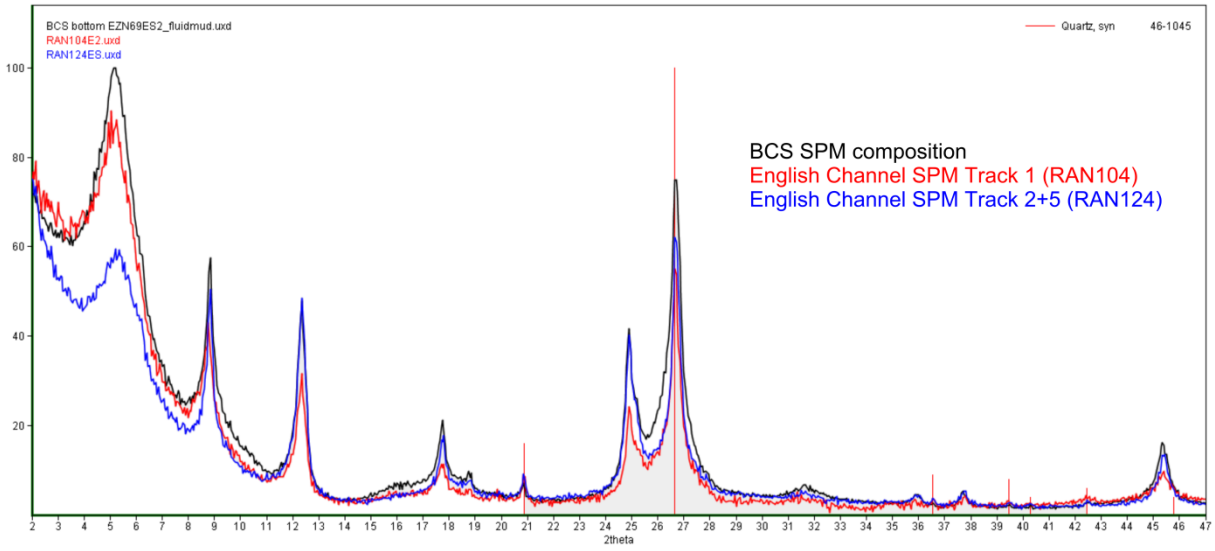

Figure 10.3. Comparison of glycolated oriented diffraction patterns <2µm of typical suspended mudplate composition on the Belgian Continental Shelf and suspension tracks south to southwest of the BCS. Track 1, shown in red, is positioned between the BCS and Calais; whereas track 2+5 is positioned central in the English Channel. The clay mineralogy of the latter contains clearly less smectite than the typical BCS composition. The red line identifies the presence of quartz in the <2µm fraction.

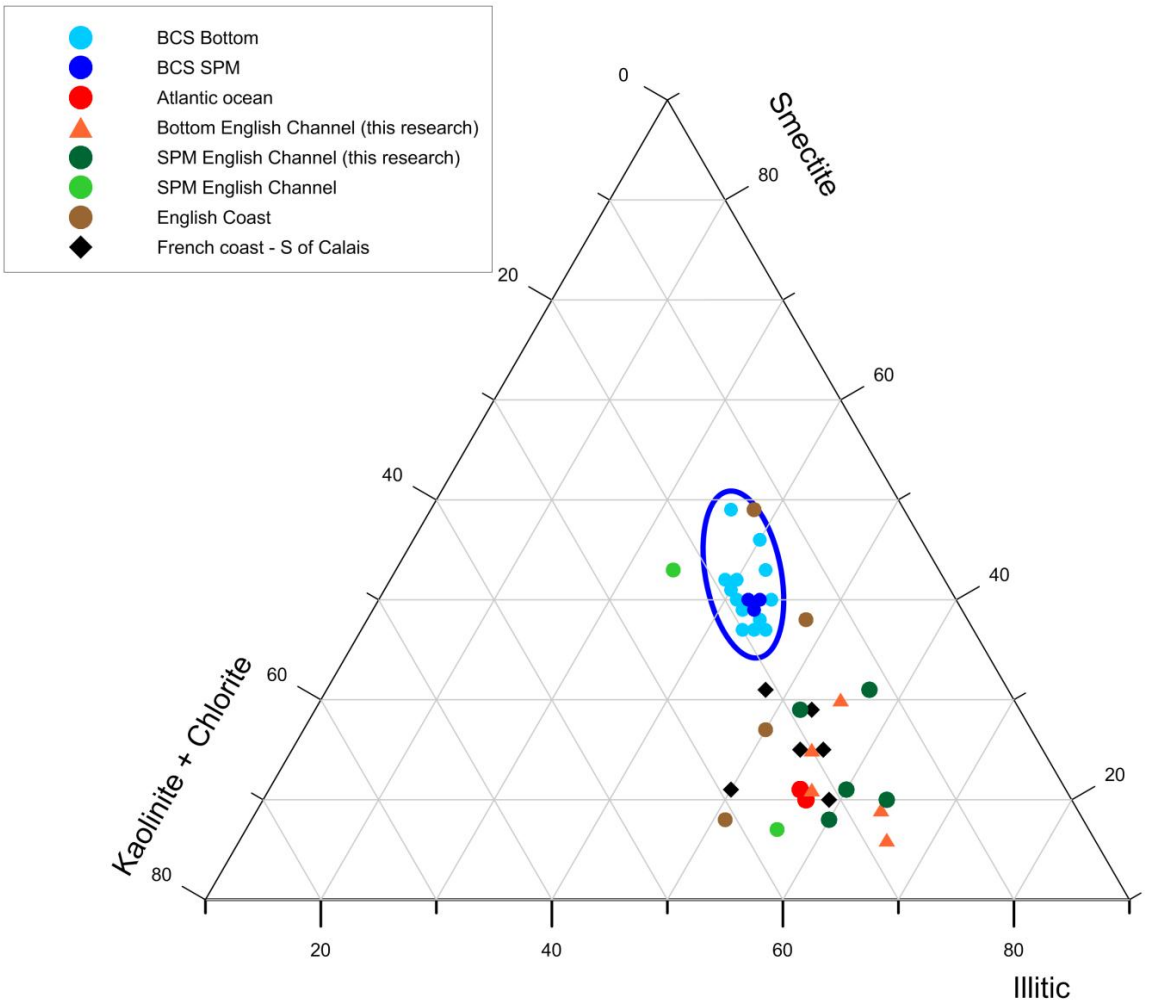

Figure 10.4. Ternary diagram illustrating the clay mineralogical composition of samples on the bottom and in suspension of the mudplate on the Belgian Continental Shelf (in blue) and bottom and suspension samples of different sources in and outside the English Channel. The scale of the ternary diagram was slightly modified to create an improved visualization of the results. Note that the axes of the ternary diagram in indicate “smectite”, “kaolinite+chlorite” and “illitic”, with illitic as the sum of illite and illite-smectite (typically 70:30 proportioned).

X.2 LATE QUATERNARY BELGIAN COASTAL PLAIN CLAY MINERALOGY

X.2.1 Holocene U6 and U4 deposits in the Belgian coastal plain

In the work of Zeelmaekers (2011) only a few samples of the Holocene deposits in the coastal plain are included. In this chapter, a more elaborate sample set consisting of Late-Holocene U6 deposits and Early-Holocene U4 deposits is analyzed for clay mineralogical composition and compared with the present-day surface muds.

X.2.1.1 Sampling

Samples of the Holocene seismostratigraphic units U4 and U6 (Mathys, 2009) were collected in four different offshore borehole locations: Stroombank SB1, Stroombank SB2, Grote Rede Gr1 and a location between the shore and the Wenduinebank SBW (Figure 10.5 and Figure 10.6). These boreholes were available for sampling from the stratigraphical collection of the Geological Survey of Belgium. In total 16 clay samples were collected of the early Holocene tidal U4 unit and the late Holocene U6 BCS mudplate deposits (Figure 10.5). The hypothesis formulated by Zeelmaekers (2011) is that these deposits have an identical clay mineralogy to the BCS bottom and suspension samples.

X.2.1.2 Bulk mineralogy

The bulk analyses show that almost 90% of the U6 deposits is made up by quartz, carbonate minerals (mainly calcite and minor aragonite, dolomite and Mg-calcite) and 2:1 Al-clays. Amorphous matter is present in the form of organic carbon and amorphous silica. The group accessory minerals consists mainly of halite and sulphides (pyrite) and sulphates (gypsum).
This composition matches very well with the typical bulk mineralogical composition of the recent weakly consolidated muddy deposits on the BCS (Figure 10.7).
The bulk mineralogy of the investigated U4 deposits is on average less clay-rich than the U6 and the recent mud deposits, and contain slightly less carbonates. Instead, quartz and feldspars are relatively more important (Figure 10.7).

X.2.1.3 Clay mineralogy <2µm

The clay mineralogical results of the Holocene U6 and U4 deposits show that these deposits are characterized by very similar clay compositions (Figure 10.8). On average, the smectite content in the U6 samples is 36% whereas it is 34% in the U4 deposits. Concerning illitic minerals, the U6 samples contain on average 29% illite-smectite and 18% illite. In the U4 samples, the average illite-smectite content is slighty lower (26%) and illite content slightly higher (23.5%). Both clay compositions are furthermore very similar to the BCS mud composition (Figure 10.8). When plotting the different clay mineralogical results in a ternary diagram together with the recent mud and suspension compositions (Figure 10.9), it can be observed that the Holocene deposits are slightly more illitic, and therefore contain less smectite, but the difference is very small. This small difference is mainly caused by the fact that illite-smectite mixed-layers are somewhat more abundant in the U4 deposits, and to a lesser degree in the U6 deposits, compared to the typical bottom and suspended composition on the BCS.

X.2.1.4 Interpretation

Although individual samples of the U6 and U4 deposits appear to be very similar in clay mineralogy to the present-day bottom and suspension samples, comparing averages of each group of samples reveals that the Early Holocene U4 samples have a higher illitic/smectite ratio compared to the recent deposits (Figure 10.10). Samples of the U4 unit contain on average 7%, and those of the U6 unit on average 4.5%, more smectite than the present-day bottom muds. It seems moreover that the clay composition has gradually evolved in time, as the U4, U6 and recent deposits line up (Figure 10.10) illustrating a gradually lower illitic/smectite ratio with time evolution.

Figure 10.5. Photograph of the U4 tidal unit in the Stroombank 2 core from 12.70m until 12.95m showing a strong tidal character of the sediment with alternating sand and clay laminae. Depths were measured from the top of the core.

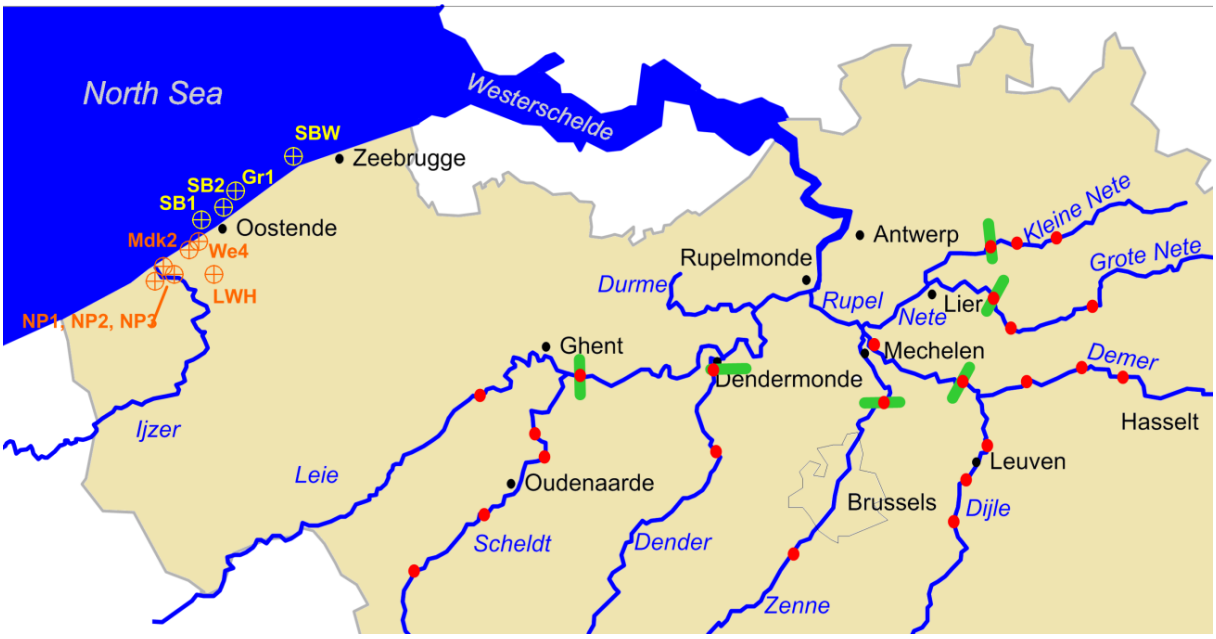

Figure 10.6. Overview of the flow area of the Scheldt river system. Black dots indicate place names. Green stripes indicate SPM sampling locations and red dots indicate bottom or riverbed sampling locations. Yellow markers indicate Holocene samples of offshore borehole locations SB1 Stroombank, SB2 Stroombank, SBW Wenduinebank and Grote Rede Gr1. Orange markers indicate borehole locations where Pleistocene deposits were sampled: Nieuwpoort 1,2,3 (NP1, NP2, NP3), Westende 4 (We4), Middelkerke 2 (Mdk2) and Leeuwenhof (LWH).

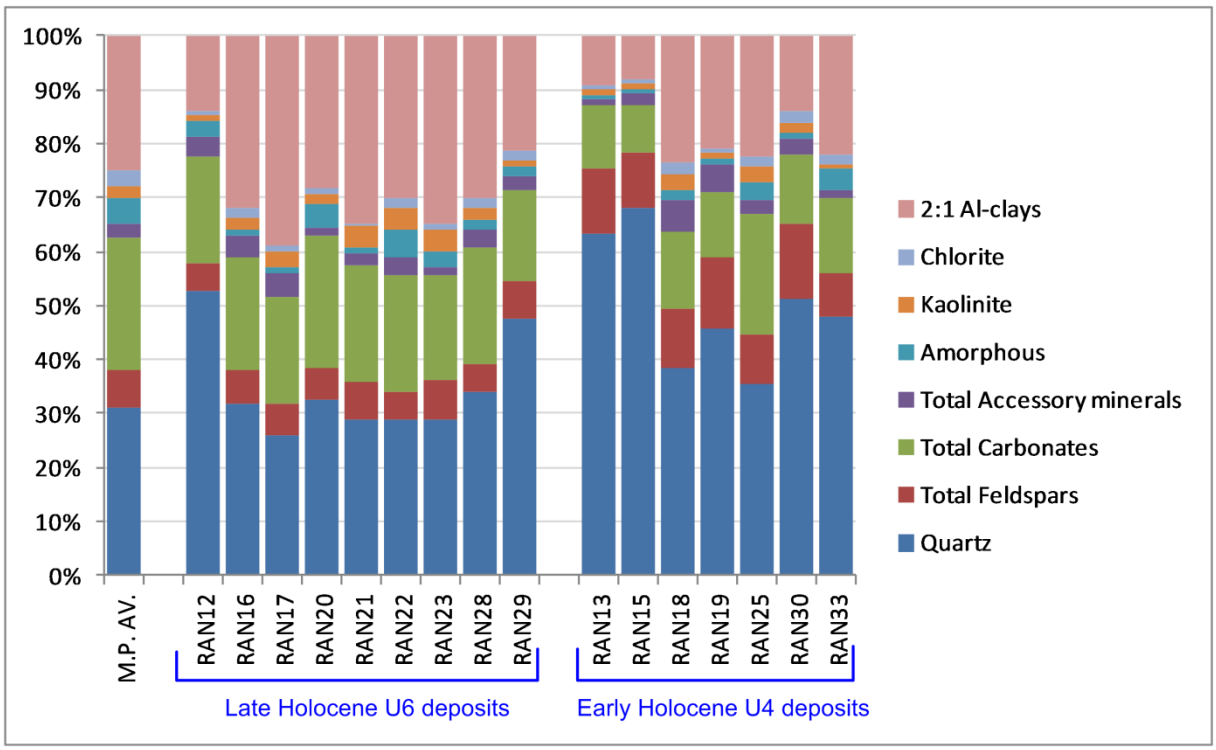

Figure 10.7. Early Holocene U4 and Late-Holocene U6 deposits: quantitative bulk results (in wt%) of individual samples. M.P. AV. represents the average composition of the BCS mudplate, i.e. the recent muddy bottom deposits.

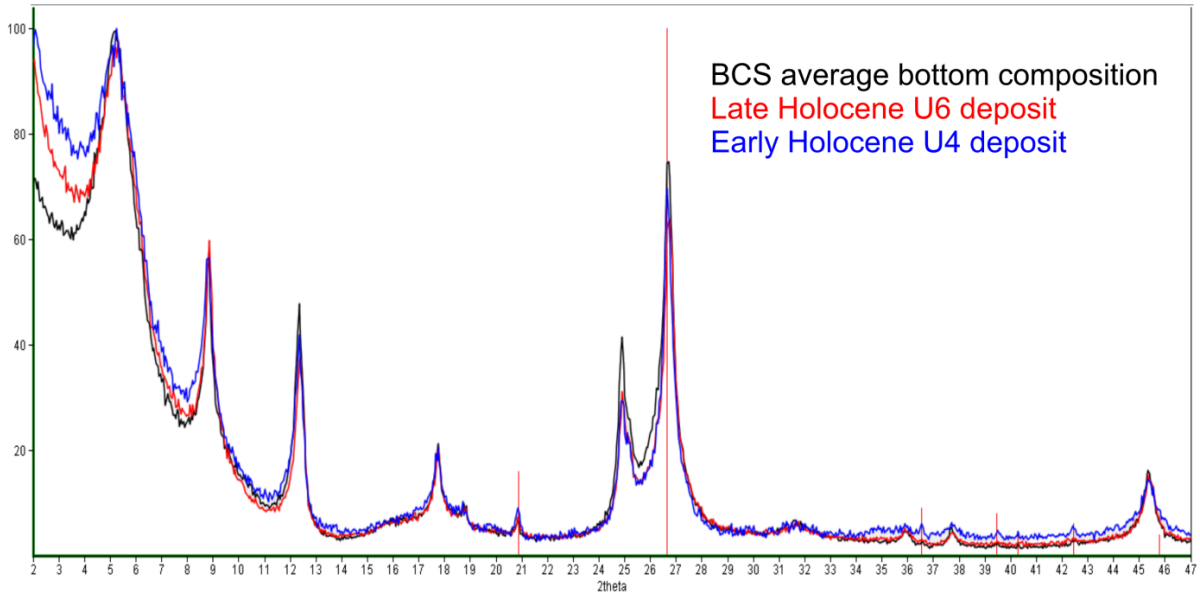

Figure 10.8. Glycolated oriented diffraction patterns <2µm of a typical U6 and U4 deposit in relation to the average bottom mud composition on the BCS. The red lines identify the presence of quartz <2µm.

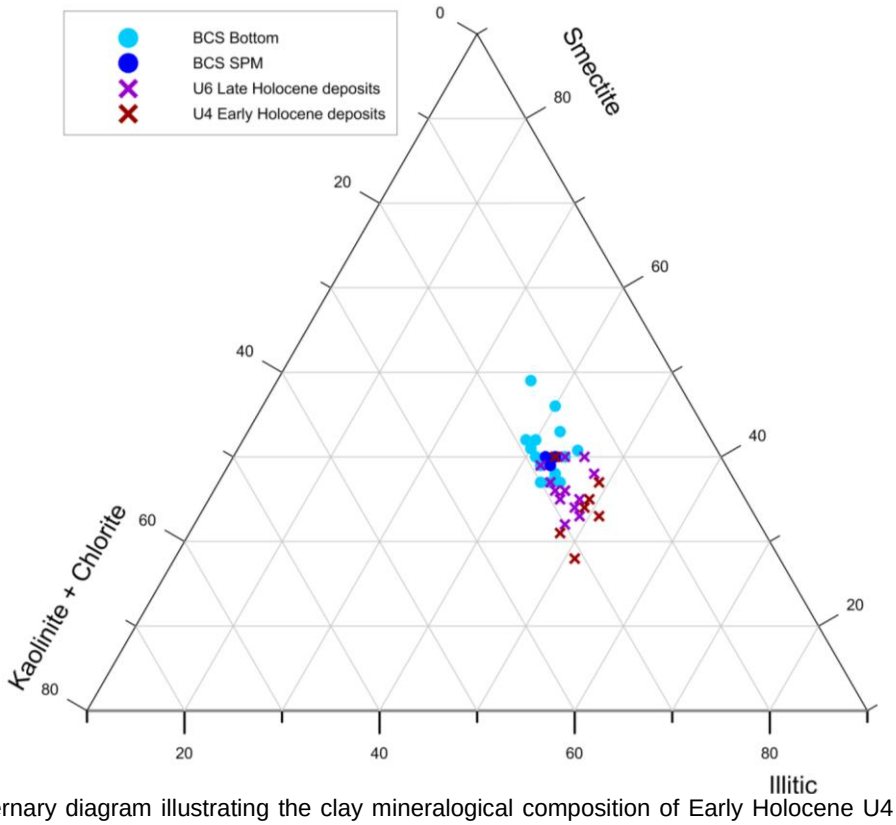

Figure 10.9. Ternary diagram illustrating the clay mineralogical composition of Early Holocene U4 samples (red crosses), Late Holocene U6 samples (purple crosses) and of the bottom and suspension samples of the Belgian Continental Shelf (blue dots). The scale of the ternary diagram was slightly modified to create an improved visualization of the results. Note that illitic represent the contribution of illite and illite-smectite.

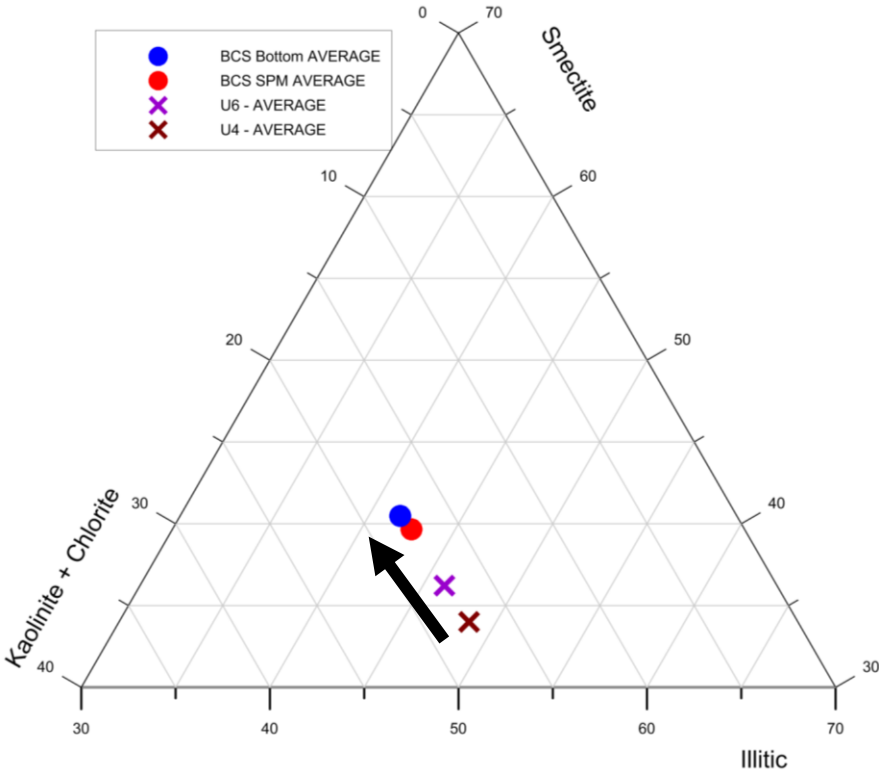

Figure 10.10. Ternary diagram illustrating the average clay mineralogical composition of Early Holocene U4 samples (red crosses), Late Holocene U6 samples (purple crosses) and of the bottom and suspension samples of the Belgian Continental Shelf (blue and red dots). The black arrow indicates a timeline.

X.2.2 Pleistocene deposits in the Belgian coastal plain

Zeelmaekers (2011) analyzed the clay mineralogy of intertidal flat deposits, which were than assumed of MIS-5e (Eemian) age but are now reinterpreted as MIS-5d (early-Weichselian) with only the lowermost sample of the Leeuwenhof core of MIS-5e (Eemian) age (F.Bogemans, pers. comm.). The clay composition of these samples is almost identical to the BCS mudplate composition (Zeelmaekers, 2011). It is suspected that the recent BCS clay mineralogy has already been installed during the Mid-Pleistocene, starting from the moment when the Paleo-Scheldt river system occupied the Flemish Valley and discharged in westward direction. Presumably this occurred for the first time during the Elsterian (~MIS12) around 450.000 years BP after the breakthrough of the proglacial lake (Gibbard, 2007; Toucanne et al., 2010). To test this hypothesis, post-Elsterian Pleistocene clay-rich deposits in the coastal plain with a reliable stratigraphy and facies interpretation should be sampled and analyzed. Pleistocene deposits in the coastal plain older than Saalian (MIS6-MIS 8) are however scarce.

X.2.2.1 Samples

Although the Pleistocene subsurface of the Belgian coastal area is a complex sedimentary system of which the stratigraphy is difficult to unravel and interpretation often open for discussions, continuous research (Baeteman et al., 2002; Mathys, 2009; Verheyden et al., 2013) allows for an improved stratigraphy of these deposits. Late Pleistocene deposits were sampled in 5 boreholes, Nieuwpoort 1, 2 and 3, Middelkerke 2 and Westende 4 (all indicated in orange on Figure 10.6). The majority of the sampled clay material has an intertidal to subtidal character and is correlated to Marine Isotope Stage 7, part of the Saalian glaciation period. Two subtidal clay samples of the Westende 4 well (13.70m-RAN46 and 13.80m-RAN47) have an MIS-5e signal (Eemian interglacial). One sample in the Nieuwpoort 1 well (12.10m – RAN38) has a clear fluvial character but most likely was deposited in a primary tidal environment during MIS 7. One additional clay sample in the Westende 4 well (11.58m – RAN45) is most likely younger than MIS5e, and therefore dates from the Weichselian glacial period. This sample originates from a fluvial channel deposit with slight tidal influence (Frieda Bogemans, pers. comm.). Two additional samples were collected in the Nieuwpoort-3 well of the Ypresian clay occurring a few meters below the Pleistocene deposits.

X.2.2.2 Bulk mineralogy

The mineralogical composition of almost all investigated samples (Figure 10.11) consists of mainly quartz (ca. 50%) and 2:1 Al-clays (ca. 25%). Feldspars are also relatively abundant (>10%) whereas carbonates are present in amounts <5%. Sample RAN45 is unusual because of its relatively high chlorite content (7%) and relatively high amounts of albite (11%) as opposed to lower microcline content (4%). Amorphous contents are generally very low (<0.5%).

X.2.2.3 Clay mineralogy <2µm

The clay mineralogical results of the investigated samples can roughly be subdivided in two categories. The first group includes all tidal MIS-7 (Saale) and MIS-5e (Eemian) samples which show very low variability in clay composition. All such samples are characterized by a very smectite-rich (>70%) composition <2µm. Illite-smectite mixed-layers occurs in proportions from 11-17%. Kaolinite layers only occur mixed-layered with smectite layers in a low abundant kaolinite-expandable structure (Figure 10.13). Chlorite is present in trace amounts as evidenced by the very weak reflection at 13.72Å after heating (Figure 10.12). Figure 10.13 demonstrates the clay model fit and quantification of a representative sample of this group. Remarkably, the composition on these samples is almost exactly the same as the clay composition encountered in Ypresian clays, which occur directly below the Pleistocene deposits in these boreholes. The high degree of similarity between these Paleogene clay compositions and the Pleistocene tidal clay compositions is evidenced by comparing their diffraction patterns (Figure 10.14).

The composition of the second group of samples significantly deviates from these smectite-rich tidal deposits. The clay mineralogy <2µm contains significantly less smectite, no kaolinite-expandable and more chlorite (Figure 10.15). Samples of this group are fluvial MIS-7 and pre-MIS5e fluvial channel deposits. Although the samples of fluvial MIS-7 contains slightly more smectite, their composition is very similar to the typical BCS mudplate composition (Figure 10.16 and Figure 10.17). The pre-MIS-5e (probably

Weichselian) sample contains clearly less smectite but contains up to 11% of chlorite (Figure 10.18).

X.2.2.4 Interpretation

The results of the different investigated Pleistocene samples allow an interpretation in relation to the provenance of the North Sea muds. The specific clay composition of the MIS-7 and MIS-5e tidal deposits, i.e. highly smectitic, the presence of kaolinite-expandable and the low variability in quantitative composition clearly links the composition of these samples to the Ypresian clays, occurring directly below the Pleistocene deposits (Figure 10.14). It is therefore most likely that Ypresian clay material was reworked in these tidal Pleistocene deposits. In a ternary diagram, these latter samples plot far away from the typical BCS composition (Figure 10.19) but instead plot very close to Ypresian clay samples and the clay composition of the currently outcropping Paleogene deposits in the northern part of the BCS.

In contrast, the MIS-7 deposits interpreted as fluvial dominated contain clearly less smectite in the <2µm fraction. These samples all occur shallower than 13m depth and plot close to, or even within, the compositional field of the BCS muds in a ternary diagram (Figure 10.19). Remarkably is that when the vertical succession in the Nieuwpoort 1 well is considered, the smectite content gradually decreases with height and therefore also with the change in sedimentary environment from tidal to fluvial (Figure 10.19). Such a relation suggests that in the tidal environments during the MIS-7 and MIS-5e periods (Saale – Eemian) the sediment material was mainly derived from Ypresian clay erosion but also that the fluvial sediment source during these times had a clay composition which very closely resembled that of the current mudplate on the BCS. In Figure 10.19, the decreasing smectite trend observed in the Nieuwpoort-1 well might therefore represent a mixing of clay compositions ranging from locally eroded smectite-rich intertidal estuarine conditions and, the typical BCS clay composition supplied by a fluvial system.

During MIS-5d (Weichselian glacial period), both fluvial (current RAN45) and intertidal clay deposits (Zeelmaekers, 2011) have a clay composition which matches the BCS mudplate composition (Figure 10.19) and the smectite-rich typical Ypresian clay composition is not preserved anymore in tidal flat deposits. It has to be noted however that the composition of sample RAN45 deviates slighty with a relatively high chlorite and plagioclase content. This might be related to the influence of chlorite-rich eolian sediment sources in northern Europe, which during glacial periods influence the composition of these deposits (see analyses of eolian cover sands in Zeelmaekers (2011)).

Nevertheless, these new results strongly suggest that the recent BCS mud composition was already installed during the Saalian, MIS-7, and that a fluvial source for these deposits is the most probable. Although the analysis of deposits older than MIS-7, e.g. Holsteinian and Elsterian, would make an even stronger case, still the results presented and discussed in this section strongly suggest that a fluvial system, most likely the Paleo-Scheldt system, discharged the clay minerals to form the clay mineral composition found in the particular mid- to late-Pleistocene fluvial deposits analyzed in this work.

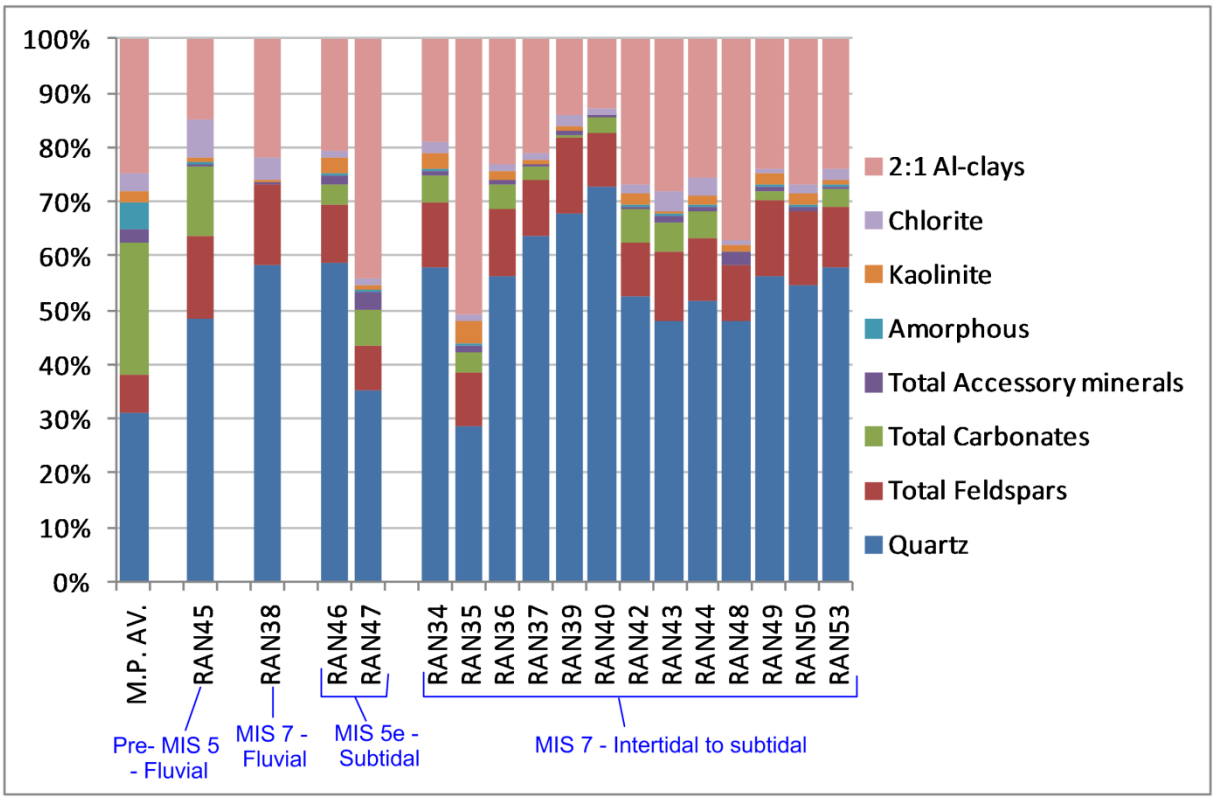

Figure 10.11. Pleistocene fluvial and tidal deposits in the Belgian coastal plain: quantitative bulk mineralogy in wt% of individual samples.

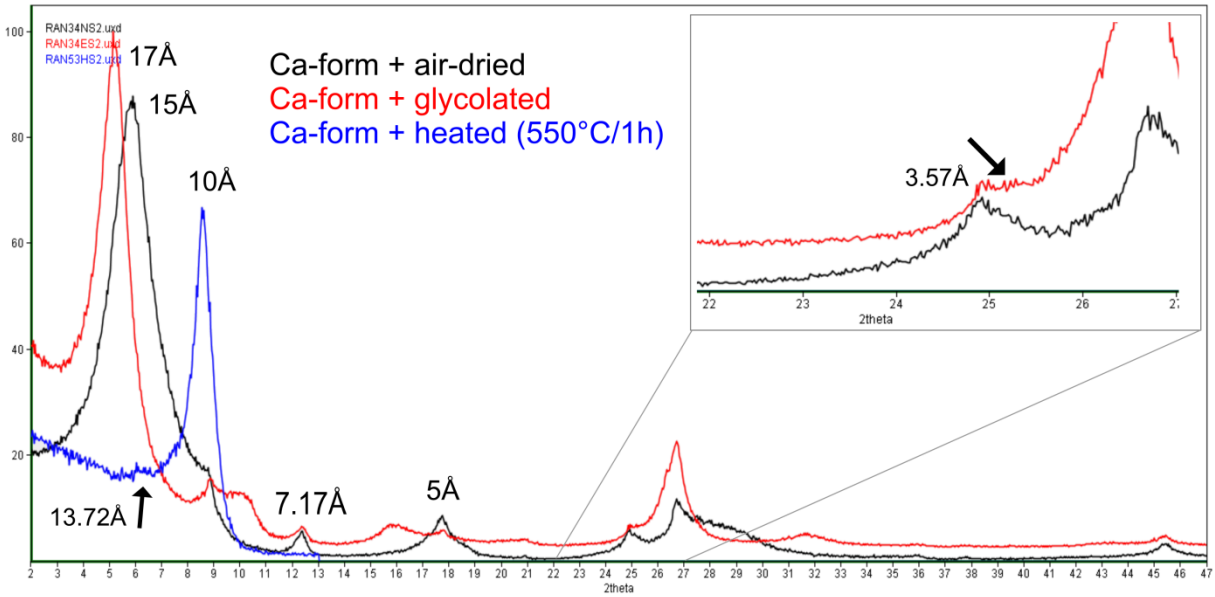

Figure 10.12. Tidal MIS-7 deposits: air dried, glycolated and heated diffraction patterns <2µm illustrating the occurrence of predominantly smectite of sample RAN34. The left arrow indicates the marginal presence of chlorite after heating whereas the zoomed in area and arrow on the right illustrates the mixed-layered nature of the kaolinite-expandable (85:15) structure with a shift of the 002-005 reflection to higher angles as a response to glycolation.

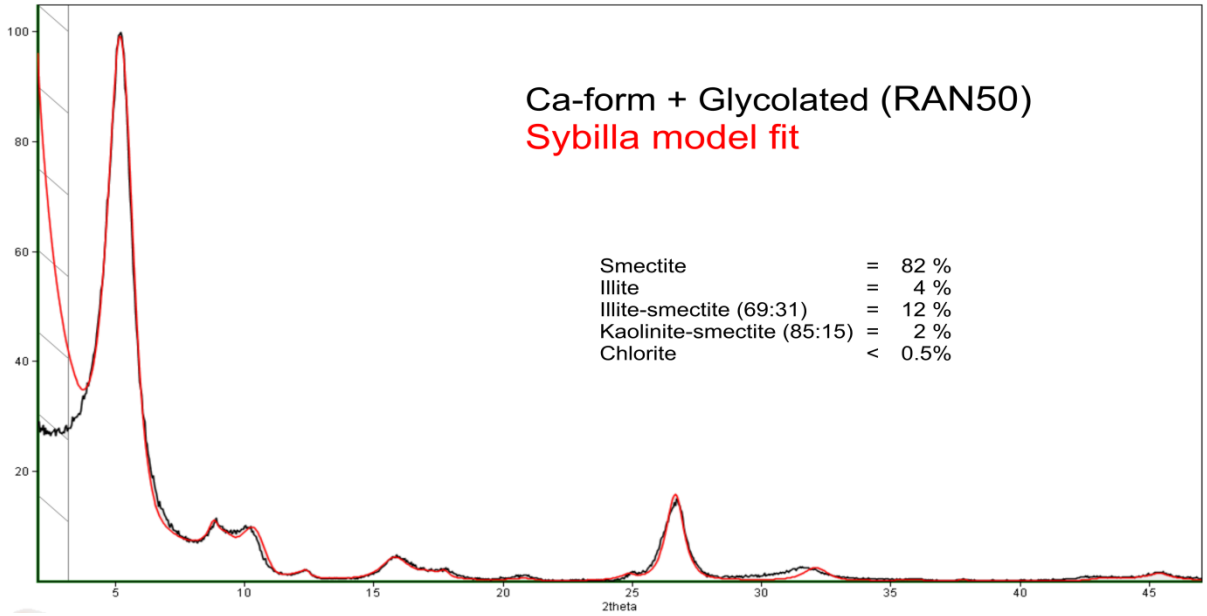

Figure 10.13. Glycolated oriented diffraction pattern <2µm of sample RAN50 (in black) and Sybilla clay model fit (red).

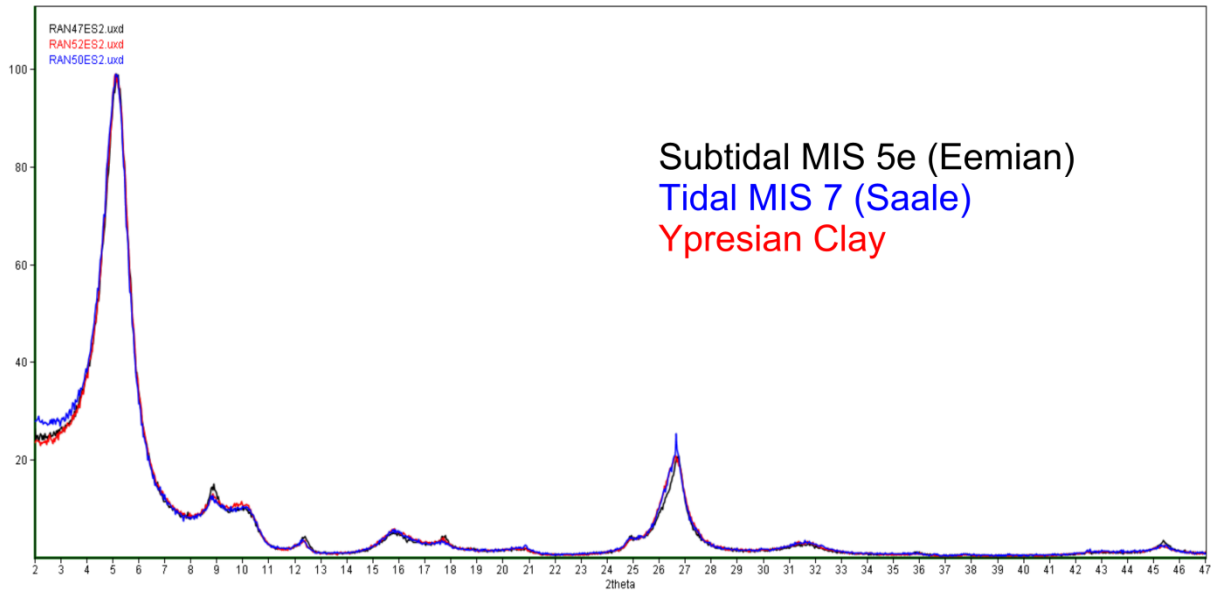

Figure 10.14. Comparison of glycolated oriented diffraction patterns <2µm of subtidal MIS 5e (black), tidal MIS7 (blue) and Ypresian clay sample (red). All three samples produce exactly the same diffraction pattern and suggest a relation.

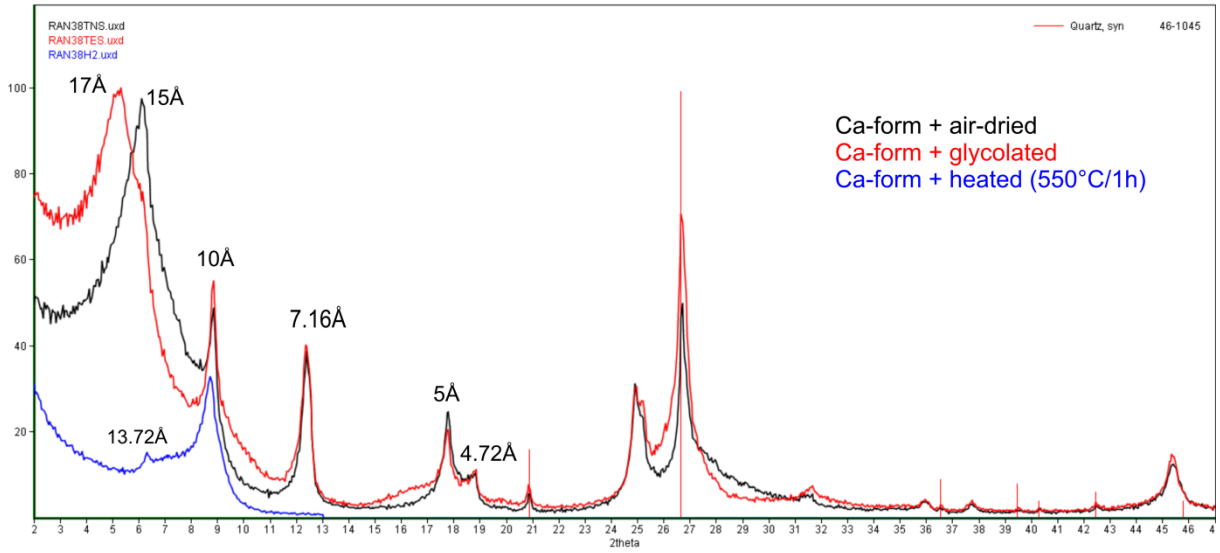

Figure 10.15. Fluvial MIS-7 deposits: air dried, glycolated and heated diffraction patterns <2µm of sample RAN38.

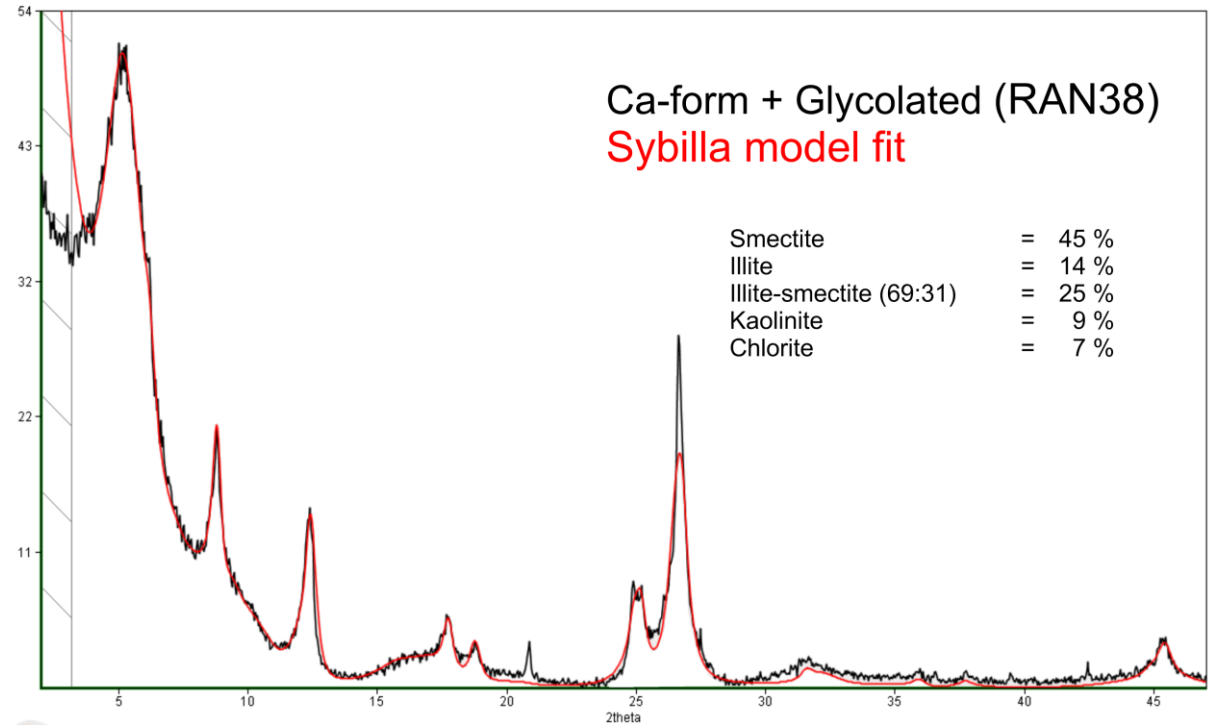

Figure 10.16. Glycolated oriented diffraction pattern <2µm of fluvial MIS-7 sample RAN38 (in black) and Sybilla clay model fit (red).

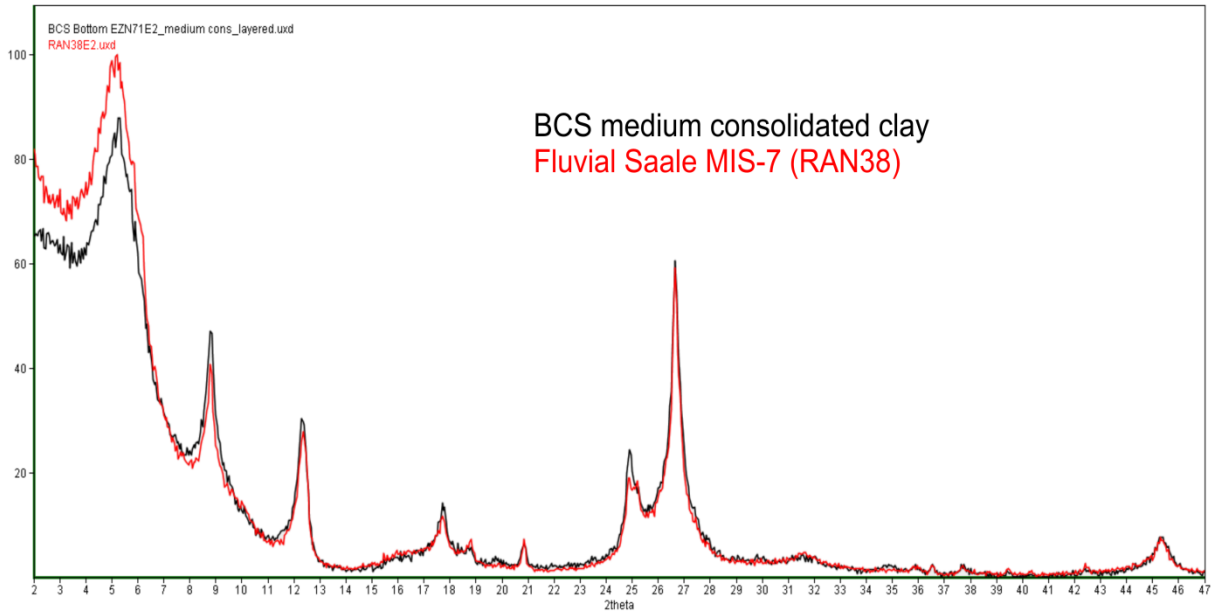

Figure 10.17. Glycolated oriented diffraction patterns <2µm of BCS medium consolidated mud and a fluvial MIS-7 sample from the Nieuwpoort-1 well (RAN38).

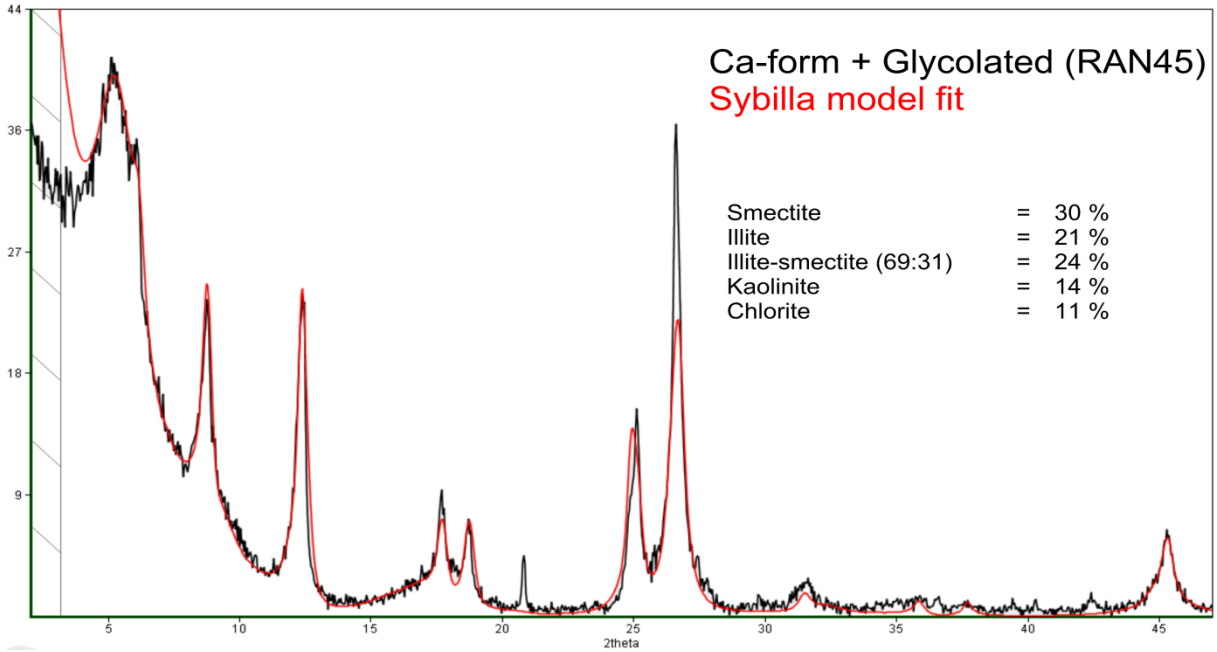

Figure 10.18. Glycolated oriented diffraction pattern <2µm of fluvial channel deposit sample of pre-MIS-5e age: RAN45 (in black) and Sybilla clay model fit (red).

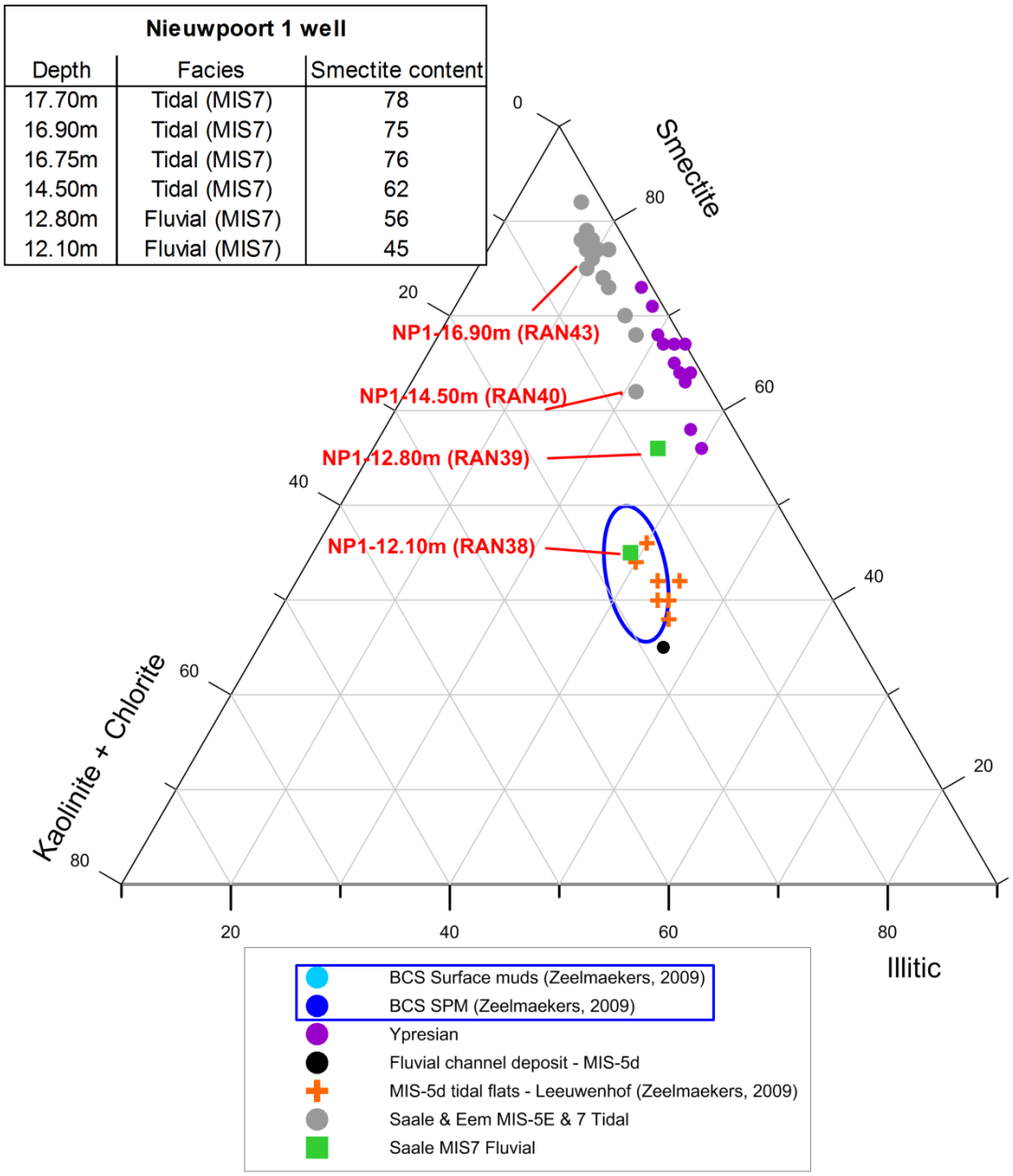

Figure 10.19. Ternary diagram of clay mineralogy <2µm comparing the typical BCS mud and suspension (blue ellipse) composition to the compositions of different Pleistocene deposits in the Belgian coastal plain. The table on the left side illustrates the increasing smectite with depth in the Nieuwpoort 1 well accompanied with facies change. Four of these samples have also been indicated on the ternary diagram in red.

X.3 THE DUTCH COASTAL PLAIN MINERALOGY

Zeelmaekers (2011) demonstrated that the present-day BCS clay composition can be found south of the BCS until Calais. A possible extension to the north, in Dutch coastal waters, was not yet investigated. In this chapter, appropriate samples will be analyzed in order to study this possible northern extension.

X.3.1 Sampling

Suspended sediment samples were collected along four tracks along the Dutch coast using the RV Belgica (campaign 2011/26). The exact location of the SPM tracks is illustrated on Figure 10.20.

X.3.2 Bulk mineralogy

Bulk mineralogy of the four SPM samples (Figure 10.21) shows a composition which is very similar to that of the recent muds on the Belgian Continental Shelf. In general, the clay content and amorphous content are slightly higher but the overall mineralogical composition of the analyzed samples is very similar.

X.3.3 Clay mineralogy <2µm

The clay composition <2µm of the sampled offshore locations shows a close match with the BCS clay composition with 38-46% smectite, 22-26% illite-smectite, 13-17% illite, 12-18% kaolinite and 3-5% chlorite. Variability is generally low but observed differences seem to be linked to geographical position. Remarkable is that the SPM samples with the most smectite (44-46%) are positioned near the Belgian Continental Shelf mud area, whereas the two more northern SPM tracks are the least smectitic (38-39%) (Figure 10.22).

X.3.4 Interpretation

From these results, it seems that the mudplate composition is not restricted to the Belgian part of the North Sea but extends up north to the Dutch coastal area. It could be interpreted that Dutch marine or fluvial sources might have contributed to the clay composition of the BCS muds. However, present-day tidal movements mainly transport water, and thus suspended sediment, in northeastern direction. It is therefore more likely that the Dutch SPM composition is an extension of the SPM above the Belgian mudplate rather than the reversed situation. This idea is supported by the more variable composition further away from the BCS mudplate.

Figure 10.20. Present-day geographical overview of the sampling of clay-rich bottom load, suspension load and boreholes containing recent, Holocene and Pleistocene deposits. Holocene samples are Early and Mid-Holocene Rhine deposits whereas the Pleistocene samples are Mid-Pleistocene Maas samples.

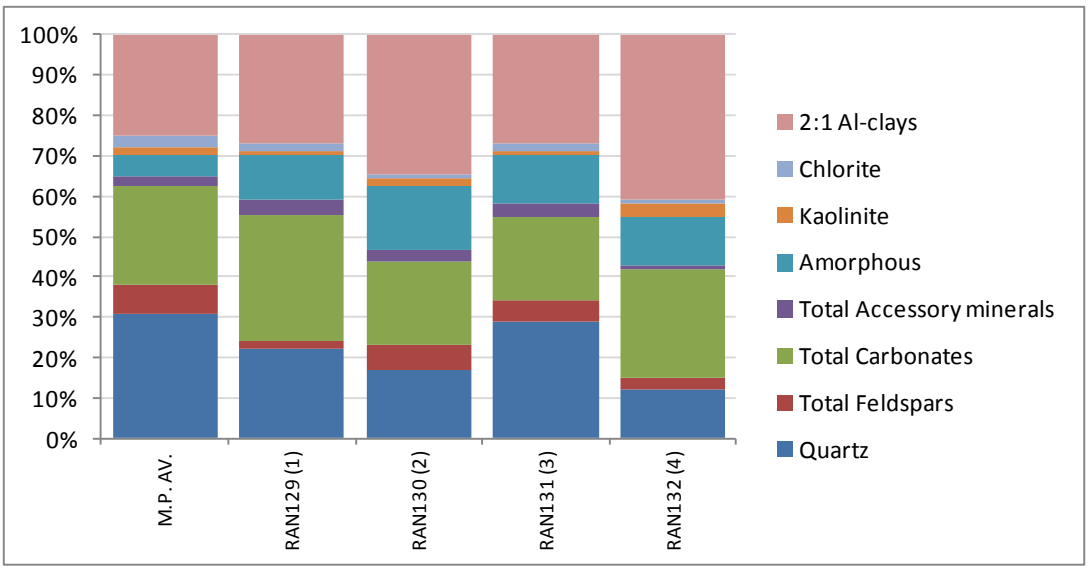

Figure 10.21. Dutch coastal SPM samples: quantitative bulk results (in wt%) of individual samples. M.P. AV. represents the average composition of the BCS mudplate, i.e. the recent muddy bottom deposits.

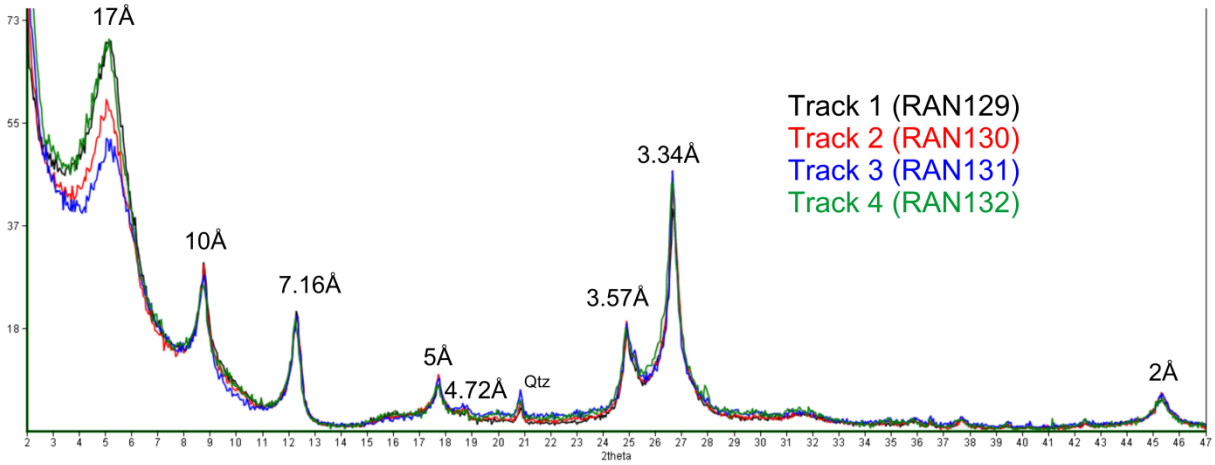

Figure 10.22. Dutch coast SPM samples: diffraction patterns of <2µm clay fraction measured on oriented slides. It is apparent that the two samples positioned closest to the BCS are characterized by higher smectite contents (see intensity of 17A-peak) compared to the more northern positioned samples.

X.4 RHINE-MEUSE RIVER SYSTEM: RECENT AND QUATERNARY CLAY MINERALOGY

One of the sediment sources which was not studied before in this context, is the Rhine-Meuse river system. Nevertheless, according to Lacroix et al. (2004) at least 5% of Rhine waters reach the Belgian Continental Shelf. It is also important to study Holocene and late-Pleistocene Rhine-Meuse deposits as in sections IX.2 and IX.3 it was demonstrated that the present-day BCS clay composition is found in Holocene and middle- to late-Pleistocene fluvial deposits on the Belgian Continental Shelf. As the Rhine-Meuse River system delivered a large mass of sediments to the southern North Sea during the glacial periods of late-Pleistocene, these deposits could possibly be reworked during the interglacials, e.g. the Holocene (Busschers, 2007). In this section, the clay mineral composition of the Rhine-Meuse system is studied from recent as well as Holocene and mid-Pleistocene deposits.

X.4.1 Samples

Present-day river samples were collected from 1994 surface samplings of the upstream Meuse and Waal rivers, indicated M1, M2 and W1 and W2 on Figure 10.20 (H. Middelkoop, pers. comm.). Holocene and mid-Pleistocene Rhine/Meuse samples were collected from drilling cores from the TNO/Deltares stratigraphic collection (Figure 10.20).

X.4.2 Bulk mineralogy

The bulk mineralogical composition of the different analyzed samples is schematized in Figure 10.23. It is apparent from this figure that the composition of the recent river sediment is very similar to that of the BCS muds, although carbonates are slightly deficient. Carbonate minerals are furthermore almost completely absent in Holocene Rhine deposits which also contain elevated amounts of amorphous components. Samples of the Mid-Pleistocene Meuse river are slightly enriched in quartz compared to more recent samples but do contain carbonate minerals although still in smaller amounts compared to the BCS muds (Figure 10.23).

X.4.3 Clay mineralogy

The clay mineralogical composition of the recent Meuse and Waal samples (Figure 10.24) is characterized by fairly low smectite contents (19-23%). The composition of both rivers is nearly identical with a dominant illite and illite-smectite mineralogy and relatively

high kaolinite and chlorite amounts. Also the clay mineralogy of the Holocene Rhine river samples and Mid-Pleistocene Meuse river samples contains relatively low smectite amounts (Figure 10.25). The Holocene Rhine ranges between 23 and 31% smectite whereas the Mid-Pleistocene Meuse deposits even contain less smectite, ranging from 13% to 24%. Compared to the more recent deposits, the clay composition contains ca. 10% less kaolinite and chlorite minerals.

X.4.4 Interpretation

The results of the recent bottom sediments in both the Meuse and Rhine rivers demonstrate that the clay composition of these rivers is significantly different from that of the Scheldt river system and the BCS muds. The clay composition of Early-Holocene Rhine and Mid-Pleistocene Meuse deposits are relatively similar to the more recent deposits with smectite contents varying between 20 and 30%. Therefore, this river system is, neither today nor in the past, a main clay supplier of the fine-grained muds at the BCS. The relatively low amount of smectite discharged by the Rhine-Meuse system could however explain the slightly less smectite-rich clay mineralogy of suspension material north of Rhine river mouth along the Dutch coast (see Figure 10.20 and Figure 10.26).

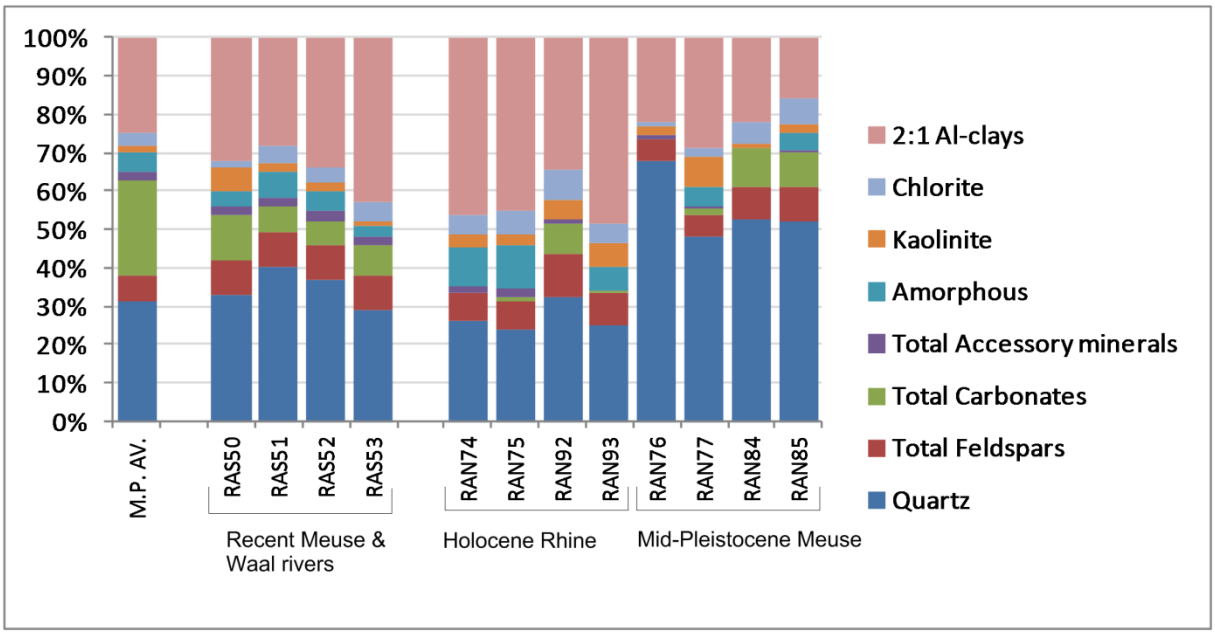

Figure 10.23. Recent Meuse and Waal, Holocene Rhine and Mid-Pleistocene Meuse: bulk mineralogical composition and comparison with the average mineralogical composition of the BCS muds.

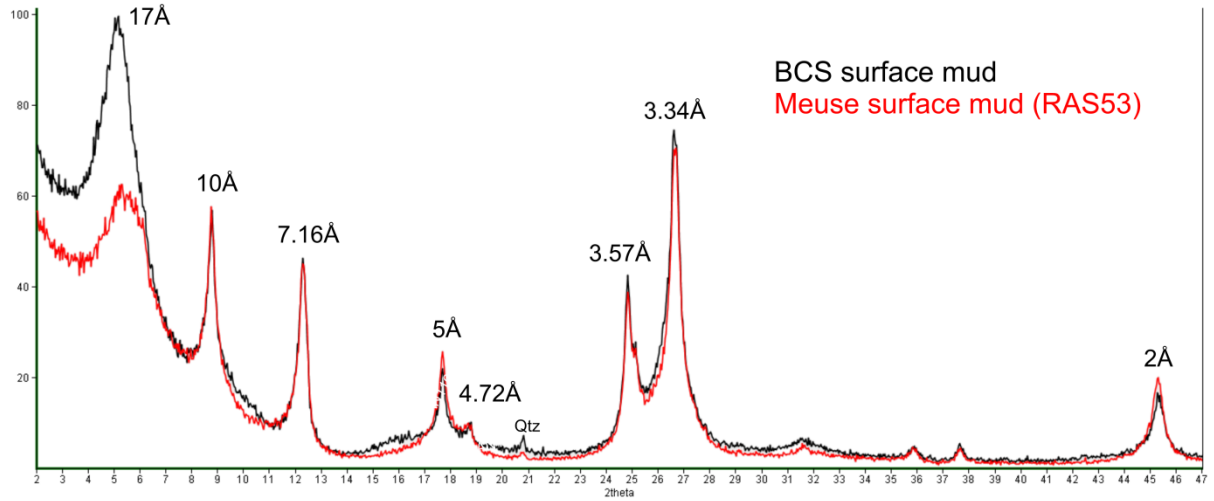

Figure 10.24. Present-day Meuse surface mud (RAS53): diffraction pattern of <2µm clay fraction measured on oriented slides. It is apparent from this figure that the Meuse composition has clearly less smectite minerals in its clay fraction compared to the BCS muds.

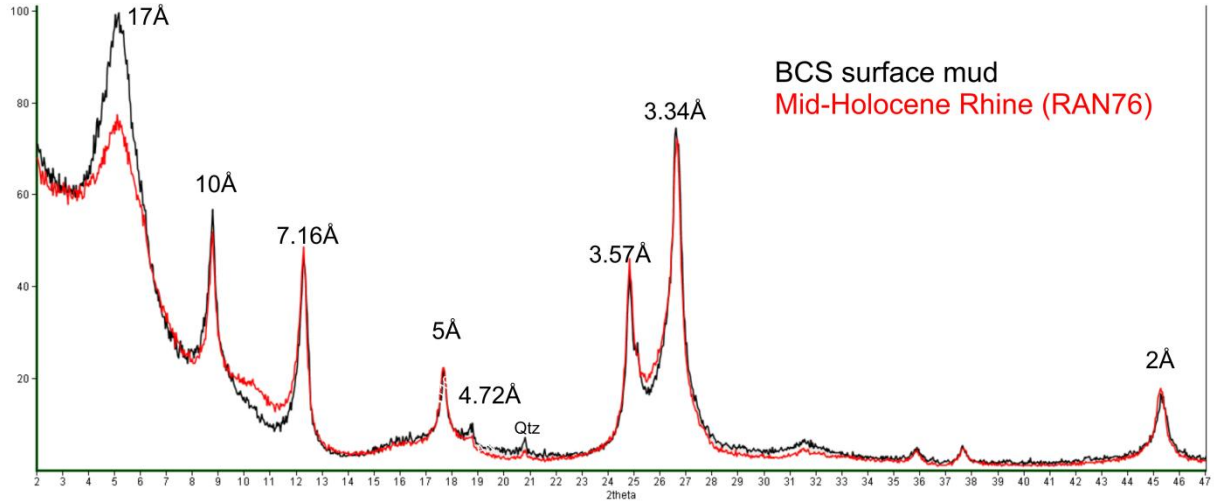

Figure 10.25. Mid-Holocene Rhine (RAN76): diffraction of <2µm clay fraction measured on oriented slides. Similar to the more recent composition, also the Holocene and the Pleistocene river clay minerals lack smectite compared to the BCS muds.

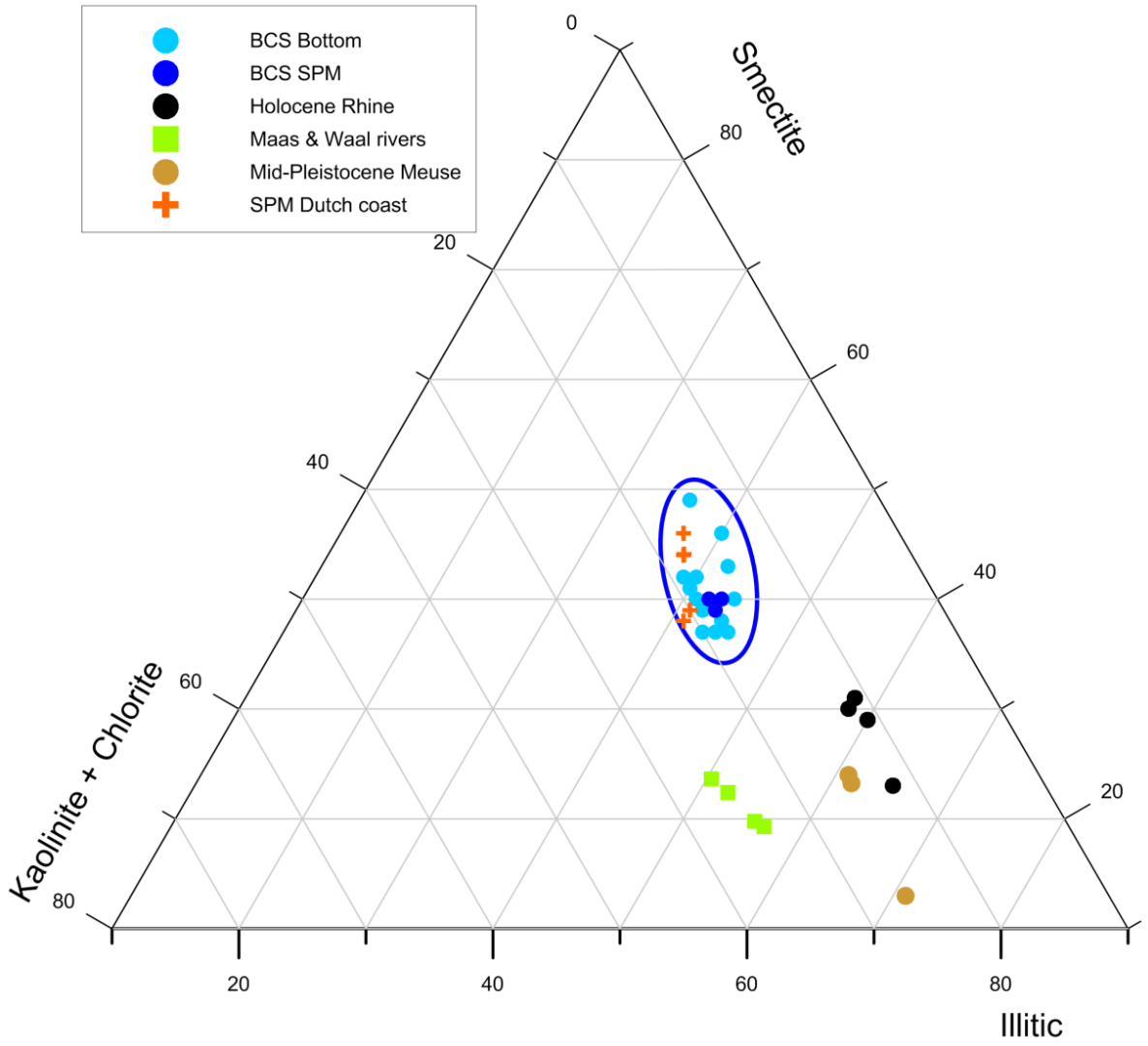

Figure 10.26. Ternary diagram comparing the BCS mud composition with the clay mineralogical composition of recent marine deposits in the Dutch coastal zone, recent upstream Meuse and Waal deposits, Early Holocene Rhine deposits and Mid-Pleistocene Meuse deposits.

X.5 THE SCHELDT RIVER SYSTEM AND THE SCHELDT ESTUARY CLAY MINERALOGY

Clay minerals from the Scheldt estuary analyzed by Zeelmaekers (2011) showed great similarity to the BCS muds. However it is commonly argued that this represents the influx of marine mud into the estuary (Reading and Collinson, 1996). To determine the pure fluvial Scheldt contribution to the estuary the tributary SPM and bottom clay mineralogy has been determined. These clay data will be recalculated towards annual clay mineral fluxes of the fluvial Scheldt river component using suspension concentrations and flow rate data.

X.5.1 Sampling

Sampling of the different tributaries of the Scheldt river system was carried out in the years 2010-2012 with a Van Veen grab for bottom and riverbed samples. Suspension samples were collected by a trough-flow centrifuge in 2012 combined with a series of suspension samples collected in 2006. The position of the samples is indicated on Figure 10.27 and Figure 10.28. Bottom and riverbed samples are collected at several positions on the tributary rivers whereas suspension samples are collected in the fluvial regime just above the fluvial-estuarine regime boundary (Figure 10.27).

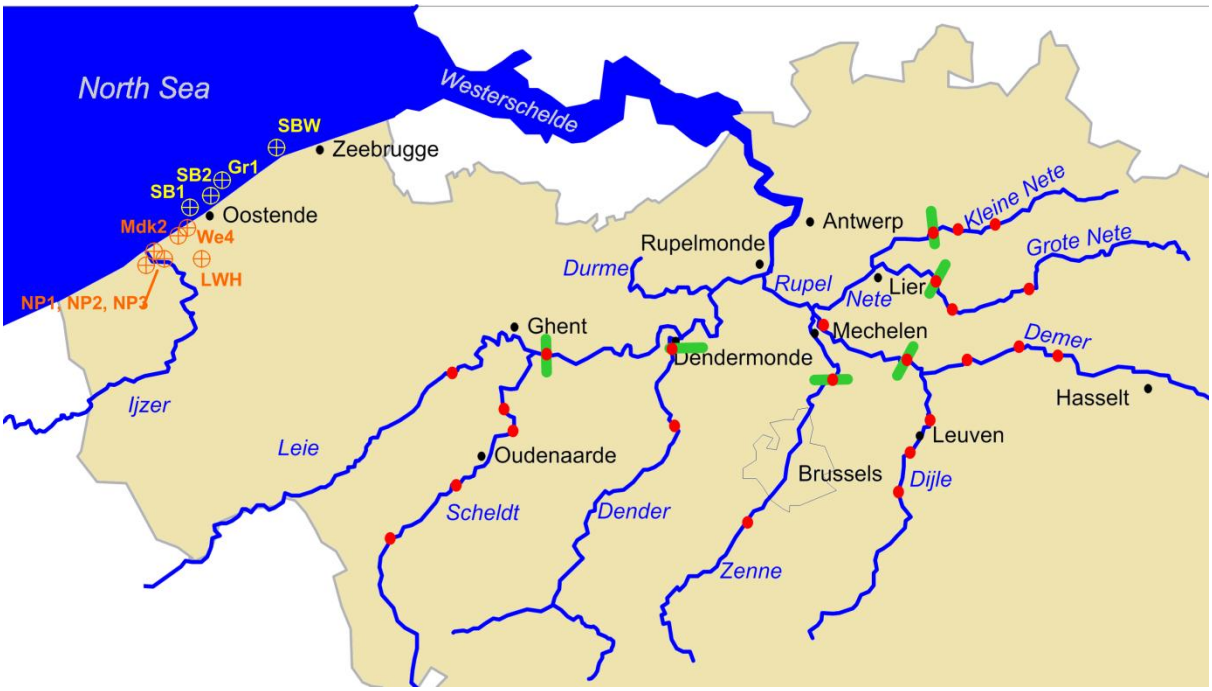

Figure 10.27. Overview of the flow area of the Scheldt river system. Black dots indicate place names. Green stripes indicate SPM sampling locations and red dots indicate bottom or riverbed sampling locations. Yellow markers indicate Holocene samples of offshore borehole locations SB1 Stroombank, SB2 Stroombank, SBW Wenduinebank and Grote Rede Gr1. Orange markers indicate borehole locations where late-Pleistocene, Weichselian-Eemian, deposits were sampled: Nieuwpoort 1,2,3 (NP1, NP2, NP3), Westende 4 (We4), Middelkerke 2 (Mdk2) and Leeuwenhof (LWH).

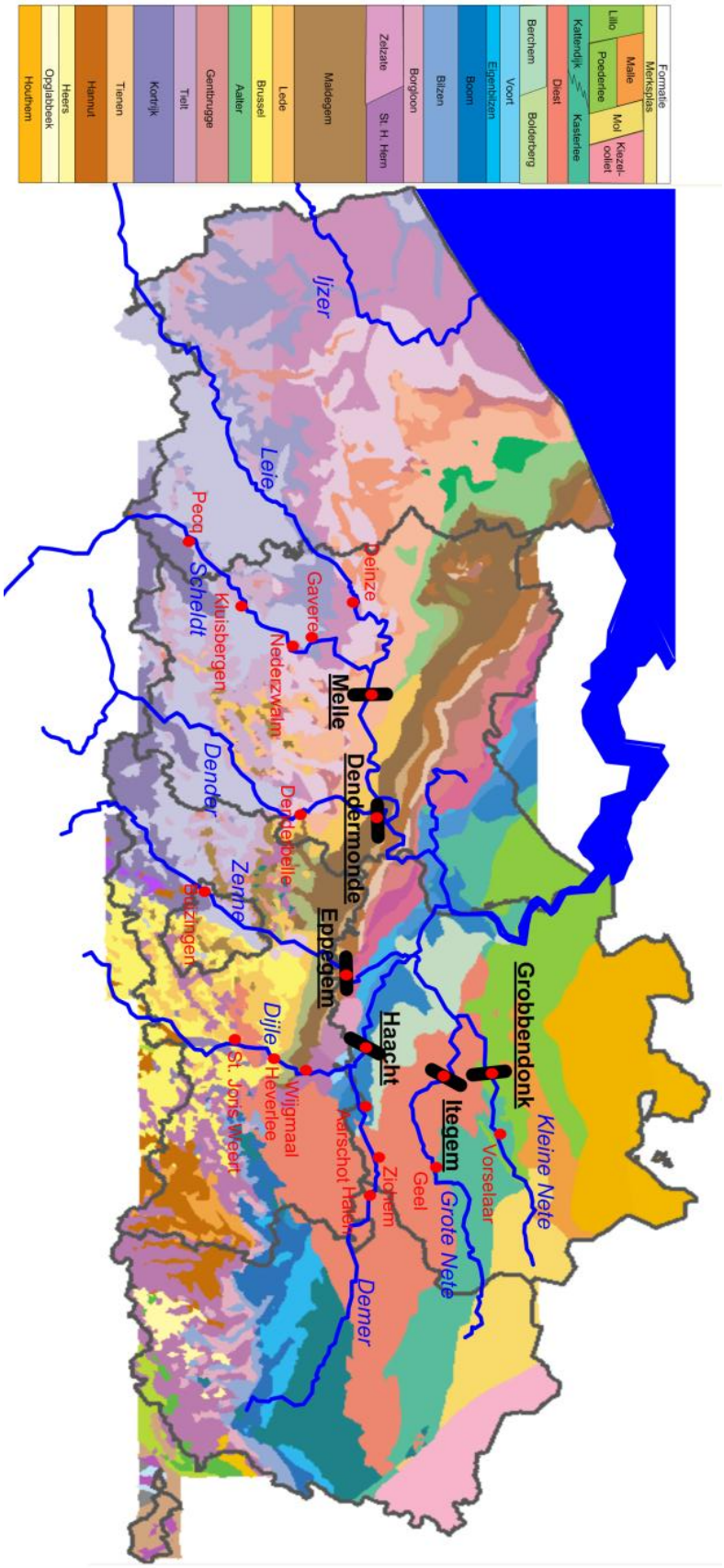

Figure 10.28. Geological map of Flanders with indication of the sampling locations of the Scheldt river system. Red points indicate bottom load samples whereas black lines indicate suspension samples at the upper boundary of the estuary. Map modified after ALBON (2009).

X.5.2 The Demer and Dijle rivers

The Demer river drains the southeastern part of Flanders (Figure 10.28) and flows into the Dijle river in Werchter, 10km north of Leuven. Slightly northwestern of this junction, in Haacht, the first salty influences are measured, the fluvial system gradually changes to an upstream estuary.

X.5.2.1 Bulk mineralogy

The bulk mineralogical composition of bottom samples of the Demer and Dijle rivers is displayed in Figure 10.29 and Figure 10.30. In general, quartz is the dominant mineral in the bottom deposits of both rivers. For the Dijle, the composition seems to become somewhat more clayey downstream (14% in Heverlee compared to 22% in Haacht). The composition of the material in suspension is even more clay-rich (40%) but also contains 17% amorphous material. This amorphous phase most likely consist of amorphous Si and organic components, which are also typical amorphous constituents in suspended particulate matter in the Scheldt estuary . The Demer bottom sediments are somewhat more quartz-rich (>70%) compared to the Dijle bottom sediments (50-66%). Furthermore, the Demer bottom sediments are characterized by <5% glauconitic minerals whereas the Dijle bottom sediments contain no glauconitic minerals. This is most likely explained by the fact the Demer erodes the Miocene glauconitic Diest Formation over a large area (Figure 10.28). After the confluence of Demer and Dijle, glauconitic minerals are not detected in bulk measurements.

X.5.2.2 Clay mineralogy <2µm

The clay composition of Dijle bottom samples along the downstream profile (Figure 10.31) is relatively stable with typically 30% smectite or more, ca. 10% kaolinite and 2% chlorite. The main variation exists in illitic components with 30-40% illite-smectite and 17-28% illite. The clay composition of the analyzed bottom load of the Demer river is slightly different (Figure 10.32). Similar to the bulk measurement data, glauconitic minerals are present in the clay fraction of the Demer bottom muds. From Halen to Zichem, the amount of glauconitic minerals is 11%, whereas in the further upstream Aarschot sample, only 6% was quantified. Typically, 35% of smectite is present and illite and illite-smectite make up 40% of the total clay mineral content. The glauconitic minerals were modeled with one glauconite-smectite phase with 27% expandable layers (higher expandable). This expandability is much larger than that encountered in the Diest D1 sand unit which is expected outcropping in this area (see Chapter 5).

At the boundary of the estuary in Haacht, when the Demer has already joined the Dijle river (Figure 10.28), the bottom clay composition consists of 39% smectite, 38% illite-smectite, 13% illite, 8% kaolinite and 2% chlorite. The clay composition of suspended material at the same position is nearly identical to the bottom mud composition. Glauconitic minerals are found neither in bottom nor in suspended material in Haacht. Possibly this is explained by the fact that from the annual tonnage of material drained by the composed Dijle-Demer river in Haacht, only 10-13% originates from the Demer (Waterbouwkundig Laboratorium, 2000; 2002). When correcting the amount of glauconite in the Demer with this factor, glauconite minerals should be present between 0.5-1% in Haacht. This amount is probably just below the detection limit in the clay mixtures typical for the Scheldt river system and explains why it is not identified in suspension in Haacht.

Analysis of suspended material sampled throughout the year 2006 moreover indicates that this SPM clay composition is very stable during the year with little or no seasonal variation (Figure 10.33). The clay composition of the SPM material in Haacht is therefore optimal to characterize the clay composition transported by the Dijle-Demer system into the estuary. This composition is consequently used for further calculations in this work when reconstructing the clay composition of all tributary rivers and mixing them to one fluvial output composition.

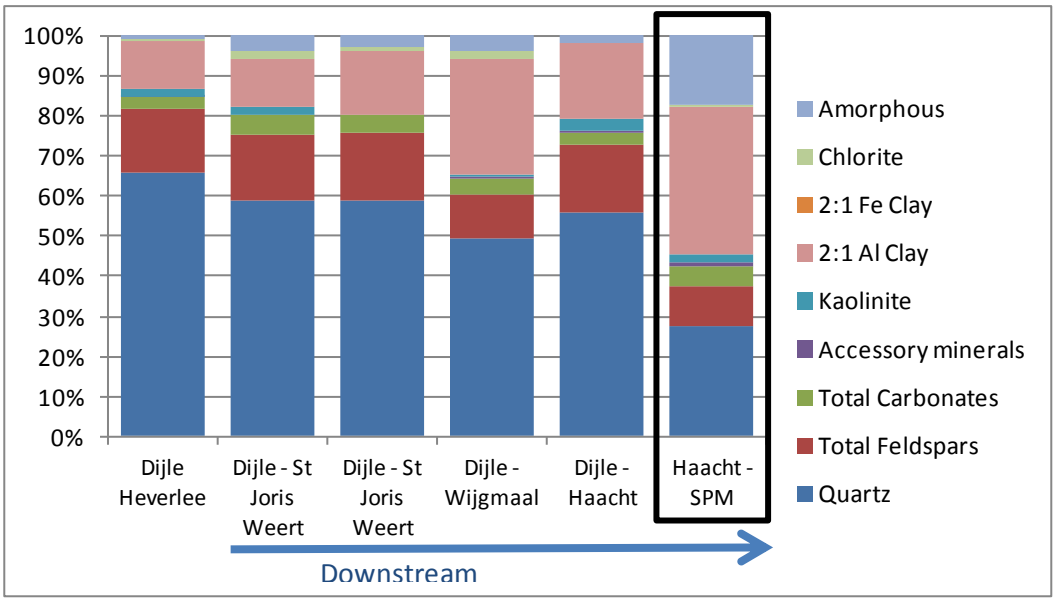

Figure 10.29. Bulk mineralogy of bottom samples of the Dijle river along the downstream track. The most right sample (black rectangle) is not bottom material but suspended material. The latter sample clearly contains more clay and amorphous components. The Demer river flow into the Dijle between the "Wijgmaal" and "Haacht" sampling position.

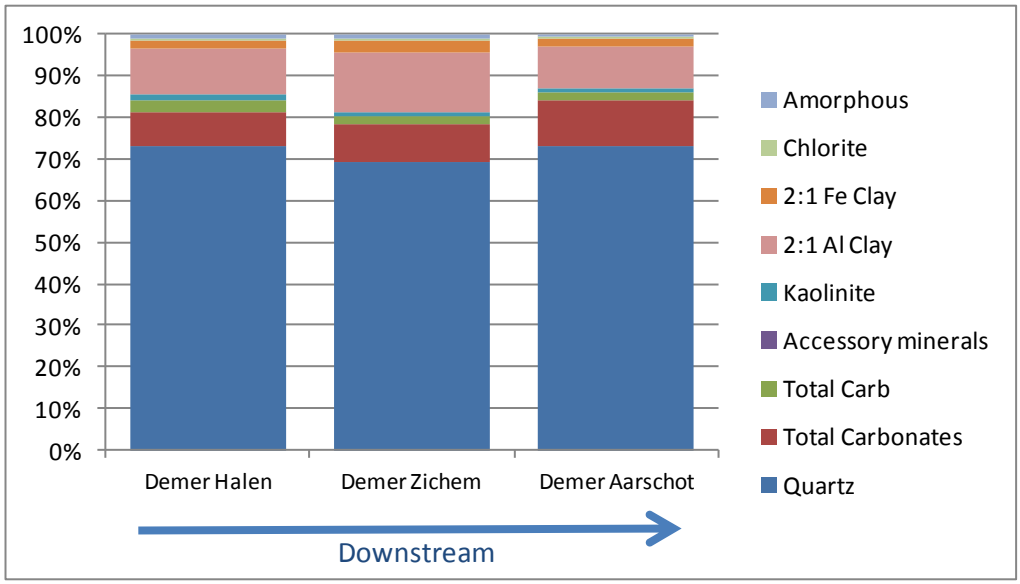

Figure 10.30. Bulk mineralogical results of bottom samples of the Demer river along the downstream profile. Quartz is very dominant. Besides the usual 2:1 Al-clay, Demer bottom samples also contains small proportions of glauconitic minerals. No SPM sampling was performed since the Demer joins the Dijle River in before the estuary border at Haacht.

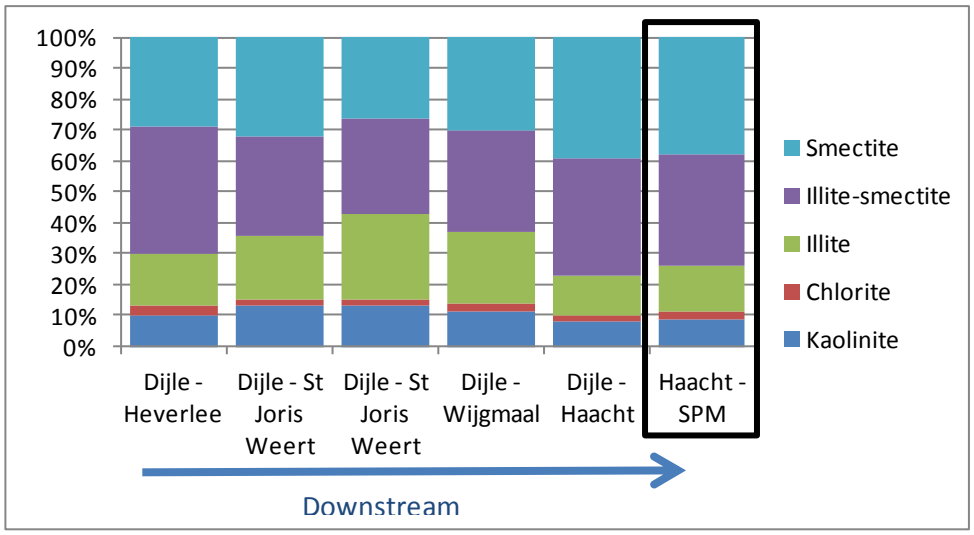

Figure 10.31. Clay mineralogical composition <2µm of bottom sediments of the Dijle river along the downstream profile. The most right sample (black rectangle) is a suspended sediment sample of which the quantitative data is used for further calculations.

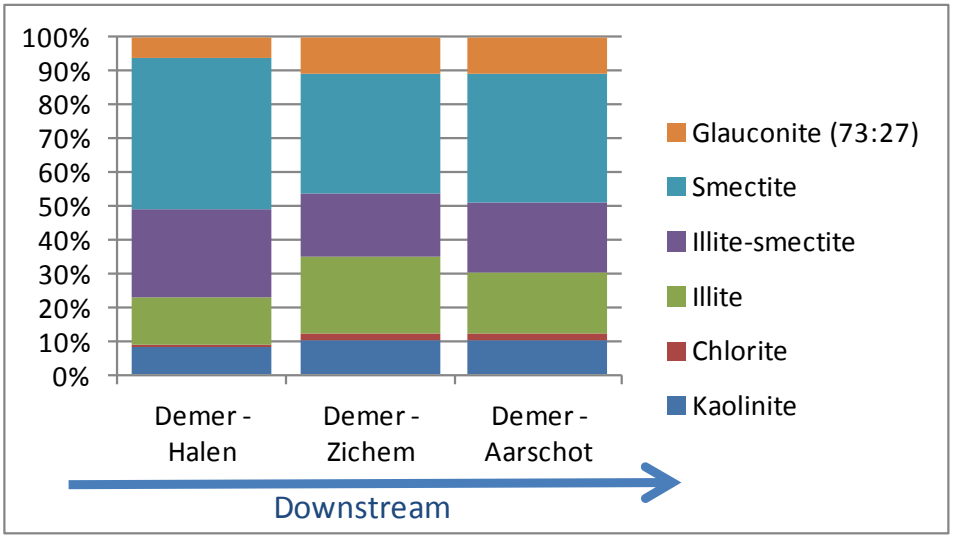

Figure 10.32. Clay mineralogical composition <2µm of bottom sediments of the Demer river along the downstream profile illustrating the presence of clay-sized glauconite-smectite.

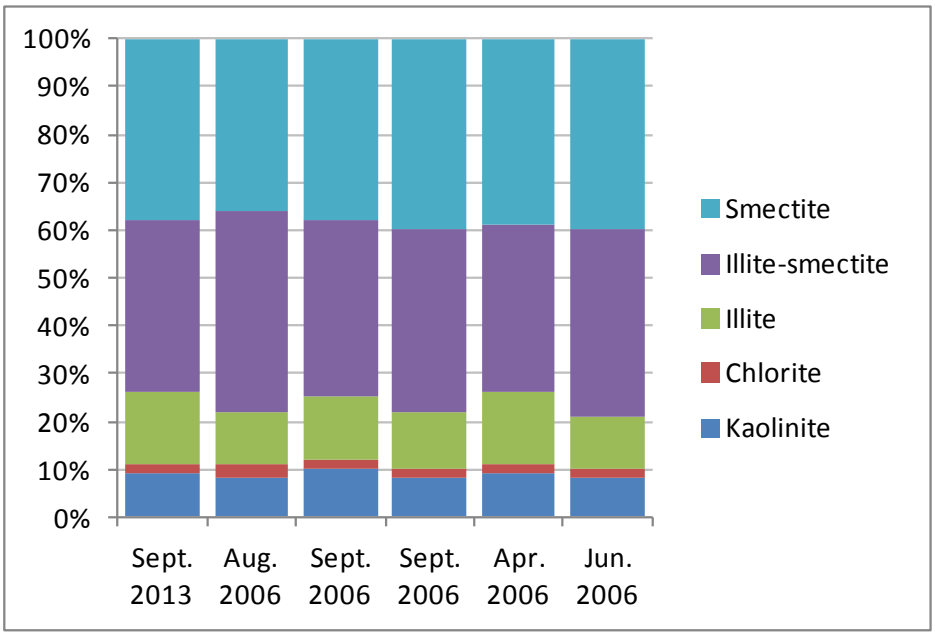

Figure 10.33. Clay composition <2µm of suspended sediment sampled in Haacht demonstrating the very low variability in clay mineralogy throughout seasons or years.

X.5.3 The Zenne river

The Zenne river drains the south-central part of Flanders and Brabant and joins the Dijle river in the estuary in Mechelen. The upper boundary of the Scheldt estuary upwards in the Zenne river is found at Eppegem (Figure 10.28).

X.5.3.1 Bulk mineralogy

The bulk mineralogical results of the bottom Zenne samples (Figure 10.34) illustrate that upstream sediments contain 41% quartz and 37% clay minerals. At the border of the estuary, in Eppegem, the amount of clay minerals has decreased to 29%. Although the total clay content is somewhat lower in Eppegem, it has to be noted that 5% chlorite is present upstream in Buizingen whereas in Eppegem only 1% is found. The mineralogical composition of the suspended sediment sampled in Eppegem also shows a relatively low clay content (26%) and amorphous components account for 20% of the total suspended sample.

X.5.3.2 Clay mineralogy <2µm

The clay composition of bottom Zenne samples is very similar to those of the Dijle river (Figure 10.35) with smectite, illite-smectite and illite all being proportioned around 30% of the total clay fraction <2µm. The composition of suspended material sampled at the estuary boundary at Eppegem is also very similar to the bottom composition, and to the Dijle SPM clay composition. Furthermore, five additional SPM samples show that the variability in clay mineralogical composition between different samples is exceptionally low (Figure 10.36). The clay mineralogy of the suspended sediment sampled in 2012 is used for further calculations.

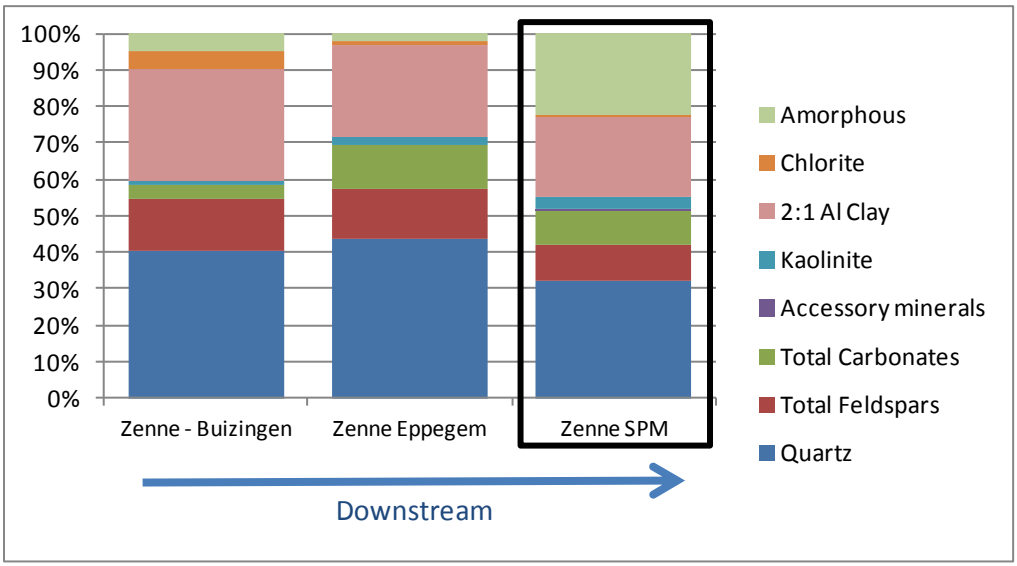

Figure 10.34. Bulk mineralogical composition of bottom sediments in the Zenne river along the downstream profile. The most right sample (black rectangle) is suspended sediment sampled in Eppegem.

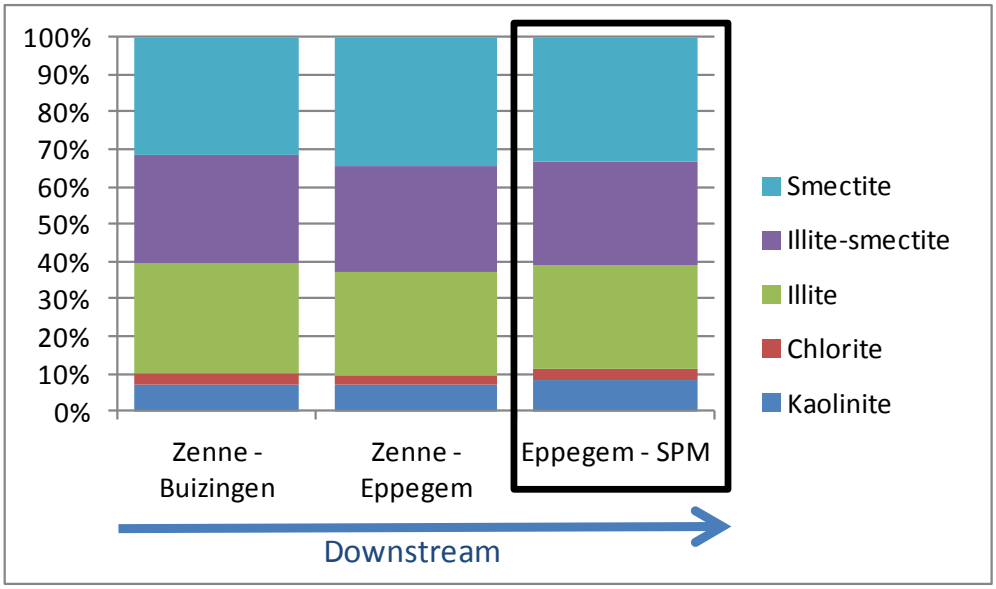

Figure 10.35. Clay mineralogical composition <2µm of bottom sediments of the Zenne rivier along the downstream profile. The most right sample is a suspended sample (black rectangle) which is used for further calculations.

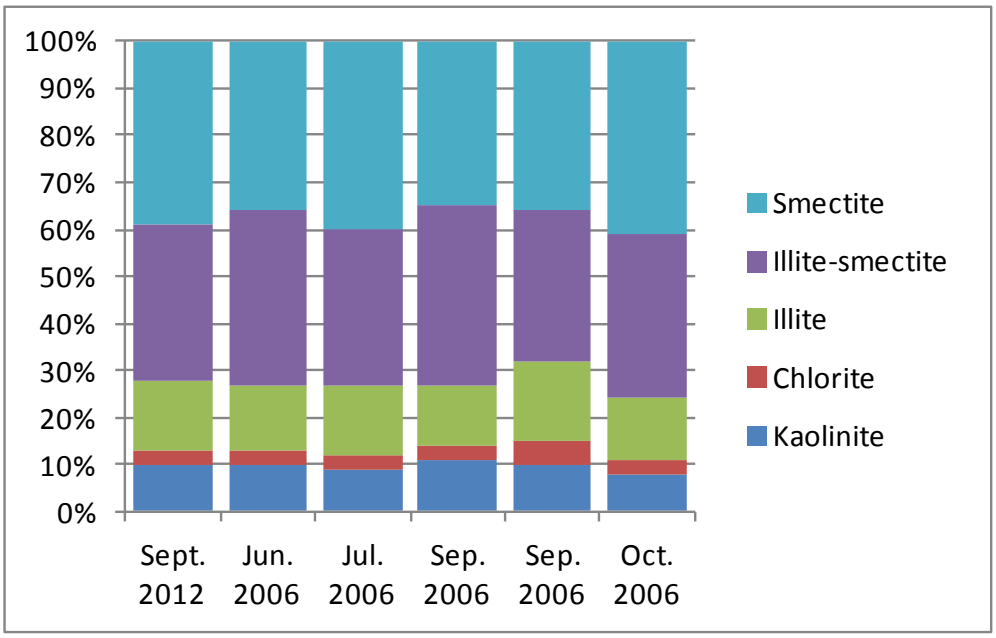

Figure 10.36. Clay composition <2µm of suspended sediment sampled in Eppegem demonstrating the very low variability in clay mineralogy throughout seasons or years.

X.5.4 Kleine and Grote Nete rivers

The Kleine and Grote Nete rivers drain the Neogene glauconitic deposits in the northwestern part of Belgium, already discussed earlier in this work. The color of the sediment in these rivers is systematically brown colored. Bottom load samples in both rivers were visually very sandy as opposed to the more muddy nature of other rivers in the Scheldt basin. This sandy bottom deposits contain pelletal glauconite and resemble, and probably represent, the Neogene deposits in the Campine basin (see chapters 5-6-7) which are being eroded by the Kleine and Grote Nete rivers. Bulk mineralogy was determined on total samples but in order to extract the <2µm fraction, bottom samples were first wet sieved <32µm (see Methodology section) before initiating the clay extraction procedure.

X.5.4.1 Bulk mineralogy

The bulk mineralogy of the Kleine Nete samples (Figure 10.37) consist predominantly of quartz (>87%) with only 6.5% clay minerals, amongst which also glauconitic minerals. The material in suspension in Grobbendonk, at the fluvial/estuary border, is less quartz-rich and contains 13% of semi-crystalline ferrihydrite.
The mineralogical composition of the Grote Nete (Figure 10.38) is similar to that of the Kleine Nete although the quartz percentage is only ca. 70%. Glauconitic minerals occur in the bottom deposits, 5% in Geel compared to 13% in Itegem at the estuary boundary. No bulk mineralogical analysis was performed on the suspended material sampled in Grobbendonk because only very little material was available.

X.5.4.2 Clay mineralogy <2µm

The clay mineralogical composition of bottom sediments of Kleine Nete (Figure 10.39) consists of elevated amounts of glauconitic minerals (45% in Vorselaar), for which both a low expandable (10% expandable layers) and a higher expandable glauconite-smectite (27% expandable layers) were necessary to model the clay mineralogical pattern. Further downstream in Grobbendonk, the amount of smectite has increased significantly and higher expandable glauconite-smectite is predominant, both in bottom and suspended sediment (Figure 10.39).
The clay composition of the Grote Nete (Figure 10.40) is similar but in this case, in the upstream sampling position in Geel, only higher expandable glauconite-smectite is present whereas at the estuary boundary in Itegem, also low expandable glauconite-smectite is present. The suspended material in Itegem is similar in composition to the bottom sediment but the ratio higher/low – expandable glauconite-smectite is somewhat higher.

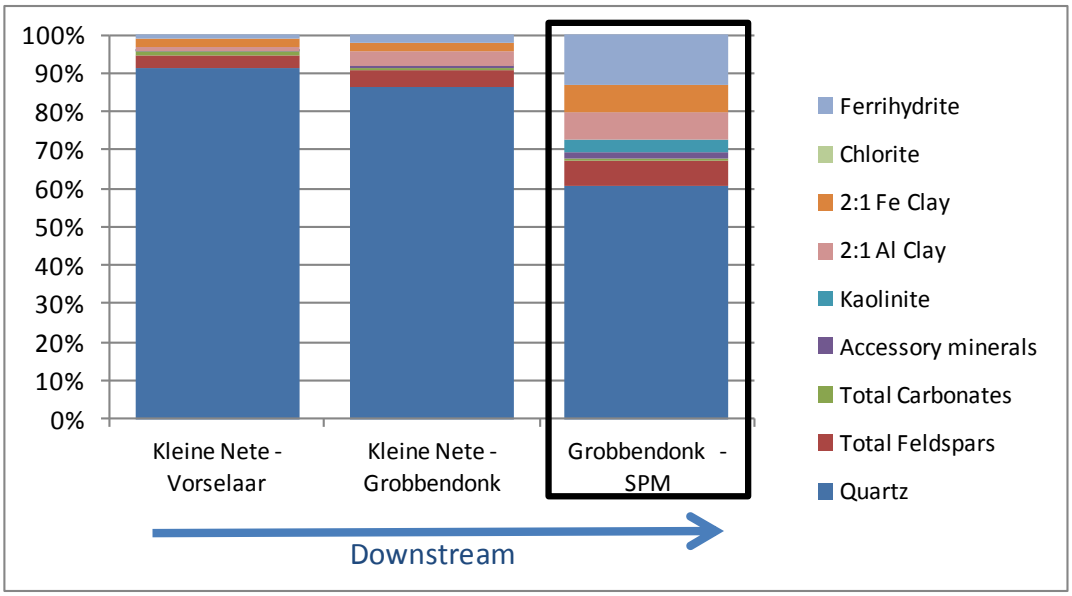

Figure 10.37. Bulk mineralogy of bottom samples of the Kleine Nete along the downstream profile which contain over 85% quartz. The most right sample (black rectangle) is a suspended sediment sampled in Itegem at the border of the estuary and the fluvial area.

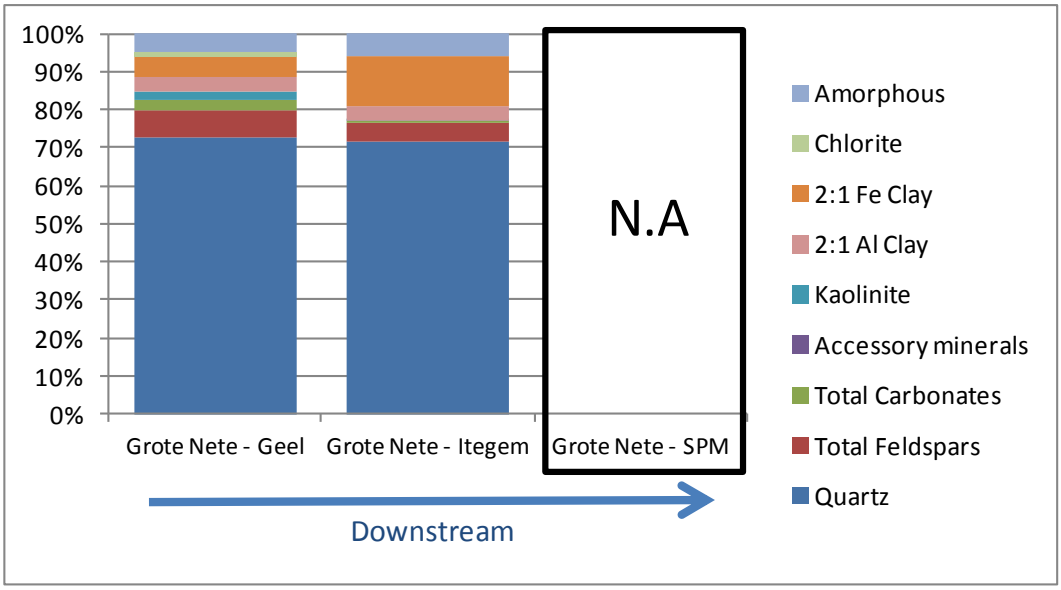

Figure 10.38. Bulk mineralogical composition <2µm of bottom sediments in the Grote Nete river along the downstream profile. The most right sample (black rectangle) is a suspended sample collected in Itegem. Only little amount of material was available from this sample and therefore it was chosen to only determine the clay mineralogy <2µm. N.A indicates “Not Analyzed”.

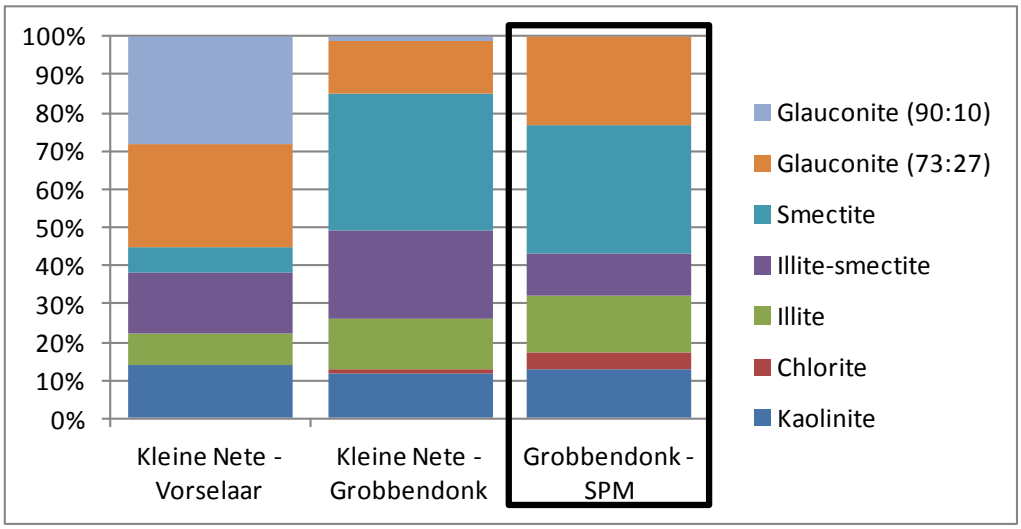

Figure 10.39. Clay mineralogical composition <2µm of bottom samples of the Kleine Nete along the downstream profile. The most right sample is suspended material sampled at Itegem.

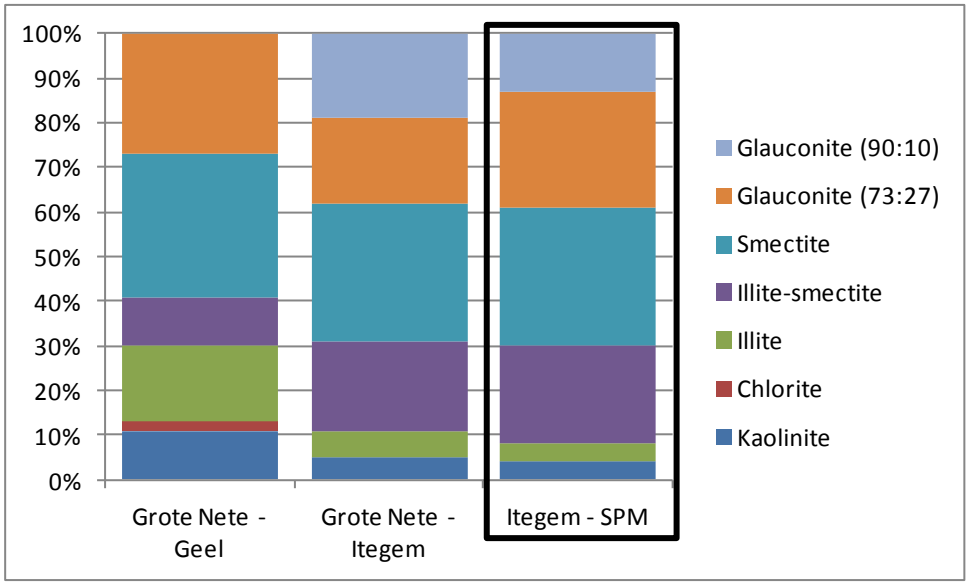

Figure 10.40. Clay mineralogical composition <2µm of bottom samples of the Grote Nete along the downstream profile. The most right sample (black rectangle) is a suspended sample collected in Itegem.

X.5.5 The Dender

The Dender flows in northern France and further in the central to central-west part of Flanders, and erodes mainly clay deposits of Ypresian age (Figure 10.28).

X.5.5.1 Bulk mineralogy

The bulk mineralogy of the bottom Dender sample in Denderleeuw (Figure 10.41) consists of 59% quartz and 15% clay minerals. Carbonates and feldspars occur in proportions of 12% and 11% respectively. The suspended material sampled at the estuary border in Dendermonde, is more clay-rich (51%) but also contains 25% amorphous components.

X.5.5.2 Clay mineralogy

The clay composition <2µm of the Dender bottom and suspended sediment is very similar (Figure 10.42), consisting of 44% and 46% smectite respectively and with slightly less illite-smectite mixed-layers occurring in the suspended sediment. Kaolinite and chlorite make up 10% of the total clay fraction in both samples.

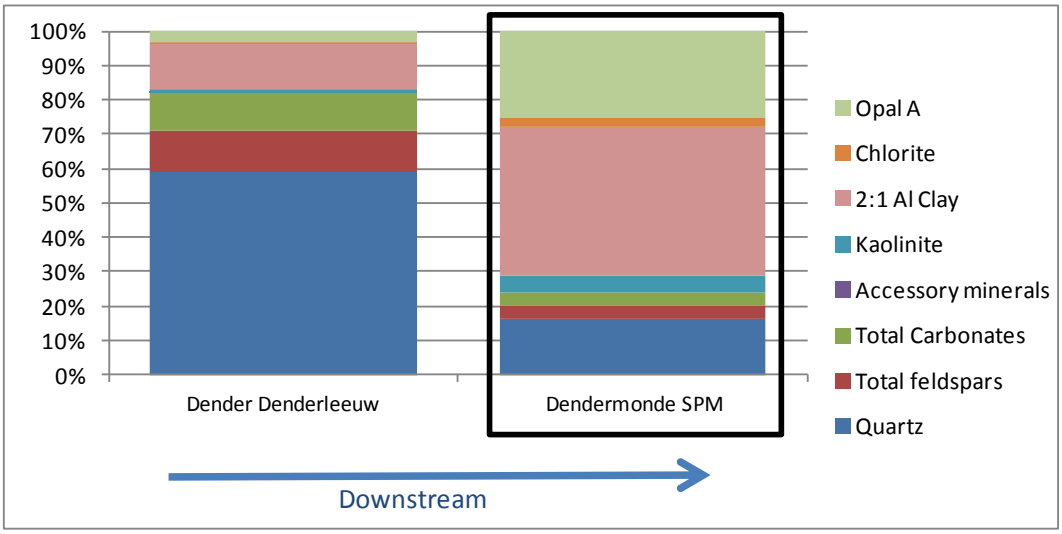

Figure 10.41. Bulk mineralogical composition of a bottom sediment sample in Denderleeuw and suspended sample at the estuary boundary in Dendermonde.

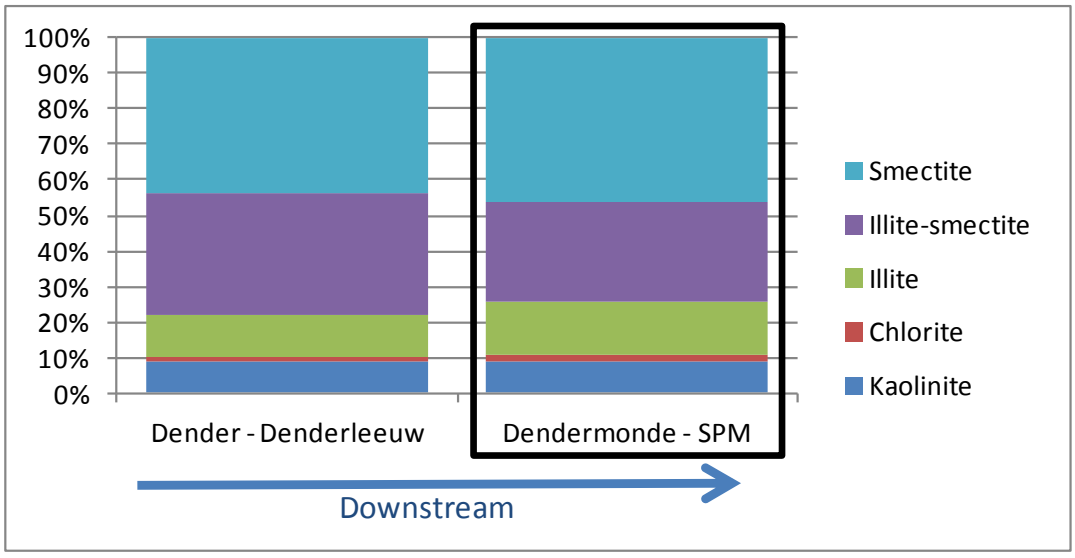

Figure 10.42. Clay mineralogical composition <2µm of bottom mud in Denderleeuw and suspended sediment collected at estuary border in Dendermonde.

X.5.6 The Scheldt and Leie rivers

The Scheldt and Leie drain the northern part of France and further upstream the northwestern part of Belgium, hereby eroding essentially the Ypresian clay deposits.

X.5.6.1 Bulk mineralogy

The mineralogical composition of the bottom samples of the Scheldt river is characterized by variable quartz/clay content along the downstream profile (Figure 10.43). Whereas upstream, in Pecq, 39% clay minerals occur, this is only 14% in Kluisbergen and around 30% clay minerals are present in Nederzwalm and Gavere. Further downstream, the Scheldt river merges with the Leie river in the vicinity of Ghent, in Melle. The bottom composition of the upstream Leie river (Figure 10.43) is quite similar to the bottom composition of the Scheldt in Gavere. Suspended sediment was collected in Melle, just across the estuary boundary. The clay content of the SPM is 38% and also 17% amorphous components were quantified. Such high amorphous were also reported in the Scheldt estuary by Chen et al.(2005).

X.5.6.2 Clay mineralogy <2µm

The clay composition of all bottom samples in both rivers is very similar (Figure 10.44). Smectite occurs between 39% and 44% and also illite-smectite is constantly present in amounts around 35%. Only 8% of illite is present upstream, which increases to 15-19% further downstream. At the SPM sampling station at estuary boundary, Melle, this typical composition is also found.

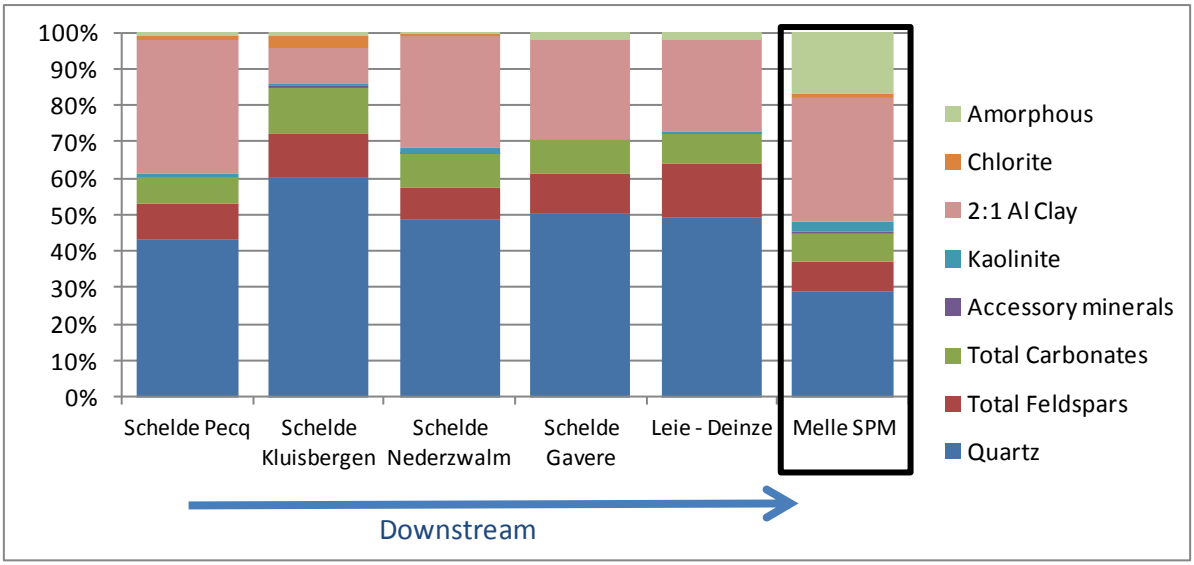

Figure 10.43. Bulk mineralogical composition of bottom sediment sampled along the downstream Schelde profile. One sample of the Leie river, collected in Deinze, was incorporated. The most right sample (black rectangle) is suspended material sampled in Melle, close to the estuary border.

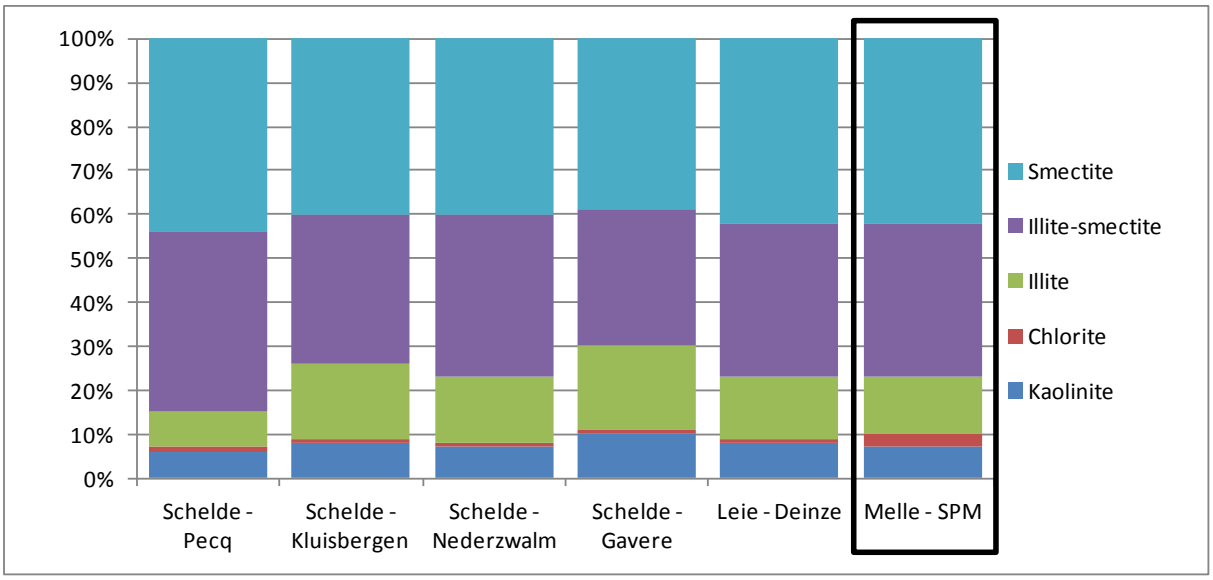

Figure 10.44. Clay mineralogical composition <2µm of bottom samples of the Scheldt along the downstream profile, one bottom sample of the Leie at Deinze and a suspended sample collected in Melle, after the confluence of Schelde and Leie. The most right sample (black rectangle) is suspended material collected in Melle right across the estuary boundary. The variability in clay composition is remarkably low. The clay composition of the SPM sample is used for further calculations.

X.5.7 Comparing the tributary river composition with the North Sea muds

The clay composition of the bottom and suspension samples of the different tributary rivers was plotted in a ternary diagram and compare with the BCS surface mud composition (Figure 10.45). It is apparent from this figure that the clay composition of the different tributaries plots close to the BCS surface muds but deviates slightly to somewhat more illitic compositions (Figure 10.45).

X.5.8 The calculated fluvial clay mineralogy of the Scheldt river system

X.5.8.1 Calculating annual sediment fluxes

Now that the clay mineral composition of the important tributary rivers outside of the estuary has been characterized, the clay data should be combined in such a way that a net output clay signal for the Scheldt fluvial system can be calculated. In order to attribute the relative importance of each tributary river, the clay data must be complemented with sediment fluxes.

Time-dependent sediment fluxes can be calculated in various ways but always require the input of suspension concentration and flow rate data for each tributary river. Such data are available at the Hydrological Information Centre Flanders ("Waterbouwkundig laboratorium"). For the sediment concentrations, it was chosen to work with data measured on "bucket-water samples" during which SPM concentrations are determined in a bucket water sample, sampled relatively close to the surface of the river. The main reason to use these data is that they are available over a prolonged time sequence, as they were continuously measured since 1992 up to 2009 and therefore provide the longest timeframe available of all sediment concentration data. During this period, sediment concentrations were measured once every week whereas flow rates were automatically measured each day at the boundary of the estuary. The used sampling locations are therefore identical to the sampling locations for clay mineral characterization. Only for the Scheldt/Leie, sediment concentrations were measured at Merelbeke, a few kilometers upstream from the flow rate measurements and sediment sampling location in Melle (Figure 10.28).

Annual sediment fluxes were calculated as proposed in Vanlierde (2013). From the initial

data, monthly averages were calculated for both sediment concentration and flow rate. Monthly sediment fluxes were subsequently calculated by multiplying the monthly average data. Finally, annual sediment fluxes were calculated as a weighted average by assigning weight factors as a function of the amount of days in each month. Through this procedure, 17 annual sediment fluxes were calculated from the year 1992 until 2009, except for the year 2005, of which most data were not or not correctly recorded.

Figure 10.46 and Table 10.1 show the annual sediment fluxes for each tributary river relative to the total annual sediment flux. It can be observed that 60% to 80% of the material transported by the fluvial Scheldt river system originates from the Scheldt/ Leie and Dijle rivers but also that a very large variability exists between different years. In 1996, the Scheldt/Leie only drained 31% whereas in 2001, more than 61% of the sediment flux in the river system origined from the Scheldt/Leie (Table 10.1). In years with less Scheldt/Leie output, material from the Dijle and Zenne becomes relatively much more important.

X.5.8.2 Net Scheldt clay mineralogical output signal

The clay mineralogical assemblages of each tributary river can now be combined with the annual sediment fluxes to result in an annual clay mineralogical output of the Scheldt river system. In order to do so, the fixed clay assemblage for each river is proportioned according to the annual sediment fluxes calculated in Table 10.1. For this purpose, the clay mineralogy of the SPM samples at the estuary boundary are used. The resulting annual clay mineralogical output signal are shown in Table 10.2.

The results have been represented as “smectite”, “kaolinite+chlorite” and “illitic”. The latter combines the contributions from illite, illite-smectite and any glauconitic minerals. This approach is justified as the different clay mineral species, and even their detailed characteristics, occurring in the different rivers are very similar.

The first important observation from these calculations is that, although large variability in annual sediment flux is observed (Figure 10.46), the clay mineralogical fluvial composition in the 1992-2009 period is very constant. The largest spread between two outer values of one of the end members is only 2%. The second observation is even more crucial, considering the relative position of the Scheldt clay composition in relation to the BCS composition (Figure 10.47). On average, the Scheldt composition contains slightly more illitic minerals (2-3%) and slightly less kaolinite+chlorite minerals but the Scheldt and BCS mudplate are overall very similar.

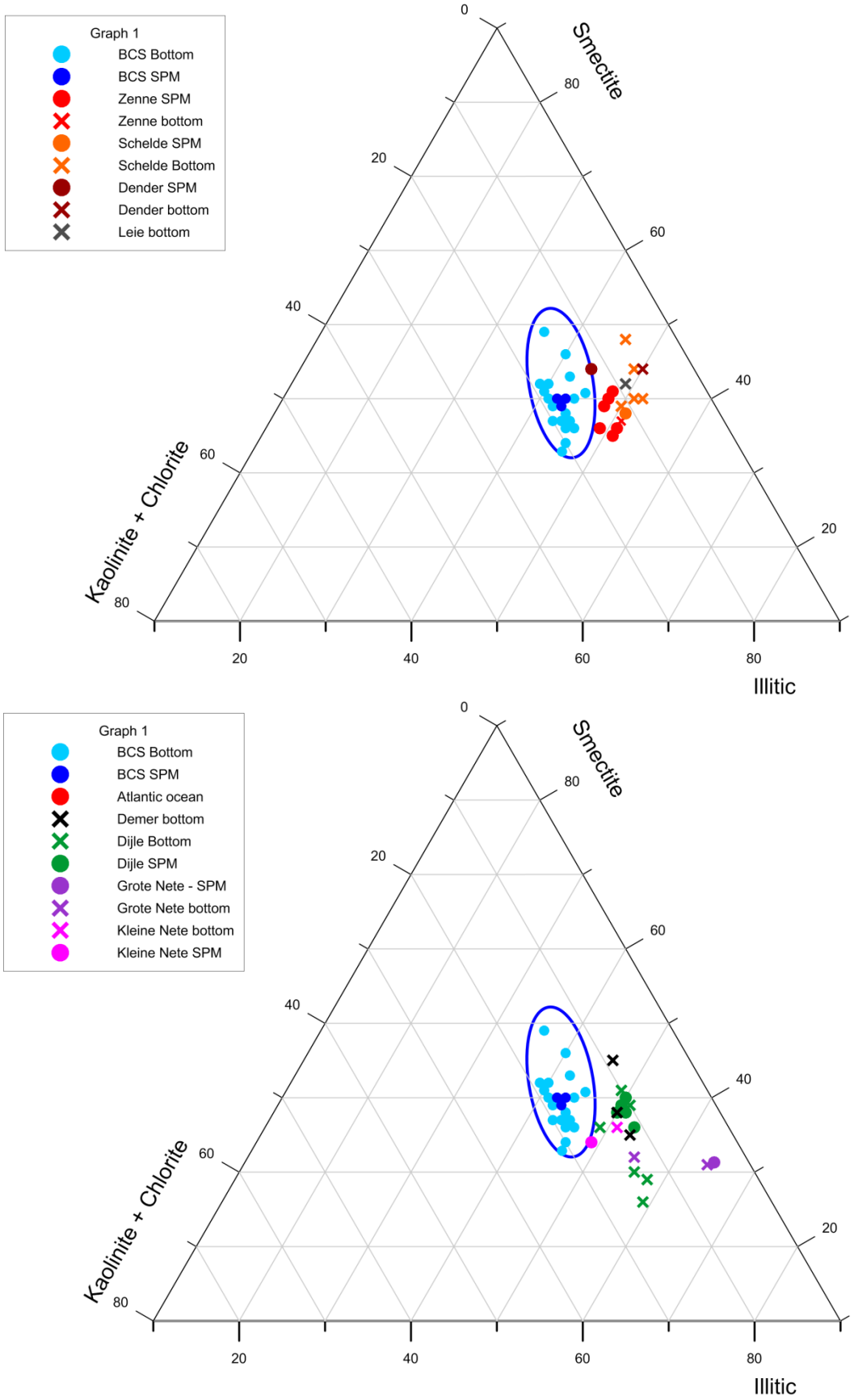

Figure 10.45. Ternary diagram demonstrating the clay mineralogy of the different tributary rivers in the Scheldt river system with respect to the North Sea mud clay composition. Upper figure shows clay composition of Scheldt, Leie and Dender and Zenne rivers. Lower figure shows clay composition of Dijle, Demer, Kleine Nete and Grote Nete.

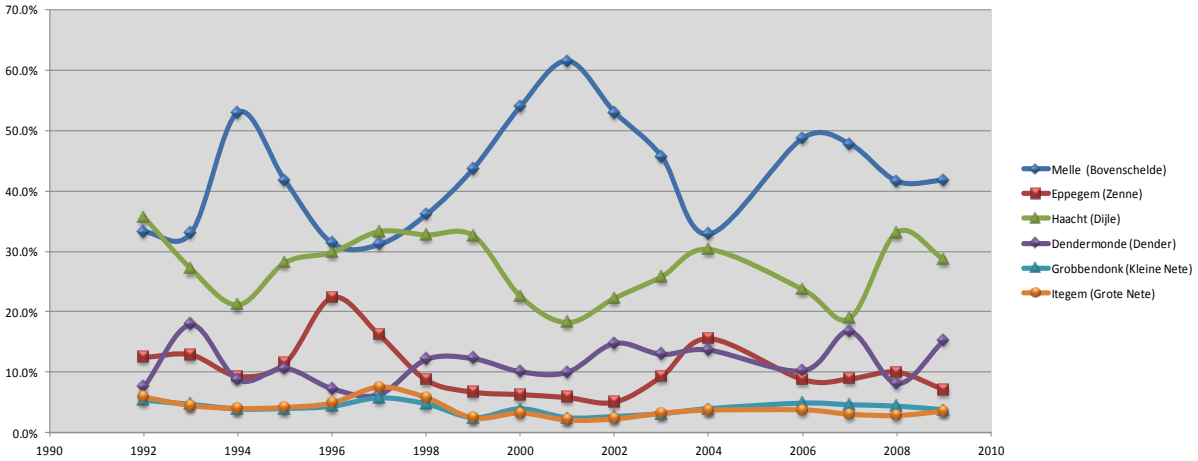

Figure 10.46: Annual sediment fluxes of each tributary river relatively to the total fluvial annual flux.

Table 10.1: Annual sediment fluxes of each tributary river, expressed relatively to the total sediment flux of the Scheldt river system. The year 1996 and 2001 have been highlighted because they represent the most extreme years. In 1996, the Scheldt/Leie only drained 31% whereas in 2001, more than 61% of the sediment flux in the River system origined from the Scheldt/Leie.

	Scheldt/Leie	Zenne	Dijle	Dender	Kl Nete	Gr Nete
1992	33.2%	12.5%	35.6%	7.5%	5.3%	5.8%
1993	33.0%	12.9%	27.1%	17.9%	4.6%	4.4%
1994	53.0%	9.3%	21.2%	8.7%	3.8%	4.0%
1995	41.7%	11.5%	28.1%	10.6%	3.9%	4.1%
1996	31.4%	22.4%	29.8%	7.3%	4.3%	4.9%
1997	31.1%	16.2%	33.2%	6.3%	5.7%	7.5%
1998	36.1%	8.7%	32.7%	12.1%	4.7%	5.7%
1999	43.7%	6.7%	32.5%	12.3%	2.4%	2.4%
2000	54.0%	6.3%	22.6%	10.1%	3.9%	3.2%
2001	61.5%	5.8%	18.2%	10.0%	2.4%	2.1%
2002	53.0%	5.0%	22.3%	14.8%	2.6%	2.3%
2003	45.7%	9.3%	25.8%	13.0%	3.1%	3.2%
2004	32.8%	15.6%	30.3%	13.7%	3.9%	3.7%
2005	/	/	/	/	/	/
2006	48.7%	8.8%	23.7%	10.2%	4.8%	3.7%
2007	47.8%	8.9%	19.0%	16.8%	4.5%	3.0%
2008	41.6%	10.0%	33.1%	8.1%	4.3%	2.8%
2009	41.8%	7.1%	28.6%	15.3%	3.7%	3.5%

Table 10.2. Annual clay mineralogical composition as Scheldt river system output in percentages. Illitic combines contributions from illite, illite-smectite and glauconite-smectite.

	Illitic	Smectite	Kaol + Chl
1992	45.2	39.08	15.71
1993	45.3	39.65	15.04
1994	46.2	39.48	14.33
1995	45.9	39.47	14.59
1996	45.7	38.92	15.37
1997	44.8	38.75	16.50
1998	45.2	39.43	15.33
1999	46.7	39.93	13.35
2000	46.3	39.69	14.00
2001	47.1	39.90	13.03
2002	46.7	40.08	13.23
2003	46.3	39.77	13.88
2004	45.8	39.51	14.64
2005	/	/	/
2006	45.9	39.52	14.61
2007	45.8	39.86	14.30
2008	46.2	39.51	14.26
2009	46.0	39.86	14.18
AVERAGE	**46.0**	**39.6**	**14.5**

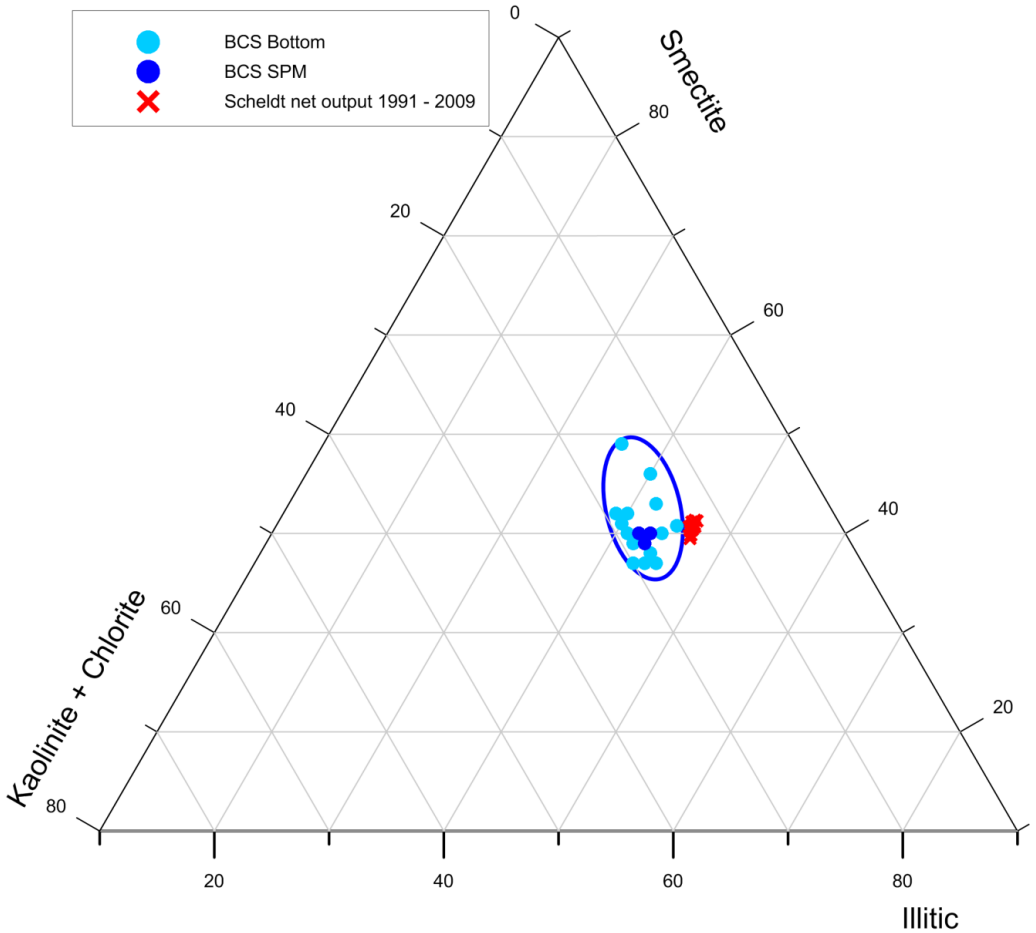

Figure 10.47. Ternary diagram comparing the clay mineralogical composition of the bottom and suspended sediments at the Belgian Continental Shelf and the calculated output fluvial clay mineralogy in the 1992-2009 period.

X.5.9 Interpretation

It is apparent from Figure 10.47 that the calculated clay composition of the present-day Scheldt river system plots very close to BCS surface mud composition. This confirms the great similarity and hence relationships between the fluvial Scheldt sediment, the Scheldt estuary muds and the BCS muds.

Nevertheless, the calculated clay composition slightly deviates from the mean BCS clay composition, as the Scheldt composition seems to be slightly more illitic and slightly less kaolinite- and chlorite-rich. Obviously there are inherent errors and uncertainties in the measurements. However, clay mineral quantification uncertainties are probably better than 2 à 3% per mineral phase. The error on the SPM and flow rate raw data is most likely limited to a minimum as the clay mineral composition of the different tributary rivers is not significantly different, as illustrated by the very small difference in calculated clay composition between the extreme years 1996 and 2005 (Figure 10.46). Also there is no reason to suppose a systematic deviation of the error in all samples to shift the composition to a few percent higher illitic minerals. However an important factor not taken into account in the comparison is the erosion within the estuary which surely will affect the estuarine clay mineralogy. In the estuary, the fluvial clay minerals are furthermore mixed with the import of the marine clay mineral component which will also modify the total output composition at the river mouth.

Zeelmaekers (2011) reported that the present-day BCS clay composition extends in suspension and in bottom sediments in the Westerscheldt up to Bath with 39-42% smectite, whereas upstream Bath, the clay mineralogy contains more than 45% smectite (45-50%) (Figure 10.48). Because the quantification of samples in this work is done following exactly the same preparation procedures and clay model parameters as Zeelmaekers (2011), systematic errors are prevented and clay mineral data of both studies can be safely compared. Although this difference is small, it is remarkable as the different tributary rivers, apart from the Dender river, all contain considerably less smectite in suspended sediment. Because also the marine component is less smectitic, the surplus in smectite must be caused by local erosion of deposits present in the estuary (Van Kessel et al., 2011). Smectite-rich clay mineral composition are known from Priabonian-Lutetian-Bartonian deposits outcropping in the estuary area (Figure 10.28 and Figure 10.48).

In the fluvial domain however, the Paleogene and Neogene erosion influence is mixed with the signal from the Quaternary cover. From the results of the Kleine and Grote Nete rivers, the presence of glauconite minerals in sand-sized and clay-sized fractions most likely origins from the glauconitic Neogene deposits outcropping in the Campine area, i.e. the Kasterlee and Poederlee Formations (see chapters V-VI-VII). Also in the Demer clay minerals, glauconite minerals were traced which is expected since the Demer erodes a large part of the Diest Formation in the eastern part of Flanders. The clay mineralogy of the other tributary rivers is, however, strikingly similar. The Leie, Scheldt, Dender and Zenne are all eroding Neogene clays of Ypresian age but their smectite content is systematically lower than 45% whereas the Ypresian clays contain over 60% smectite in the <2µm fraction (Figure 10.48), which indicates that also clay minerals from Quaternary deposits covering the Ypresian clays in the river valleys influence the clay composition of these rivers.

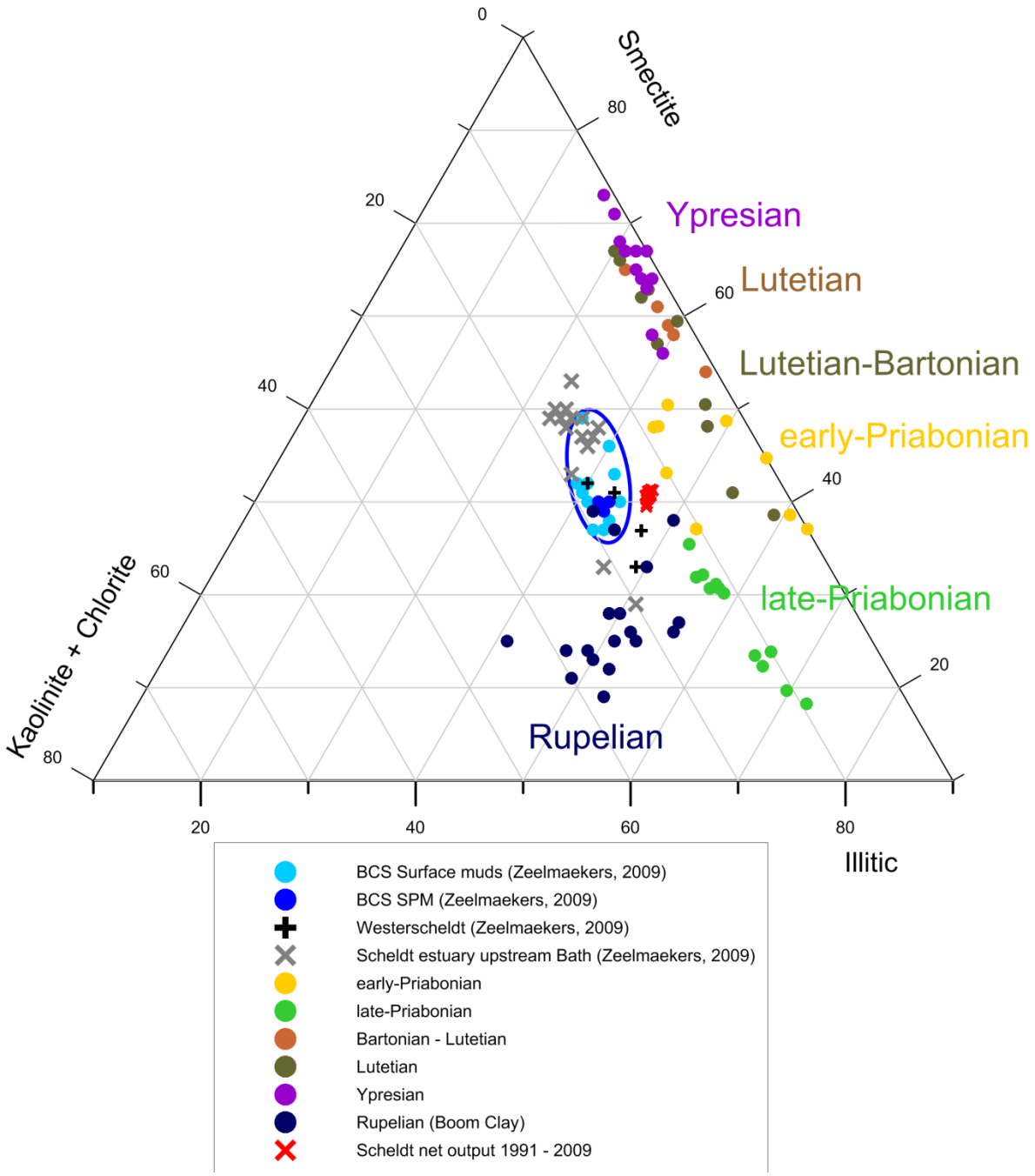

Figure 10.48. Ternary diagram comparing the BCS surface mud composition with calculated Scheldt river system composition, the Westerschelde composition and the Scheldt estuary composition upstream Bath. Clay mineral data of the most important clay-rich Cenozoic deposits outcropping in the Scheldt basin are also plotted, showing the clay mineralogical evolution in Paleogene stratigraphy in Belgium (after Zeelmaekers, 2009).

Chapter XI
Discussion & Conclusion

XI.1 THE PROVENANCE OF THE PRESENT-DAY BCS MUDS

In the sections above, the clay mineralogical results of both present-day and past sediment sources were presented. The use of quantitative clay mineralogy as a provenance indicator has proven its value in marine, tidal and fluvial environments (Sandler and Herut, 2000; Ramaswamy et al., 2007; Liu et al., 2008; Pache et al., 2008; Dou et al., 2010; Kessarkar et al., 2010; Liu et al., 2010; Howell et al., 2014; Li et al., 2014). Also in this research it was shown that quantitative clay mineralogy allows to differentiate between different sediment sources.

It was demonstrated that the Scheldt river system is the only potential source with a clay mineral composition corresponding to the BCS mud composition (Figure 10.1). Other investigated sources, such as the English Channel and the Rhine river system have a significantly different clay mineral composition. In general, smectite minerals are lacking in both the Meuse-Waal deposits as well as in the different English Channel sources. Zeelmaekers (2011) already pointed to the Scheldt estuary as main clay supplier. It was however uncertain whether the estuary samples studied by Zeelmaekers (2011) were reflecting the fluvial output sediment signal or the marine input signal. In this research, the clay mineralogy <2µm of the different upstream tributaries of the Scheldt river system was combined with annual sediment fluxes to result in an annual clay mineralogical output composition for the fluvial Scheldt river system. This Scheldt output composition corresponds to the present-day BCS mud composition (Figure 10.47), which points to the Scheldt river system as a main clay supplier.
Two options remain to explain the present-day situation. Either the recent mud deposits are directly discharged from the Scheldt river system, transported through the Westerscheldt and deposited at the shelf or, the recent muds are reworked from the Holocene deposits.
Almost all arguments point to the latter hypothesis. Many authors already stated that most of the Holocene and recent deposits on the shelf and in the coastal area are the result of constant reworking of older Holocene and Pleistocene deposits (Gossé,1977; Van Alphen ,1990; Salden and Mulder,1996; Beets and van der Spek, 2000; Mathys, 2009). Furthermore, Fettweis and Van den Eynde (2003) have demonstrated that the shelf area is dominantly controlled by erosion processes rather than active deposition. Also mud balance models of the Scheldt river system systematically predict that presently no, or insignificant, amounts of fluvial-derived mud is transported out of the estuary (Verlaan et al., 1997; Van Maldeghem,1993; Reading and Collinson, 1996; Taverniers,2000; Van Alphen,2000; Vanlede et al., 2009). Whenever muddy sediment is presently being transported out of the estuary into the marine area, this muddy sediment is composed of marine material, which was deposited in the estuary during earlier marine inflow, and not of recently discharged fluvial mud. Such a situation cannot be persistent on a geological time-scale but due to the anthropogenic deepening of navigation channels in the estuary, the inflow of marine waters has doubled compared to the natural situation (Salden, 2000; Chen et al., 2005) which causes fluvial discharged mud to be deposited much higher up in the estuary or even in the fluvial regime itself, e.g. the siltation of the Westerscheldt, the Antwerp harbor and Scheldt river in the Gentbrugge-Melle area (Piesschaert et al., 2009). It is nevertheless not excluded that very small amounts of fresh fluvial mud reach the North Sea during extreme tidal and/or weather conditions.

For all of the reasons discussed above, it is not unreasonable to assume that the Scheldt river system presently does not actively discharge fluvial mud into the North Sea area but massively did before.

The fact that the Scheldt river system is the main clay supplier of the BCS muds seems in contradiction with the results of hydrodynamic modelling (see for instance Fettweis and Van

den Eynde, 2003; Fettweis et al., 2007) which indicate that presently the water reaching the BCS mainly originates from the English Channel area.

The crucial factor to understand why this is not a contradiction is the factor time. Presently, the BCS does not receive fresh fluvial mud whereas English Channel waters flow over the BCS. As the clay composition of the bottom mud on the BCS does not correspond to the composition of the English Channel waters, this must mean that none, or only minimal amounts, of the English Channel SPM are being deposited on the BCS. Instead, these suspensions are either transport further to the north in the North Sea or transported back to the English Channel following the tidal wave regime.

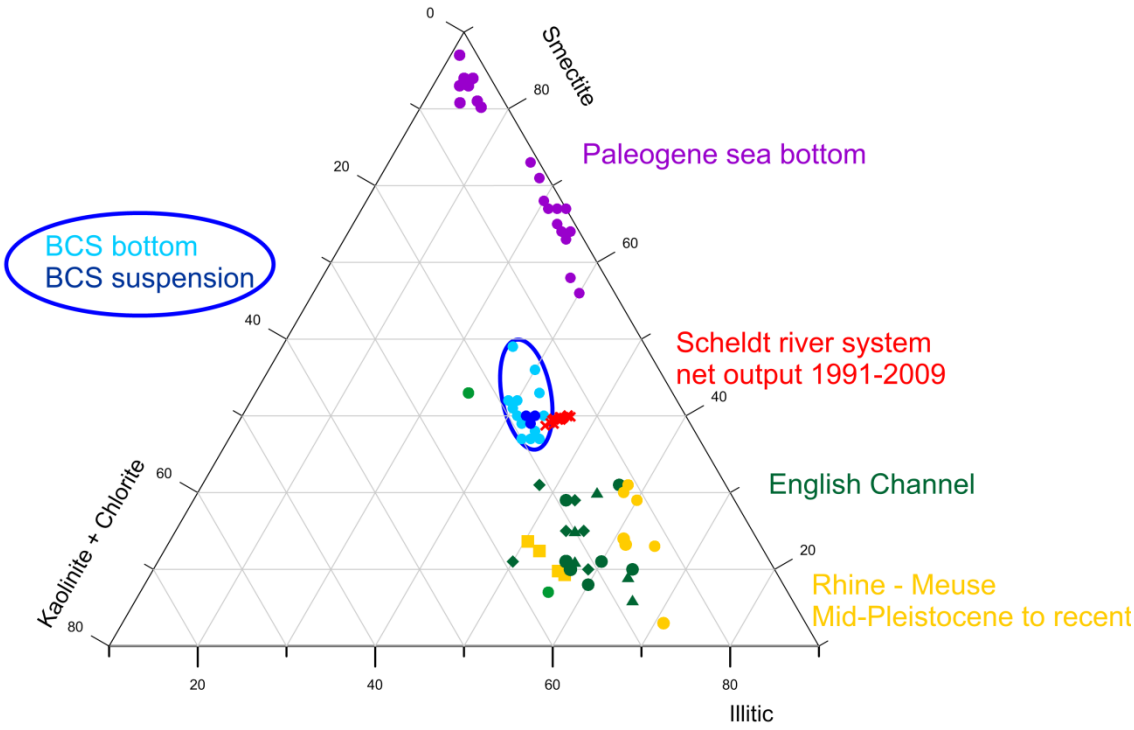

Figure 10.1. Ternary diagram comparing the BCS bottom and suspension composition with that of the different analyzed source areas.

XI.2 THE PROVENANCE OF THE BCS CLAY MINERALOGY DURING THE QUATERNARY

In this research also Holocene and middle- to late-Pleistocene deposits were studied to better document the Quaternary evolution in clay mineralogy and understand why the present-day clay composition also occurs in these older deposits.

In this research, the analysis of early-Holocene U4 deposits shows that their composition is very similar to that the U6 mudplate deposits and to that of the recent mud deposits, although there is on average a slight deviation. Although the difference is small, this could suggest an influence of a less-smectite rich clay source during the early-Holocene, e.g. the Rhine-Meuse system or the English Channel. Despite such smaller scaled influence, the large majority of clay is still delivered by the Scheldt river system.

For the Pleistocene sample set analyzed in this work, among which Weichselian, Eemian and Saalian deposits of the coastal plain, it was demonstrated that the clay mineralogy of the deposits formed in tidal environments is identical to that of the underlying Ypresian clays suggesting local reworking. This clay composition however gradually transitions in the BCS mud composition whenever the sedimentary environment becomes more fluvial (Figure 10.19). This confirms that a fluvial source, the Scheldt river system, was already discharging mud towards during the Saalian (MIS-7) to what is presently the BCS.

XI.3 CONCLUSION

This research has identified and addressed the remaining issues in the study of the BCS muds provenance after the work of Fontaine (2004), Gregoir (2005) and Zeelmaekers (2011). All results and interpretations shown above indicate that a fluvial source, the Scheldt river system, is responsible for the deposition of fine-grained sediments on the shelf and in the coastal area both during the Quaternary as well as presently. It is clear from the results that the particular Scheldt clay mineralogy was already established ca. 200.000 years ago during the Saalian (MIS-7). This means that the clay material eroded and discharged as SPM by the river system was already present in the river valleys before this time.
It is most likely that the clay composition found on the BCS today, was first formed when the paleo-Scheldt system connected all tributary rivers into one river system, subsequently discharged in westward direction, occupying the Flemish Valley. Before, the clay composition could not have existed because this composition can only be formed if the composition of the different tributaries is combined.

Although no deposits older than Saalian (MIS-7) were analyzed, the Scheldt clay composition was probably first introduced in the coastal plain during the Elsterian (MIS-12) after the first proglacial lake breakthrough (ca. 450.000y BP). Since this time , sediment transported by the river system was held nearby the coast during warm periods of high sea level. Depending on local hydrodynamics, the muds could be deposited like in the U6 mudplate or eroded during periods of increased storm activity. During the latest glacial, most deposits are eroded and later sporadically reworked in coastal plain or shelf deposits, such as the mudplate U6 deposits. During the late-Holocene, the Scheldt changed its course and eventually discharged into the Westerschelde. It is believed that presently, the Scheldt river system does not actively discharge fluvial mud into the North Sea, because of anthropogenic influence, but massively did before.

CONCLUSIONS & FUTURE PERSPECTIVES

In this work it was demonstrated how the systematic quantitative analysis of clay minerals yields a better understanding of specific geological and stratigraphical issues.

In the first part, a reliable and accurate method for the X-ray diffraction analysis of clay minerals, and glauconite minerals in particular, was established. Especially the decomposition and separate quantification of the 060-region in random oriented powder diffraction patterns was found a powerful tool for the characterization of glauconite-bearing sediments. It was shown that pelletal glauconite is able to disintegrate to clay-sized glauconite during intensive preparation procedures. Nevertheless, the large majority, at least 80%, of clay-sized glauconite in Neogene deposits in Belgium is introduced in the sediment by natural processes instead of artificially introduced during preparation procedures. To minimize contaminations, the clay mineralogy of pelletal glauconite-bearing sediments is systematically studied on size fractions <32µm, hereby isolating the large majority of pelletal glauconite, present in size fractions >32µm.

In the second part, quantitative clay and glauconite mineralogy was used for lithostratigraphic characterization of formation and specifically to better define stratigraphic boundaries between formations and subunits.

It was demonstrated that the clay mineral analyses for the Berchem Fm do not add information to the traditional stratigraphy as the clay mineral content in all members of the Berchem Fm, as well as in the Houthalen to Genk Members of the Bolderberg, is very constant with a smectite-rich assemblage.

In contrast, lithology and clay mineralogy within different parts of the Diest Fm was found to be very heterogeneous. The Deurne and Dessel Members have almost identical clay mineralogical and sediment petrological characteristics compared to those of the Berchem and the marine Bolderberg Formation indicating important reworking. A major break in clay mineralogy is observed in the Diest sand member, with the introduction of coarse clastics, and a glauconite-smectite dominated clay mineralogy. Different litho-units were recognized in the Diest sand member, named Diest D1-D4, of which the lowermost D1 unit is the most extensive unit composed of the coarse, loose, typical “Diest sand”. No difference was found between the Campine Diest D1 sand and the Hageland Diest sand. In the western part of the Campine basin, a clayey and pelletal glauconite-poor facies occurs, which were defined as the Diest D2 and D3 units. At the top of the Diest Formation, the Diest D4 unit is defined based on the presence of Fe-vermiculite, indicating the weathered, but not in-situ, origin of the sediments This unit was however not found in the southern part, such as in outcrops in Olen, Heist or the Hageland area where the Diest D1 unit forms the top of the Formation.

At the base of the Kasterlee Formation, a transition zone is found in which characteristics typical for the top Diest Fm gradually transition into typical Kasterlee Fm characteristics pointing to substantial reworking. It is likely that this reworking and the absence of the weathered Diest D4 unit in the southern part of the basin is related to the emersion of the Diest Fm during the Late-Miocene as a consequence of the ongoing subsidence of the Campine basin and the uplift of the Caledonian Brabant Massif. The lateral distribution of the weathered Diest D4 unit and the transition unit within the basin is not known and should be further mapped in order to be able to draw further conclusions.

Clay mineralogy of the Kasterlee Fm is dominated by glauconite-smectite although also kaolinite is significantly higher compared to the Diest Fm, which indicates an increased influence from the continent. The Pliocene Mol Fm consists of a kaolinite-dominated clay mineralogy which is continentally-derived.

In the Poederlee Formation, different types of clay mineralogical assemblages were found. At the base, reworked Kasterlee material was observed in Lichtaart. New, smectite-rich Poederlee sediment was found in outcropping

Poederlee deposits. In the Fe-sandstone facies of the Poederlee Formation, Fe-vermiculite and kaolinite-expandable indicate intensive weathering. This weathering also affected pelletal glauconite, of which the mineralogical composition consists of not only glauconite-smectite but also of Fe-vermiculite. The stratigraphy of the Poederlee Fm needs further study in order to map the lateral distribution of these different facies.

Several paleogeographic conclusions can be made from the clay mineral characterization:

1) Marine detrital clay is mainly transported from the North Sea and typically results in smectite-rich clay assemblages during the Miocene.
2) Continentally-derived clays were encountered in the Opgrimbie facies of the Bolderberg Fm, the Mol Fm and in the top Flemish hill sand deposits. The clay composition of all of the former deposits consists dominantly of kaolinite and illite which originates from the Ardennes-Rhenish massif in the south to southeast.
3) Substantial amounts of clay minerals have a reworked origin, such as the Deurne and Dessel Member of the Diest Fm and the basal deposits of the Kasterlee and Poederlee Formations. Glauconite-smectite in the Mol Formation is also considered as reworked. Pelletal glauconite was also massively reworked in the Neogene, except within the Antwerp Member.
4) Clay-sized glauconite-smectite has no detrital origin but instead is locally derived from pelletal glauconite abrasion or disintegration upon energetic transport. It occurs exclusively in the clay fraction of sands and never in clay intercalations. The mineralogy of clay-sized glauconite is systematically more expandable indicating the increased reactivity compared with pelletal glauconite.
5) Chemical weathering products (Fe-vermiculite) were observed in the Diest D4 unit and in the clay fraction and pelletal glauconite of deposits in the top of the Poederlee Fm. These weathering products most likely origin from eroded soils.

The paleogeographic significance of the clay minerals was however not worked in detailed and this topic should be addressed in future studies.

An interesting observation is also that pelletal glauconite seems to be massively reworked and when being mechanically weathered by transport, clay-sized glauconite is formed, mineralogically almost identical to pelletal glauconite. In the top of the Poederlee Fm however, chemical weathering of pelletal glauconite resulted in the presence of Fe-vermiculite. Such chemical weathering of pelletal glauconite is not observed in weathered glauconite pellets in the Miocene and suggests a link with climatic conditions.

Aside from unit characterization, the systematic clay mineralogical analyses allow to (1) unravel a more concise and detailed stratigraphic positioning, (2) make robust correlations between boreholes and, (3) define reliably boundaries between different formations and subunits. It was furthermore demonstrated that the defined boundaries are also levels characterized by an important change in paleoenvironment and that boundaries can also be correlated to gamma-ray and resistivity signatures.

It is also recommended that the stratigraphy of the Diest Fm is changed to incorporate the Diest sand member. The Veerle Fm is proposed with Deurne, Dessel and Diest Members. Within the Diest Member, the Hageland Diest sand is a separate facies as well as the clayey, glauconite-poor sands in the western part of the Campine. It is also recommended that , because of the lithological heterogeneity within units, boundary stratotypes are defined instead of unit stratotypes.

In the third part of this research, quantitative clay mineralogy was studied to find the provenance of recent mud deposits at the Belgian Continental Shelf. As all other potential source areas are characterized by a significantly different clay mineral composition, the Scheldt river system is the only possible provenance source. Analysis and combination of the clay mineral composition of the different tributary rivers of the Scheldt river system confirms that the fluvial composition matches the BCS mud composition. Although the Scheldt is presently not discharging fluvial mud to the BCS, it must have massively discharged mud in the past before anthropogenic influence. The BCS mud composition can indeed be traced back to Holocene and late-Pleistocene (Saalian-MIS-7) times. Logically, the clay composition was first introduced in the coastal plain when the paleo-Scheldt river system united all tributary rivers during which

the current Scheldt river clay composition was formed for the first time.
As the Scheldt river system was the main suspect at the start of this research, the study focused on the clay mineral characterization of the different tributaries of the Scheldt system. In the western part of the Campine, the Demer and Kleine and Grote Nete erode the Neogene deposits studied in part II, especially the Diest, Kasterlee and Poederlee Formations. Consequently, the relatively large amounts of glauconite-smectite present in these deposits was eroded and found at the bottom and in suspension of these rivers. In suspension material of the Kleine and Grote Nete rivers, substantial amounts of ferrihydrite were found which are logically related to the weathering of glauconite minerals. It is presently unclear how this glauconite weathering is related to the mechanical and chemical weathering of glauconite minerals encountered in the Neogene deposits. Possibly, there is a link with the ruling climatic conditions at the time of weathering.

It is clear that in this work many problems were clarified but also that several issues remain open questions which should be addressed in future studies. Such a continued research should therefore also focus on the occurrence of formations and units across international borders in order to make reliable interpretations and draw extensive and detailed conclusions regarding paleogeographic, tectonic and climatic evolution of the southern North sea during the Neogene and the Quaternary.

BIBLIOGRAPHY

Websites

International Commission on Stratigraphy: http://www.stratigraphy.org ; last consulted January 2015.

National Stratigraphic Commission Belgium: http://www.natstratcommBelgium.drupalgardens.com ; last consulted January 2015.

Literature

Adriaens, R. (2009) Mineralogical and crystal-chemical analysis of glauconites in the Upper-Cretaceous and Cenozoic strata of the Southern North Sea basin. Unpublished master thesis, University of Leuven, Leuven, België, 105pp.

Adriaens, R., Vandenberghe, N. and Elsen, J. (2014). Natural clay-sized glauconite in the Neogene deposits of the Campine basin (Belgium). *Clays and Clay Minerals*, **62**, 35-52.

Afdeling Land en Bodembescherming, Ondergrond, Natuurlijke rijkdommen (ALBON) (2009). Tertiair Geologische kaart Vlaanderen, Vlaamse Overheid, Departemend LNE.

Anderson, J.U. (1963). An improved pretreatment for mineralogical analyses of samples containing organic matter. *Clays and Clay Minerals*, **10**, 380-388.

Andresen, K.J., O.R. Clausen, and M. Huuse, 2009, A giant (5.3×107m3) middle Miocene (c. 15 Ma) sediment mound (M1) above the Siri Canyon, Norwegian–Danish Basin: Origin and significance, *Marine and Petroleum Geology*, **26** (8), 1640-1655.

Annell, I., Thybo, H., Rasmussen, E. (2012). A synthesis of Cenozoic sedimentation in the North Sea. *Basin Research*, **24**, 154-179.

Amorosi, A. (1997) Detecting compositional, spatial, and temporal attributes of glaucony: a tool for provenance research. *Sedimentary Geology* **109**, 135-153.

Aplin, A.C., Matenaar, I.F., McCarty, D.K., van der Pluijm, B.A. (2006). Influence of mechanical compaction and clay mineral diagenesis on the microfabric and pore scale properties of deep-water Gulf of Mexico mudstones. *Clays and Clay Minerals*, **54,** 500-514.

Auden, J.B. (1933). Vindhyan sedimentation in the Son Valley, Mirzapur district. India Geological Survey Mem. 62, pt. 2, 250pp.

Baeteman, C. and De Gans , W. (eds), (1993). Fieldmeeting 1993 Quaternary Shorelines in Belgium and the Netherlands, September 18-25. INQUA Subcommission on shorelines of Northwestern Europe. Geological Survey of Belgium, Geological Survey of the Netherlands, Earth technology Institute. Ministry Economic Affairs Brussels, 185pp.

Baeteman, C. (1999). The Holocene depositional history of the Ijzer paleo-valley (Western Belgian coastal plain) with reference to the factors controlling the formation of intercalated peat beds. *Geologica Belgica*, **2**, 39-72.

Baeteman, C., Scott, D.B. and Van Strydonck, M. (2002). Changes in coastal zone processes at a high sea-level stand: a late-Holocene example from Belgium. *Journal of Quaternary Science*, **17**, 547-559.

Bailey, S.W. (1980) Summary of recommendations of AIPEA nomenclature committee. *Clays and Clay minerals*, **65**, 1-7.

Bailey, S.W. (1988) Hydrous phyllosilicates (exclusive of micas). *Reviews in Mineralogy*, **19**, 725.

Baioumy, H. and Boulis, S. (2012) Non-pelletal glauconite from the Campanian Qusseir Formation, Egypt: Implication for glauconitisation. *Sedimentary Geology*, **249**, 1-9.

Baldermann, A., Grathoff, G.H., Nickel, C. (2012) Micromileu-controlled glauconitisation in fecal pellets at Oker (Central Germany). *Clay Minerals,* **47**, 513-538.

Bardon, C., Bieber, M.T, Cuiec, L., Jacquin, C., Courbot, A., Deneuville, G., Simon, J.M., Voirin, J.M., Espy., M., Nectoux, A., Pellerin, A. (1983). Recommandations pour la détermination expérimentale de la capacité d'échange de cations des milieux argileux. *Revue de L' Institut Francais Du Pétrole*, **38**, 621-626.

Bastin, A. (1966). Sedimentpetrologie van de Zanden van Edegem en de Zanden van Antwerpen. *Het Ingenieursblad*, Koninklijke Vlaamse Ingenieursvereniging, **35**/17, 547-550.

Bell, D. H. and Goodell, H. G. (1967) A comparative study of glauconite and the associated clay fraction in modern marine sediments. Sedimentology, **9**, 169-202.

Beets, D.J. and van der Spek, A.J.F. (2000). The Holocene evolution of the barrier and the back-barrier basins of Belgium and the Netherlands as a function of late Weichselian morphology, relative sea-level rise and sediment supply. Netherlands *Journal of Geosciences*, **79**, 3-16.

Berckmans, A. and Wouters, L. (2003). Werkvergadering mbt de stratigrafische indeling van de boring Dessel II. NIRAS nota 2003-2819.

Berg-Madsen, V. (1983) High-alumina glaucony from the middle Cambrian of Öland and Bornholm, Southern Baltoscandia. *Journal of Sedimentary Petrology*, **53**/3, 875–893.

Bergmann J., Friedel P., Kleeberg R. (1998). BGMN — a new fundamental parameters based Rietveld program for laboratory X-ray sources, it's use in quantitative analysis and structure investigations. *Commission of Powder Diffraction Newsletter*, **20**, 5–8.

Blundell, D.J., Freeman, R. and Mueller, S. (1992). *A continent revealed: The European geotraverse, structure and dynamic evolution*. Cambridge University Press, Cambridge.

Bornhold, B.D., Giresse, P. (1985). Glauconitic sediments on the continental shelf of Vancouver Island, British Columbia, Canada. *Journal of Sedimentary Petrology* , **55**, 653-664.

Brindley, G.W., Brown, G. (1980). *Crystal structures of clay minerals and their X-ray identification*. London, Mineralogical Society, 495pp.

Broothaers, L. (2000). Zandboek Vlaanderen. Dienst Natuurlijke Rijkdommen, Vlaamse Overheid, 115pp.

Buckley, H. A., Bevan, J. C., Brown, K. M., Johnson, L. R., Farmer, V. C. (1978) Glauconite and celadonite: two separate mineral species. *Mineralogical Magazine,* **42**, 373-382.

Buffel, P.,Vandenberghe, N., Goolaerts, S. and Laga P. (2001). The Pliocene sediments in 4 boreholes in the Turnhout area (North-Belgium): the relationship with the Lillo and Mol Formations. *Aardkundige Mededelingen*, **11**, University Press Leuven, 1-8.

Burst, J.F., (1958). Mineral heterogeneity of glauconite pellets. *American Mineralogist* , **43**, p481-497.

Busschers, F.S., Kasse, C., van Balen, R.T., Vandenberghe, J., Cohen, K.M, Weerts, D.J.T., Wallinga, J., Johns, C., Cleveringa, P. and Bunnik, F.P.M. (2007). Late Pleistocene evolution of the Rhine-Meuse system in the Southern North Sea basin: imprints of climate change, sea-level oscillation and glacio-eustacy. *Quaternary Science Reviews*, **26**, 3216-3248.

Cecil, M.R., Ducea, M.N. (2011). K-Ca ages of authigenic sediments: examples from Paleozoïc glauconite and applications to low-temperature thermochronometry. *International Journal of Earth Sciences*, Vol. **100**, Issue 8, 1783-1790.

Chafetz, H.S. and Reid, A. (2000). Syndepositional, shallow water precipitation of glauconitic minerals. *Sedimentary Geology*, **136**, 29-42.

Chamley, H. (1989*). Clay sedimentology*. Springer-Verlag, 623pp.

Chen, M.S.; Wartel, S.; Van Eck, B.T.M.; van Maldegem, D. (2005). Suspended matter in the Scheldt estuary. *Hydrobiologia ,***540,** 79-104.

Claret, F.,Sakharov, B.A.,Drits, V.A.,Velde, B., Meunier, A., Griffault, L. and Lanson, B. (2004). Clay minerals in the Meuse-Haute Marne underground laboratory (France): possible influence of organic matter on clay mineral evolution. *Clays and Clay minerals*, **52**, 515-535.

Curtis, C.D. (1995). Post-depositional evolution of mudstones I: early days and parental influences. *Journal of Geological Society*, **152**, 577-586.

De Batist, M. and Versteeg, W.H. (1999). Seismic stratigraphy of the Mesozoic and Cenozoic in northern Belgium: main results of a high-resolution reflection seismic survey along rivers and canals. *Geologie en Mijnbouw*, **77**, 17-37.

De Heinzelin, J. (1964). Le réseau hydrographique de la région gallo-belge au Néogene. Essais de reconstitution. *Bulletin de la Société belge de Géologie, de Paléontologie et d'Hydrologie*, **72**, 137-148.

De Man, E. and Van Simaeys, S. (2004). Late Oligocene Warming Event in the southern North Sea Basin: benthic foraminifera as paleotemperature proxies. *Netherlands Journal of Geosciences*, **83**, 227-239.

De Man , E., Van Simaeys, S., Vandenberghe, N., Harris, W.B. and Wampler, J.M. (2010). On the nature and chronostratigraphic position of the Rupelian and Chattian stratotypes in the southern North Sea Basin. *Episodes* , **33** (1), 3-14.

De Meuter, F.J. and Laga, P. (1976) Lithostratigraphy and biostratigraphy based on benthonic foraminifera of the Neogene deposits of northern Belgium. *Bulletin de Société belge Géologie*, **85**: 133–152.

De Schepper, S., Head, M.J. and Louwye, S. (2010). Pliocene dinoflagellate cyst stratigraphy, palaeoecology and sequence stratigraphy of the Tunnel-Canal Dock, Belgium. *Geological Magazine*, **146**, 92-112.

DeMaster, D.J. (1981). The supply and accumulation of silica in the marine environment. *Geochimica et Cosmochimica Acta*, **45**, 1715–1732.

Demyttenaere, R. (1988). De Post-Paleozoïsche geologische geschiedenis van Noord-België. Doctoraatsthesis, K.U.Leuven.

Demyttenaere, R. (1989). The Post-Paleozoic Geological History of North-Eastern Belgium. *Mededelingen Koninklijke Academie Wetenschappen Letteren en Schone Kunsten van België, Klasse Wetenschappen*, **51** (4), 51-81.

Dohrmann, R., Kaufhold, S. (2009). Three new, quick CEC methods for determining the amounts of exchangeable calcium cations in calcareous clays. *Clays and Clay Minerals*, **57**, 338-352.

Dohrmann, R., Kaufhold, S. (2010). Determinations of exchangeable calcium of calcareous and gypsiferous bentonites. *Clays and Clay Minerals*, **58**, 79-88.

Dohrmann, R., Rüping, K.B., Kleber, M., Ufer, K. and Jahn, R. (2009). Variation of preferred orientation in oriented clay mounts as a result of sample preparation and composition. *Clays and Clay Minerals*, **57** (6), 686-694.

Dou, Y., Yang, S., Liu, Z., Clift, P.D., Yu, H., Berne, S. and Shi, X. (2010). *Palaeogeography, Palaeoclimatology, Palaeoecology,* **288**, 108-117.

Drits, V.A., Sakharov, B.A. (1976). X-*ray Structural Analysis of Mixed-Layer Minerals.* Nauka, Moscow.

Drits, V.A., Lindgreen, H., Sakharov, B.A., Salyn, A.L. (1997). Sequential structure transformation of illite-smectite-vermiculite during diagenesis of Upper Jurassic shales, North Sea. *Clay Minerals*, **33,** 351-371.

Dudas, M.J. , Harward, M.E. (1971). Effect of dissolution treatment on standard and soil clays. *Soil Science Society of America Proceedings*, **35**, 134-140.

Eberl, D.D. (2003) *User's guide to RockJock—a program for determining quantitative mineralogy from x-ray diffraction data*. Open File Report 2003–**78**. Washington DC, United States Geological Survey, 55pp.

Eberl, D.D., Środoń, J., Lee, M., Nadeau, P. H., Northrop, H. R. (1987). Sericite from the Silverton caldera, Colorado: Correlation among structure, composition, origin, and particle thickness. *American Mineralogist*, **72**, 914-934.

El Albani, A. (2005) Unusual occurrence of glauconite in a shallow lagoonal environment (Lower Cretaceous, northern Aquitaine Basin, SW France). *Terra Nova*, **17**, 537-544.

Esquevin, J. (1969). Influence de la composition chimique des illites sur leur cristallinité. *Bulletin du Centre des Recherces de Pau*, **3**, no.1, 147pp.

Fettweis, M and Van den Eynde, D. (2003). The mud deposits and the high turbidity in the Belgian-Dutch coastal zone, southern bight of the North Sea. *Continental Shelf Research*, **23**, 669-691.

Fetweiss, M., Nechad, B. and Van den Eynde, D. (2007). An estimate of the suspended particulate matter (SPM) transport in the southern North Sea using SeaWiFS images, in situ measurements and numerical model results. *Continental Shelf Research*, 27, 1568-1583.

Fobe, B. (1995). Lithologie en lithostratigrafie van de Formatie van Kasterlee (Plioceen van de Kempen), *Natuurwetenschappelijk Tijdschrift*, **75**(2), 35-45.

Folk, R.L. (1980*). Petrology of sedimentary rocks*. Hemphill Publishing Company, Austin, Texas, 182 pp.

Fontaine, K. (2004). Waar komt het slib voor de Belgische kust vandaan ? Een kleimineralogische benadering. Licentiaatsthesis KULeuven, 118pp.

Geets, S. and De Breuck, W. (1991). De zware-mineraleninhoud van Belgische Mesozoïsche en Cenozoïsche afzettingen. G. Neogeen. *Natuurwetenschappelijk Tijdschrift (Gent)* **73**, 3-37.

Geets, S. (1962). Stratigrafische positie van het Poederliaan in de Antwerpse Kempen. *Natuurwetenschappelijk tijdschrift*, **44**, 143-152.

Gibbard, P.L. (2007). Europe cut adrift. *Nature*, **448**, 259-260.

Gilson, G. (1900). Exploration de la mer sur les côtes de la Belgique en 1899. *Mémoires du Musées Royal d'Histoire Naturelle de Belgique*, **I**, 81pp. *(in French)*

Gonzalez, R., Dias, J.M.A., Lobo, F., and Mendes, I. (2004). Sedimentological and paleoenvironmental characterization of transgressive sediments on the Guadiana Shelf (Northern Gulf of Cadiz, SW Iberia). *Quaternary International*, **120**, 133-144.

Gossé, J.G. (1977). A preliminary investigation into the possibility of erosion in the area of the Flemish Banks. FA 7702, RIKZ, The Netherlands.

Gradstein, F.M., Ogg, J.G., Schmitz, M.D., Ogg, G.M. (2012). *The Geologic Time Scale*, Elsevier, Amsterdam, 1176pp.

Grim, R.E. (1962). *Applied clay mineralogy*: McGraw Hill, New York, 422 p.

Gulbrandsen, R.A., Goldich, S.S., Thomas, H.H. (1963). Glauconite from the Precambrian belt series, Montana. *Science*, **140**, 390-391.

Gulinck, M. (1960). Un gisement de kiezeloolithes à Lichtaart (Kempen). Comparaison avec les cailloutis à kiezeloolithes des collines flamandes. *Bulletin de la société belge de Géologie*, **59**, 191-204.

Gulinck, M. (1963). Symposium sur la Stratigraphie du Néogène nordique, Gand 1961. Essai d'une carte géologique de la Campine. Etat de nos connaissances sur la natures des terrains néogènes recoupés par sondages. *Mémoires de la Société belge de Géologie,* serie in-8, **6**, 30-39.

Gulinck, M. (1964b). Boring te Neeroeteren (Groeve Knippenberg) 64W-234. Archives Belgian Geological Survey , Brussels.

Gulinck, M. (1964a). Lithological description and stratigraphic interpretation of the Westerlo 60e215 borehole. Open access report, Databank Ondergrond Vlaanderen.

Gulinck, M. and Laga, P. (1975). Boring te Mol 31W237. Archives Belgian Geological Survey , Brussels.

Gulinck, M. and Laga,P. (1975a). Lithological description and foraminifera investigation of the Oostmalle - Rijkevorsel 16e153 borehole. Unpublished notes of P. Laga. Belgian Geological Survey.

Gulinck, M. and Laga,P. (1975b). Lithological description and foraminifera investigation of the Essen 1e42 borehole. Unpublished notes of P. Laga. Belgian Geological Survey.

Gulinck, M., Geets, S. Van Voorthuysen, J.H. (1964). Note sur les sondages du Centre Nucléaire à Mol. *Bulletin de la Société belge de Géologie*, **72**, 283-294.

Gullentops F. (1957). L'origine des colines du Hageland. *Bulletin Société belge de Géologie*, **65**, 81-85.

Gullentops F. (1963). Etude de divers facies quatemaires et tertiaires dans le Nord et l'Est de la Belgique. Excursion O-P, *6e Congrès International de Sédimentologie*, Belgique et Pays-Bas, 7pp.

Gullentops, F. (1988). Neogene . *In:* I*.A.S. 9th European Regional Meeting, Excursion Guidebook Leuven-Belgium, Sept. 1988* (Herbosch A., editor), Belgian Geological Survey, Brussels, 226 and 255-260.

Gullentops, F., Moens,M., Ringelé, A. and Sengier, R. (1976). Geologische kenmerken van de suspensie en de sedimenten. In: Nihoul, J.C.J. and Gullentops,F. Project Zee/ Projet Mer, Volume 4: Sedimentologie. Brussels, Science Policy Office, 1-137.

Gullentops,F. and Huyghebaert, L. (1999). A profile through the Pliocene of Northern Kempen, Belgium. Aardkundige Mededelingen , *University Press Leuven*, **9** , 191-202.

Gullentops, F., Bogemans, F., De Moor, F., Paulissen, E. and Pissart, A. (2001). Quaternary lithostratigraphic units (Belgium). *Geologica Belgica*, **4**, 153-164.

Halet, F. (1935). A propos des formations dites Casterliennes des environs d'Hérenthals en Campine. *Bulletin de la Société belge de Géologie*, **45**, 290-297.

Harris, W.B., Fullager, P.D., and Tovo, L.T. (2007). Significance of young Paleocene Rb-Sr glauconite dates from the Lang Syne Formation, Savannah River site, South-Carolina. *Southeastern Geology*, **37**, 55-72.

Harward, M.E. and Brindley, G.W. (1965). Swelling properties of synthetic smectite in relation to lattice substitutions. *Clays and Clay Minerals*, **13**, 209–222.

Hill, R.J., Howard, C.J. (1987). Quantitative phase analysis from neutron powder diffraction data using the Rietveld method. *Journal of Applied Crystallography*, **20**, 467-474.

Hillier, S. (1999). Use of an air brush to spray dry samples for X-ray powder diffraction. *Clay Minerals*, **34**, 127-135.

Houthuys, R. (2011). A sedimentary model of the Brussels sands, Eocene, Belgium. *Geologica Belgica*, **14**, 55-74.

Houthuys, R. (2014). A reinterpretation of the Neogene emersion of central Belgium based on the sedimentary environment of the Diest Formation and the origin of the drainage pattern. *Geologica Belgica*, **17**, 211-235.

Howell, A.L., Bentley Sr., S.J., Xu, K., Ferell Jr., R.E., Muhammad, Z. and Septama, E. (2014). Fine sediment mineralogy as a tracer of latest Quaternary sediment delivery to a dynamic continental marin: Pandora Through, Gulf of Papua, Papua New Guinea. *Marine Geology*, **357**, 108-122.

Hubert,F., Caner, L, Meunier, A., Lanson, B. (2009). Advances in characterization of the soil clay mineralogy using X-ray diffraction: from decomposition to profile fitting. *European Journal of Soil Science*, **60**, 1093-1105.

Hubert, F., Caner, L., Meunier, A., Ferrage, E. (2012). Unraveling complex <2µm clay mineralogy from soils using X-ray diffraction profile modeling on particle-size sub-fractions: Implications for soil pedogenesis and reactivity. *American Mineralogist*, **97**, 384-398.

Huyghebaert, B. and Nolf, D. (1979)**.** Otolithes de Téléostèens et biostratigraphie des Sables de Zonderschot (Miocène Moyen de la Belgique). *Mededelingen van de Werkgroep voor Tertiaire en Kwartaire Geologie,* **16**, 59-100.

Ireland, B.J., Curtis, C.D., Whiteman, J.A. (1983) Compositional variation within some glauconites and illites and implications for their stability and origins. *Sedimentology*, **30**, 769-786.

Irion, G. and Zölmer, V., 1999. Clay mineral associations in fine grained surface sediments of the North Sea*. Journal of Sea Research*, **41**, 119-12.

ISO (2006). Petroleum and natural gas industries – Completion fluids and materials. Part 2: Measurement of properties of proppants used in hydraulic fracturing and gravel-packing operations. ISO 13503-2: 2006(E). International Organisation for Standardisation, Geneva, Switzerland.

Ivanovskaya, T.A. and Geptner, A.R. (2004). Glauconite at different stages of lithogenesis in Lower Cambrian rocks of Western Lithuania

Jackson, M.L., 1975. Soil chemical analysis – Advanced course, 2nd edition. Published by the author, Madison, Wisconsin, 895pp.

Japsen, P. And Chalmers, J.A. (2000). Neogene uplift and tectonics around the North Atlantic: overview. *Global and Planetary Change*, **24**, 165-173.

Johnson, H.D and Baldwin, C.T. (2006). Shallow clastic seas In: Reading, H.G. (editor) *Sedimentary environments: Processes, Facies and Stratigraphy*, third edition, Blackwell Science, UK, 232-280.

Kessarkar, P.M., Purnachandra Rao, V., Shynu, R., Mehdra, P. and Viegas, B.E. (2010). *Estuaries and Coasts*, **33**, 30-44.

Ketzer, J.M., Morad, S., Nystuen, J.P., De Ros, L.F. (2003). The role of the Cimmerian unconformity (Early Cretaceous) in the kaolinization and related reservoir-quality evolution in Triassic sandstones of the Snorre Field, North Sea, in R.H Worden and S. Morad. (eds*.), Clay Cements in Sandstones: IAS Special Publication*, 34: Oxford, UK, International Association of Sedimentologists - Blackwell Scientific Publications, 353-374.

King, C. (2006). Paleogene and Neogene: uplift and a cooling climate. In: The Geology of England and Wales (Brenchley, P.J. and Rawson, P.F., editors). The Geological Society of London, 561pp.

Kleeberg, R., Monecke, T., Hillier, S. (2008). Preferred orientation of mineral grains in sample mounts for quantitative XRD measurements: how random are powder samples? *Clays and Clay Minerals*, **56**, 404-415.

Komadel, P., Lear, P.R., Stucki, J.W. (1990). Reduction and reoxidation of nontronite: extent of reduction and reaction rates. *Clays and Clay Minerals*, **38**, 203-208.

Krumbein, W.C. and Sloss, L.L. (1963). *Stratigraphy and sedimentation*. Second Edition. W.H. Freeman and Company, San Francisco, 660 pp.

Kuhlmann, G. (2004). High resolution stratigraphy and paleoenvironmental changes in the southern North Sea during the Neogene – An integrated study of the Late-Cenozoïc marine deposits from the northern part of the Dutch offshore area. Thesis Utrecht University, *Geologica Ultraiectina, Mededelingen van de Faculteit Aardwetenschappen*, **245**, 205pp.

Labat, S., Gedeon, M., Beerten, K. and Maes, T. (2011). Dessel-5 borehole: technical aspects and hydrogeological investigations. SCK-CEC external report, 39pp.

Lacroix, G., Ruddick, K., Ozer, J., Lancelot, C. (2004). Modeling the impact of the Scheldt and Rhine/Meuse plumes on the salinity distribution in Belgian waters (Southern North Sea). *Journal of Sea Research*, **52**, 149-163.

Laenen, B. (1997). The Geochemical Signature of Relative sea-Level Cycles Recognized in the Boom Clay. Doctoral thesis, University of Leuven, 3 volumes.

Laga, P. (1970). Stratigrafie van de marine Plio-Pleistocene afzettingen uit de omgeving van Antwerpen met een bijzondere studie van de formaminiferen. Master thesis, KULeuven.

Laga, P. (1972). Een fossielhoudende zandsteen in de Zanden van Diest te Olmen (Antwerpse Kempen). *Bulletin de la Société belge de Géologie*, **81**, 251-254.

Laga, P. (1975). Geologisch Profiel Meerle-Olen-Houwaert. PGL 75/104/1 Archives Belgian geological Survey, Brussels

Laga, P. and De Meuter, F.J. (1972). A foraminiferal fauna found in the lower member of the Diest Formation of borings of the Antwerp Kempen – *Bull. Soc. Belge Géol., Pal. Hydrol*., **81**, 211–220
Laga, P. and Notebaert, K. (1981). Boring Weelde 8E 133. Archives Belgian Geological Survey , Brussels.

Laga P, Louwye S, Geets S. 2001. Paleogene and Neogene lithostratigraphic units (Belgium). In Guide to a revised lithostratigraphic scale of Belgium, Bultynck P, Dejonghe L (eds). Geologica Belgica 4(1–2): 135–152.

Laird, D. and Fleming, P. (2008) Analysis of layer charge, cation and anion exchange capacaties, and synthesis of reduced charge clays. Pp 485-508 in: *Methods of soil analysis, part 5: Mineralogical methods* (Ulery, A.L., Drees, L.R., editors). Soil Science Society of America book series number **5**, Madison.

Li, Y., Li, A-C., Huang, P., Xu, F-J., Zheng, X-F. (2014). Clay minerals in surface sediment of the north Yellow Sea and their implication to provenance and transportation. *Continental Shelf Research*, **90**, 33-40.

Lindgreen, H., Drits, V.A., Sakharov, B.A., Jakobsen, H.J., Salyn, A.L.,Dainyak, L.G. and Kroyer,H. (2002). The structure and diagenetic transformation of illite-smectite and chlorite-smectite from NorthSea Cretaceous-Tertiary chalk. *Clay Minerals*, **37**, 429-450.

Liu, Z., Tuo, S., Colin, C., Liu, J.T., Huang, C., Selvaraj, K., Arthur Chen, C., Zhao, Y., Siringan, F.P., Boulay, S. and Chen, Z. (2008). Detrital fine-grained sediment contribution from Taiwan to the northern South China Sea and its relation to regional ocean circulation. *Marine Geology*, **255**, 149-155.

Liu, J.P., Xue, Z., Ross, K., Wang, J., Yang, Z.S., Li, A.C. and Gao, S. (2009). Fate of sediments delivered to the sea by Asian large rivers: Long-distance transport and formation of remote alongshore clinothems. *SEPM The Sedimentary Record*, **7**, 4-9.

Liu, Z., Colin, C., Li, X., Zhao, Y., Tuo, S., Chen, Z., Siringan, F.P., Liu, J.T., Huang, C., You, C. and Huang, K. (2010). *Marine Geology*, **277**, 48-60.

Louwye, S. (2000). Dinoflagellate cysts and acritarchs from the Miocene Zonderschot sands, Northern Belgium: stratigraphic significance and correlation with contiguous areas. *Geologica Belgica*, **3**, 55-65.

Louwye, S. (2001). New species of dinoflagellate cysts from the Berchem formation, Miocene, northern Belgium (southern North Sea basin). *Geobios*, **34**, Issue 2, 121-130.

Louwye, S. (2002). Dinoflagellate cyst biostratigraphy of the Upper Miocene Deurne Sands (Diest Formation) of northern Belgium, southern North Sea Basin. *Geological Journal*, **37**,55-67.

Louwye, S. (2005) The Early and Middle Miocene transgression at the southern border of the North Sea Basin (northern Belgium). *Geological Journal*, **40**, 441- 456.

Louwye, S. and De Schepper, S. (2010). The Miocene–Pliocene hiatus in the southern North Sea Basin (northern Belgium) revealed by dinoflagellate cysts. *Geological Magazine*, **5**, 760-776.

Louwye, S. and Laga, P. (1998). Dinoflagellate cysts of the shallow marine Neogene succession in the Kalmthout well, northern Belgium. *Bulletin of the Geological Society of Denmark*, **45**, 73-86.

Louwye, S. and Laga, P. (2008). Dinoflagellate cyst stratigraphy and palaeoenvironment of the marginal marine Middle and Upper Miocene of the eastern Campine area, northern Belgium (southern North Sea basin). *Geological Journal*, **43**, 75-94

Louwye, S., De Coninck, J., and Verniers, S. (1999) Dinoflagellate cyst stratigraphy and depositional history of Miocene and Lower Pliocene formations in northern Belgium (southern North Sea basin). *Geologie en Mijnbouw*, **78**, 31-46.

Louwye, S., De Conick, J., and Verniers, J. (2000) Shallow marine Lower and Middle Miocene deposits at the southern margin of the North Sea Basin (northern Belgium): dinoflagellate cyst biostratigraphy and depositional history. *Geological Magazine,* **137**, 381-394.

Louwye, S., De Schepper, S., Laga, P., and Vandenberghe, N. (2007). The Upper Miocene of the southern North Sea Basin (northern Belgium): a palaeoenvironmental and stratigraphical reconstruction using dinoflagellate cysts. *Geological Magazine.* **144**(1), 33-52.

Louwye, S., Marquet, R., Bosselaers, M., Lambert, O. (2010). Stratigraphy of an Early-Middle Miocene sequence near Antwerp in northern Belgium (southern North Sea Basin). *Geologica Belgica*, **13** (3), 269-284.

Malla, P. B., Douglas, L. A. (1987). Problems in identification of montmorillonite and beidellite. *Clays and Clay Minerals*, **35**(3), 232-236.

Maréchal, R. (1993). A new lithostratigraphic scale for the Palaeogene of Belgium. *Bulletin de la Société belge de Géologie*, **102**(1-2), 215-229.

Martini, E. and Müller, C. (1973). Nannoplankton-Gemeinschaften im Miozän and Pliozän des Nordseebeckens. *Neues Jahrbuch Geologie und Paläontologie*, **9**, 555-564.

Mathys, M; (2009). The Quaternary geological evolution of the Belgian Continentel Shelf, southern North Sea. Doctoral dissertation, University of Ghent, 382pp.

Matthijs, J., Lanckacker, T., De Koninck, R., Deckers, J., Lagrou, D. and Broothaers, M. (2013). Geologisch 3D lagenmodel van Vlaanderen en het Brussels Hoofdstedelijk Gewest – versie 2, G3Dv2. Studie uitgevoerd door VITO in opdracht van de Vlaamse overheid, Departement Leefmilieu, Natuur en Energie, Afdeling Land en Bodembescherming, Ondergrond, Natuurlijke Rijkdommen, VITO-rapport 2013/R/ETE/43.

McRae, S.C. (1972). Glauconite. *Earth-Science Reviews*, **8**, 397-440.

Mehra, O.P, Jackson, O.M. (1960). Iron oxide removal from soils and clays by a dithionite-citrate-system buffered with sodium bicarbonate. *Clays and Clay Minerals*, **7**, 317-327.

Méring, J. (1949). L'Inté reference des Rayons X dans les systems à stratification dé sordonnée. *Acta Crystallographica*, **2**, 371-377.

Meunier, A. (2005) *Clays*. Springer-Verlag, Berlin, 472 pp.

Meunier, A., El Albani, A. (2007). The glauconite-Fe-illite-Fe-smectite problem : a critical review. *Terra Nova*, **19**, 95-104.

Michon, L., Van Balen, R., Merle, O., Pagnier, H. (2003). Cenozoïc evolution of the Roer Valley Rift System integrated at a European scale. *Tectonophysics*, **367**, 101-126.

Missiaen, T., Murphy, S., Loncke, L. and Henriet, J.-P. (2002). Very high-resolution seismic mapping of shallow gas in the Belgian coastal zone. *Continental Shelf Research*, **22**, 2291-2301.

Moore, D.M., Reynolds, R.C., Jr. (1997). *X-ray diffraction and the identification and analysis of clay minerals*. Oxford University Press, Oxford-New York, 378pp.

Mosser-Ruck, R., Devineau, K., Charpentier, D. And Cathelineau, M. (2005). Effects of ethylene glycol saturation protocols on XRD patterns: a critical review and discussion. *Clays and Clay Minerals*, **53**, 631-638.

Mostaert, F. and De Moor, G. (1989). Eemian and Holocene sedimentary sequences on the Belgian coast and their meaning for sea level reconstruction. In: J.P. Henriet and G.D. Moor (Editors), The Quaternary and Tertiary Geology of the Southern Bight, North Sea. Ministry of Economic Affairs, Belgian Geological Survey, Gent, 137-148.

Mostaert, F. , Auffret, J.P., De Batist, M., Henriet, J.P., Moons, A., Sevens,E., Van den Broeke, I. and Verschuren, M. (1989). Quaternary shelf deposits and drainage patterns off the French and Belgian Coasts. In: J.P. Henriet and G.D. Moor (Editors), The Quaternary and Tertiary Geology of the Southern Bight, North Sea. Ministry of Economic Affairs, Belgian Geological Survey, Gent, 111-118.

Mozley, P.S. (1989). Relation between depositional environment and the elemental composition of early diagenetic siderite. *Geology*, 17, 704-706.

Mikutta, R., Kleber, M., Kaiser, K., Jahn, R. (2005). Organic matter removal from soils using hydrogen peroxide, sodium hypochlorite, and disodium peroxdisulfate. *Soil Science Society of America Journal*, **69**, 120-135.

Mystkowski, K., Środoń, J., McCarty, D.K. (2002). *Application of evolutionary programming to automatic XRD quantitative analysis of clay-bearing rocks*: The Clay Minerals Society 39th Annual Meeting, Boulder, CO, Abstracts with program.

Nechad, B., Fettweis, M., Francken, M. and Van den Eynde, D. (2003). Suspended particulate matter mapping from multitemporal Sa Wifs imagery of the Southern North Sea – SEBAB project. Multitemp 2003 workshop held in Ispra, 16-18 July.

Nihoul, J.C.J. (1975). Effect of tidal stress on residual circulation and mud deposition in the Southern Bight of the North Sea. *Review of Pure and Applied Geophysics*, **113**, 577–591.

Nybakk, E. and Fabricius, I.A. (2001). Excess conductivity of glauconite. 6th Nordic symposium on petrophysics, Tronheim, Norway.

Odin, G.S., (1982) *Numerical dating in stratigraphy.* Wiley Interscience, New York, 1094 pp.

Odin, G.S., Hunziker, J.C., Keppens, E., Laga, P.G., and Pasteels, P. (1974) Analyse radiométrique de glauconies par les méthodes au strontium et a l'argon; L'Oligo-Miocène de Belgique. *Bulletin de Société belge Géologie*, **83**, 1, 35-48.

Odin, G.S. and Giresse, P. (1972). Formation de mineraux phylliteux (berthierine, smectites ferrifères, glauconite ouverte) dans les sediments du Golf de Guinée. *Comptes Rendus de l'Académie des sciences, série D: Sciences naturelles*, **275**, 177-180

Odin, G.S. and Lamboy, M. (1988). Glaucony from the margin of northwestern Spain. In: *Green Marine Clays: Developments in Sedimentology* (G.S. Odin, editor). Elsevier, Amsterdam, 249-275.

Odin, G.S.and Matter A. (1981). De glauconiarum origine, *Sedimentology*, **28**, 611–641.

Odin, G.S.and Fullager P.D. (1988). Geological significance of glaucony facies. Pp295-332 in: *Green marine clays* (G.S. Odin, editor). Developments inSedimentology, **45**, Elsevier, Amsterdam.

Odom, I.E. (1976). Microstructure, mineralogy and chemistry of Cambrian glauconite pellets and glauconite, Central USA. *Clays and Clay minerals*, Vol. **24**, 232-238.

Omotoso, O., McCarthy, D.K., Hillier, S., Kleeberg, R. (2006). Some successful approaches to quantitative mineral analysis as revealed by the 3th Reynolds Cup contest. *Clays and Clay Minerals*, **54**, 748-760.

Orsini, L., Remi, J.-C. (1976). Utilisation du chlorure de cobaltihexammine pour la détermination simultanée de la capacité d'échange et des bases échangeables des sols. *Science du Sol*, **4**, 269-275.

Pache, T., Brockamp, O. and Clauer, N. (2008). Varied pathways of river-borne clay minerals in a near-shore marine region : A case study of sediments from the Elbe- and Wester rivers, and the SE North Sea. *Estuarine, Coastal and Shelf Science*, **78**, 563-575.

Piesschaert F., Van Braeckel A., Mertens W., Mikkelsen J., Spanoghe G., Speybroeck J., Vandevoorde B. and Van den Bergh E. (2009). Scheldetraject Gentbrugge-Melle; ecologische potenties in het bovenstrooms Zeescheldetraject. Rapporten van het Instituut voor Natuur-en Bosonderzoek 2009 (INBO.R.2009.47). Instituut voor Natuur-en Bosonderzoek, Brussel.

Pillans, B. and Gibbard, P. (2012). The Quaternary Period. Pp979-1010 in: The Geologic Time Scale 2012 (Gradstein, F.M., Ogg, J.G., Schmitz, MD. And Ogg, G., eds.), Elsevier, Amsterdam.

Porrenga, D.H. (1966). Clay minerals in recent sediments of the Niger delta. Pp 221-233 in: Clays and Clay minerals: proceedings of the 14th National Conference on Clays and Clay Minerals (S.W. Bailey, ed.), Clay Mineral Society, Berkeley.

Ramaswamy, V., Nagender Nath, B., Vethamony, P. and Illangovan, D. (2007). Source and dispersal of suspended sediment in the macro-tidal Gulf of Kachchh. *Marine Pollution Bulletin*, **54**, 708-719.

Rasmussen, E.S., Dybkjaer, K. and Piasecki, S. (2010). Lithostratigraphy of the Upper Oligocene – Miocene succession of Denmark. *Geological Survey of Denmark and Greenland Bulletin*, **22**, 1-92.

Rasmussen, E.S. and Dybkjaer, K. (2014). Patterns of Cenozoïc sediment flux from western Scandinavia: discussion. *Basin Research*, **26**, 338-346.

Renngarten, N.V., Rateev, M.A., Shutov, V.D., and Drits, V.A. (1978). Lithology and Clay Mineralogy of Sediments from Site 337, DSDP Leg 38. *DSDP Supplement to Volumes*

38-39-40-41, Deep Sea Drilling Project Report and Publications.

Reading, H.G. and Collinson, J.D. (1996). Clastic coasts. In: Reading, H.G. (editor) *Sedimentary environments: Processes, Facies and Stratigraphy*, third edition, Blackwell Science, UK, 154-232.

Reynolds, R.C., Jr. (1986). The Lorentz-Polarization factor and preferred orientation in oriented clay aggregates. *Clays and Clay Minerals*, **34**, 359–367.

Robert, M.M.M and Barshad, I. (1972). Note des membres et correspondants et notes présentées ou transmises par leur soins minéralogie – Sur les propriétés et la determination des minéraux argileux 2/1 expansibles (vermiculites-smectites). *C.R. Academie Scientific de Paris,* **275**, 3p.

Robinson, G.W. (1922). Note on the mechanical analysis of humus soils. *Journal of Agricultural Science*, **12** , 287.

Rögl, F. (1999), Mediterranean and Paratethys:Facts and hypotheses of an Oligocene to Miocene paleogeography (short overview), *Geologica Carpathica*, **50**(4), 330– 349.

Rosenblum, S. , Brownfield, I.K (2000). Magnetic susceptibilities of minerals. USGS open file report 99-529, 37pp.

Ruffel, A., McKinley, J.M. and Worden, R.H. (2002). Comparison of clay mineral stratigraphy to other proxy paleoclimate indicators in the Mesozoic of NW Europe. *Philosophical Transactions of the Royal Society A: Mathematical, Physical and Engineering Sciences*, **360**, 675-693.

Saccone, L., Conley, D.J., Sauer, D. (2006). Methodologies for amorphous silica analysis. *Journal of Geochemical Exploration*, **88**, 235-238.

Sakharov, B.A., Lindgreen, H., Salyn, A.L., Drits, V.A. (1999). Determination of illite-smectite structures using multispecimen X-ray diffraction profile fitting. *Clays and Clay Minerals*, **47**, 555-566.

Sakharov, B.A., Dubińska, E., Bylina, P., Kozubowsk, J.A., Kaproń, G. and Frontczak-Baniewicz,M. (2004). Serpentine-smectite interstratified minerals from Lower Silesia (WS Poland). *Clays and Clay Minerals*, **52**, 55-65.

Salden R.M. (2000). Effecten van systeemingrepen op de water- en bodemkwaliteit van de Westerschelde. Rapport RIKZ/2000.006, 41pp.

Salden, R.M., Mulder, H.P.J. (1996). De slibbalans voor de Nederlandse kustwateren onder invloed van slibonttrekking als gevolg van strengere kwaliteitstoetsing van baggerspecie. OS-96.116X, RIKZ, The Netherlands.

Sandler, A. and Herut, B. (2000). Composition of clays along the continental shelf off Isreal: contribution of the Nile versus local sources. *Marine Geology*, **167**, 339-354.

Scarlett, N.V.Y, Madsen, I.C (2006). Quantification of phases with partial or no known crystal structures*. Powder diffraction*, **21**, 278-284.

Schiltz, M., Vandenberghe, N. and Gullentops, F. 1993. *Tertiairgeologische kaart van België, Vlaams gewest, Kaartblad 16 Lier 1/50000*. In opdracht van de Belgische Geologische Dienst en het Ministerie van de Vlaamse Gemeenschap, Afdeling natuurlijke Rijkdommen en Energie.

Schwertmann, U. (1964). Differenzierung der Eisenoxide des Bodens durch Extraktion mit Ammoniumoxalat-Lösung. *Journal of Plant Nutrition and Soil Science*, **105**, 194–202.

Seed**,** D.P. (1968) The analysis of the clay content of some glauconite oceanic sediments. Journal of Sedimentary Petrology, **38**: 229-231.

Sels, O., Claes, S. and Gullentops, F. (2001). Toelichtingen bij de Geologische Kaart van België,Vlaams Gewest Kaartblad 18-10, Maaseik (en Beverbeek) 1:50000. Ministerie van de Vlaamse Gemeenschap, ANRE, Brussel, België 50p.

Schäfer, A., Utescher, T. and Mörs, T. (2004). Stratigraphy of the Cenozoic Lower Rhine Basin, nortwestern Germany. *Newsletter on Stratigraphy*, **40**, 73-110**.**

Schäfer, A. and Utescher, T. (2014). Origin, sediment fill, and sequence stratigraphy of the Cenozoic Lower Rhine Basin (Germany) interpreted from well logs. *Zeitschrift der Deutschen Gesellschaft für Geowissenschaften*, **165**, 287-314.

Shang, C., Zelazny, L.W. (2008) Selective dissolution techniques for mineral analysis of soils and sediments. Pp 33-80 in: *Methods of soil analysis, part 5: Mineralogical methods* (Ulery, A.L., Drees, L.R., editors). Soil Science Society of America book series number **5**, Madison.

Sissingh, W. (2003). Tertiary paleogeographic and of the Rhenish tectonostratigraphic evolution triple Junction. *Palaeogeography Palaeoclimatology Palaeoecology,* **196** (1-2), 229-263.

Sissingh, W. (2006). Tertiary Evolution of the West European Platform: syn-kinematic stratigraphy and palaeogeography. *Netherlands Journal of Geology/Geologie en Mijnbouw* **85**, 131pp.

Soers, E., Gullentops, F., Geets, S., De Moor, G., Malherbe, B. and Broothaers, L. (1996). Bouwzand. *In: Delfstoffen in Vlaanderen (F. Gullentops and L. Wouters, editors*). Vlaams Energieagentschap, 175pp.

Soukup, D.A., Buck, B.J., Harris, W. (2008) Preparing soils for mineralogical analysis. Pp 13-32 in: *Methods of soil analysis, part 5: Mineralogical methods* (Ulery, A.L., Drees, L.R., editors). Soil Science Society of America book series number **5**, Madison.

Środoń, J., Drits, V.A., McCarty, D.K., Hsieh, J.C.C., Eberl, D.D. (2001). Quantitative XRD analysis of clay-rich rocks from random preparations. *Clays and Clay Minerals*, **49**, 514-528.

Środoń, J., and McCarty, D.K. (2008). Surface area and layer charge of smectite from CEC and EGME/H_2O-retention measurements. *Clays and Clay Minerals*, **56** (2), 155–174.

Stessels (1866). Carte générale des bancs de Flandre compris entre Gravelines et l'embouchure de l'Escaut. Ministre des affaires étrangères, Anvers, Belgium. *(in French)*

Storer, D.A. (1984). A simple high sample volume ashing procedure for determining soil organic matter. *Communications in Soil Science and Plant Analysis*, **15**, 759-772.

Suquet, H., De la Calle, C. and Pezerat, H. (1975). Swelling and structural organization of saponite. *Clays and Clay Minerals*, **23**, 1–9.

Svoboda J. (2004). *Magnetic techniques for the treatment of materials*. Kluwers Academic Publishers, Dordrecht. 656 pp.

Tavernier R. and de Heinzelin J. (1962). Introduction au Néogène de la Belgique. *In: Symposium sur la stratigraphie du Néogène nordique (*de Heinzelin J. and Tavernier R., editors). Mémoire Société belge de Géologie, **6**, 7-30.

Tavernier, R. and De Moor, G. (1974). L'Evolution du Bassin de l'Escaut. In : P. Macar and F. Gullentops (Editors), L'Evolution Quaternaire des bassins fluviaux de la Mer du Nord Méridoniale. Cent. Soc. Géol. Belg., Liège, 159-233.

Taverniers, E. (2000). Beneden-Zeeschelde: slibbalans 1999. *Verslag AMS*, 2000.04. Ministerie van de Vlaamse Gemeenschap. Departement Leefmilieu en Infrastructuur. Administratie Waterwegen en Zeewezen. Afdeling Maritieme Schelde: Antwerpen. 35pp.

Tebbens, LA., Veldkamp, A. and Kroonenberg, S.B. (2000). Natural compositional variation of the river Meuse (Maas) suspended load : a 13ka bulk geochemical record from the upper Kreftenheye and Betuwe Formations in northern Limburg. *Netherlands Journal of Geosciences*, **79**, 391-409.

Tedrow, J.C.F. (1986) *Soils of New Jersey*. Robert E. Krieger Publishing Company, Malabar , Florida, 479 pp.

Tedrow, J.C.F. (2002) *Greensand and greensand soils of New Jersey: a review.* Department of Ecology, Evolution and Natural Resources Rutgers University, New Brunswick, 40 pp.

Titschack, J., Goetz-Neunhoeffer, F., Neubauer, J. (2011). Magnesium quantification in calcites (CaMgCO3) by Rietveld-based XRD analysis: Revisting a well-established method. *American Mineralogist*, **96**, 1028-1038.

Toucanne, S., Zaragosi, S., Bourillet, J-F., Marieu, V., Cremer, M., Eynaud, F., Turon, J-L. and Gibbard, P. (2010). The first estimation of the Fleuve Manche palaeoriver discharge during the last deglaciation: Evidence for Fennoscandian ice sheet meltwater flow in the English Channel ca. 20-18ka age. *Earth and Planetary Science Letters*, **290**, 459-473.

Ufer, K., Stanjek, H., Roth, G., Dohrmann, R., Kleeberg, R., Kaufhold, S. (2008). Quantitative phase analysis of bentonits by the Rietveld method. *Clays and Clay Minerals*, **56(2)**, 272-282.

Udgata, D.B.P. (2007) Glauconite as an indicator of sequence stratigraphic packages in a lower Paleocene passive-margin shelf succession, Central Alabama. Master thesis, Auburn University, 124 pp.

URS (2002). Lithological description and stratigraphic interpretation of the Beerse borehole. URS Internal report.

Utescher, T., Ashraf, A.R., Dreist, A., Dybkjær, K., Mosbrugger, V., Pross, J. and Wilde, V. (2012). Variability of Neogene Continental Climates in Northwest Europe. A Detailed Study Based on Microfloras. *Turkish Journal of Earth Sciences*, **21**, 289–314.

Van Alphen, J.S.L.J. (1990). A mud balance for Belgian-Dutch coastal waters between 1969 and 1986, Netherlands Journal of Sea Research, **25**, 19-30.

Van Calster P. (1960). Het sedimentatiemilieu van het Diestiaan ten noorden van Leuven. Unpublished licentiaatsthesis K.U. Leuven , Belgium.

Van Kessel,T. , Vanlede, J. and De Kok, J. (2011). Development of a mud transport model for the Scheldt estuary. *Continental Shelf Research*, **31**, 165-181.

Van Lancker, V., Deleu, S., Bellec, V., Le Bot, S., Verfaillie, E., Fettweis, M., Van den Eynde, D., Francken, F., Pison, V., Wartel, S., Monbaliu, J., Portilla, J., Lanckneus, J., Moerkerke, G. and Degraer, S. (2004). Management, research and budgeting of aggregates in shelf seas related to end-users (Marebasse). Belgian Science Policy, Scientific Report Year 2, 144pp.

Van Lancker, V., Du Four I, Degraer S, Fettweis M, Francken F, Van den Eynde D, Devolder M, Luyten P, Monbaliu J, Toorman E, Portilla J, Ullmann A, Verwaest, T, Janssens J, Vanlede J, Vincx, M, Rabaut M, Houziaux J.-S, Mallaerts T, Vandenberghe N, Zeelmaekers, E, and Goffin, A. (2009). QUantification of Erosion/Sedimentation patterns to Trace the natural versus anthropogenic sediment dynamics (QUEST4D). Final Report Phase 1. Brussels, Belgian Science Policy, 63pp. + annexes. (Research Programme Science for a Sustainable Development).

Van Loon, A.J., (2009). Unravelling the enigmas of the 'silver sands' in the Dutch/German/Belgian border area. *Netherlands Journal of Geosciences*, **88**, 133-145.

Van Maldegem, D. (1993). De slibbalans van het Schelde-estuarium. Studierapport Rijkswaterstaat, Dienst Getijdewateren, Nota GWAO-91.081.

Van Mierlo, C-J. (1897). Quelques mots sur le régime de la côte devant Heyst. *Annales de l'association des ingénieurs sortis des écoles spéciales de Gand*, tome **XX**, 4e livraison. *(in French)*

Van Ranst, E. and De Coninck, F. (1983). Evolution of glauconite in imperfectly drained soils of the Belgian Campine. *Zeitschrift fur Pflanzenernahrung and Bodenkunde,* **146**, 415-426.

Van Vliet-Lanoë, B., Vandenberghe, N., Laurent, M., Laignel, B., Lauriat-Rage, A., Louwye, S., Mansy, J.-L., Mercier, D., Hallégouët, B., Laga , P., Laquement, F., Meilliez, F., Michel, Y., Moguedet, G. and

Vidier, J.-P. (2002). Palaeogeographic evolution of norhwestern Europe during the Upper Cenozoic. *Geodiversitas,* **24**, 511-541.

Van Vliet-Lanoë, B., Gosselin, G., Mansy, J.-L., Bourdillon, C., Meurisse-Fort, M., Henriet, J.-P., Le Roy P. and Trentesaux, A. (2010). A renewed Cenozoic story of the Strait of Dover. *Annales Société Géologique du Nord,* **17** (2ième série) ,59-80.

Vandenberghe, N., Laga, P., Steurbaut, E., Hardenbol, J. and Vail, P. (1998). Sequence stratigraphy of the Tertiary at the southern border of the North Sea Basin in Belgium, *in*: *Mesozoic and Cenozoic Sequence Stratigraphy of European Basins. (De Graciansky, P-C., Hardenbol, J., Jacquin, T., Vail*, P.R., editors), SEPM, Special Publication, **60**, 119-154.

Vandenberghe, N., Van Simaeys, S., Steurbaut, E., Jagt, J., and Felder, P. (2004) Stratigraphic architecture of the Upper Cretaceous and Cenozoic along the southern border of the North Sea Basin in Belgium. *Netherlands journal of geosciences-geologie en mijnbouw,* **83** (3), 155-171.

Vandenberghe, N., Laga, P., Louwye, S., Vanhoorne, R., Marquet, R., De Meuter, F., Wouters, K. and Hagemann, H.W. (2005). Stratigraphic interpretation of the Neogene marine-continental record in the Maaseik well (49W0220) in the Roer valley Graben, NE Belgium. *Mémoirs of the Geological Survey of Belgium*, **52**, 39p.

Vandenberghe, N. and Mertens, J. (2013). Differentiating between tectonic and eustatic signals in the Rupelian Boom Clay cycles (Lower Oligocene, Southern North Sea Basin). *Newsletters on Stratigraphy* , **46**, 319-337.

Vandenberghe, N., Harris, W.B., Wampler, J.M., Houthuys, R., Louwye, S., Adriaens, R., Vos, K., Lanckacker, T., Matthijs, J., Deckers, J., Verhaegen, J., Laga, P., Westerhoff, W. and Munsterman, D. (2014). The implications of K-Ar glauconite dating of the Diest Formation on the paleogeography of the Uper Miocene in Belgium. *Geologica Belgica*, **17**, 161-174.

Vandenbroek, E. (1882). Diestien, Casterlien, Scaldesien. *Societé malacologique de Belgique*, **17**, 103-108.

Vanderaveroet, P., Averbuch, O, Deconinck, J.F. and Chamley, H. (1999). A record of glacial/interglacial alternations in Pleistocene sediments off New Jersey expressed by clay mineralogy, grain-size and magnetic susceptibility data, *Marine Geology*, **159**, 79-92.

Vanlede, J., Schramkowski, G., De Mulder, T. and Mostaert, F. (2009). Mud transport model for the Scheldt estuary: Hydrodynamics report. *WL Rapporten*, 756_06. Waterbouwkundig Laboratorium: Antwerp.

Vanlierde, E. (2013). Sediment concentrations, fluxes and source apportionment: methodology assessment and applications in Nete and Demer tributary basins (River Scheldt basin, Belgium). Doctoral dissertation, Ghent University, 328pp.

Varentsov, I.M., Sakharov, B.A. and Eliseeva T.G. (1983). Clay components of postmiddle Jurassic sediments of the southwest Atlantic, Deep Sea Drilling Project, Leg 71: depositional history and authigenic transformations. *DSDP Volumes 71, Deep Sea Drilling Project Report and Publications*.

Verlaan, PA.J., Donze, M. and Kulk, P. (1997). Marine versus fluvial suspended matter in the Scheldt estuary. *Estuarine, Coastal and Shelf Science*, **46**, 873-883.

Velde, B. (1985) Clay minerals. A physicochemical explanation of their occurrence. *Developments in Sedimentology*, **40**. Elsevier, Amsterdam, 427 pp.

Velde, B. and Meunier, A. (2008) *The origin of clay minerals in soils and weathered rocks*. Springer Verlag, Berlin, 406 pp.

Verhaegen, J., Adriaens, R., Louwye, S., Vandenberghe,N. and Vos,K. (2014). Sediment petrological study supporting the presence of the Kasterlee Formation in the Heist-op-den-Berg and Beerzel hills, southern Antwerp Campine, Belgium. *Geologica Belgica*, **17**, 323-332.

Verheyden S., Bogemans F., Backeljau T., Baeteman C. (2013). Lithostratigraphic and geochemical study of coastal deposits in Belgium. Implications for the age of the deposits and for bivalve-speleothem compared environmental reconstruction. *Geophysical Research Abstracts,* **15**, EGU2013-2853-1.(poster)

Viani,B.E., Roth, C.B. and Low, P.F. (1985). Direction measurement of the relation between swelling pressure and interlayer distance in Li-vermiculite. *Clays and Clay Minerals*, **33**, 244-250.

Vos, K. (in preparation). Dynamic image analysis using a Camsizer.

Vos, Zeiler (2008). Overstromingsgeschiedenis van zuidwest-Nederland, interactie tussen natuurlijke en antropogene processen. *Grondboor en hamer*, **62**, 86-96.

Walker, G.F. (1957). On the differentiation of vermiculite and smectites in clays. *Clay Minerals Bulletin*, **3**, 154–163

Walker, G.F. (1958). Reactions of expanding lattice clay minerals with glycerol and ethylene glycol. *Clay Minerals Bulletin*, **3**, 302–313

Walkley, A., Black, I.A. (1934). An examination of Degtjareff method for determining soil organic matter and a proposed modification of the chromic acid titration method. *Soil Science*, **37**, 29-37.

Weaver, C.E., Pollard, L.D. (1973) The Chemistry of Clay Minerals. *Developments in Sedimentology,* **15**, Elsevier Scientific Publishing Company, Amsterdam, London, New York, 213 pp.

Wong, T., de Lugt, I.R., Kuhlmann, G. and Overeem, I. (2007). Tertiary *in: Geology of the Netherlands* (Wong, T., Batjes, D.A.J, de Jager, J., editors). Royal Netherlands academy of arts and sciences, 354pp.

Wouters, L. and Schiltz, M. (2011). Overview of the field investigations in and around the nuclear site of Mol-Dessel. ONDRAF/NIRAS open report, 100pp + annexes.

Yans, J. (2003). Chronologie des sédiments kaoliniques à faciès wealdien (barrémien moyen et albien supérieur ; Bassin de Mons) et de la saprolite polyphasée (crétacé inférieur et miocène inférieur) de la Haute-Lesse (Belgique). Implications géodynamiques et paléoclimatiques. Doctoral dissertation, University of Mons,

Zachos, J. C., Pagani, M., Sloan, L., Billups, K., and Thomas, E. (2001). Trends, rhythms, and aberrations in global climate 65 Ma to present. *Science*, **292**, 686-693.

Zagwijn, .W.H. (1992). The beginning of the Ice Age in Europe at its major subdivisions. *Quaternary Science Reviews*, **406**, 583-591.

Zaitseva, T.S., Gorokhov, I.M., Ivanovskaya, T.A., Zyvagina, B.B., Mel'nikov, N.N., Yakovleva, O.V. (2005). Mineralogy, mössbauer characteristics and K-Ar isotopic age of glauconite from the Lower Cambrian sediments, Western Lithuania. *Lithology and Mineral resources*,Vol. **40**, No. 4, 353-363.

Zeelmaekers, E. (2011). Computerized qualitative and quantitative clay mineralogy: Introduction and application to known geological cases. Doctoral dissertation, University of Leuven, 397 pp.

Ziegler, P.A. and Dèzes, P. (2005). Neogene uplift of Variscan Massifs in the Alpine foreland: Timing and controlling mechanisms. *6th EUCOR-URGENT meeting*, Mt. St. Odile.

List of publications

Adriaens, R., Vandenberghe, N. and Elsen, J. (2014). Natural clay-sized glauconite in the Neogene deposits of the Campine basin (Belgium). *Clays and Clay Minerals*, 62, 35-52.

Snellings, R., Mertens, G., Adriaens, R. and Elsen, J. (2013). In situ synchrotron X-ray powder diffraction study of the early age hydration of cements blended with zeolitite and quartzite fines and water-reducing agent. *Applied Clay Science*, 72, 124-131.

Haerinck, T., Adriaens, R. , Debacker, T.N., Hirt, A.M. and Sintubin, M. (2013). Paramagnetic metamorphic mineral assemblages controlling AMS in low-grade deformed metasediments and the implications with respect to the use of AMS as a strain marker. *Journal of the Geological Society of London*, 170, 263-280.

Ronchi, B., Barao, L., Vandevenne, F., Van Gaelen, N., Verheyen, D., Adriaens, R., Batelaan, O., Dassargues, A., Struyf, E., Diels, J. and Govers, G. (2013). Opal-Ct precipitation in a clayey soil explained by geochemical transport model of dissolved Si (Blégny, Belgium). *Mineralogical Magazine*, 77, 2082-2082.

Verstrynge, E., Adriaens, R., Elsen, J. and Van Balen, K. (2014). Multi-scale analysis on the influence of moisture on the mechanical behavior of ferruginous sandstone. *Construction and Building Materials*, 54, 78-90.

Vandenberghe, N., Harris, W.B., Wampler, J.M., Houthuys, R., Louwye, S., Adriaens, R., Vos, K., Lanckacker, T., Matthijs, J., Deckers, J., Verhaegen, J., Laga, P., Westerhoff, W. and Munsterman, D. (2014). The implications of K-Ar glauconite dating of the Diest Formation on the paleogeography of the Upper Miocene in Belgium. *Geologica Belgica*, **17**, 161-174.

A. Licht, M. van Cappelle, H. A. Abels, J.B. Ladant, J. Trabucho-Alexandre, C. France-Lanord, Y. Donnadieu, J. Vandenberghe, T. Rigaudier, C. Lécuyer, D. Terry Jr., R. Adriaens, A. Boura, Z. Guo, Aung Naing Soe, J. Quade, G. Dupont-Nivet, J.-J. Jaeger. Asian monsoons in a late Eocene greenhouse world. *Nature*, **513**, 501-506.

Verhaegen, J., Adriaens, R., Louwye, S., Vandenberghe, N. and Vos, K. (2014). Sediment petrological study supporting the presence of the Kasterlee Formation in the Heist-op-den-Berg and Beerzel hills, southern Antwerp Campine, Belgium. *Geologica Belgica*, **17**, 323-332.

Ronchi B., Adriaens R., Barao L., Vandevenne F., Van Gaelen N., Verheyen D., Clymans W., Batelaan O., Dassargues A. Govers G., Struyf E. and Diels J., under review for publication in *Geoderma*. Land use impact on the biogeochemical cycle of Si in temperate climates: authigenic clay formation (Belgium).

Adriaens, R. , Ronchi, B., Mertens, G., Vandenberghe, N. and Elsen, J., in preparation for *Geologica Belgica*. Halloysite occurrence at the contact of Oligocene sand infillings and karstified Cretaceous calcarenites in Hinnisdael caves, Vechmaal (E of Belgium).

Zeelmaekers, E., Honty, M., Derkowski, A., Środoń, J., De Craen, M., Vandenberghe, N., Adriaens, R. and Wouters, L. - *under review for publication in Clay Minerals.* Qualitative and quantitative mineralogical composition of the Rupelian Boom Clay in Belgium.

Barrie, E. , Cappuyns, V. , Vassilieva, E. , Adriaens, R., Hollanders, S. , Garcés, D. , Carrion, D. , Parra, C. , Paredes, C., Pontikes, Y., Elsen, J. and Machiels, L. – in preparation. Potential of meta-halloysite and volcanic glass based polymers for the encapsulation of tailings from gold extraction (Ecuador).